UNIVERSITÄT
ZU KÖLN

Studies on Nitrogenous Sulfates

Inaugural-Dissertation

zur

Erlangung des Doktorgrades

(Dr. rer. nat.)

der Mathematisch-Naturwissenschaftlichen Fakultät

der Universität zu Köln

vorgelegt von

Tobias Rennebaum

aus Köln

Köln, 2024

Submission date:	01.07.2024
Disputation date:	10.09.2024
First reviewer and examiner:	Prof. Dr. Mathias S. Wickleder
Second reviewer and examiner:	Prof. Dr. Uwe Ruschewitz
Chair of the thesis defense committee:	Prof. Dr. Stephanie Kath-Schorr

„Nur einem glücklichen Zufalle ist es zu danken, dass der Schreiber dieser Zeilen vor Unheil bewahrt blieb“

Theodor Curtius (**1890**, „Über die Stickstoffwasserstoffsäure (Azoimid) N_3H“)

Zusammenfassung

Die vorliegende Dissertation behandelt das chemische Gebiet der stickstoffhaltigen Derivate der Schwefelsäure. Durch formale Substitution einer Hydroxylgruppe (–OH) durch Stickstoff bzw. einer Aminogruppe (–NH_2) erhält man einen strukturellen Baustein, der eine Vielzahl an bekannten und denkbaren Verbindungen repräsentiert. Insgesamt wurden vier Teilbereiche in dieser Arbeit synthetisch und analytisch elaboriert.

Durch Reaktionen der Stickstoffquellen $P_3N_3Cl_6$ und $(S_3N_2Cl)Cl$ mit verschiedenen Metallsalzen in flüssigem Schwefeltrioxid wurde eine Vielzahl an Verbindungen mit ringförmigen Nitridosulfatanionen erhalten. Dabei handelt es sich sowohl um Komplexverbindungen als auch um klassisch ionische Strukturen. Die strukturelle Aufklärung der Verbindungen erfolgte weitestgehend kristallographisch. Die in den Strukturen enthaltenden Anionen $[S_3NO_8]^-$, $[S_4N_2O_{10}]^{2-}$, $[S_4NO_{11}]^-$, $[S_4N_3O_9]^{3-}$ und $[S_4N_3O_8Cl]^{2-}$ weisen allesamt eine ähnliches Strukturmotiv auf. Ferner gelang es eine phosphorhaltige Verbindung mit der Konstitution $S_6N_4O_{13}H_2{\cdot}P_2O_3Cl_4$ aus dem Reaktionssystem $SO_3/P_3N_3Cl_6$ zu isolieren.

Im zweiten Teil wurden die Sulfonate des Hydrazins systematisch untersucht. Diese Verbindungsklasse ist schon lange Zeit bekannt, jedoch mangelt es an einer ausführlichen analytischen Betrachtung. Als einfach sulfonierte Hydrazinverbindungen wurde die zwitterionische Hydrazinmonosulfonsäure und dessen Bariumsalz ausführlich charakterisiert.
Des Weiteren wurden das Hydrazindisulfonat, $[(SO_3)HNNH(SO_3)]^{2-}$, und das isomere Hydrazin-*iso*-disulfonat, $[H_2NN(SO_3)_2]^{2-}$, in verschiedenen Salzen ausführlich analysiert und verglichen. Zuletzt wurde das schwerzugängliche Hydrazintetrasulfonat, $[(SO_3)_2NN(SO_3)_2]^{4-}$, synthetisiert und in zwei verschiedenen Verbindungen charakterisiert. Die strukturelle Aufklärung aller Hydrazinsulfonate erfolgte durch Einkristalldiffraktometrie. Darauf aufbauend erfolgte eine Phasenanalyse der kristallinen Produkte mit der *Rietveld*-Methode. Zudem wurde das thermische Zersetzungsverhalten betrachtet sowie die schwingungsspektroskopischen Eigenschaften unter Zuhilfenahme von quantenmechanischen Berechnungen ausgearbeitet.

Das Azidosulfat $[SO_3N_3]^-$ stellt ein ebenfalls bekanntes aber ebenso nicht tiefgründig analysiertes Anion in der Literatur dar. Durch zwei verschiedene Herangehensweisen wurden die Verbindungen $(TBA)_3(N_3)_3[SO_3N_3]$, $(TBA)[SO_3N_3]$, $K[SO_3N_3]$ und $Na_3[SO_3N_3]_3(CH_3CN)$ dargestellt und mittels Einkristallstrukturanalyse aufgeklärt. $K[SO_3N_3]$ wurde hierbei in größeren Mengen erhalten, was eine umfangreiche Untersuchung mittels spektroskopischer sowie thermischer Methoden ermöglichte.

Im letzten Kapitel wurden drei neue gemischt kationische hochsymmetrische Verbindungen des Nitrido-*tris*-sulfates, $[N(SO_3)_3]^{3-}$, ausgehend von $K_3[N(SO_3)_3](H_2O)_2$ aus alkalischem Medium dargestellt. $K_3[N(SO_3)_3](H_2O)_2$ wurde mit Röntgenmethoden analysiert und das thermische Verhalten untersucht. Dabei wurde die Empfindlichkeit des $[N(SO_3)_3]^{3-}$ Anions gegenüber Hydrolyse in Salzmetathesen bestätigt.

Abstract

This dissertation deals with the chemical compound class of nitrogen-containing derivatives of sulfuric acid. The formal substitution of a hydroxyl group (-OH) by nitrogen or an amino group ($-NH_2$) yields a structural entity that represents a large number of known and conceivable compounds. In total four sub-areas were synthetically and analytically elaborated in this work.

By reactions of the nitrogen sources $P_3N_3Cl_6$ and $(S_3N_2Cl)Cl$ with metal salts in liquid sulfur trioxide, various compounds with cyclic nitridosulfate anions were obtained. These are both complex compounds and classic ionic structures. Structural elucidation was mainly carried out by single crystal X-ray diffraction. The yielded anions $[S_3NO_8]^-$, $[S_4N_2O_{10}]^{2-}$, $[S_4NO_{11}]^-$, $[S_4N_3O_9]^{3-}$ and $[S_4N_3O_8Cl]^{2-}$ exhibit a similar structure motif. Additionally, it was possible to isolate a phosphorus-containing compound with the constitution of $S_6N_4O_{13}H_2{\cdot}P_2O_3Cl_4$ from the reaction system $SO_3/P_3N_3Cl_6$.

The second part of this thesis covers the systematic studies on the sulfonates of hydrazine. The sulfonates have been known for a long time but lack completely of analytical data. The zwitterionic hydrazine monosulfonic acid and its barium salt were characterized in detail as monosulfonated compounds. Furthermore, the hydrazine disulfonate, $[(SO_3)HNNH(SO_3)]^{2-}$, and isomeric hydrazine *iso*-disulfonate, $[H_2NN(SO_3)_2]^{2-}$, in various salts were analyzed and compared structurally. Finally, the elusive hydrazine tetrasulfonate anion was synthesized and investigated in two compounds. The structure determination off all hydrazine sulfonates was carried out by single crystal X-ray diffraction. This was followed by a phase analysis of the crystalline compounds using the *Rietveld* method. In addition, the thermal decomposition behavior was examined and the vibrational spectroscopic properties were worked out with the aid of quantum mechanical calculations.

Thirdly, the azidosulfate anion, $[SO_3N_3]^-$, was focused on, which is also a known but not thoroughly analyzed anion in the literature. Using different approaches, the compounds $(TBA)_3(N_3)_3[SO_3N_3]$, $(TBA)[SO_3N_3]$, $K[SO_3N_3]$ and $Na_3[SO_3N_3]_3(CH_3CN)$ were synthesized and elucidated using single crystal XRD. $K[SO_3N_3]$ was obtained in larger quantities, which enabled a comprehensive study by spectroscopic and thermal methods.

In the last chapter, three new mixed cationic highly symmetric compounds of the nitrido-*tris*-sulfate $[N(SO_3)_3]^{3-}$ were prepared from $K_3[N(SO_3)_3](H_2O)_2$ in alkaline medium. $K_3[N(SO_3)_3](H_2O)_2$ was analyzed by X-ray methods and the thermal behavior was investigated. The sensitivity towards hydrolysis of the $[N(SO_3)_3]^{3-}$ anion was also confirmed in salt metathesis.

List of Abbreviations

A	Alkali metal
(A)	Acceptor
as	Antisymmetric
BASF	Batch scale factor
br	Bridging
Calcd.	Calculated
CCDC	Cambridge Crystallographic Data Centre
CIF	Crystallographic Information File
CN	Coordination Number
CSD	Cambridge Structural Database
(D)	Donor
DSC	Differential Scanning Calorimetry
en	Ethane-1,2-diamine
Eq.	Equivalents
Exp.	Experimental
FEP	Fluorinated ethylene propylene (copolymer)
GooF	Goodness of fit
Hal	Halogen
K	Kelvin
M	Metal
Max	Maximum
NMR	Nuclear Magnetic Resonance
OAc	Acetate
Obsd.	Observed
p.	Page
Py	Pyridine
Py-H	Pyridinium
$Py{\cdot}SO_3$	Pyridine sulfur trioxide complex
PTFE	Polytetrafluoroethylene
P-XRD	Powder X-ray diffraction
R	Organic Rest
s	symmetric
SC-XRD	Single crystal X-ray diffraction
t	Terminal
T	Temperature
TBA	Tetrabutylammonium, $[N(C_4H_9)_4]^+$
TG	Thermogravimetry
TGA	Thermogravimetric Analysis
TMS	Trimethylsilyl
XRD	X-ray diffraction

Table of Contents

1 Introduction

The mineral acid sulfuric acid (H_2SO_4), its salts and derivatives are of enormous importance for today's industry and research. A production amount of 2.9 million tons in Germany and around 200 million tons worldwide for just sulfuric acid makes it the inorganic chemical with largest production volume.[1-2] Starting from burning elemental sulfur the acid is produced in large scales in the so-called "double contact double absorption" process.[3] From there the acid is used in a variety of chemical processes as the production of fertilizers and other mineral acids as phosphoric or hydrochloric acid. The structure-chemical properties of the sulfuric acid and its anhydride, sulfur trioxide (SO_3), were gradually investigated over the course of the last century. While the first solid-state modification of SO_3 was already reported in 1941, a precise solid-state structure of sulfuric acid was described in 1965 followed by some reinvestigations (see Figure 1).[4-9] The structure of disulfuric acid, $H_2S_2O_7$, was just revealed in 1991 by *Hönle*.[10] Aside from the corresponding classical anions, the sulfates (SO_4^{2-}) and hydrogensulfates (HSO_4^-), the polysulfates with the general equation $[S_nO_{3n+1}]^{2-}$ represent a fundamental compound class. They were thoroughly studied from trisulfates ($n = 3$) to hexasulfates ($n = 6$) in recent years by *Wickleder et al.* after the first publication of the nitrosonium trisulfate, $(NO)_2[S_3O_{10}]$, dates back to 1954.[11-17]

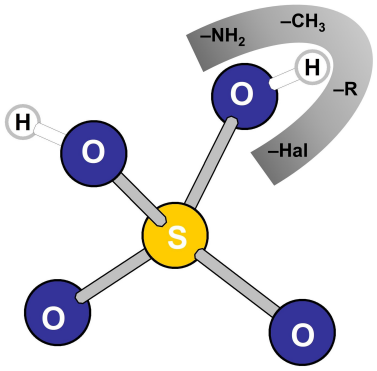

Figure 1: Structure of H_2SO_4 in the solid-state (*Kemnitz et al.*[8]), which represents the fundamental structural component for derivatization in this work.

When the derivatives of sulfuric acid by a formal substitution of one hydroxyl group are included, important compounds like the organic sulfonic acids R-SO_3H (R = organic rest), halogen sulfonic acids X-SO_3H (X = halogen) or the nitrogenous sulfonic acid R_2N-SO_3H (R = organic/inorganic rest) can be pointed out. The most prominent nitrogen derivative is the so-called sulfamic or amidosulfuric acid, which is commonly used as a descaler and has zwitterionic structure in the solid state.[18-19] It can be formally seen as the adduct between the Lewis acid SO_3 and Lewis base NH_3 and further nitrogenous sulfonates can be derived from it. Thus, a stepwise deprotonation leads to three anions, namely amidosulfate, imidosulfate and nitridosulfate of which the latter two are barely described in the literature.[20-21] A formal substitution of the protons by SO_3 groups leads in turn to the anions imido-*bis*-sulfate $[HN(SO_3)_2]^{2-}$ and nitrido-*tris*-sulfate $[N(SO_3)_3]^{3-}$, which are also rarely mentioned

in the literature. The entire concept can be elaborated further with nitrogenous Lewis bases as e.g. hydrazine (N_2H_4) or azide (N_3^-).[22-24] Sulfonates of hydrazine and azide are lacking of a proper structural-chemical analysis in the literature as well.

Wickleder and *van Gerven* recently succeeded in synthesizing the cage-shaped molecule $S_6N_2O_{15}$, which represents formally the anhydride of the unknown nitrido-*tris*-sulfuric acid, $[N(SO_3H)_3]$.[25] Prepared in a solvothermal reaction between SO_3 and $P_3N_3Cl_6$ this synthesis route provides a basis for further nitrogenous sulfates. Based on this, the anions $[S_6N_3O_{14}]^-$, $[S_3NO_8]^-$ and $[S_4N_2O_{10}]^{2-}$ were yielded by adding metals salts to mixtures of SO_3 and $P_3N_3Cl_6$.[26] The structural characteristic of these cyclic anions are the vertex-connected $[SO_4]$ and $[SO_3N]$ tetrahedra. However, the control and mechanistical interpretation of these reactions is quite challenging due to the harsh conditions.

Overall, the topic of nitrogenous sulfates still offers great potential for research. This includes compounds which are known for decades, but their chemical and structural properties have hardly been investigated. In turn, there is still space for new structures that do not only exist on paper, which was shown lately.[25] This work is fundamentally dedicated to this issue and therefore considers methods that have already proven to be successful in the past as well as state-of-the-art synthetic, theoretical and analytical approaches.

2 State of Knowledge

2.1 Sulfur Trioxide

As the anhydride of sulfuric acid, sulfur trioxide (SO_3) holds an important industrial status. In the industrial "double contact double absorption" (DCDA) process introduced by the Bayer AG in 1963 it is produced in millions of tons annually.[3,27] In this process sulfur dioxide (SO_2), which is beforehand prepared by burning of elemental sulfur or roasting of metal sulfides, is catalytically oxidized to SO_3 by a catalyst with vanadium(V) oxide (V_2O_5) as an active component. In this process, conversion efficiencies above 99% are achieved.[28] If SO_3 is passed into sulfuric acid polysulfuric acids with the general formula $H_2S_nO_{3n+1}$ are formed. This mixture is then hydrolyzed to sulfuric acid by stepwise addition of water.[29-30] Sulfuric acid with free SO_3 portions (commercially 20%-65%) is commonly known under the names "fuming sulfuric acid" or "oleum".

Gaseous SO_3 as a monomer has a trigonal-planar (D_{3h}) structure. The monomeric form is in a pressure- and temperature-dependent equilibrium with the cyclic trimeric form, S_3O_9. This equilibrium exists both in the gaseous and liquid phase but in the gaseous phase monomeric SO_3 is dominant.[31] At 44.5 °C (1013 hPa) the gaseous form condenses to a liquid, which crystallizes at 16.86 °C to rhombic γ-SO_3.[27,32] In total three polymorphs of SO_3 are known in the solid state. They are called α-, β- and γ-SO_3, respectively. The ice-like γ-modification consists of three connected SO_3 molecules forming a six-membered ring of vertex-connected [SO_4] tetrahedra (see Figure 2).[4,7] Presence of traces of water (≈ 10^{-3} mol%) induces the formation of the asbestos-like looking α- and β-SO_3 modifications.[33] The crystallographic analysis of β-SO_3 shows a polymeric structure of vertex-connected [SO_4] tetrahedrons with an unknown chain length (see Figure 2).[5] Therefore it can be defined as a polysulfuric acid with the formula $H(OSO_2)_nOH$ (n ≈ 10^5).

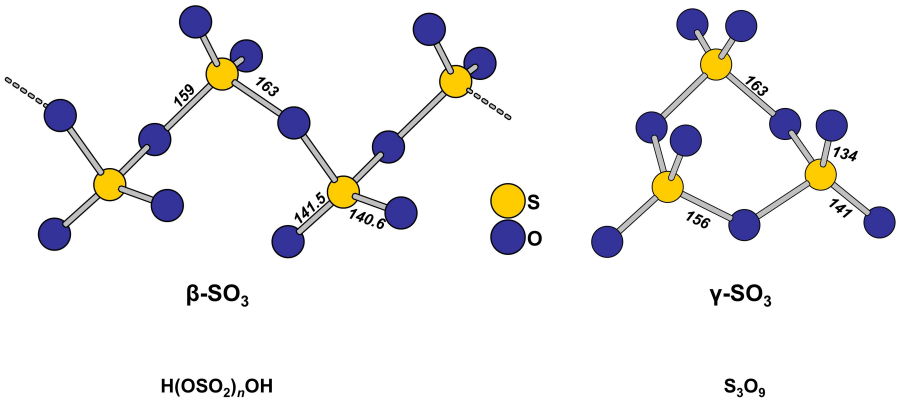

Figure 2: Solid-state structures of the SO_3 polymorphs β- and γ-SO_3.[4-5] Selected bond lengths in pm are shown in italics.

The α-SO_3 modification is crystallographically not examined, however a cross-linkage of the polysulfuric chains seems reasonable since it has the higher melting point with 62.2 °C compared to the β-SO_3 with 32.5 °C.[33] Additives, such as boric acid, thionyl chloride, silica or sulfonic acids,

can prevent the polymerization of SO_3.[27,29] Handling of pure SO_3 is difficult and dangerous due to its strong Lewis acidic character and oxidizing strength. It reacts violently with traces of water by forming sulfuric acid and with oxides, the high electron-affinity promotes the formation of sulfates. In addition, with several Lewis bases as e.g. pyridine, ammonia, 1,4-dioxane, trimethylamine, triphenylphosphin or tetrasulfur tetranitride it forms donor–acceptor adducts (see Figure 3).[34-38] These adducts can be applied as sulfonation reagents with less reactive nature compared to fuming sulfuric acid or pure SO_3.[34,37]

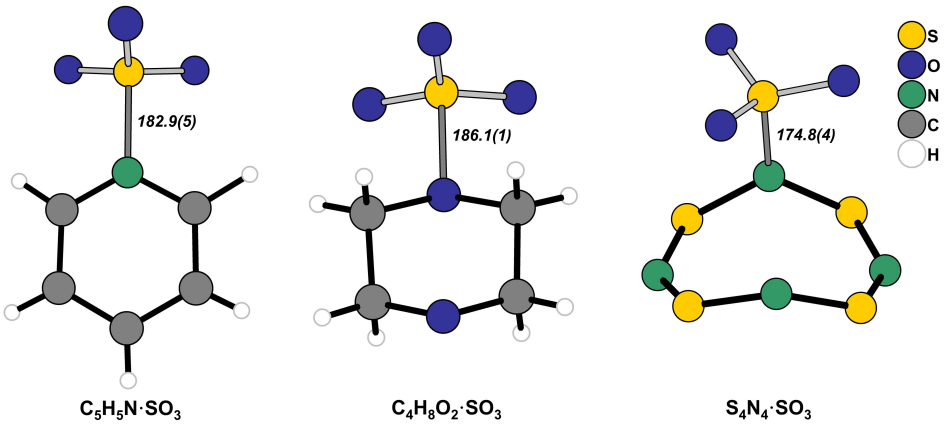

Figure 3: Structure of the SO_3 adducts of pyridine (left), 1,4-dioxane (middle) and S_4N_4 (right) obtained from single crystal X-ray diffraction.[34-35,38] The donor–acceptor distances (S–N, S–O) are in pm.

SO_3 can also act as an electron-donating ligand for strong Lewis acids as $SbCl_3$[39], $SbCl_5$[40] and $AsCl_3$[41]. Furthermore, it can oxidize e.g. elemental iodine to I_4^{2+}, Pd^0 to Pd^{2+}, S_8 to SO_2 and P_4 to P_4O_{10}, to name just a few examples.[42-44] On a laboratory scale SO_3 is accessible by distillation of commercially available fuming sulfuric acid with a free SO_3 content of 20% or 65%. The distillation over hot P_4O_{10} enables additional drying and further decomposition of H_2SO_4 to SO_3 under formation of polyphosphoric acids.[45-47]

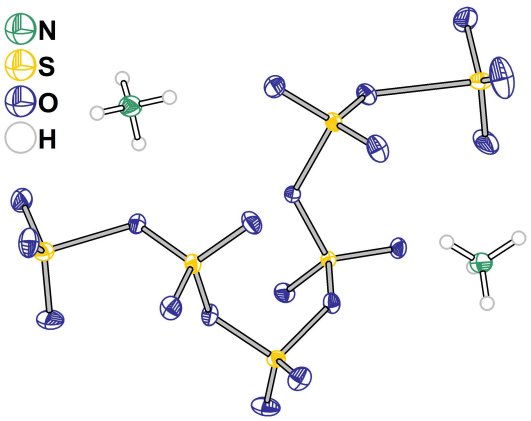

Figure 4: Structure of the hexasulfate $(NH_4)_2[S_6O_{19}]$ obtained by *Wickleder et al.*[15] The thermal ellipsoids are set to probability level of 70%.

In reactions between pure SO_3 and cations, polysulfates with the general constitution $[S_nO_{3n+1}]^{2-}$ can be prepared. *Wickleder* and coworkers provided many contributions on this subject with structure of

trisulfates up to hexasulfates (hexasulfate see Figure 4, p. 4).[13,15-17,43] A structural characteristic of these anions are alternating bond lengths between sulfur and the bridging oxygen atoms. A higher chain-length increases the terminal O^{br}–S bond lengths and the terminal [SO_3] units are increasingly adopting trigonal-planar geometry.[15]

2.2 Sulfonic Acids of Ammonia

The most prominent nitrogen derivative of sulfuric acid is the amidosulfuric acid, H_3NSO_3, also called sulfamic acid.[48] The acid can be interpreted either as the amide of sulfuric acid or as a sulfonic derivative of ammonia. The first report on the acid dates back to 1834 which describes the reaction between dry ammonia and SO_3.[49] The properties and synthesis were later analyzed in more detail by *E. Berglund* and *F. Raschig*.[50-51] *Raschig* prepared it in a reaction between hydroxylamine and sulfurous acid, H_2SO_3.[52] *Baumgarten* published a synthetical route in 1936, which is still used by the industry today.[53-54] In this process urea is treated with fuming sulfuric acid yielding H_2NSO_3H, CO_2 and $NH_4(HSO_4)$ (see Scheme 1).[53]

$$H_2SO_4 + OC(NH_2)_2 + SO_3 \xrightarrow{130\ °C} 2\ H_3NSO_3 + CO_2$$

Scheme 1: Industrial synthesis of the amidosulfuric acid (H_3NSO_3) starting from urea.[54]

Under ambient conditions the acid is solid with a melting point of 205 °C.[51] The high melting point results from the zwitterionic nature of the acid in the solid state according to $^{+}H_3N–SO_3^{-}$, which was proven by single crystal X-ray and neutron diffraction as well as vibrational spectroscopy.[18,55-56] Along the N–S bond a staggered conformation is present resulting in a molecular symmetry C_{3v}. The N–S bond has a length of 176.84(8) pm and is therefore significantly longer compared to the amidosulfate anion (167 pm) and sulfamide (162 pm).[57-58] With a pK_a value of around 1, it can be considered a strong acid.[59-60] In aqueous solution, the acid is stable at ambient temperatures but undergoes hydrolysis to NH_3 and H_2SO_4 at higher temperatures.[60-61] Its acidic properties and good handling also aroused the interest of the chemical industry.[60] Upon today the acid is used in practice as a commercially available descaler, metal cleaner and a common standard in the acidimetry with a worldwide production quantity of almost 100000 metric tons per year.[54] Additionally, it is an important NO_2^- scavenger as it reacts quantitatively with the latter in a comproportionation to form N_2 and $[HSO_4]^-$.[62-63]

$$NO_2^- + H_3NSO_3 \longrightarrow N_2 + HSO_4^- + H_2O$$

Scheme 2: Reaction of nitrite with amidosulfuric acid.

Single crystals of the acid have recently received attention as a material for nonlinear optical applications.[64]

As a triprotic acid, three anions can be derived, namely the amidosulfate, $[H_2NSO_3]^-$, the imidosulfate, $[HNSO_3]^{2-}$ and nitridosulfate, $[NSO_3]^{3-}$ (see Figure 5). The latter two are isoelectronic to $[HPO_4]^{2-}$ and $[PO_4]^{3-}$, respectively. The amidosulfates can be easily prepared in presence of oxides, hydroxides and carbonates and are widely reported in literature.[56,61,65-66]

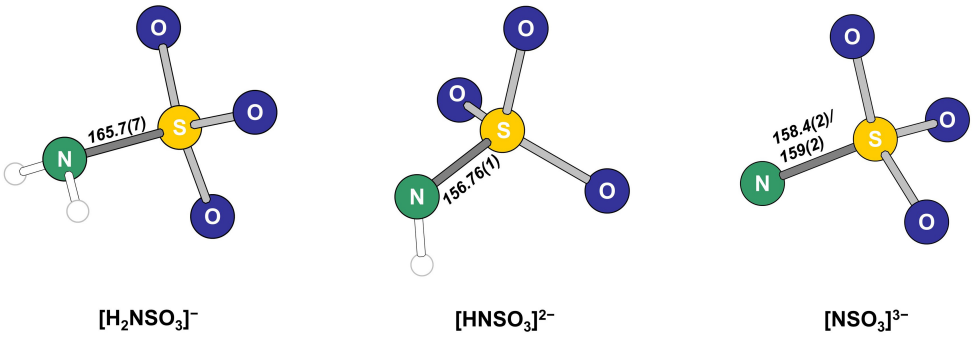

Figure 5: Structures of the anions $[H_2NSO_3]^-$, $[HNSO_3]^{2-}$ and $[NSO_3]^{3-}$. The structures were obtained from SC-XRD analysis of the compounds $Na[H_2NSO_3]$[67], $Na_2[HN(SO_3)_2]$[21] and $Ag_3[NSO_3](H_2O)$[68]. The S–N distances (italics) are in pm.

Apart from classical metal salts, *Wickleder* obtained several amidosulfates of trivalent rare-earth elements, e.g. $Nd[H_2NSO_3](SO_4)(H_2O)_{1.5}$, $Nd[H_2NSO_3](H_2O)_2$ and $La[H_2NSO_3]_3$ which were prepared by simple evaporation of solutions containing Ln^{3+} cations and amidosulfuric acid.[69-71] Lately, *Höppe et al.* reported on the preparation and thermal behavior of new alkaline-earth amidosulfates.[66] They outlined that a small amount of tetrasulfur tetranitride, S_4N_4, is formed during the thermal decomposition. Thus, the thermal decomposition of amidosulfates represents an alternative route to prepare S_4N_4, without the need to start from sulfur halides or elemental sulfur.

The second protolysis step of amidosulfuric acid, the imidosulfate anion $[HNSO_3]^{2-}$, is only accessible under stronger alkaline conditions. The mixed cationic imidosulfates, $AgK[HNSO_3](H_2O)$ and $AgNa[HNSO_3](H_2O)$ were reported in the early 20th century.[72-73] These salts were accessed by reacting NH_3SO_3 with $AgNO_3$ in NaOH and KOH, respectively. *Wickleder et al.* contributed to this compound class with the salts $Na_2[HNSO_3]$, $K_2[HNSO_3]$ and $BaNa_2[HNSO_3]_2$.[21] These imidosulfates were obtained by solvothermal reactions between NH_3SO_3 and the respective bases NaOH, KOH or $Ba(OH)_2$ in PTFE tubes. The SC-XRD data shows that the S–N bond lengths reveal values of 156.12(6) pm (K^+-salt), 156.76(1) pm (Na^+-salt) and 156.01(6) pm (Ba^{2+}/Na^+-salt). The distances, which are in the range of 160-166 pm, are therefore slightly shorter than in comparable amidosulfates.[65-67,70]

For the nitridosulfates, $[NSO_3]^{3-}$, even less literature entries can be found. Only two crystal structures containing this anion, namely $Ag_3[NSO_3](H_2O)$ and $Ag_3[NSO_3](NH_3)_3(H_2O)_2$ are know so far, both reported by *Belaj* in 1987.[68,74] Their synthesis was achieved by adding $AgNO_3$ to an solution of $K[H_2NSO_3]$ with a high concentration of ammonia. The unique $[SO_3N]^{3-}$ anions within the structure have a distorted tetrahedral geometry with S−N distances of 158.4(2)-159(2) pm and S−O distances of 146(2)-150(2) pm.

$Li_3[NSO_3]$ as a third nitridosulfate was reported by *Kurzman* in 2013.[20] This compound was prepared within a ball mill reaction of $Li[H_2NSO_3]$ with two equivalents of $LiNH_2$ and LiH, respectively. The structure was analyzed by *Rietveld* refinement of neutron powder diffraction data. The structure adopts the low-temperature modification (*β, Pmn*2_1) of the isoelectronic Li_3PO_4. The successful synthesis was supported by means of infrared spectroscopy and thermal analysis (TG/DSC). Additionally, by impedance spectroscopy and cyclic voltammetry it turned out that $Li_3[NSO_3]$ is a weak ionic conductor with an extrapolated room temperature conductivity around 10^{-14} S·cm^{-1}.[20]

The amidosulfuric acid can be conceived as derivative of ammonia by replacing one hydrogen atom by a $[HSO_3]$ group. Substitution of the other two protons by $[HSO_3]$ yields the formal acids, called imido-*bis*-sulfuric acid $HN(SO_3H)_2$ and nitrido-*tris*-sulfuric acid $N(SO_3H)_3$. These acids were mentioned in the literature since the end of the 19th century but neither they were isolated nor analytically confirmed up to now.[52,61,75] However, the corresponding bases, the imido-*bis*-sulfate $[HN(SO_3)_2]^{2-}$ and nitrido-*tris*-sulfate $[N(SO_3)_3]^{3-}$ are reported mainly as salts of ammonium and potassium.[61,76-78] The ammonium salt can be obtained if gaseous or solid SO_3 reacts with gaseous or liquid NH_3. Analytically, there is hardly any data on these compounds. Only the structures $K_3[N(SO_3)_3](H_2O)_2$[79-81] and $K_2[HN(SO_3)_2]$[82-84] have been examined by SC-XRD and spectroscopic methods. The nitrido-*tris*-sulfate $K_3[N(SO_3)_3](H_2O)_2$ can be prepared in a simple reaction in water between KNO_2 and $K_2S_2O_5$ or $KHSO_3$.

$$KNO_2 + 2\,K_2S_2O_5 + 2\,H_2O \longrightarrow K_3[N(SO_3)_3](H_2O)_2 + K_2SO_3$$

$$[N(SO_3)_3]^{3-} + H_2O \xrightarrow{H^+} [HN(SO_3)_2]^{2-} + SO_4^{2-} + H^+$$

Scheme 3: Preparation of $K_3[N(SO_3)_3](H_2O)_2$ according to *Sisler et al.* and hydrolysis of the $[N(SO_3)_3]^{3-}$ anion to $[HN(SO_3)_2]^{2-}$.[61,78]

The $[N(SO_3)_3]^{3-}$ anion can only be stabilized in aqueous alkaline solutions and undergoes hydrolysis to $[HN(SO_3)_2]^{2-}$ under neutral and acidic conditions.[82] So $K_2[HN(SO_3)_2]$ simply forms by keeping $K_3[N(SO_3)_3](H_2O)_2$ in neutral aqueous solution for a while. It can even convert into $K[H_2NSO_3]$ in strongly acidic media. By deprotonation of $K_2[HN(SO_3)_2]$ using potassium hydroxide, the nitrido-*bis*-sulfate, $K_3[N(SO_3)_2](H_2O)$ is synthesized.[84] The $[N(SO_3)_2]^{3-}$ anion can also be included in the series of sulfates of ammonia and is just analyzed by SC-XRD in form of the potassium salt.[84-85] Like $[N(SO_3)_3]^{3-}$, it is very prone to hydrolysis.

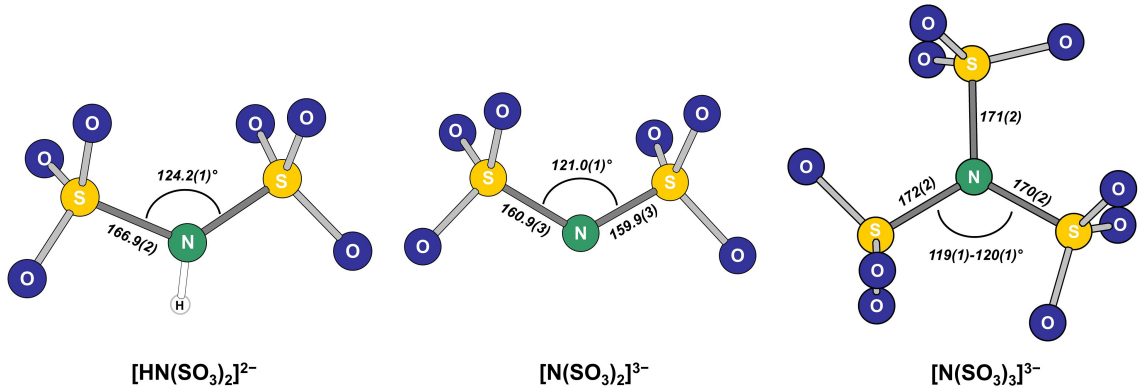

Figure 6: Structures of the anions $[HN(SO_3)_2]^{2-}$, $[N(SO_3)_2]^{3-}$ and $[N(SO_3)_3]^{3-}$ with observed ∠S–N–S angles and bond lengths for S–N (italics, in pm). The structures were obtained from SC-XRD analysis of the compounds $K_2[HN(SO_3)_2]$[84], $K_3[N(SO_3)_2](H_2O)$[85] and $K_3[N(SO_3)_3](H_2O)_2$[79].

The observed S–N distances in these anions have values of 166.9(2) pm for $[HN(SO_3)_2]^{2-}$, 160.9(3)/159.9(3) pm for $[N(SO_3)_2]^{3-}$ and 170(2)-172(2) pm for $[N(SO_3)_3]^{3-}$ (see Figure 6). The significantly shorter S–N bond length in $[N(SO_3)_2]^{3-}$ results from π-bonding of the lone pair orbitals of nitrogen to the unfilled 3d orbitals of sulfur.[85] The $[N(SO_3)_3]^{3-}$ can be assigned to point symmetry C_{3h} in the solid state. Overall, it is apparent that there are hardly any known and analyzed compounds in this category. *Van Gerven* and *Wickleder* recently contributed to this structural class by synthesizing the molecule $S_6N_2O_{15}$ (see Figure 7, p. 9).[25] This remarkable cage-shaped molecule represents the anhydride of the formal nitrido-*tris*-sulfuric acid, $N(SO_3H)_3$. The molecule can be prepared from a reaction between liquid SO_3 and aromatic hexachlorophosphazene ($P_3N_3Cl_6$) in sealed glass ampoules at 80 °C. Although the reaction mechanism remains unclear and by-products were not identified, the desired compound can be reproduced as a colorless crystalline solid. In 1954 *Goehring et al.* already reported about the reaction of SO_3 and $P_3N_3Cl_6$ in research for SO_3 Lewis acid-base adducts. Three equivalents of SO_3 were condensed onto $P_3N_3Cl_6$ at 40 °C and a resulting compound with the stoichiometry $P_3N_3Cl_6 \cdot 3\ SO_3$ was gravimetrically determined which decomposed at higher temperatures. However, there is no supporting analytical data on this SO_3 adduct up to now. The similarity of $S_6N_2O_{15}$ to the nitrido-*tris*-sulfate mentioned above results from the structural peculiarity that the two nitrogen atoms are surrounded in a trigonal planar manner by three $[SO_3]$ groups. The nitrogen atoms are connected via three $[S_2O_5]$ units which can be expressed by the formula $N[O_2S(O)_\mu SO_2]_3N$ for clarity.[25] The S–N bonds occupy similar values of 170.6(2)-171.6(2) pm and within the three S–O–S bridges distances of 161.8-163.8 pm and angles of about 125° are observed. In contrast, the terminal S–O bonds only take values of around 140 pm. The trigonal planar NS_3 units hint that the lone-pair of nitrogen is used for π-bonding to the sulfur atoms. Theoretical calculations reveal C_{3h} symmetry of the molecule but in solid state only C_1 is found.

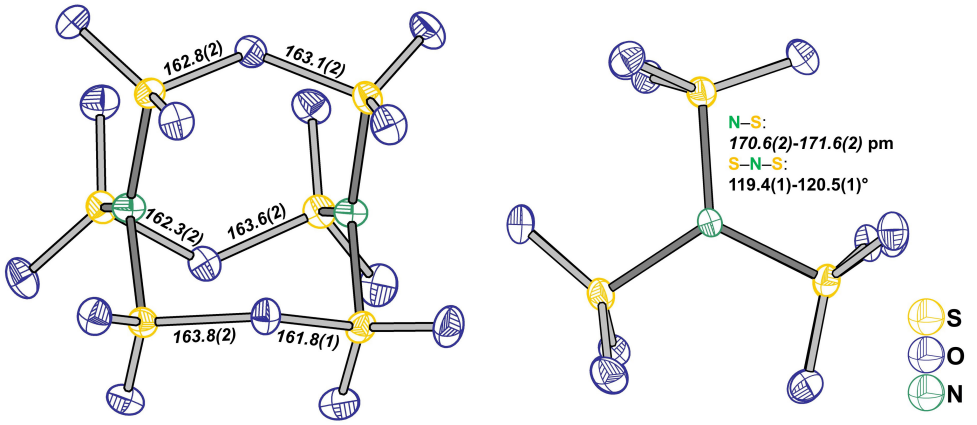

Figure 7: Molecular structure of $S_6N_2O_{15}$ along two viewing directions. Selected bond lengths (italics, in pm) and angles are depicted. The thermal ellipsoids are set to a probability level of 70%. $S_6N_2O_{15}$ crystallizes in the monoclinic space group *C*2/*c* with cell parameters a = 1243.70(4) pm, b = 711.61(2) pm, c = 2696.4(1) pm, β = 95.148(1)° and V = 2.3768(1) nm^3.[25]

The preparation of $S_6N_2O_{15}$ led to further investigations of this reaction system. It was shown that in presence of metal salts, anions with the same structural motif can be formed.[26] Accordingly, the reaction of KCl with $P_3N_3Cl_6$ and SO_3 yielded the compound $K[S_3NO_8]$, which was analyzed by SC-XRD. The novel anion, $[S_3NO_8]^-$, can be derived structurally from trimeric γ-SO_3 (S_3O_9) with one bridging nitrogen atom being substituted by nitrogen. In a reaction with CsCl the anion $[S_6N_3O_{14}]^-$ was formed, which in turn can be derived from molecular $S_6N_2O_{15}$ according to the same principle. In this cage-shaped anion the bonding parameters are slightly different. The N–S bonds within the $[NS_3]$ fragments range from 168.4(4) pm to 179.6(4) pm. Particularly the N–S bonds to the sulfur atoms, which are part of the $[O_2SNSO_2]$ bridges, are elongated exhibiting values of 179.6(4) pm and 178.9(3) pm. Within the bridge, the S–N^{br} bonds are shorter (157.5(3) pm and 159.9(3) pm) compared to the opposite bridging S–O^{br} bond (161.9(3)-163.0(3) pm).

Also the unique cyclic anion $[S_4N_2O_{10}]^{2-}$ was structurally analyzed as part of the compound $(NH_4)[Au(S_4N_2O_{10})_2](SO_3)$.[26] This complex was isolated in form of yellow crystals formed via a solvothermal reaction between $AuCl_3$, SO_3 and $P_3N_3Cl_6$. SC-XRD analysis revealed trivalent gold centers, which are coordinated by two bidentate $[S_4N_2O_{10}]^{2-}$ anions in a square-planar manner. The structure of $[S_4N_2O_{10}]^{2-}$ can accurately be derived from SeO_3, which is a tetramer in the solid state according to Se_4O_{12}.[86] Conceptionally, the latter anions can be described as condensation products between sulfate $[SO_4]^{2-}$ and amidosulfate $[H_2NSO_3]^-$ tetrahedra with different ratios. This concept will be discussed in more detail as part of this thesis. These class of anions will be called cyclic nitridosulfate anions in course of this work.

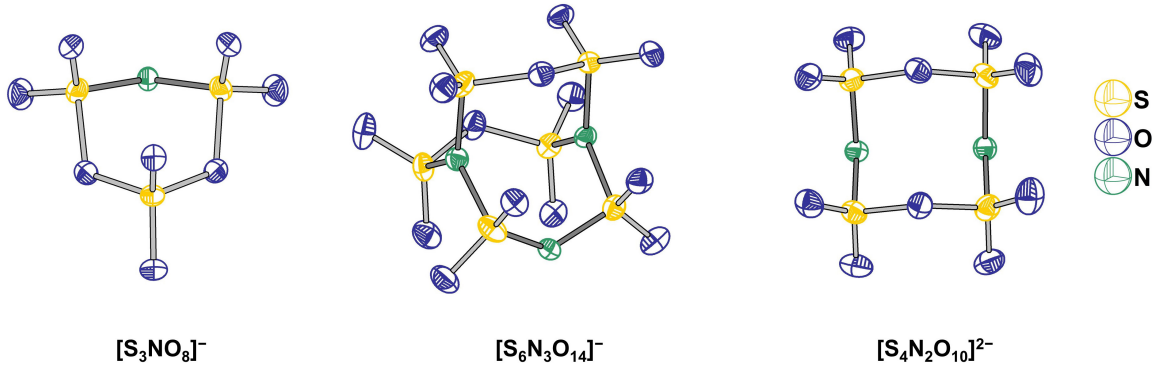

Figure 8: Structure of the cyclic anions $[S_3NO_8]^-$, $[S_6N_3O_{14}]^-$ and $[S_4N_2O_{10}]^{2-}$.[26] The anions were analyzed as part of the compounds $K[S_3NO_9]$, $Cs[S_6N_3O_{14}]$ and $(NH_4)[Au(S_4N_2O_{10})_2](SO_3)$ by SC-XRD. Displacement ellipsoids are shown at 70% probability.

Generally, there are not many examples for ternary S–N–O ring-based systems prepared in reactions with SO_3 and N-containing compounds in literature. The trisulfur dinitrogen pentoxide, $S_3N_2O_5$, was prepared by *Goehring et al.*[87] in 1954 for the first time followed by a structural XRD analysis in 1979 by *Roesky et al.*[88]. It is prepared via sublimation of a S_4N_4/ SO_3 mixture at 70 °C. The cyclic molecule consists of six-membered ring in which one sulfur atom and two $[SO_2]$ moieties, which are linked via two bridging nitrogen and one oxygen atom (see Figure 9). The bridging oxygen atom protrudes slightly from the ring plane. The S−N distances S(IV)–N^{br} are shortened about 10 pm compared to the adjacent S(VI)–N^{br} bonds.

Another well-described cyclic [SNO] compound is the trisulfimide anion $[S_3N_3O_6]^{3-}$ as it is reported in the structures $Ag_3[S_3N_3O_6](H_2O)$[89-90] and $(NH_4)_3[S_3N_3O_6]$[91-92]. It is accessible by thermal rearrangement of sulfamide, $SO_2(NH_2)_2$, at 180 °C. Its chair-shaped solid-state structure is isosteric to that of γ-SO_3. The S−N distances take up similar values of around 160 pm.

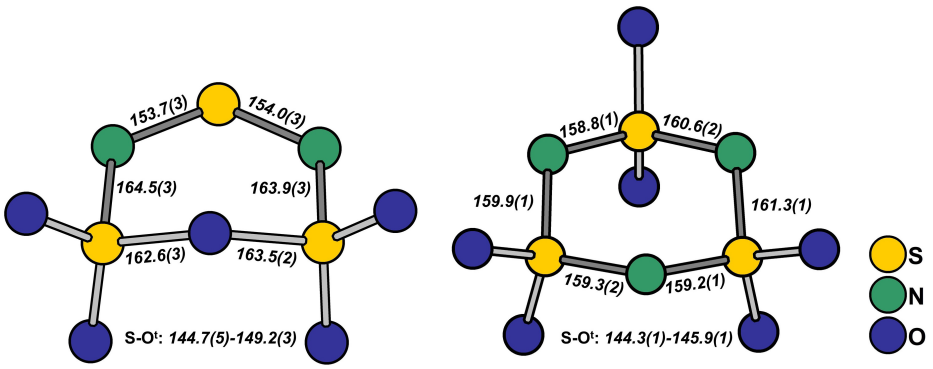

Figure 9: Structure of $S_3N_2O_5$[88] (left) and $[S_3N_3O_6]^{3-}$[91] (right) with bond lengths (italics, in pm) obtained from SC-XRD.

2.3 Hydrazine Sulfonates

As a related compound to ammonia, hydrazine (N_2H_4) is also a suitable candidate for the preparation of nitrogen-based sulfuric acid. The molecule itself deserves a very important role in past and present chemical research and industry. The first report about hydrazine dates back to 1887 wherein *Curtius* in his manuscript "Ueber das Diamid (Hydrazin)" outlined the preparation and properties of hydrazine and hydrazinium sulfate ($N_2H_6SO_4$) and chloride ($N_2H_6Cl_2$).[93]

Afterwards, its importance increased rapidly. As an endothermic molecule with nitrogen in the oxidation state −2, it highly favors to form to N_2. In World War II, the Germans recognized its potential as a rocket fuel.[94] Pure hydrazine is hypergolic in contact with oxidizers, such as HNO_3, and today derivatives as monomethyl hydrazine (MMH) and asymmetrical dimethyl hydrazine (UDMH) are applied as propellants for rockets. Industrially, hydrazine and its derivatives are also used as foaming agents, as pesticides and fungicides, and in the synthesis of pharmaceuticals and organic compounds.[95-97] The synthesis of hydrazine can be carried out in different routes, however the *Raschig* or more modern *Bayer* process is of large-scale industrial significance.[98] In the *Raschig* process ClO^- reacts with ammonia to N_2H_4, water and chloride according to the net equation. As an intermediate monochloramine (H_2NCl) is formed, which undergoes a nucleophilic substitution with further ammonia to yield N_2H_4.[99-100] Pure hydrazine undergoes autoxidation in presence of O_2 to N_2 and H_2O and coupled with its carcinogenic, toxic and explosive character it is hard to handle on a laboratory scale. Upon heating, it disproportionates explosively to ammonia and nitrogen (see Scheme 4).

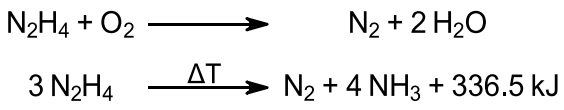

Scheme 4: Autoxidation (top) and thermal disproportionation (bottom) of hydrazine.

More established is the commercially available hydrazine hydrate ($N_2H_4 \cdot H_2O$, 64% N_2H_4), which is much safer to work with and shows similar reaction properties.[94] As strong base it forms the cations $N_2H_5^+$ and $N_2H_6^{2+}$ under acidic conditions. Most prominent salts are $(N_2H_6)SO_4$, N_2H_5Cl and $N_2H_6Cl_2$. Since hydrazine has four electrons to donate, it is a strong reducing agent, which is frequently used in organic chemistry, e.g. in the famous *Wolff-Kishner* reduction wherein carbonyl groups are reduced to methylene groups.[95]

In hydrazine the [NH_2] moieties can rotate along the N–N single bond. In the energy profile, the molecule has energetic minima at dihedral angles (∠H–N–N–H) of 100° and 260° (*gauche*, synclinal/anticlinal). That the antiperiplanar (or *trans*) conformation is not energetically favored relies on preferred hyperconjugative ($n \rightarrow \sigma^*$) and steric interactions in the *gauche* modification.[101] Structurally, only rather old SC-XRD datasets are available for hydrazine[102] and its hydrate[103]. Therein N–N bond lengths of 146 pm for N_2H_4 and 144.7 pm for its hydrate are found.

The four protons of hydrazine can be replaced by other functional groups. Organic moieties are widely represented but for hydrazine sulfonic acids and sulfonates there are just few scientific contributions that only deal with synthesis and simple elemental analysis. In 1914 *Traube* and *Vockerodt* covered the synthesis of hydrazine monosulfonic acid (NH_2NHSO_3H) and azidosulfuric acid (N_3SO_3H) in their publication "Über Hydrazino und Azido-sulfonsäure".[22] They treated dry hydrazine in a pure state with gaseous SO_3. The obtained solid was analyzed to be the hydrazinium salt of the hydrazine monosulfonic acid formulated as $(N_2H_5)(NH_2NHSO_3)$. In order to yield the hydrazine monosulfonic acid, first the barium salt, $Ba(NH_2NHSO_3)_2(H_2O)_2$, was generated by treatment with $Ba(OH)_2$. The Ba^{2+} ions were removed with H_2SO_4 to yield finally the free acid, NH_2NHSO_3H as a solid compound with a decomposition temperature of 217 °C. Furthermore, *Traube* and *Vockerodt* were able to isolate the azidosulfate, $K[SO_3N_3]$, which will be discussed later in *2.4*. *Raschig* and *Pellens* reported on the double sulfonated hydrazine, the hydrazine disulfonate, $[(SO_3)HNNH(SO_3)]^{2-}$.[23] They already distinguished between the two isomers, the symmetrical disulfonate ($[(SO_3)HNNH(SO_3)]^{2-}$) and non-symmetrical disulfonate or *iso*-disulfonate ($[H_2NN(SO_3)_2]^{2-}$). $[(SO_3)HNNH(SO_3)]^{2-}$ was isolated as the pyridinium salt by reacting $(N_2H_6)(SO_4)$ with $ClSO_3H$ in pyridine. In 1958 the whole hydrazine sulfonic acid chemistry was considered in more detail by *Meuwsen* and *Tischer*.[24] Their route to synthesize NH_2NHSO_3H included the sulfonation of $N_2H_4 \cdot H_2O$ with the pyridine sulfur trioxide complex ($Py \cdot SO_3$) and precipitation with acetic acid.

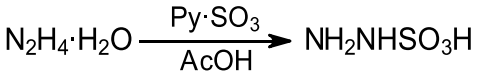

Scheme 5: Preparation of hydrazine monosulfonic acid according to *Meuwsen* and *Tischer*.[24]

Additionally, they reported in more detail on the synthesis of hydrazine disulfonates and the isomeric *iso*-disulfonate. Unlike the symmetrical disulfonate, the *iso*-disulfonate, $[H_2NN(SO_3)_2]^{2-}$ is not accessible by sulfonation of hydrazine. It was created via coupling of the amine group of hydroxylamine-*O*-sulfonic acid (H_2NOSO_3H) with the nitrido-*bis*-sulfate $K_3[N(SO_3)_2](H_2O)$ in alkaline medium.[24]

The preparation of the hydrazine trisulfonate and tetrasulfonate was also conducted for the first time.[24] The tetrasulfonate was prepared according to a peculiar oxidation reaction between $(Py\text{-}H)_2[(SO_3)HNNH(SO_3)]$ and NaOCl, while the trisulfonate was accessed by sulfonating the *iso*-disulfonate with $Py \cdot SO_3$. The prepared hydrazine sulfonates were analyzed by means of elemental analysis and their stability towards hydrolysis and oxidation was tested. The hydrazine tetrasulfonate, $K_4[(SO_3)_2NN(SO_3)_2](H_2O)$ was identified to be resistant towards hydrolysis and oxidation with $KMnO_4$, I_2/KI and $[Ag(NH_3)_2]^+$.

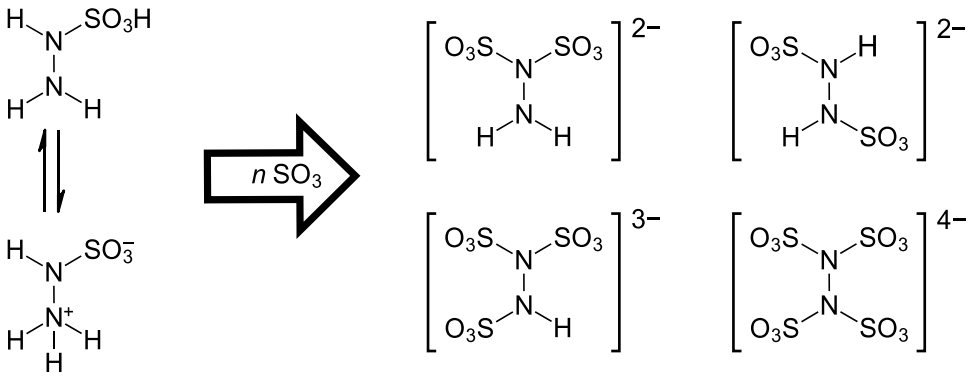

Figure 10: Structural formulas of the hydrazine sulfonic acid (left) and hydrazine di-, *iso*-di-, tri- and tetrasulfonates (right) synthesized according to *Meuwsen* and *Tischer*.[24] On the left, the zwitterionic structure of NH_2NHSO_3H is depicted proposed by *Audrieth* and *West*.[104]

IR analysis of the solid hydrazine monosulfonic acid indicated the presence of $[NH_3^+]$ deformation bands at 1638 cm^{-1} and 1541 cm^{-1}. *Audrieth* and *West* derived the zwitterionic nature of the acid from this just like the amidosulfuric acid.[104] Furthermore, they analyzed the acidity and calculated a pK_a value of 3.85. Therefore, the acid strength is slightly lower than that of the amidosulfuric acid but stronger compared to acetic acid. Further structural and analytical details on the acid and its derivatives are not available in literature.

2.4 Azidosulfates

The third class of compounds covered in this work are the Lewis acid-base adducts of azides and SO_3, namely azidosulfates with the formula $[SO_3N_3]^-$. The azide anion (N_3^-) as the corresponding base of hydrazoic acid (HN_3) is categorized as a pseudo-halide and resembles the chloride anion. Azide chemistry was initiated by *Curtius* in the end of the 19th century who yielded N_3^- in reactions of hydrazine functions with $NaNO_2$.[105]

Hitherto, a large number of binary azides are known, e.g. for all main group elements except for sulfur, selenium and nitrogen.[106] It can be distinguished between covalent azides, e.g. $Si(N_3)_4$ and $B(N_3)_3$, and azides with a more ionic character, such as salts of alkali metals.[107] Hydrazoic acid and azides tend to decompose thermally, some even explosively, which has already been warned about by *Curtius*.[105] Particularly heavy metal azides, such as e.g. AgN_3, and covalent azides are highly explosive at ambient conditions and can detonate by simple impact, which makes them suitable as a primary explosive.[105,107-108] As a Lewis base it can easily attached to Lewis acids. In the preparative chemistry trimethylsilyl (TMS) azide (Me_3SiN_3) is a useful reagent to transfer N_3^-.[109] It is commercially available, is soluble in most organic solvents and metathesis with chlorides are straightforward since volatile Me_3SiCl is formed.

As already pointed out the first report about the $[SO_3N_3]^-$ was made by *Traube* and *Vockerodt*.[22] They prepared the anion by the reaction of hydrazine monosulfonic acid and KNO_2 in a manner of a diazotization reaction.

$$NH_2NHSO_3H + KNO_2 \xrightarrow{H_2O} K[SO_3N_3] + 2\,H_2O$$

Scheme 6: Preparation of $K[SO_3N_3]$ according to *Traube* and *Vockerodt*.[22]

The resulting salt $K[SO_3N_3]$ was yielded in form of colorless prismatic crystals, which were sensitive towards heat and mineral acids. Further routes to yield the anion are reported. *Beck* prepared $Na[SO_3N_3]$ by storing NaN_3 with oleum (70% SO_3) in a desiccator to accumulate the SO_3 on the azide.[110] Via reaction of NaN_3 with chlorosulfonic acid ($ClSO_3H$) also $Na[SO_3N_3]$ is formed, with HCl as the byproduct.[111]

Lehmann et al. isolated $K[SO_3N_3]$ via alkaline hydrolysis of disulfuryl azide $S_2O_5(N_3)_2$.[112] According to this report $S_2O_5(N_3)_2$ can be synthesized by heating KN_3 in boiling SO_3 under reflux cooling. It is described as a liquid that detonates above 80 °C. However, no further properties and literature entries for this compound can be found. In 2002 *Christe et al.* discussed $[SO_3N_3]^-$ in more depth, especially with regard to analytical data.[113] They prepared the anions $[SO_2N_3]^-$, $[(SO_2)_2N_3]^-$ and $[SO_3N_3]^-$ out of solutions of SO_2 as salts of Cs^+ and $[N(CH_3)_4]^+$. The anions were analyzed by ^{14}N-NMR and vibrational spectroscopy. They also examined the adduct $Cs[SO_2N_3]\cdot Cs[SO_3N_3]$ by SC-XRD providing the first example of a solid-state structure of $[SO_3N_3]^-$. The single crystal of $Cs[SO_2N_3]\cdot Cs[SO_3N_3]$ was formed in an FEP tube containing liquid SO_2 and CsN_3. The co-crystallization of both anions in one structure allows a good comparison. The S–N distance in $[SO_3N_3]^-$ is 175(1) pm and 198(1) pm in $[SO_2N_3]^-$ (see Figure 11).

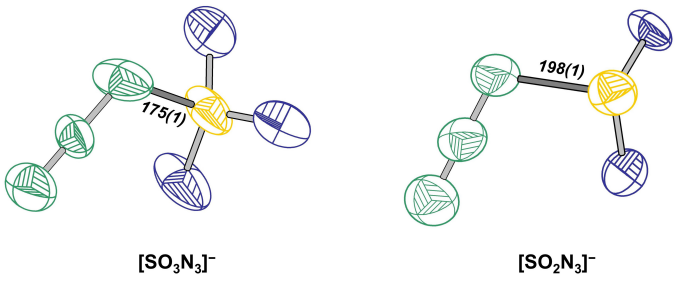

Figure 11: Structure of the anions $[SO_3N_3]^-$ (left) and $[SO_2N_3]^-$ (right) obtained from single crystal XRD of the compound $Cs[SO_2N_3]\cdot Cs[SO_3N_3]$.[113] Probability of the thermal ellipsoids is set to 70%. Interatomic distances are in pm.

Since SO_3 is the stronger Lewis acid than SO_2, interaction of SO_3 and N_3^- is expectedly stronger. This was also verified by quantum mechanical calculations. Experimental IR and *Raman* spectroscopy supported with theoretical data supplied characteristic vibrational modes for $[N_3]$ at 2134 cm^{-1} (ν_{as}) and 1278 cm^{-1} (ν_s) and for S–N at 464 cm^{-1} (ν_s). Additionally, $Cs[SO_3N_3]$ was synthesized as a pure compound. For that $CsSO_3Cl$ was stirred in liquid $(TMS)N_3$ at room temperature (see Scheme 7). The volatile by-product (TMS)Cl was removed under reduced pressure to obtain phase-pure $Cs[SO_3N_3]$, which was monitored by *Raman* spectroscopy. A SC-XRD dataset of a pure azidosulfate is not known up to now. Data on thermal stability of this compounds are also not available.

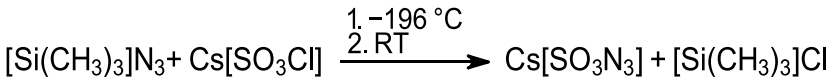

Scheme 7: Synthesis of $Cs[SO_3N_3]$ according to *Christe et al.*.[113]

Christe et al. pushed the SO_2/N_3 system even further by synthesizing $Cs[(SO_2)_2N_3]$.[114] Yellow crystals of this compound were grown from CsN_3 in liquid SO_2 at −64 °C. SC-XRD data of $[(SO_2)_2N_3]^-$ shows weak S–N bonding with distances of 242.7(4) pm and 220.1(5) pm. *Zeng et al.* were also able to attach two azide group on SO_2.[115] The explosive sulfuryl diazide $O_2N(N_3)_2$ is accessible by the reaction of NaN_3 and SO_2Cl_2 and fractional condensation at −30 °C.

In principle the azide anion should hold also up to attach two $[SO_3]$ groups according to $[N_3(SO_3)_2]^-$. It is very likely that this is also a thermally very unstable compound and thus can only be isolated at low temperatures.

3 Objective

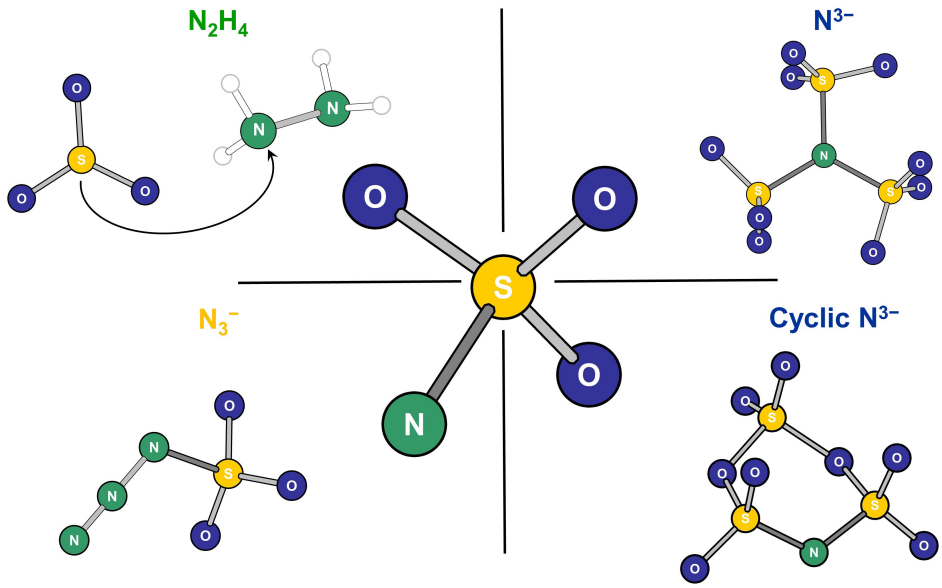

Figure 12: Depiction of the four chemical categories of nitrogenous sulfates examined in the context of this work.

The elaborated state of nitrogenous sulfates in the introductory part hints at the fact there is plenty of scope for research in this area. The principal objective was therefore to extend the state of knowledge with assistance of known and new methods. Thematically, the work can be categorized into four areas: the cyclic nitridosulfates, the hydrazine sulfonates, azidosulfates and nitrido-*tris*-sulfates.

Reactions between $P_3N_3Cl_6$ and metal salts in SO_3 already turned out to be promising route to gain access to cyclic nitridosulfates. As there are hardly any literature data or procedures in this regard, the whole issue can be developed in many ways. This synthetic route was pursued further by using especially transition metals. In previous work the square-planar aurate complex $[Au(S_4N_2O_{10})_2]^-$ with the bidentate anion $[S_4N_2O_{10}]^{2-}$ was isolated for the first time.[26] Based on this the reproducibility of the anion $[S_4N_2O_{10}]^{2-}$ was to be scrutinized with different Au^{3+}-salts. Also alkali metals salts were considered, since reactions with CsCl and KCl yielded the anions $[S_6N_3O_{14}]^-$ and $[S_3NO_8]^-$, which are isosteric to $S_6N_2O_{15}$[25] and S_3O_9[7], respectively. Additionally, unknown phosphorus species in this reaction leaves room for further investigations. In terms of methodology, the preparation of liquid SO_3 for the reactions using the distillation apparatus was mandatory. The reaction components were to be treated with the liquid SO_3 in closed glass vessels in a solvothermal approach. The aggressive nature of SO_3 and labile products complicate an appropriate analysis. However, via this approach single crystal formation was to be facilitated.

When it comes to the hydrazine sulfonic acid and its derivatives there are indeed reports, which, however, date back to the 1950s without any detailed analytical data. These procedures with

modifications were to be applied to prepare the hydrazine monosulfonate up to fully substituted hydrazine tetrasulfonate. The mono- and disulfonate can be obtained by sulfonation with common reagents as $Py{\cdot}SO_3$ and $ClSO_3H$. For the disulfonate different approaches have to be applied to yield the isomeric *iso*-disulfonate $[H_2NN(SO_3)_2]^{2-}$ and disulfonate $[(SO_3)HNNH(SO_3)]^{2-}$. Especially the synthesis of the highly negatively charged hydrazine tri- and tetrasulfonate appears not to be straightforward, since they cannot be prepared by simple sulfonation but via oxidation of the disulfonates. After preparation of the aforementioned compounds, the focus was on detailed analysis, which includes structural and spectroscopic methods. Their thermal and hydrolysis stability was to be evaluated for further applications.

The azide anion as a classical Lewis base and pseudo halide is highly predestined to bond to Lewis acidic SO_3. $[SO_3N_3]^-$ has various mentions in literature but up to know only one single crystal structure of the mixed compound, $Cs[SO_3N_3]{\cdot}Cs[SO_2N_3]$, is known.[113] Different approaches to yield the anion are available. On the one hand, sulfonation of N_3^- with pure SO_3 or SO_3 adducts as $Py{\cdot}SO_3$ is expedient. Albeit it is advisable to avoid the presence of H_2O since formation of H_2SO_4 in turn leads to formation of explosive HN_3. A more convenient method is the ion exchange reaction between chlorosulfates ($[ClSO_3]^-$) and $(TMS)N_3$. The latter is proven to be a readily available reagent, which is used to transfer azide groups on chlorides e.g. acyl chlorides (RCOCl) by forming volatile (TMS)Cl.[116] Also in this compound class, the analysis of the structure-property relationship was the paramount objective.

At last, the also long known nitrido-*tris*-sulfate anion $[N(SO_3)_3]^{3-}$ was scrutinized. $K_3[N(SO_3)_3](H_2O)_2$ is the only compound in this structural class that is well documented in the literature and was thus to be synthesized first. It can be prepared by reacting $K_2S_2O_5$ and KNO_2 under alkaline conditions. A phase-pure synthesis and more detailed analysis of the latter was aimed and then salt metathesis were to be carried out to exchange the potassium by other metals.

4 Results and Discussion

4.1 Nitrogen Source $(S_3N_2Cl)Cl$

As already highlighted in the introduction, aromatic $P_3N_3Cl_6$ was already suitable as a nitrogen source for the preparation of polymeric nitridosulfate anions. In course of this work the sulfur-nitride chloride thiodithiazyl dichloride $(S_3N_2Cl)Cl$ was considered as another possible nitrogenous compound.

$(S_3N_2Cl)Cl$, which consists of the cyclic cation $(S_3N_2Cl)^+$ and Cl^- as counter-anion, is well-known since the end of the 19th century.[117] In the 1960s, a detailed preparation procedure and the crystal structure were published.[118-119] In the following preparation and analysis of $(S_3N_2Cl)Cl$ is examined with the support of current X-ray methods including SC-XRD and P-XRD with *Rietveld* refinement.

$(S_3N_2Cl)Cl$ was prepared according to a modified procedure of *Jolly et al*.[118] Accordingly, NH_4Cl was heated in S_2Cl_2 under inert conditions. In an attached sublimation tube the product deposited as a crystalline orange-brown solid in phase-pure yield of 2% (Literature 20%[120]). The proposed mechanism is a gas phase reaction involving S_2Cl_2 and NSCl (thiazyl chloride).[118] The compound rapidly decomposes under ambient conditions.

$$2\,NH_4Cl + 4\,S_2Cl_2 \xrightarrow{138\,^\circ C} (S_3N_2Cl)Cl + 8\,HCl + 5\,S$$

Scheme 8: Reaction equation of the preparation of $(S_3N_2Cl)Cl$ according to *Jolly et al.*.[120]

Single crystals of $(S_3N_2Cl)Cl$ were already formed by the gas phase deposition. To obtain a more reliable dataset with anisotropic refinement, SC-XRD analysis of $(S_3N_2Cl)Cl$ was carried out (see Table 1, p. 18 and Figure 13, p. 19).

Table 1: Selected crystallographic data of $(S_3N_2Cl)Cl$ compared to the dataset of *Zalkin et al.* and cell parameters obtained from a *Rietveld* refinement.[119]

	$(S_3N_2Cl)Cl$	**$(S_3N_2Cl)Cl$[119]**	***Rietveld* Refinement**
Temperature	100 K	RT	RT
Crystal System	Monoclinic	Monoclinic	Monoclinic
Space Group	$P2_1$	$P2_1$	$P2_1$
a / pm	547.00(3)	654.6	550.93(2)
b / pm	850.67(5)	860.0	860.45(4)
c / pm	650.44(4)	550.8	655.02(3)
β / °	102.348(3)	102.37	102.375(3)
V / nm^3	0.29566(3)	0.310	0.30329(2)
Z	2	2	2
R values	R_1 (all data) = 0.0167; wR_2 (all data) = 0.0384	-	R_{wp} = 10.08 %; R_{exp} = 11.14%; R_p= 7.72%
BASF	0.36(12)	-	-
GooF	1.120	-	0.905

The compound crystallizes in the acentric monoclinic space group $P2_1$ and the structure was refined as an inversion twin with proportion of 36% of the inversion component. The cell dimensions are in the range of the structure solution of *Zalkin et al.*[119]

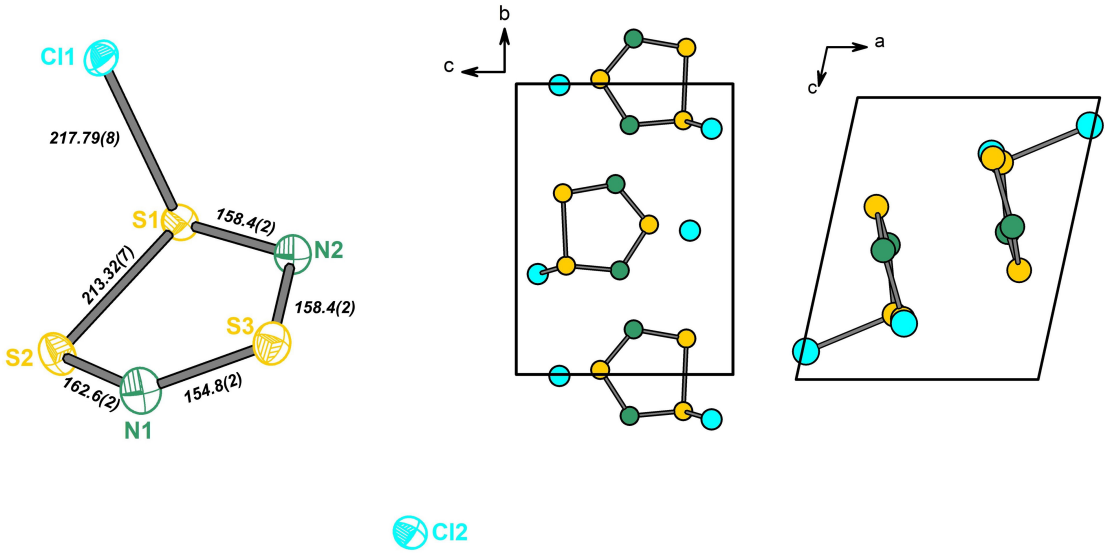

Figure 13: Structure of $(S_3N_2Cl)Cl$ (left) and view of the extended unit cell along the crystallographic axes *a* (middle) and *b* (right). In the picture bond lengths (italics, in pm) are given. The thermal ellipsoids are set to a probability level of 70%.

In the structure, one crystallographically distinguishable $S_3N_2Cl^+$ cation and one Cl^- anion can be found. The observed distances and angles correspond well with those of *Zalkin et al.*[119] Within the five-membered ring of the cation bond lengths of 213.32(7) pm for S1−S2, 162.6(2) pm for S2−N1, 154.8(2) pm for N1−S3, 161.8(2) pm for N2-S3 and 158.4(2) pm for N2-S1 are found. The S1–Cl1 distance is the longest with a value of 217.79(8) pm. The closest contact of Cl2 with the cation amounts to 287.22(9) pm (Cl2–S3). Looking at the crystal structure a layered orientation is recognizable. The $S_3N_2Cl^+$ moieties based on the orientation of S1–Cl1 are arranged in the same direction within the layers.

The powder data of the crystalline product was examined by means of a *Rietveld* refinement to verify the crystalline phase-purity. The *Rietveld* fit shows crystalline phase-purity for $(S_3N_2Cl)Cl$ (see Figure 14, p. 20). After the preparation, $(S_3N_2Cl)Cl$ was then used in solvothermal reactions with SO_3 (see 4.2.5, p. 38).

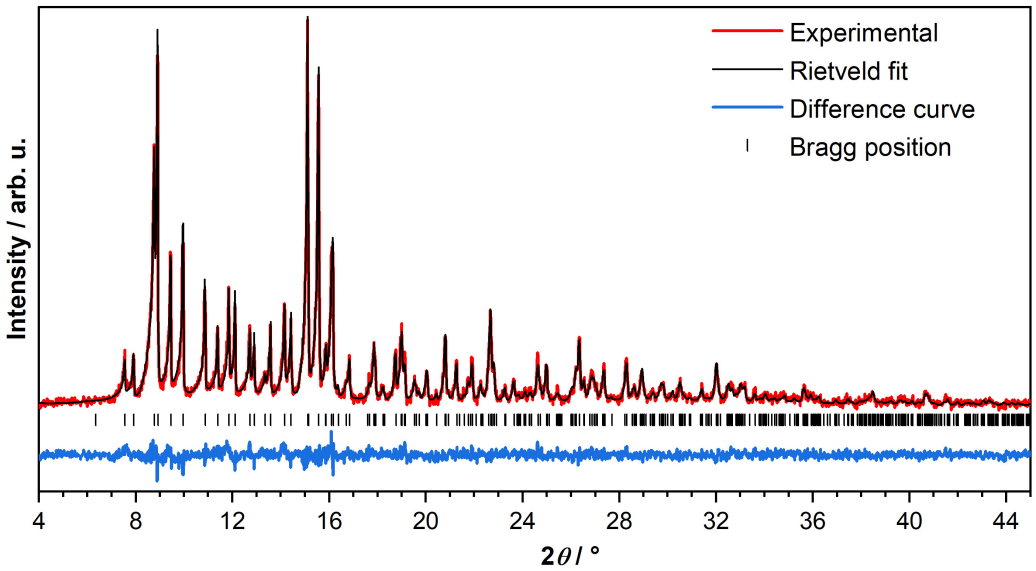

Figure 14: Powder X-ray diffraction pattern of $(S_3N_2Cl)Cl$ (red) with *Rietveld* refinement (black), difference curve (blue) and *Bragg* positions (black strokes). The powder was measured in an 0.3 mm capillary with Mo-$K_{\alpha 1}$ (λ = 70.930 pm) radiation. The cell parameters *a*, *b*, *c* and β were refined (see Table 1, p. 18).

4.2 Cyclic Nitridosulfate Anions and $S_6N_4O_{13}H_2 \cdot P_2O_3Cl_4$

4.2.1 $S_6N_4O_{13}H_2 \cdot P_2O_3Cl_4$

In the reaction between $P_3N_3Cl_6$ and SO_3 at 80 °C the sulfur nitride oxide, $S_6N_2O_{15}$, is the only product phase identified so far.[25] The harsh reaction medium due to the presence of SO_3 makes the investigation of the reaction quite difficult. One of the questions that arises is the whereabout of phosphorus and chlorine, which are part of the reactant. In addition to colorless crystalline $S_6N_2O_{15}$, a slightly yellowish liquid was always observed in the reaction ampoules, which presumably contains the remaining elements. Interestingly, crystallization of SO_3 to its polymeric form did not occur in presence of $P_3N_3Cl_6$. So it seems reasonable, that a phosphorus derivative participates as polymerization inhibitor.[36] A test $^{31}P(H)$ NMR spectrum of this yellow liquid (in CD_2Cl_2) obtained from a reaction between AuCl, $P_3N_3Cl_6$ and SO_3 showed many signals in the range of −31 ppm to 11 ppm (see Figure 99, p. 162). Normally, phosphorus oxychlorides resonate in this range while phosphorus chlorides are shifted to higher frequencies.[121-122] For $P_3N_3Cl_6$ a chemical shift of δ = 19.3 ppm (in CH_2Cl_2) is reported for the phosphorus.[123] NMR spectroscopic examination generally proved to be difficult due to reactions of the standard dried solvents with the SO_3 containing samples. 1954 *Goehring et al.* already reported about the $P_3N_3Cl_6 \cdot 3SO_3$ adduct by distilling SO_3 (at 40 °C) on $P_3N_3Cl_6$ at ambient conditions.[124] They removed surplus SO_3 under reduced pressure at 25 °C and the remaining material was identified gravimetrically as $P_3N_3Cl_6 \cdot 3SO_3$. Hence, attempts were made to reproduce this adduct. For that, around ten equivalents of liquid SO_3 were added to $P_3N_3Cl_6$ in a glass vessel under liquid nitrogen cooling.

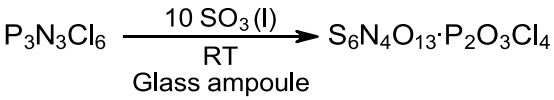

Scheme 9: Synthesis of $S_6N_4O_{13}H_2 \cdot P_2O_3Cl_4$ in a solvothermal synthesis with SO_3.

The reaction vessel was fused under reduced pressure and was stored at room temperature for one week. A colorless syrup-like mass with a few colorless single crystals on the glass wall above formed during this period. Via structure analysis by SC-XRD the crystals were partially assigned to the known phase $S_6N_2O_{15}$ but also to a new phase according to the composition $S_6N_4O_{13}H_2 \cdot P_2O_3Cl_4$ (see Figure 15, p. 22). In a further reaction attempt, $S_6N_4O_{13}H_2 \cdot P_2O_3Cl_4$ was also identified but again in the form of isolated single crystals. The crystal structure was solved in space group $P2_1/n$ with four formula units per unit cell and reliable quality factors were obtained (see Table 2, p. 22). Chemically this compound consists of molecular $S_6N_4O_{13}H_2$ and $P_2O_3Cl_4$, which exhibit intermolecular interaction by hydrogen bonding. While $S_6N_4O_{13}H_2$ represents a new type of molecule, $P_2O_3Cl_4$ is a literature-known condensed phosphorus(V) oxychloride.

Table 2: Selected crystallographic data of $S_6N_4O_{13}H_2 \cdot P_2O_3Cl_4$.

$S_6N_4O_{13}H_2 \cdot P_2O_3Cl_4$	
Temperature	100 K
Crystal System	Monoclinic
Space Group	$P2_1/n$
a / pm	1148.20(5)
b / pm	1383.87(7)
c / pm	1337.94(6)
β / pm	103.184(2)°
V / nm^3	2.0699(2)
Z	4
R_1 (all data); wR_2 (all data)	0.0401; 0.0770
GooF	1.109

It was already presumed that the phosphorus of $P_3N_3Cl_6$ is transformed to an oxychloride in the presence of SO_3, but now the first structural proof is demonstrated.[25]

The first report of so called pyrophosphoryl chloride or diphosphoryl chloride dates back to 1891.[125] Preparation of the latter and higher condensed phosphoryl chlorides were then further elaborated.[126-128] Diphosphoryl chloride and polyphosphoryl chlorides can be accessed when $POCl_3$ reacts with P_4O_{10}. The degree of condensation is controlled by stoichiometry of the reactants and separation can be achieved by fractional distillation. Structural examination of $P_2O_3Cl_4$ is only given by *Raman* and ^{31}P NMR spectroscopy up to now.[129-131]

$S_6N_4O_{13}H_2$ is a nitrogen-richer derivative of $S_6N_2O_{15}$ with two [NH] fragments that replace two bridging oxygen atoms.

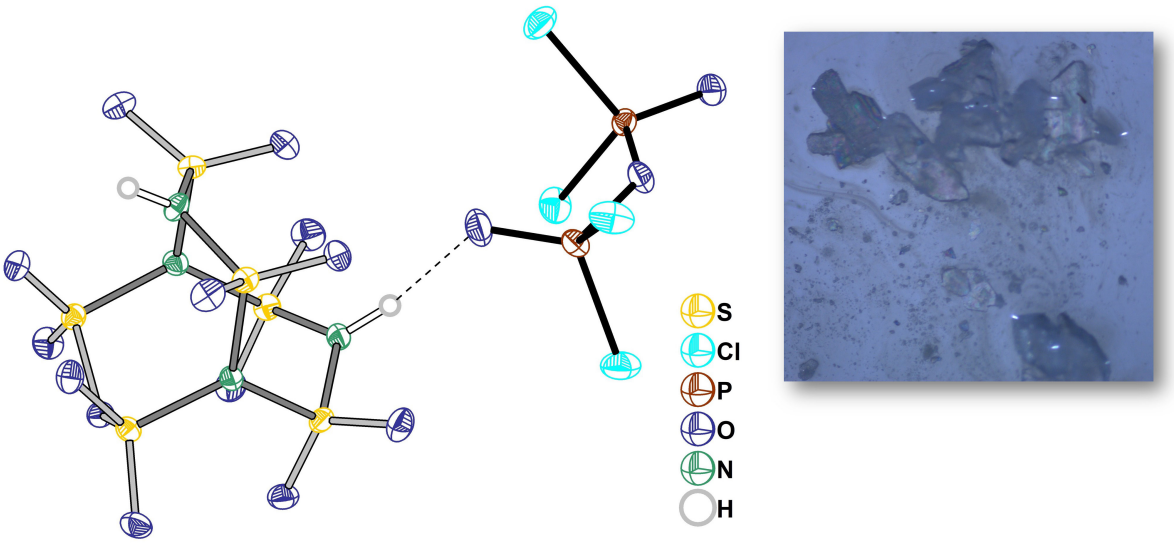

Figure 15: Structure of $S_6N_4O_{13}H_2 \cdot P_2O_3Cl_4$ (left) and microscope image of decomposing single crystals (right) from the reaction ampoule. The thermal ellipsoids are set to a probability level of 70%.

The presence of the protons is worth discussing since only proton-free reagents were used in the synthesis and the experiments were done under inert conditions. Nevertheless, it cannot be ruled out that traces of water may get into the SO_3 distillation apparatus. In the burette where the liquid SO_3 is collected, γ-SO_3 sometimes crystallizes to polymeric α/β-SO_3 over time, which indicates the minor

presence of water. From a crystallographic perspective the two [NH] (N3, N4) groups are clearly indicated. Free refinement of nitrogen atoms at these two positions leads to an occupancy close to one while the occupancy drops to 0.82 for both positions when oxygen atoms are refined. There is also distinct remaining electron density near N3 and N4 suitable for free refinement of hydrogen atoms. A directional interaction between N···O–P is also visible and will be discussed later on. The [NH] groups create a neutral molecule, which fits to the whole structural model.

The crystal structure consists of one crystallographically unique $S_6N_4O_{13}H_2$ and $P_2O_3Cl_4$ molecule with all atoms located on general sites (*Wyckoff 4e*). $P_2O_3Cl_4$ consists of two [$POCl_2$] subunits connected by a bridging oxygen atom (O2) (see Figure 16). The P–Cl bonds are much longer with values of 195.26(2)-196.12(6) pm compared to the terminal P–O^t bonds with 148.8(2) pm and 145.6(1) pm. The P–Cl distance is therefore in the range of other solid state structures of phosphorus(V) oxychlorides, such as $POCl_3$.[132-133] In the starting material $P_3N_3Cl_6$ the P–Cl distance is 198 pm.[134] The bridging bonds P–O^{br} are 159.70(1) pm and 159.71(1) pm and are as expected longer than the terminal ones. The two [$POCl_2$] moieties are angled towards each other with ∠P1–O2–P2 of 131°. By viewing along the P···P axis an antiperiplanar orientation of the [$POCl_2$] groups is evident, which creates a maximal spacing between the [PCl_2] units. The angles within the [PCl_2O_2] tetrahedra are subjected to deviations with Cl–P–Cl of 106-107°, O–P–O of 109-112° and O–P–Cl of 103-115.9°.

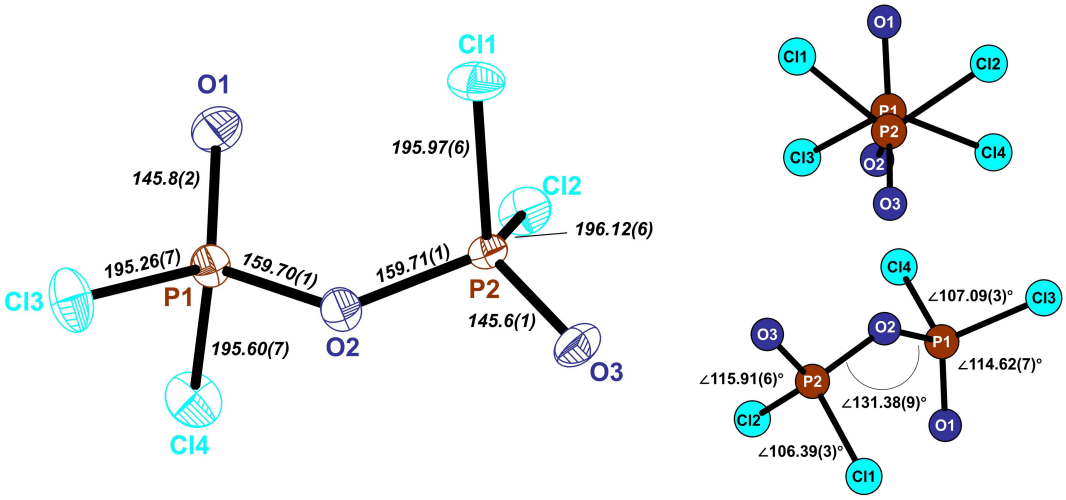

Figure 16: Structure and labeling of the $P_2O_3Cl_4$ along different viewing directions with selected bond lengths (italics, in pm) and angles.

$S_6N_4O_{13}H_2$ adopts a bicyclic cage structure similar to the shape of $S_6N_2O_{15}$ (see Figure 17, p. 24). The backbone of the bicycle has the same configuration of bicyclo[3,3,3]undecane.[135] Structurally, the molecule is composed of two [$N(SO_2)_3$] units, which are connected via two bridging nitrogen atoms (N3, N4) and one oxygen atom (O36).

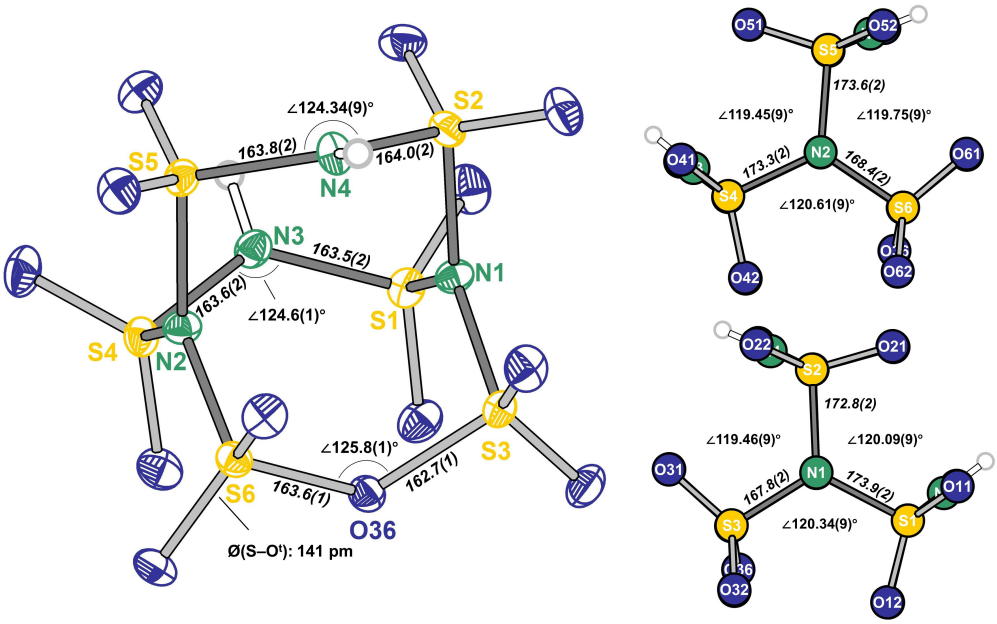

Figure 17: Structure and labeling of molecular $S_6N_4O_{13}H_2$ from three different perspectives with selected bond lengths (italics, in pm) and angles.

In the solid state the molecule has C_1 symmetry but is rather close to a symmetry of C_s. Within the two S–N–S bridges the distances of 163.5(2)-164.0(2) pm and angles of 124.34(9)° and 124.6(1)° are observed. The S–O–S bridge shows only slight deviation from this with a distance of 163.6(1) pm and 162.7(1) pm and an angle of 125.8(1)°. The respective values for $S_6N_2O_{15}$ are also within this range. For the trigonal planar [NS_3] unit major differences are recognizable. The distances of nitrogen N1 and N2 to the sulfur atoms of the S–N–S bridges (S1, S2, S4, S5) are significantly longer with 172.8(2)-173.9(2) pm compared to S3 and S6 of the S–O–S bridge with 168.4(2) pm and 167.8(2) pm. The observed angles in the trigonal plane range from 119.45(9)° to 120.61(9)°, which implies minor distortion from an ideal trigonal planar geometry. Based on this structural evidence, it can be assumed that the lone pairs of N1 and N2 take part in π-bonding to the sulfur atoms as known for $S_6N_2O_{15}$ and $[N(SO_3)_3]^{3-}$.[25,79] The distances for the terminal S–O^t bonds are 141 pm on average without major discrepancies. Though a shape-wise similarity to $S_6N_2O_{15}$ is given, overall the mentioned values of $S_6N_4O_{13}H_2$ indicate a significant difference.

A mutual stabilization of the two molecules is provided by hydrogen bonding between secondary amines and the oxygen atoms of $P_2O_3Cl_4$. Each $P_2O_3Cl_4$ forms two hydrogen bonds with two neighboring $S_6N_4O_{13}H_2$ molecules, which results in a chain-like pattern in the crystal structure (see Figure 18, p. 25). The observed donor(N)–acceptor(O) distances are 264.8(2) pm (O1···N3) and 266.5(2) pm (O3···N4) and the respective angles (∠N-H···O) are 165(1)° and 170(1)°. This classifies them as electrostatic hydrogen bonds.[136-137]

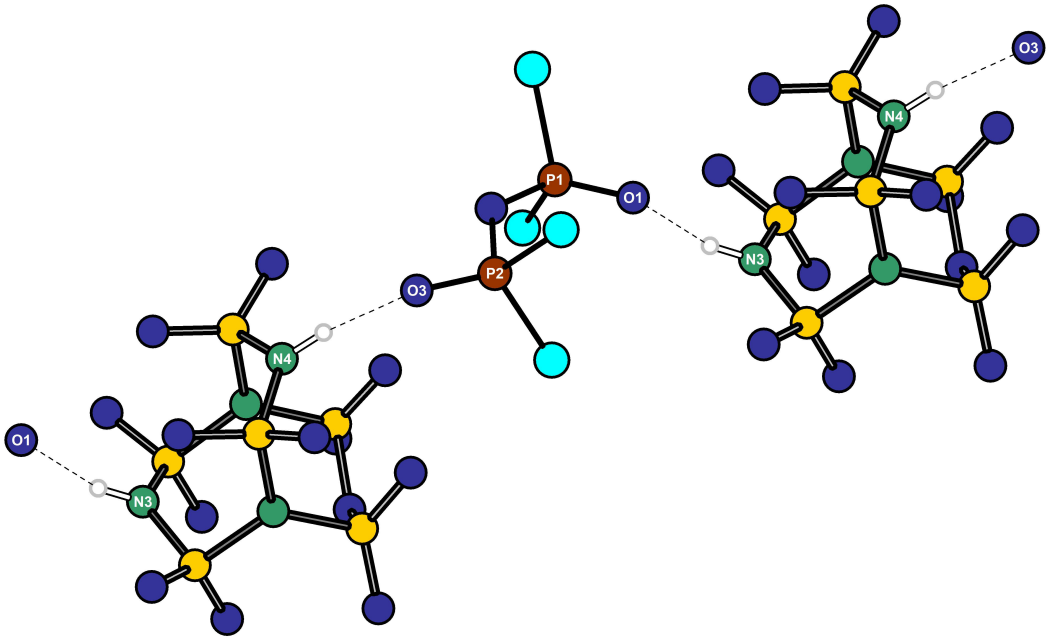

Figure 18: Illustration of the interaction of $P_2O_3Cl_4$ with the two neighboring $S_6N_4O_{13}H_2$ molecules via hydrogen bonding.

$P_2O_3Cl_4$ is neighbored by six more $S_6N_4O_{13}H_2$ molecules and by one $P_2O_3Cl_4$ molecule but without a considerable interaction (see Figure 19). Closest contact for the $P_2O_3Cl_4$ molecules is observed between Cl3 and O3 with a distance of 325.1(1) pm.

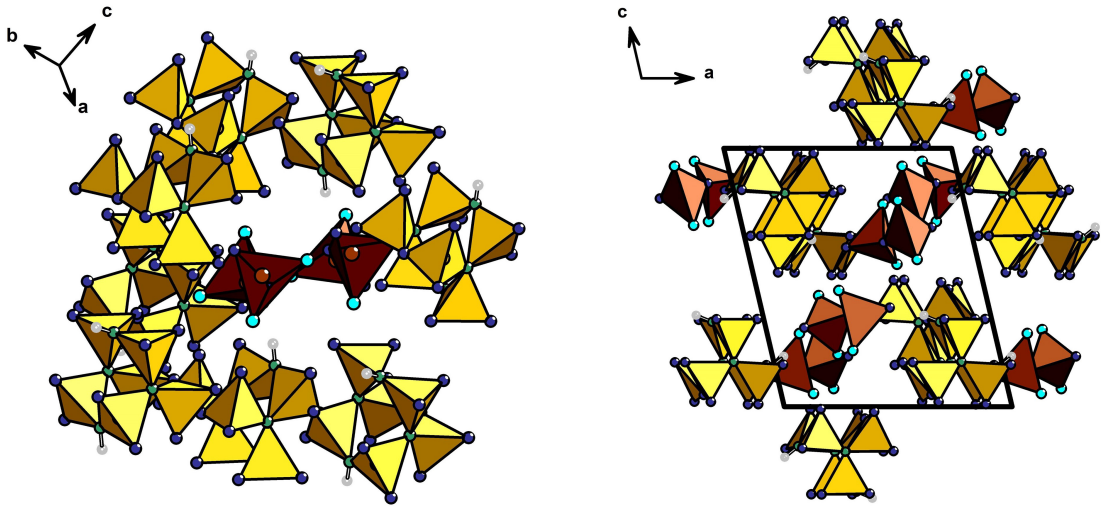

Figure 19: On the left the surrounding of one $P_2O_3Cl_4$ is highlighted and on the right the extended unit cell along the crystallographic *b* axis is depicted. The surrounding of phosphorus (brown) and sulfur (yellow) are shown as tetrahedra to provide a better perspective.

4.2.2 Rb[S3NO8] and Ag[S3NO8]

Based on previous results further reactions between $P_3N_3Cl_6$ and compounds of monovalent cations were performed.[26] As a starting material the chlorides RbCl and AgCl were used. These were reacted with $P_3N_3Cl_6$ and liquid SO_3 in sealed glass ampoules at 80 °C. Out of both attempts a few colorless crystals were generated in the ampoule. The crystals were very sensitive towards moisture and had to be quickly mounted on a diffractometer to avoid decomposition. Via SC-XRD examination of the crystals, the structures $Ag[S_3NO_8]$ (see Figure 20, p. 27) and $Rb[S_3NO_8]$ (see Figure 22, p. 28) were found. The Ag^+-salt crystallizes in the orthorhombic space group *Pnma* with four formula units per unit cell. The Rb^+-salt also crystallizes in the orthorhombic lattice but in the acentric space group $P2_12_12_1$ with twelve formula units per unit cell.

Scheme 10: Preparation of $Ag[S_3NO_8]$ (left) and $Rb[S_3NO_8]$ (right) in a solvothermal synthesis with liquid SO_3.

In the refinement process of $Rb[S_3NO_8]$ a *Flack* X parameter near to 50% indicated the occurrence of inversion twinning. The applied law for inversion twins resulted in a significant improvement in quality parameters of the refinement. A brief listing of the important SC-XRD parameters of the two compounds is shown below (see Table 3, page 26).

Table 3: Selected crystallographic data of $Ag[S_3NO_8]$ and $Rb[S_3NO_8]$ from this work and $K[S_3NO_8]$ from previous work.[26]

	$Ag[S_3NO_8]$	**$Rb[S_3NO_8]$**	**$K[S_3NO_8]$[26]**
Crystal System	Orthorhombic	Orthorhombic	Orthorhombic
Space Group	*Pnma*	$P2_12_12_1$	*Pnma*
a / pm	860.03(4)	928.77(4)	761.60(4)
b / pm	942.33(5)	961.37(5)	841.08(4)
c / pm	860.19(4)	2545.8(1)	1162.09(6)
V / nm³	0.69713(6)	2.2731(2)	0.74440(7)
Z	4	12	4
R_1 (all data); wR_2 (all data)	0.0149; 0.0383	0.0875; 0.0895	0.0640; 0.0642
BASF	-	0.52(2)	-
GooF	1.094	1.014	1.114

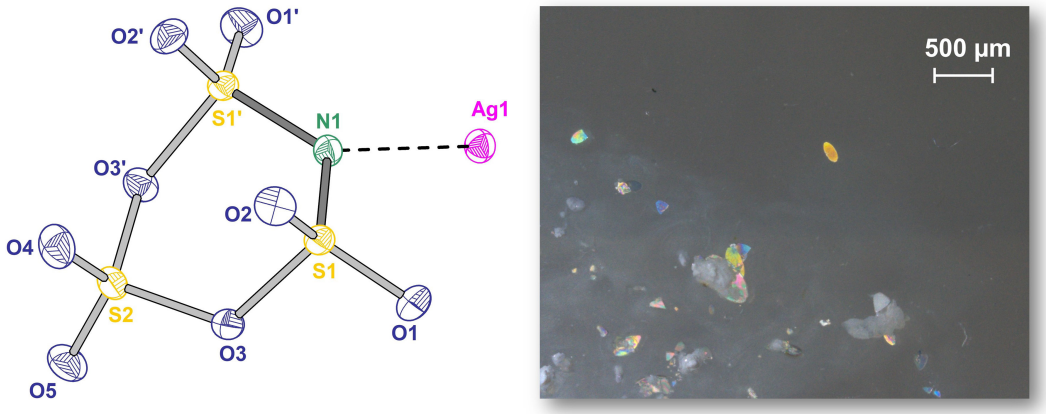

Figure 20: Structure and labeling of $Ag[S_3NO_8]$ in ellipsoidal representation (left). On the right a microscope image of the latter is shown. The thermal ellipsoid probability is set to 70%.

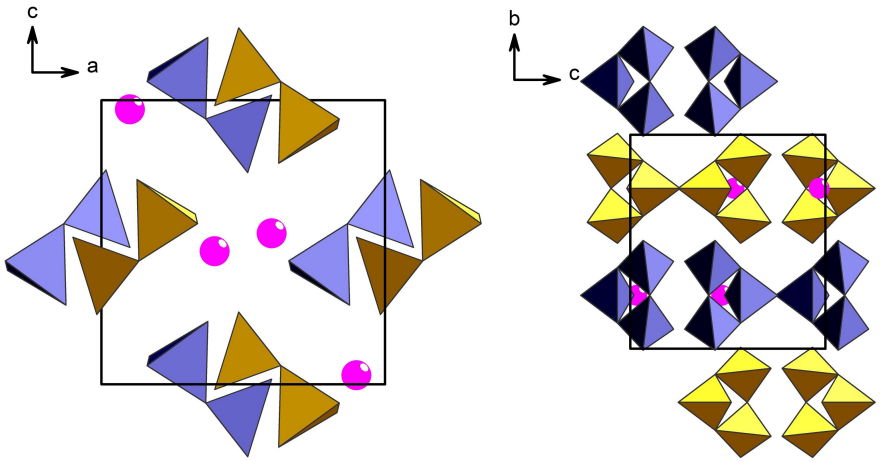

Figure 21: Representation of the extended unit cell along the crystallographic axes *b* and *a* of $Ag[S_3NO_8]$. The $[S_3NO_8]^-$ anions are shown in polyhedron representation in two different colors (indigo and gold) to provide a better perspective.

In both salts the cyclic anion $[S_3NO_8]^-$ is present, which was crystallographically determined in $K[S_3NO_8]$ for the first time.[26] Structurally, it can be described as vertex-connected tetrahedra of two $[SO_4]$ units and one $[SO_3N]$ unit, resulting in a six-membered ring. Thus, it has solid-state structure similarity to γ-SO_3 with one bridging oxygen atom being replaced by a nitrogen atom.[4] The shape is also found for the trisulfimide, $[S_3N_3O_6]^{3-}$, which in contrast contains three bridging nitrogen atoms in its composition.[91,138] The cyclotriphosphate (or trimetaphosphate), $[P_3O_9]^{3-}$, also adopts a similar configuration in the solid-state.[139-141] In the silver salt one $[S_3NO_8]^-$ anion can be distinguished crystallographically while in the rubidium salt three unique anions are found.

In $Ag[S_3NO_8]$ the atoms Ag1, N1, S2, O4 and O5 are located at special sites (*Wyckoff* position *4c*, mirror plane) and S1, O1, O2 and O3 are on general sites (*Wyckoff* position *8d*). In $Rb[S_3NO_8]$ all atoms occupy general sites (*Wyckoff* position *4a*).

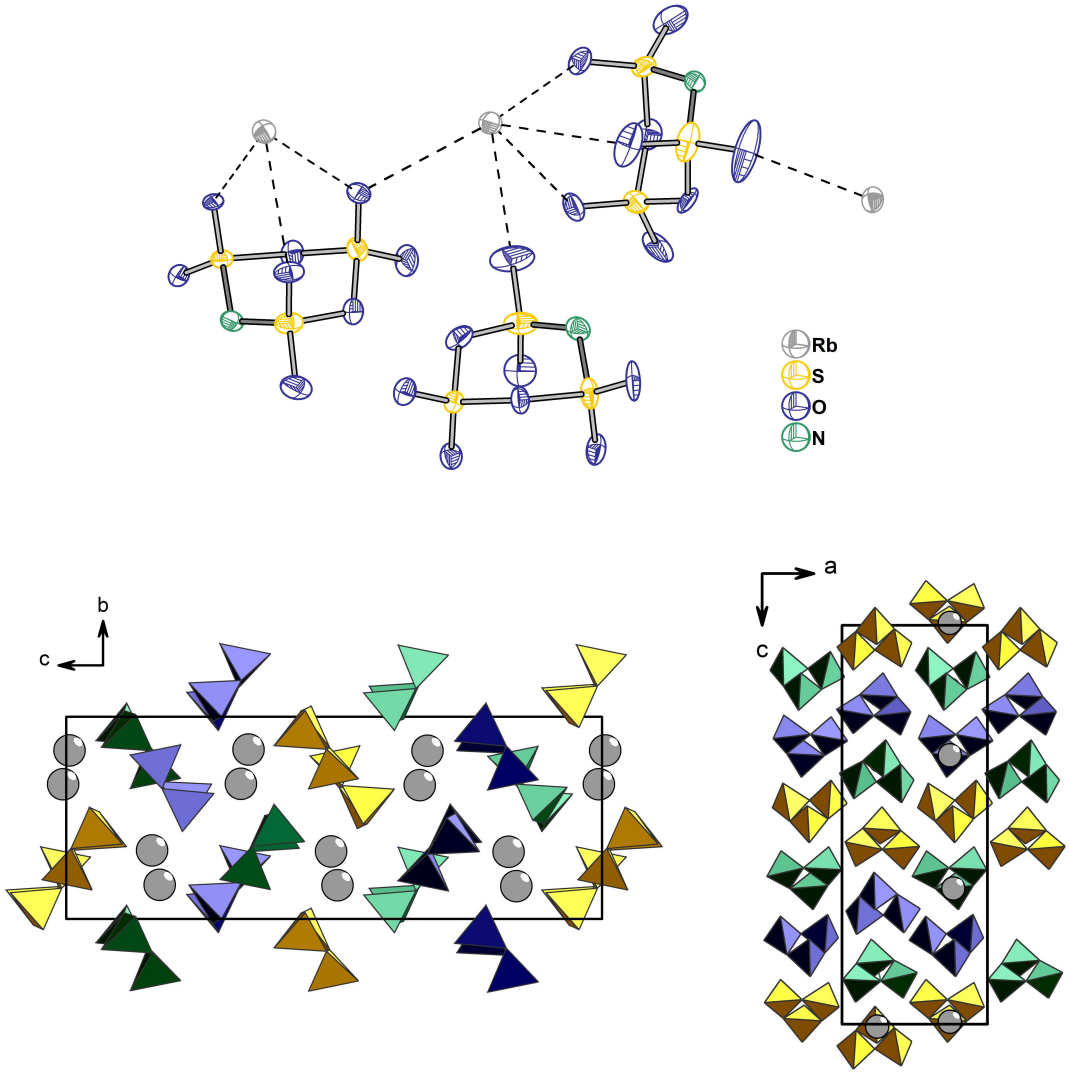

Figure 22: Asymmetric unit of $Rb[S_3NO_8]$ with thermal ellipsoids shown at 70% probability (top). Extended unit cell of $Rb[S_3NO_8]$ along the crystallographic axes *a* and *b* (bottom). The three crystallographically distinguishable $[S_3NO_8]^-$ anions are shown in polyhedron representation, each in different color (indigo, gold, green) to provide a better perspective.

By comparing the anions of the two compounds, similar bonding properties can be observed (see Figure 23, p. 29). In both cases, a deviation between the terminal bonds and bridging bonds is noticeable. The S–N distances amount to 158.21(8) pm in the Ag^+-salt and range from 155.5(9)-160.3(8) pm in the Rb^+-salt. For the bridging bonds $S–O^{br}$ values between 157.7(7) pm and 170.4(8) pm for $Rb[S_3NO_8]$ and 158.3(1)-169.2(1) pm for $Ag[S_3NO_8]$ are found. In contrast the terminal $S–O^t$ bond lengths are much shorter with values in the range of 141.3(2)-142.2(1) pm ($Ag[S_3NO_8]$) and 139.9(8)-143.2(9) pm ($Rb[S_3NO_8]$). They are also shorter than the respective $P–O^t$ bonds observed in the $[P_3O_9]^{3-}$ anions, which have mean distances near to 150 pm.[139,141] In the structurally comparable literature-known trisulfimides S–N distances of 158.8(1)-161.3(1) pm for $(NH_4)_3[S_3N_3O_6]$[91] and 163.1(5)-163.6(6) pm for $Ag_3[S_3N_3O_6](H_2O)_3$[138] are found.

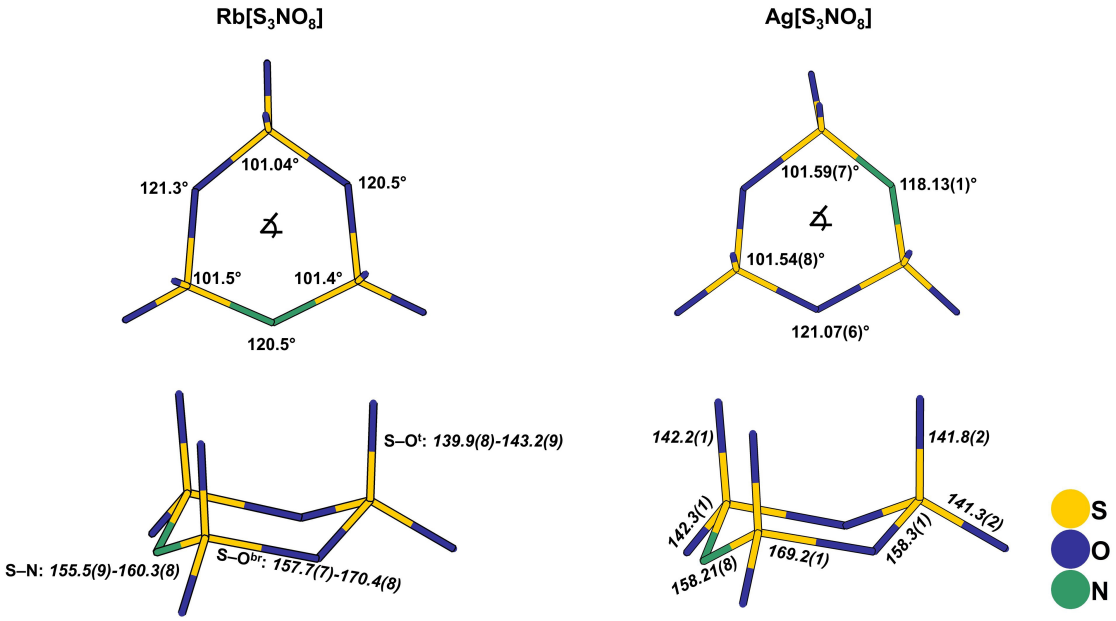

Figure 23: Wires and sticks representation of $[S_3NO_8]^-$ found in the structures of $Rb[S_3NO_8]$ (left) and $Ag[S_3NO_8]$ (right) with bond angles (mean values for Rb^+ salt) and bond lengths (italics, in pm).

In the six-membered ring the angles between the sulfur atoms ($S–N^{br}–S$, $S–O^{br}–S$) are in the range of 120° whereas the angles between the bridging atoms ($N^{br}–S–O^{br}$, $O^{br}–S–O^{br}$) are shorter with values around 101° for both compounds (see Figure 23).

Considering the ionic interactions, a difference between both compounds becomes apparent (see Figure 24 and Figure 25, p. 30). Ag^+ shows the strongest interaction to the bridging atom N1 with a distance of 239.0(1) pm. Rb^+ interacts more strongly with oxygen atoms. This can be explained by the circumstance that Ag^+ is the softer acid compared to Rb^+.[91]

The Ag–N interaction is also observed in $Ag_3[S_3N_3O_6](H_2O)_3$ with distances of 232.4(4) pm and 242.7(5) pm.[138] In total the silver cation is sevenfold coordinated by six oxygen and one nitrogen according to an analysis with *CHARDI*[142] leading to a non-specified polyhedron, which was examined with the program *Polynator*[143]. The Ag–O distances take up values of 249.3(1)-260.4(1) pm, which indicates a weaker interaction as between Ag and N. The three rubidium cations in the structure are in twelvefold coordination by oxygen and nitrogen and no distinctive coordination polyhedron can be identified according to *Polynator*[143]. Rb–O distances range from 289.4(8) pm up to 371.7(8) pm and Rb–N distances lie in between 324.9(8) pm and 327.8(8) pm. This is in accordance with the larger ionic radius of Rb^+ compared to Ag^+.[144-145]

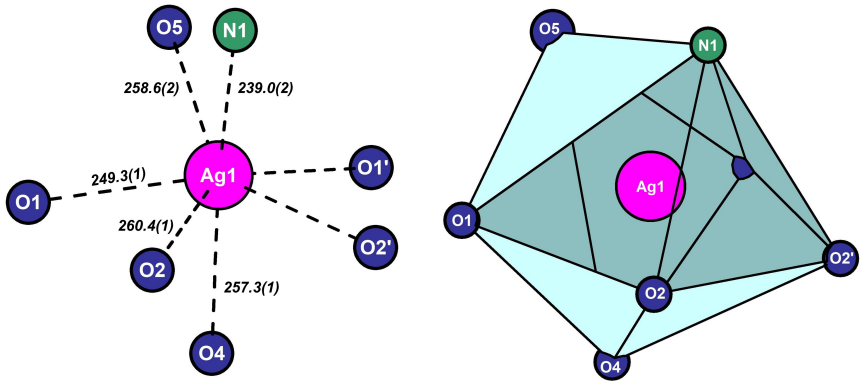

Figure 24: Coordination sphere of Ag^+ in $Ag[S_3NO_8]$ with atomic distances (italics, in pm).

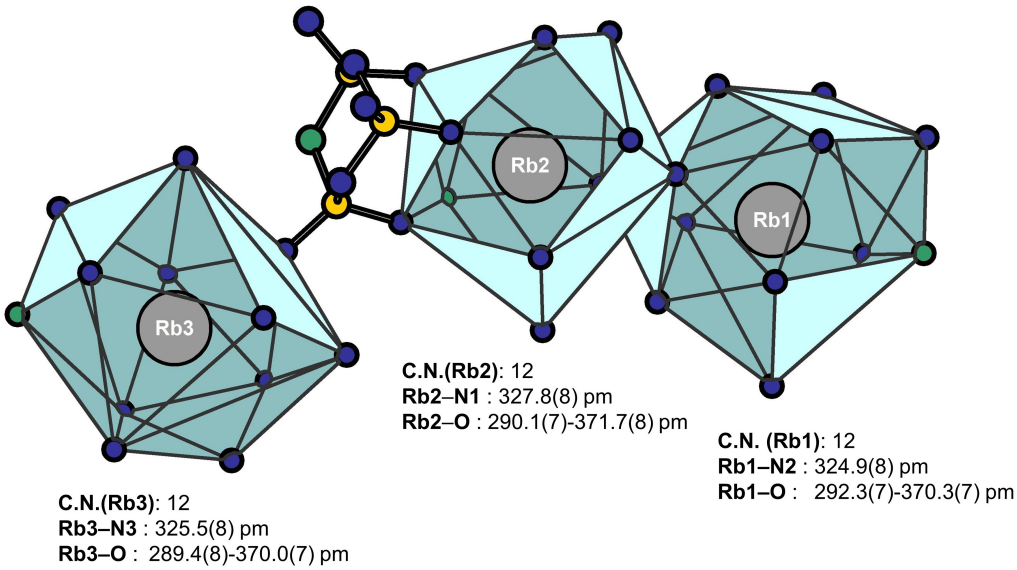

Figure 25: Depiction of the coordination sphere as polyhedra of the three unique Rb^+ in $Rb[S_3NO_8]$ with listing of the coordination numbers (CN, determined with *CHARDI*[142]) and atomic distances.

4.2.3 Na[S4NO11]

$P_3N_3Cl_6$ and SO_3 were also reacted with sodium, and lithium salts to complete the series of alkali metal compounds. For lithium no cyclic nitridosulfate anions could be obtained, even though numerous Li^+ salts were used as starting materials. Reactions with lithium compounds led to the formation of the pentasulfate, $Li_2[S_5O_{16}]$, which has already been reported by *Wickleder et al.* as a crystalline phase resulting from a reaction between Li_2SO_4 and SO_3.[16] In reactions with sodium-containing reactants, NaCl showed no reaction, but with Na_2O small colorless crystals were formed. The crystals were extremely sensitive towards ambient conditions and even under argon atmosphere after being released from the ampoule. SC-XRD analysis of one single crystal revealed a structure with the composition $Na[S_4NO_{11}]$ (see Figure 26, p. 32).

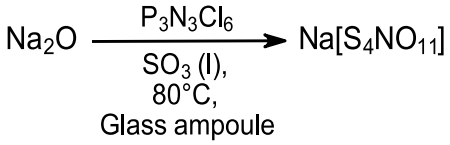

Scheme 11: Preparation of $Na[S_4NO_{11}]$ in a solvothermal synthesis with SO_3.

The crystal structure was solved in the monoclinic space group $P2_1/n$ with four formula units per unit cell (see Table 4). All atoms occupy general sites (*Wyckoff 4e*). One unique Na^+ and $[S_4NO_{11}]^-$ are observed in the unit cell.

Table 4: Selected crystallographic data of $Na[S_4NO_{11}]$.

Na[S4NO11]	
Crystal System	Monoclinic
Space Group	$P2_1/n$
a / pm	734.58(4)
b / pm	1337.59(7)
c / pm	944.86(5)
β / °	101.525(2)
V / nm^3	0.90967(8)
Z	4
R_1 (all data); wR_2 (all data)	0.0308; 0.0729
GooF	1.116

$[S_4NO_{11}]^-$ represents a novel anion and can be categorized as a polymeric nitridosulfate in terms of its structural composition. Formally it derives from $[S_3NO_8]^-$ with one $[SO_3]$ fragment inserted into the ring leading to an eight-membered ring. The solid-state conformation is thus isosteric to that of SeO_3 with its tetrameric Se_4O_{12} ring structure.[86] The pure ring itself has a boat-boat conformation, also found for cyclooctane.[146] An analogous structure to $A[S_3NO_8]$ (A = Ag^+, K^+, Rb^+) was not obtained in case of sodium. Why unlike to K^+, Rb^+ and Ag^+ this anion was formed in the presence of Na^+ remains unclear and can only be guessed at. The nature of the cation may decisive, i.e. the ionic radius and Lewis acidity are parameters to consider.

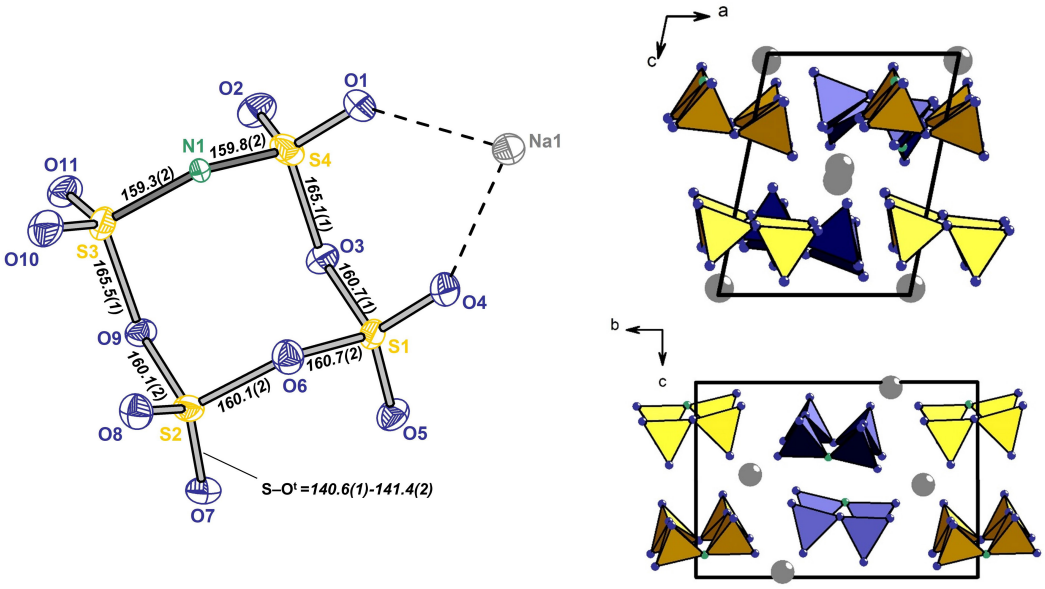

Figure 26: Structure and labeling of $Na[S_4NO_{11}]$ (left) and crystal structure along crystallographic axis *b* and *a* (right). The thermal ellipsoids are set to probability level of 70%. Selected bong lengths (italics, in pm) are shown.

The differentiation of nitrogen and oxygen atoms by X-ray diffraction is not very reliable due to the similar atomic form factors. One argument for the presence of nitrogen is to create a total charge of −1 of the anion. The isotropic refinement of the bridging atoms with an occupancy set to be free suggests that the nitrogen atom lies in between S4 and S3. The two S–N^{br} bonds in the anion have lengths of 159.3(2) pm and 159.8(2) pm. The S–O^{br} are slightly longer with values of 160.1(2) pm to 165.5(1) pm. The terminal bonds S–O^{t} are in turn shortened with values around 141 pm. The angles in the ring between the sulfur atoms (S–O–S, S–N–S) are in between 124-125° whereas the angles between the bridging atoms (O^{br}–S–O^{br}, O^{br}–S–N^{br}) lie close to 102°. The anion adopts a "boat-boat" conformation (see Figure 27). All sulfur atoms lie almost on the same plane with a torsion angle of 1.2° (S–S–S–S). The two pairs of parallel bridging atoms (O6/N1 and O9/O3) protrude from this plane in opposite directions with distances ranging from 74 pm to 75 pm.

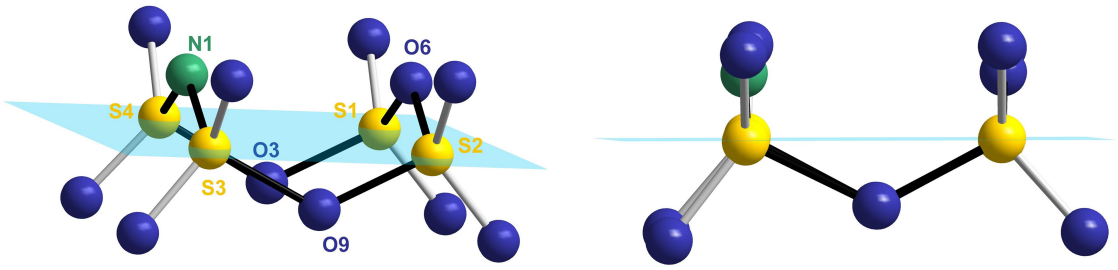

Figure 27: Structure of $[S_4NO_{11}]^-$ with plane through the sulfur atoms along two viewing directions. Bonds that are part of the ring are shown in black.

The sodium cation is sevenfold coordinated by oxygen atoms of in total six $[S_4NO_{11}]^-$ anions according to *CHARDI*[142] (see Figure 28). Observed distances for Na–O lie within 233.8(2) pm

(Na1–O4) up to 262.3(2) pm (Na1–O1). The polyhedron can be described approximately as a monocapped trigonal prism but with considerable distortion with a calculated value δ = 8.778 (*Polynator*[143]).

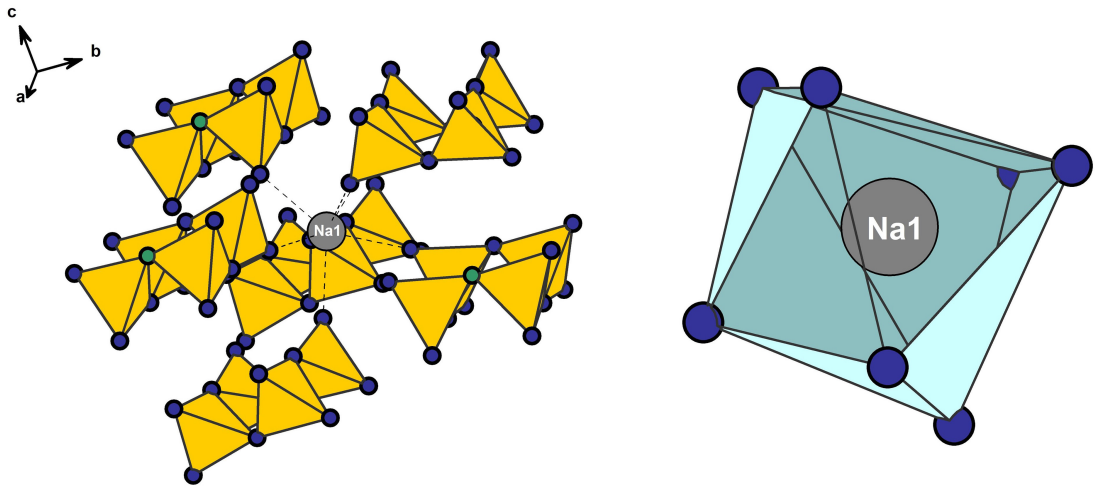

Figure 28: Coordination sphere of Na^+ in $Na[S_4NO_{11}]$.

4.2.4 Publication 1

The Unprecedented $[S_4N_2O_{10}]^{2-}$ Anion in the Molecular Gold Complexes $[Au_2Br_2(S_4N_2O_{10})_2]$ and $[Au_2Cl_2(S_4N_2O_{10})_2](S_2O_5Cl_2)$

Tobias Rennebaum, David van Gerven, and Mathias S. Wickleder

Chem. Eur. J. **2022**, *28*, e202202171, 1-3.

The following publication describes the synthesis and characterization of the isosteric molecular gold complexes $[Au_2Br_2(S_4N_2O_{10})_2]$ and $[Au_2Cl_2(S_4N_2O_{10})_2](S_2O_5Cl_2)$. The syntheses succeeded by reaction of the gold halides $AuCl_3$ and $AuBr_3$ with $P_3N_3Cl_6$ in liquid SO_3 at elevated temperature. The structures of both compounds were thoroughly elucidated by single crystal X-ray diffraction. Additionally, *Raman* spectroscopy on single crystals was performed. With the assistance of DFT calculations the structure model was verified, and *Raman* modes were assigned. The supplementary information (see 8.1, p. 163) contains the synthetic procedures and all detailed analytical data.
The principal author Tobias Rennebaum carried out all syntheses, evaluated the analytical data and did the theoretical calculations. Dr. David van Gerven helped to resolve the two-component twinned structure of $[Au_2Br_2(S_4N_2O_{10})_2]$. Prof. Dr. Wickleder is the supervisor of this work, the corresponding author of this publication and co-authored and proofread the manuscript.
Thankfully acknowledged are the single crystal XRD measurements by Silke Kremer (University of Cologne), introduction to *Raman* microscopy by Christoph Lenting (University of Cologne) and laboratory support by Felix Croé (University of Cologne).

Chemistry–A European Journal
Research Article
doi.org/10.1002/chem.202202171
Chemistry Europe
European Chemical Societies Publishing
www.chemeurj.org

The Unprecedented $[S_4N_2O_{10}]^{2-}$ Anion in the Molecular Gold Complexes $[Au_2Br_2(S_4N_2O_{10})_2]$ and $[Au_2Cl_2(S_4N_2O_{10})_2](S_2O_5Cl_2)$

Tobias Rennebaum,[a] David van Gerven,[a] and Mathias S. Wickleder*[a]

Abstract: The reaction of hexachlorophosphazene, $P_3N_3Cl_6$, with SO_3 and the gold halides $AuCl_3$ and $AuBr_3$, respectively, leads to the new cyclic anionic tetramer, $[S_4N_2O_{10}]^{2-}$, which is coordinated to Au^{3+} in the dimeric complexes $[Au_2X_2(S_4N_2O_{10})_2]$ (X=Cl, Br). The $[S_4N_2O_{10}]^{2-}$ anion can be seen as the condensation product of two sulfate anions, $[SO_4]^{2-}$, and two amidosulfate anions, $[NH_2SO_3]^-$.

Introduction

Amidosulfuric acid, NH_2SO_3H, also known as sulfamic acid, is the most simple nitrogen derivative of sulfuric acid. It can be seen either as the amide of sulfuric acid or as a sulfonic acid derivative of ammonia, NH_3. In this case, a $[HSO_3]$ group replaces one hydrogen atom of NH_3. Also the remaining hydrogen atoms can be substituted, leading to imido-*bis*-sulfuric acid, $NH(SO_3H)_2$, and nitrido-*tris*-sulfuric acid, $N(SO_3H)_3$. While NH_2SO_3H and its salts are well studied and frequently used, $NH(SO_3H)_2$ and $N(SO_3H)_3$ are not known as neat acids, and also the knowledge on their salts is very limited.[1–5] The nature of the S–N bond still leaves a plenty of scope for novel SN compounds which was recently demonstrated by the synthesis of the tetraimido sulfuric acid, $H_2S(NtBu)_4$ and the sulfur nitride oxide, $S_6N_2O_{15}$.[6–7] With $S_6N_2O_{15}$ we shed some more light on the higher sulfonic acids of ammonia, because this cage-type molecule is the anhydride of $N(SO_3H)_3$.[7] It shows the two nitrogen atoms connected by three $[S_2O_5]$ bridges according to $N\{S(O)_2O(O)_2S\}_3N$. $S_6N_2O_{15}$ forms in the reaction of hexachlorophosphazene, $P_3N_3Cl_6$, and SO_3. The ability of $P_3N_3Cl_6$ to act as a Lewis base in the reaction with SO_3 under formation of $P_3N_3Cl_6\cdot 3\,SO_3$ has already been described in 1954.[8] It is reasonable to assume that this compound is the first step of the reaction that leads to $S_6N_2O_{15}$. It is not understood, how the decomposition of $P_3N_3Cl_6\cdot 3\,SO_3$ occurs and thus, scrutiny of the reaction appears to be reasonable. In course of our investigations, we also explored the presence of various metals in the reaction mixture. It turned out that the reaction of $P_3N_3Cl_6$ with SO_3 leads to the formation of the previously unknown anion $[S_4N_2O_{10}]^{2-}$ when $AuCl_3$ and $AuBr_3$, respectively, are added to the reaction mixture. The reaction sequence is not clear up to now. However, we assume that the formation of the adduct $P_3N_3Cl_6\cdot 3\,SO_3$ will also be the step in this reaction. If $S_6N_2O_{15}$ is an intermediate of the reaction or if the Au^{3+} ions interact directly in the decomposition of $P_3N_3Cl_6\cdot 3\,SO_3$ is currently under investigation. Therefore, we started to perform especially NMR investigations and in situ Raman measurements. However, this is challenging due to the unconventional SO_3 solvent.

Results and Discussion

The $[S_4N_2O_{10}]^{2-}$ anion can be traced back to the aforementioned imido-*bis*-sulfuric acid $NH(SO_3H)_2$. The anhydride of this acid would be the cyclic dimer $NH\{S(O)_2O(O)_2S\}_2NH$. The hydrogen atoms of the [NH] groups are still acidic and the gold complexes with the anion $[S_4N_2O_{10}]^{2-}$ are, thus, the first representative of a salt of this new acid.

The $[S_4N_2O_{10}]^{2-}$ anion is a ring consisting of four vertex-connected tetrahedra (Figure 1). The backbone of the ring consists of two S–N–S and two S–O–S bridges with bonding angles around 123° in both cases. The distances within these bridges are slightly, but significantly, different displaying mean values S–N of 166.4(6) pm and S–O of 163.4(6) pm (see caption of Figure 1 and supporting information). The S–O distances are in line with reported values for disulfates,[9–11] while the values for the S–N bonds are larger than found for the potassium nitrido-*bis*-sulfate, $K_3[N(SO_3)_2]\cdot H_2O$, which show values of 160 pm.[1,12]

This difference can be attributed to the strong bonding of the $[S_4N_2O_{10}]^{2-}$ anion to the Au^{3+} ions in the presented molecules $[Au_2X_2(S_4N_2O_{10})_2]$ (X=Cl, Br). In these complexes two gold atoms are connected to dimers which are terminated by two $[S_4N_2O_{10}]^{2-}$ anions (Figure 2 and Figure 3). The latter act as chelating ligands and the distances Au–N range from 201.8(4) to 203.9(3) pm (X=Cl) and 203.6(7) to 205.1(7) pm (X=Br). The distances to the bridging halide anions are about 232.5(1) pm (X=Cl) and 243.3(1) pm (X=Br) and are in accordance with the observations for the trihalides AuX_3, which show also dimeric

[a] T. Rennebaum, Dr. D. van Gerven, Prof. M. S. Wickleder
University of Cologne
Institute of Inorganic Chemistry
Greinstr. 6, 50939 Cologne (Germany)
E-mail: mathias.wickleder@uni-koeln.de

Supporting information for this article is available on the WWW under https://doi.org/10.1002/chem.202202171

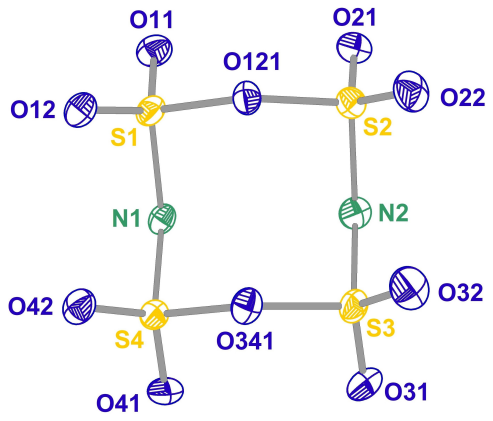

Figure 1. Structure and labelling of the $[S_4N_2O_{10}]^{2-}$ as observed in the dimeric $[Au_2Cl_2(S_4N_2O_{10})_2]$ molecule. Selected distances (in pm) and angles (in °) compared to theoretical values (in *italics*): S(1–4)–$O_{terminal}$ (O11,O12; O21, O22; O31, O32; O41, O42) 139.7(3)-141.1(3)/*142.2*, S1–O121 164.0(3)/*164.83*, S2–O121 162.1(3)/*164.81*, S3–O341 163.8(3)/*164.82*, S4–O341 162.7(3)/*164.85*, N1–S1 166.9(4)/*168.29;* N1–S4 166.0(4)/*168.32*, N2–S2 166.6(4)/*168.29*, N2–S3 166.5(4)/*168.33*; S1–O121–S2 123.4(2)/*123.6*; S3–O341–S4 123.0(2)/*123.5*; S1–N1–S4 122.6(2)/*123.5*; S2–N2–S3 123.1(2)/*123.54*. The thermal ellipsoids are set to a 70% probability level.

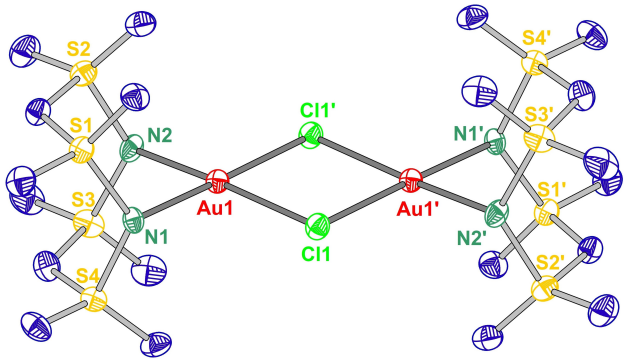

Figure 2. Structure and labelling of the molecular dimer $[Au_2Cl_2(S_4N_2O_{10})_2]$ in the crystal structure of $[Au_2Cl_2(S_4N_2O_{10})_2](S_2O_5Cl_2)_2$. Selected distances (in pm) an angles (in °) within the $\{N_2AuCl_2AuN_2\}$ moiety compared to theoretical values (in *italics*): Au1–Cl1 232.6(1)/*234.72*, Au1–Cl1' 232.4(1)/*234.67*; Au1–N1 203.9(3)/*201.87*, Au1–N2 201.8(4)/*201.83*; N1–Au1–N2 86.3(2)/*86.23*; Cl1–Au1–Cl1' 87.0(4)/*85.53*; N1–Au1–Cl1 94.5(1)/*94.16*, N2–Au1–Cl1' 92.2(1)/*94.08* (data for the respective bromide are given in the supplement). The thermal ellipsoids are set to 70% probability level.

structures according to Au_2X_6.[13–14] The distances and angles within the complexes $[Au_2X_2(S_4N_2O_{10})_2]$ (*X*=Cl, Br) are well reflected by quantum mechanical calculations (see captions of Figures 2 and 3, and Supporting Information). As expected, the calculations result in D_{2h} symmetry for the molecules, while in the solid state they exhibit only C_i (*X*=Cl, space group *C*2/*c*) or even C_1 symmetry (*X*=Br, space group *P*1).

While the bromide $[Au_2Br_2(S_4N_2O_{10})_2]$ crystallises as a pure compound, the chloride contains additional $S_2O_5Cl_2$ molecules in the crystal structure. Interestingly, this molecule, even if long known, has been characterised thoroughly only very recently.[15] According to these investigations, different possible conformers of the molecule are stable and the solid state structures reveal strong polymorphism. The disulfuryl dichloride molecule in $[Au_2Cl_2(S_4N_2O_{10})_2](S_2O_5Cl_2)_2$ appears as the so-called *anti*-conformer and the observed bond and angle parameters match very well the reported findings for the pure compound.[15]

The new $[S_4N_2O_{10}]^{2-}$ anion is the first example of a cyclic anion consisting of condensed $[SO_4]^{2-}$ and $[NH_2SO_3]^-$ tetrahedra, because the above mentioned imido-*bis*- and nitrido-*tris*-sulfate are monomeric species. The condensation of only $[NH_2SO_3]^-$ ions is known in form of the cyclic trimer $[S_3N_3O_6]^{3-}$ and tetramer $[S_4N_4O_8]^{4-}$.[16–17] It is worthwhile to mention that there are other anions in the system S/N/O.[18] However, these anions are usually not composed of linked tetrahedra. The anions $[S_3N_3O_6]^{3-}$ and $[S_4N_4O_8]^{4-}$ are usually prepared by heating sulfamide, $SO_2(NH_2)_2$, to a temperature between 180 and 210 °C. However, because the synthesis is not straightforward, the number of these anions is very limited. On the other hand, the condensation of $[SO_4]^{2-}$ tetrahedra can only lead to linear polysulfates $[S_nO_{3n+1}]^{2-}$ ($n=2$–6).[19–23] Cyclization would result in neutral molecules and with S_3O_9, the so-called ice-type SO_3 (or γ-SO_3), there is one known example.[24,25] The combination of the different $[SO_4]^{2-}$ and $[NH_2SO_3]^-$ tetrahedral, respectively, is not known up to now, probably because no suitable preparative pathway is known. According to our findings the route using $P_3N_3Cl_6$ as a Lewis base and SO_3 as a Lewis acid is very promising in this respect. In principle, numerous variations in the condensation of $[SO_4]^{2-}$ and $[NH_2SO_3]^-$ tetrahedra are thinkable, bearing the potential of a large number of new anions. However, even if the systematic approach seems to be sound, the synthesis of defined products turns out to be not that simple. Concerning the new $[S_4N_2O_{10}]^{2-}$ anion it is of importance to obtain further compounds. We are especially interested in the salts with simple monovalent cations that would allow studying the anion without complexation.

Experimental

Full details of synthesis, characterisation and quantum chemical calculations can be found in the Supporting Information.

Deposition Number(s) 2154742 (for $[Au_2Cl_2(S_4N_2O_{10})_2](S_2O_5Cl_2)_2$) and 2154741 (for $[Au_2Br_2(S_4N_2O_{10})_2]$) contain(s) the supplementary crystallographic data for this paper. These data are provided free of charge by the joint Cambridge Crystallographic Data Centre and Fachinformationszentrum Karlsruhe Access Structures service.

Acknowledgements

We acknowledge Silke Kremer (University of Cologne) for the single-crystal X-ray diffraction data collection and Christoph Lenting (University of Cologne) for the support with the Raman measurements. Furthermore, we are indebted to Felix Croé for technical assistance. Open Access funding enabled and organized by Projekt DEAL.

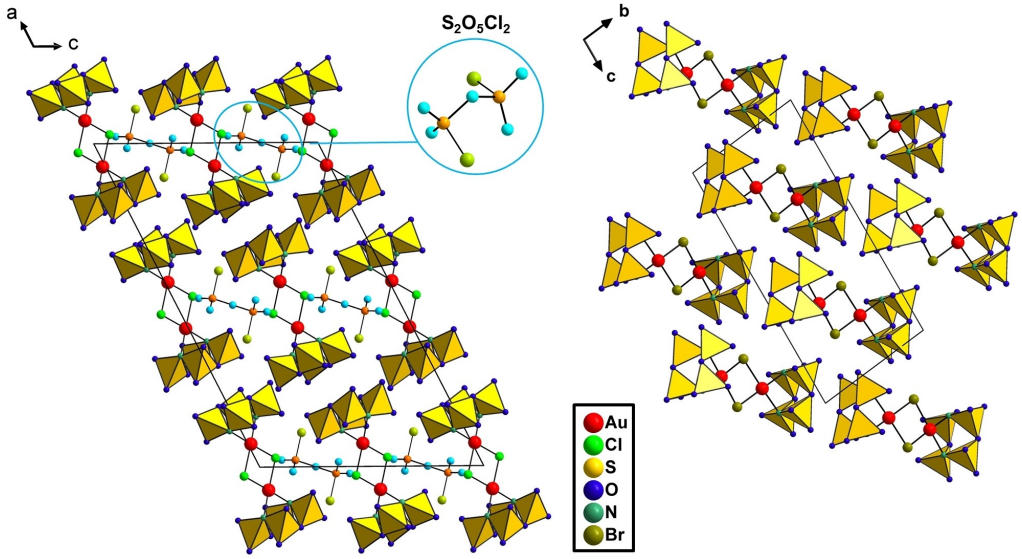

Figure 3. Crystal structures of $[Au_2Cl_2(S_4N_2O_{10})_2](S_2O_5Cl_2)_2$ (left) and $[Au_2Br_2(S_4N_2O_{10})_2]$ (right). In the monoclinic chloride compound the dimers show inversion symmetry, in the triclinic bromide the complexes are located on general sites bearing no symmetry elements. The crystal structure of the chloride compound contains additional $S_2O_5Cl_2$ molecules, as emphasized in different colours in the left part of the figure. To provide a better overview the $[SO_3N]$ moieties are illustrated as polyhedra. (crystallographic details are given in the Supporting Information).

Conflict of Interest

The authors declare no conflict of interest.

Data Availability Statement

The data that support the findings of this study are available from the corresponding author upon reasonable request.

Keywords: sulfur trioxide · gold · sulfuric acid · amidosulfate · solvothermal synthesis

[1] P. Barbier, Y. Parent, G. Mairesse, *Acta Crystallogr. Sect. B* **1979**, *35*, 1308–1312.
[2] D. W. J. Cruickshank, D. W. Jones, *Acta Crystallogr.* **1963**, *16*, 877–883.
[3] H. Sisler, L. F. Audrieth, *J. Am. Chem. Soc.* **1938**, *60*, 1947–1948.
[4] H. Sisler, L. F. Audrieth, U. S. Branson, W. C. Johnson, *Inorg. Synth.*, **1946**, pp. 182–183.
[5] J. V. Tillack, C. H. L. Kennard, *J. Chem. Soc. A* **1970**, 1637–1640.
[6] J. Jung, A. Münch, R. Herbst-Irmer, D. Stalke, *Angew. Chem. Int. Ed.* **2021**, *60*, 5679–5682; *Angew. Chem.* **2021**, *133*, 5742–5746.
[7] D. van Gerven, M. S. Wickleder, *Angew. Chem. Int. Ed.* **2020**, *59*, 17169–17171; *Angew. Chem.* **2020**, *132*, 17320–17323.
[8] M. Goehring, H. Hohenschutz, R. Appel, *Z. Naturforsch. B* **1954**, *9*, 678–681.
[9] C. Logemann, M. S. Wickleder, *Z. Kristallogr. New Cryst. Struct.* **2013**, *228*, 161–162.
[10] C. Logemann, J. Witt, D. Gunzelmann, J. Senker, M. S. Wickleder, *Z. Anorg. Allg. Chem.* **2012**, *638*, 2053–2061.
[11] A. Weiz, J. Bruns, M. S. Wickleder, *Eur. J. Inorg. Chem.* **2014**, *2014*, 172–177.
[12] J. R. Hall, R. A. Johnson, C. H. L. Kennard, G. Smith, B. W. Skelton, A. H. White, *J. Chem. Soc. Dalton Trans.* **1980**, 1091–1097.
[13] K.-P. Lörcher, J. Strähle, *Z. Naturforsch. B* **1975**, *30*, 662–664.
[14] P. Schwerdtfeger, P. D. W. Boyd, S. Brienne, A. K. Burrell, *Inorg. Chem.* **1992**, *31*, 3411–3422.
[15] A. Moreno Betancourt, J. Schwabedissen, R. M. Romano, C. O. Della Védova, H. Beckers, H. Willner, H.-G. Stammler, N. W. Mitzel, *Chem. Eur. J.* **2018**, *24*, 10409–10421.
[16] C. Leben, M. Jansen, *Z. Naturforsch. B* **1999**, *54*, 757.
[17] V. E. Sokol, M. A. Porai-Koshits, M. A. Kop′eva, I. A. Rozanov, *Koordinatsionnaya Khimiya* **1985**, *11*, 370–377.
[18] T. Chivers, R. S. Laitinen, *Chem. Soc. Rev.* **2017**, *46*, 5182–5192.
[19] J. Bruns, M. Eul, R. Pöttgen, M. S. Wickleder, *Angew. Chem. Int. Ed.* **2012**, *51*, 2204–2207; *Angew. Chem.* **2012**, *214*, 2247–2250.
[20] C. Logemann, T. Klüner, M. S. Wickleder, *Angew. Chem. Int. Ed.* **2012**, *51*, 4997–5000; *Angew. Chem.* **2012**, *124*, 5082–5085.
[21] C. Logemann, T. Klüner, M. S. Wickleder, *Z. Anorg. Allg. Chem.* **2012**, *638*, 758–762.
[22] L. V. Schindler, A. Becker, M. Wieckhusen, T. Klüner, M. S. Wickleder, *Angew. Chem. Int. Ed.* **2016**, *55*, 16165–16167; *Angew. Chem.* **2016**, *128*, 16399–16401.
[23] L. V. Schindler, M. Struckmann, A. Becker, M. S. Wickleder, *Eur. J. Inorg. Chem.* **2017**, *2017*, 958–964.
[24] W. S. McDonald, D. W. J. Cruickshank, *Acta Crystallogr.* **1967**, *22*, 48–51.
[25] R. Westrik, C. H. Mac Gillavry, *Recl. Trav. Chim. Pays-Bas* **1941**, *60*, 794–810.

Manuscript received: July 12, 2022
Accepted manuscript online: August 17, 2022
Version of record online: September 19, 2022

4.2.5 $(NS_2)[Au(S_4N_2O_{10})_2]$

Aside from the dimeric Au^{3+} complexes, monomeric species were prepared during this thesis. Various reactions between $(S_3N_2Cl)Cl$ and SO_3 with different stoichiometries were performed to examine whether $(S_3N_2Cl)Cl$ is also applicable to generate polymeric nitridosulfates and to attempt the reproduction of $S_6N_2O_{15}$. These reactions resulted in the formation of a more or less viscous liquid in the reaction ampoule, which was not further analyzed due to its very reactive behavior. However, in presence of metal salts the formation of solid material was observed. The reaction between $AuCl_3$, $(S_3N_2Cl)Cl$ and SO_3 yielded a yellow crystalline solid. A very small yellow rod-shaped single crystal was analyzed by SC-XRD and solved and refined as the structure with the composition $(NS_2)[Au(S_4N_2O_{10})_2]$ (see Figure 29, p. 39). This compound crystallizes in the monoclinic space group *C*2/*c* with two formula units per unit cell (for more details see Table 5).

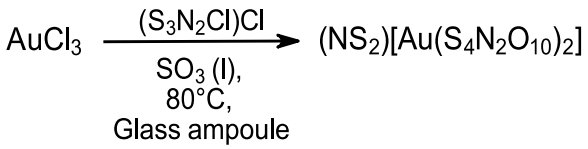

Scheme 12: Preparation of $(NS_2)[Au(S_4N_2O_{10})_2]$ in a solvothermal synthesis with SO_3.

The crystal showed twofold twinning (twin law: 0 0 −1, 0−1 0, −1 0 0) with a fractional contribution of the second component of 0.0555(7). Chemically, the compound is composed of the cation $(NS_2)^+$ and the anionic aurate complex $[Au(S_4N_2O_{10})_2]^-$. In the cell one unique $[S_4N_2O_{10}]$ fragment, one gold atom and one [NS] fragment are observed. Au1 (*Wyckoff 4d*) and N1 (*Wyckoff 4c*) lie on a center of inversion and the other atoms on general sites (*Wyckoff 8f*). The opposite $[S_4N_2O_{10}]^{2-}$ ligand of the complex and sulfur atom (S5') of the cation are projected by inversion.

Table 5: Selected crystallographic data of $(NS_2)[Au(S_4N_2O_{10})_2]$.

$(NS_2)[Au(S_4N_2O_{10})_2]$	
Crystal System	Monoclinic
Space Group	*C*2/*c*
a / pm	1305.95(7)
b / pm	1278.69(6)
c / pm	1304.34(7)
β / °	113.399(2)
V / nm³	1.9990(2)
Z	4
R_1 (all data); wR_2 (all data)	0.0226; 0.0423
GooF	1.077
BASF	0.0555(7)

The $(NS_2)^+$ ion, also called dithionitronium, represents the valence isoelectronic analogue of the nitronium cation, $(NO_2)^+$. It was isolated in the compound $(NS_2)(SbCl_6)$ by *Faggiani et al.* for the first time.[147] They reacted various cyclic sulfur imide derivatives (S_7NH, 1,4-$S_6N_2H_2$ and S_7NBCl_2) with $SbCl_5$ in liquid SO_2 to obtain the aforementioned compound. Up to now the cation is only

described in SC-XRD structures with weakly-coordinating bases, which are $(NS_2)SbCl_6$[147], $(NS_2)AlCl_4$[148] and $(NS_2)AsF_6$[149]. Although the $(NS_2)^+$ cation shows a diverse chemistry, it is rather difficult to prepare.[150] In this work the cation was presumably formed from $(S_3N_2Cl)Cl$, which already contains a pre-built S–N–S moiety.

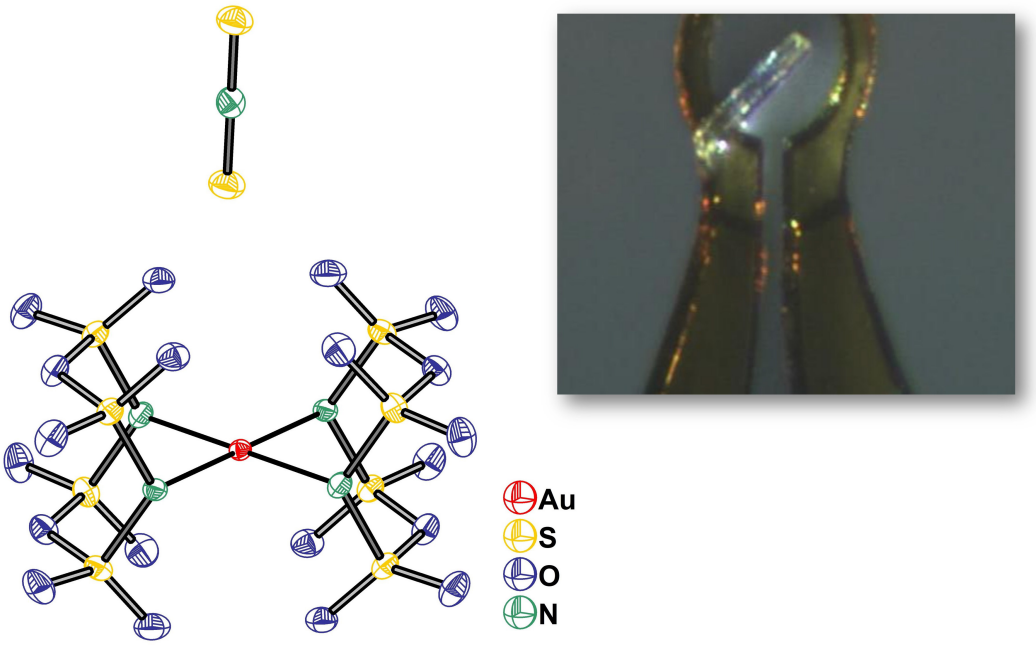

Figure 29: Structure (left) and picture of the measured single crystal on the micromount (right) of $(NS_2)[Au(S_4N_2O_{10})_2]$. The light yellowish crystal had the dimension of 0.029 x 0.033 x 0.141 mm. The thermal ellipsoids are set to a probability level of 70%.

In the literature compounds, the cation adopts a linear configuration with S–N distances ranging from 146.3(4) pm to 148.0(3) pm. In the gold complex perfect $D_{\infty h}$ symmetry for the cation is also observed (see Figure 30, p. 40). Therein the S–N bond length is slightly increased compared to the literature-known data with a value of 149.48(8) pm. The cations are neighbored by six $[S_4N_2O_{10}]^{2-}$ ligands and shows only minor interactions with the latter. Closest contact to ligand oxygen atom lies between S5 and O1 with 296.1(2) pm. The linear cation is oriented along the crystallographic *b*-axis pointing towards the Au^{3+} centers. The presence of NO_2^+ can be excluded due to the different atomic form factors of oxygen and sulfur. Additionally, N–O distances in NO_2^+ are typically around 110 pm.[14] The gold atom Au1 is surrounded in a square-planar manner by the nitrogen atoms N2 and N3 of $[S_4N_2O_{10}]^{2-}$. This coordination is typical for Au^{3+}, which is electronically a d^8 system. By a coordination polyhedron analysis with dynamic models using *Polynator*[143] a distortion from a regular square-planar geometry for $[AuN_4]$ is identified with $\delta = 4.677$. The shape is represented by an ideal parallelogram (2/*m*) with $\delta = 0.000$. This is also confirmed by the bonding situation. The Au–N distances are 205.2(2) pm and 206.3(2) pm and the observed angles are 84.6(1)° for N3–Au1–N2 and 95.37(9)° for N2–Au1–N3'. The Au–N distances are slightly longer in comparison to the observed distances of $[Au_2Br_2(S_4N_2O_{10})_2]$ (203.6(7)-205.1(7) pm) and $[Au_2Cl_2(S_4N_2O_{10})_2](S_2O_5Cl_2)$ (201.8(4)-203.9(3) pm).[151]

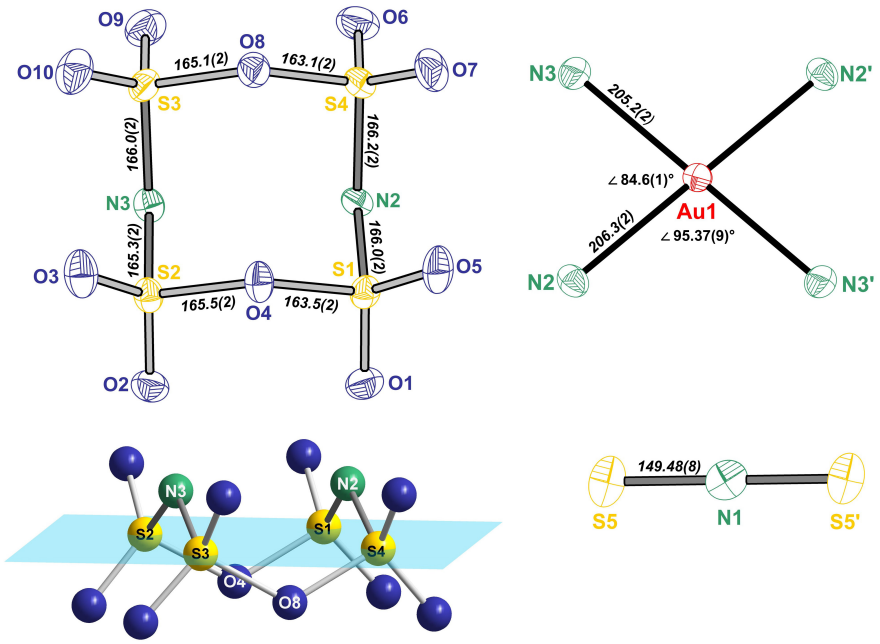

Figure 30: Structural components of the compound $(NS_2)[Au(S_4N_2O_{10})_2]$ with labeling and selected bond lengths (italics, in pm) and angles. The thermal ellipsoids are set to probability level of 70%. A plane through the sulfur atoms of $[S_4N_2O_{10}]^{2-}$ is shown at the bottom left.

The $[S_4N_2O_{10}]^{2-}$ anion acts as a chelating ligand and shows similar conformation compared to the dimeric gold compounds (see 4.2.4, p. 34) and $[S_4NO_{11}]^-$. Values of the bridging bonds are 165.3(2)-166.2(2) pm for S–N^{br} and 163.1(2)-165.5(2) pm for S–O^{br}. Their difference results from the strong bonding of N3 and N2 to Au1, which was already discussed for the dimeric gold compounds.[151] The terminal bonds between sulfur and oxygen are shortened in comparison to the bridging ones with values of 140.6(2)-141.3(2) pm. The bonding angles within the two S–O^{br}–S and S–N^{br}–S bridges are ranging from 118.9(1)° to 122.6(1)°. The bonding angles for O^{br}–S–N^{br} are again significantly shorter with values around 102°. As already pointed out, the cations are orientated vertically to the Au^{3+} centers and the aurate units are stacked offset to each other from layer to layer (see Figure 31, p. 40).

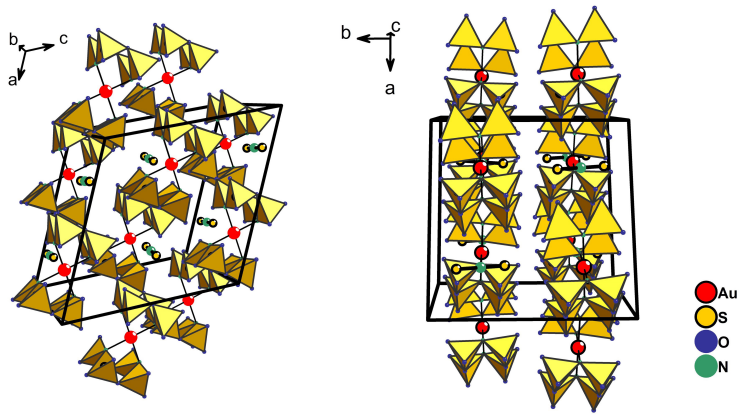

Figure 31: Crystal structure of $(NS_2)[Au(S_4N_2O_{10})_2]$ along two perspectives. The $[SO_3N]$ tetrahedra of the ligands are shown as yellow polyhedra to provide a better perspective.

4.2.6 K[Au(S4N2O10)(S3NO8)Cl]

Considering the aforementioned results with gold halides, other gold compounds were tested in the reaction system of $P_3N_3Cl_6$ and SO_3 to check whether other reagents are usable to prepare gold complexes with cyclic nitridosulfates. The reaction of $K[AuCl_4]$ with $P_3N_3Cl_6$ in SO_3 yielded small yellow single crystals in between polycrystalline and liquid material. Crystallographic analysis of one crystal revealed the structure $K[Au(S_4N_2O_{10})(S_3NO_8)Cl]$.

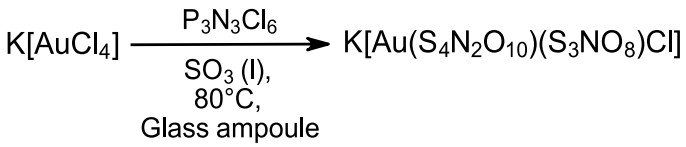

Scheme 13: Preparation of $K[Au(S_4N_2O_{10})(S_3NO_8)Cl]$ in a solvothermal synthesis with SO_3.

The aurate complex $[Au(S_4N_2O_{10})(S_3NO_8)Cl]^-$ is the first example of a heteroleptic gold complex with two different cyclic nitridosulfates ($[S_4N_2O_{10}]^{2-}$ and $[S_3NO_8]^-$) coordinating (see Figure 32, p. 42). The structure was solved and refined in the monoclinic crystal system with the space group $P2_1/c$ (for more details see Table 6).

Table 6: Selected crystallographic data of $K[Au(S_4N_2O_{10})(S_3NO_8)Cl]$.

K[Au(S4N2O10)(S3NO8)Cl]	
Crystal System	Monoclinic
Space Group	$P2_1/c$
a / pm	803.32(4)
b / pm	1544.70(8)
c / pm	1532.20(8)
β / °	104.736(2)
V / nm^3	1.8388(2)
Z	4
R_1 (all data); wR_2 (all data)	0.0486; 0.0926
GooF	1.040

While the formation of $[Au(S_4N_2O_{10})(S_3NO_8)Cl]^-$ appears randomly, the reproducibility of the anions $[S_4N_2O_{10}]^{2-}$ and $[S_3NO_8]^-$ is confirmed by this structure. In the structure one crystallographically unique K^+ and $[Au(S_4N_2O_{10})(S_3NO_8)Cl]^-$ are observed, respectively. $[S_3NO_8]^-$ and $[S_4N_2O_{10}]^{2-}$ coordinate via the bridging nitrogen atoms to Au^{3+}, however $[S_4N_2O_{10}]^{2-}$ is attached in a bidentate manner. One chlorine atom is additionally coordinated to fill the square-planar coordination sphere. Within the $[AuN_3Cl]$ moiety the Au1–Cl1 distance is the longest with 224.1(1) pm (see Figure 33). In $AuCl_3$, which forms the dimer Au_2Cl_6 in solid state, the distances between gold and the two terminal chlorine atoms are in the same range with 225(1) pm and 224(1) pm. In contrast, the bridging bonds (Au–Cl^{br}) are close to 233(1) pm.[152]

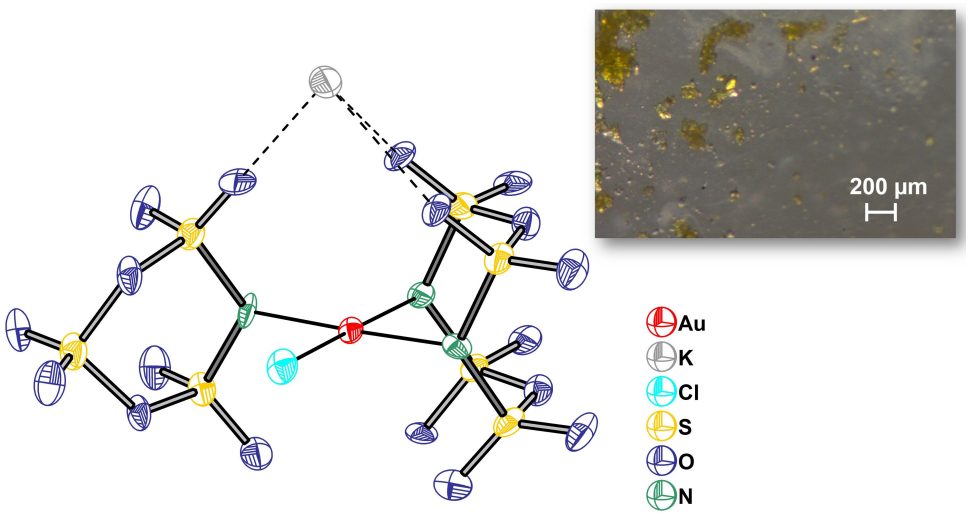

Figure 32: Structure (left) and microscope image of single crystals (top right) of $K[Au(S_4N_2O_{10})(S_3NO_8)Cl]$. The thermal ellipsoids are set to a probability level of 70%.

The Au–N distances have values of 204.7(6) pm (Au1–N1), 207.6(6) pm (Au1–N2) and 203.6(6) pm (Au1–N3). The measured angles between the gold atom further indicate a distorted square-planar geometry with observed angles of 91.0(2)° (N3–Au1–Cl1), 85.3(3)° (N3–Au1–Cl1), 92.0(2)° (N1–Au1–Cl1) and 91.8(3)° (N1–Au1–N2). A shape analysis with *Polynator*[143] yielded a distortion value of $\delta = 4.850$ for the regular square planar plane. It can be more accurately be described as a trapezoid (*mm*2) with $\delta = 3.089$.

The anion $[S_4N_2O_{10}]^{2-}$ is structurally related to those previously described for the gold structures. The backbone is again an eight-membered ring with "boat-boat" conformation. The $S–N^{br}$ distances are in the range of 164.0(7) pm to 166.0(7) pm, while the $S–O^{br}$ distances range from 163.5(6) pm to 164.2(6) pm. The slighlty longer $S–N^{br}$ bonds result from the coordination of nitrogen to gold as already observed in the other discussed gold structures. The terminal bonds between sulfur an oxygen take up values around 141 pm. The ring also exhibits the deviation in angles in between the sulfur atoms ($S–N^{br}–S$, $S–O^{br}–S$) and the bridging atoms ($N^{br}–S–O^{br}$) (see Figure 33, p. 42).

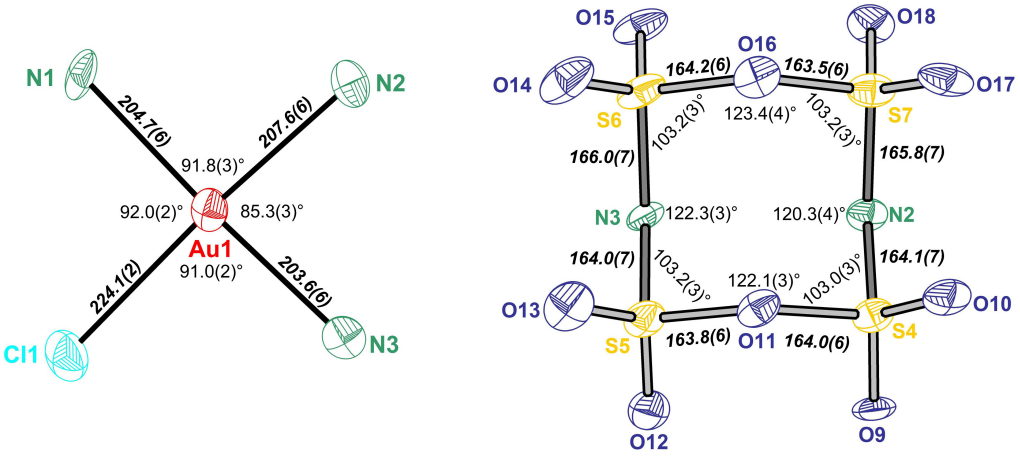

Figure 33: On the left, the square-planar $[AuN_3Cl]$ unit is shown with bond lengths (italics, in pm) and angles. On the right, the ligand $[S_4N_2O_{10}]^{2-}$ is depicted with observed bond lengths (italics, in pm) and angles within the eight-membered ring.

The $[S_3NO_8]^-$ anion has a backbone of a six-membered ring with a chair-like conformation comparable to the silver and rubidium structures discussed above (see Figure 34). In the bridges, the S–N^{br} distances are quite similar with 164.1(7) pm and 163.4(7) pm. The S–O^{br} bond lengths show variations with values of 160.7(6) pm (S3–O2), 160.8(6) pm (S3–O6), 165.0(6) pm (S1–O6) and 165.1(6) pm (S2–O2). The terminal S–O^t bonds are in the range of 139.7(6) pm to 141.7(6) pm. The angles between the terminal oxygen atoms average to 123°. Overall the bonding properties are quite similar to the aforementioned and discussed $[S_3NO_8]^-$ anions.

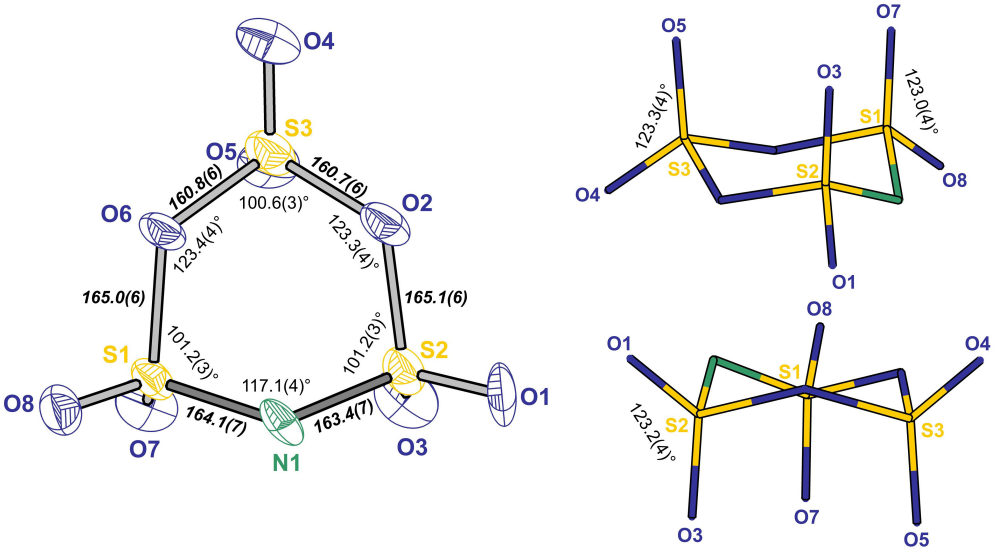

Figure 34: Structure and labeling of $[S_3NO_8]^-$ (left) with selected bond lengths (italics, in pm) angles in the six-membered ring. Wires and sticks representation of $[S_3NO_8]^-$ (right) along two viewing directions with selected angles between the terminal bonds (O^t–S–O^t).

Nine oxygen atoms of three $[S_3NO_8]^-$ and three $[S_4N_2O_{10}]^{2-}$ were assigned to the coordination sphere of K1 with the aid of the program *CHARDI*[142] (see Figure 35, p. 43). Distances within the calculated coordination are in between 278.7(6) pm and 321.4(6) pm. $[S_4N_2O_{10}]^{2-}$ shows coordination in a bidentate manner, while $[S_3NO_8]^-$ interacts in a monodentate manner. The resulting $[KO_9]$ polyhedron has an unspecified shape.

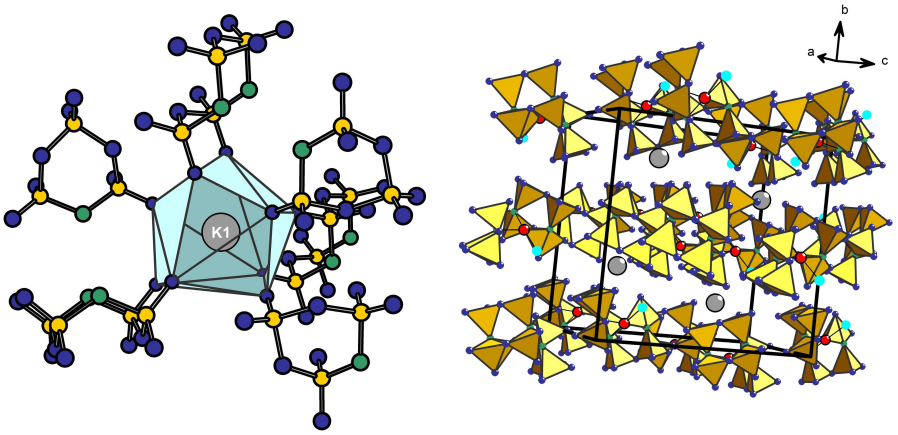

Figure 35: Coordination sphere of K^+ (left) and crystal structure of $K[Au(S_4N_2O_{10})(S_3NO_8)Cl]$ in central projection (right).

4.2.7 $K_2[Pt(S_4N_3O_9)_2](SO_3)_2$

In order to extend the chemistry of the cyclic nitridosulfates, other precious metal salts were used in syntheses with SO_3 and $P_3N_3Cl_6$. The element platinum proved to be suitable to form complexes with those anions. In one reaction between $K_2[PtCl_6]$ and $P_3N_3Cl_6$ in SO_3 the compound $K_2[Pt(S_4N_3O_9)_2](SO_3)_2$ was identified as a reaction product.

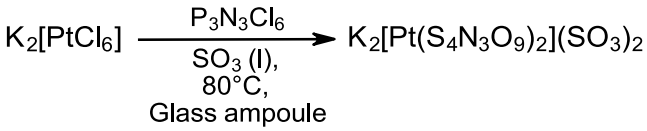

Scheme 14: Preparation of $K_2[Pt(S_4N_3O_9)_2](SO_3)_2$ in a solvothermal synthesis with SO_3.

The reaction was performed in a sealed glass ampoule at 80 °C and during the cooling process, small yellow single crystals were formed. The isolated single crystals tended to decompose when exposed to ambient conditions. During the unit cell determination twinning was recognized. The crystal structure of one crystal was solved and refined in the monoclinic space group *C*2/*c* (for more details see Table 7, p. 44).

Table 7: Selected crystallographic data of $K_2[Pt(S_4N_3O_9)_2](SO_3)_2$.

$K_2[Pt(S_4N_3O_9)_2](SO_3)_2$	
Crystal System	Monoclinic
Space Group	*C*2/*c*
a / pm	1439.4(1)
b / pm	1211.0(1)
c / pm	1458.2(1)
β / °	104.744(4)
V / nm^3	2.4580(4)
Z	4
R_1 (all data); wR_2 (all data)	0.0513; 0.1126
GooF	1.134
BASF	0.073(3)

In the refinement process a second domain was found according to the twin law (1 0 ½, 0 −1 0, 0 0 −1) with a fractional proportion of 7.6%. In the asymmetric unit one distinguishable platinum atom (Pt1), one potassium cation (K1), one SO_3 group and one $[S_4N_3O_9]^{3-}$ are present. Pt1 lies at a center of inversion (*Wyckoff 4a*), while the other atoms are located at general sites (*Wyckoff 8f*). The platinum atom is sixfold coordinated by two $[S_4N_3O_9]^{3-}$ ligands, each coordinating in a tridentate manner (see Figure 36, p. 45). The platinate complex has a total charge of 2− and the Pt center is in the oxidation state +4. Potassium acts as countercation and two additional SO_3 molecules crystallize as solvent molecules in the structure.

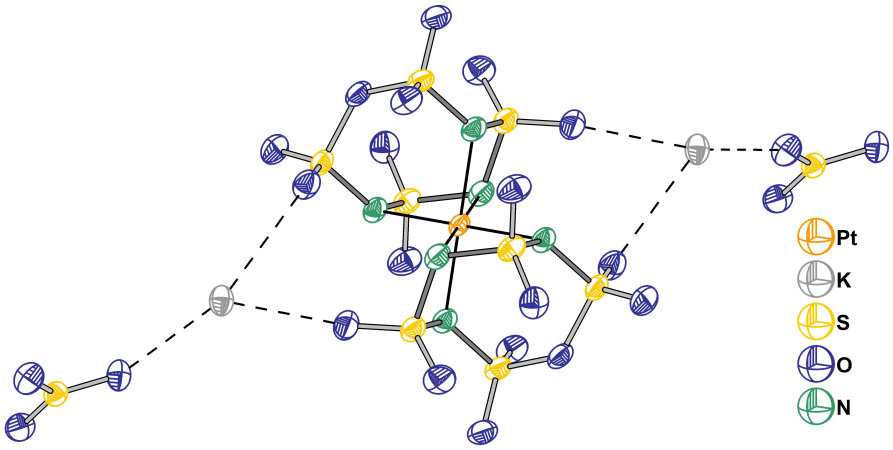

Figure 36: Structure of $K_2[Pt(S_4N_3O_9)_2](SO_3)_2$ with thermal ellipsoids set to a probability level of 70%.

Special about this compound is the created anion $[S_4N_3O_9]^{3-}$, which extends the row of cyclic nitridosulfates. In principle, it has the structure of $[S_4N_2O_{10}]^{2-}$ with one additional nitrogen atom instead of oxygen in the ring, though the conformation is different due to the three-fold coordination by the nitrogen atoms. The anion does not exhibit the aforementioned "boat-boat" conformation since the three nitrogen atoms of the S–N–S bridges are all pointing towards the platinum center. The quality of the SC-XRD dataset provides an accurate determination of bridging nitrogen sites with regard to the chemical occupancy. The S–N distances show variations with observed values in between 162.0(4) pm (S4–N3) and 170.8(5) pm (S2–N2) (for more details see Figure 37, p. 45). Distances for S–O^{br} are 164.1(7) pm and 165.8(7) pm. With around 141 pm the terminal bonds (S–O^t) are shortened. By comparing the angles between the sulfur atoms (S–N–S, S–O–S) it becomes evident that the angle S5–N1–S2 with 118.6(3)° is shorter than the other angles, which are in between 122.2(2)° to 124.3(2)° (see Figure 37). Additionally, the angles between the bridging atoms N3–S5–N1 (93.(2)°) and N2–S2–N1 (92.7(2)°) are much shorter than the opposite angles N3–S4–O34 (104.6(2)°) and N2–S4–O34 (104.9(2)°).

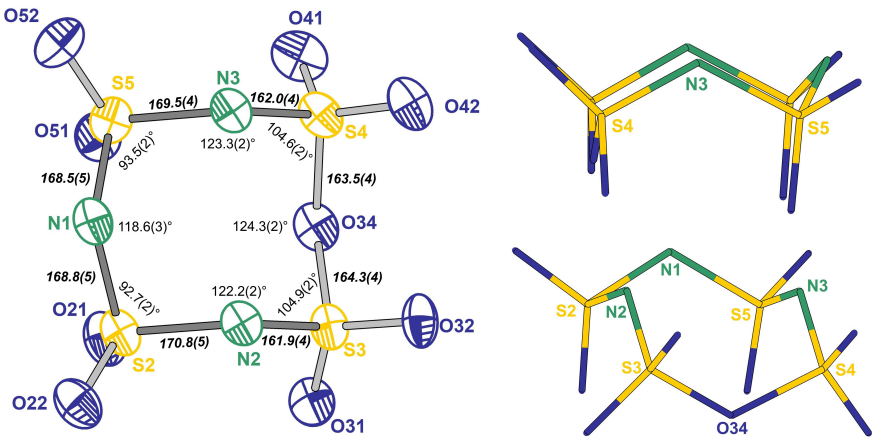

Figure 37: On the left, structure and labeling of $[S_4N_3O_9]^{3-}$ in ellipsoidal representation (probability 70 %) with distances (italics, in pm) and angles (italics) observed in the ring. On the right, wires/sticks representation of the anion is shown along two different perspectives.

Accompanied by the coordination of N1 to platinum, a change of shape of the anion is visible compared to the previously discussed bidentate anions. The three unique interatomic distances between platinum and nitrogen are 208.5(4) pm (Pt1–N1), 205.1(4) pm (Pt1–N2) and 205.2(4) pm (Pt1–N3) (see Figure 38). Comparable platinum complexes with [SO_3N] based ligands are not reported in literature. In platinum(IV) complexes with only N-coordinating ligands distances for Pt–N of 200 pm to 207 pm are observed, eg. in $[Pt(N_3)_4(en)]$[153], $[Pt(NH_3)_2(C_5H_9N_2)_2](ClO_4)_2$[154] and $[Pt(C_{12}H_{30}N_8)](S_2O_6)_2(H_2O)_{2.5}$[155].

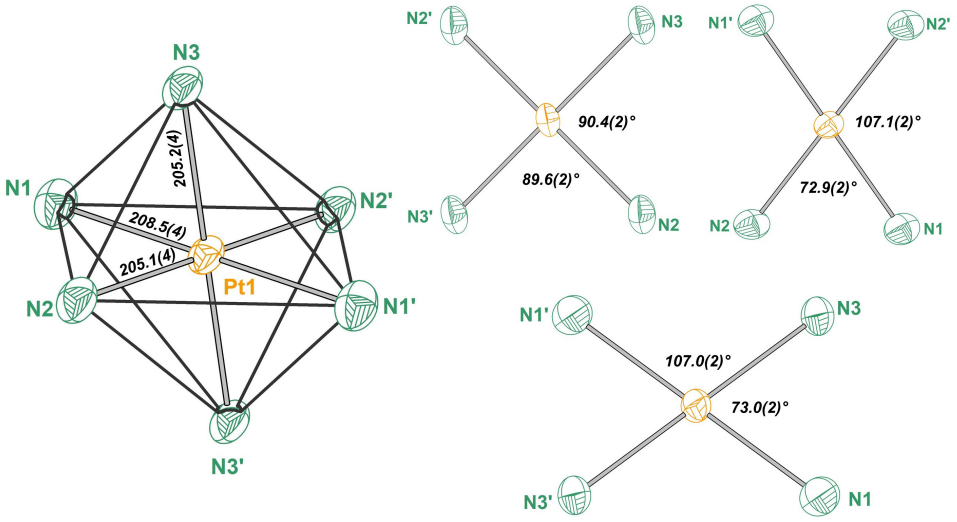

Figure 38: Coordination sphere of platinum in $K_2[Pt(S_4N_3O_9)_2](SO_3)_2$ (left) with atomic distances (italics, in pm) and angles spanned by the coordinating nitrogen atoms (left).

The [PtN_6] polyhedron is highly distorted from the platonic octahedron. By calculations by the program *Polynator* the shape can best be described as a trigonal antiprism with a medium distortion value $\delta = 8.992$ (octahedron (platonic) $\delta = 17.426$).[143] The bond angles spanned by the coordinating nitrogen atoms indicate this distortion, too. The angles deviate significantly from the ideal angle of 90° in the octahedron, ranging from 73.9(2)° to 107.9(2)°. The potassium cation shows interaction to nine oxygen atoms in total deriving from the ligands and SO_3 (see Figure 39, p. 46).

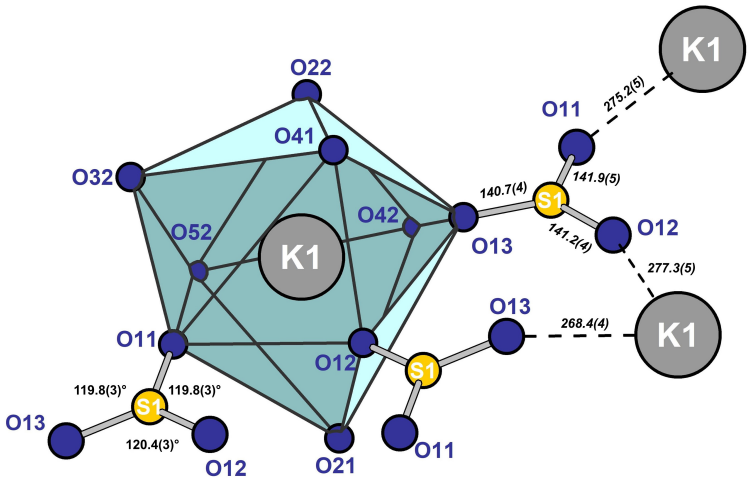

Figure 39: Coordination sphere of the potassium cation and structure of the SO_3 molecules with bond lengths (italics, in pm) and angles observed in $K_2[Pt(S_4N_3O_9)_2](SO_3)_2$.

The shape of the coordination sphere most closely resembles a tricapped trigonal prism with $\delta = 12.157$ (monocapped tetragonal antiprism $\delta = 15.159$). Shortest K–O distance lies between K1 and O13 (from SO_3) with 268.4(4) pm, while longest distance is at 307.7(4) pm between K1 and O42. The sulfur trioxide molecule interacts both as Lewis acid and base, which is evident from its position in the crystal structure (see Figure 40, p. 47). The SO_3 molecules are embedded within the $[S_4N_3O_9]^{3-}$ ligand with a directional but weak interaction of S1 with O51 (270.6 pm) and O31 (259.9 pm). Interaction between K1 and the three oxygen atoms of SO_3 is based on distances of 268.4(4) pm, 272.2(5) pm and 277.3(5) pm. The SO_3 molecule itself shows almost perfect trigonal-planar D_{3h} symmetry in the structure. The angles spanned by oxygen are near to 120° and the S–O distances have values of 140.7(4) pm, 140.7(4) pm and 141.9(5) pm. In $[Au_2Cl_4][B(S_2O_7)_2](SO_3)$[156], for example, the observed S–O distances for the free SO_3 molecule are bit shorter (139.0(5) and 137.4(8) pm) since the oxygen atoms are not participating in coordination.

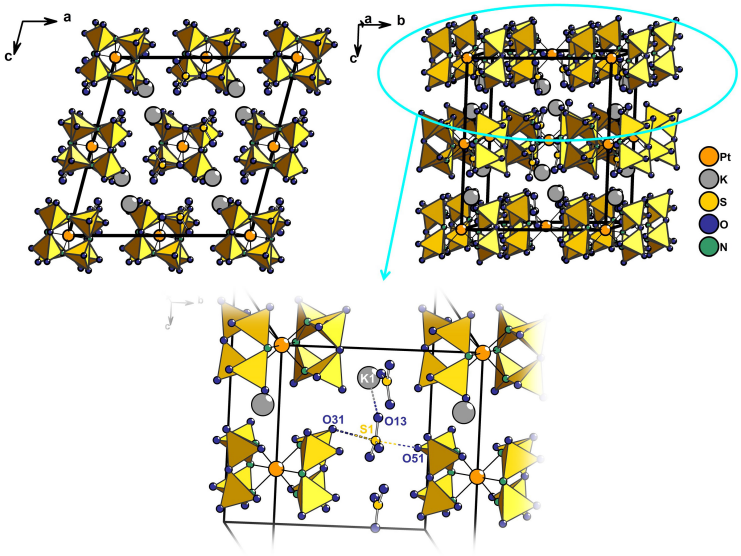

Figure 40: Crystal structure of $K_2[Pt(S_4N_3O_9)_2](SO_3)_2$ along two viewing directions (top) with emphasis on the free SO_3 molecule interaction (bottom).

In the experimental *Raman* spectrum measured on a single crystal, vibrations in the region of 100 cm^{-1} to 1445 cm^{-1} are detected (see Figure 41, p. 48). Based on the single crystal structure, a geometry optimization of the platinate structure, $[Pt(S_4N_3O_9)_2]^{2-}$, was performed on DFT level using the basis set def2-TZVPP (see 7.3.2, p. 129). The optimized structure was used to calculate vibrational frequencies for an approximate assignment of the experimental bands due to the lack of literature-known data. The bands between 1397-1445 cm^{-1} result from antisymmetric stretching vibrations of the $[SO_2]$ moieties, which include the terminal S–O^t bonds. The intense band at 1253 cm^{-1} is based on symmetric stretching from the latter group.

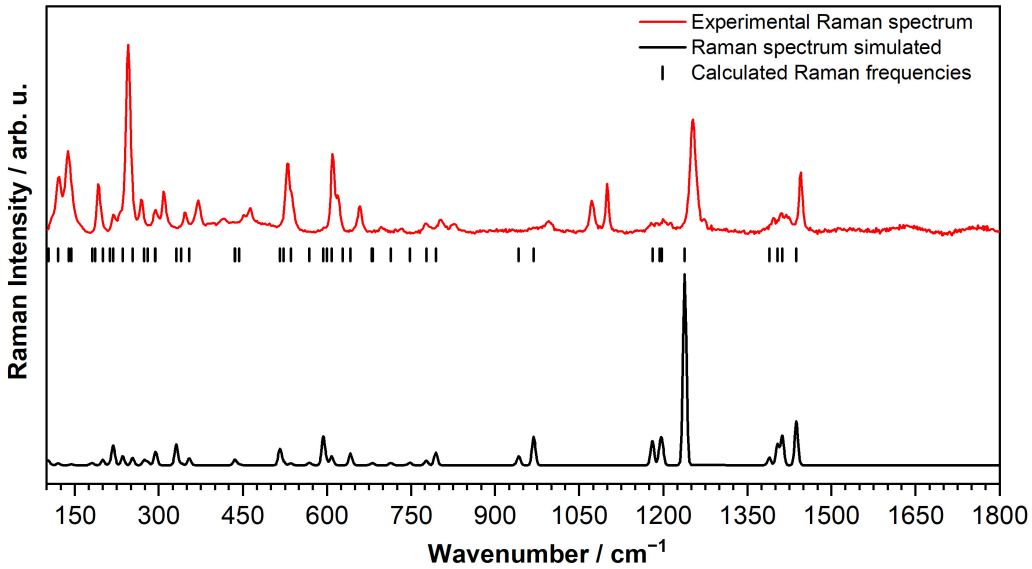

Figure 41: *Raman* spectrum of $K_2[Pt(S_4N_3O_9)_2](SO_3)_2$ recorded on a single crystal with a green laser (λ = 532 nm) at RT.

The small broad band around 1200 cm^{-1} represents the symmetric vibrations of the [SO_2] units but with different stretching phases of the groups. The bands at 1100 cm^{-1} and 1072 cm^{-1} belong to the symmetric stretching vibrations of the free SO_3 molecules.[157] The small band at 996 cm^{-1} occurs from ν_{as}(SN) combined with deformation of [PtN_4]. In between 776 cm^{-1} and 803 cm^{-1} wagging modes of the [PtN_6] unit and at 695 cm^{-1} symmetrical stretching of the [PtN_6] unit can be assigned. The band at 658 cm^{-1} results from symmetric stretching vibration of axial [N–Pt–N] and at 610-620 cm^{-1} symmetric S–N^{br} stretching is present. At lower wavenumbers complex deformation modes of the whole $[Pt(S_4N_3O_9)_2]^{2-}$ fragment occur.

Table 8: Assignment of the *Raman* bands of $K_2[Pt(S_4N_3O_9)_2](SO_3)_2$ with calculated values from a geometry optimization of $[Pt(S_4N_3O_9)_2]^{2-}$.

Assignment	Exp. *Raman* / cm^{-1}	Calcd. / cm^{-1}
$\nu_{as}(SO_2)$	1445	1437
	1410	1432
	1397	1403
$\nu_s(SO_2)$	1253	1273
	1200	1197
ν_s(free SO_3)	1100	-
	1072	
ν_{as}(SN)	996	968
	960	941
ω (PtN)	803	793
	776	776
		748
$\nu_s(PtN_4)$	695	713
$\nu_s(PtN_2)_{axial}$	658	641
ω (SO_2)	610	608
δ [$Pt(S_4N_3O_9)_2$]	530	593
	463	535
	414	435

Assignment	Exp. *Raman* / cm^{-1}	Calcd. / cm^{-1}
	370	353
	347	339
	309	330
	293	294
	269	252
	245	235
	219	218
	192	199
	139	195
	120	143
		120

4.2.8 $[Pt(S_4N_3O_8Cl)_2]$

Wickleder et al. already demonstrated in 2004 that elemental platinum can be oxidized with concentrated sulfuric acid in a sealed glass tube to yield the binary sulfate, $Pt_2(SO_4)_2(HSO_4)_2$.[158] Hence, platinum powder was also considered as a starting material. Accordingly, fine powdered platinum (platinum black), $P_3N_3Cl_6$ and liquid SO_3 were reacted in a sealed glass tube. In this reaction small pale-yellow crystals next to a yellow liquid were obtained. The elemental platinum was not fully converted in this reaction as a black residue remained.

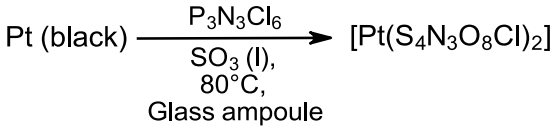

Scheme 15: Preparation of $[Pt(S_4N_3O_8Cl)_2]$ in a solvothermal synthesis with SO_3.

By crystallographic analysis of the single crystals, the structure of a tetravalent platinum complex with the formula $[Pt(S_4N_3O_8Cl)_2]$ was determined (see Figure 42). Coarser-grained platinum powder showed no reaction and even with platinum black, $[Pt(S_4N_3O_8Cl)_2]$ could hardly be reproduced. The particle size thus appears to be decisive for the oxidation of elemental platinum by SO_3.

During the structural solution and refinement, a significant rest electron density of 4.22 $e \cdot Å^{-3}$ remained and could not be reasonably resolved by twinning or disorder. A second crystal showed the same artifact. The rest electron density peak is located in between the $[S_4N_3O_8Cl]^{2-}$ fragments next to O141 with a distance of 153.7 pm. Taking this into account the structure should nevertheless be discussed as the remaining crystal parameters indicate a high quality of the dataset.
The complex crystallizes in the monoclinic space group $P2_1/n$ with four formula units per unit cell (for more details see Table 9). The cell contains one unique Pt atom (Pt1) and two unique $[S_4N_3O_8Cl]^{2-}$ ligands.

Table 9: Selected crystallographic data of $[Pt(S_4N_3O_8Cl)_2]$.

$[Pt(S_4N_3O_8Cl)_2]$	
Crystal System	Monoclinic
Space Group	$P2_1/n$
a / pm	745.78(4)
b / pm	1380.84(6)
c / pm	1912.37(9)
β / °	101.133(2)
V / nm^3	1.9323(2)
Z	4
R_1 (all data); wR_2 (all data)	0.0250; 0.0606
GooF	1.089

$[S_4N_3O_8Cl]^{2-}$ exhibits the previously discussed backbone of an eight-membered ring with four sulfur atoms connected by three bridging nitrogen and one bridging oxygen atom (Figure 42, p. 51).

Conditioned by the presence of chlorine in the anion, three bridging nitrogen atoms are needed to create a double negative charge, if a Pt^{4+} center is considered. The bridging atoms coordinating to the Pt center in both anions could be assigned to nitrogen, although it was not possible to differentiate precisely between oxygen and nitrogen for the other bridging atoms.

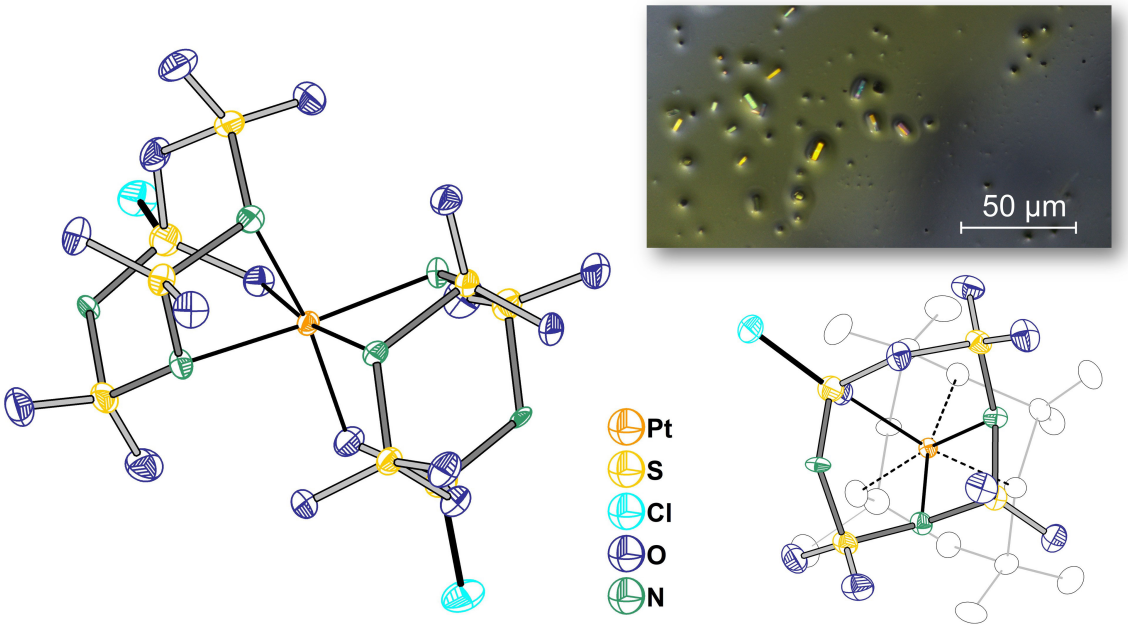

Figure 42: Structure from two viewing perspectives and microscope image of the single crystals of $[Pt(S_4N_3O_8Cl)_2]$. The thermal ellipsoids are set at 70% probability.

The special feature of this anion is the inserted chlorine atom bonded to sulfur. Chlorine species from a $SO_3/P_3N_3Cl_6$ mixture was already observed in form of the chlorosulfonic anhydride, $S_2O_5Cl_2$, in $[Au_2Cl_2(S_4N_2O_{10})_2](S_2O_5Cl_2)]$.[151] Hence, it seems plausible that a $[SO_2Cl]$ fragment took part in the formation of the anion. Formally, it represents the corresponding base of the condensation of one chlorosulfonic acid ($ClSO_3H$) and three amidosulfonic acid (H_3NSO_3) molecules according to "$H_2S_4N_3O_8Cl$".

Particularly striking are the sulfur–chlorine distances with values of 192.7(1) pm for S1–Cl1 and 191.6(2) pm for S6–Cl2 (Figure 43, p. 52). In the crystal structure of $S_2O_5Cl_2$ the S–Cl bonds take up values of around 196-197 pm, while within the anti-conformer, observed in $[Au_2Cl_2(S_4N_2O_{10})_2](S_2O_5Cl_2)]$, a distance of 196.3(2) pm was found.[151,159] A literature-known and comparable molecule is the imido-*bis*-sulfonate ($[HN(SO_3)_2]^-$) congener, the imido-*bis*-sulfuric acid chloride, $HN(SO_2Cl)_2$.[160-161] Therein the found distance for S−Cl are 198.8(1) pm and 198.94(9) pm. Concerning the terminal S–O^t bond lengths, distances for S1–O11 and S6–O61 are enlarged with 150.4(2) pm and 150.5(2) pm compared to the other terminal S–O^t bonds, which are in the range close to 140 pm.

The longer distance is due to the coordination to the platinum center. In the eight-membered ring, a variation within 156.6(3) pm to 171.6(3) pm for the bridging bond lengths is observed. The distances

between sulfur atoms to the coordinating nitrogen atoms (N2, N3, N4 and N5) are also larger than the opposite bonds involving N1, O141, N6 and O561.

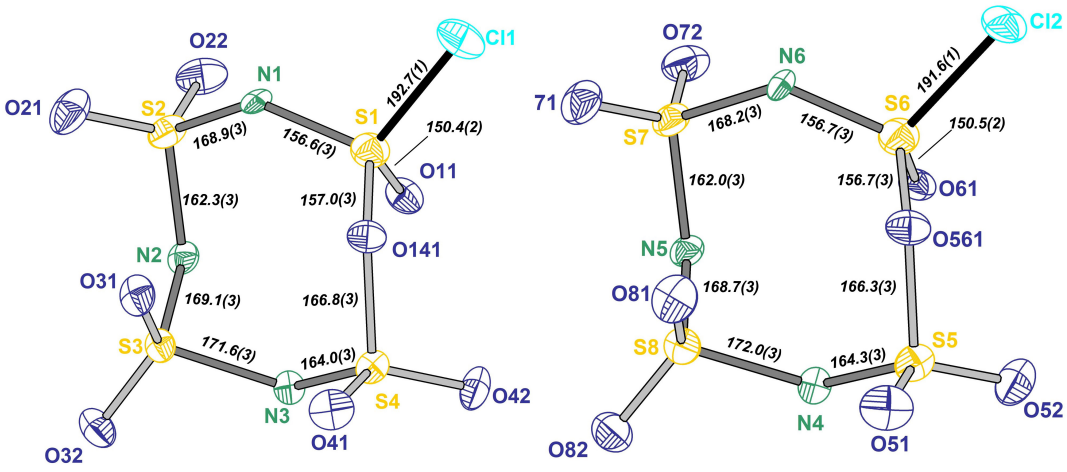

Figure 43: Structure and labeling of the two crystallographically distinguishable $[S_4N_3O_8Cl]^{2-}$ anions with selected bond lengths (italics, in pm). The thermal ellipsoids are set to a probability of 70%.

The bonds next to the chlorine bonded sulfur atom S1–N1 and S6−N6 have values of 156.6(3) pm and 156.7(3) pm, while in $HN(SO_2Cl)_2$ S–N distances of 164.9(2) pm and 163.9(2) pm are reported.[160] However, it must be noted that the bonding situation is very different due to the presence of the proton and the lack of coordination. The rings are even more distorted than in $[Pt(S_4N_3O_9)_2]^{2-}$. Angles between the sulfur atoms are 119.4(2)-125.2(2)° and between the bridging atoms (N^{br}–S–N^{br}, O^{br}–S–N^{br}) 89.5(1)-105.8(2)°. The smallest angles are observed for N5–S8–N4 (89.5(1)°) and N2–S3–N3 (89.9(1)°).

Comparable to $[Pt(S_4N_3O_9)_2]^{2-}$ the Pt1 center is surrounded in an octahedral manner by two bridging nitrogen atoms (N2, N3, N4 and N5) and one terminal oxygen atom (O11, O61) of each anion (see Figure 44, p. 52). The atomic distances are 201.7(3) pm up to 207.3(2) pm, with Pt1–O11 being the longest and Pt1–N3 the shortest distance.

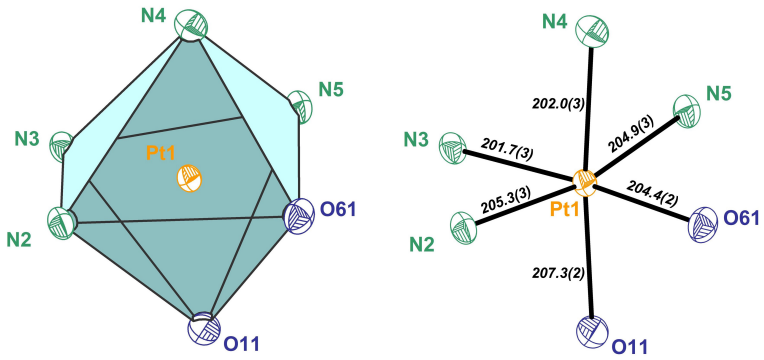

Figure 44: $[PtN_4O_2]$ coordination polyhedron (left) and observed distances (in pm) within coordination (right).

The distortion is emphasized by the angles between the opposite atoms with observed values of 168.0(1)° (N5–Pt1–N2), 171.0(1)° (N4–Pt1–O11) and 170.5(1)° (N3–Pt1–O61). According to an

analysis with *Polynator*[143] the octahedron can be described as a twisted trigonal prism (δ = 5.770) rather than trigonal antiprism (δ = 9.039) (octahedron platonic: δ = 12.512).

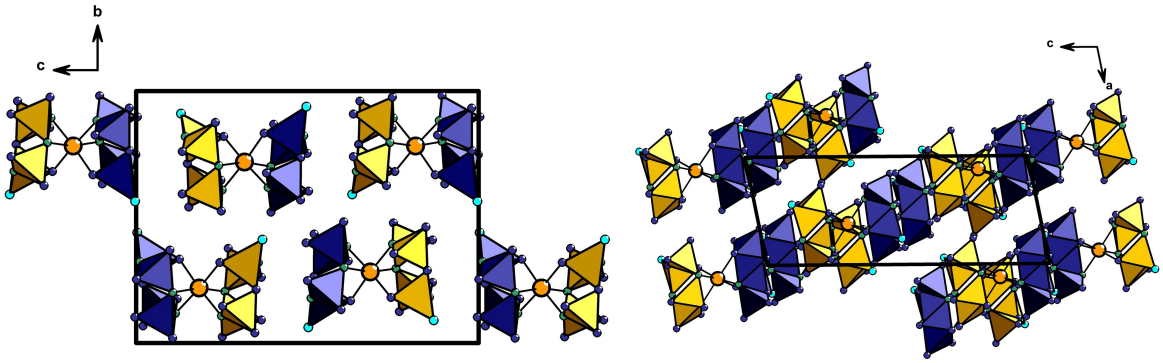

Figure 45: Unit cell along the crystallographic axes *a* (left) and *b* (right). Both crystallographically distinguishable $[S_4N_3O_8Cl]^{2-}$ anions are illustrated with tetrahedrons in different colors to provide a better perspective.

In the crystal structure, the platinum complexes are stacked in layers with no apparent interaction between the complexes (see Figure 45). From one single crystal, a *Raman* spectrum was recorded (see Figure 84, p. 124). Vibrations are observed from 116 cm^{-1} to 1471 cm^{-1}. A precise allocation of the complex *Raman* modes proves to be difficult due to a lack of literature and theoretical data. A geometry optimization by DFT gas phase calculation of the complex failed, since one bridging S–O^{br} bond was always split up during the process. The bands in between 1200 cm^{-1} and 1500 cm^{-1} can be attributed to symmetric and antisymmetric stretching of the $[SO_2]$ units.

4.2.9 Chapter Summary

In SO_3 based solvothermal synthesis between metal salts and nitrogen-containing reagents, such as $P_3N_3Cl_6$ and $(S_3N_2Cl)Cl$, compounds with various novel nitrogenous sulfates as anions were successfully synthesized and structurally characterized. Their ring-shape conformation and chemical composition is a striking and common feature in these compounds. The anion $[S_3NO_8]^-$, characterized as salts of Ag^+ and Rb^+ is structurally related to γ-SO_3 (S_3O_9), trisulfimide ($[S_3N_3O_6]^{3-}$) and trimetaphosphates ($[P_3O_9]^{3-}$). With Na^+ the anion $[S_4NO_{11}]^-$ was yielded, which exhibits one more SO_3 in the ring and corresponds to the Se_4O_{12} structure. Substitution of one bridging oxygen atom in $[S_4NO_{11}]^-$ with a nitrogen atom leads to the anion $[S_4N_2O_{10}]^{2-}$, which was characterized in various Au^{3+} complexes. Even more nitrogen-rich are the anions $[S_4N_3O_9]^{3-}$ and $[S_4N_3O_8Cl]^{2-}$, successfully examined within octahedral Pt^{4+} complexes, starting from $K_2[PtCl_6]$ and Pt^0, respectively. In case of $[S_4N_3O_8Cl]^{2-}$ chlorine was inserted into the scaffold. As a further chlorine-containing compound the chlorosulfonic anhydride ($S_2O_5Cl_2$) was crystallized in the compound $[Au_2Cl_2(S_4N_2O_{10})_2](S_2O_5Cl_2)$. Furthermore, it was found that $(S_3N_2Cl)Cl$ can also be used as a nitrogen source for the synthesis of $[S_4N_2O_{10}]^{2-}$.

Finally, a phosphorus compound, generated by the reaction system, could be analyzed. The phosphorus oxychloride, $P_2O_3Cl_4$, was co-crystallized with molecular $S_6N_4O_{13}H_2$, both interacting via hydrogen bonding. Although $P_2O_3Cl_4$ is a long-known compound, it is structurally examined in this work for the first time. The cage-shaped $S_6N_4O_{13}H_2$ represents a structural derivative of $S_6N_2O_{15}$ with two amino groups [NH] in the bridges.

Conceptually, it has already been emphasized in the publication of $Au_2Br_2(S_4N_2O_{10})_2]$ and $[Au_2Cl_2(S_4N_2O_{10})_2](S_2O_5Cl_2)$ that the cyclic anions can be regarded as condensation products of sulfuric acid and amidosulfonic acid. $[S_4N_2O_{10}]^{2-}$ is the corresponding base of the condensation of two H_2SO_4 and two NH_3SO_3 molecules. In comparison, $[S_4NO_{11}]^-$ can formally be derived as the corresponding anion of the condensation product of three H_2SO_4 and one NH_3SO_3 molecules. This formal concept with different ratios of H_2SO_4/NH_3SO_3 for known monomeric and cyclic $[NSO_3]$ structures is illustrated in Table 10 (p. 55). It should be noted, however, that none of these structures have yet been produced by means of such condensation reaction and the formal acids are most likely unstable.

Table 10: Overview of literature-known and here in this work presented [NSO_3] based monomeric and cyclic structures, which are considered as condensation products between H_2SO_4 and NH_3SO_3 and between HSO_3Cl and NH_3SO_3.

Ratio H_2SO_4/ NH_3SO_3	Sum	$-H_2O$	Chemical formula of the acid	Anion or Molecule
1:1	$H_5S_2NO_7$	1	$H_3S_2NO_6$	**$[N(SO_3)_2]^{3-}$**[85] 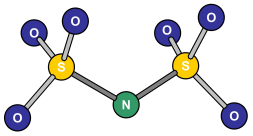
2:2	$H_{10}S_4N_2O_{14}$	4	$H_2S_4N_2O_{10}$	**$[S_4N_2O_{10}]^{2-}$** 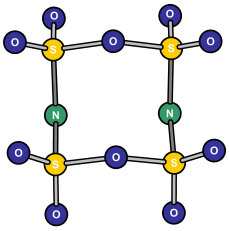
3:3	$H_{15}S_6N_3O_{21}$	7	$HS_6N_3O_{14}$	**$[S_6N_3O_{14}]^{-}$**[26] 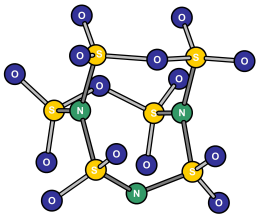
2:4	$H_{16}S_6N_4O_{20}$	7	$H_2S_6N_4O_{13}$	**$H_2S_6N_4O_{13}$** 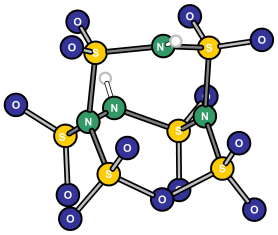
2:1	$H_7S_3NO_{11}$	2	$H_3S_3NO_9$	**$[N(SO_3)_3]^{3-}$**[79] 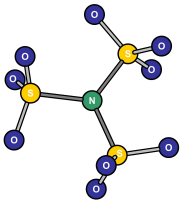

Ratio H_2SO_4/ NH_3SO_3	Sum	$-H_2O$	Chemical formula of the acid	Anion or Molecule
2:1	$H_7S_3NO_{11}$	3	HS_3NO_8	**$[S_3NO_8]^-$** 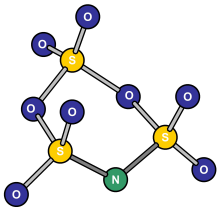
4:2	$H_{14}S_6N_2O_{22}$	7	$S_6N_2O_{15}$	**$S_6N_2O_{15}$**[25] 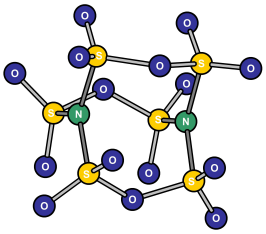
3:1	$H_9S_4NO_{15}$	4	HS_4NO_{11}	**$[S_4NO_{11}]^-$** 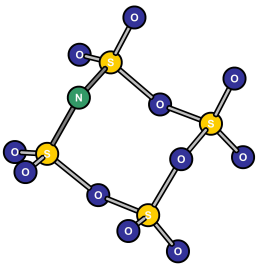
0:3	$H_9S_3N_3O_9$	3	$H_3S_3N_3O_6$	**$[S_3N_3O_6]^{3-}$**[91] 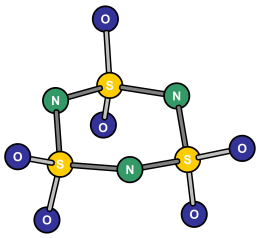
1:3	$H_{11}S_4N_3O_{13}$	4	$H_3S_4N_3O_9$	**$[S_4N_3O_9]^{3-}$** 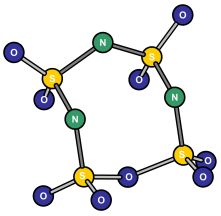

Absolute ratio HSO_3Cl/ NH_3SO_3	**Sum**	**$-H_2O$**	**Chemical formula of the acid**	**Anion or Molecule**
1:3	$H_{10}S_4N_3O_{12}Cl$	4	$H_2S_4N_3O_8Cl$	**$[S_4N_3O_8Cl]^{2-}$** 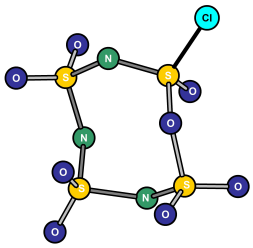

4.3 Hydrazine Sulfonates

4.3.1 Publication 2

Hydrazine Sulfonic Acid, $NH_3NH(SO_3)$, the Bigger Sibling of Sulfamic Acid

Tobias Rennebaum, David van Gerven, Sean S. Sebastian, and Mathias S. Wickleder

Chem. Eur. J. **2024**, *30*, e202302526, 1-4.

In the following publication, the zwitterionic hydrazine sulfonic acid and its barium salt are introduced. The synthesis of both compounds starting from $N_2H_4{\cdot}H_2O$ and $Py{\cdot}SO_3$ is described and a detailed analysis by X-ray crystallography, *Raman* spectroscopy, thermal methods (TG/DSC) and theoretical calculations is presented. The supplementary information contains the detailed synthesis procedures and analytical data (see 8.2, p. 181).

The principal author Tobias Rennebaum carried out all syntheses, evaluated the analytical data and co-wrote the manuscript. Dr. David van Gerven performed the quantum mechanical calculations. Sean S. Sebastian did the *Hirshfeld* surface analysis. Prof. Dr. Wickleder is the supervisor of this work, corresponding author of this publication and co-authored and proofread the manuscript.

Thankfully acknowledged are the single crystal and powder XRD measurements by Silke Kremer (University of Cologne) and Daniel Moog (University of Cologne), introduction to *Raman* microscopy by Christoph Lenting (University of Cologne) and laboratory support by Daniel Streup (University of Cologne).

Chemistry–A European Journal
Research Article
doi.org/10.1002/chem.202302526
Chemistry Europe
European Chemical Societies Publishing
www.chemeurj.org

Hydrazine Sulfonic Acid, $NH_3NH(SO_3)$, the Bigger Sibling of Sulfamic Acid

Tobias Rennebaum,[a] David van Gerven,[a] Sean S. Sebastian,[a] and Mathias S. Wickleder*[a]

The reaction of hydrazine hydrate, $N_2H_4 \cdot H_2O$, and SO_3 leads to hydrazine sulfonic acid ($Pca2_1$, $a = 849.59(4)$ pm, $b = 482.18(2)$ pm, $c = 832.17(4)$ pm). Structure elucidation reveals the zwitter-anionic nature of the compound according to $NH_3NH(SO_3)$. With the barium salt $Ba[NH_2NH(SO_3)]_2(H_2O)$, a first salt of hydrazine sulfonic acid has been prepared ($P\bar{1}$, $a = 489.75(5)$ pm, $b = 737.52(7)$ pm, $c = 1317.4(1)$ pm, $\alpha = 88.238(4)°$, $\beta = 84.761(4)°$, $\gamma = 79.701(4)°$). The compounds were characterized by vibrational spectroscopy, DFT calculations and thermal analyses.

Introduction

The best-investigated nitrogen derivative of sulfuric acid is the so-called sulfamic acid, NH_2SO_3H.[1–3] The compound can be either seen as the amide of sulfuric acid or as the simplest sulfonic acid of ammonia, NH_3. Formally, it derives from the latter by inserting an SO_3 molecule in an N–H bond. Following this idea, further sulfonic acids can be derived from NH_3, namely imido-bis-sulfuric acid, $NH(SO_3H)_2$ and nitrido-tris-sulfuric acid, $N(SO_3H)_3$. These compounds are not known as neat acids but a very limited number of their salts has been reported.[4–8] Furthermore, we recently presented the anhydride of $N(SO_3H)_3$, that is, the cage-shaped molecule $S_6N_2O_{15}$.[9] In principle, the idea of the derivatisation of NH_3 under formation of sulfonic acids should also hold for the ammonia congener hydrazine, N_2H_4. Indeed, sulfonic acid derivatives of hydrazine were first reported almost 100 years ago,[10–11] and again in more detail in the 1950s.[12] However, up to now, neither one of these acids nor one of their salts have been structurally characterized. In course of our investigations on nitrogen-based derivatives of sulfuric acid we became also interested in these scarcely described hydrazine species. This work is not only inspired by our conviction that there is fundamental importance on the investigation of these compounds, but also by the awareness that new anions will lead to compounds with hitherto unknown properties.

According to the above-mentioned early reports, a suitable starting material for the preparation of hydrazine sulfonic acid seemed to be the hydrazine hydrate $N_2H_4 \cdot H_2O$, which is a commercial compound. The handling of this hydrate is more convenient compared to the use of neat hydrazine. However, in reactions with SO_3 the presence of H_2O in the reaction mixture might be a problem due to the formation of the very stable hydrazinium ion, $[N_2H_6]^{2+}$. Indeed, our first attempts in the reactions of $N_2H_4 \cdot H_2O$ with SO_3 led usually to hydrazinium polysulfates like $[N_2H_6][S_3O_{10}]$.[13] Finally, we could gain hydrazine sulfonic acid, NH_3NHSO_3, as crystalline material in the reaction of the pyridine complex $py \cdot SO_3$ with $N_2H_4 \cdot H_2O$ in acetic acid.

Results and Discussion

The structure of $NH_3NH(SO_3)$ has been elucidated from X-ray single-crystal data (Table 1). According to the Rietveld refinement of X-ray powder data, the obtained acid is phase pure. The quality of X-ray data allows for the free refinement of the

Table 1. Crystallographic data of the investigated compounds.[a]

Compound	$NH_3NH(SO_3)$	$Ba[NH_2NH(SO_3)]_2(H_2O)$
T [K]	100.0(2)	100.0(2)
crystal system	orthorhombic	triclinic
space group	$Pca2_1$	$P\bar{1}$
a [pm]	849.59(4)	498.75(5)
b [pm]	482.18(2)	737.52(7)
c [pm]	832.17(4)	1317.4(1)
α [°]		88.238(4)
β [°]		84.761(4)
γ [°]		79.701(4)
V [nm^3]	0.34090(3)	0.46618(8)
Z	4	2
Final R indexes	$R_1 = 0.0170$	$R_1 = 0.0331$
(all data)	$wR_2 = 0.0452$	$wR_2 = 0.0649$
R_{int}	0.0523	0.0652
Goof	1.164	1.026
CCDC no.	2225901	2225900

[a] Full data can be found in the Supporting Information.

[a] T. Rennebaum, Dr. D. van Gerven, S. S. Sebastian, Prof. M. S. Wickleder
University of Cologne, Institute of Inorganic Chemistry
Greinstr. 6, 50939 Cologne (Germany)
E-mail: mathias.wickleder@uni-koeln.de
Homepage: www.mwickleder.de

Supporting information for this article is available on the WWW under https://doi.org/10.1002/chem.202302526

hydrogen atoms, revealing that the acid adopts a zwitterionic structure in the solid state (Figure 1 and the Supporting Information). In this respect, the new acid resembles the findings for sulfamic acid, which is also a zwitterionic compound in the solid state. The distance between the nitrogen atoms in the $NH_3NH(SO_3)$ molecule is 145.0(2) pm, which is almost the value as reported for hydrazine, N_2H_4,[14] and its hydrate.[15] The S–N bond has a length of 168.5(2) pm, which is significantly shorter than the respective value of 178.84(8) pm observed for sulfamic acid (see also the Supporting Information).[16] The observed distances are in quite good agreement with the respective theoretical values (see caption of Figure 1). In the solid state, the zwitterionic $NH_3NH(SO_3)$ molecules are arranged in a way that the negatively charged $[SO_3]$ moieties and the positively charges $[NH_3]$ groups are pointing towards each other. Although the main attraction between the molecules is essentially ionic, the formation of hydrogen bonds is likely according to the distances between the N-donor atoms and the oxygen atoms of the $[SO_3]$ groups as acceptors (Figure 2). The respective donor-acceptor distances N–O range from 278.6(2) to 318.4(2) pm, that is, they are only medium strong or even weak.

The presence of hydrogen bonds is also corroborated by a Hirshfeld surface analysis (HS). The concept of HS allows to specify the space occupied by a molecule in a crystal structure by dividing the electron density of the crystal structure into molecular fragments of electron densities. The Hirshfeld surface analysis for the hydrazine sulfonic acid, $NH_3NH(SO_3)$, was conducted with the program-package *CrystalExplorer 21.5*.[17,18] All covalent hydrogen bond lengths were set to normalized values (1.009 Å for N–H) by the program prior to the calculation. The electron densities for each atom type were taken from the basis sets calculated by Koga et al.[19] and the surfaces were generated on the very high setting for the number of used grid points. The dark-red regions around the NH and NH_3 moieties of the $NH_3NH(SO_3)$ molecule and one of the O atom of the $[SO_3]$ group indicate the presence of the N–H···O interaction in crystal packing (Figure 3).

The Raman spectrum of the new acid shows a number of bands that could be assigned based on a frequency analysis by quantum mechanical calculations (see the Supporting Information). Although the observed normal modes are quite complex, some bands are strongly stamped by vibrations of either the $[NH_3NH]$ or the $[SO_3]$ entity of the molecule. Thus, between 500 and 650 cm^{-1} the typical deformation modes of the $[SO_3]$ group occur, while the corresponding stretching vibrations are found between 1200 and 1400 cm^{-1}. The most important modes of the $[NH_3NH]$ moiety occur between 1600 and 1700 cm^{-1} (NH_3 deformation) and above 3000 cm^{-1} (N–H stretching). The latter show the strongest deviations from the calculated values, probably due to the observed hydrogen bonds.

The thermal decomposition of $NH_3NH(SO_3)$ occurs in the small temperature range between 209 and 241 °C, accompanied by two exothermic signals and a mass loss of 58% (see the Supporting Information). According to the observed mass loss it is very likely that $(NH_4)_2SO_4$ is the decomposition product of the acid. Upon further heating $(NH_4)_2SO_4$ decomposes in a broad temperature range leading to H_2SO_4 and NH_3.

The anion of the new acid could be studied in the barium salt $Ba[NH_2NH(SO_3)]_2(H_2O)$ (Table 1), that forms if $Ba(OH)_2$ is added to the above-mentioned reaction mixture for the acid preparation (see supplement). The $[NH_2NH(SO_3)]^-$ anion (Figure 1) shows essentially the same bond length and angles as the acid. The N–N distance is slightly shorter (143.8(5) pm) and the S–O bond lengths are in average slightly enlarged (Figure 1 and Supportimg Information). The Ba^{2+} ions are in tenfold coordination if distances up to 310 pm are included. With a distance of 296.7(4) pm also a nitrogen atom of the $[NH_2NH-$

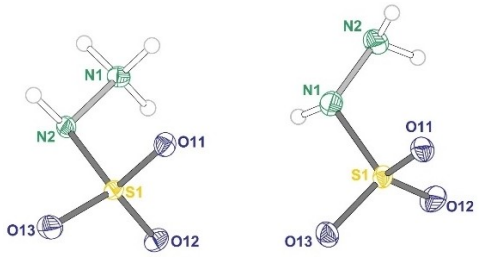

Figure 1. Structure and labelling of the $NH_3NH(SO_3)$ molecule (left) and the $[NH_2NHSO_3]^-$ anion (right). Selected distances [pm] and angles [°] compared to theoretical values (in italics): NH_3–$NHSO_3$ molecule: S1–O11 146.3(2)/*145.9*, S1–O12 144.8(1)/*147.0*, S1–O13 144.6(2)/*143.6*, S1–N2 168.5(2)/*180.9*, N1–N2 145.0(2)/*143.9*, N2–S1–O11 107.42(9)/*103.02*, N2–S1–O12 105.28(8)/*98.90*, N2–S1–O13 101.01(9)/*99.61*, S1–N2–N1 112.2(1)/*99.58*. $[NH_2$–$NHSO_3]^-$ anion: S1–O11 146.3(3)/*146.2*, S1–O12 144.4(3)/*146.1*, S1–O13 146.1(3)/*147.4*, S1–N1 166.4(4)/*164.2*, N1–N2 143.8(5)/*142.4*, N1–S1–O11 105.0(2)/*103.68*, N1–S1–O12 108.9(2)/*105.06*, N2–S1–O13 104.4(2)/*102.21*, S1–N2–N1 113.3(3)/*112.04*; full data are given in the Supporting Information.

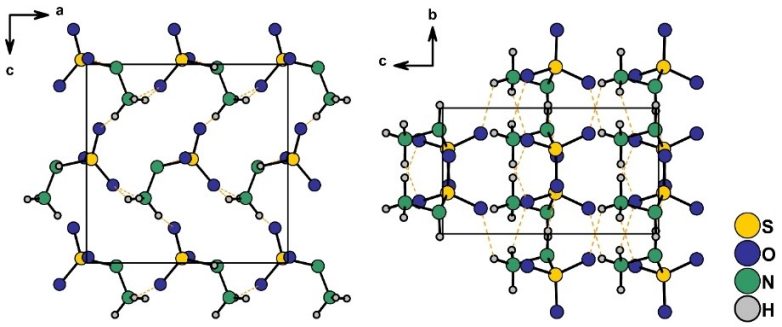

Figure 2. Solid-state structure of $NH_3NH(SO_3)$. The hatched lines emphasize hydrogen bonds with donor-acceptor distances N–O up to 320 pm (see the Supporting Information for details).

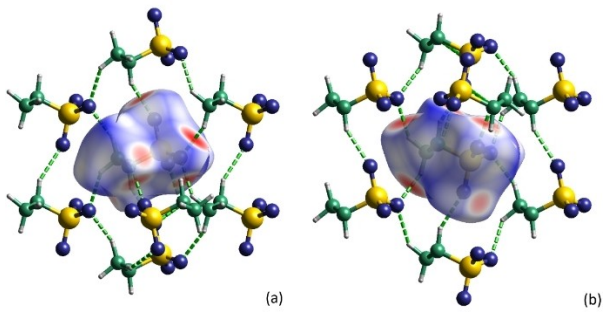

Figure 3. Hirshfeld isosurface around $NH_3NH(SO_3)$ with the d_{norm} mapping in its crystal structure viewed a) along and b) against the crystallographic *c*-axis, with eight contacting $NH_3NH(SO_3)$ units forming hydrogen bonds (green) to the central unit.

$(SO_3)]^-$ anion is part of the coordination sphere. In the crystal structure of $Ba[NH_2NH(SO_3)]_2(H_2O)$, the anions and the crystal water molecules form several hydrogen bonds which are, however, not strong with respect to the donor-acceptor distances between 276.9(5) and 328.8(6) pm (Figure 4).

The thermal analysis of $Ba[NH_2NH(SO_3)]_2(H_2O)$ shows, that after dehydration the decomposition at about 200 °C is strongly exothermic and gives $BaSO_4$ as the residue. According to the observed masses the volatile decomposition products are SO_2, H_2O, and NH_3 (see the Supporting Information). Thus, the decomposition can be described by the equation $Ba[NH_2NH(SO_3)]_2 \rightarrow BaSO_4 + SO_2 + N_2 + 2\ NH_3$.

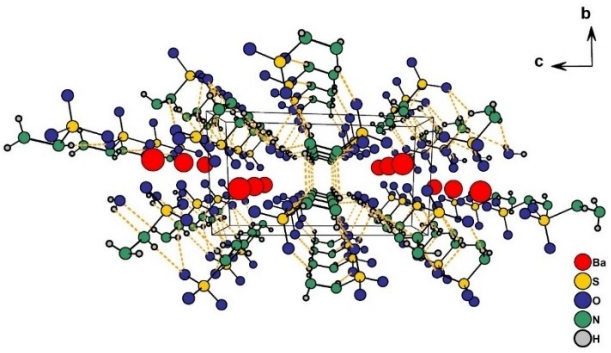

Figure 4. Crystal structure of $Ba[NH_2NH(SO_3)]_2(H_2O)$. The hatched lines emphasize hydrogen bonds with hydrogen-acceptor bonds of up to 280 pm (see the Supporting Information for details).

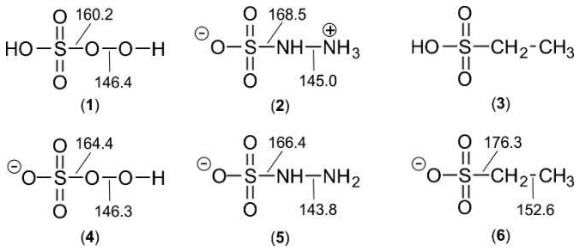

Figure 5. Comparison of the hydrazine sulfonic acid (**2**) and hydrazine monosulfonate (**5**) with their congeners peroxosulfuric acid (**1**),[17] hydrogen peroxosulfate (**4**),[18] and ethane sulfonic acid (**3**), ethane monosulfonate (**6**).[20] Compound **3** is not known as neat acid but only in the form of its salt (**6**).

Hydrazine sulfonic acid is not only the bigger sibling of sulfamic acid, but also the congener of peroxosulfuric acid (Caro's acid) and ethane sulfuric acid (Figure 5). Peroxosulfuric acid is structurally known as neat compound and in form of the two hydrogen peroxosulfates $K[HSO_5](H_2O)$ and $K_5[HSO_5]_2[HSO_4][SO_4]$,[20–22] while ethane sulfonic acid is only reported in form of its salts.[23–25]

According to the description in the introduction that the formation of sulfuric acid derivatives can be seen as insertion reactions of SO_3 into N–H bonds, the above-mentioned acids can be seen as SO_3 insertions into the O–H and C–H bonds of H_2O_2 and C_2H_6, respectively. Thus, for H_2O_2 a second sulfuric acid derivative is thinkable, namely $O_2(SO_3H)_2$, that is, peroxodisulfuric acid, $H_2S_2O_8$.[26] Consequently, ethane can form up to six sulfonic acids, and N_2H_4 should have four sulfuric acid derivatives. In this work, the first of these acids has been comprehensively studied, studies concerning the remaining species are in progress.

Conclusions

In this paper, we have presented the synthesis and the characterization of hydrazine sulfonic acid. The compound has a zwitterionic structure, similar to its lighter congener, sulfamic acid. This access to the new acid gave us the option to prepare its salts, and the barium compound $Ba[NH_2NH(SO_3)]_2(H_2O)$ has been characterized as a first example. Systematically, hydrazine sulfonic acid, $NH_3NH(SO_3)$, fills the gap between peroxosulfuric acid, $HOO(SO_3H)$, and ethane sulfonic acid, $CH_3CH_2(SO_3H)$. Further investigations are being devoted to further compounds of the new acid and their properties.

Experimental Section

The reaction of $N_2H_4 \cdot H_2O$ with the complex $py \cdot SO_3$ (py = pyridine) leads to colourless crystals of hydrazine sulfonic acid, $NH_3NH(SO_3)$. In the presence of $Ba(OH)_2$, the barium salt $Ba[NH_2NH(SO_3)]_2(H_2O)$ is formed under similar conditions. Single-crystal structure determinations have been performed on a Bruker D8 VENTURE KAPPA diffractometer using $Mo_{K\alpha 1}$ radiation (71.073 pm). The intensity data were processed using the programs APEX4, SAINT and SADABS.[27–29] The structure solution was performed using the SHELX suite.[30] Deposition Numbers 2225900 (for $Ba[NH_2NH(SO_3)]_2(H_2O)$) and 2225901 (for $NH_3NH(SO_3)$) contain the supplementary crystallographic data for this paper. These data are provided free of charge by the joint Cambridge Crystallographic Data Centre and Fachinformationszentrum Karlsruhe Access Structures service. X-ray powder data were measured by using a STADI P diffractometer (STOE) and $Mo_{K\alpha}$ radiation. The data were processed using WinXPOW (version 3.12) and TOPAS 5.[31,32] For the thermal analyses the analyser STA 409 (NETZSCH) coupled with a quadrupole mass spectrometer (QMS 421, BALZERS) was used. Raman spectroscopic data were collected with an in*Via* Qotor confocal RAMAN microscope by Renishaw GmbH (Pliezhausen, DE). Quantum mechanical calculations were performed using the ORCA program.[33,34] The Hirshfeld surface analysis for the hydrazine sulfonic acid the program-package CrystalExplorer 21.5. was used.[17–19] Full details of synthesis, characterization and quantum chemical calculations can be found in the Supporting Information.

Acknowledgements

Open Access funding enabled and organized by Projekt DEAL.

Conflict of Interests

The authors declare no conflict of interest.

Data Availability Statement

The data that support the findings of this study are available from the corresponding author upon reasonable request.

Keywords: hydrazines · hydrazine sulfonates · structural analyses · sulfonic acid · thermal analyses

[1] L. F. Audrieth, M. Sveda, H. H. Sisler, M. J. Butler, *Chem. Rev.* **1940**, *26*, 49–94.
[2] R. Sass, *Acta Crystallogr.* **1960**, *13*, 320–324.
[3] B. Singh, M. Shkir, S. AlFaify, A. Kaushal, N. Nasani, I. Bdikin, H. Shoukry, I. S. Yahia, H. Algarni, *J. Mol. Struct.* **2016**, *1119*, 365–372.
[4] P. Barbier, Y. Parent, G. Mairesse, *Acta Crystallogr. Sect. B* **1979**, *35*, 1308–1312.
[5] D. W. J. Cruickshank, D. W. Jones, *Acta Crystallogr.* **1963**, *16*, 877–883.
[6] J. R. Hall, R. A. Johnson, C. H. L. Kennard, G. Smith, B. W. Skelton, A. H. White, *J. Chem. Soc. Dalton Trans.* **1980**, 1091–1097.
[7] H. Sisler, L. F. Audrieth, U. S. Branson, W. C. Johnson, *Inorg. Synth.* **1946**, *2*, 182–183.
[8] H. H. Sisler, L. F. Audrieth, J. A. Lower, W. C. Fernelius, *Inorg. Synth.* **1946**, *2*, 179–181.
[9] D. van Gerven, M. S. Wickleder, *Angew. Chem. Int. Ed.* **2020**, *59*, 17169–17171; *Angew. Chem.* **2020**, *132*, 17320–17323.
[10] E. Konrad, L. Pellens, *Ber. Dtsch. Chem. Ges.* **1926**, *59*, 135–138.
[11] W. Traube, A. Vockerodt, *Ber. Dtsch. Chem. Ges.* **1914**, *47*, 938–944.
[12] A. Meuwsen, H. Tischer, *Z. Anorg. Allg. Chem.* **1958**, *294*, 282–293.
[13] T. Rennebaum, M. Wickleder, unpublished results.
[14] R. L. Collin, W. N. Lipscomb, *Acta Crystallogr.* **1951**, *4*, 10–14.
[15] R. Liminga, I. Olovsson, *Acta Crystallogr.* **1964**, *17*, 1523–1528.
[16] A. F. Cameron, F. D. Duncanson, *Acta Crystallogr. Sect. B* **1976**, *32*, 1563–1564.
[17] P. R. Spackman, M. J. Turner, J. J. McKinnon, S. K. Wolff, D. J. Grimwood, D. Jayatilaka, M. A. Spackman, *J. Appl. Crystallogr.* **2021**, *54*, 1006–1011.
[18] M. A. Spackman, D. Jayatilaka, *CrystEngComm* **2009**, *11*, 19–32.
[19] T. Koga, K. Kanayama, T. Watanabe, T. Imai, A. J. Thakkar, *Theor. Chim. Acta* **2000**, *104*, 411–413.
[20] O. Ermer, C. Röbke, *Helv. Chim. Acta* **2003**, *86*, 2908–2913.
[21] W. Frank, B. Bertsch-Frank, *Angew. Chem. Int. Ed.* **1992**, *31*, 436–437.
[22] E. O. Schlemper, R. C. Thompson, C. K. Fair, F. K. Ross, E. H. Appelman, L. J. Basile, *Acta Crystallogr. Sect. C* **1984**, *40*, 1781–1785.
[23] K. Matuszek, R. Vijayaraghavan, C. M. Forsyth, S. Mahadevan, M. Kar, D. R. MacFarlane, *ChemSusChem* **2020**, *13*, 159–164.
[24] R. Shankar, R. Singh, S. Mendiratta, A. K. Jassal, G. Kociok-Köhn, K. C. Molloy, *Eur. J. Inorg. Chem.* **2017**, *2017*, 2081–2087.
[25] R. Singh, G. Kociok-Köhn, A. Kaur Jassal, L. Singh, *Polyhedron* **2020**, *175*, 114200.
[26] T. E. Gilewski, P. J. Leszczynski, A. Budzianowski, Z. Mazej, A. Grzelak, T. Jaron, W. Grochala, *Dalton Trans.* **2016**, *45*, 18202–18207.
[27] Bruker, *Apex4*. Bruker AXS Inc., Madison, Wisconsin **2021**.
[28] Bruker, *SAINT V8.40B*, BrukerAXS Inc., Madison, Wisconsin 2019.
[29] L. Krause, R. Herbst-Irmer, G. M. Sheldrick, D. Stalke, *J. Appl. Crystallogr.* **2015**, *48*, 3–10.
[30] G. M. Sheldrick, *Acta Crystallogr. Sect. A* **2015**, *71*, 3–8.
[31] *WinXPOW*, Stoe & Cie, Darmstadt **2007**.
[32] A. A. Coelho, *J. Appl. Crystallogr.* **2018**, *51*, 210–218.
[33] F. Neese, F. Wennmohs, U. Becker, C. Riplinger, *J. Chem. Phys.* **2020**, *152*, 224108.
[34] T. H. Dunning Jr., *J. Chem. Phys.* **1989**, *90*, 1007–1023.

Manuscript received: September 21, 2023
Accepted manuscript online: October 3, 2023
Version of record online: November 10, 2023

4.3.2 Publication 3

N_2H_4 Derived Sulfonic Acids: Hydrazine Disulfonate, $[(SO_3)HNNH(SO_3)]^{2-}$, and Hydrazine *Iso*-disulfonate, $[H_2NN(SO_3)_2]^{2-}$

Tobias Rennebaum, David van Gerven, Felix C. H. Herwede, and Mathias S. Wickleder

Chem. Eur. J. **2024**, *30*, e202402337, 1-8.

The following publication reports comprehensively on the preparation and analysis of the hydrazine disulfonate $[(SO_3)HNNH(SO_3)]^{2-}$ and hydrazine iso-disulfonate $[H_2NN(SO_3)_2]^{2-}$ in various compounds. The different approaches to the synthesis of the two isomeric anions are explained and the obtained compounds are analyzed by single crystal and powder X-ray diffraction. On this basis, an in-depth structural comparison of the anions is carried out. In addition, the thermal behavior of the salts is presented and *Raman* spectroscopic properties are characterized with the assistance of DFT calculations. The supplementary information contains the detailed synthesis procedures and analytical data (see 8.3, p. 200)

The principal author Tobias Rennebaum carried out all syntheses, evaluated the analytical data and co-wrote the manuscript. Dr. David van Gerven performed the quantum mechanical calculations. Felix C. H. Herwede helped with the synthesis of the salts and prepared $Ba[H_2NN(SO_3)_2](H_2O)_2$ in a phase-pure state. Prof. Dr. Mathias S. Wickleder is the supervisor of this work, corresponding author of the publication and co-authored and proofread the manuscript.
Thankfully acknowledged are the single crystal and powder XRD measurements by Silke Kremer (University of Cologne) and Daniel Moog (University of Cologne), introduction to *Raman* microscopy by Christoph Lenting (University of Cologne) and laboratory support by Krunal Kanani (University of Cologne).

Chemistry–A European Journal
Research Article
doi.org/10.1002/chem.202402337
Chemistry Europe
European Chemical Societies Publishing
www.chemeurj.org

N_2H_4 Derived Sulfonic Acids: Hydrazine Disulfonate, $[(SO_3)HNNH(SO_3)]^{2-}$, and Hydrazine *Iso*-disulfonate, $[H_2NN(SO_3)_2]^{2-}$

Tobias Rennebaum,[a] David van Gerven,[a] Felix C. H. Herwede,[a] and Mathias S. Wickleder*[a]

The reaction of hydrazinium sulfate and chlorosulfonic acid in pyridine leads to the pyridinium salt of the hydrazine disulfonate anion, $[(SO_3)HNNH(SO_3)]^{2-}$. The salt is the starting material for the preparation of further hydrazine disulfonates, for example of alkaline metals and barium. In all compounds, the $[(SO_3)HNNH(SO_3)]^{2-}$ anion adopts the *gauche* conformation. The conformer is chiral but all of the investigated compounds crystallize as racemates. The disulfonate anion can occur in another constitution with the two sulfonate groups attached to only one nitrogen atom. This so-called hydrazine *iso*-disulfonate, $[H_2NN(SO_3)_2]^{2-}$, has been prepared through a substitution reaction between potassium imidodisulfonate, $K_2[HN(SO_3)_2]$, and hydroxylamine-*O*-sulfonic acid, H_2NOSO_3H. The hydrazine *iso*-disulfonate anion has been crystallized as potassium and barium compound, respectively. The compounds were characterized by XRD, vibrational spectroscopy, DFT calculations and thermal analyses.

Introduction

Nitrogen-containing derivatives of sulfuric acid are an important class of compounds for both fundamental research and industrial application. For example, amidosulfonic acid, NH_2SO_3H (no. **2** in Figure 1), is a well-known and frequently used chemical descaler.[1–3] The acid can be considered as the amide of sulfuric acid or as the simplest sulfonic acid of ammonia, NH_3 (**1**).[4–6] It derives from the latter by inserting an SO_3 molecule into an N–H bond. Recently, we could show that also in hydrazine, N_2H_4 (**5**), SO_3 can be inserted in an N–H bond by the reaction of $N_2H_4{\cdot}H_2O$ with py·SO_3 (py = pyridine) leading to hydrazine sulfonic acid, NH_2NHSO_3H (**6**).[7] In analogy to NH_2SO_3H, also NH_2NHSO_3H is a zwitterionic molecule, what explains that both acids are solids under ambient condition. In NH_2SO_3H, further insertion of SO_3 into N–H bonds is thinkable leading to imido-*bis*-sulfuric acid, $NH(SO_3H)_2$ (**3**), and nitrido-*tris*-sulfuric acid, $N(SO_3H)_3$ (**4**), as NH_3 derivatives. They are not known as neat acids, but a very limited number of their salts have been reported.[8–14] Furthermore, we have characterized the anhydride of $N(SO_3H)_3$, namely the cage-shaped molecule $S_6N_2O_{15}$.[15] In analogy to the successive sulfonation of NH_2SO_3H also NH_2NHSO_3H can be further sulfonated leading to di- (**7**), tri- (**9**), and tetrasulfonic acid (**10**) of hydrazine (Figure 1). It is worthwhile to mention that hydrazine disulfonic acid exhibits two different isomers, the symmetric species $(HO_3S)HNNH(SO_3H)$ (**7**), and the so-called *iso*-disulfonic acid, $H_2NN(SO_3H)_2$ (**8**). The name has been introduced by *Meuwsen* and *Tischer* who reported on hydrazine sulfonic acids in 1958.[16] Their work was inspired by early findings of *Traube* et al. and *Konrad* et al. published already in 1914 and 1926, respectively.[17,18] With respect on the importance of hydrazine on one hand, and on sulfuric acid derivatives on the other hand, it is remarkable that no investigations have been conducted to investigate these text book examples since more than 65 years. We here present a comprehensive study on the two isomers of hydrazine disulfonic acid, including their thermal behavior, vibrational spectroscopy, and quantum mechanical studies.

Results and Discussion

Syntheses

In a slight deviation of the literature procedure, the anion of the acid **7** has been synthesized by the reaction of chlorosulfonic acid, $ClSO_3H$, and hydrazinium sulfate, $(N_2H_6)(SO_4)$, in pyridine as the pyridinium salt $(C_5H_6N)_2[(SO_3)HNNH(SO_3)]$[16]:

$$(N_2H_6)SO_4 + 2\,ClSO_3H + 4\,C_5H_5N \xrightarrow[\text{1. 0 °C, 2h}\ \text{2. 80 °C, 30 min}]{\text{Pyridine}} (C_5H_6N)_2[(SO_3)HNNH(SO_3)] + 2\,HCl + (C_5H_6N)_2SO_4$$

Subsequently, the pyridinium cation could be exchanged by the alkaline metal ions K^+, Rb^+, and Cs^+, as well as by Ba^{2+}. All compounds were obtained as crystalline materials which are single-phase according to their powder X-ray diffraction patterns and elemental analyses (cf. supporting information). Important crystallographic data and the yields are collected in Table 1.

[a] T. Rennebaum, D. v. Gerven, F. C. H. Herwede, M. S. Wickleder
University of Cologne, Institute of Inorganic Chemistry, Greinstr. 6, 50939 Cologne, Germany
E-mail: mathias.wickleder@uni-koeln.de

Supporting information for this article is available on the WWW under https://doi.org/10.1002/chem.202402337

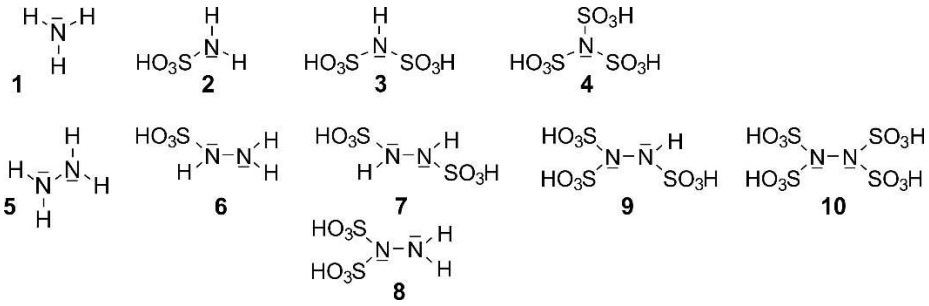

Figure 1. Sulfonic acids of ammonia, NH_3 (**1**), and hydrazine, N_2H_4 (**5**). Formally, the acids are formed by insertion of SO_3 into the N–H bonds of the two molecules. It must be noted that disulfonic acid of hydrazine should exist in two different isomers, **7** and **8**. The anions of these acids are discussed in this work.

Table 1. Selected crystallographic data and yields of the hydrazine disulfonates, $(C_5H_6N)_2[(SO_3)HNNH(SO_3)]$ (**I**), $K_2[(SO_3)HNNH(SO_3)](H_2O)$ (**II**), $Rb_2[(SO_3)HNNH(SO_3)](H_2O)$ (**III**), $Cs_2[(SO_3)HNNH(SO_3)](H_2O)$ (**IV**), $(NH_4)_2[(SO_3)HNNH(SO_3)](H_2O)$ (**V**) and $Ba[(SO_3)HNNH(SO_3)](H_2O)_2$ (**VI**).

Compound	I	II	III	IV	V	VI
T/K	100.0(2)	100.0(2)	100.0(2)	100.0(2)	101.0	101.0
Crystal System	*orthorhombic*	*orthorhombic*	*orthorhombic*	*orthorhombic*	*orthorhombic*	*orthorhombic*
Space group	*Pccn*	$Pna2_1$	*Pnma*	$Cmc2_1$	*Pnma*	*Ama*2
a/pm	1844.7(2)	2060.81(6)	2134.3(1)	590.97(3)	2105.4(1)	1130.63(5)
b/pm	871.01(8)	714.36(2)	580.23(3)	2225.2(1)	579.26(2)	1570.83(8)
c/pm	917.71(6)	570.43(1)	734.57(4)	764.64(4)	739.74(3)	467.45(2)
V/nm^3	1.4745(2)	0.83976(4)	0.90966(9)	1.00554(9)	0.90216(6)	0.83020(7)
Z	4	4	4	4	4	4
Final R indexes [all data]	$R_1 = 0.0492$, $wR_2 = 0.0986$	$R_1 = 0.0179$, $wR_2 = 0.0441$	$R_1 = 0.0250$, $wR_2 = 0.0533$	$R_1 = 0.0422$, $wR_2 = 0.1149$	$R_1 = 0.0394$, $wR_2 = 0.0924$	$R_1 = 0.143$, $wR_2 = 0.0249$
R_{int}	0.0547	0.0351	0.0458	0.0594	0.0465	0.0682
Flack X	–	0.04(2)	–	−0.02(2)	–	0.03(1)
GoF	1.104	1.162	1.090	1.188	1.074	0.989
CCDC number	2292310	2292309	2292312	2292313	2292311	2292308
Yield	59%	31%	54%	41%	53%	96%

The preparation of the hydrazine *iso*-disulfonate anion requires a three-step reaction.[16] First, the potassium imido-*bis*-sulfonate, $K_2[HN(SO_3)_2]$, is prepared which is then reacted with the hydroxylamine-*O*-sulfonic acid, H_2NOSO_3H yielding the potassium *iso*-disulfonate, $K_2[H_2NN(SO_3)_2]$:

$$2\,K_2S_2O_5 + KNO_2 + 2\,H_2O \xrightarrow[80\,^\circ C]{H_2O} K_3[N(SO_3)_3](H_2O)_2 + K_2SO_3$$

$$K_3[N(SO_3)_3](H_2O)_2 \xrightarrow[RT,\,2\,d]{1\,M\,H_2SO_4} K_2[HN(SO_3)_2] + H_2O + KHSO_4$$

$$K_2[HN(SO_3)_2] + 2\,KOH + H_2NOSO_3H \xrightarrow[1.\,3\,h,\,0\,^\circ C;\ 2.\,72\,h,\,RT;\ 3.\,KOH,\,0\,^\circ C]{H_2O} K_2[H_2NN(SO_3)_2] + K_2SO_4 + 2\,H_2O$$

The barium salt, $Ba[H_2NN(SO_3)_2](H_2O)_2$, is formed by salt metathesis with $BaCl_2$. Also the two *iso*-disulfonates are phase pure according to X-ray powder diffraction and elemental analyses (cf. supporting information). The crystallographic data and yields for the two compounds are collected in Table 2.

Table 2. Selected crystallographic data and yields for the hydrazine *iso*-disulfonates $K_2[H_2NN(SO_3)_2]$ and $Ba[H_2NN(SO_3)_2](H_2O)_2$.

Compound	$K_2[H_2NN(SO_3)_2]$	$Ba[H_2NN(SO_3)_2](H_2O)_2$
T/K	100.0(2)	100.0(2)
Crystal System	*orthorhombic*	*orthorhombic*
Space group	$P2_12_12_1$	*Pbca*
a/pm	551.21(3)	980.52(5)
b/pm	950.14(4)	1026.09(6)
c/pm	1419.29(7)	1668.31(9)
V/nm^3	0.74332(6)	1.6785(2)
Z	4	8
Final R indexes [all data]	$R_1 = 0.0238$, $wR_2 = 0.0570$	$R_1 = 0.0246$, $wR_2 = 0.0562$
R_{int}	0.0484	0.0403
GoF	1.097	1.135
Flack X	−0.05(3)	–
CCDC number	2292297	2292298
Yield	55%	45%

Hydrazine Disulfonate, $[(SO_3)HNNH(SO_3)]^{2-}$

As described above, pyridinium hydrazine disulfonate, $(C_5H_6N)_2[(SO_3)HNNH(SO_3)]$, is the first compound that forms during our synthetic approach. The pyridinium cation is only weakly coordinated to the anion by a moderate hydrogen bond (Figure 2). Thus, the salt is ideal for a detailed inspection of the undisturbed hydrazine disulfonate anion. In the crystal structure of $(C_5H_6N)_2[(SO_3)HNNH(SO_3)]$ the hydrazine disulfonate anion shows C_2 symmetry with the twofold axis oriented perpendicular to the N–N bond. The distance N–N in the anion is found at 141.9(3) pm while the bond length N–S shows a value of 167.7(2) pm. The respective values for the previously reported hydrazine monosulfonate are 144.3(5) and 165.9(4) pm, i.e. the N–N bond is significantly shorter in the disulfonate while the S–N bond length increases slightly upon the second sulfonation.[7] The S–O bond lengths are essentially the same in the monosulfonate and the disulfonate, displaying values between 144 and 146 pm. The most interesting feature of the anion is the torsion angle S–N–N–S which shows a value of 135.3(6)°. Thus, the orientation of the two $[SO_3HN]$ moieties with respect to each other leads to a *gauche* conformer of the anion. It is worthwhile to mention that also in hydrazine, N_2H_4, the *gauche* conformer has been shown to be the most stable one.[19] In the *gauche* conformation the hydrazine disulfonate anion exhibits two stereo centres located at the two nitrogen atoms leading to an (*R*, *R*) and an (*S*, *S*) enantiomer, respectively. $(C_5H_6N)_2[(SO_3)HNNH(SO_3)]$ crystallizes with orthorhombic symmetry (space group *Pccn*) as a racemate and the two enantiomers are correlated by a glide plane perpendicular to the [001] axis of the orthorhombic unit cell (Figure 2).

The hydrazine disulfonate anions in $A_2[(SO_3)HNNH(SO_3)](H_2O)$ with A=K, Rb, Cs, NH_4 and the barium salt $Ba[(SO_3)HNNH(SO_3)](H_2O)_2$ have similar bond parameters as discussed above for the pyridinium compound. However, the N–N bond increases slightly with the increasing size of the A^+ cations up to a value of 143.7(4) pm. More significant is the growth of the S–N bond lengths from 167.7(2) pm in the pyridinium salt up to 177(2) pm in the Cs^+ compound. The dihedral angles S–N–N–S in the *gauche* type anions range from 134.2° (Ba^{2+} salt) to 143.0° (Cs^+ salt). As found for the pyridinium compound, all of the investigated salts are racemates. Although some of the observed space groups do not bear inversion symmetry, none of them belongs to the *Sohnke* type space groups, which are mandatory for enantiopure solids. The cations in the hydrazine disulfonates are coordinated by oxygen atoms of the $[SO_3]$ groups and of the H_2O molecules. The coordination numbers range from 9 to 11 (cf. supporting information).

Hydrazine *iso*-disulfonate, $[H_2NN(SO_3)_2]^{2-}$

In the two hydrazine *iso*-disulfonates $K_2[H_2NN(SO_3)_2]$ and $Ba[H_2NN(SO_3)_2](H_2O)_2)$ the bonding parameters in the anion are quite similar. The S–N bond lengths range from 169.8(2)–

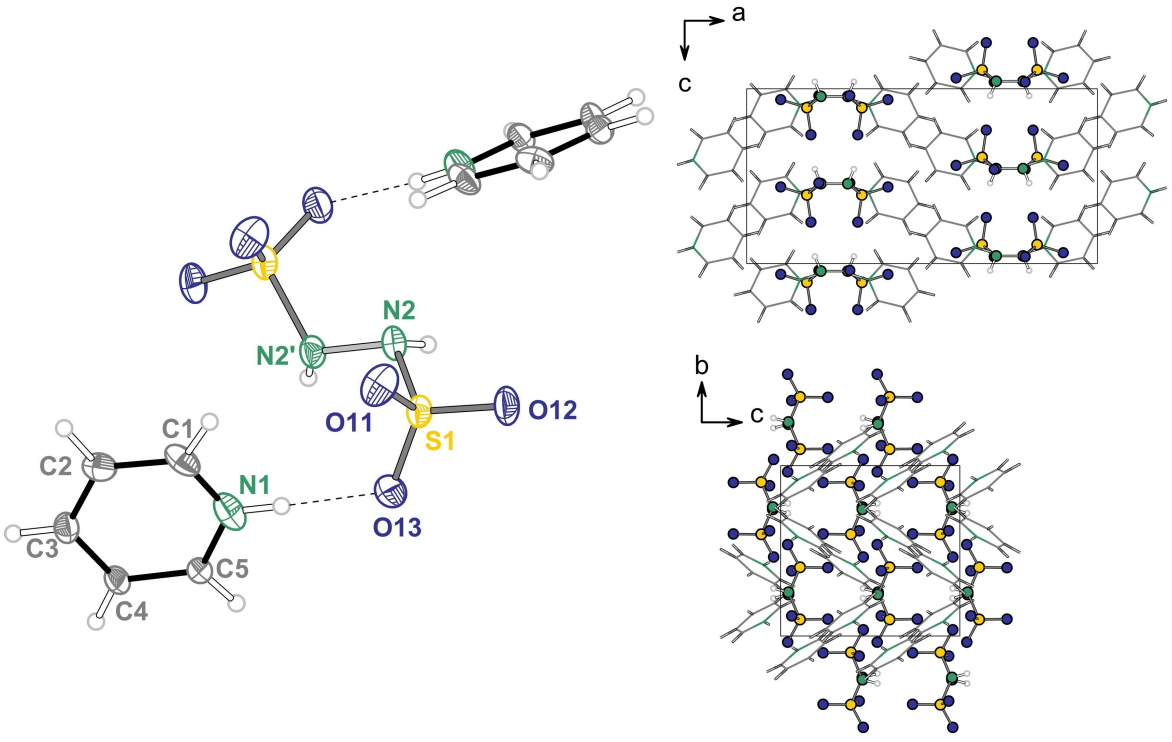

Figure 2. Structure of $(C_5H_6N)_2[(SO_3)HNNH(SO_3)]$ (left) and extended unit cells along the crystallographic *b*-axis (top right) and *a*-axis (bottom right). The thermal ellipsoid probability is set to 70%. Selected distances (in pm) and angles (in °): N2–N2′ 141.9(3), S1–N2 167.7(2), S1–O11 146.6(1), S1–O12 144.5(1), S1–O13 144.6(1), N1–C1 133.6(3), N1–C5 133.5(2), C1–C2 137.7(3), C2–C3 138.7(3), C3–C4 138.5(3), C4–C5 137.5(3), N1···O13 269.2(1), N1–H1···O13 171(1), N1–N2–S1 112.3(1), O11–S1–N2 108.32(8), O12–S1–N2 102.26(8), O13–S1–N2 105.76(8), S1–N2–N2′–S1′ 135.3(6).

171.6(2) pm and N–N bonds are essentially equal with values of 143.5(2) and 143.6(3) pm, respectively. The nitrogen atom N2 is surrounded by the two sulfonate groups and one adjacent nitrogen atom (N1) in a distorted trigonal-pyramidal manner with observed angles ∠S1–N2–S2 of 122.7(1)° (K^+) and 116.34(9)° (Ba^{2+}), ∠N1–N2–S1 of 106.5(1)° (K^+) and 113.8(1)° (Ba^{2+}), and ∠N1–N2–S2 of 112.2(1)° (K^+) and 109.2(1)° (Ba^{2+}) (Figure 3, right part). The coordination numbers for the metal ions are found in the typical range between 9 and 11. For $K_2[H_2NN(SO_3)_2]$ also the nitrogen atom of the NH_2 group takes part in the K^+ coordination with a distance K–N of 305.5 pm. The comparison of the hydrazine disulfonate and the hydrazine *iso*-disulfonate anion should be done for the respective potassium compounds (Figures 3 and 4). It turned out that the distance N–N is identical in both anions while the observed S–N bonds are slightly longer in the *iso*-disulfonate displaying values of 170.7(2) and 171.1(2) pm, respectively. These values are very similar to those of the imido-*bis*-sulfonate anion (cf. **3** in Figure 1) found in the potassium compound $K_2[HN(SO_3)_2]$.[11] Further deprotonation of the imido-*bis*-sulfonate anion leads to the nitrido-*bis*-sulfonate anion $[N(SO_3)_2]^{3-}$ which is known as the salt $K_3[N(SO_3)_2](H_2O)$.[11,12] In this anion the S–N bond is significantly shorter (≈160 pm). Table 3 summarizes the important bonding parameters of the discussed compounds and the nitrogen-containing disulfonates known so far.

Thermal Behaviour

The thermal behaviour of the hydrazine disulfonates $(C_5H_6N)_2[(SO_3)HNNH(SO_3)]$, $A_2[(SO_3)HNNH(SO_3)](H_2O)$ (A=K, Rb), and $Ba[(SO_3)HNNH(SO_3)](H_2O)_2$ as well as of the *iso*-disulfonate $K_2[H_2NN(SO_3)_2]$ has been investigated by DSC measurements coupled with mass spectrometry. The decomposition of the pyridinum hydrazine disulfonate $(C_5H_6N)_2[(SO_3)HNNH(SO_3)]$ starts at 100 °C with an endothermic step, directly followed by

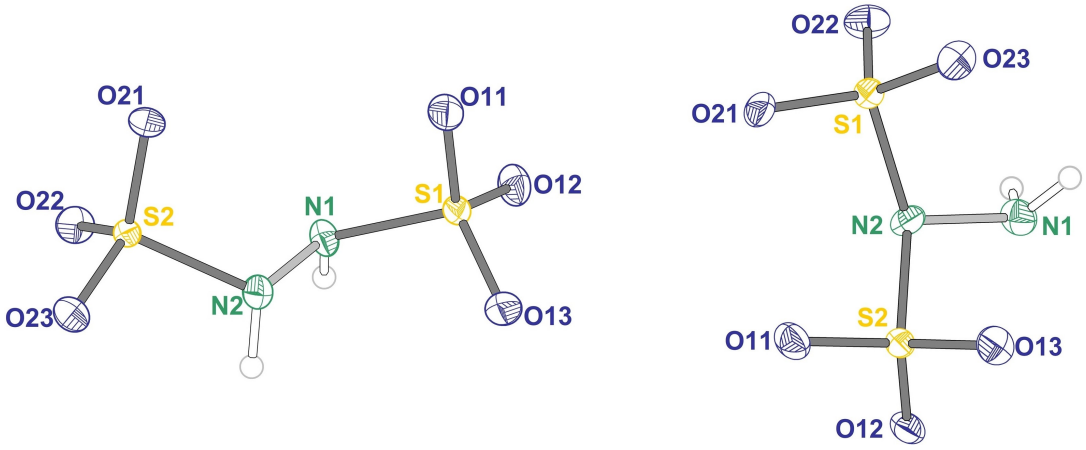

Figure 3. Structure and labelling of the hydrazine disulfonate anion, $[(SO_3)HNNH(SO_3)]^{2-}$ (left) of the structure $K_2[(SO_3)HNNH(SO_3)](H_2O)$, and the hydrazine *iso*–disulfonate anion, $[H_2NN(SO_3)_2]^{2-}$ (right) of the structure $K_2[H_2NN(SO_3)_2]$. The probability of the thermal ellipsoids is set to 70%. Selected distances (in pm) and angles (in °) compared to the theoretical values (in *italics*): **$[(SO_3)HNNH(SO_3)]^{2-}$**: S1–N1 167.8(2)/*169.8*, S2–N2 168.7(2)/*169.8*, N1–N2 142.6(3)/*137.3*, S1–O11 144.8(2)/*146.2*, S1–O12 144.9(2)/*146.2*, S1–O13 145.2(2)/ *144.6*, S2–O21 144.9(2)/*146.2*, S2–O22 145.6(2)/*146.2*, S2–O23 145.0(2)/*144.6*, S1–N1–N2 111.9(2)/*119.7*, S2–N2–N1 111.8(2)/*119.7*, O11–S1–N1 105.2(1)/*106.9*, O12–S1–N1 101.3(1)/*99.7*, O13–S1–N1 110.2(1)/*107.4*, O21–S2–N2 104.7(1)/*106.9*, O22–S2–N2 110.0(1)/*107.3*, O23–S2–N2 100.8(1)/*99.7*, S1–N1–N2–S2 134.3(1)/*135.4*. **$[H_2NN(SO_3)_2]^{2-}$**: S1–N2 170.7(2)/*175.4*, S2–N2 171.1(2)/*175.9*, N1–N2 143.6(3)/*142.7*, S1–O11 144.4(2)/*145.7*, S1–O12 145.1(2)/*146.6*, S1–O13 145.4(2)/*147.1*, S2–O21 145.5(2)/*145.6*, S2–O22 144.9(2)/*148.0*, S2–O23 145.3(2)/*146.8*, S2–N2–S1 122.7(1)/*123.4*, N1–N2–S1 106.5(1)/*107.0*, N1–N2–S2 112.2(1)/*109.3*, O21–S2–N2 106.5(1)/*106.7*, O22–S2–N2 102.35(9)/*99.7*, O23–S2–N2 106.5(1)/*108.6*, O11–S1–N2 105.9(9)/*105.2*, O12–S1–N2 102.1(9)/*103.0*, O13–S1–N2 107.5(1)/*105.7*.

Table 3. Selected bonding parameters of the disulfonates discussed in this paper and in literature.

Compound	N–N/pm	S–N/pm	S–O/pm	S–N–N–S/ °	S–N–S/ °
$(C_5H_6N)_2[(SO_3)HNNH(SO_3)]$	141.9(3)	167.7(2)	144.5(1)–146.(1)	135.3(6)	–
$K_2[(SO_3)HNNH(SO_3)](H_2O)$	142.6(3)	168.7(2), 167.8(2)	144.8(2)–145.7(2)	134.3(1)	–
$Rb_2[(SO_3)HNNH(SO_3)](H_2O)$	142.4(5)	172.5(4), 173.6(4)	144.3(2)–144.9(2)	139.3(2)	–
$Cs_2[(SO_3)HNNH(SO_3)](H_2O)$	143(3)	177(2), 173(2)	143(1)–145(1)	143.0(3)	–
$(NH_4)_2[(SO_3)HNNH(SO_3)](H_2O)$	143.2(4)	170.9(3), 173.3(3)	143.8(2)–144.5(2)	141.8(2)	–
$Ba[(SO_3)HNNH(SO_3)](H_2O)_2$	143.7(4)	168.5(2)	144.2(2)–145.8(2)	134.2(1)	–
$K_2[H_2NN(SO_3)_2]$	143.6(3)	170.7(2), 171.1(2)	144.4(2)–145.4(2)	–	122.7(1)
$Ba[H_2NN(SO_3)_2](H_2O)_2$	143.5(2)	169.8(2), 171.6(2)	144.3(1)–145.8(1)	–	116.34(9)
$K_2[HN(SO_3)_2]$[11]	–	166.9(2)	144.6(3)–145.1(2)	–	124.2(1)
$K_3[N(SO_3)_2](H_2O)$[12]	–	159.9(3), 160.9(3)	145.6(3)–147.5(2)	–	121.0(1)

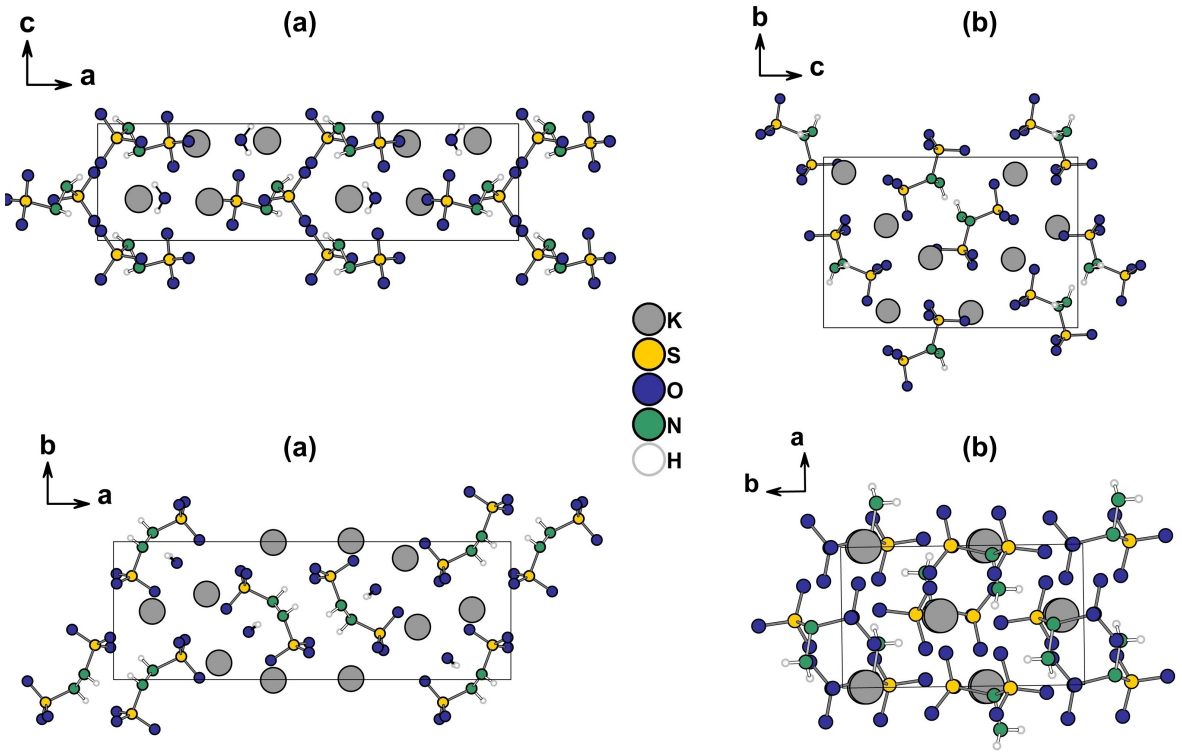

Figure 4. Solid state structure of $K_2[(SO_3)HNNH(SO_3)](H_2O)$ (a) along the crystallographic *c*- and *b*-axis and $K_2[H_2NN(SO_3)_2]$ (b) along the crystallographic *a*- and *b*-axis.

an exothermic reaction (Figure S17 in the supporting information). The mass loss after these two steps is 72% and sulfuric acid, H_2SO_4, can be assumed as residual. This assumption fits to the next step in the DCS/TG curve, which shows a maximum at 301 °C in line with the known decomposition characteristics of H_2SO_4.

The decomposition of the alkaline metal hydrazine disulfonates $A_2[(SO_3)HNNH(SO_3)](H_2O)$ (A=K, Rb) is quite similar. For example, the decomposition of $K_2[(SO_3)HNNH(SO_3)](H_2O)$ starts with the release of crystal water starting at 135 °C, accompanied by a mass loss of 6.3% (theory: 6.1%) (Figure 5). As expected, the observed masses of the fragments in the mass spectrometer are m/z = 18 (H_2O) and m/z = 17 (OH). The anhydrous salt decomposes exothermally starting at 207 °C and the most prominent fragments in the mass spectrum are m/z = 64 (SO_2) and m/z = 48 (SO). The residue is identified by powder X-ray diffraction as K_2SO_4. As can be seen from the TG curve there is still a smooth mass loss after the main decomposition step. A similar effect can be seen in the measurement of the Rb compound. A possible explanation would be, that $(NH_4)_2SO_4$ forms as a second decomposition product which is known to decompose above 250 °C.[20] However, there is no valid prove for this assumption up to now.

A very unique thermal behaviour is found for the barium compound $Ba[(SO_3)HNNH(SO_3)](H_2O)_2$. Unexpectedly, not an endothermic peak typical for a dehydration process is observed, but an exothermic peak with a maximum slightly below 100 °C. This peak is not accompanied with a significant mass loss. The final decomposition above 200 °C leads to $BaSO_4$ as shown by X-ray powder diffraction. In order to get further insight into this exothermic reaction below 100 °C, we repeated the measurement but stopped it at 100 °C. Surprisingly, the X-ray powder diffractogram of the residue at this temperature shows a mixture of $BaSO_4$ and hydrazinium sulfate, $(N_2H_6)SO_4$ (cf. supplement). The diffractogram is not of the best quality, however, the treatment of the residue with H_2O gives a non-soluble residue ($BaSO_4$) and a solution of which $(N_2H_6)SO_4$ could be crystallized. Thus the reaction that occurs in the solid state can be formulated as $Ba[(SO_3)HNNH(SO_3)](H_2O)_2 \rightarrow (N_2H_6)SO_4 + BaSO_4$.

The hydrazine *iso*-disulfonate $K_2[H_2NN(SO_3)_2]$ decomposes essentially in a one-step process displaying an exothermic peak in the DSC curve at a maximum of 229 °C (Figure 6). This is essentially the same temperature as observed for the respective disulfonate $K_2[(SO_3)HNNH(SO_3)](H_2O)$. The ion current of the mass spectrometer for the SO and SO_2 fragments, respectively, show that the decomposition is probably more complex than the DSC peak suggests. The decomposition residue is K_2SO_4 as confirmed by X-ray powder diffraction (see supporting information).

Raman Spectroscopy

The expected Raman bands for the hydrazine disulfonates and *iso*-disulfonates were derived from quantum mechanical calculations within density functional theory (DFT, see supporting information). Although the calculations have been performed in

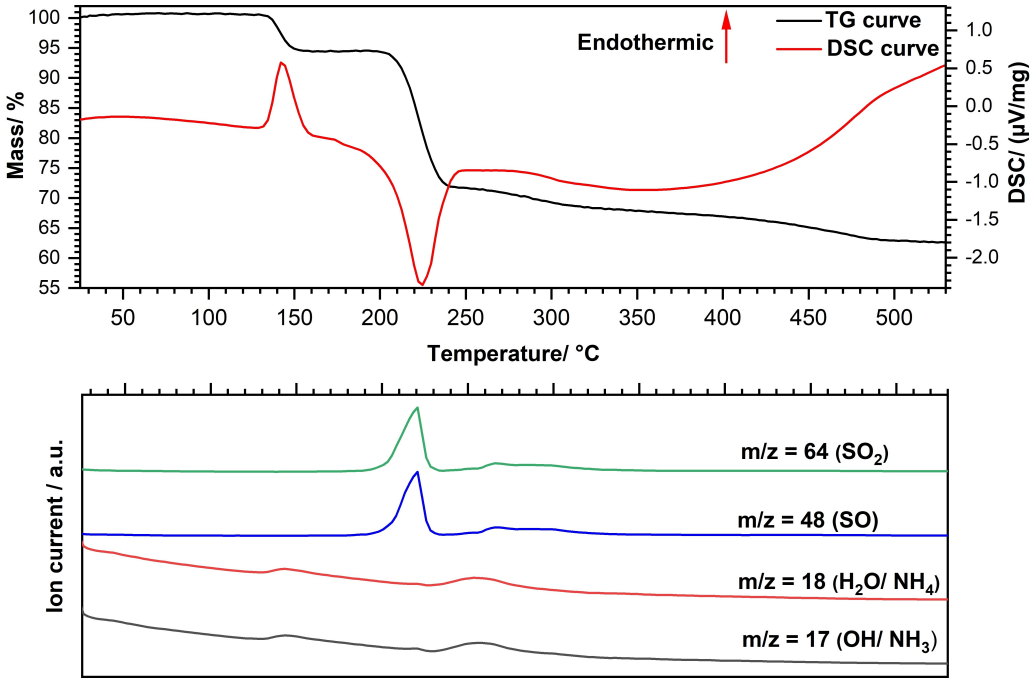

Figure 5. Thermal analysis of $K_2[(SO_3)HNNH(SO_3)](H_2O)$ (heating rate 5 K min^{-1}, argon flow 80 ml min^{-1}) combined with an ion current measurement (below) of selected m/z values.

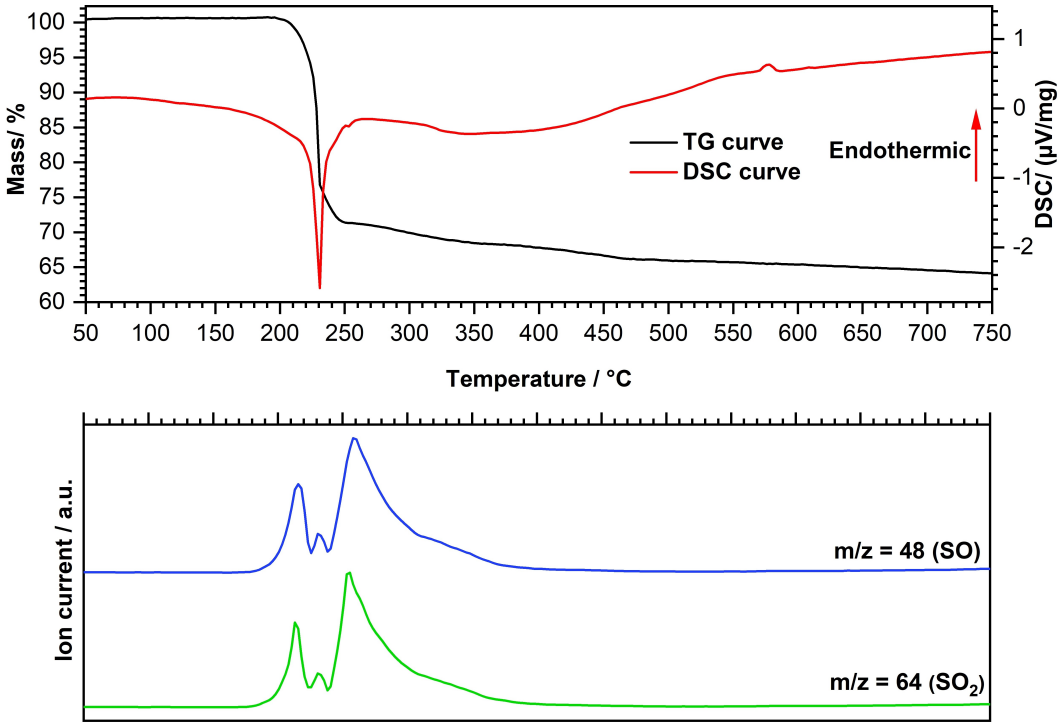

Figure 6. Thermal analysis (on top) of $K_2[H_2NN(SO_3)_2]$ (heating rate 6 K min^{-1}, argon flow 80 ml min^{-1}) combined with an ion current measurement (below) of selected m/z values.

a gas phase approximation for both anions, the obtained data allow for a reliable assignment of the observed bands. The example of $K_2[(SO_3)HNNH(SO_3)](H_2O)$ (Figure 7) shows the stretching vibrations of the $[SO_3]$ moieties in the range from 1223 to 1255 cm^{-1} (asymmetric) and at 1042 and 1068 cm^{-1}, respectively (symmetric). The deformation vibrations are found at 593 and 640 cm^{-1}. The most interesting vibrations for the new anion are those with participation of the nitrogen atom. They occur in the potassium compound at 1213 cm^{-1} for the N–N vibration and at 737 and 889 cm^{-1} for the asymmetric and

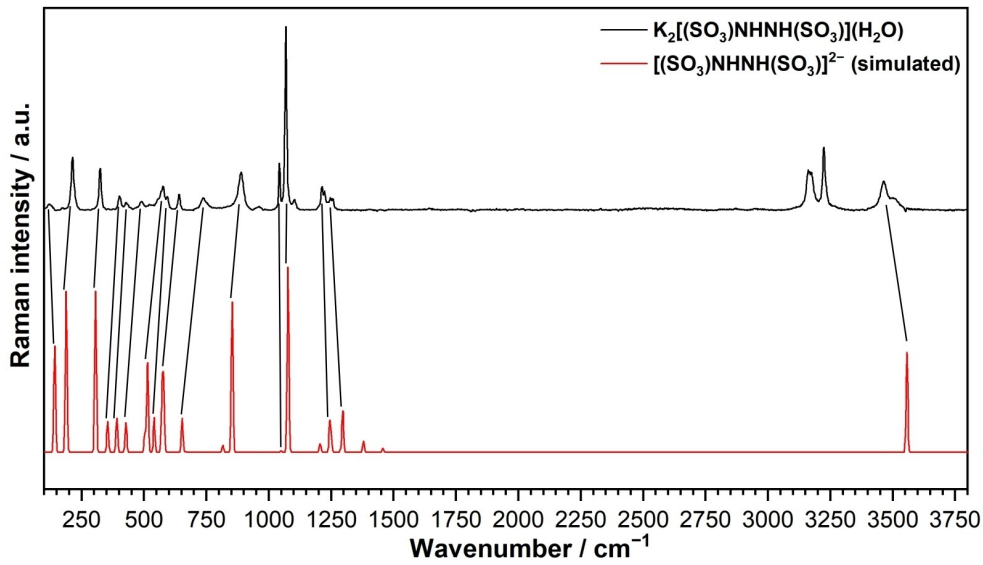

Figure 7. Raman spectrum of for $K_2[(SO_3)HNNH(SO_3)](H_2O)$ (black) compared to the simulated spectrum based on DFT calculation in the gas phase approximation.

symmetric stretching vibrations of the S–N bonds. Finally, the N–H bond stretching vibrations are observed around 3500 cm^{-1}. The observed values differ only slightly for the respective salts of the other investigated metals. For the hydrazine *iso*-disulfonate in $K_2[H_2NN(SO_3)_2]$ the N–N vibration is observed at 914 cm^{-1} while the streching mode S–N occurs at 712 cm^{-1}. The vibration modes of the $[SO_3]$ are seen in the same range as observed for $K_2[(SO_3)HNNH(SO_3)](H_2O)$. Full data for all compounds can be found in the supporting information.

Conclusions

The hydrazine disulfonates have been characterized comprehensively for the first time. Formally, the anions are derived from hydrazine, N_2H_4, by insertion of SO_3 into N–H bonds. Two structural isomers could be obtained, namely the hydrazine disulfonate $[(SO_3)HNNH(SO_3)]^{2-}$ and the hydrazine *iso*-disulfonate, $[H_2NN(SO_3)_2]^{2-}$. With respect to the position of the $[SO_3]$ groups in relation to each other, the hydrazine disulfonate $[(SO_3)HNNH(SO_3)]^{2-}$ anion has a *gauche* conformation, i.e. the anion is chiral. All of the compounds obtained so far are racemates, however, the formation of enantiopure compounds should be possible. Another question that needs to be answered is, if further SO_3 insertions in N–H bonds of the hydrazine molecule can be achieved, giving finally the hydrazine tetrasulfonate anion $[(SO_3)_2NN(SO_3)_2]^{4-}$.

Experimental Section

Caution: $(N_2H_6)SO_4$ is carcinogenic and toxic upon contact with the skin and causes severe skin burns and eye damage. As a reducing agent, it can react violently with oxidizing agents. $ClSO_3H$, is a very strong acid which reacts violently with water and causes severe skin burns and eye damage.

$(C_5H_6N)_2[(SO_3)HNNH(SO_3)]$ was prepared in a reaction between $(N_2H_6)SO_4$ (1.00 eq.) and $ClSO_3H$ (2.72 eq.) in pyridine.[16] Aqueous solutions of $(C_5H_6N)_2[(SO_3)HNNH(SO_3)]$ (1.00 eq.) were reacted with KOH (excess), RbOH (2.00 eq.), CsOH (2.00 eq.), NH_3 (excess) and $Ba(OH)_2$ (1.02 eq.) to yield the hydrazine disulfonates $A_2[(SO_3)HNNH(SO_3)](H_2O)$ (A=K, Rb, Cs, NH_4) and $Ba[(SO_3)HNNH(SO_3)](H_2O)_2$ in a crystalline phase-pure form, respectively.

$K_2[H_2NN(SO_3)_2]$ was synthesized in a two-step reaction. First $K_2[HN(SO_3)_2]$ was synthesized by the reaction of $K_2S_2O_5$ (2.00 eq.) and KNO_2 (1.00 eq.) at 80 °C. $K_2[HN(SO_3)_2]$ (1.00 eq) was reacted with H_2NOSO_3H (1.00 eq.) in a KOH solution to obtain $K_2[H_2NN(SO_3)_2]$. Through salt metathesis with $BaCl_2{\cdot}2H_2O$, $K_2[H_2NN(SO_3)_2]$ was transformed to $Ba[H_2NN(SO_3)_2](H_2O)_2$. Single crystal structure determination of the compounds has been performed on a Bruker D8 VENTURE KAPPA diffractometer using MoK_α radiation (λ = 71.073 pm). The integration was done with SAINT and a multi-scan absorption correction using SADABS was applied.[21,22] The structure solution was performed in the software Olex2 by intrinsic phasing (SHELXT) and the structural model was refined by least squares methods using SHELXL.[23,24]

The deposition numbers 2292310 for $(C_5H_6N)_2[(SO_3)HNNH(SO_3)]$, 2292309 for $K_2[(SO_3)HNNH(SO_3)](H_2O)$, 2292312 for $Rb_2[(SO_3)HNNH(SO_3)](H_2O)$, 2292313 for $Cs_2[(SO_3)HNNH(SO_3)](H_2O)$, 2292311 for $(NH_4)_2[(SO_3)HNNH(SO_3)](H_2O)$, 2292308 for $Ba[(SO_3)HNNH(SO_3)](H_2O)_2$, 2292297 for $K_2[H_2NN(SO_3)_2]$ and 2292298 for $Ba[H_2NN(SO_3)_2](H_2O)_2$ contain the supplementary crystallographic data for this paper. These data are provided free of charge by the joint Cambridge Crystallographic Data Centre and Fachinformationszentrum Karlsruhe Access Structures Services.[25] X-ray powder data were measured with a *STOE STADI P* (Mo-$K_{\alpha1}$, λ = 70.930 pm) and a *Rigaku Miniflex* (Cu-K_α, $\lambda(K_{\alpha1})$ = 154.1 pm, $\lambda(K_{\alpha2})$ = 154.4 pm) diffractometer. The data was processed using *WinXPOW* (version 3.12) and *SmartLab Studio II*.[26,27] The Rietveld refinements were performed with the program *jEdit* using *TOPAS5*.[28–30] For the thermal analyses the analyzer STA 409 (*NETZSCH*) coupled with a quadrupole mass spectrometer (QMS 421, BALZERS) was used. Raman spectroscopic data were collected with *inVia Qotor confocal RAMAN microscope* by Renishaw GmbH. Quantum mechanical calculations were done using the *ORCA 5.0.3* program.[31] Elemental

analysis (CHNS) was performed with an elemental analyzer *Euro EA 300* (*EuroVector S. p. A.*). Full details of the syntheses, characterizations and quantum mechanical calculations can be found in the Supporting Information.

Supporting Information Summary

Additional supporting information can be found online in the Supporting Information section at the end of this article.

Acknowledgements

Open Access funding enabled and organized by Projekt DEAL.

Conflict of Interests

The authors declare no conflict of interest.

Data Availability Statement

The data that support the findings of this study are available from the corresponding author upon reasonable request.

Keywords: Sulfonic acid · hydrazine · sulfonation · crystal structures · thermal analyses

[1] G. A. Benson, W. J. Spillane, *Chem. Rev.* **1980**, *80*, 151–186.
[2] M. Cupery, *Ind. Eng. Chem.* **1938**, *30*, 627–631.
[3] L. F. Audrieth, M. Sveda, H. H. Sisler, M. J. Butler, *Chem. Rev.* **1940**, *26*, 49–94.
[4] L. B. Clapp, *J. Chem. Educ.* **1943**, *20*, 189.
[5] R. Sass, *Acta Crystallogr.* **1960**, *13*, 320–324.
[6] K. Yoshikubo, M. Suzuki, *Kirk-Othmer Encyclopedia of Chemical Technology*, John Wiley & Sons, 2000, New Jersey, US.
[7] T. Rennebaum, D. van Gerven, S. S. Sebastian, M. S. Wickleder, *Chem. Eur. J.* **2024**, *30*, e202302526.
[8] H. Sisler, L. F. Audrieth, *J. Am. Chem. Soc.* **1938**, *60*, 1947–1948.
[9] H. Sisler, L. F. Audrieth, U. S. Branson, W. C. Johnson, *Inorganic Synthesis, Vol. 2*, 1946, McGraw-Hill, New York, US, p. 182–183.
[10] H. H. Sisler, L. F. Audrieth, J. A. Lower, W. C. Fernelius, *Inorganic Synthesis., Vol. 2*, 1946, McGraw-Hill, New York, US, p. 179–181.
[11] P. Barbier, Y. Parent, G. Mairesse, *Acta Crystallogr. Sect. B.* **1979**, *35*, 1308–1312.
[12] J. R. Hall, R. A. Johnson, C. H. L. Kennard, G. Smith, B. W. Skelton, A. H. White, *J. Chem. Soc., Dalton Trans.* **1980**, 1091–1097.
[13] J. V. Tillack, C. H. L. Kennard, *J. Chem. Soc. A.* **1970**, 1637–1640.
[14] G. A. Jeffrey, D. W. Jones, *Acta Crystallogr.* **1956**, *9*, 283–289.
[15] D. van Gerven, M. S. Wickleder, *Angew. Chem. Int. Ed.* **2020**, *59*, 17169–17171, *Angew. Chem.* **2020**, *132*, 17320–17323.
[16] A. Meuwsen, H. Tischer, *Z. Anorg. Allg. Chem.* **1958**, *294*, 282–293.
[17] W. Traube, A. Vockerodt, *Ber. Dtsch. Chem. Ges.* **1914**, *47*, 938–944.
[18] E. Konrad, L. Pellens, *Ber. Dtsch. Chem. Ges.* **1926**, *59*, 135–138.
[19] L. Song, M. Liu, W. Wu, Q. Zhang, Y. Mo, *J. Chem. Theory Comput.* **2005**, *1*, 394–402.
[20] R. Kiyoura, K. Urano, *Ind. Eng. Chem. Process Des. Dev.* **1970**, *9*, 489–494.
[21] Bruker A. X. S., *Saint V8.40B* **2012**, Madsion, Winconsin, USA.
[22] L. Krause, R. Herbst-Irmer, G. M. Sheldrick, D. Stalke, *J. Appl. Crystallogr.* **2015**, *48*, 3–10.
[23] G. Sheldrick, *Acta Crystallogr. Sec. A* **2015**, *71*, 3–8.
[24] O. V. Dolomanov, L. J. Bourhis, R. J. Gildea, J. A. K. Howard, H. Puschmann, *J. Appl. Crystallogr.* **2009**, *42*, 339–341.
[25] C. R. Groom, I. J. Bruno, M. P. Lightfoot, S. C. Ward, *Acta Crystallogr. Sect. B.* **2016**, *72*, 171–179.
[26] Rigaku Corporation, *SmartLab Studio II 4.4.295.0* **2014**, Tokyo, Japan.
[27] STOE & Cie GmbH, *WinXPOW 3.6.0.1* **2018**, Darmstadt, Germany.
[28] A. A. Coelho, *TOPAS Academic v6* **2016**.
[29] A. Coelho, *J. Appl. Crystallogr.* **2018**, *51*, 210–218.
[30] B. S. Hulbert, W. M. Kriven, *J. Appl. Crystallogr.* **2023**, *56*, 576.
[31] F. Neese, F. Wennmohs, U. Becker, C. Riplinger, *J. Chem. Phys.* **2020**, *152*, 224108 (1-18)..

Manuscript received: June 18, 2024
Accepted manuscript online: August 22, 2024
Version of record online: October 23, 2024

4.3.3 Hydrazine Tetrasulfonate $[(SO_3)_2NN(SO_3)_2]^{4-}$: $K_4[(SO_3)_2NN(SO_3)_2](H_2O)$ and $K_4[(SO_3)_2NN(SO_3)_2](H_2O)_2$

The previous publications and the works of *Meuwsen et al.*[24] already stated that a hydrazine-tetrasulfonate, as a fully substituted hydrazine sulfonate, can be synthesized. The basic idea came from the work of *Pellens et al.*[23] in their work "Zur Kenntnis der Oxydation des Hydrazins, I.: Azodisulfonsaures Kalium". Therein, on the one hand, the synthesis $(Py–H)[(SO_3)HNNH(SO_3)]$ (cf. 4.3.2, p. 63) was described for the first time. This compound was treated with an alkaline NaOCl solution and KCl under cooling at −40 °C. The resulting yellow product with the tendency to explode was analyzed as an azo-disulfonate, according to $K_2[O_3SN{=}NSO_3]$. This oxidation aroused the interest of *Meuwsen* and *Tischer* and by slightly modifying the reaction procedure they prepared $K_4[(SO_3)_2NN(SO_3)_2](H_2O)$, which was solely confirmed by elemental analysis.

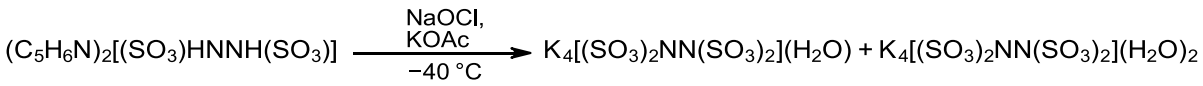

Scheme 16: Synthesis $K_4[(SO_3)_2NN(SO_3)_2](H_2O)$ and $K_4[(SO_3)_2NN(SO_3)_2](H_2O)_2$ according to a modified procedure of *Meuwsen* and *Tischer*.[24]

The procedure of *Meuwsen* was considered as part of this work to isolate the hydrazine tetrasulfonate. First $(Py–H)_2[(SO_3)HNNH(SO_3)]$ was prepared according to *4.3.2*. The phase-pure salt was dissolved in an aqueous solution of NaOH (2%). Under cooling at −40 °C a NaOCl solution (13%) was slowly added to the pyridinium salt. During the addition, the ice-cream mass locally took on a lemon yellow color (Figure 82, p. 119), which faded after warming up to RT. After treatment with KOAc the resulting solid was washed and recrystallized several times from NH_3-solution. In one crystallization batch colorless, rod-shaped crystals were obtained (see Figure 46, p. 73). These were examined by single crystal XRD and similar cell parameters of a monoclinic *C*-centered structure with a = 1280.6 pm, b = 431.7 pm, c = 1554.3 pm and β = 93.3° was determined (for more details see Table 11, p. 73). The data evaluation of one crystal yielded the structure of the potassium hydrazine tetrasulfonate dihydrate, $K_4[(SO_3)_2NN(SO_3)_2](H_2O)_2$. The structure was solved in the space group *C*2/*c* with four formula units per unit cell (for more details see Table 11, p. 73). It was checked by P-XRD if the crystalline compound was obtained phase-pure. For that several crystallization batches were collected to obtain a sufficient amount for a P-XRD measurement. In a *Rietveld* refinement of the P-XRD, dominant external reflections were observed, which could not be assigned to a literature-known and plausible phase. A second look at the crystallization batches revealed crystals with a different morphology (see Figure 46, p. 73). SC-XRD analysis of the latter showed a triclinic cell and the structure solution unveiled the monohydrate, $K_4[(SO_3)_2NN(SO_3)_2](H_2O)$, already reported by *Meuwsen* and *Tischer*.[24] This compound crystallizes in the space group $P\bar{1}$ with eight formula units per unit cell (see Table 11, p. 73).

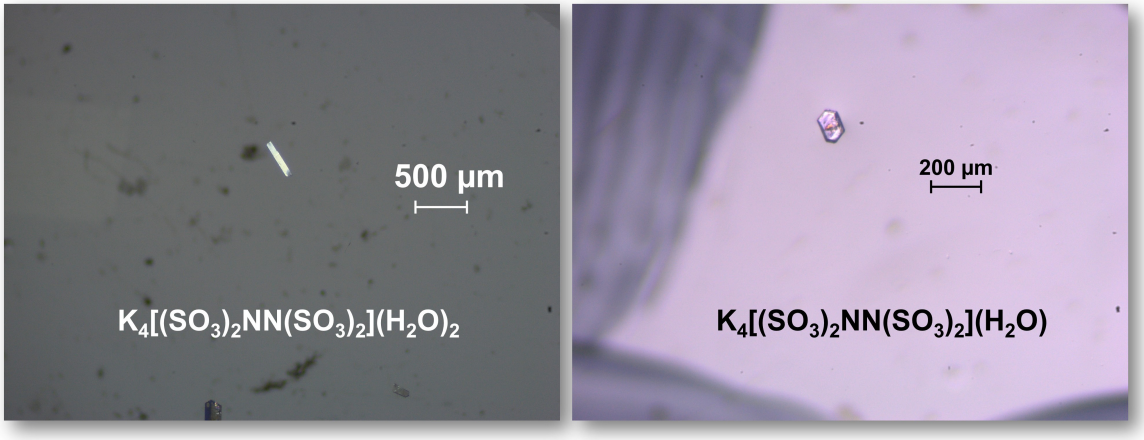

Figure 46: Light microscope images of single crystals of $K_4[(SO_3)_2NN(SO_3)_2](H_2O)_2$ (left) and $K_4[(SO_3)_2NN(SO_3)_2](H_2O)$ (right).

The monohydrate crystallizes in a large cell with a *c*-axis of 3034.2(2) pm length. The structure was refined as a twin (−1 0 0, 0 −1 0, 1 1 1) and during refinement rotational disorder of four [SO_3] groups was treated.

Table 11: Selected crystallographic data of the two hydrazine tetrasulfonates, $K_4[(SO_3)_2NN(SO_3)_2](H_2O)_2$ and $K_4[(SO_3)_2NN(SO_3)_2](H_2O)$.

	$K_4[(SO_3)_2NN(SO_3)_2](H_2O)_2$	**$K_4[(SO_3)_2NN(SO_3)_2](H_2O)$**
Crystal System	Monoclinic	Triclinic
Space Group	*C*2/*c*	$P\bar{1}$
a / pm	1280.62(8)	712.11(5)
b / pm	731.69(4)	1307.98(9)
c / pm	1554.3(1)	3034.2(2)
α / °	-	102.354(3)
β / °	93.333(2)	96.504(3)
γ / °	-	90.880(2)
V / nm³	1.4539(2)	2.740.6(3)
Z	4	8
R_1 (all data); wR_2 (all data)	0.0480; 0.0817	0.0362; 0.0792
GooF	1.091	1.036
BASF	-	0.2777(5)

By the X-ray analysis a structural evidence for the hydrazine tetrasulfonate anion $[(SO_3)_2NN(SO_3)_2]^{4-}$ is provided for the first time. Nevertheless, the synthesis turned out not to be straightforward with poor yield and by-products already reported by *Meuwsen* and *Tischer*. As one certain by-product a literature-known dithionate with the composition $NaK_5(S_2O_6)_2Cl_2$ was crystallographically identified (see 7.4.12, p. 146).[162-163] This compound underlines the complex redox chemistry occurring in this reaction. Mechanistically, it can be proposed that hypochlorite first oxidizes the N–N moiety under liberation of SO_3. Then, free SO_3 from the cleaved anion binds again to nitrogen to form partially the tetrasulfonate since no external SO_3 is added to the reaction.

In the crystal structure of $K_4[(SO_3)_2NN(SO_3)_2](H_2O)_2$ all atoms are located at general sites (*Wyckoff 8f*). Two potassium cations, one water molecule and one $[N(SO_3)_2]$ moiety can be distinguished from a crystallographic perspective (see Figure 47). In the large triclinic unit cell of the monohydrate sixteen K^+, four $[(SO_3)_2NN(SO_3)_2]^{4-}$ anions and four water molecules are distinguishable and all atoms are located at general sites (*Wyckoff 2i*) (see Figure 48).

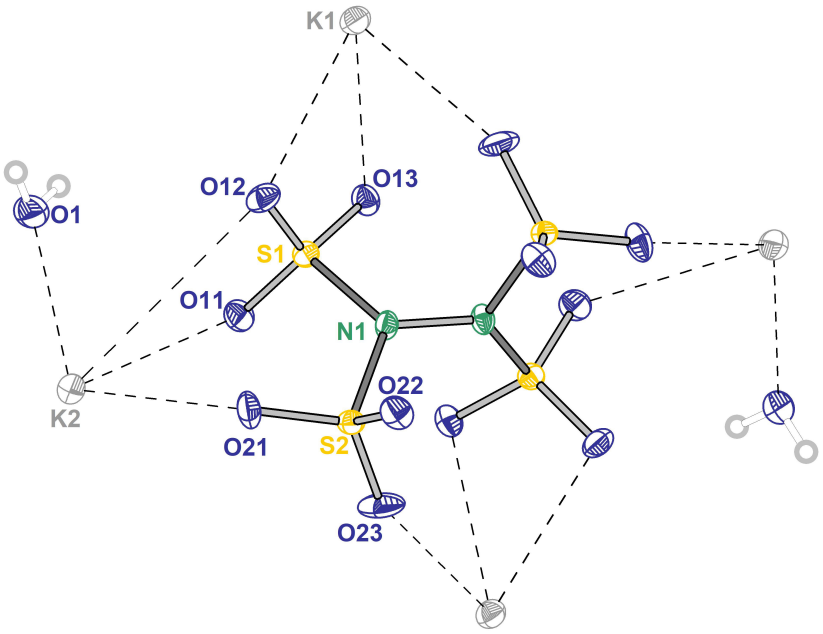

Figure 47: Structure of $K_4[(SO_3)_2NN(SO_3)_2](H_2O)_2$ with labeling of the crystallographic unique atoms. The thermal ellipsoids are set to a probability level of 70%.

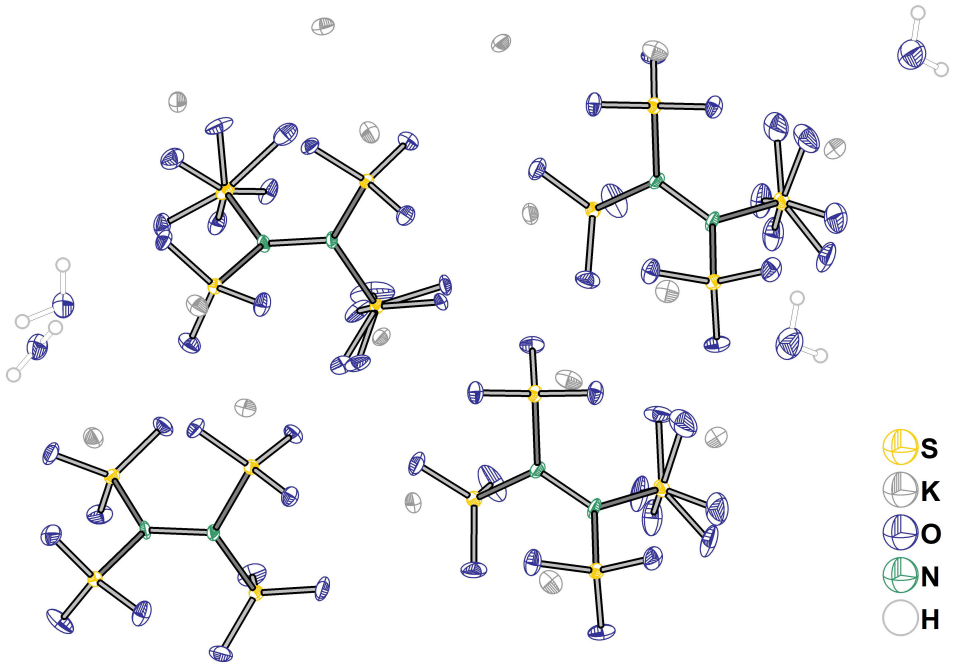

Figure 48: Asymmetric unit of triclinic $K_4[(SO_3)_2NN(SO_3)_2](H_2O)$. The thermal ellipsoids are set to a probability level of 70%.

A brief listing and comparison of the bonding parameters observed in both structures is shown in Table 12 (p. 76). Shape and bond properties of $[(SO_3)_2NN(SO_3)_2]^{4-}$ observed in both structures are similar (see Figure 49, p. 75 and Figure 50, p. 76). The distances between the nitrogen atoms are ranging from 137.2(3) pm to 138.5(5) pm. In the comparable hydrazine monosulfonate and disulfonate/*iso*-disulfonate elucidated before, these bonds are significant longer with 143.8(5) pm for $Ba[NH_2NH(SO_3)](H_2O)$ and 141.99(3)-143.7(4) pm for the hydrazine disulfonates and *iso*-disulfonates. Bond lengths for S–N range from 170.5(2) pm to 173.4(2) pm and are thus significantly longer than in the monosulfonate (166.4(4) pm) but coincide with the disulfonates (167.7(2)-173.6(4) pm). The angles spanned between the nitrogen atoms (∠S–N–N, ∠S–N–S) are within 116.1(2)° to 121.5(1)°. Analysis of the coordination geometry via *Polynator* suggests a distorted isoceles triangle (*mm*2) geometry for the crystallographically distinguishable $[S_2NN]$ fragments (see Table 12). This stands in contrast to the observations in the lower-substituted hydrazine sulfonates where the nitrogen atoms have a more trigonal-pyramidal surrounding, resulting from the lone-pairs steric demand. In the tetrasulfonate the trigonal-planar surrounding can be explained by the steric demand of the four sulfonate groups and delocalized π-bonding of the nitrogen lone pairs. This would also explain the contraction of the N–N bond. The bonding situation is well reflected by a quantum chemical gas-phase calculation. A geometry optimization for the isolated anion yielded similar bond lengths and angles (see Table 12). Only the S–N distances are enlarged with about 4-6 pm, which can be attributed to the not considered ionic interactions.

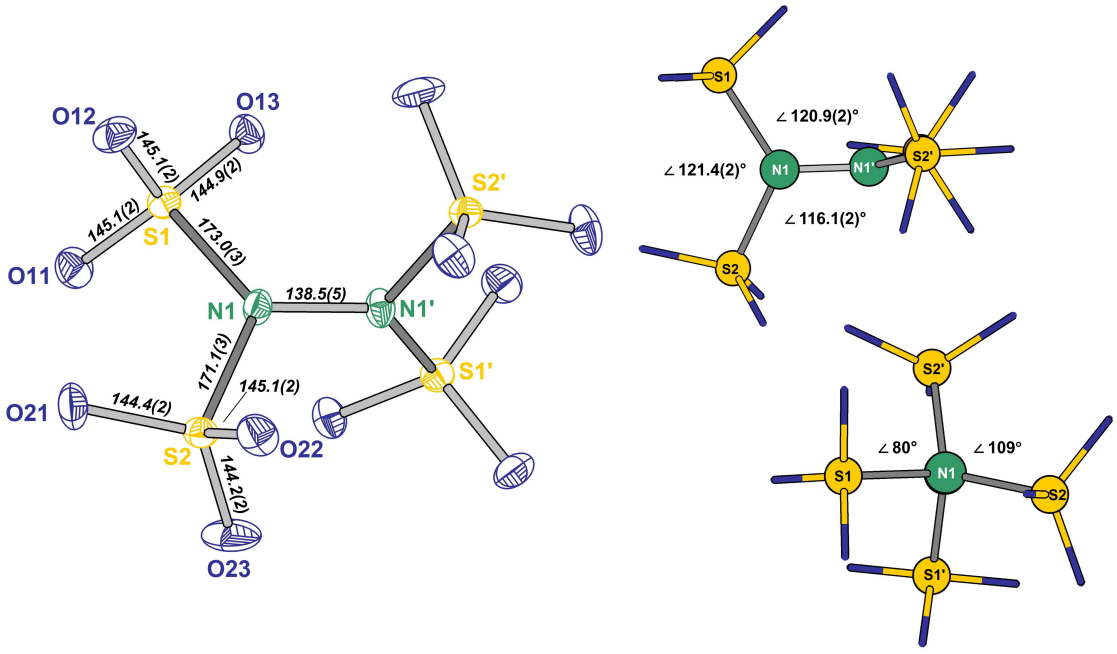

Figure 49: Structure and labeling of $[(SO_3)_2NN(SO_3)_2]^{4-}$ observed in $K_4[(SO_3)_2NN(SO_3)_2](H_2O)_2$. On the left the anion in ellipsoid (probability 70%) representation is shown with bond lengths (italics, in pm). On the right a wires and sticks representation of the anion is depicted with angles within the $[NNS_2]$ unit and dihedral angles (S1–N1–N1'–S2', S2–N1–N1'–S2').

Table 12: Selected bonding parameters observed in the hydrazine tetrasulfonates, $K_4[(SO_3)_2NN(SO_3)_2](H_2O)_2$ and $K_4[(SO_3)_2NN(SO_3)_2](H_2O)$ compared to a geometry optimization of the anion $[(SO_3)_2NN(SO_3)_2]^{4-}$ (see 7.3.1, p. 128).

	$K_4[(SO_3)_2NN(SO_3)_2](H_2O)_2$	$K_4[(SO_3)_2NN(SO_3)_2](H_2O)$	$[(SO_3)_2NN(SO_3)_2]^{4-}$
N–N / pm	138.5(5)	137.6(3)/137.6(3)/138.0(3)/137.2(3)	136.05
S–N / pm	171.1(3)/173.0(3)	170.5(2)-173.4(2)	177.6/179.2
S–O / pm	144.9(2)-145.1(2)	139(1)-150(1) (Ø 144.3)	141.1-147.3
K–O / pm	270.5(2)-323.8(3)	250(1)-361.8(2)	-
S–N–N–S / °	80/ 109	72.3(2)-110.0(2)	83.7/103.3
S–N–N / °	116.1(2)/120.9(2)	116.2(1)-120.8(2)	121.1/119.4
S–N–S / °	121.4(2)	118.6(1)-123.5(1)	118.7
O(D)…O(A) / pm	294.2(4)/282.3(4)	277.0/320.0	-
Shape δ $[NNS_2]$[143]	Isoceles triangle: 4.979 Triangle: 9.413	Isoceles triangle: 2.695-5.321 Triangle: 8.627-10.176	-

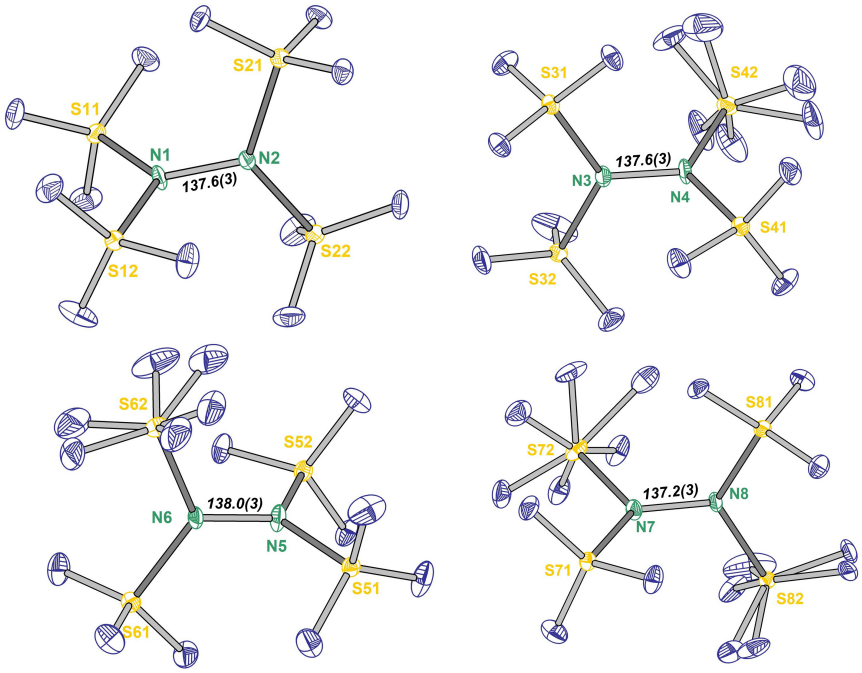

Figure 50: Depiction of the four unique $[(SO_3)_2NN(SO_3)_2]^{4-}$ anions observed in $K_4[(SO_3)_2NN(SO_3)_2](H_2O)$. The thermal ellipsoids are set to a probability level of 70%. The N–N distances are given in pm. At the $[SO_3]$ moieties of sulfur atoms S42, S62, S72 and S82 rotational disorder for the oxygen atoms was observed with a determined occupancy distribution of 0.67/0.33, 0.77/0.23, 0.92/0.08 and 0.82/0.18, respectively.

The relative orientation of the sulfonate groups can be expressed by the dihedral angle S–N–N–S. In both structures these angles are in between 72.3(2)° and 110.0(2)°. The $[O_3SNSO_3]$ units are positioned almost perpendicular to each other, which ensures steric distance. In the sulfonate groups of the dihydrate S–O distances of 144.9(2) pm to 145.1(2) pm are present. The monohydrate exhibits rotational disorder in four sulfonate groups of S42, S62, S72 and S82, which was indicated by significant rest electron density in between the oxygen atoms (see Figure 50). By modelling of the disorder S–O distances in the range of 139(1) pm to 150(1) pm are yielded.

Coordination to the potassium cations only takes place by the oxygen atoms of the sulfonate groups. In the dihydrate K1 has nine oxygen atoms and K2 eight oxygen atoms in their respective coordination spheres with distances of 270.5(2) pm up to 323.8(3) pm (see Figure 51). In this context,

no specific coordination polyhedra could be assigned. The sixteen unique K^+ in the monohydrate show a similar coordination pattern when the modulated oxygen atoms from disorder are not considered (see Figure 52).

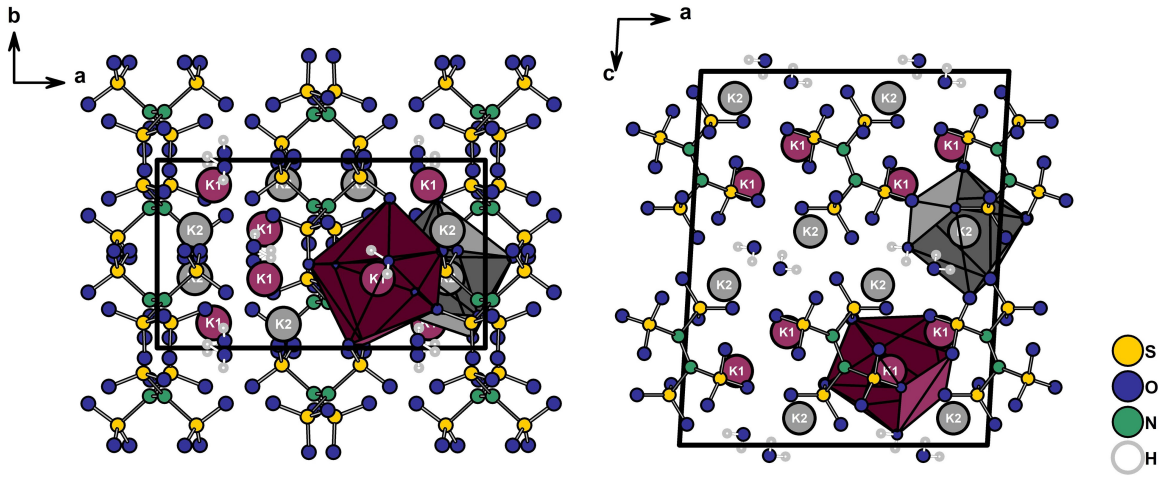

Figure 51: Crystal structure of $K_4[(SO_3)_2NN(SO_3)_2](H_2O)_2$ along the crystallographic axes *b* and *c*. The crystallographic distinguishable potassium cations are shown in different colors K1 (plum) and K2 (grey).

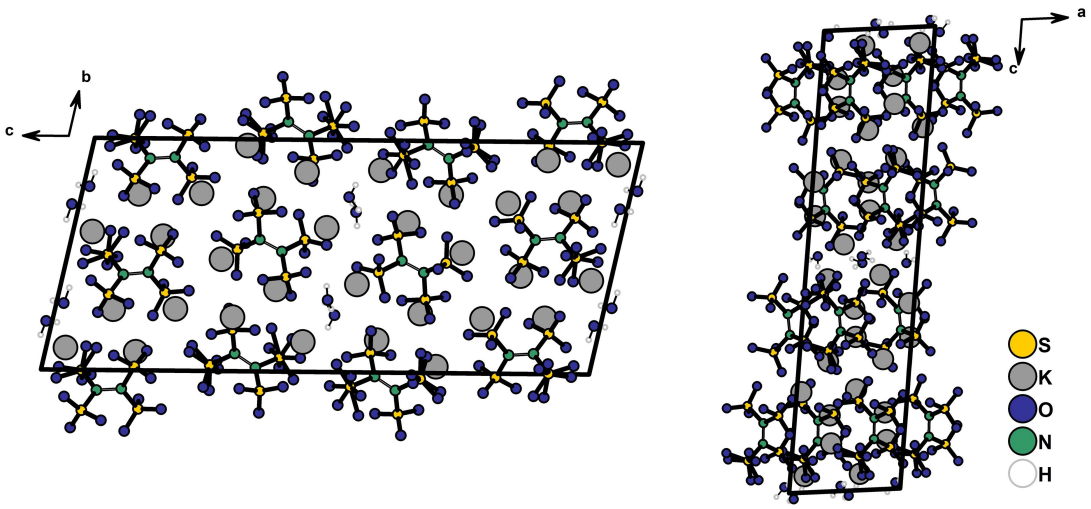

Figure 52: Crystal structure of $K_4[(SO_3)_2NN(SO_3)_2](H_2O)$ along the crystallographic axes *a* and *b*.

The water molecules in both structures participate in the coordination to K^+ and show hydrogen bonding to the sulfonate groups. In the dihydrate O(donor)–O(acceptor) distances of 294.2(4) pm (O1–O23) and 282.3(4) pm (O1–O21) with angles (∠O–H···O) of 155° and 172°, respectively, are found. This classifies them as medium strong with mainly electrostatic character.[136-137] For the monohydrate donor–acceptor distances in between 277.0 pm and 320.0 pm are found. Noteworthy, is the close contact of the two water oxygen atoms O3 and O5 to each other with a distance of 298.2(3) pm and an angle ∠O–H···O of 151°.

As already pointed out the P-XRD of the crystallization batch could not be assigned to a single phase. For that reason, a quantitative analysis of the P-XRD by the *Rietveld* method was conducted (see Figure 53). The monoclinic and triclinic cell were included for the refinement. The measured

powder suffers from amorphous background that remained even after additional recrystallization steps.

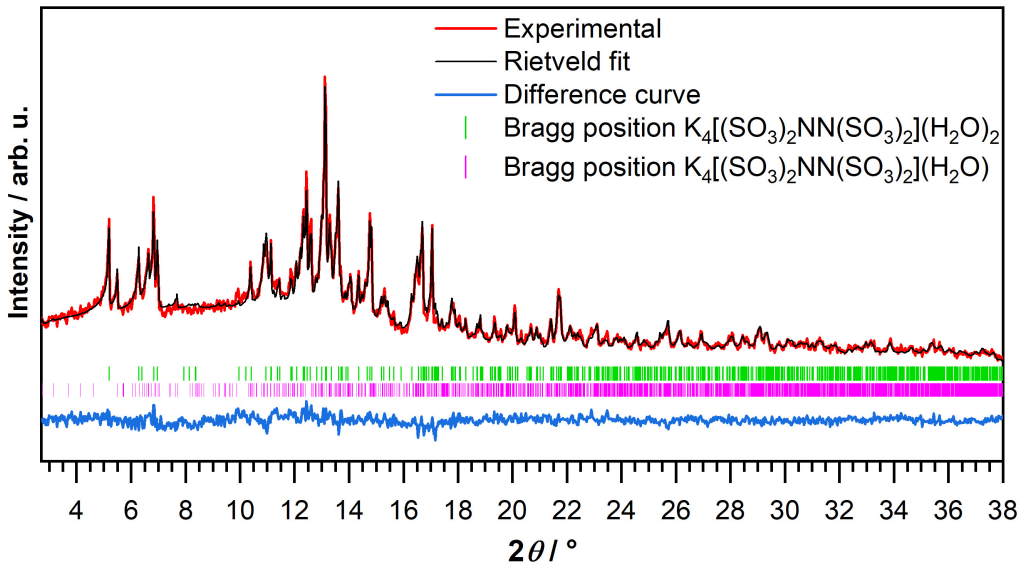

Figure 53: Experimental powder X-ray diffraction pattern of the two hydrazine tetrasulfonates with *Rietveld* refinement. The powder was measured in an 0.3 mm capillary with Mo-$K_{\alpha 1}$ (λ = 70.930 pm) radiation. For both structures all cell parameters were refined.

The refinement fit curve shows a good agreement to the experimental diffractogram with all dominant reflections being included. A fractional crystalline distribution of 43.81% for the monohydrate and 56.19% for the dihydrate was determined to be present in the powder sample (see Table 13).

Table 13: Cell data and refinement parameters obtained from the *Rietveld* powder analysis of the structures $K_4[(SO_3)_2NN(SO_3)_2](H_2O)$ and $K_4[(SO_3)_2NN(SO_3)_2](H_2O)_2$.

***Rietveld* Analysis**	**$K_4[(SO_3)_2NN(SO_3)_2](H_2O)$**	**$K_4[(SO_3)_2NN(SO_3)_2](H_2O)_2$**
Crystal System	Triclinic	Monoclinic
Space Group	$P\bar{1}$	$C2/c$
a / pm	715.7(2)	1297.1(1)
b / pm	1322.6(4)	729.94(6)
c / pm	3050(1)	1567.0(2)
α / °	102.45(7)	-
β / °	96.57(7)	93.112(9)
γ / °	90.70(2)	-
V / nm^3	2799(2)	1.4814(2)
Z	2	4
Fraction	43.8%	56.2%
R values	R_{wp} = 5.96 %; R_{exp} = 4.69%; R_p= 4.73%	
GooF	1.27	

Separation of the two phases by selective recrystallization from water was not possible. For $K_4[(SO_3)_2NN(SO_3)_2](H_2O)_2$ a single crystal was isolated and a *Raman* spectrum was recorded (see Figure 54, p. 79). For the assignment of the observed vibrations, a DFT gas phase-calculation of the

free $[(SO_3)_2NN(SO_3)_2]^{4-}$ anion was conducted. Although this does not include ionic interactions, a rough comparison can be made (see Table 14, p. 79).

The spectrum shows a number of bands between 240 cm^{-1} and 1310 cm^{-1}. Stretching vibration ν_s(NH) and ν_{as}(NH) are, as expected, not observed as in the hydrazine mono- and disulfonate anion (above 3000 cm^{-1}, see 4.3.1, p.58 and 4.3.2, p. 63). Interestingly, the bands for the O–H stretching vibration from the water molecules are not visible in the spectrum, either. This may be due to the low *Raman* activity of the water molecule. Antisymmetric stretching vibrations of $[SO_2]$ moieties lie in between 1231-1309 cm^{-1}. The most intense band at 1092 cm^{-1} is due to the symmetrical stretching vibration of the sulfonate group. The very small band at 1037 cm^{-1} is also $\nu_s(SO_3)$ but with different phases of the groups. The small bands at 866 cm^{-1} and 852 cm^{-1} result from antisymmetric stretching of S–N, while the more intense band at 707 cm^{-1} origins from symmetrical S–N stretching combined with wagging of the sulfonate groups. Bands below 700 cm^{-1} are rather complex deformation modes. The weak broad band within 540-641cm^{-1} originates from wagging and scissoring modes of the sulfonate groups. At lower wavenumbers the deformation modes of the whole $[(SO_3)_2NN(SO_3)_2]^{4-}$ unit and twisting mode of SO_3 occur. At 241 cm^{-1} simple S–N stretching without deformation modes is determined.

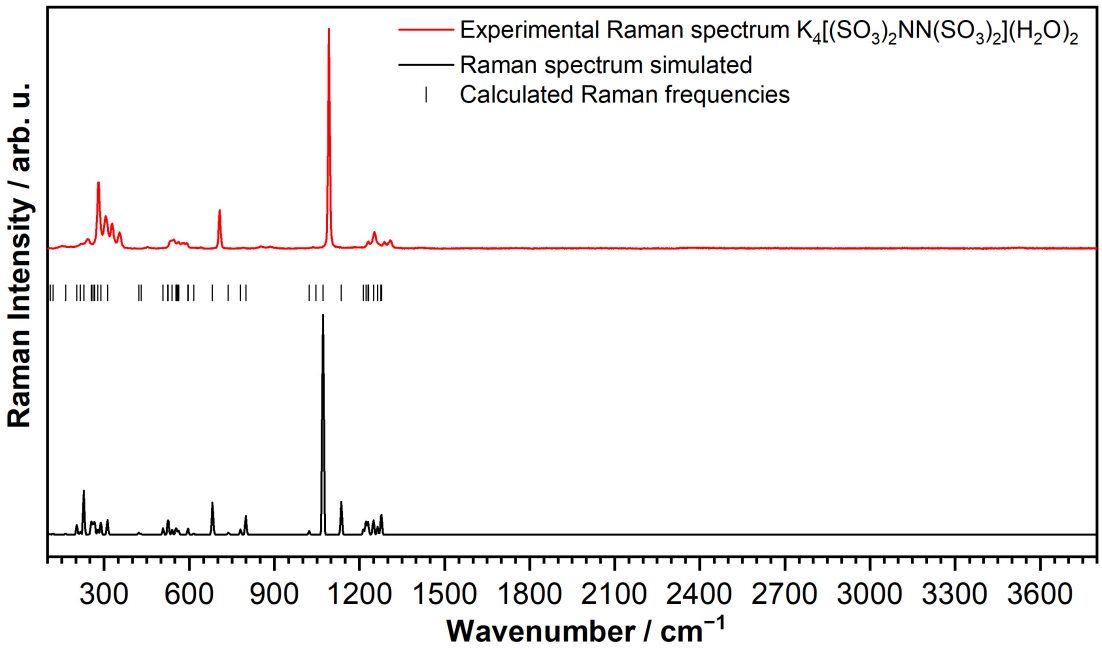

Figure 54: *Raman* spectrum of $K_4[(SO_3)_2NN(SO_3)_2](H_2O)_2$ recorded on a single crystal with a green laser (λ = 532 nm) at RT.

Table 14: Assignment of the experimental *Raman* bands of $K_4[(SO_3)_2NN(SO_3)_2](H_2O)_2$ with calculated values from a geometry optimization.

Assignment	Exp. *Raman* / cm^{-1}	Calcd. / cm^{-1}
$\nu_{as}(SO_2)$	1309	1277
	1288	1275
	1253	1263
	1231	1249

Assignment	**Exp. *Raman* / cm^{-1}**	**Calcd. / cm^{-1}**
		1222
		1213
ν_s(N–N)	-	1135
ν_s(SO_3) / ν_s(N–N)	1092	1071
ν_s(SO_3)	1037	1046
		1023
ν_{as}(SN)	866	799
	852	780
		738
ν_s(SN) + ω (SO_3)	707	682
ω (SO_3)	641	615
	590	595
δ(SO_3)	581	560
	563	555
	540	525
		507
τ(SO_3)	306	288
	280	277
		254
ν_s(SN)	241	227

4.3.4 Chapter Summary

In the context of sulfonates of hydrazine, various compound were yielded and analyzed as part of this work (see Table 15). As monosulfonated hydrazine compounds, hydrazine monosulfonic acid, $NH_3NH(SO_3)$, and its corresponding anion $[NH_2NH(SO_3)]^-$ in form of $Ba[NH_2NH(SO_3)]_2(H_2O)$ were successfully prepared and analyzed. With the observed zwitterionic nature in the solid state the acid is structurally related to sulfamic acid. Though the preparation was reported long ago[22], the new structural and analytical findings add another classic inorganic small molecule to the textbook knowledge. The acid and its corresponding anion are chiral with the stereocenter at the central nitrogen atom. However both compounds are not present in an enantiomerically pure form since symmetry operations of the second kind are found in the structures ($Pca2_1$ for the acid and $P\bar{1}$ for the Ba^{2+}-salt).[164]

Table 15: Overview of the hydrazine sulfonates analyzed in this work with observed interatomic distances between sulfur and nitrogen and between nitrogen and nitrogen. For the hydrazine disulfonates, the distances are only given in ranges.

Hydrazine Sulfonates	Analyzed Compounds	S–N / pm	N–N / pm
Mono 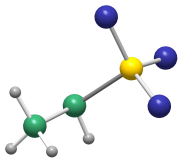	$NH_3NH(SO_3)$	168.5(2)	145.0(2)
	$Ba[NH_2NH(SO_3)]_2(H_2O)$	166.4(4)/165.9(4)	144.3(3)/143.8(5)
Di 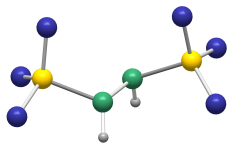	$(C_5H_6N)_2[(SO_3)HNNH(SO_3)]$ $A_2[(SO_3)HNNH(SO_3)](H_2O)$ (A= (NH_4), K, Rb, Cs) $Ba[(SO_3)HNNH(SO_3)](H_2O)_2$	167.7(2)-177(2)	141.9(3)-143.7(4)
Iso-di 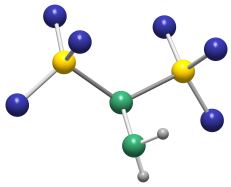	$K_2[H_2NN(SO_3)_2]$	170.7(2)/171.1(2)	143.6(3)
	$Ba[H_2NN(SO_3)_2](H_2O)_2$	169.8(2)/171.6(2)	143.5(2)
Tetra 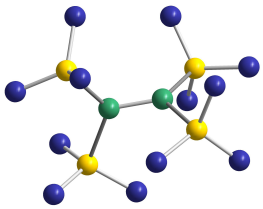	$K_4[(SO_3)_2NN(SO_3)_2](H_2O)$	170.5(2)-173.4(2)	137.2(2)/138.5(5)
	$K_4[(SO_3)_2NN(SO_3)_2](H_2O)_2$		
			

The distances between the nitrogen atoms are 145.0(2) pm (acid) and 143.8(5)/144.3(5) pm (Ba^{2+}-salt) and between the sulfur and nitrogen atoms 168.5(2) pm (acid) and 166.4(4)/165.9(4) pm (Ba^{2+}-salt). The compounds were isolated single phase pure, the thermal behavior was outlined and by *Raman* spectroscopic analysis, the vibrational modes in comparison with quantum mechanical calculations were correlated. Syntheses of the acid and the barium salt starting from $Py{\cdot}SO_3$ are unfortunately not straightforward and suffer from poor yield and formation of by-products, which are hard to separate. The pure acid is stable up to 209 °C. Above this temperature decomposition occurs, producing the intermediate $(NH_4)_2SO_4$, directly followed by exothermic conversion to H_2SO_4. The barium salt undergoes dehydration in the first step and starts to decompose to $BaSO_4$ at 200 °C. For the acids, additionally a *Hirshfeld* surface analysis was conducted, which revealed a pronounced hydrogen bonding in the structure.

The syntheses of hydrazine disulfonates and *iso*-disulfonates, on the other hand were much more convenient. Concerning the hydrazine disulfonates, first $(C_5H_6N)_2[(SO_3)HNNH(SO_3)]$ was isolated in a sufficient yield by sulfonating $N_2H_6SO_4$ with $ClSO_3H$ in pyridine. In alkaline salt metathesis with the pyridinium salt numerous salts (NH_4^+, K^+, Rb^+, Cs^+ and Ba^{2+}) were prepared, analyzed and compared. The compounds were all obtained as hydrates. Analyzed single crystals of the alkali (K^+, Rb^+, Cs^+) salts and the ammonium salt have similar cell parameters with deviation due to the size of the cations.

The single crystal XRD examination further unveiled the chirality of $[(SO_3)HNNH(SO_3)]^{2-}$ with stereocenters at the nitrogen atoms. For all salts no enantiomerically pure crystallization was observed, as they do not crystallize in *Sohncke* type space groups. The N–N bond undergoes a slight contraction compared to the monosulfonated derivatives. Upon heating the alkali and alkaline earth hydrazine disulfonates decompose to the corresponding sulfates. The barium salt, $Ba[(SO_3)HNNH(SO_3)](H_2O)_2$ cannot be thermally dehydrated and converts to $BaSO_4$ and $(N_2H_6)SO_4$ at 100 °C.

Aside from the disulfonate, the synthesis and structure of isomeric *iso*-disulfonate, $[H_2NN(SO_3)_2]^{2-}$, was elaborated. Synthetically, a different approach was required to achieve double substitution on the same nitrogen atom. The $[N(SO_3)_2]$ fragment is pre-assembled in the imido-*bis*-sulfonate $K_2[K[HN(SO_3)_2]$, which was coupled with H_2NOSO_3H under alkaline conditions to form $[H_2NN(SO_3)_2]^{2-}$. The potassium salt, $K_2[H_2NN(SO_3)_2]$, was obtained single-phase pure and XRD structure analysis proved the presence of two SO_3 groups at the same nitrogen atom. It further showed similar thermal behavior as $K_2[(SO_3)HNNH(SO_3)](H_2O)$ with decomposition of the hydrazine unit starting at 220 °C and forming K_2SO_4 as remaining phase. Salt metathesis with $BaCl_2$ was suitable for the preparation of $Ba[H_2NN(SO_3)_2](H_2O)_2$. According to a *Rietveld* refinement this compound was also isolated in a crystallographically phase-pure form. The *iso*-disulfonate N–N bond lengths are similar to those observed in the other hydrazine disulfonates.

As a third species the elusive hydrazine tetrasulfonate anion was elucidated in two structures, namely $K_4[(SO_3)_2NN(SO_3)_2](H_2O)_2$ and $K_4[(SO_3)_2NN(SO_3)_2](H_2O)$.

By reacting $(C_5H_6N)_2[(SO_3)HNNH(SO_3)]$ and NaOCl very small amounts of the tetrasulfonate were generated. The proposed labile azo-disulfonate $[O_3SN{=}NSO_3]^{2-}$ could not be isolated.[23] The structures of the two hydrates were distinguished by single crystal XRD. The *Rietveld* analysis of a crystalline powder sample proved co-crystallization of the monohydrate and dihydrate. *Raman* analysis of a single crystal shows a clean spectrum with no presence of N–H stretching vibration.

4.4 Azidosulfates

4.4.1 $(TBA)_4(N_3)_3[SO_3N_3]$ and $(TBA)[SO_3N_3]$

Recently, *Wickleder et al.* presented the hitherto unknown cyanidosulfate anion $[SO_3CN]^-$.[165] The anion was stabilized in the salt $(TBA)[SO_3CN]$ (TBA = $[N(C_4H_9)_4]^+$) and the preparation was achieved by sulfonation of (TBA)CN with $Py{\cdot}SO_3$ in 1,4-dioxane. Advantages are the high solubility of TBA-salts in organic solvents and the mild sulfonating ability of $Py{\cdot}SO_3$. First experiments on sulfonation of azides as NaN_3 with liquid SO_3 has led to explosive reactions and was therefore avoided as a route for further experiments.

$$[N(C_4H_9)_4]N_3 + (C_5H_5N){\cdot}SO_3 \xrightarrow[40\ °C]{n\text{-hexane}} [N(C_4H_9)_4][SO_3N_3] + C_5H_5N$$

Scheme 17: Synthesis of $(TBA)[SO_3N_3]$.

Considering the results for $(TBA)[SO_3CN]$, commercially available $(TBA)(N_3)$ was used in sulfonating reactions with $Py{\cdot}SO_3$ with different solvents. A reaction between $(TBA)(N_3)$ (1.00 eq.) and $Py{\cdot}SO_3$ (1.00 eq.) in *n*-hexane performed in sealed glass ampoules at 40 °C yielded colorless single crystals. The crystals were assigned to recrystallized $Py{\cdot}SO_3$ and to the novel compound $(TBA)_4(N_3)_3[SO_3N_3]$. This mixed anionic species provided the second structural evidence for the $[SO_3N_3]^-$ anion (see Figure 55, p.85). More experiments on this reaction were done by the author and *A. N. Udaya* who obtained $(TBA)[SO_3N_3]$ by increasing the stoichiometric amount of $Py{\cdot}SO_3$ (1.10 eq.). $(TBA)[SO_3N_3]$ hence represents the first pure azidosulfate crystallographically described (see Figure 56, p. 85).

$(TBA)_4(N_3)_3[SO_3N_3]$ crystallizes in the monoclinic space group $P2_1/c$ with four formula units per unit cell. The large unit cell (V = 7.5503(5) nm^3), which can be deduced to the bulky $(TBA)^+$ cation. $(TBA)[SO_3N_3]$ was solved in the same space group, but the unit cell is significantly smaller (V = 2.7406(3) nm^3). In Table 16 selected crystallographic data of both compounds are compared.

Table 16: Selected crystallographic data of the two azidosulfates, $(TBA)_4(N_3)_3[SO_3N_3]$ and $(TBA)[SO_3N_3]$.

	$(TBA)_4(N_3)_3[SO_3N_3]$	**$(TBA)[SO_3N_3]$**
Crystal System	Monoclinic	Monoclinic
Space Group	$P2_1/c$	$P2_1/c$
a / pm	1280.40(5)	976.02(4)
b / pm	2704.5(1)	1281.46(6)
c / pm	2208.49(9)	1747.82(8)
β / °	100.682(2)	104.973(2)
V / nm^3	7.5503(5)	2.7406(3)
Z	4	4
R_1 (all data); wR_2 (all data)	0.1020; 0.2610	0.0551; 0.1129
GooF	1.041	1.062

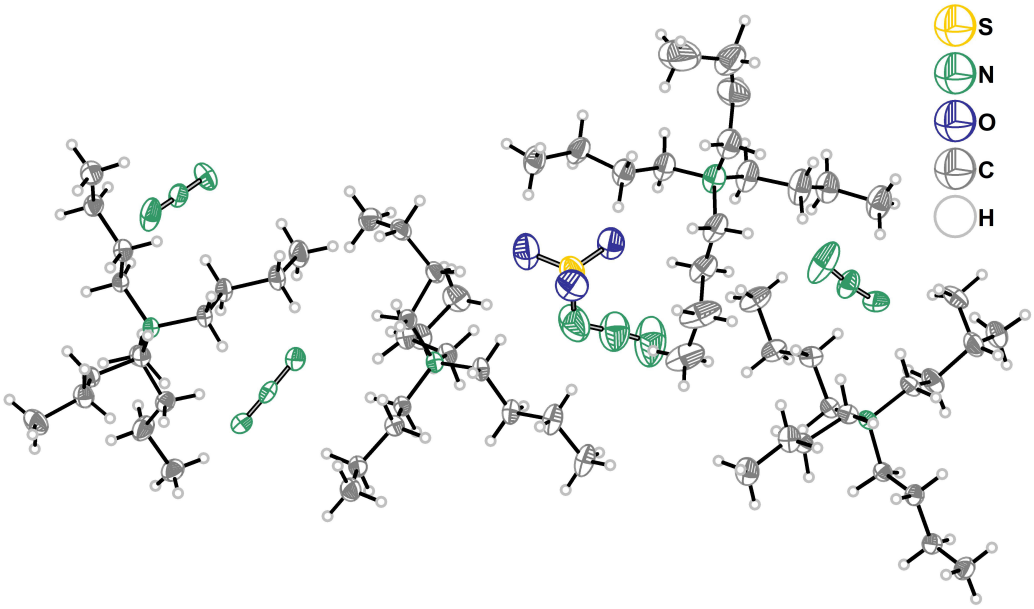

Figure 55: Asymmetric unit of $(TBA)_4(N_3)_3[SO_3N_3]$ with thermal ellipsoids set to a probability level of 50%.

During refinement of $(TBA)_4(N_3)_3[SO_3N_3]$ rotational disorder at one butyl chain was treated. A position of a terminal carbon atom was split into two with occupancies of 43% (C57) and 57% (C56). Four $(TBA)^+$, three N_3^- and one $[SO_3N_3]^-$ are crystallographically distinguishable in the cell and all atoms lie on general sites (*Wyckoff 4e*).

In $(TBA)[SO_3N_3]$ no disorder was observed and overall good quality factors for the refinement were achieved. The crystal structure contains one unique $(TBA)^+$ and one unique $[SO_3N_3]^-$ located at general sites (*Wyckoff 4e*). The $(TBA)^+$ cation shows no special structural features. The nitrogen atom (N4) is surrounded by four butyl-chains ($-C_4H_9$) in a tetrahedral manner. Within the chains the carbon atoms lie almost on the same plane with dihedral angles (∠C–C−C–C) near to 180°.

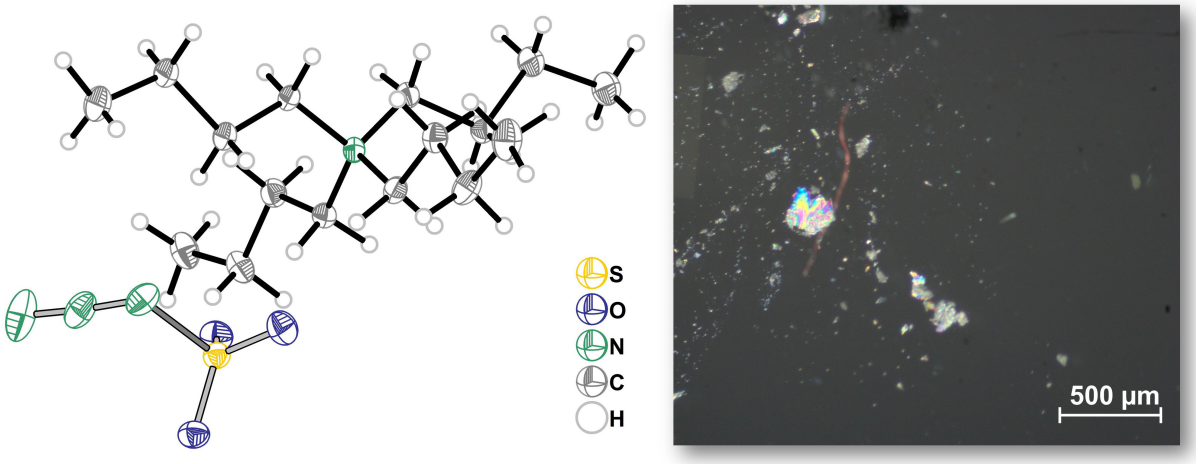

Figure 56: Structure of $(TBA)[SO_3N_3]$ (left) and light microscope image of the measured single crystal. Thermal ellipsoids are set to a probability level of 50%.

In $(TBA)_4(N_3)_3[SO_3N_3]$ some butyl chains are skewed (∠C–C−C–C: 60°-80°) due to the disorder and packing in the crystal structure.

A structural comparison of $[SO_3N_3]^-$ found in both structures is illustrated in Figure 57. The observed S–N distances for $[SO_3N_3]^-$ are 171.9(5) pm in $(TBA)_4(N_3)_3[SO_3N_3]$ (S1–N13) and 174.8(1) pm in $(TBA)[SO_3N_3]$ (S1–N1). In the disordered azidosulfate observed by *Christe et al.*[113] ($Cs[SO_3N_3]\cdot Cs[SO_2N_3]$), a length of 175.4(1) pm was found.

In the sulfonate groups of both anions the S–O distances are in between 140.2(3) pm and 144.4(3) pm. In the azido group, asymmetry in the N–N bonds is visible, also described in the literature-known azidosulfate. The terminal N–N distances are 113.0(2) pm (N2-N3) and 113.6(6) pm (N13–N15), whereas the adjacent distances are 123.4(2) pm (N1-N2) and 122.7(6) pm (N13-N14), respectively. The covalent azides show similar bonding characteristics with bond orders that are in between 1-2 for the short bond (N_α–N_β) and 2-3 for the longer bond (N_β–N_γ).[107,166] There is also minor bending of the azide group with angles of 175.3(2)° (∠N3–N2–N1) and 175.2(6)° (∠N15–N14–N13). In contrast, for ionic azides linear $D_{\infty h}$ symmetry for the $[N_3]$ moieties is mostly observed with symmetrical N–N distances of around 117 pm (e.g. NaN_3 or NH_4N_3).[109,167-169] The free azide anions in the structure $(TBA)_4(N_3)_3[SO_3N_3]$ exhibit no perfect $D_{\infty h}$ symmetry and the N–N distances are ranging from 114.2(3) pm to 118.3(5) pm.

The azide groups in both structures are positioned angled to the SO_3 groups, which was already observed by *Christe*[113] (see Figure 57). The angles found for ∠S–N−N are 112.4(4)° (S1–N13–N14) and 111.7(1)° (S1–N1–N2) (*Christe*: 114.5°). One visible difference is the position of $[N_3]$ in relation to the oxygen atoms in both structures. By viewing along the S–N bond in $(TBA)[SO_3N_3]$, $[N_3]$ is almost located in between the oxygen atoms O3 and O2 and *trans* oriented to O1 (∠N2–N1−S1–O1: 174.9(1)°).

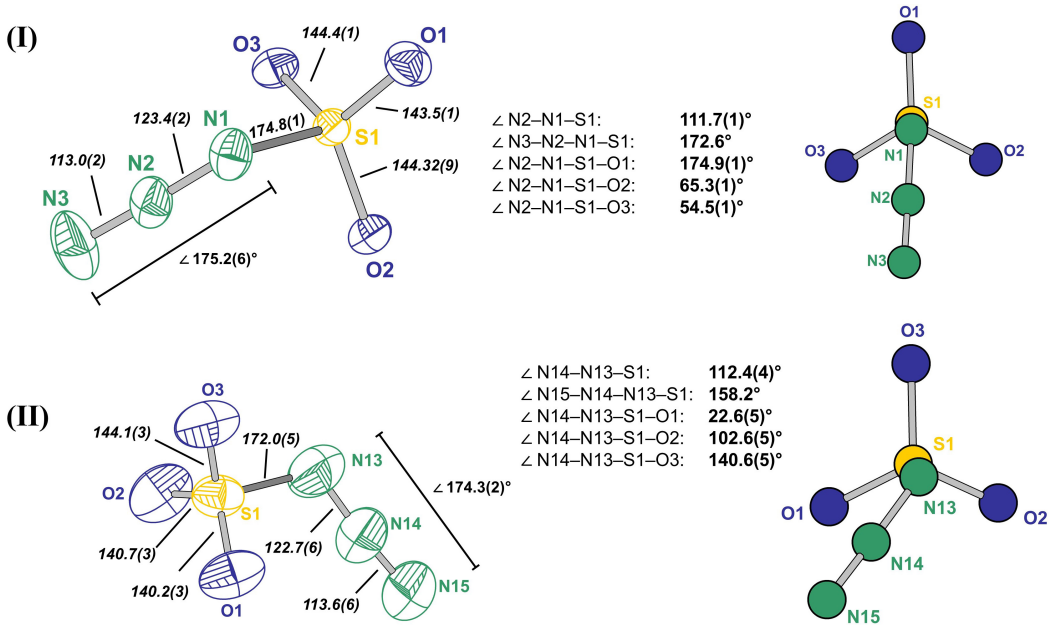

Figure 57: Structure and labeling of the two $[SO_3N_3]^-$ anions found in $(TBA)[SO_3N_3]$ (**I**) and $(TBA)_4(N_3)_3[SO_3N_3]$ (**II**) with selected bond lengths (italics, in pm) and angles. On the right, both anions are depicted along the N–S bond.

In $(TBA)_4(N_3)_3[SO_3N_3]$, the $[N_3]$ moiety is more shifted towards O1 in a *cis* like manner (∠N14–N13–S1–O1: 22.6(5)°). This orientation was also reported by *Christe*[113] and further discussed with the quantum mechanical calculations (MP2/6-31+G(d) level of theory). The weak S–N bonding results in pronounced rotation along S–N and *cis* or *trans* orientation is mainly influenced by interactions with cations and packing in the crystal structure. The weak S–N bond is associated with a distorted tetrahedral arrangement around the sulfur atoms.

In the crystal structure of $(TBA)[SO_3N_3]$ the azidosulfate anions are packed between the bulky TBA cations showing minor interaction (Figure 58). Closest donor–acceptor contact between the anion and the butyl chains is 329.99(2) pm (O3–C5) and in total six TBA cations are surrounding $[SO_3N_3]^-$.

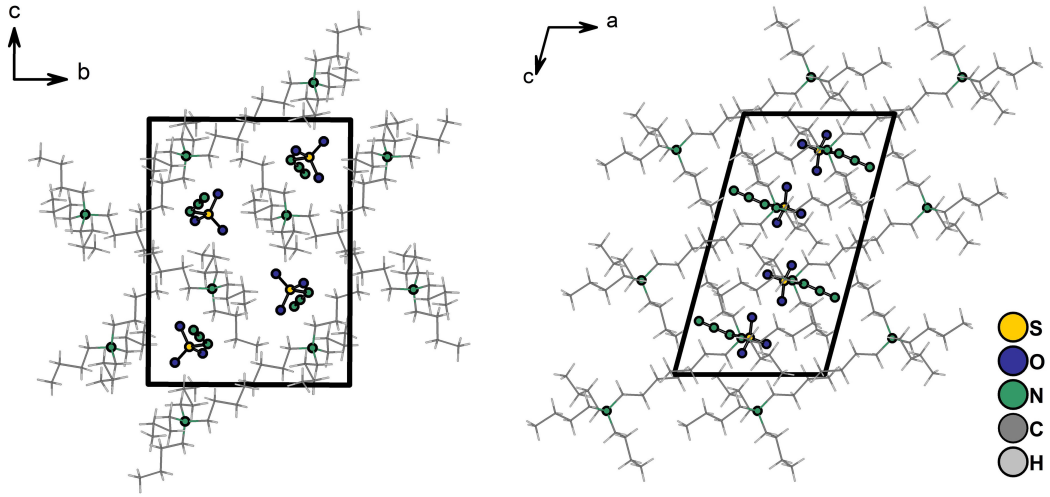

Figure 58: Crystal structure cut-out of $(TBA)[SO_3N_3]$ along the crystallographic axes *a* (left) and *b* (right). The butyl chains are depicted in a wire-stick representation.

In $(TBA)_4(N_3)_3[SO_3N_3]$ incorporation of $[SO_3N_3]^-$ in between six TBA cations is observed and the closest contact to the butyl chain is 318.(6) pm (N15–C61) (see Figure 59).

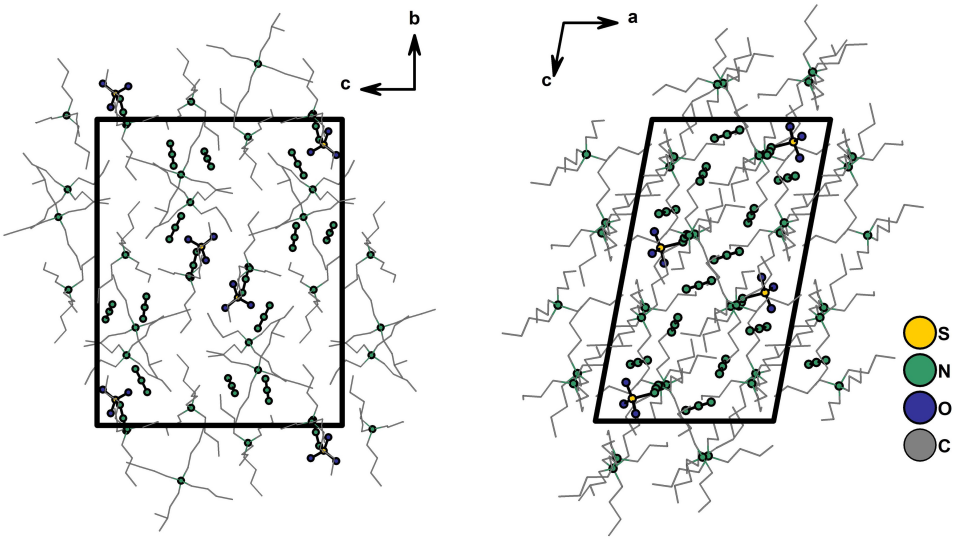

Figure 59: Extended unit cell of $(TBA)_4(N_3)_3[SO_3N_3]$ along the crystallographic axes *a* and *b*. Hydrogen atoms were omitted for clarity. The butyl chains are depicted in a wires and sticks representation.

4.4.2 $K[SO_3N_3]$

For the preparation of literature-known but analytical scarcely investigated $K[SO_3N_3]$, a different synthetic route was chosen than the previously mentioned one. *Christe et al.* already prepared $Cs[SO_3N_3]$ by reacting $Cs[SO_3Cl]$ with $(TMS)N_3$.[113] The basic driving force behind this reaction is the formation of volatile and stable (TMS)Cl, which can be easily separated from the formed azidosulfate. $Cs[SO_3N_3]$ was solely investigated by *Raman* spectroscopy and no further structural evidence has yet been given.

$$K[SO_3Cl] + (TMS)N_3 \xrightarrow[RT]{MeCN} K[SO_3N_3] + (TMS)Cl$$

Scheme 18: Synthesis of $K[SO_3N_3]$ starting from $K[SO_3Cl]$ and $(TMS)N_3$.

Referring to this procedure, $K[SO_3Cl]$ was considered as a starting material to prepare $K[SO_3N_3]$. The chlorosulfate was previously synthesized in the research group by treating $KHSO_4$ with $SOCl_2$. In this reaction gaseous HCl and SO_2 are formed as by-products leaving behind phase-pure $K[SO_3Cl]$. In order to yield single crystals of $K[SO_3N_3]$, a solvothermal approach was carried out. A glass ampoule was loaded with one equivalent of $K[SO_3Cl]$ and an excess of $(TMS)N_3$ (6.50 eq.) under inert conditions in an argon glove box. Additionally, a few drops of dried MeCN were added to increase solubility of $K[SO_3Cl]$. The sealed reaction ampoule was only gently heated to 45 °C to avoid decomposition of the azide. During cooling a suspension was formed and few crystals deposited on the ampoule wall. The crystals had a platelet-like shape and were strongly intergrown. SC-XRD data examination finally revealed the structure of $K[SO_3N_3]$. Thus, the synthesis of $K[SO_3N_3]$ was scaled up in a *Schlenk* tube to yield larger amounts of $K[SO_3N_3]$ for analytical investigations. Therefore, $K[SO_3Cl]$ was stirred in an excess of $(TMS)N_3$ and MeCN for 48 h in an argon flow. Afterwards the volatile components were removed under reduced pressure and the residual phase was analyzed to be phase-pure $K[SO_3N_3]$, which was yielded as a colorless solid (see Figure 60, p. 89). The compound can be handled under ambient conditions only for a limited time since it was observed that single crystals which were exposed to air slowly decomposed to K_2SO_4 after a week.

A comparison of an X-ray powder dataset (RT) with the low temperature single crystal dataset (100 K) via *Rietveld* refinement (discussion will follow in the later part) showed large discrepancies in the assignment of the reflections. The cause of this was suspected to be a phase transition occurring at higher temperatures. Indeed, a single crystal measurement at 250 K revealed different unit cell parameters for $K[SO_3N_3]$ (for comparison see Table 17, p. 89). The crystallographic *a*-axis is elongated by 68 pm and the monoclinic angle adopts a value of 108.582(2)° compared to 90.83(1)° of the 100 K dataset. This symmetry change was then also confirmed in a *Rietveld* refinement.

During the SC-XRD analysis of the 100 K dataset (**b**), a second domain was observed in the cell analysis and the data integration and absorption correction was done as a two-component twin. The structure of $K[SO_3N_3]$ was solved in the monoclinic crystal system with a symmetry best described by the space group $P2_1/c$. The asymmetric unit consists of one potassium cation and one $[SO_3N_3]^-$ anion and all atoms are located at general sites (*Wyckoff 4e*) of the unit cell. At 250 K (**a**) the compound also crystallizes in the monoclinic space group $P2_1/c$ with the differences in cell parameters already mentioned. Therein all atoms are located at *Wyckoff* sites *4e*, too.

Table 17: Selected single crystal data of $K[SO_3N_3]$ measured at 250 K (**a**) and 100 K (**b**).

	$K[SO_3N_3]$ (a)	**$K[SO_3N_3]$ (b)**
Temperature	250 K	100 K
Crystal System	Monoclinic	Monoclinic
Space Group	$P2_1/c$	$P2_1/c$
a / pm	985.70(5)	917.8(3)
b / pm	718.09(3)	708.3(2)
c / pm	744.79(3)	743.7(2)
β / °	108.582(2)	90.83(1)
V / nm^3	0.49970(4)	0.4834(2)
Z	4	4
R_1 (all data); wR_2 (all data)	0.0388, 0.0695	0.1052; 0.1382
GooF	1.057	1.109

As expected, the anisotropic displacement parameters are smaller within the low-temperature structure. The solid state structures of $[SO_3N_3]^-$ are quite similar in their bonding properties and are comparable to the two aforementioned $[SO_3N_3]^-$ structures (see Figure 60). The S–N distances are 171.1(2)(**a**)/171.0(6)(**b**) pm.

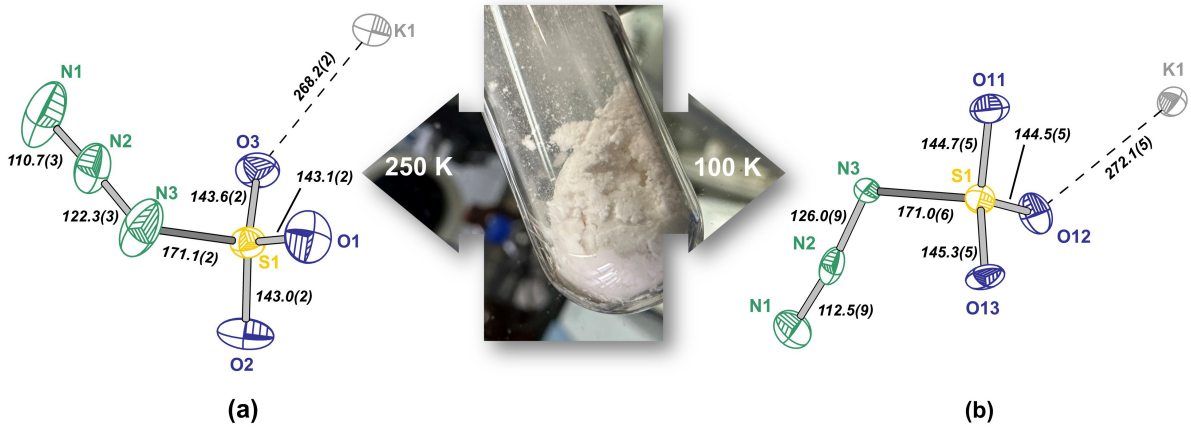

Figure 60: Structure and labeling of $K[SO_3N_3]$ measured at 250 K (**a**) (left) and 100 K (**b**) (right) with atomic distances (italics, in pm). The thermal ellipsoids are set to a probability level of 50%. In the center powdered $K[SO_3N_3]$ is shown.

An angled position of the $[N_3]$ unit to SO_3 is also recognizable with a measured angle ∠S1–N3–N2 of 114.6(5)°(**a**)/114.9(2)°(**b**) (see Figure 61). Covalent bonding of the azide, again, results in different N–N distances with 122.3(3)(**a**)/126.0(9)(**b**) pm (N3–N2) and 110.7(3)(**a**)/112.5(9)(**b**) pm (N2–N1).

N_3 has no linear shape and is slightly bended according to an angle of 174.1(3)°(**a**)/173.5(7)°(**b**). The sulfonate groups in both modifications have common S−O distances between 143.6(2) pm and 145.3(5) pm. The main structural difference between the low and high temperature modification is the relative orientation of the azide group to the SO_3 group (see Figure 61).

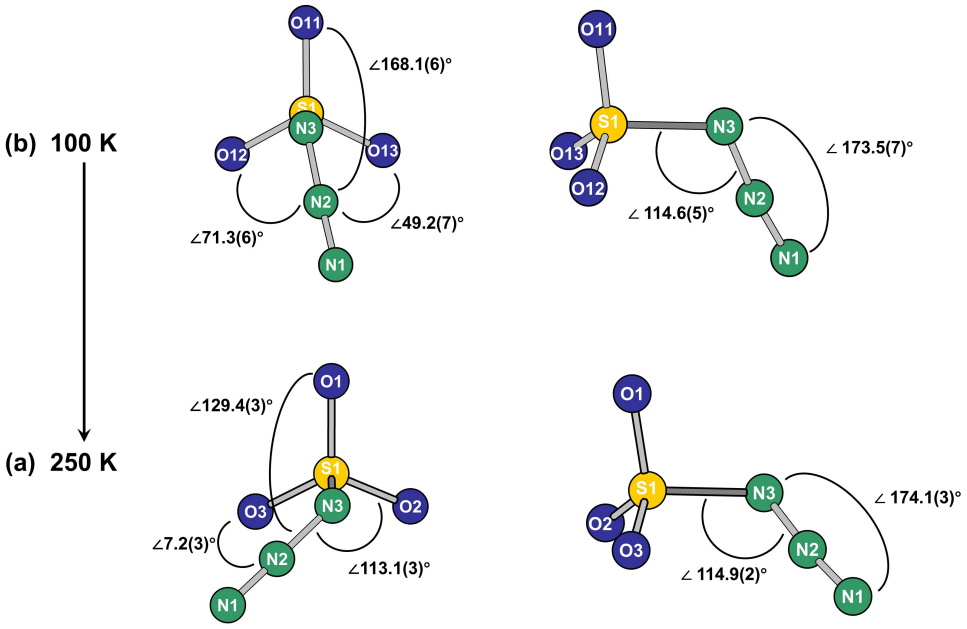

Figure 61: Structure of $[SO_3N_3]^-$ observed at 100 K (**b**) (top) and 250 K (**a**) (bottom), each along two viewing directions with marked angles (∠S–N–N, ∠N–N–N) and dihedral angles (∠N–N–S–O).

For (**b**) a view along the N3−S1 bond shows that N_3 is oriented almost in an antiperiplanar manner to O11 (168.1(6)°) and lies in between O12 and O13. The smallest dihedral angle for (**b**) is 49.2(7)° (∠N2–N3–S1–O13). In contrast, the anion within the high-temperature modification (**a**) has a synperiplanar (*cis*) orientation of N_3 to oxygen O3 with an observed dihedral angle ∠N2–N3–S1–O3 of 7.2(3)°. This temperature-induced rotation along the S–N bond can thus be regarded as the main cause of the symmetry change.

In Figure 62 (p. 91) the unit cell depiction of both structures illustrates the different orientation of the azide groups viewed along the crystallographic *b*-axis. For both modifications, however, the $[N_3]$ groups are oriented towards each other, while the $[SO_3]$ groups are oriented to the cationic potassium sites.

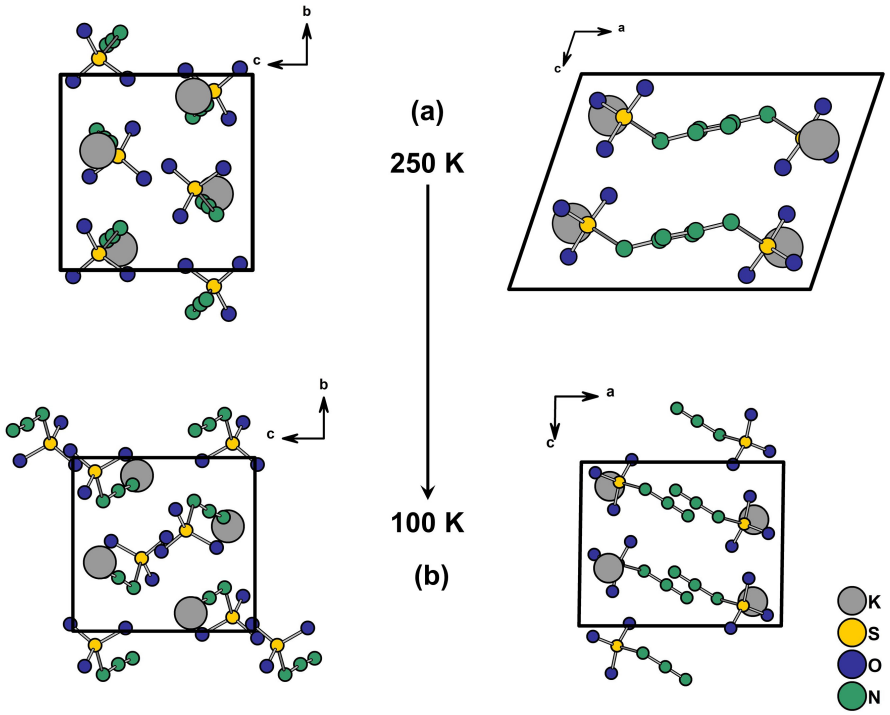

Figure 62: Extended unit cell of $K[SO_3N_3]$ (**a**) (top)/(**b**) (bottom) viewed along the crystallographic axes *a* (left) and *b* (right).

In both structures, the potassium cations are tenfold coordinated by eight oxygen and two nitrogen atoms according to a *CHARDI* analysis (see Figure 63).[142] K–O distances are in the same range with 272.1(5)-298.8(5) pm for (**b**) and 268.2(2)-303.0(2) pm for (**a**). Relevant distances to nitrogen are 301.9(8) pm (N1) and 298.4(6) pm (N3) for the low temperature structure.

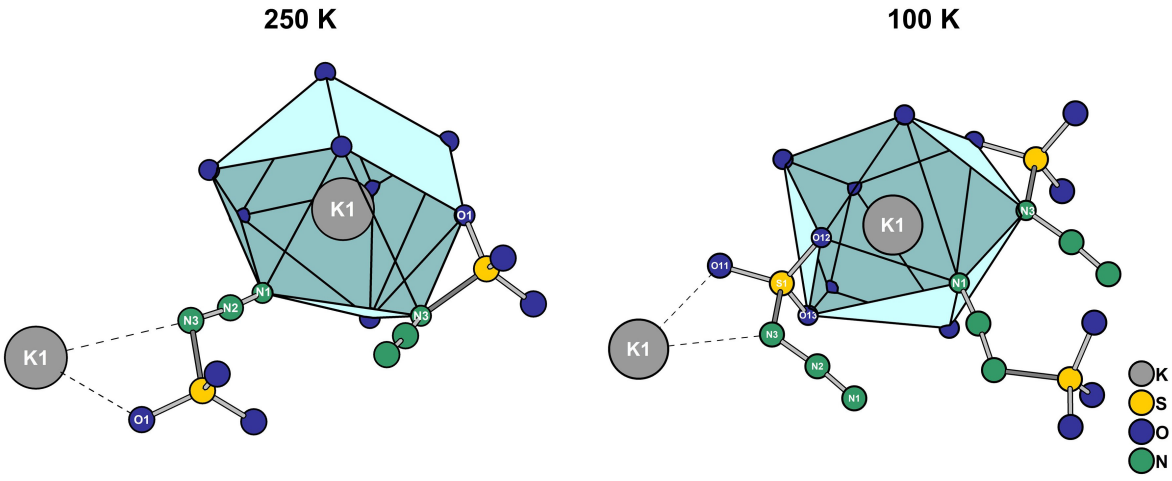

Figure 63: Coordination sphere of the potassium cation observed in the two structures measured at 250 K (**a**) (left) and 100 K (**b**) (right) with illustration of the polyhedra.

In the 250 K structure distances of 300.6(2) pm (N1) and 340.8(3) pm (N3) are found within the coordination sphere. In both cases a monodentate and bidentate coordination of $[SO_3N_3]^-$ takes place. In the bidentate case, the coordination occurs both via O⁀O and N⁀O. The resulting coordination polyhedra have no specific or approximate geometric shape, which was checked with *Polynator*.

In order to verify crystalline phase-purity, a *Rietveld* refinement a powder sample was performed (see Figure 64). A sufficient refinement with the low temperature phase was not achieved for crystallographic causes already mentioned. The refinement with the SC-dataset collected at 250 K shows a good profile fitting with all dominant reflections of the diffractogram being assigned and only minor deviations in the intensities. For the reflections at 11.5° (hkl (020) and (002)) and 12.7° (hkl (021)) the greatest discrepancies are observed. Refinement with a preferred orientation for these reflections could not rectify the differences in intensities.

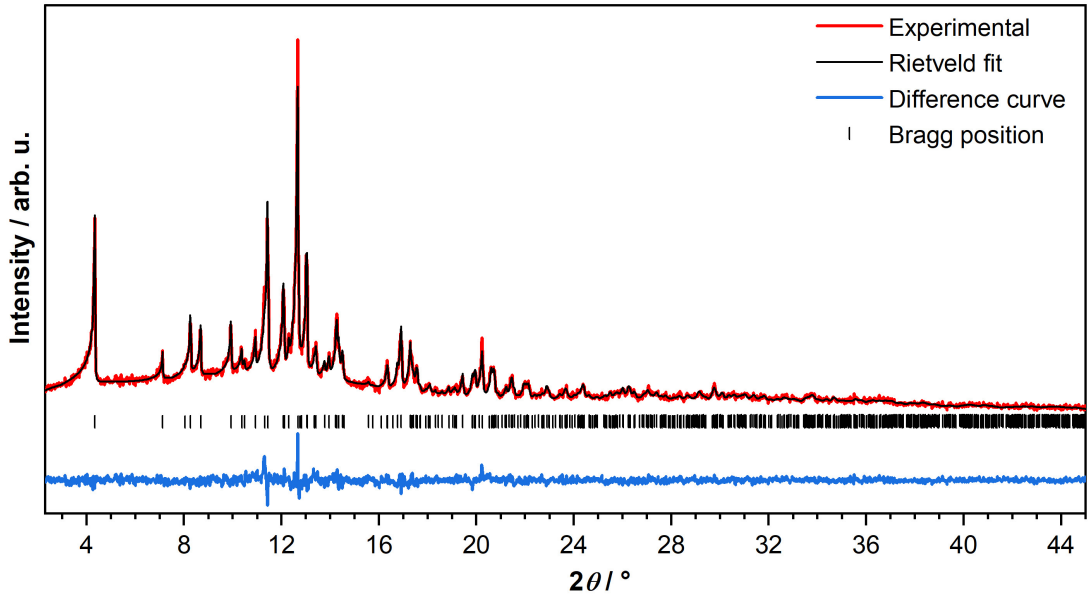

Figure 64: Experimental powder X-ray diffraction pattern of $K[SO_3N_3]$ with *Rietveld* refinement using single crystal data of (**a**). The powder was measured in an 0.3 mm capillary with Mo-$K_{\alpha 1}$ (λ = 70.930 pm) radiation at room temperature. The cell parameters *a*, *b*, *c* and *β* and the positions off all atoms excluding N1 were refined.

The refined cell parameters do not deviate greatly from the measured ones and the profile factors are of high quality (see Table 18).

Table 18: Cell parameters and profile factors from the *Rietveld* refinement of $K[SO_3N_3]$ (**a**) compared to the original cell parameters of $K[SO_3N_3]$ (**a**).

	***Rietveld* Refinement**	**$K[SO_3N_3]$ (a)**
Temperature	RT	250 K
Crystal System	Monoclinic	Monoclinic
Space Group	$P2_1/c$	$P2_1/c$
a / pm	983.59(6)	985.70(5)
b / pm	720.40(4)	718.09(3)
c / pm	747.40(5)	744.79(3)
β / °	107.688(7)	108.582(2)
V / nm^3	0.50456(6)	0.49970(4)
R values	R_{wp} = 6.74%; R_{exp} = 6.72%; R_p= 5.25%	
GooF	1.003	

Additionally, an IR and *Raman* spectroscopic analysis of $K[SO_3N_3]$ was performed (see Figure 65). The IR spectrum was recorded on a powdered sample and *Raman* spectrum on a single crystal. The assignment was done with theoretical values of the anion (MP2 and B3LYP level of theory) and experimental values of the compound $CsSO_3N_3$ reported by *Christe et al*. In addition, a calculation within this work at PBE0 level of theory was conducted (for more details see 7.3.3, p.130 and 6.9, p.116). The positions of the bands of both spectra correspond well. Due to device-specific limitations, the IR measurement ends at 400 cm^{-1}.

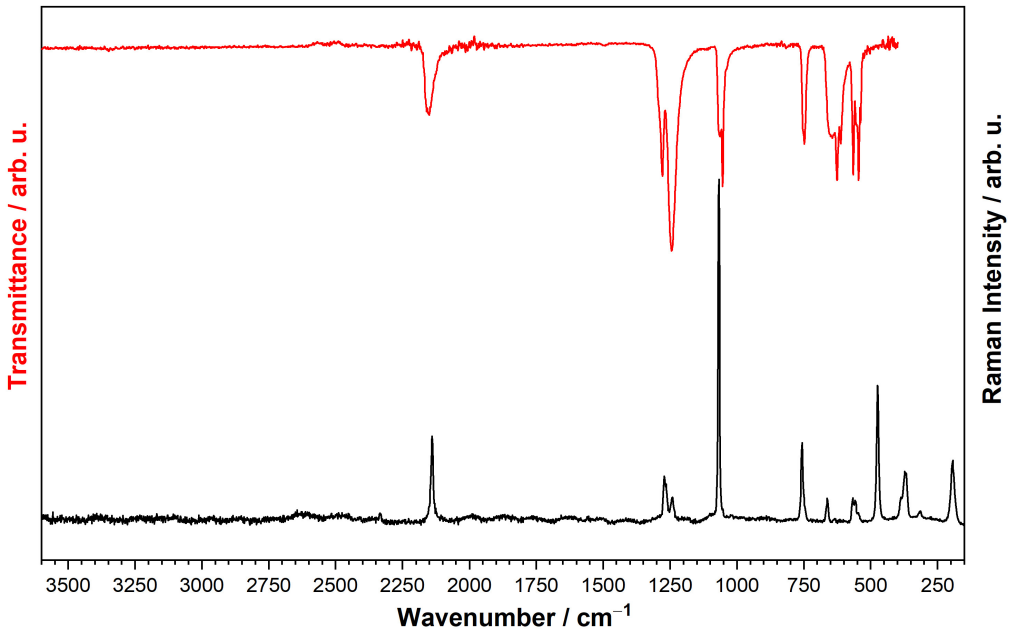

Figure 65: *Raman* (bottom) and IR (top) spectrum of $K[SO_3N_3]$. The *Raman* spectrum was measured on a single crystal using a green laser (λ = 532 nm) at RT.

In the IR spectrum of powdered $K[SO_3N_3]$ no bands for C–H stretching vibrations of residual TMS above 3000 cm^{-1} are visible. The characteristic antisymmetric stretching bands of the azide group are located at 2150 cm^{-1} (IR) and 2140 cm^{-1} (*Raman*). Symmetric stretching vibrations of the SO_3 groups are present at 1278 cm^{-1} (IR) and 1271 cm^{-1} (*Raman*). The $\nu_s(SO_3)$ is visible at 1064 cm^{-1} and 1066 cm^{-1} in form of strong bands. Further bands of deformation modes of the azide and sulfonate groups are in between 500-760 cm^{-1} (see Table 19). The band at 474 cm^{-1} in the *Raman* spectrum results from symmetric stretching vibration of S–N.

Table 19: Assignment of the experimental Raman and IR bands of $K[SO_3N_3]$ with calculated values from a geometry optimization (see 7.3.3, p. 130).

Assignment	Exp. IR / cm^{-1}	Exp. *Raman* / cm^{-1}	Calcd. / cm^{-1}
$\nu_{as}(N_3)$	2150s	2140	2262
$\nu_s(N_3)$	1278s	1271	1365
$\nu_{as}(N_3)$	1243vs	1241	1313
$\nu_s(SO_3)$	1064sh 1053s	1066	1064
$\delta(N_3)$ in plane	747s	758	748
$\delta(N_3)$ out of plane	650sh	662	639

Assignment	Exp. IR / cm^{-1}	Exp. *Raman* / cm^{-1}	Calcd. / cm^{-1}
$\delta(SO_3)$ umbrella	625s 613s	-	611
$\delta(SO_2)$	565s 552sh 544s 538sh	567 558 547	543 542
ν_s(S–N)	-	474	415
$\tau(SO_3)$	-	387 372	345
$\omega(SO_3)$	-	313	336
$\delta(SN_3)$	-	193	142

Thermal behavior of $K[SO_3N_3]$ was additionally investigated after assurance of phase-purity (see Figure 66 and Table 20). Azides in general tend to explode upon heat exposure, sometimes even upon mechanical impact, and must therefore be handled with caution. For $K[SO_3N_3]$ the only verified thermal information is that it explodes with an intense sound under heating at ambient conditions.[22] This could be attested during preparation of capillaries for P-XRD measurements, where explosions of $K[SO_3N_3]$ were noticed. Considering that, a thermogravimetric analysis (TG-DSC) of a 13.5 mg sample with a heating rate of 5 $K \cdot min^{-1}$ up to 1000 °C under an argon flow. Under these parameters, the compound showed no explosive decomposition. Overall, the azidosulfate undergoes a three-step thermal decomposition down to a remaining mass of 53.5%, which plateaus during the cooling process.

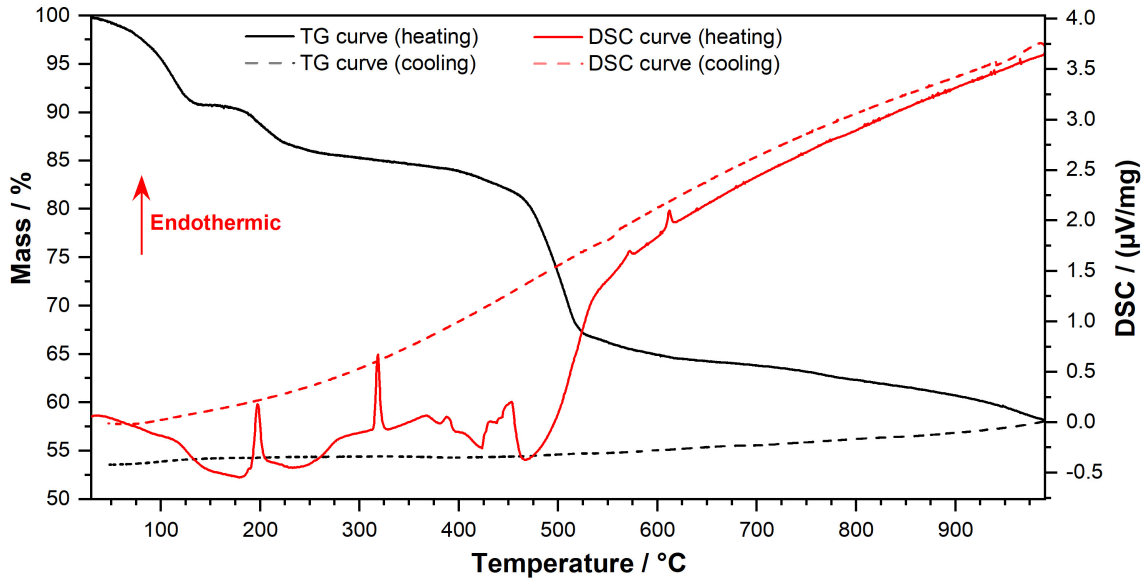

Figure 66: TG/ DSC measurement of $K[SO_3N_3]$. The sample was measured in a corundum crucible with a heating rate of 5 $K \cdot min^{-1}$ under an argon flow (80 $mL \cdot min^{-1}$).

In the TG curve the first decomposition step starts at 84 °C and finishes at around 150 °C accompanied by a small broad endothermic signal. In this step a mass loss of 9% is observed. This is immediately followed by an endothermic step (peak: 197 °C), which starts at 192.5 °C and ends around 202.6 °C.

Table 20: Assignment of the thermal decomposition/ transition steps $K[SO_3N_3]$.

DSC/ Step	T_{onset}/ °C	T_{end}/ °C	T_{max}/ °C	Mass loss/ (obsd./*calc.*) %	Proposed transitions/ decomposition
I	82.2	148.5	107.3	9.0	Formation of $K_2S_2O_7$ (O_2 impurities)
II	192.5	202.6	197.4	5.7	Formation of $K_2S_2O_7$ + Enantiotropic solid–solid transition γ→ β
III	314.9	318.7	322.2	-	Enantiotropic solid–solid transition β→ α
IV	383.2	387.9	393.9	-	Melting of $K_2S_2O_7$
V	454.0	513.9	466.9	31.2/ *31*	Broad decomposition of $K_2S_2O_7$ to K_2SO_4
Total				45.9/ *46*	Residual phase: K_2SO_4

In this step a mass loss of 5.7% occurs. In the following plateau of the TG curve a strong endothermic signal, starting at 315 °C with a peak at 319 °C and a small endothermic signal, starting at 384 °C, are visible in the DSC curve. From there on a last decomposition step over a broad temperature range proceeds (up to 1000 °C). It starts at 454 °C accompanied with a broad exothermic signal. The resulting phase was assigned to K_2SO_4 by powder XRD (see 7.2.1, p. 125), which agrees with the observed total mass loss. Further attempts were then made to isolate the intermediate steps. For this purpose, one sample was heated to 230 °C and held at this temperature while monitoring the TG curve. As soon as the stable plateau was reached, the measurement was stopped and the resulting phase was analyzed by powder XRD. The reflections were assigned to high-crystalline phase-pure $K_2S_2O_7$ (see 7.2.2, p. 125). This is further confirmed by the DSC curve. The endothermic signals at 197.4 °C and 319 °C are enantiotropic solid–solid transitions of $K_2S_2O_7$ according to γ→β and β→α, respectively.[170-173] And the small endothermic signal starting at 383 °C indicates the melting of $K_2S_2O_7$.[173] Formation of the latter, however, indicates the presence of O_2 in the TG chamber since $K[SO_3N_3]$ cannot convert stoichiometrically to $K_2S_2O_7$.

In another TG analysis a sample of $K[SO_3N_3]$ was heating up to 130 °C and the temperature was maintained for 30 min to isolate the first plateau. In this step a vanishing of the $\nu_{as}(N_3)$ band in the IR spectrum was already observed (see 7.1.1, p. 124). This strongly indicates that the azide group already undergoes decomposition in the first step. In total a decomposition equation according to $2\ K[SO_3N_3] \longrightarrow K_2SO_4 + SO_2 + 3\ N_2$ can be stated. The thermal lability was also recognized by recrystallization of $K[SO_3N_3]$ from warm ethanol (60 °C). *Traube et al.* reported the yield of a phase-pure product by this method, while this is not confirmed for the herein concluded experiments, which showed the formation of potassium ethyl sulfate single crystals instead.[22]

4.4.3 $Na_3[SO_3N_3]_3(CH_3CN)$

The preparation of the aforementioned TBA azidosulfates have shown that $Py{\cdot}SO_3$ can be used to sulfonate azides. Accordingly, $Py{\cdot}SO_3$ based syntheses with alkali metal azides were conducted. Sulfonation of NaN_3 with this SO_3 reagent in dry acetonitrile yielded $Na_3[SO_3N_3]_3(CH_3CN)$. Acetonitrile as aprotic polar solvent turned out to be sufficient to dissolve quantities required for the reaction of NaN_3 and $Py{\cdot}SO_3$.

$$3\,NaN_3 + 3\,(C_5H_5N){\cdot}SO_3 + CH_3CN \xrightarrow[40\,^\circ C]{CH_3CN} Na_3[SO_3N_3]_3(CH_3CN) + 3\,C_5H_5N$$

Scheme 19: Synthesis of $Na_3[SO_3N_3]_3(CH_3CN)$.

$Na_3[SO_3N_3]_3(CH_3CN)$ was analyzed by SC-XRD and crystallizes in the triclinic crystal system ($P\bar{1}$) with two formula units per unit cell (see Table 21).

Table 21: Selected crystallographic data of $Na_3[SO_3N_3]_3(CH_3CN)$.

$Na_3[SO_3N_3]_3(CH_3CN)$	
Crystal System	Triclinic
Space Group	$P\bar{1}$
a / pm	684.15(5)
b / pm	1029.88(8)
c / pm	1265.6(1)
α / °	107.137(3)
β / °	90.83(1)
γ / °	109.295(3)
V / nm^3	0.7732(1)
Z	2
R_1 (all data); wR_2 (all data)	0.0301; 0.0672
GooF	1.111

MeCN was inserted in the structure as a solvent with one molecule of MeCN per three formula units of the sodium azidosulfate (see Figure 67, p. 96).

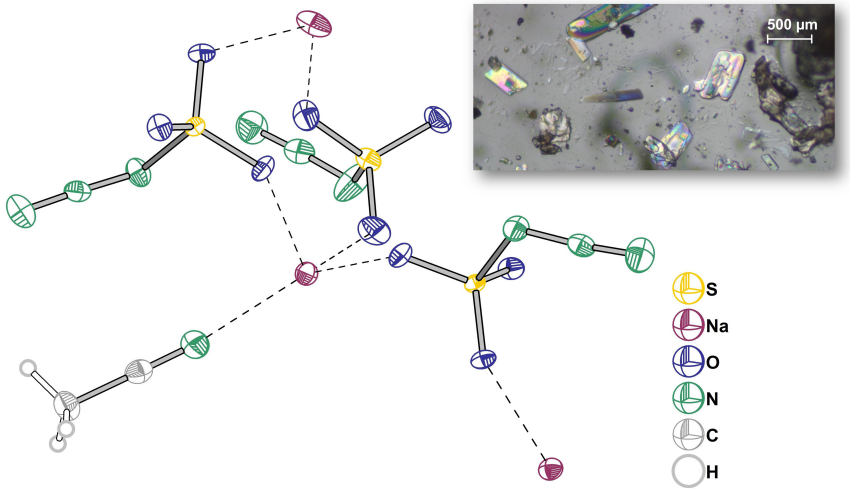

Figure 67: Structure (left) and microscope image of single crystals (top right) of $Na_3[SO_3N_3]_3(CH_3CN)$.

In the cell all atoms located at general sites (*Wyckoff 2i*). Basically, the three distinct $[SO_3N_3]^-$ show similar structural parameters as the previously discussed anions (see Figure 68, p.97). The S–N distances show minor deviations with values of 170.5(1) pm (N5–S1), 171.0(1) pm (N7–S2) and 171.7(1) pm (N10–S3). The S–O distances are approximately 144 pm and a distorted tetrahedral environment around the sulfur atom is formed. Bending of all N_3 groups is also existent with ∠N–N–N angles of 173.1(1)°, 174.0(2)° and 173.4(1)° and the orientation of N_3 towards the SO_3 group is angled with ∠N–N–S around 115°.

Striking again is the difference in the configuration of the $[N_3]$ groups relative to the oxygen atoms (see Figure 68). In two anions the $[N_3]$ groups and oxygen O1 and O4 are arranged to each other in a *syn*-periplanar manner (∠N3–N4–S1–O1: 5.8(1)°, ∠N6–N7–S2–O4: 7.5(2)°). In the other anion, $[N_3]$ is arranged in between O9 and O8 and has antiperiplanar configuration towards O7 (∠N9–N10–S3–O7: 172.4(1)°).

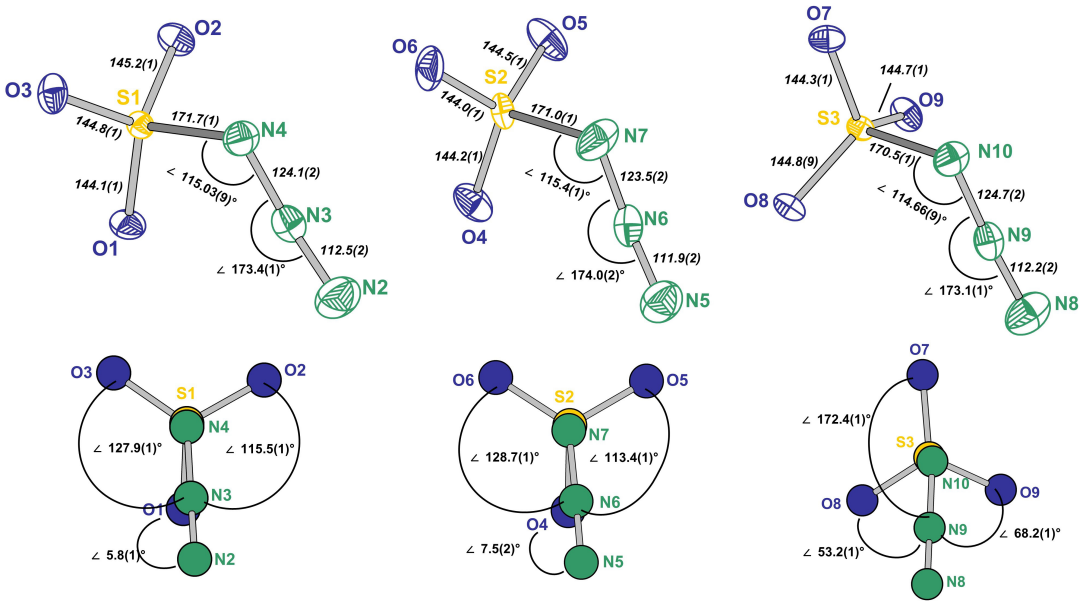

Figure 68: Structure and labeling of the three distinct $[SO_3N_3]^-$ anions observed in $Na_3[SO_3N_3]_3(CH_3CN)$. Top: depiction of the anions with bond lengths (italics, in pm) and selected angles. Bottom: anions depicted along the N–S bond with marked dihedral angles (N–N–S–O).

This observation can again be explained by a low rotation barrier along the S–N bond, which results from weak S–N bonding. In agreement to previous findings, $[N_3]$ moieties are again oriented towards each other, while the $[SO_3]$ groups are directed towards the cationic sites (see Figure 69, p.98). The sodium cations dominantly interact with the sulfonate oxygen atoms with Na–O distances observed from 230.3(1) pm up to 302.0(1) pm (see Figure 70, p. 98).

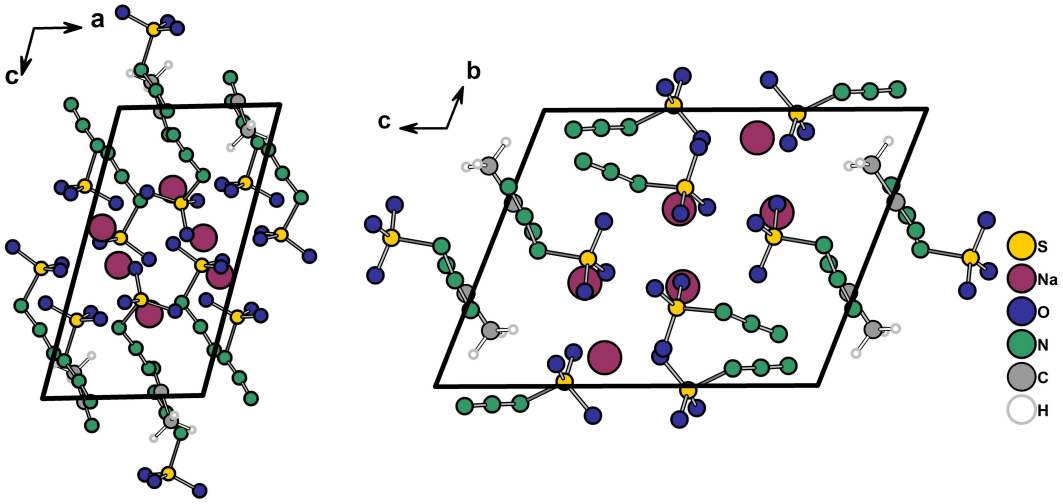

Figure 69: Extended unit cell of $Na_3[SO_3N_3]_3(CH_3CN)$ viewed along the crystallographic axes *b* and *a*.

The nitrogen atoms also coordinate, more specifically between N10 and N7 of the azides and Na3 with a distance of 300.0(1) pm and 321.4(2) pm, respectively. The acetonitrile coordinates to Na1 via N1 with an atomic distance of 239.6(1) pm. Overall, coordination numbers for sodium range from five (Na1) over six (Na2) to eight (Na3) (see Figure 70). For Na2 and Na3 no distinct polyhedron can be found, but for Na1 a distorted trigonal bipyramidal surrounding can be detected (δ = 17.30). Another description for the geometry would be a trigonal heterobipyramid (δ = 16.79).

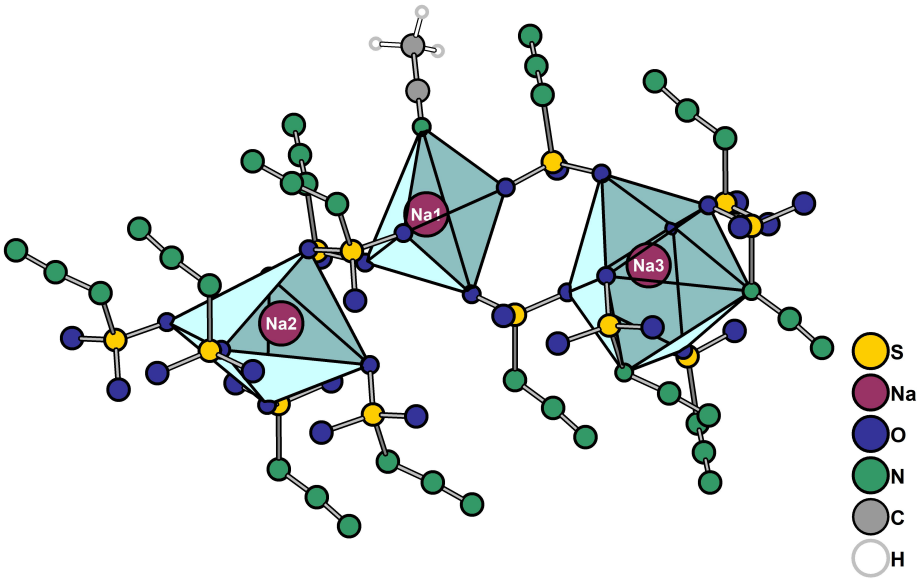

Figure 70: Coordination spheres around the three unique sodium atoms in the crystal structure of $Na_3[SO_3N_3]_3(CH_3CN)$.

4.4.4 Chapter Summary

The $[SO_3N_3]^-$ anion was examined crystallographically in four structures, namely $(TBA)_4(N_3)_3[SO_3N_3]$ $(TBA)[SO_3N_3]$, $K[SO_3N_3]$ and $Na_3[SO_3N_3]_3(CH_3CN)$. The syntheses were achieved in sulfonation reactions of azides using $Py{\cdot}SO_3$ and in an exchange reaction between $TMS(N_3)$ and $K[SO_3Cl]$. The latter reaction route is the more efficient and convenient. Structurally, all $[SO_3N_3]^-$ anions show similar bonding properties with S–N distances ranging from 170.5(1) pm to 174.8(1) pm and an angled position of $[N_3]$ relative to the $[SO_3]$ moieties. The azide units also exhibit the properties of covalently bonded azides with an asymmetry in the N–N distances and minor bending from the linear shape. The striking difference is the relative position of the N_3 towards SO_3, which results from a low rotation barrier along the S–N bond. For $K[SO_3N_3]$ two different crystalline phases were analyzed. The low-temperature phase at 100 K and high-temperature phase at 250 K differ due to the above-mentioned rotation along the S–N bond. $K[SO_3N_3]$ was also covered by vibrational spectroscopy, which revealed full conversion to $K[SO_3N_3]$ without impurity from TMS. *Rietveld* refinement of powder data proved crystalline phase purity. In a thermogravimetric analysis of the K^+-salt a stability up to 80 °C was detected. The compound decomposes first to $K_2S_2O_7$ and finally (T > 400 °C) to K_2SO_4 in presence of oxygen.

4.5 High Symmetrical Nitrido-*tris*-sulfates

4.5.1 Overview

In the introductory part higher SO_3 substituted ammonia derivatives were already addressed. The anions $[HN(SO_3)_2]^{2-}$, $[N(SO_3)_3]^{3-}$ and $[N(SO_3)_2]^{3-}$, which can be chemically converted into each other, in summary, are only scarcely described in literature as pointed out in 2.2 (p. 5). This chapter focuses on the phase-pure preparation of $K_3[N(SO_3)_3](H_2O)_2$ and presents three new alkali metal based mixed-cationic nitrido-*tris*-sulfates derived from $K_3[N(SO_3)_3](H_2O)_2$. Obtained from alkaline solvothermal synthesis these compounds were only accessed in yields of single crystals. Parts of the following results were part of a Bachelor thesis[174] that was co-supervised by the author. Experimental work for $K_2Na[N(SO_3)_3]$ and $K_{1.2}Rb_{1.8}[N(SO_3)_3]$ was partially carried out by *A. N. Udaya* and structural examination by the author. Accordingly, a more detailed description together with $Cs_2K[N(SO_3)_3]$ is carried out in this chapter.

4.5.2 Preparation and Phase Analysis of $K_3[N(SO_3)_3](H_2O)_2$

The synthesis of $K_3[N(SO_3)_3](H_2O)_2$ was first described by *Claus* and *Koch*[175] in 1869 and then in more detail by *Sisler et al.* in 1946.[78] A slightly modified procedure according to the latter findings was applied to prepare $K_3[N(SO_3)_3](H_2O)_2$. First, dissolved $K_2S_2O_5$ was reacted with a solution of KNO_2. After addition of KNO_2, $K_3[N(SO_3)_3](H_2O)_2$ immediately precipitated. The suspension must be kept alkaline to avoid the formation of $K_2[HN(SO_3)_2]$ due to hydrolysis. $K_2[NH(SO_3)_2]$ is rapidly formed under ambient conditions and absence of KOH (see *Rietveld* Refinement, p. 127). By further purification, $K_3[N(SO_3)_3](H_2O)_2$ was obtained in a yield of 48%.

$$KNO_2 + 2\,K_2S_2O_5 + 2\,H_2O \xrightarrow[50°C]{KOH} K_3[N(SO_3)_3](H_2O)_2 + K_2SO_3$$

Scheme 20: Synthesis of $K_3[N(SO_3)_3](H_2O)_2$.[78]

The compound was analyzed by SC-XRD to get an anisotropically refined dataset. The cell parameters coincide with the measurement of *Tillack* and *Kennard* from 1970.[79] The anion has three unique S–N bonds with lengths of 169.3(5) pm, 170.0(5) pm and 172.0(5) pm and the symmetry approximates to C_{3h} (see 7.4.18, p.153).

A *Rietveld* refinement of a powder sample was carried out including the SC dataset (see Figure 71 and Table 22, p. 101). The sample showed good crystallinity and the refinement curve fits well to the diffractogram with no significant intensity deviations recognizable in the difference curve.

Table 22: Selected crystallographic data of $K_3[N(SO_3)_3](H_2O)_2$ compared to the dataset of *Tillack et al.* and refined cell parameters obtained from a *Rietveld* refinement.

	$K_3[N(SO_3)_3](H_2O)_2$	**$K_3[N(SO_3)_3](H_2O)_2$[79]**	***Rietveld***
Crystal System	Orthorhombic	Orthorhombic	Orthorhombic
Space Group	*Pnma*	*Pnma*	*Pnma*
T/ K	100	RT	-
a / pm	1107.77(3)	1118(1)	1117
b / pm	569.76(1)	577.6(7)	576.50(3)
c / pm	1797.53(5)	1806(1)	1806.6(1)
V / nm^3	1.13453(5)	1.16624	1.164(1)
Z	4	4	4
R values	R_1 (all data) = 0.0603; wR_2 (all data) = 0.1192	-	R_{wp} = 9.59%; R_{exp} = 9.03%; R_p= 7.51%
GooF	1.20	-	1.06

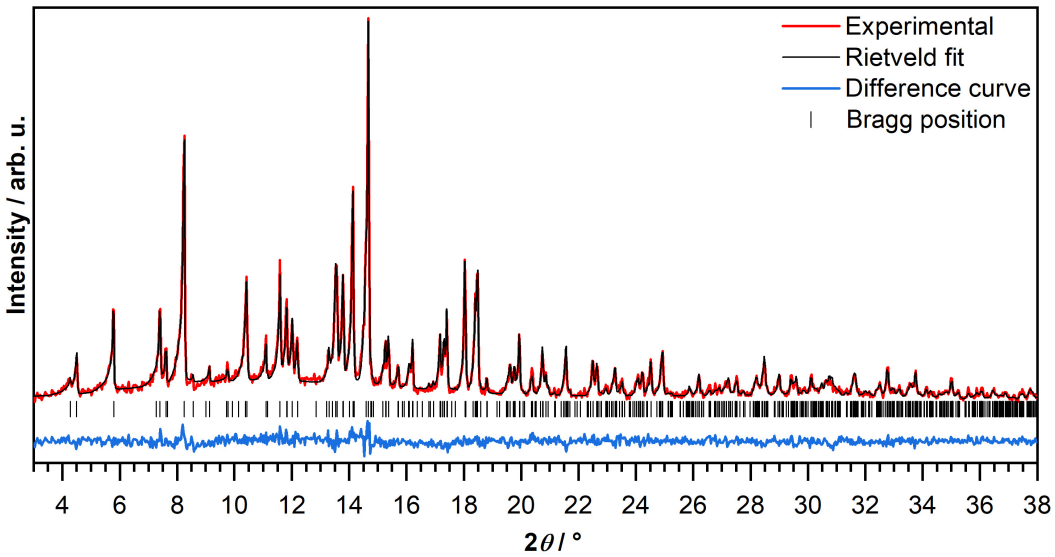

Figure 71: Experimental powder X-ray diffraction pattern of $K_3[N(SO_3)_3](H_2O)_2$ with *Rietveld* refinement. The powder was measured in an 0.3 mm capillary with Mo-$K_{\alpha1}$ (λ = 70.930 pm) radiation at RT. The cell parameters *a*, *b*, *c* and β were refined.

The refined cell parameters are well reflected by the measurement of *Tillack* and *Kennard*[79], which was also a measurement at RT. An elemental (CHNS) analysis confirmed the purity of the compound. TG/ DSC analysis of a powder sample shows that the compound is stable up to 150 °C (see 7.5.1, p.161). From there on, multiple signals in the DSC curve occur with a slight mass loss (4%). This can be deduced to the formation of $K_2S_2O_7$, which was confirmed by P-XRD (see 7.2.4, p.126) of a sample heated to 370 °C. At 360 °C melting of $K_2S_2O_7$ starts and at 463 °C the disulfate decomposes slowly to K_2SO_4 under liberation of SO_3 to a remaining mass of 65%. The presence of K_2SO_4 was also verified by powder P-XRD (see 7.2.3, p. 126). Consequently, $K_3[N(SO_3)_3](H_2O)_2$ cannot be dehydrated by a thermal approach.

4.5.3 $K_2Na[N(SO_3)_3]$, $K_{1.2}Rb_{1.8}[N(SO_3)_3]$ and $Cs_2K[N(SO_3)_3]$

After examination of $K_3[N(SO_3)_3](H_2O)_2$, it was used in further reactions. A variety of salt metatheses in aqueous solutions have been carried out to substitute potassium by another metal cation. Metal perchlorates and 18-crown-6 were used to separate potassium. These reactions led to the formation of metal sulfates and amidosulfates. This confirms the hydrolytic sensitivity and lability of $[N(SO_3)_3]^{3-}$. Only alkaline hydrothermal syntheses made it possible to synthesize new compounds of the anion. $K_3[N(SO_3)_3](H_2O)_2$ was reacted with the bases NaOH, RbOH and CsOH, respectively, in small amounts of water (see Scheme 21). The reactions were completed in sealed glass ampoules at 65 °C in tube furnaces. During this process, colorless single crystals with visibly different morphologies formed in all three reactions. Crystals with a triangular and hexagonal shape stood out in particular.

$$K_3[N(SO_3)_3](H_2O)_2 \xrightarrow[65\ °C]{NaOH} K_2Na[N(SO_3)_3]$$

$$K_3[N(SO_3)_3](H_2O)_2 \xrightarrow[65\ °C]{RbOH} K_{1.2}Rb_{1.8}[N(SO_3)_3]$$

$$K_3[N(SO_3)_3](H_2O)_2 \xrightarrow[65\ °C]{CsOH} Cs_2K[N(SO_3)_3]$$

Scheme 21: Syntheses of the nitrido-*tris*-sulfates $K_2Na[N(SO_3)_3]$, $K_{1.2}Rb_{1.8}[N(SO_3)_3]$ and $Cs_2K[N(SO_3)_3]$.

Analysis of single crystals yielded the structures of $K_2Na[N(SO_3)_3]$, $K_{1.2}Rb_{1.8}[N(SO_3)_3]$ and $Cs_2K[N(SO_3)_3]$, respectively. In addition to that, literature known sulfates as by-products were detected. Thus, this synthesis method is not suitable for a phase-pure preparation of this novel nitrido-*tris*-sulfates.

The new compounds exhibit a high symmetry by crystallizing in the hexagonal crystal family (see Table 23). The crystal structure of $K_2Na[N(SO_3)_3]$ and $K_{1.2}Rb_{1.8}[N(SO_3)_3]$ are isotypic since both crystallize in the hexagonal space group $P6_3/m$ and have similar cell parameters (see Figure 72, p. 103). The cell volume of $K_{1.2}Rb_{1.8}[N(SO_3)_3]$ is about 11% larger than $K_2Na[N(SO_3)_3]$ which results from the larger cationic radius of Rb^+ compared to Na^+. In the structure of $K_2Na[N(SO_3)_3]$ merohedral twinning (0−10, −100, 001) was identified.

Table 23: Selected crystallographic data of $K_2Na[N(SO_3)_3]$, $K_{1.2}Rb_{1.8}[N(SO_3)_3]$ and $Cs_2K[N(SO_3)_3]$.

	$K_2Na[N(SO_3)_3]$	**$K_{1.2}Rb_{1.8}[N(SO_3)_3]$**	**$Cs_2K[N(SO_3)_3]$**
Crystal System	Hexagonal	Hexagonal	Trigonal
Space Group	$P6_3/m$	$P6_3/m$	$R3c$
a / pm	714.49(3)	748.21(2)	778.14(3)
c / pm	1000.40(5)	1011.98(5)	3075.7(2)
γ / °	120	120	120
V / nm^3	0.44228(4)	0.49062(4)	1.6129(2)
Z	2	2	6
R_1 (all data); wR_2 (all data);	0.0180; 0.0457	0.0356; 0.0689	0.0230; 0.0503
BASF	0.246(1)	-	0.08(5); 0,42(4); 0.05(5)
GooF	1.167	1.154	1.231

In $K_{1.2}Rb_{1.8}[N(SO_3)_3]$ the cationic sites are occupied in a mixed ratio. The observed total occupancy of K^+ to Rb^+ amounts to 1.2:1.8. The substitutional disorder of the cationic sites can be attributed to their similar ionic radii.[145,176]

The unit cell of $Cs_2K[N(SO_3)_3]$ (see Figure 73) has *c*-axis three times as long as the other two structures and crystallizes in the trigonal crystal system with a rhombohedral lattice. The acentric space group *R*3*c* describes the symmetry in the crystal structure. During data refinement of $Cs_2K[N(SO_3)_3]$ merohedral plus racemic twinning was treated, which leads to a total of four domains (see Table 23, p. 102). A summary of important bonding parameters observed for the three structures is listed in Table 24 (p. 105)

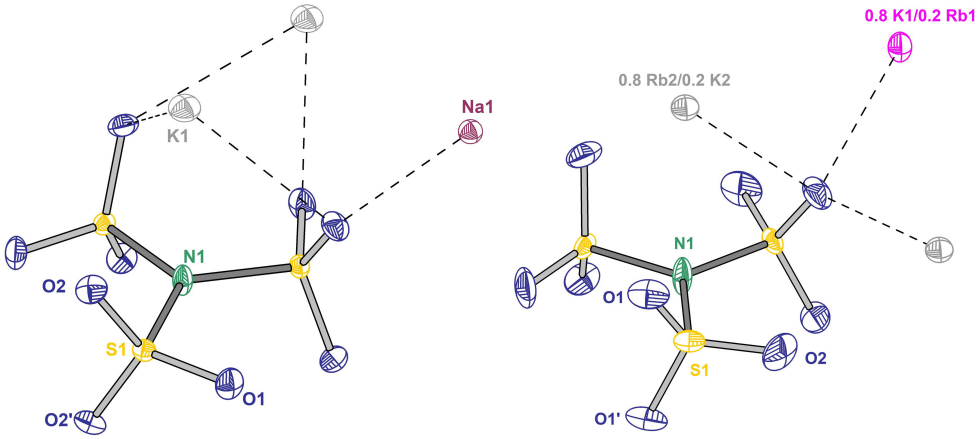

Figure 72: Structure of the two isotypic compounds $K_2Na[N(SO_3)_3]$ (left) and $K_{1.2}Rb_{1.8}[N(SO_3)_3]$ (right) with labeling of the crystallographically unique atoms. The thermal ellipsoids are set to a probability level of 70%.

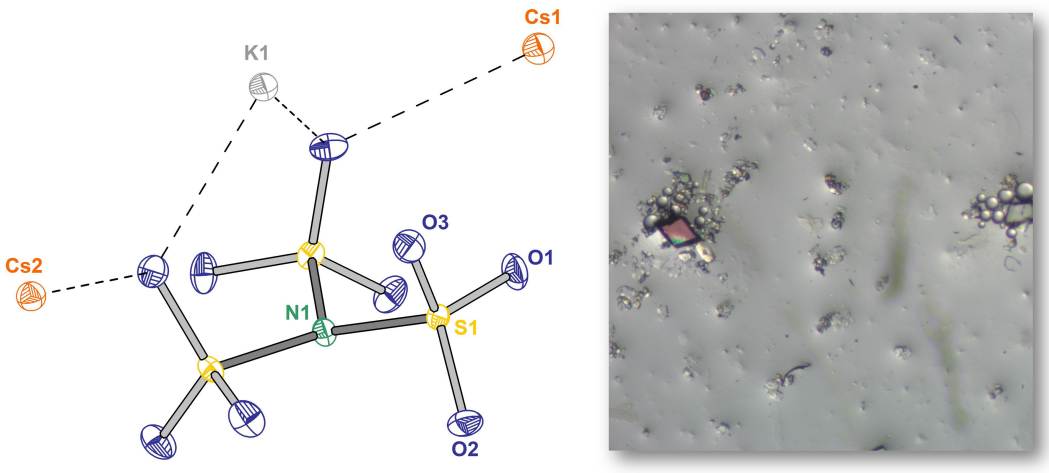

Figure 73: Structure of $Cs_2K[N(SO_3)_3]$ with labeling of the crystallographically unique atoms (left). The thermal ellipsoids are set to a probability level of 70%. On the right a light microscope image of a single crystal ($Cs_2K[N(SO_3)_3]$) is shown.

Most atoms are located on special sites in the structures. In $K_2Na[N(SO_3)_3]$ the atom K1 lies on a threefold rotational axis (*Wyckoff 4f*), Na1 on a threefold rotoinversion axis (*Wyckoff 2b*), N1 on a sixfold rotoinversion axis (*Wyckoff 2c*) and S1 as well as the oxygen atom O1 on a mirror plane

(*Wyckoff 6h*). Only O1 lies on a general site (*Wyckoff 12i*). For $K_{1.2}Rb_{1.8}[N(SO_3)_3]$ similar site symmetries are observed. For the mixed cationic sites ratios of 0.8 K^+ to 0.2 Rb^+ for K1/Rb1 (*Wyckoff 2b*) and 0.8 Rb^+ to 0.2 K^+ for Rb2/K2 (*Wyckoff 4f*) were set.

The $[N(SO_3)_3]^{3-}$ anions have perfect C_{3h} symmetry in the two isotypic structures with nitrogen being surrounded by sulfur in a trigonal planar geometry with an angle ∠S–N–S of 120° (see Figure 74). The observed distances between the sulfur and nitrogen atoms are 171.11(4) pm ($K_2Na[N(SO_3)_3]$) and 170.7(1) pm ($K_{1.2}Rb_{1.8}[N(SO_3)_3]$). The sulfonate groups show common S–O distances within 144-145 pm. The observed distances are consistent with those found in $K_3[N(SO_3)_3](H_2O)_2$.

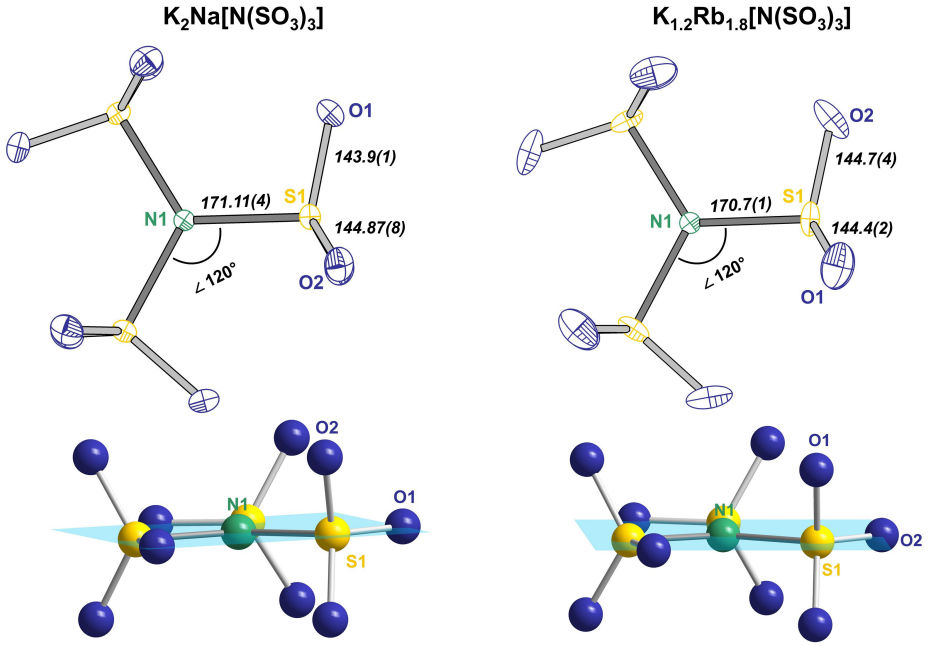

Figure 74: Depiction of the $[N(SO_3)_3]^{3-}$ anions observed in $K_2Na[N(SO_3)_3]$ (top left) and $K_{1.2}Rb_{1.8}[N(SO_3)_3]$ (top right) with bond lengths (italics, in pm) and angles. Additionally, planes through the atoms N1, S1, O1 (bottom left) and N1, S1, O2 (bottom right) are shown.

On the contrary, $[N(SO_3)_3]^{3-}$ within the cesium-containing salt has a lower symmetry with a point group C_3. The atoms N1, Cs1, Cs2 and K1 all lie on a threefold rotational axis (*Wyckoff 6a*). The atoms of the sulfonate group S1, O1, O2 and O3 are on general sites (*Wyckoff 18b*). The angle ∠S1–N1–S1' has a value of 177.6(2)° and the nitrogen atom (N1) protrudes slightly from the plane spanned by the three sulfur atoms (see Figure 75, p. 105). The $[NS_3]$ geometry is actually no longer a regular triangle ($\delta = 7.844$) as in the two previous structures but a tripod ($\delta = 0$) according to an analysis with *Polynator*[143] (see Table 24). Accordingly, a directional interaction between Cs1 and N1 is recognizable at an interatomic distance of 338(1) pm, which is accompanied by a symmetry loss of the anion. However, the observed S–N distance of 171.9(2) pm and S–O distances around 145 pm coincide to those found in the other $[N(SO_3)_3]^{3-}$ anions.

All three observed S–N distances are significantly longer than in $[HN(SO_3]_2]^{2-}$[83] (166.5 pm) and $[N(SO_3)_2]^{3-}$[85] (160.4(3) pm) but shorter than in zwitterionic sulfamic acid (178.84(8) pm)[151].

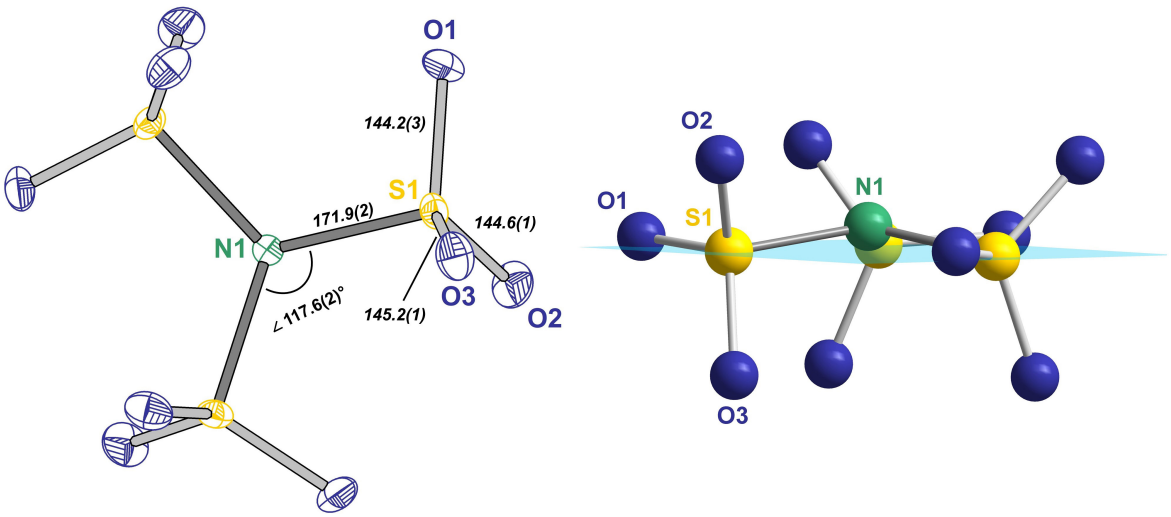

Figure 75: Structure of $[N(SO_3)_3]^{3-}$ observed in $Cs_2K[N(SO_3)_3]$ with bond lengths (italics, in pm) and angle ∠S1–N1–S1'. On the left, a plane through the three sulfur atoms is depicted.

Table 24: Selected bonding parameters observed in the structures $K_2Na[N(SO_3)_3]$, $K_{1.2}Rb_{1.8}[N(SO_3)_3]$ and $Cs_2K[N(SO_3)_3]$ and values of the polyhedron analysis calculated with *Polynator*[143].

	$K_2Na[N(SO_3)_3]$	**$K_{1.2}Rb_{1.8}[N(SO_3)_3]$**	**$Cs_2K[N(SO_3)_3]$**
S–N / pm	171.11(4)	170.7(1)	171.9(2)
S–O / pm	143.9(1)/144.87(8)	144.7(4)/144.4(2)	145.2(3)/144.6(3)/144.2(3)
S–N–S / °	120	120	117.6(2)
N–S–O / °	102.75(5)/105.14(4)	104.9(1)/104.1(2)	105.2(1)/105.3(3)/104.7(3
A–O / pm	**K–O**: 268.60(9)-319.86(8) **Na–O**: 239.01(8)	**K/Rb–O**: 278.4(2)-354.5(3)	**K–O**: 275.9(3)-292.3(3) **Cs–O**: 301.5(3)-381.5(4)
A–N / pm	**K–N**: 316.10(4)	**K/Rb–N:** 330.29(2)	**K–N**: 355(1) **Cs–N**: 338(1)
***δ*[NS_3]**	0 (regular triangle)	0 (regular triangle)	7.844 (regular triangle) 0 (tripod, 3*m*)
***δ*[AO_x]**	[$Na1O_6$]: 0 (trigonal antiprism) 5.3 (octahedron platonic)	[$(Rb1/K1)O_{12}$] 0 (cuboctahedron) 6.80 (icosahedron)	[$Cs1O_{12}$] 9.39 (cuboctahedron) 11.90 (icosahedron)

In the structures distinct ionic interactions can be noticed, which was examined with *CHARDI*.[142] In $K_2Na[N(SO_3)_3]$, Na1 is in sixfold coordination by O2 with a interatomic distance of 239.01(8) pm (see Figure 76, p. 106). The resulting polyhedron can nearly be described as a distorted octahedron due to measured angles ∠O2–Na1–O2 of 86° and 94°. With the program *Polynator*[143] a perfect trigonal antiprismatic shape was calculated ($\delta = 0.00$).

K1 is in tenfold coordination by O1 and O2 with distances of 268.60(9) pm up to 319.86(8) pm. There is also coordination by N1 at a distance of 316.10(4) pm. A certain coordination polyhedron cannot be assigned for K1. By viewing along the crystallographic *a*-axis alternating layers of $[N(SO_3)_3]^{3-}$ anions and layers of cations become evident.

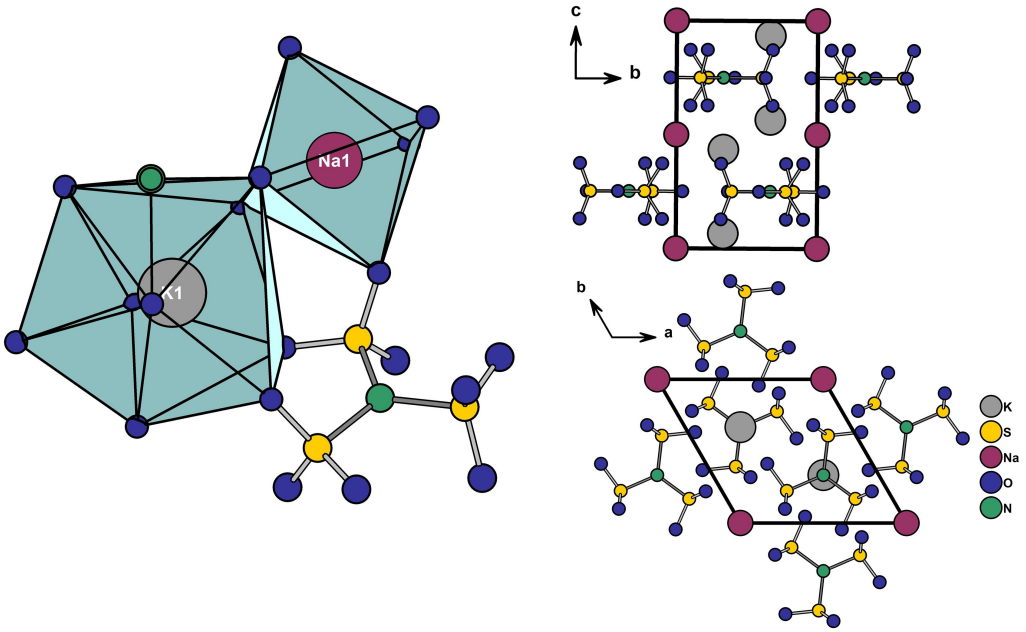

Figure 76: Depiction of the coordination sphere of K^+ and Na^+ in $K_2Na[N(SO_3)_3]$ shown as polyhedra (left) and extended unit cell of $K_2Na[N(SO_3)_3]$ along the crystallographic *a*-axis (top right) and *c*-axis (bottom right).

For $K_{1.2}Rb_{1.8}[N(SO_3)_3]$ the rubidium richer site Rb2/K2 is coordinated in a tenfold manner by O1, O2 and N1 and the potassium richer site is in a 12-fold coordination only by O1 and O2 (see Figure 77). Within coordination spheres distances of 278-354.5(3) pm for Rb/K–O and 330.29(2) pm for Rb/K–N are observed. Same packing as in isotype $K_2Na[N(SO_3)_3]$ is visible.

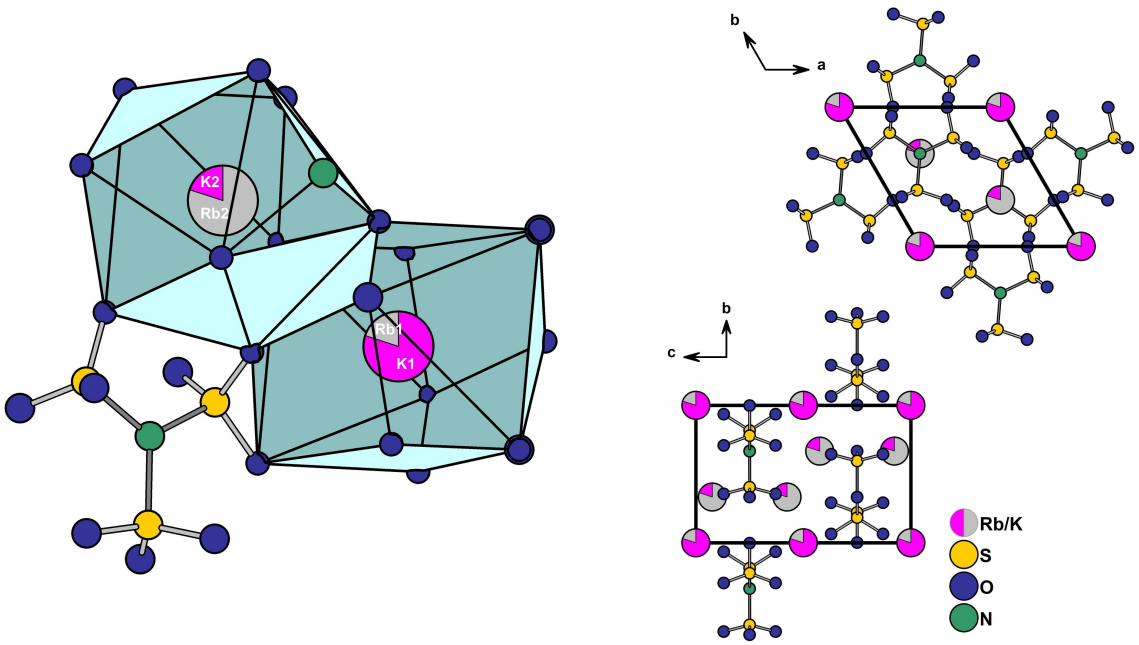

Figure 77: Depiction of the coordination sphere of the cationic sites Rb1/K1 and Rb2/K2 in $K_{1.2}Rb_{1.8}[N(SO_3)_3]$ shown as polyhedra (left) and the extended unit cell of $K_{1.2}Rb_{1.8}[N(SO_3)_3]$ viewed along the *c*-axis (top right) and *a*-axis (bottom right).

In $Cs_2K[N(SO_3)_3]$ Cs2 is surrounded by twelve oxygen atoms with a distance ranging from 301.5(3) pm to 381.5(4) pm with a shape closest to a cuboctahedron (δ = 9.39). For Cs1 also coordination by N1 (338(1) pm) is observed and the 13-fold coordination cannot be assigned to a geometric shape. In the coordination sphere of K1 nine oxygen atoms (275.9(3)-292.3(3) pm) and one nitrogen atom (355(1) pm) is present. Identical to the two other structures, alternating layers of anions and cations are visible along the crystallographic axis *c* (see Figure 78).

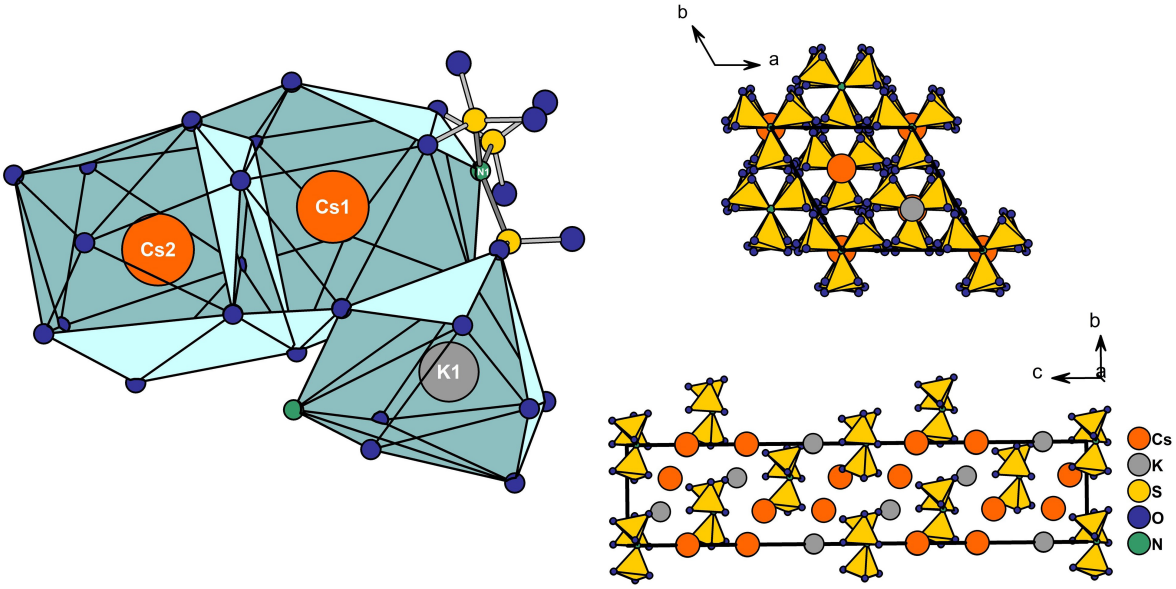

Figure 78: Depiction of the coordination sphere of Cs^+ and K^+ shown as polyhedra (left) and extended unit cell of $Cs_2K[N(SO_3)_3]$ viewed along the crystallographic *c*-axis (top right) and *a*-axis (bottom right).

5 Summary of the Results and Future Prospects

In the context of the studies presented, the scientific area of nitrogenous sulfates was developed in different directions. The paramount chemical moiety [NSO_3] was examined in structures of hydrazine sulfonates, cyclic nitridosulfates, azidosulfates and nitrido-*tris*-sulfates (see Figure 79).

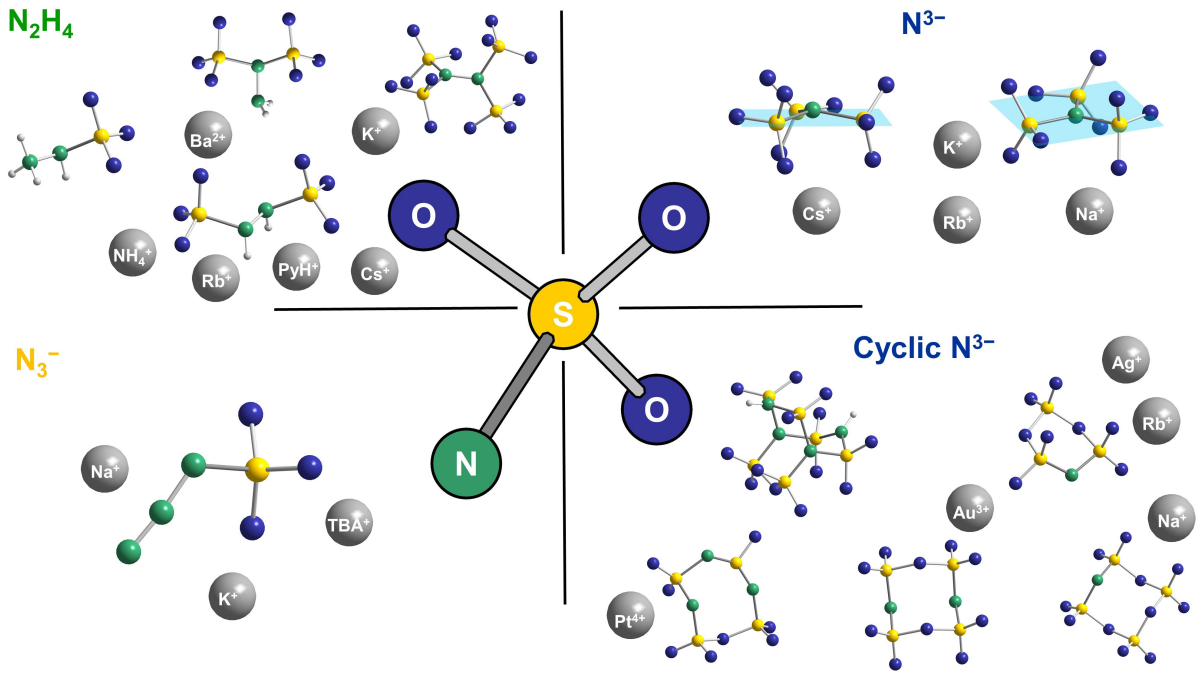

Figure 79: Overview of the four structural categories covered in this work with depictions of the examined anionic structures and corresponding cations.

In total, nine structures with cyclic nitridosulfate anions were obtained in reactions between $P_3N_3Cl_6$ and metal salts in liquid SO_3. Relying on previous results, $[S_3NO_8]^-$ was successfully reproduced in the structures $Rb[S_3NO_8]$ and $Ag[S_3NO_8]$. $[S_3NO_8]^-$ has a chair-shaped configuration in the solid-state and is similar to S_3O_9.[7] The bridging bond lengths are varying in the structures, with $S–N^{br}$ slightly shorter than $S–O^{br}$. Within the silver salt, strong coordination by the nitrogen atom is visible with an interatomic distance of 239.0(2) pm. In a reaction with Na_2O the novel anion $[S_4NO_{11}]^-$ with Na^+ as the counter-cation was obtained. $[S_4NO_{11}]^-$ has a backbone of an eight-membered ring and is one SO_3 molecule richer than $[S_3NO_8]^-$. It further has similarity to the solid Se_4O_{12} structure.[86] The two $S–N^{br}$ bonds in the anion have lengths of 159.3(2) pm and 159.8(2) pm.

Cyclic nitridosulfates were also analyzed in various square-planar gold complexes. The dimeric complexes $[Au_2Br_2(S_4N_2O_{10})_2]$ and $[Au_2Cl_2(S_4N_2O_{10})_2](S_2O_5Cl_2)$ were synthesized by reactions between $P_3N_3Cl_6$, SO_3 and the gold halides $AuBr_3$ and $AuCl_3$, respectively. Both exhibit the anion $[S_4N_2O_{10}]^{2-}$, which has a backbone of an eight-membered ring and coordinates via two bridging nitrogen atoms to the Au^{3+} centers.

$[S_4N_2O_{10}]^{2-}$ and $[S_3NO_8]^-$ were also observed in the structure $K[Au(S_4N_2O_{10})(S_3NO_8)Cl]$. This complex was prepared using $K[AuCl_4]$ as starting reactant. In the $[Au(S_4N_2O_{10})(S_3NO_8)Cl]^-$, $[S_3NO_8]^-$ coordinates through the bridging nitrogen atom to Au^{3+}, while $[S_4N_2O_{10}]^{2-}$ bidentately

coordinates via N⁀N. Moreover, it was demonstrated with $(S_3N_2Cl)Cl$ that another nitrogen containing reactant can be used to create cyclic nitridosulfate anions. Reaction of the latter with $AuCl_3$ and SO_3 yielded single crystals of $(NS_2)[Au(S_4N_2O_{10})_2]$. The homoleptic square-planar complex $[Au(S_4N_2O_{10})_2]^-$ is stabilized by the scarcely reported dithionitronium, NS_2^+. It is related to valence isoelectronic NO_2^+ and could so far only be obtained in salts with weakly coordinating bases, such as $[SbCl_6]^-$ and $[AsF_6]^-$.

In reactions with elemental platinum and $K_2[PtCl_6]$ the compounds $[Pt(S_4N_3O_8Cl)_2]$ and $K_2[Pt(S_4N_3O_9)_2](SO_3)_2$ were prepared. In both compounds the Pt^{4+} centers are coordinated in a sixfold manner. $[S_4N_3O_9]^{3-}$ has three bridging nitrogen atoms and can structurally be derived from $[S_4N_2O_{10}]^{2-}$. In $[S_4N_3O_8Cl]^{2-}$ chlorine was inserted at a terminal position (Ø(S–Cl) = 192.2 pm) in the cyclic anion for the first time. The structure model of $[Pt(S_4N_3O_8Cl)_2]$ still requires a more detailed consideration as there is significant rest electron density in between the ligands.

In further experiments with reactions of $P_3N_3Cl_6$ and SO_3 at RT, the compound $S_6N_4O_{13}H_2{\cdot}P_2O_3Cl_4$ was obtained. Thus, the remaining phosphorus could be structurally proven for the first time. Molecular $P_2O_3Cl_4$ is a long-known compound, but is structurally described in a single crystal structure in this work for the first time. It shows hydrogen bonding to the molecule $S_6N_4O_{13}H_2$. The latter compound is a cage-type molecule with similarity to $S_6N_2O_{15}$. While $S_6N_2O_{15}$ has three bridging oxygen atoms, $S_6N_4O_{13}H_2$ has two bridging [NH] moieties instead. Altogether, the named structures considerably complement the pool of cyclic nitrogenous sulfates, and show that there is still great potential in this structural category.

What remains a challenge is the controlled synthesis of products. Though the anions $[S_4N_2O_{10}]^{2-}$ and $[S_3NO_8]^-$ appeared in different structures, only yields on single crystal basis were obtained so far. Additionally, the complex by-products are not yet fully investigated. This is made particularly difficult by the reactive nature of SO_3 and the dynamic reaction process in the closed glass vessels. The reaction parameters certainly still offer a lot of scope for adjustment since most of the reactions were performed at 80 °C and using similar quantities of SO_3. Further adjustments can be made by selection of the nitrogen source. E.g. S_4N_4 as a chlorine and phosphorus-free compound might be a better alternative also with regard to the known adduct $S_4N_4{\cdot}SO_3$.[38] However, the explosive nature of this nitride must be taken into account. In order to obtain a better solubility of the components and achieve a more selective addition of SO_3, reactions in liquid SO_2 should be considered. Since the anions can be regarded as condensation products of NH_3SO_3 and H_2SO_4, solid-state reactions of e.g. (hydrogen)sulfates and NH_3SO_3 might lead to these anions, too.

In the second part the hydrazine sulfonates were systematically studied in various structures. The hydrazine monosulfonic acid and its barium salt, $Ba[NH_2NH(SO_3)](H_2O)$, were obtained by sulfonation of hydrazine monohydrate with $Py{\cdot}SO_3$. The zwitterionic nature of the acid ($^+H_3N–NH–SO_3^-$) was proven by SC-XRD and crystalline phase-purity confirmed by *Rietveld* refinement. The

acid was refined as an inversion twin and has a chiral center at the central nitrogen atom. In the solid-state distinct hydrogen bonding is evident for both structures. Especially for the acid, this in an important stabilizing parameter in the solid state, which was also emphasized by a *Hirshfeld* surface analysis. Thermal stability up to 209 °C for the acid was determined. The Ba^{2+}-salt shows first dehydration at 110 °C, followed by decomposition to $BaSO_4$ at 200 °C. Problematic in course of this studies were the poor yields of the compounds. Aqueous reactions with $Py{\cdot}SO_3$ forms by-products, such as sulfates, and for larger-scaled syntheses, the synthetic strategy should be reconsidered. In contrast, the synthesis of the symmetrical hydrazine disulfonates was much more straightforward. From the reaction between $ClSO_3H$ and $N_2H_6(SO_4)$ in pyridine, the pyridinium salt, $(Py–H)_2[(SO_3)HNNH(SO_3)]$, was synthesized. This compound was converted into other salts by predominantly alkaline salt metatheses. The salts of monovalent cations with the general composition $A_2[(SO_3)HNNH(SO_3)](H_2O)$ (A= (NH_4), K, Rb, Cs) and $Ba[(SO_3)HNNH(SOs_3)](H_2O)_2$ were prepared. Structural commonality is the SO_3 substitution on opposite nitrogen positions with observed dihedral angle ∠S–N–N–S within 134.2(1)-143.0(3)°. $[(SO_3)HNNH(SO_3)]^{2-}$ has two stereocenters located at the nitrogen atoms. In all salts, no enantiomerically pure crystallization was found. The isomeric hydrazine *iso*-disulfonate $[H_2NN(SO_3)_2]^{2-}$ was also prepared and analyzed in salts of K^+ and Ba^{2+}. This was achieved by connecting the nitrido-*bis*-sulfate unit $[N(SO_3)_3]^{3-}$ and the amine moiety of H_2NOSO_3H. $K_2[H_2NN(SO_3)_2]$ and $Ba[H_2NN(SO_3)_2](H_2O)$ were both obtained phase-pure from purification. $K_2[H_2NN(SO_3)_2]$ showed similar thermal stability as $K_2[(SO_3)HNNH(SO_3)](H_2O)$ (dehydrated) in an thermal analysis. The N−N and S–N distances coincide with those of the disulfonates with values within 142-144 pm and 167-177 pm, respectively. The hydrazine tetrasulfonate anion $[(SO_3)_2NN(SO_3)_2]^{4-}$ was studied in the two compounds $K_4[(SO_3)_2NN(SO_3)_2](H_2O)$ and $K_4[(SO_3)_2NN(SO_3)_2](H_2O)_2$. Preparation of the tetrasulfonates was achieved in an oxidation reaction between $(Py–H)_2[(SO_3)HNNH(SO_3)]$ and NaOCl with final KOAc quenching. The mechanism of the reactions is not yet fully grasped and the synthesis provides a low yield. The observed lemon-yellow compound, which formed during the synthesis while cooling at −40 °C, and possibly is caused from an azo compound[23], has not yet been isolated. Both structures were analyzed and compared by SC-XRD. By the fourfold substitution, the N–N bond undergoes a contraction with found distances in between 137.2(3) pm to 138.5(5) pm, while the S–N bond distances are similar as in the hydrazine disulfonates. The two $[N(SO_3)_2]$ units of the anion are almost perpendicular to each other and the nitrogen atoms are surrounded in a slightly distorted trigonal planar manner. With a *Rietveld* refinement both phases were quantified and vibrational modes of $K_4[(SO_3)_2NN(SO_3)_2](H_2O)_2$ were evaluated by *Raman* spectroscopy. Thermal analysis has not yet been carried out due to insufficient yield and failure to separate the two hydrates. This should be taken into consideration for further investigations. Apart from that, salt metatheses with the potassium salt should be carried out in the future. Investigations of other salts of the hydrazine tetrasulfonate may allow an even more detailed analysis of the highly negative charged anion and

creates a basis for comparison. The remaining gap, the hydrazine trisulfonate, could not be synthesized within this work.
Now that some salts of hydrazine sulfonates have been examined in detail, the reaction characteristics are of interest since they might, e.g., be used as selective reduction reagents.

Lewis acid base reactions between azides and SO_3 were successfully conducted to prepare four compounds with azidosulfates. The two tertbutyl ammonium salts (TBA)$[SO_3N_3]$ and $(TBA)_4(N_3)_3[SO_3N_3]$ were prepared by sulfonating (TBA)N_3 with Py·SO_3 in closed reaction glass vessels. Although these reactions do not enable complete turnover, $[SO_3N_3]^-$ is crystallographically characterized in a pure and non-disordered structure for the first time. It was also succeeded in sulfonating NaN_3 in MeCN via this route leading to $Na_3[SO_3N_3]_3(CH_3CN)$. A more facile synthesis is the exchange reaction between chlorosulfonates and (TMS)N_3, which was adapted from *Christe*[113]. This was demonstrated for $K[SO_3N_3]$ using $K[SO_3Cl]$ as reactant. Phase purity of the compound was confirmed by crystallographic, spectroscopic and thermal methods. $K[SO_3N_3]$ is thermally sensitive as it begins to decompose at around 80 °C, first forming $K_2S_2O_7$ (oxygen presence) and then K_2SO_4. All $[SO_3N_3]^-$ structures show comparable bonding properties with S–N distances in between 170.5(1) pm an 174.8(1) pm and an angled orientation of the $[N_3]$ towards $[SO_3]$. Since this structural compound class is still limited to a few salts, further investigations are recommended, especially with regard to the synthetic route via chlorosulfonates. This route should be beneficial to synthesize a variety of metal and nonmetal azidosulfates, which might have pronounced spectroscopic properties or are mild primary explosives, i.e. they can be used for applications. Of course, the limited class of known chlorosulfates has to be extended, too.[177-179] Other pseudohalides like cyanide (CN^-), isocyanate (NCO^-) or thiocyanate (SCN^-) also fit into this concept and should be pursued further due to the lack of investigations.[165]

Finally, three new highly symmetrical nitrido-*tris*-sulfates were synthesized in this work. For this purpose, literature-known $K_3[N(SO_3)_3](H_2O)_2$[78] was prepared and re-evaluated. The latter was then treated with the bases NaOH, RbOH and CsOH, which lead to $K_2Na[N(SO_3)_3]$, $K_{1.2}Rb_{1.8}[N(SO_3)_3]$ and $Cs_2K[N(SO_3)_3]$, respectively. All three compounds crystallize in the hexagonal crystal family. $K_2Na[N(SO_3)_3]$ and $K_{1.2}Rb_{1.8}[N(SO_3)_3]$ are isotypic structures, crystallizing in the space group $P6_3/m$ with similar cell parameters. For $[N(SO_3)_3]^{3-}$ in $K_2Na[N(SO_3)_3]$ and $K_{1.2}Rb_{1.8}[N(SO_3)_3]$ C_{3h} point symmetry was observed in the solid state. The ideal trigonal-planar geometry indicates that the lone pair of nitrogen involves in π-bonding to the sulfur atoms. For $Cs_2K[N(SO_3)_3]$ C_3 symmetry was found since the nitrogen atom protrudes slightly from the plane spanned by the three sulfur atoms.
S–N distances for the anion were found in between 170.9(2) pm and 171.9(2) pm and are in good agreement to those in $K_3[N(SO_3)_3](H_2O)_2$ and $S_6N_2O_{15}$[25]. Unfortunately, these compounds were not analyzed further, since they were obtained on a single crystal scale with alkali metal sulfates as by-

products. $[N(SO_3)_3]^{3-}$ proved to be a very labile anion under neutral and alkaline conditions, which hampered salts metatheses with transition and rare earth elements. As consequence, the focus should be on establishing stabilizing reaction conditions in the future. Reactions in non-aqueous systems will probably be difficult to realize due to the high negative charge of the anion. Since it is still a considerably under-represented anion, further research is remunerative. This might lead to novel compounds with unexpected thermal, spectroscopic and structural properties.

6 Experimental Part

6.1 SO_3 Distillation Apparatus and Reaction Glass Ampoules

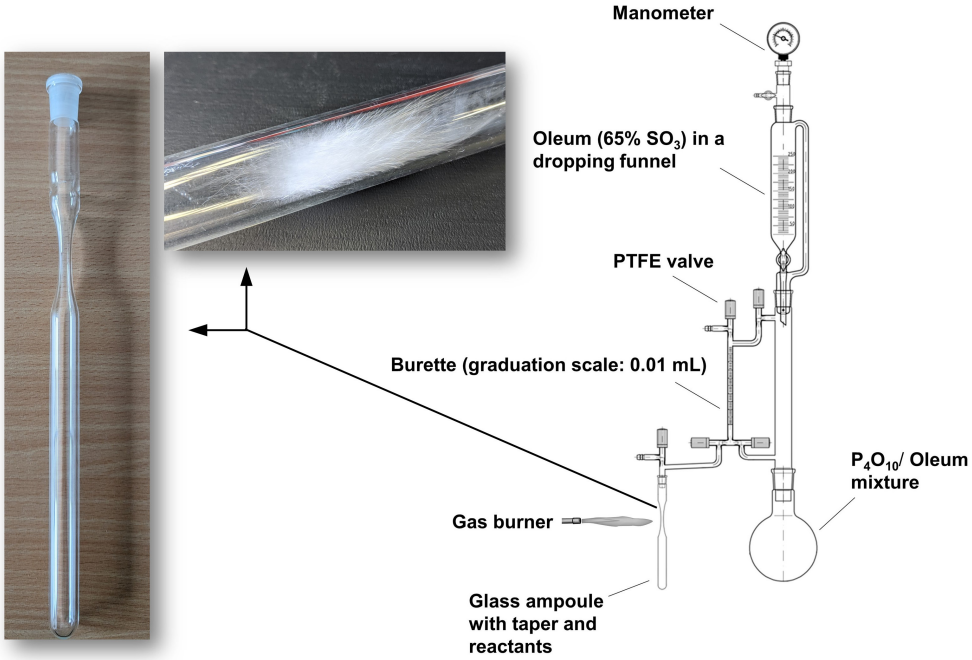

Figure 80: Schematic representation of the distillation apparatus (right) used in this work for the preparation of liquid SO_3 (γ) and its transfer into a reaction vessel. On the left on picture of an empty glass ampoule used in course of this work and of an SO_3 loaded ampoule with asbestos-like α/β-SO_3 are shown. The apparatus was designed by *van Gerven*.[180]

Liquid SO_3 was yielded by distillation of commercially obtained fuming sulfuric acid (65% SO_3). The distillation was done in an apparatus designed by *D. v. Gerven* (see Figure 80). The whole apparatus consists of borosilicate glass (3.3) and is operated under inert conditions (N_2) using *Schlenk* technique while the pressure is monitored by a manometer. The apparatus is connected to the *Schlenk* line by FEP tubes. The valves for operating the individual sections are made of SO_3 resistant PTFE. Before start-up all components must be baked out under reduced pressure (10^{-3} mbar) to get rid of water traces. Via a dropping funnel the oleum is added to a flask containing P_4O_{10}. The latter is an effective agent, which can dry H_2SO_4 at higher temperatures to form additional gaseous SO_3. The flask with P_4O_{10} is constantly heated to 130 °C during the distillation. The vaporized SO_3 is transferred through a connecting piece to a volumetric burette (graduation scale: 0.01 mL) where it condenses. The burette allows to transfer almost stoichiometric quantities to the reaction vessel. From there on the liquid SO_3 can be transferred to a connected (ground glass joint) reaction vessel with reactants. During the SO_3 addition, it is recommended to cool the reaction vessel with liquid nitrogen in order to avoid violent reactions and to trap the SO_3 as thoroughly as possible. In case of glass ampoules for solvothermal synthesis, the ampoule is evacuated under reduced pressure and fused at the tapered site with a gas burner. Afterwards the reaction vessels were put in reaction furnaces. In order to isolate the reaction products, the ampoules were first cooled with liquid nitrogen to reduce

the SO_3 pressure. The vessels were opened with a glass cutter and the reaction products, such as single crystals, were carefully scooped out with a spatula under inert or ambient conditions.

The applied reaction ampoules were made of 3.3 borosilicate glass (wall thickness ≈ 1.8 mm, outer diameter ≈16 mm) with a determined average volume of 20 cm^3. In order to determine and control the pressure and SO_3 amount in the gas phase of the ampoule, the saturated vapor pressure of SO_3 at certain temperatures was calculated using the *Antoine* equation:

$$log_{10}(p) = A - \left(\frac{B}{C + T}\right)$$

where p denotes the pressure, T the temperature and A, B and C empirical parameters (for SO_3: A = 4.20515, B = 892.175, C = −103.564).[181-182] E.g. at 80 °C a vapor pressure of $4.27 \cdot 10^5$ Pa for SO_3 is calculated. Under assumption that SO_3 acts like in ideal gas, the amount of substance of SO_3 to saturate the gas phase can be determined according to the ideal gas law:

$$n = \frac{pV}{RT}$$

where n denotes the amount of substance, V the volume in the fused glass ampoule, R the gas constant. For 80 °C, $4.27 \cdot 10^5$ Pa and a volume of 20 cm^3, approximately 2.90 mmol (0.121 mL, $\rho(SO_3)$[46] = 1.92 $g \cdot cm^{-3}$) SO_3 is required to saturate the gas phase of the reaction ampoule. This quantity is therefore not available as solvent during the solvothermal syntheses and was added to the calculated stoichiometric quantities of SO_3 (see 6.13.3, p. 120).

6.2 Single Crystal X-ray Diffraction and Structure Determination

Single crystal structure determination was performed on a Bruker D8 VENTURE KAPPA diffractometer with a microfocus sealed tube using multilayer mirror as monochromator and a Bruker PHOTON III detector. As characteristic X-ray radiation MoK_α (λ= 71.073 pm) was used for the measurements. Before the measurements, the crystals were prepared in perfluorinated ether (Fomblin® YR-180) and selected with the aid of a light microscope with a polarization filter. The crystals were fixed on a micromount with a 150 µm polymer loop and adjusted to the X-ray beam with optional cooling down to 100 K. The images with the intensity data were processed using the software *APEX4*[183] and *APEX5*[184]. The frames were integrated with *Bruker SAINT*[185] software package using a narrow-frame algorithm. Absorption effects were corrected using *SADABS*[186] for the multi-scan absorption correction. The structure solution and refinement was done with the software *OLEX2*[187]. Dual methods using *SHELXT*[188] were used for structure solution and full-matrix least-squares methods against F^2 using *SHELXL*[189] for the refinement. All illustrations of the crystal structures were made with the program *Diamond 4*[190] using the CIF as input file.

6.3 Powder X-ray Diffraction and Rietveld Refinement

For sample measurements with **Mo-$K_{\alpha1}$ radiation** (λ = 70.930 pm) a *STOE Stadi P* diffractometer (*STOE & Cie* GmbH, Darmstadt, DE) was used. The samples were prepared in 3.3 borosilicate glass capillaries with an outer diameter of 0.3 mm and 0.5 mm. The reflections were measured with a silicon-based *Dectris Mythen 1K* detector (*Dectris Ltd*, Baden-Daettwil, CH) in *Debye-Scherrer* geometry at RT. The data was processed with *WinXPOW* (version 3.6)[191]. Theoretical patterns were simulated with *WinXPOW* (version 3.6)[191] using *Debye-Scherrer* geometry, a Germanium monochromator, *Pseudo-Voigt* profile function (Gauss Component: 0.5) and the CIF as an input file. **Cu-K_{α} radiation** ($\lambda(K_{\alpha1})$ = 154.1 pm, $\lambda(K_{\alpha2})$= 154.4 pm) measurements were performed on a *RIGAKU MiniFlex* diffractometer with a *HyPix-400 MF 2D* hybrid detector in Bragg-Brentano geometry at RT. The samples were prepared on flat low background glass or monocrystalline silicon holders. Processing of the data was conducted with *SmartLab Studio II*.[192]
The *Rietveld* refinements were done with the program *jEdit* using *TOPAS5*[193-195] as an input file. As a background polynomial, *Chebyshev* polynomials (5th order) of the first kind were applied in all refinements. The lattice parameters and atomic sites were read from the CIFs created in this work or downloaded from the ICSD/CSD.

6.4 Raman Spectroscopy

The *Raman* spectra were recorded with an *inVia Qotor confocal Raman microscope* equipped with 10x, 50x and 100x magnification lenses from Renishaw GmbH (Pliezhausen, DE). The spectra were measured on selected single crystals and powder samples using a green laser (λ= 532 nm, 100 mW) and varying exposure times at RT. The data was processed and corrected with *WiRE 5.1*[196] software.

6.5 Infrared Spectroscopy

Under ambient conditions IR spectra were recorded on *a PerkinElmer FTIR-UART TWO* spectrometer at RT. Processing of the data was done with the program *Spectrum*[197]. Measurements under Argon atmosphere in a glove box were done with a *Bruker Alpha II* using *OPUS*[198] software.

6.6 Thermal Analysis

The thermal analyzer *STA 409C* (*NETZSCH*) coupled with a quadrupole mass spectrometer (*QMS 421*, *BALZERS*) was used for thermal analyses. All measurements were done in corundum crucibles on a DSC/TG sample holder under an Argon flow of 80 ml·min^{-1}. The ion current measurements were carried out in a scanning mode with predefined *m*/*z* values. The data was processed with *NETZSCH Proteus*[199].

6.7 CHNS Analysis

The carbon, hydrogen, nitrogen and sulfur content of the samples were determined with an elemental analyzer *Euro EA 300* of *EuroVector S. p. A.*. About 1-2 mg of the sample were loaded in a tin cartridge (V =177 mm^3) together with vanadium pentoxide. Via an autosampler, the closed cartridge was transferred to the reactor and heated to 1000 °C in an oxygen flow. The formed gases were separated by gas chromatography (column temperature 75 °C) with helium as a carrier gas (148-152 $mL \cdot min^{-1}$). The fractions were quantitatively analyzed with the program *Callidus 5.1*. Calibration was done with sulfanilamide as a standard. Two measurements for each sample were performed and the mean value was determined.

6.8 NMR Spectroscopy

The $^{31}P\{^{1}H\}$ NMR spectrum was recorded on a Bruker *Avance Neo 400* spectrometer at 162 MHz. The data was processed using *MestReNova* (version: 14.3.3) software. The sample was prepared in a *GPE Scientific*™ *J Young* NMR tube (5 mm) with a PTFE valve in an argon glovebox.

6.9 Quantum Mechanical Calculations

Theoretical calculations were carried out with the software packages *Orca 5.0.3*[200] and *TmoleX 4.2*[201]. The atomic coordinates (xyz) were extracted from the CIF files and used as input file for the geometry optimization. For the geometry optimization and calculation of vibrational frequencies of compounds the following quantum mechanical parameters were used:

$[Pt(S_4N_3O_9)_2]^{2-}$: *Orca 5.0.3*, DFT, PBE0 exchange-correlation functional, basis set def2-TZVPP[202-204].

$[SO_3N_3]^-$: *TmoleX 4.2*, DFT, PBE0 exchange-correlation functional, basis set cc-pVTZ[204-206].

$[(SO_3)_2NN(SO_3)_2]^{4-}$: *Orca 5.0.3*, DFT, PBE0 exchange-correlation functional, basis set cc-pVTZ[204-206].

6.10 Polyhedron Analysis with *Polynator*

The program *Polynator*[143] was used to investigate the polyhedra formed by the coordination sphere of the cations. The program identifies coordination polyhedra of an atomic arrangement and calculates the distortions δ. The program allows to fit dynamic models with free parameters set to any number, which is in contrast to earlier program *SHAPE*[207-208] which uses rigid models. The distortion is defined by the following equation:

$$\delta = 100 \cdot \left(\frac{\sum_i |a_i - v_i|^2}{\sum_i |a_i - c|^2} \right)^{1/2},$$

where a_i denotes an atom vector, v_i the vector of its corresponding model vertex and c the centroid of all atom vectors. A value of $\delta = 0$ implies a perfect fit between atom vectors and the model and values above $\delta = 30$ should not be interpreted for the description of the atom arrangement. The generated CIFs were used as an input file for the polyhedral analysis.

6.11 Coordination Number Determination with *CHARDI*

The charge distribution analysis of the ionic structures was conducted with *CHARDI2015*.[142] In this method a Madelung-type approach is applied. The charge distribution is determined under consideration of the formal oxidation numbers of the cations and anions. The atoms are set as point charges, and the oxidation number of the cations are distributed among the anions and the resulting value is distributed back. For the coordination polyhedron the effective coordination number (Econ, *Hoppe*[209], 1979) is determined, which includes both the number of the atoms bonded and also the strength of each bond. For the analysis of the datasets the CIF files with specification of the oxidation numbers of the atoms were loaded as input files.

6.12 Chemicals

Commercially available chemicals used for the reactions are listed below. All other chemicals were prepared in course of this work or have already been prepared in the working group before.

Table 25: List of commercially acquired chemicals used within this work.

Chemical	Purity	Supplier
$AuCl_3$	99%	SIGMA-Aldrich Chemie GmbH, D-89555 Steinheim
$AuBr_3$	99%	SIGMA-Aldrich Chemie GmbH, D-89555 Steinheim
$K[AuCl_4]$	98%	Acros Organics
$P_3N_3Cl_6$	99%	SIGMA-Aldrich Chemie GmbH, D-89555 Steinheim
Fuming sulfuric acid (60% SO_3)	100%	VWR Chemicals, B-3001 Geldenaaksebaan
NaOCl (aqueous solution)	11-15% available chlorine	ThermoFisher GmbH, DE-76870 Kandel
$(TBA)N_3$	≥95%	TCI EUROPE N. V., B-2070 Zwijndrecht,
$(TMS)N_3$	≥95%	TCI EUROPE N. V., B-2070 Zwijndrecht
$(C_5H_5N)(SO_3)$	97%	SIGMA-Aldrich Chemie GmbH, D-89555 Steinheim
P_4O_{10}	≥98%	VWR Chemicals, B-3001 Geldenaaksebaan
HSO_3Cl	99%	ThermoFisher GmbH, DE-76870 Kandel
Hydroxylamine-*O*-sulfonic Acid	99.99%	SIGMA-Aldrich Chemie GmbH, D-89555 Steinheim
Sulfur Monochloride (S_2Cl_2)	98%	SIGMA-Aldrich Chemie GmbH, D-89555 Steinheim
Hydrazine Hydrate (64% N_2H_4)	100%	ThermoFisher GmbH, DE-76870 Kandel
NaN_3	99%	Riedel-de Haën AG, D-3016 Seelze 1
Platinum (black) (≤ 20 µm)	98.7%	Carl Roth GmbH Co. KG, D-76185 Karlsruhe
$K_2[PtCl_6]$	40% (Pt)	Acros Organics

6.13 Syntheses

6.13.1 $(S_3N_2Cl)Cl$

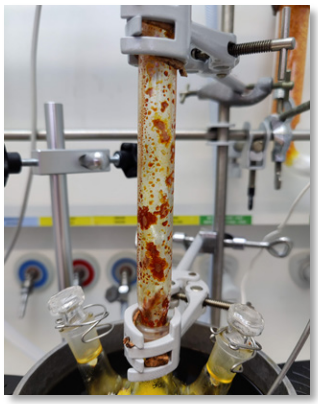

Figure 81: Picture of the sublimation tube during the reaction of NH_4Cl and S_2Cl_2 at 140 °C. At this moment, the orange-brown solid already indicated the presence of $(S_3N_2Cl)Cl$.

25.00 g (0.467 mol, 3.00 eq.) NH_4Cl and 12.5 mL (0.156 mol, 1.00 eq.) S_2Cl_2 were placed in a dried three-necked flask with a connected glass sublimation tube on top. The mixture was stirred at 138 °C for 22 h under inert conditions in a constant argon flow. During this time period an orange-brownish crystalline solid deposited on wall of the glass sublimation tube. The product was scraped off the tube under inert conditions and a crystalline phase-pure product was determined in a yield of 2%.

6.13.2 $K_4[(SO_3)_2NN(SO_3)_2](H_2O)$ and $K_4[(SO_3)_2NN(SO_3)_2](H_2O)_2$

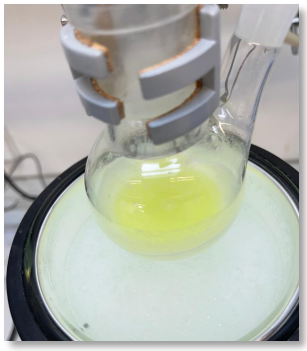

Figure 82: Flask with reaction mixture of $(C_5H_6N)_2[(SO_3)HNNH(SO_3)]$ and NaOCl. The yellow color appeared during addition of the NaOCl-solution at −40 °C.

2.00 g (5.71 mmol, 1.00 eq.) $(C_5H_6N)_2[(SO_3)HNNH(SO_3)]$ was placed in a round bottom flask and dissolved in 10 mL of a 2%-NaOH solution. The solution was cooled to −40 °C (isopropanol/ dry ice) and then 4.10 mL (8.56 mmol, 1.50 eq.) of a 13% NaOCl-solution was added dropwise over a period of 25 min. The color of the reaction mixture changed to an intense yellow, which faded after 10 min of the complete addition of NaOCl. The mixture was allowed to reach RT and stirred for further 30 min. Then 1.12 g (11.42 mmol, 2.00 eq.) KOAc in 10 mL water was added to the mixture

and the formed precipitate was filtered and washed with a 1 M KOH solution. The crude product was solved in warm water and recrystallized in the refrigerator. From the recrystallization a colorless solid was obtained, which contained $K_4[(SO_3)_2NN(SO_3)_2](H_2O)$ and $K_4[(SO_3)_2NN(SO_3)_2](H_2O)_2$. The quantitative *Rietveld* refinement analysis of a powder sample revealed a distribution of 56.2% for $K_4[(SO_3)_2NN(SO_3)_2](H_2O)_2$ and 43.8% for $K_4[(SO_3)_2NN(SO_3)_2](H_2O)$. The product mixture was obtained in a yield of 3.6% (110 mg, 0.206 mmol).

6.13.3 Solvothermal Syntheses with SO_3 in Sealed Glass Vessels

Table 26: Tabular list of reactions with SO_3 in sealed glass reaction vessels (3.3 borosilicate). For the respective products of this work the weighed portions of the reactants, the maximum temperature in the furnace and the timed furnace program (heating↗|holding →|cooling ↘) are listed. $\rho(SO_3)^{[46]} = 1.92\ g{\cdot}cm^{-3}$.

Product	Reactants	T/ ° C	↗|→|↘ / h
$S_6N_4O_{13}H_2{\cdot}P_2O_3Cl_4$	**$P_3N_3Cl_6$:** 200 mg, 0.574 mmol, 1.00 eq. **SO_3:** 0.26 ml, 6.230 mmol, 10.86 eq	RT	-| 72 | -
$Rb[S_3NO_8]$	**$P_3N_3Cl_6$:** 288 mg, 0.807 mmol, 1.00 eq. **RbCl:** 100 mg, 0.827 mmol, 1.00 eq. **SO_3 :** 0.52 ml**,** 12.67 mmol, 15.70 eq.	80	10 | 60 | 100
$Ag[S_3NO_8]$	**$P_3N_3Cl_6$:** 122 mg, 0.349 mmol, 1.00 eq. **AgCl:** 50 mg, 0.349 mmol, 1.00 eq. **SO_3:** 0.33 mL, 7.91 mmol, 20.00 eq.	80	10 | 60 | 100
$Na[S_4NO_{11}]$	**$P_3N_3Cl_6$:** 281 mg, 0.807 mmol, 1.00 eq. **Na_2O:** 50 mg, 0.807 mmol, 1.00 eq. **SO_3:** 0.52 mL, 12.71 mmol, 15.75 eq.	80	10 | 60 | 100
$K[Au(S_4N_2O_{10})(S_3NO_8)Cl]$	**$P_3N_3Cl_6$**: 23 mg, 0.066 mmol, 1.00 eq. **$K[AuCl_4]$:** 25 mg, 0.066 mmol, 1.00 eq. **SO_3:** 0.32 mL, 7.76 mmol, 116.28 eq.	80	10 | 48 | 100
$(NS_2)[Au(S_4N_2O_{10})_2]$	**$(S_3N_2Cl)Cl$:** 15.5 mg, 0.079 mmol, 1.04 eq. **$AuCl_3$:** 23 mg, 0.076 mmol, 1.00 eq. **SO_3:** 0.22 mL, 5.28 mmol, 69.50 eq.	80	10 | 24 | 80
$K_2[Pt(S_4N_3O_9)_2](SO_3)_2$	**$P_3N_3Cl_6$:** 22 mg, 0.062 mmol, 1.00 eq. **$K_2[PtCl_6]$**: 30 mg, 0.062 mmol, 1.00 eq. **SO_3:** 0.21 mL, 5.04 mmol, 81.30 eq.	80	10 | 48 | 24
$[Pt(S_4N_3O_8Cl)_2]$	**Pt (black):** 25 mg, 0.128 mmol, 1.00 eq. **$P_3N_3Cl_6$:** 45 mg, 0.128 mmol, 1.00 eq. **SO_3:** 0.24 mL, 5.04 mmol, 45.00 eq	100	10 | 48 | 100

6.13.4 $(TBA)_4(N_3)_3[SO_3N_3]$

15.0 mg (0.052 mmol, 1.00 eq.) $[N(C_4H_9)_4]N_3$, 8.0 mg (0.052 mmol, 1.00 eq) $(C_5H_5N)(SO_3)$ and 0.5 mL dried *n*-hexane were added to a small snap cap vial in an argon glove box. The mixture was stirred for one day and the *n*-hexane was allowed to evaporate isothermally at RT for one week. By evaporation a colorless solid and a few colorless single crystals were formed. The single crystal XRD analysis revealed the structure of $(TBA)(N_3)_3[SO_3N_3]$.

6.13.5 $(TBA)[SO_3N_3]$

In an argon glove box 30.0 mg (0.105 mmol, 1.00 eq.) $[N(C_4H_9)_4]N_3$, 18.5 mg (0.116 mmol, 1.10 eq) $(C_5H_5N)(SO_3)$ and 1.0 mL dried *n*-hexane were added to a glass ampoule (3.3 borosilicate). The reaction components were cooled with liquid nitrogen and the ampoule was sealed under reduced pressure (10^{-3} mbar) with a gas burner. The closed reaction vessel was then heated to 40 °C within 2 h (0.16 °C·min^{-1}) in a tube furnace. The temperature was maintained for 4 h and then a cooling period to RT within 20 h was initiated. After cooling a colorless amorphous solid with single crystals in between was observed. The SC-XRD analysis revealed the structure of $(TBA)[SO_3N_3]$.

6.13.6 $K[SO_3N_3]$

Single Crystal Preparation: 20.0 mg (0.130 mmol, 1.00 eq.) KSO_3Cl (prepared in the working group), 110 µL (96.8 mg, 0.840 mmol, 6.50 eq.) $(TMS)N_3$ (>95%, TCI Europe) and 150 µL MeCN were placed in a glass ampoule. The mixture was frozen under liquid nitrogen cooling and the ampoule was sealed under reduced pressure (10^{-3} mbar). The ampoule was placed in a tube furnace and was heated from 20 °C to 45 °C within 4 h. This temperature was maintained for further 24 h and then the ampoule was allowed to cool down to RT with a rate of 1.05 °C/ h to enable crystallization. Via the furnace treatment a suspension with a few colorless crystals were formed.

Upscaled-Preparation: In a Schlenk tube 280 mg (1.810 mmol, 1.00 eq.) KSO_3Cl, 0.6 mL (4.46 mmol, 2.52 eq.) $(CH_3)_3SiN_3$ and 2 mL of MeCN were placed. The mixture was stirred for 20 h in a constant argon flow at RT and afterwards all volatile components were removed under reduced pressure. The compound was obtained as a colorless solid in a yield of 91% (265 mg, 1.65 mmol).

6.13.7 $Na_3[SO_3N_3]_3(MeCN)$

120 mg (0.75 mmol, 1.00 eq.) $(C_5H_5N)(SO_3)$, 70 mg (1.08 mmol, 1.44 eq.) NaN_3 and about 1 mL dried MeCN were transferred into a glass ampoule (3.3 borosilicate) in an argon glovebox. The mixture was frozen with liquid nitrogen and then the ampoule was sealed under reduced pressure (10^{-3} mbar) with a gas burner. The sealed glass vessel was heated up to 40 °C within 2 h in a tube

furnace. The temperature of 40 °C was kept for 6 h and finally the vessel was cooled to RT within 8 h. In this process colorless single crystals were formed, which were identified as $(C_5H_5N)(SO_3)$ (recrystallized) and the new compound $Na_3[SO_3N_3]_3(MeCN)$.

6.13.8 $K_3[N(SO_3)_3](H_2O)_2$

10.00 g (44.98 mmol, 2.04 eq.) $K_2S_2O_5$ was dissolved in 24.0 mL water under heating at 50 °C. Simultaneously, 1.87 g (22.00 mmol, 1.00 eq.) KNO_2 was dissolved in 5 mL water. The KNO_2 solution was poured into the warm $KHSO_3$ solution. Within one minute of stirring a cloudy colorless precipitate was formed. 20 mL of KOH (2 mol/L) were directly added to the suspension to stabilize the product. Afterwards the crude solid product was filtered, washed with small portions of water and ethanol and finally dried under reduced pressure (10^{-3} mbar) for several hours. $K_3[N(SO_3)_3](H_2O)_2$ was obtained as a colorless flocculent solid in a total yield of 48% (4.25 g, 10.45 mmol).

Elemental Analysis (C/H/N/S; found/ *calcd*. in %): N 3.43/ *3.44*; C 0/ *0*; H 0.55/ *0.99*, S 23.74/ *23.60*.

6.13.9 $K_2Na[N(SO_3)_3]$

50 mg (0.12 mmol, 1.00 eq.) $K_3[N(SO_3)_3](H_2O)_2$ and 15 mg (0.38 mmol, 3.16 eq.) NaOH were placed in a glass ampoule and 1 ml water was added. The mixture was frozen with liquid nitrogen and the ampoule sealed under reduced pressure (10^{-3} mbar). In a tube furnace the reaction vessel was heated to 65 °C within 4 h. After maintaining the temperature for 4 h a cooling period to RT within 10 h was conducted. Colorless trigonal single crystals formed on the glass wall, which were analyzed and assigned to $K_2Na[N(SO_3)_3]$.

6.13.10 $K_{1.2}Rb_{1.8}[N(SO_3)_3]$

30 mg (0.073 mmol, 1.00 eq.) $K_3[N(SO_3)_3](H_2O)_2$, 26 mg (0.216 mmol, 3.00 eq.) $RbOH{\cdot}H_2O$ and a few drops of water (0.5 mL) were placed in a glass ampoule. The ampoule was sealed under reduced pressure (10^{-3} mbar) and cooling of the mixture by liquid nitrogen. The reaction vessel was heated to 65 °C within 2 h, the temperature was maintained for 4 h and cooling to RT was completed within 11 h. During this process hexagonal colorless crystals were formed, which were analyzed and assigned to $K_{1.2}Rb_{1.8}[N(SO_3)_3]$.

6.13.11 $Cs_2K[N(SO_3)_3]$

100 mg (0.245 mmol, 1.00 eq.) $K_3[N(SO_3)_3](H_2O)_2$, 165 mg (0.988 mmol, 4.03 eq.) $CsOH \cdot H_2O$ and 0.2 mL water were loaded into a glass ampoule. After cooling the mixture with liquid nitrogen, the ampoule was sealed under reduced pressure (10^{-3} mbar). In a tube furnace the reaction ampoule was heated up to 65 °C in a period of 2 h and the temperature was hold for further 24 h. Then a cooling period to RT within 40 hours was initiated to enable crystallization. On the glass wall colorless crystals were formed, which were assigned to $Cs_2K[N(SO_3)_3]$.

7 Analytical Data

7.1 Vibrational Spectroscopy

7.1.1 $K[SO_3N_3]$

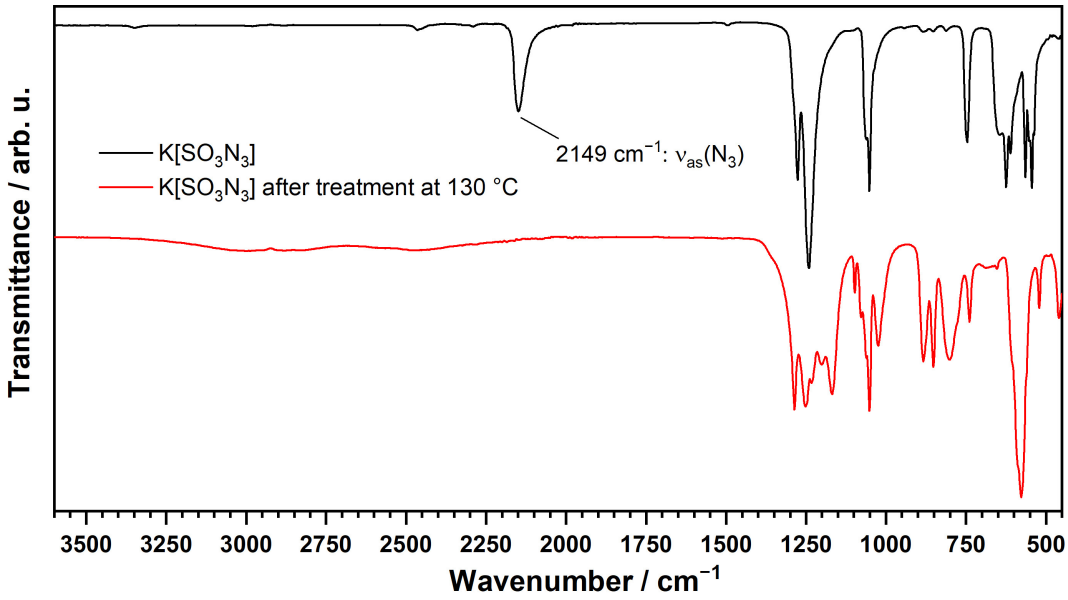

Figure 83: IR spectrum of $K[SO_3N_3]$ recorded before and after treatment at 130 °C (TGA analysis).

7.1.2 $[Pt(S_4N_3O_8Cl)_2]$

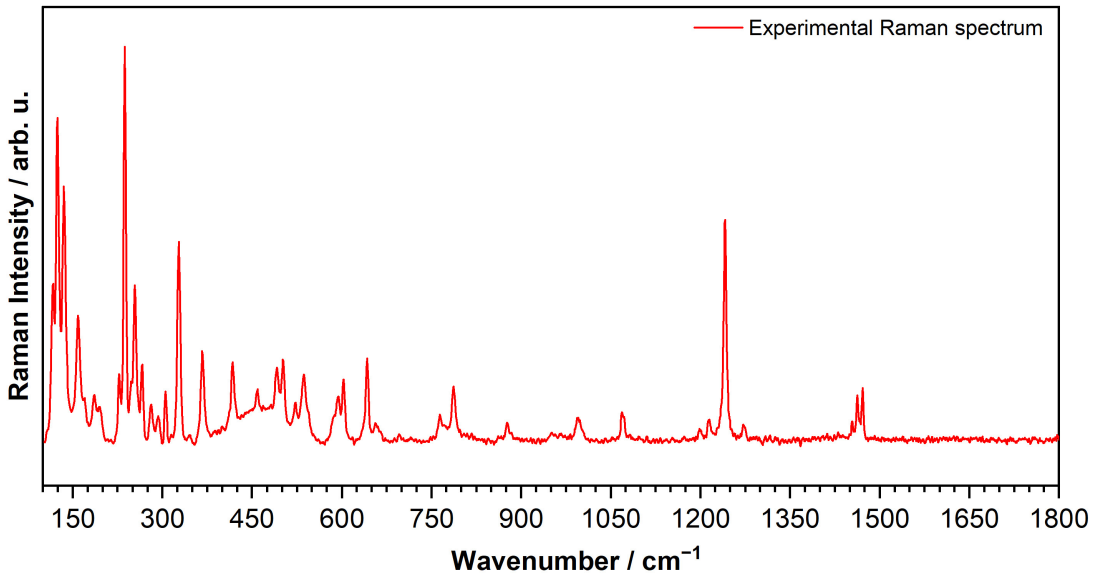

Figure 84: *Raman* spectrum of $[Pt(S_4N_3O_8Cl)_2]$ recorded on a single crystal.

7.2 Powder X-ray Diffraction

7.2.1 K[SO$_3$N$_3$] (TGA residue, T$_{max}$ = 1000 °C)

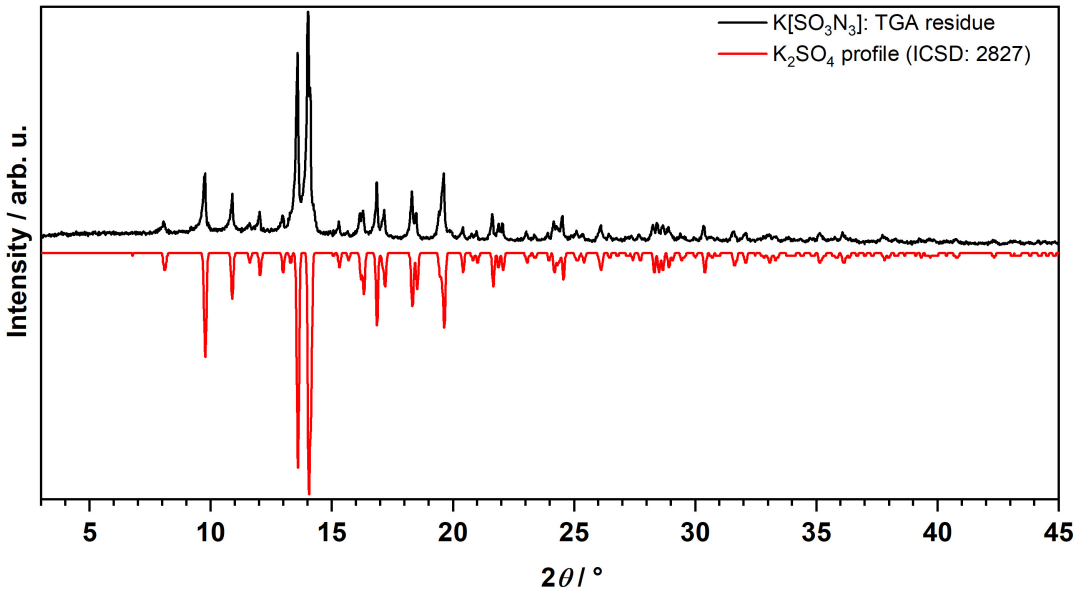

Figure 85: Experimental powder X-ray diffractogram of the residue from the thermogravimetric analysis of K[SO$_3$N$_3$] (T$_{max}$= 1000 °C) compared to a simulated diffractogram (using *WinXPOW*[191]) of K$_2$SO$_4$. The powder was measured in an 0.3 mm glass capillary with Mo-K$_{\alpha1}$ (λ = 70.930 pm) radiation. The K$_2$SO$_4$ profile was simulated from single crystal data of K$_2$SO$_4$ (ICSD: 2827) using *WinXPOW*.

7.2.2 K[SO$_3$N$_3$] (TGA residue, T$_{max}$ = 230 °C)

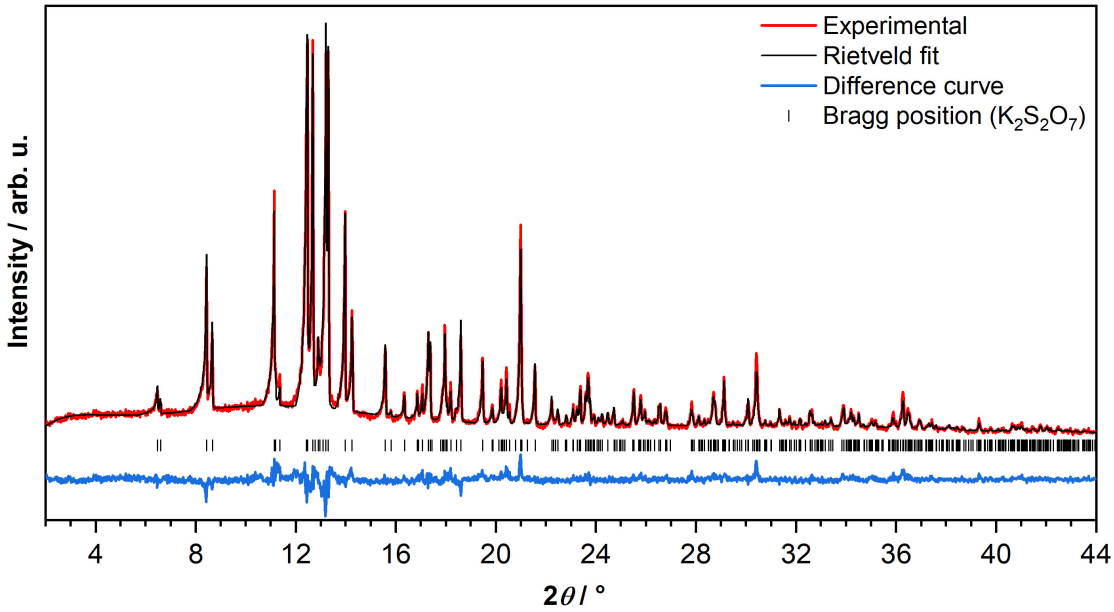

Figure 86: Experimental powder X-ray diffractogram of K[SO$_3$N$_3$] heated to 230 °C in an TG analysis with *Rietveld* refinement. For the refinement the single crystal data of K$_2$S$_2$O$_7$ (ICSD: 249741) was used. The powder was measured in an 0.3 mm glass capillary with Mo-K$_{\alpha1}$ (λ = 70.930 pm) radiation. The cell parameters *a*, *b*, *c* and β were refined. The following profile factors were obtained: R_{wp} = 7.80%, R_{exp} = 6.25%, R_p = 6.15%, GooF = 1.25. Cell parameters after refinement: *C*2/*c*, *a* = 1236.11(3) pm, *b* = 731.37(3) pm, *c* = 728.80(2) pm, β = 93.14(2)°, *V* = 0.65790(3) nm^3.

7.2.3 $K_3[N(SO_3)_3](H_2O)_2$ (TGA residue, T_{max} = 1000 °C)

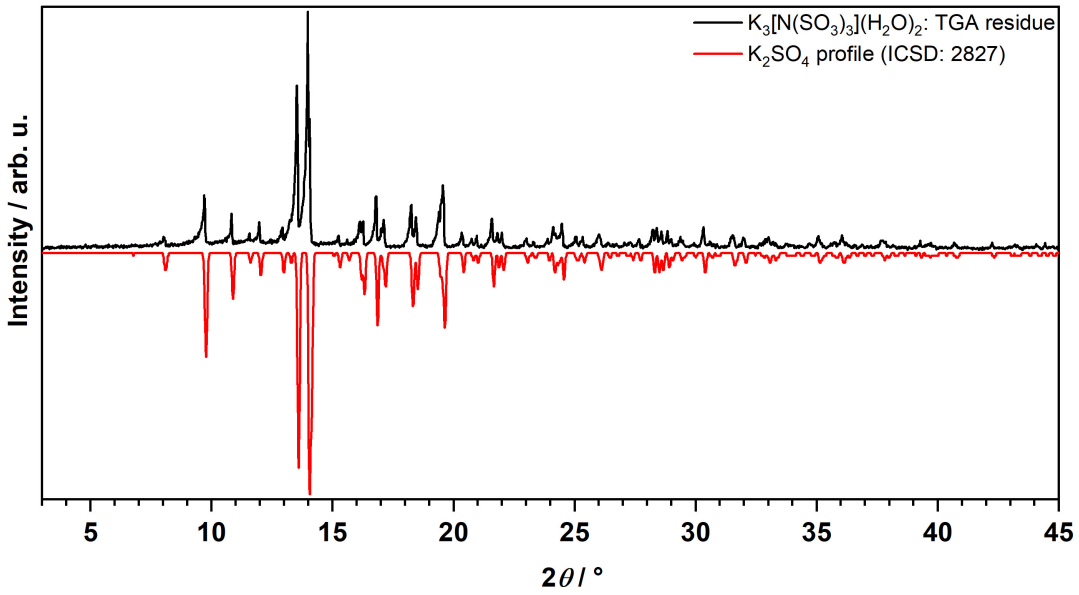

Figure 87: Experimental powder X-ray diffractogram of the residue from the thermogravimetric analysis (T_{max}= 1000 °C) of $K_3[N(SO_3)_3](H_2O)_2$ compared to a simulated diffractogram (using *WinXPOW*[191]) of K_2SO_4. The powder was measured in an 0.3 mm glass capillary with Mo-$K_{\alpha1}$ (λ = 70.930 pm) radiation. The K_2SO_4 profile was simulated from single crystal data of K_2SO_4 (ICSD: 2827) using *WinXPOW*.

7.2.4 $K_3[N(SO_3)_3](H_2O)_2$ (TGA residue, T_{max} = 370 °C)

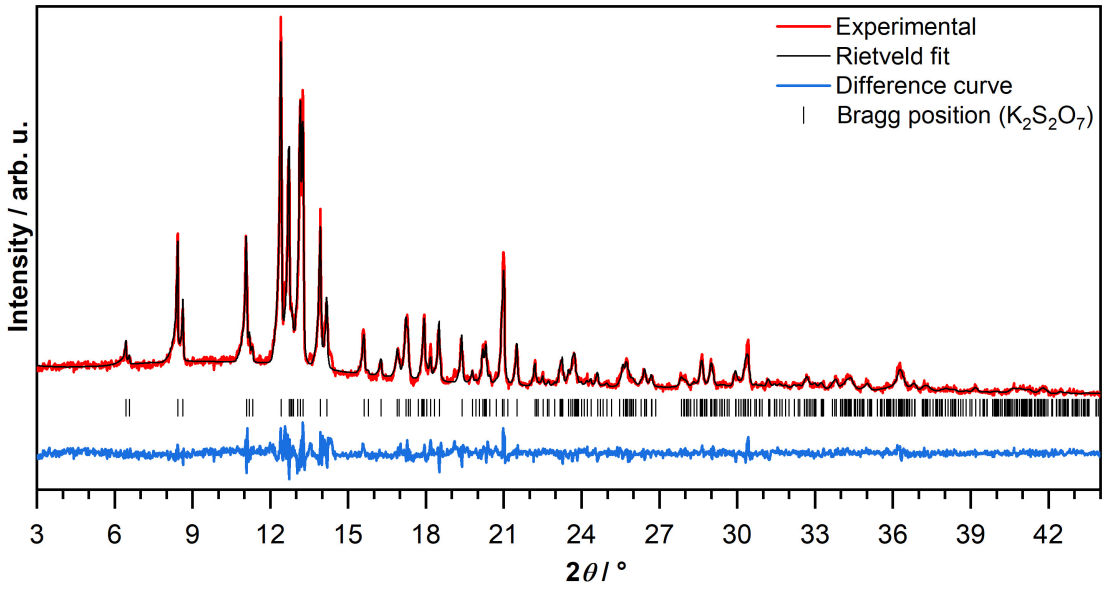

Figure 88: Experimental powder X-ray diffractogram of $K_3[N(SO_3)_3](H_2O)_2$ heated to 370 °C in an TG analysis with *Rietveld* refinement. For the refinement the single crystal data of $K_2S_2O_7$ (ICSD: 249741) was used. The powder was measured in an 0.3 mm glass capillary with Mo-$K_{\alpha1}$ (λ = 70.930 pm) radiation. The cell parameters *a*, *b*, *c*, β and all atomic positions were refined. The following profile factors were obtained: R_{wp} = 8.70%, R_{exp} = 6.39%, R_p = 6.70%, GooF = 1.25. Cell parameters after refinement: *C*2/*c*, *a* = 1239.47(8) pm, *b* = 734.84(5) pm, *c* = 727.70(6) pm, β = 92.710(4)°, *V* = 0.66206(8) nm^3.

7.2.5 $K_2[HN(SO_3)_2]$

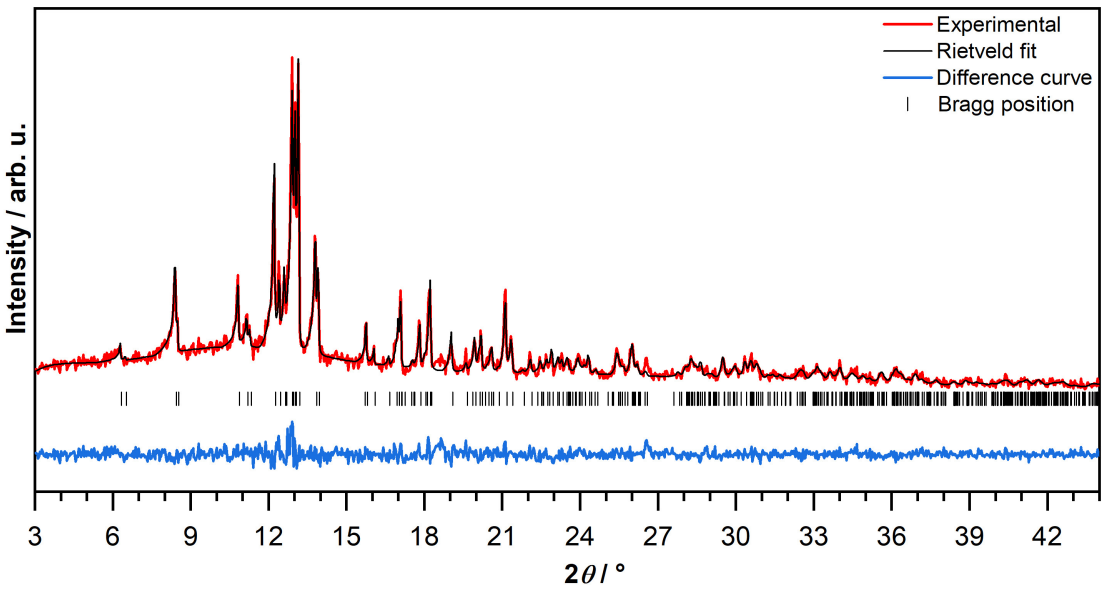

Figure 89: Experimental powder X-ray diffractogram of $K_2[HN(SO_3)_2]$ with *Rietveld* refinement. $K_2[HN(SO_3)_2]$ was obtained by storing $K[N(SO_3)_3](H_2O)_2$ in an aqueous solution for a few hours. For the refinement the single crystal data of $K_2[HN(SO_3)_2]$ (see 7.4.19, p.156) was used. The powder was measured in an 0.3 mm glass capillary with Mo-$K_{\alpha1}$ (λ = 70.930 pm) radiation. The cell parameters *a*, *b*, *c*, and β all atomic positions of K, S and O were refined. The following profile factors were obtained: R_{wp} = 10.69%, R_{exp} = 6.94%, R_p = 8.20%, GooF = 1.54. Cell parameters after refinement: *C*2/*c*, *a* = 1246.4(2) pm, *b* = 748.4(1) pm, *c* = 719.06(9) pm, β = 91.230(9)°, *V* = 0.6705(2) nm^3.

7.3 Results from Quantum Mechanical Calculations

7.3.1 $[(SO_3)_2NN(SO_3)_2]^{4-}$

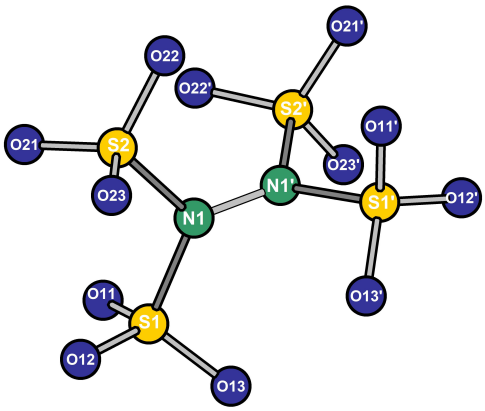

Figure 90: Structure of $[(SO_3)_2NN(SO_3)_2]^{4-}$ obtained from a geometry optimization (see 6.9, p. 116).

Table 27: Atomic coordinates of $[(SO_3)_2NN(SO_3)_2]^{4-}$ obtained from the geometry optimization.

Atom	*x*	*y*	*z*	Atom	*x*	*y*	*z*
N1	5.5232	5.56058	10.98778	O21'	6.62942	7.38451	14.0504
N1'	5.92766	5.56055	12.28675	O22	4.05482	7.59376	11.5466
O11	7.57638	5.38232	9.33002	O22'	7.39592	7.59388	11.72812
O11'	3.87436	5.38245	13.94439	O23	3.08223	5.90238	10.07262
O12	5.44677	4.35756	8.72035	O23'	8.36873	5.90227	13.20167
O12'	6.00389	4.35766	14.55424	S1	6.42178	4.60023	9.79446
O13	6.8277	3.3803	10.49815	S1'	5.02897	4.6003	13.48006
O13'	4.62305	3.38035	12.77641	S2	4.27173	6.70467	10.40731
O21	4.82161	7.38482	9.22437	S2'	7.17917	6.70459	12.86727

Table 28: Bond lengths for $[(SO_3)_2NN(SO_3)_2]^{4-}$ obtained from the geometry optimization.

Atom–Atom	Length/ pm
N1–N1'	136
N1–S1	177.6
N1–S2	179.2
S1–O11	147
S1–O12	147.1
S1–O13	146.6
S2–O21	147.1
S2–O22	146.1
S2–O23	147.3

7.3.2 $[Pt(S_4N_3O_9)_2]^{2-}$

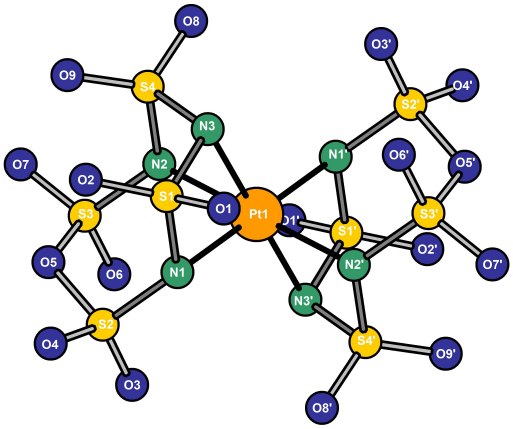

Figure 91: Structure of $[Pt(S_4N_3O_9)_2]^{2-}$ obtained from a geometry optimization (see 6.9, p. 116).

Table 29: Atomic coordinates of $[Pt(S_4N_3O_9)_2]^{2-}$ obtained from a geometry optimization.

Atom	*x*	*y*	*z*	Atom	*x*	*y*	*z*
N1	5.85764	7.5369	5.69186	O6'	2.86532	4.39308	5.13358
N1'	4.82472	4.57287	8.40977	O7	6.29236	9.54977	9.67657
N2	5.38182	7.50842	8.53096	O7'	4.39091	2.5601	4.42503
N2'	5.30104	4.60158	5.57073	O8	2.94332	7.35893	9.18069
N3	3.65952	7.29803	6.77998	O8'	7.73965	4.75166	4.92167
N3'	7.02293	4.81213	7.32224	O9	3.69669	9.50488	8.22044
O1	3.77221	7.38694	4.27619	O9'	6.98651	2.60545	5.88153
O1'	6.90981	4.7228	9.826	Pt1	5.34125	6.05497	7.05071
O2	4.14365	9.52266	5.45768	S1	4.27089	8.0981	5.41188
O2'	6.53885	2.58722	8.64408	S1'	6.41146	4.01177	8.69009
O3	8.30334	7.76079	6.06251	S2	7.12341	8.54296	5.89818
O3'	2.37909	4.34866	8.03886	S2'	3.55911	3.56666	8.20331
O4	7.06506	9.60814	4.94702	S3	6.64889	8.50675	8.76685
O4'	3.61748	2.50145	9.15443	S3'	4.03414	3.60305	5.33472
O5	6.82218	9.32536	7.33199	S4	3.79282	8.07848	8.28354
O5'	3.86071	2.78437	6.76949	S4'	6.89007	4.03182	5.81852
O6	7.81765	7.71661	8.96787				

Table 30: Bond lengths for $[Pt(S_4N_3O_9)_2]^{2-}$ obtained from a geometry optimization.

Atom–Atom	Length/ pm	Atom–Atom	Length/ pm
Pt1–N1	207.6	O1–S1	143
Pt1–N2	207.5	O5–S3	166.1
Pt1–N3	210.9	S2–O5	166.1
N1–S1	170.6	S2–O3	142.5
N1–S2	163	S2–O4	142.9
N2–S4	170.6	S3–O7	142.9
N2–S3	163	S3–O6	142.5
N3–S4	169.9	S4–O8	143
N3–S1	169.9	S4–O9	143.1

7.3.3 $[SO_3N_3]^-$

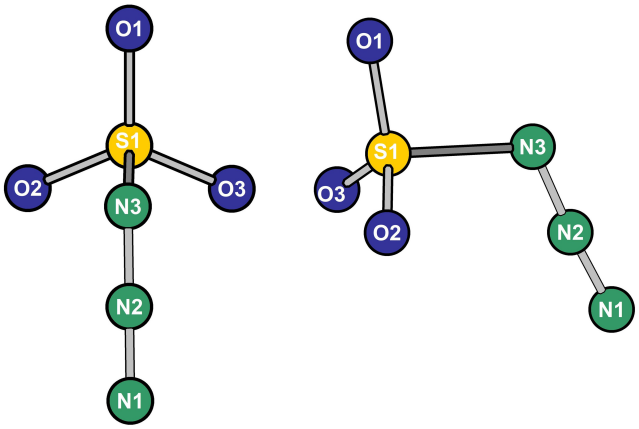

Figure 92: Structure of $[SO_3N_3]^-$ obtained from a geometry optimization (see 6.9, p. 116).

Table 31: Atomic coordinates for $[SO_3N_3]^-$ obtained from the geometry optimization.

Atom	*x*	*y*	*z*
S1	4.82471	2.58076	2.38937
O3	5.37921	1.68136	1.3897
O2	4.63448	2.00032	3.70928
O1	3.78423	3.47923	1.9319
N3	6.17591	3.78065	2.65885
N2	7.20925	3.28164	3.03828
N1	8.21174	2.88747	3.39475
N1	8.21174	2.88747	3.39475

Table 32: Bond lengths for $[SO_3N_3]^-$ obtained from the geometry optimization.

Atom–Atom	Length/ pm
N2–N1	113.5
N3–N2	120.9
S1-N3	182.7
S1-O1	144.9
S1-O2	145.4
S1-O3	145.5

7.4 Single Crystal X-ray Diffraction

In the following the single crystal data tables with the most important information are listed. For structures, which are not uploaded to the CCDC database, also more detailed information as the atomic coordinates, anisotropic displacement parameters, selected bond lengths and angles are given. For all single crystal structures uploaded to the CCDC database[210], the CSD deposition number is provided to retrieve the crystallographic information file (CIF).

7.4.1 $(S_3N_2Cl)Cl$

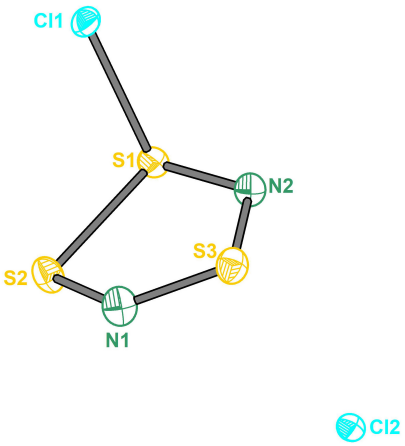

Figure 93: Structure and labeling of $(S_3N_2Cl)Cl$. The thermal ellipsoids are set to a probability level of 70%.

Table 33: Crystallographic data of $(S_3N_2Cl)Cl$.

Empirical formula	$Cl_2N_2S_3$	
Formula weight	195.10 g · mol^{-1}	
Temperature	100.0(2) K	
Wavelength	71.073 pm (Mo-K$_\alpha$)	
Crystal system	monoclinic	
Space group	$P2_1$ (4)	
Unit cell dimensions	a = 547.00(3) pm	
	b = 850.67(5) pm	β = 102.348(3)°
	c = 650.44(4) pm	
Volume	0.29566(3) nm^3	
Z	2	
Density (calculated)	2.192 g · cm^{-3}	
Absorption coefficient μ	2.023 mm^{-1}	
F(000)	192.0	
Crystal size	0.19 × 0.06 × 0.04 mm^3	
2θ range/ °	6.412 to 54.924	
Index ranges	$-7 \leq h \leq 7$, $-11 \leq k \leq 11$, $-8 \leq l \leq 8$	
Reflections collected	14666	
Independent reflections	1344 [R_{int}= 0.0503, R_σ= 0.0280]	
Completeness to theta = 27.46°	100%	
Absorption correction	multiscan	
Max. and min. transmission	0.751 and 0.572	

Refinement method	least-squares
Data / restraints / parameters	1344/1/65
Goodness-of-fit on F^2	1.120
Final R indices [$I \geq 2\sigma(I)$]	$R_1 = 0.0166$, $wR_2 = 0.0384$
R indices (all data)	$R_1 = 0.0167$, $wR_2 = 0.0384$
Largest diff. peak and hole	$0.51/-0.33$ e · Å^{-3}
BASF	0.36(12)

Table 34: Atomic coordinates and equivalent isotropic displacement parameters [pm^2 x 10^4] for (S_3N_2Cl)Cl. *U(eq)* is defined as one third of the trace of the orthogonalized U_{ij} tensor**.**

Atom	***x***	***y***	***z***	U_{eq}
Cl2	0.6046(1)	0.49499(7)	0.19856(8)	0.0129(1)
S2	0.3862(1)	0.62384(6)	0.78514(8)	0.0123(1)
S3	0.1765(1)	0.51582(7)	0.38718(9)	0.0124(1)
S1	0.3484(1)	0.37427(6)	0.77008(8)	0.0111(1)
Cl1	0.0163(1)	0.34560(7)	0.90082(9)	0.0174(1)
N2	0.2585(4)	0.3578(2)	0.5229(3)	0.0132(4)
N1	0.2440(4)	0.6550(2)	0.5422(3)	0.0136(4)

Table 35: Anisotropic displacement parameters [pm^2 × 10^4] for (S_3N_2Cl)Cl. The anisotropic displacement factor exponent takes the form: $-2\pi^2$ [h^2 a*^{2}U_{11} + 2 h k a* b* U_{12} +…].

Atom	U_{11}	U_{22}	U_{33}	U_{23}	U_{13}	U_{12}
Cl2	0.0125(2)	0.0125(2)	0.0130(2)	0.0005(2)	0.0013(2)	−0.0004(2)
S2	0.0147(3)	0.0099(3)	0.0109(3)	−0.0004(2)	−0.0005(2)	−0.0003(2)
S3	0.0111(3)	0.0148(2)	0.0105(3)	−0.0014(2)	0.0009(2)	0.0003(2)
S1	0.0116(3)	0.0098(3)	0.0120(3)	−0.0004(2)	0.0031(2)	−0.0006(2)
Cl1	0.0149(3)	0.0233(3)	0.0153(3)	−0.0049(2)	0.0058(2)	−0.0050(2)
N2	0.0141(9)	0.0130(9)	0.0133(9)	−0.0024(8)	0.0047(7)	−0.0017(8)
N1	0.014(1)	0.013(1)	0.0120(9)	0.0006(7)	0.0000(8)	0.0025(8)

Table 36: Selected experimental bond lengths [pm] for (S_3N_2Cl)Cl.

Atom–Atom	**Length/ pm**
S2–S1	213.32(7)
S2–N1	162.6(2)
S3–N2	161.8(2)
S3–N1	154.8(2)
S1–Cl1	217.79(8)
S1–N2	158.4(2)

Table 37: Selected experimental bond angles [°] for (S_3N_2Cl)Cl.

Atom–Atom–Atom	**Angle/ °**
N1–S2–S1	95.52(7)
N1–S3–N2	106.3(1)
S2–S1–Cl1	100.03(3)
N2–S1–S2	98.08(8)
N2–S1–Cl1	106.42(8)
S1–N2–S3	118.0(1)
S3–N1–S2	120.4(1)

7.4.2 $(S_6N_4O_{13}H_2)\cdot(P_2O_3Cl_4)$

Table 38: Crystallographic data of $(S_6N_4O_{13}H_2)\cdot(P_2O_3Cl_4)$.

Empirical formula	$Cl_4H_2N_4O_{16}P_2S_6$
Formula weight	710.16 g · mol^{-1}
Temperature	100.00 K
Wavelength	71.073 pm (Mo-Kα)
Crystal system	monoclinic
Space group	$P2_1/n$ (14)
Unit cell dimensions	a = 1148.20(5) pm
	b = 1383.87(7) pm β = 103.184(2)°
	c = 1337.94(6) pm
Volume	2.0699(2) nm^3
Z	4
Density (calculated)	2.279 g · cm^{-3}
Absorption coefficient μ	1.415 mm^{-1}
F(000)	1408.0
Crystal size	0.209 × 0.166 × 0.1 mm^3
2θ range/ °	4.226 to 64.998°
Index ranges	−17 ≤ h ≤ 17, −20 ≤ k ≤ 20, −20 ≤ l ≤ 20
Reflections collected	74019
Independent reflections	7497 [R_{int}= 0.0537, R_σ= 0.0271]
Completeness to theta = 27.46°	100%
Absorption correction	multiscan
Max. and min. transmission	0.751 and 0.572
Refinement method	least-squares
Data / restraints / parameters	7497/0/289
Goodness-of-fit on F^2	1.109
Final R indices [$I \geq 2\sigma(I)$]	R_1 = 0.0325, wR_2 = 0.0714
R indices (all data)	R_1 = 0.0401, wR_2 = 0.0770
Largest diff. peak and hole	0.65/−0.53 e · Å^{-3}
CSD Number	2358807

7.4.3 Rb[S$_3$NO$_8$]

Table 39: Crystallographic data of Rb[S_3NO_8].

Empirical formula	NO_8RbS_3
Formula weight	323.66 g · mol^{-1}
Temperature	100.0(2) K
Wavelength	71.073 pm (Mo-Kα)
Crystal system	orthorhombic
Space group	$P2_12_12_1$ (19)
Unit cell dimensions	a = 928.77(4) pm
	b = 961.37(5) pm
	c = 2545.8(1) pm
Volume	2.2731(2) nm^3
Z	12
Density (calculated)	2.837 g · cm^{-3}
Absorption coefficient μ	7.378 mm^{-1}
F(000)	1872
Crystal size	0.16 × 0.153 × 0.126 mm^3
2θ range/ °	4.528 to 64.106
Index ranges	−13 ≤ h ≤ 13, −14≤ k ≤ 13, −37 ≤ l ≤ 37
Reflections collected	49348
Independent reflections	7155 [R_{int}= 0.0719, R_σ= 0.0606]
Completeness to theta = 32.05°	100%
Absorption correction	multiscan
Max. and min. transmission	0.746 and 0.542
Refinement method	least-squares
Data / restraints / parameters	7155/0/353
Goodness-of-fit on F^2	1.025
Final R indices [$I \geq 2\sigma(I)$]	R_1 = 0.0462, wR_2 = 0.0766
R indices (all data)	R_1 = 0.0875, wR_2 = 0.0895
Largest diff. peak and hole	0.88/−0.81 e · Å^{-3}
BASF	0.52(2)
CSD Number	2341238

7.4.4 Ag[S_3NO_8]

Table 40: Crystallographic data of Ag[S_3NO_8].

Empirical formula	$AgNO_8S_3$
Formula weight	346.06 g · mol^{-1}
Temperature	100.0(2) K
Wavelength	71.073 pm (Mo-K_α)
Crystal system	orthorhombic
Space group	*Pnma* (62)
Unit cell dimensions	a = 860.03(4) pm
	b = 942.33(5) pm
	c = 860.19(4) pm
Volume	0.69713(6) nm^3
Z	4
Density (calculated)	3.297 g · cm^{-3}
Absorption coefficient μ	3.807 mm^{-1}
F(000)	664.0
Crystal size	0.4 × 0.19 × 0.02 mm^3
2θ range/ °	6.414 to 60.988
Index ranges	$-12 \leq h \leq 12$, $-13 \leq k \leq 13$, $-12 \leq l \leq 11$
Reflections collected	24861
Independent reflections	1123 [R_{int}= 0.0479, R_σ= 0.0181]
Completeness to theta = 30.49°	99.6%
Absorption correction	multiscan
Max. and min. transmission	0.746 and 0.539
Refinement method	least-squares
Data / restraints / parameters	1123/0/67
Goodness-of-fit on F^2	1.094
Final R indices [$I \geq 2\sigma(I)$]	R_1 = 0.0146, wR_2 = 0.0382
R indices (all data)	R_1 = 0.0149, wR_2 = 0.0383
Largest diff. peak and hole	0.64/−0.52 e · $Å^{-3}$
CSD Number	2341239

7.4.5 Na[S$_4$NO$_{11}$]

Table 41: Crystallographic data of Na[S$_4$NO$_{11}$].

Empirical formula	$NNaO_{11}S_4$
Formula weight	341.24 g · mol^{-1}
Temperature	100.0(2) K
Wavelength	71.073 pm (Mo-Kα)
Crystal system	monoclinic
Space group	$P2_1/n$ (14)
Unit cell dimensions	a = 734.58(4) pm b = 1337.59(7) pm β = 101.525(2)° c = 944.86(5) pm
Volume	0.90967(8) nm^3
Z	4
Density (calculated)	2.492 g · cm^{-3}
Absorption coefficient μ	1.153 mm^{-1}
F(000)	680.0
Crystal size	0.22 × 0.138 × 0.082 mm^3
2θ range/ °	5.352 to 57.996
Index ranges	−10 ≤ h ≤ 9, −18≤ k ≤ 18, −12 ≤ l ≤ 12
Reflections collected	242516
Independent reflections	2417 [R_{int}= 0.0476, R_σ= 0.0187]
Completeness to theta = 29.00°	99.8%
Absorption correction	multiscan
Max. and min. transmission	0.747 and 0.580
Refinement method	least-squares
Data / restraints / parameters	2417/0/154
Goodness-of-fit on F^2	1.116
Final R indices [$I \geq 2\sigma(I)$]	R_1 = 0.0284, wR_2 = 0.0715
R indices (all data)	R_1 = 0.0308, wR_2 = 0.0729
Largest diff. peak and hole	0.81/−0.40 e · Å^{-3}
CSD Number	2341237

7.4.6 $(NS_2)[Au(S_4N_2O_{10})_2]$

Table 42: Crystallographic data of $(NS_2)[Au(S_4N_2O_{10})_2]$.

Empirical formula	$AuN_5O_{20}S_{10}$
Formula weight	907.62 g · mol^{-1}
Temperature	100.0(2) K
Wavelength	71.073 pm (Mo-Kα)
Crystal system	monoclinic
Space group	*C*2/*c* (15)
Unit cell dimensions	*a* = 1305.95(7) pm
	b = 1278.69(6) pm β = 113.399(2)°
	c = 1304.34(7) pm
Volume	1.9990(2) nm^3
Z	4
Density (calculated)	3.016 g · cm^{-3}
Absorption coefficient μ	8.518 mm^{-1}
F(000)	1736.0
Crystal size	0.141 × 0.0033 × 0.029 mm^3
2θ range/ °	4.658 to 57.952
Index ranges	−17 ≤ h ≤ 17, −17≤ k ≤ 17, −17 ≤ l ≤ 17
Reflections collected	16135
Independent reflections	2646 [R_{int}= 0.0318, R_σ= 0.0275]
Completeness to theta = 28.98°	99.4%
Absorption correction	multiscan
Max. and min. transmission	0.747 and 0.628
Refinement method	least-squares
Data / restraints / parameters	2646/0/167
Goodness-of-fit on F^2	1.077
Final *R* indices [$I \geq 2\sigma(I)$]	R_1 = 0.0181, wR_2 = 0.0395
R indices (all data)	R_1 = 0.0226, wR_2 = 0.0423
Largest diff. peak and hole	0.64/−1.47 e · Å^{-3}
BASF	0.0555(7)
CSD Number	2341067

7.4.7 K[Au(S$_4$N$_2$O$_{10}$)(S$_3$NO$_8$)Cl]

Table 43: Crystallographic data of K[Au(S$_4$N$_2$O$_{10}$)(S$_3$NO$_8$)Cl].

Empirical formula	$AuClKN_3O_{18}S_7$
Formula weight	825.97 g · mol^{-1}
Temperature	100.0(2) K
Wavelength	71.073 pm (Mo-Kα)
Crystal system	monoclinic
Space group	$P2_1/c$ (14)
Unit cell dimensions	a = 803.32(4) pm
	b = 1544.70(8) pm β = 104.736(2)°
	c = 1532.20(8) pm
Volume	1.8388(2) nm^3
Z	4
Density (calculated)	2.984 g · cm^{-3}
Absorption coefficient μ	9.266 mm^{-1}
F(000)	1568.0
Crystal size	0.278 × 0.081 × 0.091 mm^3
2θ range/ °	3.808 to 52.992
Index ranges	−10 ≤ h ≤ 10, −13≤ k ≤ 19, −16 ≤ l ≤ 19
Reflections collected	16702
Independent reflections	3795 [R_{int}= 0.0570, R_σ= 0.0474]
Completeness to theta = 26.50°	99.9%
Absorption correction	multiscan
Max. and min. transmission	0.747 and 0.171
Refinement method	least-squares
Data / restraints / parameters	3795/0/280
Goodness-of-fit on F^2	1.040
Final R indices [$I \geq 2\sigma(I)$]	R_1 = 0.0398, wR_2 = 0.0884
R indices (all data)	R_1 = 0.0486, wR_2 = 0.0926
Largest diff. peak and hole	1.84/−1.63 e · Å^{-3}
CSD Number	2341236

7.4.8 $K_2[Pt(S_4N_3O_9)_2](SO_3)_2$

Table 44: Crystallographic data of $K_2[Pt(S_4N_3O_9)_2](SO_3)_2$.

Empirical formula	$K_2N_6O_{24}PtS_{10}$	
Formula weight	1061.95 g · mol^{-1}	
Temperature	100.0(2) K	
Wavelength	71.073 pm (Mo-Kα)	
Crystal system	monoclinic	
Space group	*C*2/*c* (15)	
Unit cell dimensions	*a* = 1439.4(1) pm	
	b = 1211.0(1) pm	β = 104.744(4)°
	c = 1458.2(1) pm	
Volume	2.4580(4) nm^3	
Z	4	
Density (calculated)	2.870 g · cm^{-3}	
Absorption coefficient μ	7.017 mm^{-1}	
F(000)	2040.0	
Crystal size	0.126 × 0.085 × 0.048 mm^3	
2θ range/ °	4.46 to 65.00	
Index ranges	−21 ≤ h ≤ 21, 0≤ k ≤ 18, 0 ≤ l ≤ 22	
Reflections collected	4432	
Independent reflections	4432 [R_{int}= 0.0617, R_σ= 0.0204]	
Completeness to theta = 25.2°	100%	
Absorption correction	multiscan	
Max. and min. transmission	0.7465 and 0.6376	
Refinement method	least-squares	
Data / restraints / parameters	4432/0/197	
Goodness-of-fit on F^2	1.134	
Final *R* indices [$I \geq 2\sigma(I)$]	R_1 = 0.0400, wR_2 = 0.0983	
R indices (all data)	R_1 = 0.0513, wR_2 = 0.1126	
Largest diff. peak and hole	2.43/−1.07 e · Å^{-3}	
BASF	0.073(3)	
CSD Number	2310249	

7.4.9 [Pt(S4N3O8Cl)2]

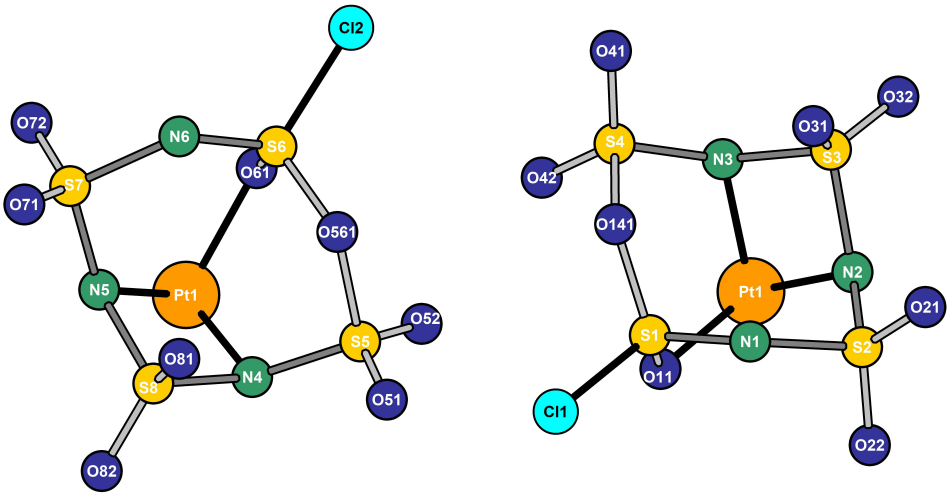

Figure 94: Labeling of [Pt(S4N3O8Cl)2] from two different directions to provide a better perspective.

Table 45: Crystallographic data of [Pt(S4N3O8Cl)2].

Empirical formula	$Cl_2N_6O_{16}PtS_8$
Formula weight	862.53 g · mol^{-1}
Temperature	100.0(2) K
Wavelength	71.073 pm (Mo-K$_\alpha$)
Crystal system	monoclinic
Space group	$P2_1/n$ (14)
Unit cell dimensions	a = 745.78(4) pm b = 1380.84(6) pm β = 101.133(2)° c = 1912.37(9) pm
Volume	1.9323(2) nm^3
Z	4
Density (calculated)	2.965 g · cm^{-3}
Absorption coefficient μ	8.498 mm^{-1}
F(000)	1640.0
Crystal size	0.221 × 0.099 × 0.08 mm^3
2θ range/ °	4.342 to 59.998
Index ranges	−10 ≤ h ≤ 10, −19≤ k ≤ 19, −26 ≤ l ≤ 26
Reflections collected	66852
Independent reflections	5586 [R_{int}= 0.0271, R_σ= 0.0143]
Completeness to theta = 30.00°	99.1%
Absorption correction	multiscan
Max. and min. transmission	0.747 and 0.474
Refinement method	least-squares
Data / restraints / parameters	5586/0/298
Goodness-of-fit on F^2	1.076
Final R indices [$I \geq 2\sigma(I)$]	R_1 = 0.0251, wR_2 = 0.0641
R indices (all data)	R_1 = 0.0255, wR_2 = 0.0644
Largest diff. peak and hole	4.22/−0.97 e · Å^{-3}

Table 46: Atomic coordinates and equivalent isotropic displacement parameters [pm^2 x 10^4] for [$Pt(S_4N_3O_8Cl)_2$]. *U(eq)* is defined as one third of the trace of the orthogonalized U_{ij} tensor**.**

Atom	*x*	*y*	*z*	U_{eq}
Pt1	0.3805(2)	0.28189(2)	0.31616(2)	0.00792(4)
S3	0.5460(1)	0.40241(5)	0.42851(4)	0.0103(1)
S4	0.1632(1)	0.35866(6)	0.42984(4)	0.0107(1)
S8	0.1906(1)	0.40530(6)	0.20999(4)	0.0123(1)
Cl2	0.5606(1)	0.08967(6)	0.13107(5)	0.0183(2)
S5	0.5732(1)	0.38254(6)	0.20209(4)	0.0132(1)
S7	0.0636(1)	0.20648(6)	0.18855(4)	0.0133(1)
S2	0.70460(1)	0.21179(6)	0.44408(4)	0.0138(2)
S6	0.43982(1)	0.18792(6)	0.17558(4)	0.0152(2)
S1	0.33326(1)	0.17208(6)	0.45386(4)	0.0147(2)
Cl1	0.23738(1)	0.06232(6)	0.49689(5)	0.0212(2)
O11	0.3028(3)	0.1675(2)	0.3739(1)	0.0134(4)
O61	0.4797(3)	0.1806(2)	0.2556(1)	0.0122(4)
O41	0.1544(3)	0.4323(2)	0.47800(1)	0.0160(5)
O32	0.6120(3)	0.4808(2)	0.3936(1)	0.0151(4)
O31	0.5649(3)	0.3971(2)	0.5038(1)	0.0144(4)
O141	0.2424(3)	0.2639(2)	0.4807(1)	0.0133(4)
O22	0.7290(4)	0.1317(2)	0.40143(1)	0.0198(5)
N1	0.5410(3)	0.1773(2)	0.4889(1)	0.0087(4)
O561	0.5046(4)	0.2881(2)	0.1497(1)	0.0150(5)
O72	0.0518(4)	0.1246(2)	0.2312(1)	0.0187(5)
O81	0.1676(4)	0.4085(2)	0.1346(1)	0.0186(5)
N5	0.1455(4)	0.2954(2)	0.2410(2)	0.0110(5)
O51	0.5588(4)	0.4601(2)	0.1537(1)	0.0197(5)
N6	0.2305(3)	0.1810(2)	0.1434(1)	0.0102(5)
O71	-0.0795(4)	0.2399(2)	0.1347(1)	0.0192(5)
O52	0.7367(3)	0.3541(2)	0.2475(1)	0.0189(5)
O82	0.1139(3)	0.4759(2)	0.2487(1)	0.0169(5)
O42	0.0110(3)	0.3251(2)	0.3803(1)	0.0153(5)
O21	0.8420(4)	0.2474(2)	0.4993(1)	0.0198(5)
N2	0.6119(4)	0.2993(2)	0.3930(1)	0.0106(5)
N4	0.4158(4)	0.3926(2)	0.2510(1)	0.0115(5)
N3	0.3251(4)	0.3826(2)	0.3854(1)	0.0096(5)

Table 47: Anisotropic displacement parameters [$pm^2 \times 10^4$] for [$Pt(S_4N_3O_8Cl)_2$]. The anisotropic displacement factor exponent takes the form: $-2\pi^2$ [$h^2 a^{*2} U_{11} + 2\ h\ k\ a^*\ b^*\ U_{12} + \ldots$].

Atom	U_{11}	U_{22}	U_{33}	U_{23}	U_{13}	U_{12}
Pt1	0.00915(6)	0.00832(6)	0.00635(6)	−0.00054(3)	0.00163(4)	−0.00035(3)
S3	0.0116(3)	0.0116(3)	0.0075(3)	−0.0007(2)	0.0011(2)	−0.0019(2)
S4	0.0104(3)	0.0135(3)	0.0086(3)	0.0002(2)	0.0024(2)	0.0010(3)
S8	0.0136(3)	0.0126(3)	0.0101(3)	0.0011(3)	0.0010(3)	0.0009(3)
Cl2	0.0208(4)	0.0176(4)	0.0190(4)	−0.0076(3)	0.0097(3)	−0.0006(3)
S5	0.0139(3)	0.0158(3)	0.0108(3)	−0.0003(3)	0.0045(3)	−0.0034(3)
S7	0.0118(3)	0.0163(4)	0.0115(3)	−0.0047(3)	0.0017(3)	−0.0033(3)
S2	0.0119(3)	0.0172(4)	0.0123(3)	0.0035(3)	0.0022(3)	0.0037(3)
S6	0.0158(4)	0.0174(4)	0.0132(3)	−0.0040(3)	0.0045(3)	−0.0015(3)
S1	0.0161(4)	0.0146(3)	0.0137(3)	0.0029(3)	0.0038(3)	0.0000(3)
Cl1	0.0271(4)	0.0163(4)	0.0219(4)	0.0062(3)	0.0091(3)	−0.0032(3)
O11	0.018(1)	0.012(1)	0.010(1)	0.0000(8)	0.0041(8)	−0.0022(8)
O61	0.014(1)	0.011(1)	0.012(1)	−0.0030(8)	0.0043(8)	0.0000(8)
O41	0.020(1)	0.018(1)	0.012(1)	−0.0022(9)	0.0063(9)	0.0029(9)
O32	0.020(1)	0.013(1)	0.013(1)	0.0002(8)	0.0034(9)	−0.0053(9)
O31	0.016(1)	0.017(1)	0.009(1)	−0.0022(8)	0.0004(8)	−0.0032(9)
O141	0.016(1)	0.013(1)	0.011(1)	0.0022(8)	0.0036(8)	0.0009(9)

Atom	U_{11}	U_{22}	U_{33}	U_{23}	U_{13}	U_{12}
O22	0.023(1)	0.018(1)	0.020(1)	0.001(1)	0.0062(10)	0.008(1)
N1	0.008(1)	0.013(1)	0.006(1)	0.0062(9)	0.0018(8)	0.0019(9)
O561	0.020(1)	0.015(1)	0.010(1)	−0.0029(8)	0.0042(9)	−0.0013(9)
O72	0.020(1)	0.016(1)	0.020(1)	−0.0034(9)	0.0053(10)	−0.006(1)
O81	0.020(1)	0.023(1)	0.011(1)	0.0035(9)	−0.0001(9)	0.001(1)
N5	0.010(1)	0.012(1)	0.010(1)	−0.0012(9)	−0.0009(9)	−0.0010(9)
O51	0.027(1)	0.019(1)	0.015(1)	0.0024(9)	0.0094(10)	−0.004(1)
N6	0.0060(1)	0.019(1)	0.007(1)	−0.0081(9)	0.0030(8)	−0.0030(9)
O71	0.015(1)	0.027(1)	0.015(1)	−0.006(1)	−0.0004(9)	−0.002(1)
O52	0.014(1)	0.027(1)	0.016(1)	−0.003(0)	0.0029(9)	−0.003(1)
O82	0.018(1)	0.015(1)	0.018(1)	−0.0010(9)	0.0036(9)	0.0023(9)
O42	0.010(1)	0.024(1)	0.012(1)	0.0014(9)	0.0001(8)	−0.0027(9)
O21	0.014(1)	0.031(1)	0.013(1)	0.005(1)	−0.0002(9)	0.001(1)
N2	0.011(1)	0.012(1)	0.0077(1)	−0.0009(9)	−0.0006(9)	−0.0003(9)
N4	0.011(1)	0.013(1)	0.011(1)	0.0011(9)	0.0021(9)	0.0000(9)
N3	0.011(1)	0.012(1)	0.007(1)	−0.0008(9)	0.0032(9)	−0.0008(9)

Table 48: Selected experimental bond lengths [pm] for $[Pt(S_4N_3O_8Cl)_2]$.

Atom–Atom	Length/ pm	Atom–Atom	Length/ pm
Pt1–O11	207.3(2)	S5–O561	166.3(3)
Pt1–O61	204.4(2)	S5–O51	140.6(3)
Pt1–N5	204.9(3)	S5–O52	140.9(3)
Pt1–N2	205.3(3)	S5–N4	164.3(3)
Pt1–N4	202.0(3)	S7–O72	140.7(3)
Pt1–N3	201.7(3)	S7–N5	162.8(3)
S3–O32	141.0(2)	S7–N6	168.2(3)
S3–O31	142.1(2)	S7–O71	141.2(3)
S3–N2	169.1(3)	S2–O22	140.6(3)
S3–N3	171.6(3)	S2–N1	168.9(3)
S4–O41	140.8(2)	S2–O21	141.0(3)
S4–O141	166.8(3)	S2–N2	162.3(3)
S4–O42	140.9(2)	S6–O61	150.5(2)
S4–N3	164.0(3)	S6–O561	157.6(3)
S8–O81	141.9(3)	S6–N6	156.7(3)
S8–N5	168.7(3)	S1–Cl1	192.7(1)
S8–O82	141.0(3)	S1–O11	150.4(2)
S8–N4	172.0(3)	S1–O141	157.0(3)
Cl2–S6	191.6(1)	S1–N1	156.6(3)

Table 49: Selected experimental bond angles [°] for $[Pt(S_4N_3O_8Cl)_2]$.

Atom–Atom–Atom	Angle/ °	Atom–Atom–Atom	Angle/ °
O61–Pt1–O11	87.1(1)	O72–S7–N6	105.4(2)
O61–Pt1–N5	91.1(1)	O72–S7–O71	124.1(1)
O61–Pt1–N2	98.0(1)	N5–S7–N6	104.4(1)
N5–Pt1–O11	98.8(1)	O71–S7–N5	110.1(2)
N5–Pt1–N2	168.0(1)	O71–S7–N6	103.0(2)
N2–Pt1–O11	89.51(1)	O22–S2–N1	105.1(2)
N4–Pt1–O11	171.0(1)	O22–S2–O21	123.5(2)
N4–Pt1–O61	93.7(1)	O22–S2–N2	108.8(2)
N4–Pt1–N5	72.2(1)	O21–S2–N1	102.2(2)
N4–Pt1–N2	99.2(1)	O21–S2–N2	110.8(2)
N3–Pt1–O11	93.6(1)	N2–S2–N1	104.5(1)
N3–Pt1–O61	170.5(1)	O61–S6–Cl2	112.7(1)
N3–Pt1–N5	98.2(1)	O61–S6–O561	111.5(1)
N3–Pt1–N2	72.5(1)	O61–S6–N6	112.4(1)

Atom–Atom–Atom	Angle/ °	Atom–Atom–Atom	Angle/ °
N3–Pt1–N4	87.15(1)	O561–S6–Cl2	106.5(1)
O32–S3–O31	123.0(1)	N–S6–Cl2	108(1)
O32–S3–N2	107.5(1)	N–S6–O561	105.8(2)
O32–S3–N3	106.6(1)	O11–S1–Cl1	113.9(1)
O31–S3–N2	112.6(2)	O11–S1–O141	112.1(1)
O31–S3–N3	112.2(1)	O11–S1–N1	112.3(1)
N2–S3–N3	89.9(1)	O141–S1–Cl1	106.1(1)
O41–S4–O141	103.2(1)	N1–S1–Cl1	105.8(1)
O41–S4–O42	123.9(2)	N1–S1–O141	106.1(1)
O41–S4–N3	110.1(2)	S1–O141–S4	124.7(2)
O42–S4–O141	106.4(1)	S1–N1–S2	123.2(2)
O42–S4–N3	107.2(1)	S6–O561–S5	125.2(2)
N3–S4–O141	104.3(1)	S7–N5–S8	122.6(2)
O81–S8–N5	113.1(2)	S6–N–S7	124.4(2)
O81–S8–N4	112.5(2)	S2–N2–S3	120.5(2)
N5–S8–N4	89.5(1)	S5–N4–S8	119.4(2)
O82–S8–O81	122.0(2)	O51–S5–N4	109.8(2)
O82–S8–N5	108.0(2)	O52–S5–O561	106.4(2)
O82–S8–N4	106.9(2)	O52–S5–N4	107.5(2)
O51–S5–O561	103.0(1)	N4–S5–O561	103.8(1)
O51–S5–O52	124.4(2)	O72–S7–N5	107.8(2)
S4–N3–S3	121.2(2)	-	-

7.4.10 $K_4[(SO_3)_2NN(SO_3)_2](H_2O)_2$

Table 50: Crystallographic data of $K_4[(SO_3)_2NN(SO_3)_2](H_2O)_2$.

Empirical formula	$H_4K_4N_2O_{14}S_4$
Formula weight	540.69 g · mol^{-1}
Temperature	100.0 K
Wavelength	71.073 pm (Mo-Kα)
Crystal system	monoclinic
Space group	*C*2/*c* (15)
Unit cell dimensions	*a* = 1280.62(8) pm
	b = 731.69(4) pm β = 93.333(2)°
	c = 1554.3(1) pm
Volume	1.4539(2) nm^3
Z	4
Density (calculated)	2.470 g · cm^{-3}
Absorption coefficient μ	1.878 mm^{-1}
F(000)	1080
Crystal size	0.5 × 0.02 × 0.01 mm^3
2θ range/ °	5.25 to 54.98
Index ranges	−16 ≤ h ≤ 16, −9 ≤ k ≤ 9, −20 ≤ l ≤ 20
Reflections collected	11911
Independent reflections	1677 [R_{int}= 0.0614, R_σ= 0.0313]
Completeness to theta = 25.24°	100%
Absorption correction	multiscan
Max. and min. transmission	0.981 and 0.956
Refinement method	least-squares
Data / restraints / parameters	1677/0/117
Goodness-of-fit on F^2	1.092
Final *R* indices [$I \geq 2\sigma(I)$]	R_1 = 0.0378, wR_2 = 0.0747
R indices (all data)	R_1 = 0.0480, wR_2 = 0.0817
Largest diff. peak and hole	0.52/−0.53 e · Å^{-3}
CSD number	2292295

7.4.11 $K_4[(SO_3)_2NN(SO_3)_2](H_2O)$

Table 51: Crystallographic data of $K_4[(SO_3)_2NN(SO_3)_2](H_2O)$.

Empirical formula	$H_2K_4N_2O_{13}S_4$	
Formula weight	522.68 g · mol^{-1}	
Temperature	100.0 K	
Wavelength	71.073 pm (Mo-K$_\alpha$)	
Crystal system	triclinic	
Space group	$P\bar{1}$ (2)	
Unit cell dimensions	a = 712.11(5) pm	α = 102.354(3)°
	b = 1307.98(9) pm	β = 96.504(3)°
	c = 3034.2(2) pm	γ = 90.880(2)°
Volume	2.7406(3) nm^3	
Z	8	
Density (calculated)	2.533 g · cm^{-3}	
Absorption coefficient μ	1.982 mm^{-1}	
F(000)	2080.0	
Crystal size	0.209 × 0.101 × 0.093 mm^3	
2θ range/ °	3.744 to 66.36	
Index ranges	−10 ≤ h ≤ 10, −20 ≤ k ≤ 20, −46 ≤ l ≤ 46	
Reflections collected	260115	
Independent reflections	20889 [R_{int}= 0.0578, R_σ= 0.0269]	
Completeness to theta = 33.18°	99.8%	
Absorption correction	multiscan	
Max. and min. transmission	0.981 and 0.956	
Refinement method	least-squares	
Data / restraints / parameters	20889/124/974	
Goodness-of-fit on F^2	1.036	
Final R indices [$I \geq 2\sigma(I)$]	R_1 = 0.0338, wR_2 = 0.0777	
R indices (all data)	R_1 = 0.0362, wR_2 = 0.0792	
Largest diff. peak and hole	0.87/−0.58 e · Å^{-3}	
BASF	0.2777(5)	
CSD number	2358809	

7.4.12 $K_5Na(S_2O_6)_2Cl_2$

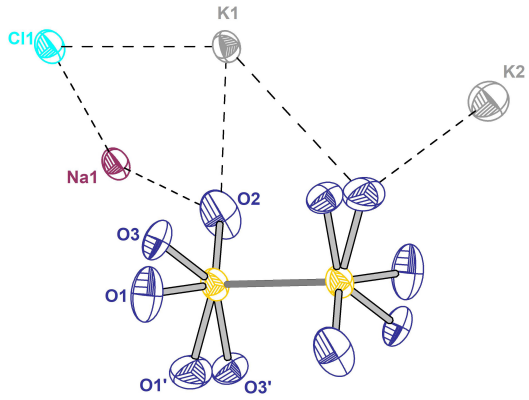

Figure 95: Structure of $K_5Na(S_2O_6)_2Cl_2$ with labeling of the unique atoms. Rotational disorder of the SO_3 moiety was treated during the refinement, which resulted in splitting of one oxygen atom in O1 (occupancy: 52%) and O3 (occupancy: 48%). Thermal ellipsoids probability is set to 70%. O2 lies on special site (*m*, *Wyckoff 8h*)

Table 52: Crystallographic data of $K_5Na(S_2O_6)_2Cl_2$.

Empirical formula	$Cl_2K_5NaO_{12}S_4$
Formula weight	609.63 g · mol^{-1}
Temperature	100.0 K
Wavelength	71.073 pm (Mo-K$_\alpha$)
Crystal system	tetragonal
Space group	*P*4/*mnc* (128)
Unit cell dimensions	*a* = 852.68(2) pm
	c = 1139.44(6) pm
Volume	0.82844(6) nm^3
Z	2
Density (calculated)	2.444 g · cm^{-3}
Absorption coefficient μ	2.231 mm^{-1}
F(000)	600
Crystal size	0.132 × 0.056 × 0.054 mm^3
2θ range/ °	5.97 to 59.96
Index ranges	$-11 \leq h \leq 11$, $-11 \leq k \leq 11$, $-14 \leq l \leq 16$
Reflections collected	8870
Independent reflections	630 [R_{int}= 0.0697, R_σ= 0.0290]
Completeness to theta = 25.24°	100%
Absorption correction	multiscan
Max. and min. transmission	0.7461 and 0.6583
Refinement method	least-squares
Data / restraints / parameters	630/0/45
Goodness-of-fit on F^2	1.146
Final *R* indices [$I \geq 2\sigma(I)$]	R_1 = 0.0311, wR_2 = 0.0614
R indices (all data)	R_1 = 0.0421, wR_2 = 0.0755
Largest diff. peak and hole	0.69/−0.47 e · Å^{-3}

Table 53: Atomic coordinates and equivalent isotropic displacement parameters [pm^2 x 10^4] for $K_5Na(S_2O_6)_2Cl_2$. *U(eq)* is defined as one third of the trace of the orthogonalized U_{ij} tensor**.**

Atom	*x*	*y*	*z*	U_{eq}
K1	0.18795(6)	0.31205(6)	0.750000	0.0138(2)
K2	0.500000	0.500000	1.000000	0.0239(4)
Cl1	0.500000	0.500000	0.7377(1)	0.0158(3)
S1	0.4296(1)	0.1015(1)	0.500000	0.0144(2)
Na1	0.500000	0.500000	0.500000	0.0141(6)
O2	0.5393(4)	0.2276(3)	0.500000	0.0323(8)
O1	0.3075(8)	0.0837(5)	0.5789(7)	0.027(2)
O3	0.3771(8)	0.0989(5)	0.6304(5)	0.017(2)

Table 54: Anisotropic displacement parameters [$pm^2 \times 10^4$] for $K_5Na(S_2O_6)_2Cl_2$. The anisotropic displacement factor exponent takes the form: $-2\pi^2$ [$h^2 a^{*2} U_{11} + 2 h k a^* b^* U_{12} + \ldots$].

Atom	U_{11}	U_{22}	U_{33}	U_{23}	U_{13}	U_{12}
K1	0.0120(2)	0.0120(2)	0.0176(4)	0.0002(2)	0.0002(2)	−0.0016(3)
K2	0.0254(6)	0.0254(6)	0.0209(8)	0.000	0.000	0.000
Cl1	0.0120(4)	0.0120(4)	0.0235(6)	0.000	0.000	0.000
S1	0.0119(4)	0.0102(4)	0.0213(5)	0.000	0.000	0.0008(3)
Na1	0.0099(9)	0.0099(9)	0.0225(15)	0.000	0.000	0.000
O2	0.020(2)	0.008(1)	0.068(3)	0.000	0.000	−0.003(1)
O1	0.030(3)	0.022(2)	0.029(4)	0.005(2)	0.015(3)	0.007(2)
O3	0.024(3)	0.014(2)	0.013(2)	−0.001(2)	0.006(2)	0.003(2)

Table 55: Selected experimental bond lengths [pm] for $K_5Na(S_2O_6)_2Cl_2$.

Atom–Atom	Length/ pm	Atom–Atom	Length/ pm
K1–Cl1	310.93(2)	Cl1–Na1	270.8(1)
K1–O1$^{\#1}$	302.7(5)	S1–S1$^{\#3}$	210.7(2)
K1–O1	293.8(5)	S1–O2	142.5(3)
K1–O3	278.6(4)	S1–O1	138.4(4)
K1–O3$^{\#1}$	285.4(4)	S1–O3	155.2(5)
K2–Cl1	298.9(1)	Na1–O2	234.7(3)
K2–O1$^{\#2}$	286.2(9)	-	-

#1: 0.5−X, 0.5+Y, 1.5−Z; #2: 0.5−Y, 0.5−X, 1.5−Z, #3: 1−X, 1−Y, +Z.

Table 56: Selected experimental bond angles [°] for $K_5Na(S_2O_6)_2Cl_2$.

Atom–Atom–Atom	Angle/ °
O2–S1–O3	101.6(2)
O1–S1–S1$^{\#1}$	109.8(2)
O3–S1–S1$^{\#1}$	98.8(2)
O1–S1–O2	125.2(3)
O1–S1–O1$^{\#2}$	81.1(8)
O1–S1–O3$^{\#2}$	113.8(6)
O3$^{\#2}$–S1–O3	146.4(6)
Cl1$^{\#3}$–Na1–Cl1	180.0
O2$^{\#4}$–Na1–O2$^{\#5}$	180.0
Na1–Cl1–K2	180.0
Cl1–K2–Cl1$^{\#6}$	180.0
O1$^{\#7}$–K2–O1$^{\#8}$	180.0

#1: 1−X, −Y, 1−Z; #2: +X, +Y, 1−Z; #3: 1−X, 1−Y, 1−Z; #4: +Y, 1−X, 1−Z; #5: 1−Y, +X, +Z; #6: 1−X, 1−Y, 2−Z; #7: 0.5+X, 0.5−Y, 0.5+Z; #8: 0.5−X, 0.5+Y, 1.5−Z.

7.4.13 (TBA)[SO_3N_3]

Table 57: Crystallographic data of (TBA)[SO_3N_3].

Empirical formula	$C_{16}H_{36}N_4O_3S$
Formula weight	364.55 g · mol^{-1}
Temperature	100.0 K
Wavelength	71.073 pm (Mo-K_α)
Crystal system	monoclinic
Space group	$P2_1/c$ (14)
Unit cell dimensions	a = 976.02(4) pm
	b = 1281.46(6) pm β = 104.973(2)°
	c = 1747.82(8) pm
Volume	2.1118(2) nm^3
Z	4
Density (calculated)	1.147 g · cm^{-3}
Absorption coefficient μ	0.173 mm^{-1}
F(000)	800.0
Crystal size	0.236 × 0.118 × 0.062 mm^3
2θ range/ °	3.99 to 59.998
Index ranges	$-13 \leq h \leq 13$, $-18 \leq k \leq 18$, $-24 \leq l \leq 24$
Reflections collected	89271
Independent reflections	6159 [R_{int}= 0.0545, R_σ= 0.0228]
Completeness to theta = 30.00°	100%
Absorption correction	multiscan
Max. and min. transmission	0.747 and 0.658
Refinement method	least-squares
Data / restraints / parameters	6159/1/221
Goodness-of-fit on F^2	1.062
Final R indices [$I \geq 2\sigma(I)$]	R_1 = 0.0412, wR_2 = 0.1026
R indices (all data)	R_1 = 0.0551, wR_2 = 0.1129
Largest diff. peak and hole	0.38/−0.37 e · $Å^{-3}$
CSD number	2310251

7.4.14 $(TBA)_4(N_3)_3[SO_3N_3]$

Table 58: Crystallographic data of $(TBA)_4(N_3)_3[SO_3N_3]$.

Empirical formula	$C_{64}H_{142}N_{16}O_3S$
Formula weight	1515.99 g · mol^{-1}
Temperature	100.0 K
Wavelength	71.073 pm (Mo-Kα)
Crystal system	monoclinic
Space group	$P2_1/c$ (14)
Unit cell dimensions	a = 1280.40(5) pm
	b = 2704.5(1) pm β = 100.682(2)°
	c = 2208.49(9) pm
Volume	7.5503(5) nm^3
Z	4
Density (calculated)	1.070 g · cm^{-3}
Absorption coefficient μ	0.094 mm^{-1}
F(000)	2712.0
Crystal size	0.61 × 0.374 × 0.347 mm^3
2θ range/ °	3.732 to 52
Index ranges	−15 ≤ h ≤ 15, −33 ≤ k ≤ 33, −27 ≤ l ≤ 27
Reflections collected	220384
Independent reflections	14820 [R_{int}= 0.0850, R_σ= 0.0385]
Completeness to theta = 26.00°	100%
Absorption correction	multiscan
Max. and min. transmission	0.747 and 0.692
Refinement method	least-squares
Data / restraints / parameters	14820/1/796
Goodness-of-fit on F^2	1.041
Final R indices [$I \geq 2\sigma(I)$]	R_1 = 0.0818, wR_2 = 0.2366
R indices (all data)	R_1 = 0.1020, wR_2 = 0.2610
Largest diff. peak and hole	1.06/−1.00 e · Å^{-3}
CSD number	2341494

7.4.15 K[SO$_3$N$_3$] (100 K)

Table 59: Crystallographic data of K[SO$_3$N$_3$] measured at 100 K.

Empirical formula	KN_3O_3S
Formula weight	161.19 g · mol^{-1}
Temperature	100.0 K
Wavelength	71.073 pm (Mo-Kα)
Crystal system	monoclinic
Space group	$P2_1/c$ (14)
Unit cell dimensions	a = 917.8(3) pm
	b = 708.3(2) pm β = 90.83(1)°
	c = 743.7(2) pm
Volume	0.4834(2) nm^3
Z	4
Density (calculated)	2.215 g · cm^{-3}
Absorption coefficient μ	1.438 mm^{-1}
F(000)	320.0
Crystal size	0.207 × 0.168 × 0.094 mm^3
2θ range/ °	7.268 to 51.97
Index ranges	−11 ≤ h ≤ 11, −0 ≤ k ≤ 8, −0 ≤ l ≤ 9
Reflections collected	951
Independent reflections	951 [R_{int}= 0.1011, R_σ= 0.1053]
Completeness to theta = 25.99°	100%
Absorption correction	multiscan
Max. and min. transmission	0.747 and 0.471
Refinement method	least-squares
Data / restraints / parameters	951/0/74
Goodness-of-fit on F^2	1.109
Final R indices [$I \geq 2\sigma(I)$]	R_1 = 0.0696, wR_2 = 0.1247
R indices (all data)	R_1 = 0.1052, wR_2 = 0.1382
Largest diff. peak and hole	0.83/−0.68 e · Å^{-3}
CSD number	2313397

7.4.16 K[SO$_3$N$_3$] (250 K)

Table 60: Crystallographic data of K[SO$_3$N$_3$] measured at 250 K.

Empirical formula	KN_3O_3S
Formula weight	161.19 g · mol^{-1}
Temperature	250 K
Wavelength	71.073 pm (Mo-K$_\alpha$)
Crystal system	monoclinic
Space group	$P2_1/c$ (14)
Unit cell dimensions	a = 985.70(5) pm
	b = 718.09(3) pm β = 108.582(2)°
	c = 744.79(3) pm
Volume	0.49970(4) nm^3
Z	4
Density (calculated)	2.143 g · cm^{-3}
Absorption coefficient μ	1.391 mm^{-1}
F(000)	320
Crystal size	0.104 × 0.092 × 0.045 mm^3
2θ range/ °	4.36 to 59.98
Index ranges	−13≤ h ≤ 13, −9 ≤ k ≤ 10, −9 ≤ l ≤ 10
Reflections collected	7998
Independent reflections	1441 [R_{int}= 0.0379, R_σ= 0.0262]
Completeness to theta = 25.24°	100%
Absorption correction	multiscan
Max. and min. transmission	0.7467 and 0.6891
Refinement method	least-squares
Data / restraints / parameters	1441/0/73
Goodness-of-fit on F^2	1.057
Final R indices [$I \geq 2\sigma(I)$]	R_1 = 0.0305, wR_2 = 0.0634
R indices (all data)	R_1 = 0.0388, wR_2 = 0.0695
Largest diff. peak and hole	0.48/−0.40 e · Å^{-3}
CSD number	2358804

7.4.17 $Na_3[SO_3N_3]_3(CH_3CN)$

Table 61: Crystallographic data of $Na_3[SO_3N_3]_3(CH_3CN)$.

Empirical formula	$C_2H_3N_{10}Na_3O_9S_3$	
Formula weight	476.29 g · mol^{-1}	
Temperature	100.0 K	
Wavelength	71.073 pm (Mo-Kα)	
Crystal system	triclinic	
Space group	$P\bar{1}$ (2)	
Unit cell dimensions	a = 684.15(5) pm	α = 107.137(3)°
	b = 1029.88(8) pm	β = 98.672(3)°
	c = 1265.6(1) pm	γ = 109.295(3)°
Volume	0.7732(1) nm^3	
Z	2	
Density (calculated)	2.046 g · cm^{-3}	
Absorption coefficient μ	0.636 mm^{-1}	
F(000)	476.0	
Crystal size	0.953 × 0.2 × 0.116 mm^3	
2θ range/ °	4.508 to 60.998	
Index ranges	$-9 \leq h \leq 9$, $-14 \leq k \leq 14$, $-18 \leq l \leq 18$	
Reflections collected	33138	
Independent reflections	4703 [R_{int}= 0.0439, R_σ= 0.0263]	
Completeness to theta = 30.50°	99.7%	
Absorption correction	multiscan	
Max. and min. transmission	0.748 and 0.684	
Refinement method	least-squares	
Data / restraints / parameters	4703/0/245	
Goodness-of-fit on F^2	1.111	
Final R indices [$I \geq 2\sigma(I)$]	R_1 = 0.0262, wR_2 = 0.0641	
R indices (all data)	R_1 = 0.0301, wR_2 = 0.0672	
Largest diff. peak and hole	0.47/−0.48 e · Å^{-3}	
CSD number	2310250	

7.4.18 $K_3[N(SO_3)_3](H_2O)_2$

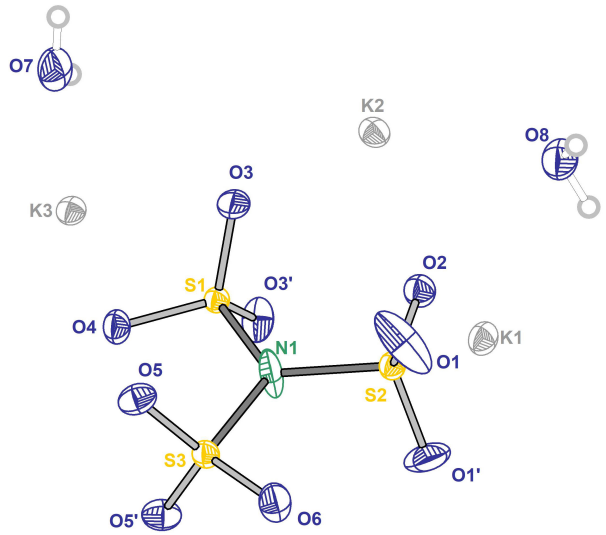

Figure 96: Structure and labeling of $K_3[N(SO_3)_3](H_2O)_2$. The thermal ellipsoids are set to a probability level of 70%.

Table 62: Crystallographic data of $K_3[N(SO_3)_3](H_2O)_2$.

Empirical formula	$H_4K_3NO_{11}S_3$
Formula weight	407.52 g · mol^{-1}
Temperature	100.0 K
Wavelength	71.073 pm (Mo-K$_\alpha$)
Crystal system	orthorhombic
Space group	*Pnma* (62)
Unit cell dimensions	a = 1107.77(3) pm
	b = 569.76(1) pm
	c = 1797.53(5) pm
Volume	1.13453(5) nm^3
Z	4
Density (calculated)	2.386 g · cm^{-3}
Absorption coefficient μ	1.807 mm^{-1}
F(000)	816.0
Crystal size	0.94 × 0.209 × 0.172 mm^3
2θ range/ °	4.32 to 66.84
Index ranges	−16 ≤ h ≤ 16, −8 ≤ k ≤ 7, −27 ≤ l ≤ 27
Reflections collected	16687
Independent reflections	2141 [R_{int}= 0.0442, R_σ= 0.0274]
Completeness to theta = 25.24°	99.6%
Absorption correction	multiscan
Max. and min. transmission	0.7466 and 0.6727
Refinement method	least-squares
Data / restraints / parameters	2141/2/109
Goodness-of-fit on F^2	1.237
Final R indices [$I \geq 2\sigma(I)$]	R_1 = 0.0447, wR_2 = 0.0989
R indices (all data)	R_1 = 0.0603, wR_2 = 0.1192
Largest diff. peak and hole	1.18/−1.09 e · Å^{-3}
Extinction coefficient	0.0051(4)

Table 63: Atomic coordinates and equivalent isotropic displacement parameters [pm^2 x 10^4] for $K_3[N(SO_3)_3](H_2O)_2$. *U(eq)* is defined as one third of the trace of the orthogonalized U_{ij} tensor**.**

Atom	*x*	*y*	*z*	U_{eq}
K2	0.52301(9)	-0.250000	0.58966(6)	0.0125(2)
K3	0.88714(9)	-0.250000	0.49201(6)	0.0111(2)
K1	0.6294(1)	0.750000	0.82698(6)	0.0138(2)
S1	0.7230(1)	0.250000	0.51527(6)	0.0086(2)
S3	0.8962(1)	0.250000	0.64243(6)	0.0101(2)
S2	0.6315(1)	0.250000	0.66788(6)	0.0099(2)
O5	0.9519(2)	0.0377(5)	0.6141(1)	0.0152(5)
O4	0.8510(3)	0.250000	0.4841(2)	0.0136(7)
O3	0.6642(2)	0.0376(5)	0.4984(2)	0.0169(5)
O2	0.5298(3)	0.250000	0.6181(2)	0.0140(7)
O8	0.3760(4)	-0.250000	0.7140(2)	0.0201(8)
O6	0.8800(3)	0.250000	0.7218(2)	0.0185(8)
O7	0.7593(4)	-0.250000	0.3612(2)	0.0224(9)
O1	0.6444(3)	0.4609(7)	0.7097(2)	0.0350(9)
N1	0.7531(4)	0.250000	0.6084(2)	0.0250(1)
H8	0.372(6)	-0.36(1)	0.741(4)	0.06(2)
H7	0.727(8)	-0.145(4)	0.346(6)	0.25(8)

Table 64: Anisotropic displacement parameters [$pm^2 \times 10^4$] for $K_3[N(SO_3)_3](H_2O)_2$. The anisotropic displacement factor exponent takes the form: $-2\pi^2$ [$h^2 a^{*2} U_{11} + 2\ h\ k\ a^*\ b^*\ U_{12} + \ldots$].

Atom	U_{11}	U_{22}	U_{33}	U_{23}	U_{13}	U_{12}
K2	0.0113(4)	0.0109(4)	0.0153(4)	0.000	−0.0003(3)	0.000
K3	0.0127(4)	0.0086(4)	0.0121(4)	0.000	0.0006(3)	0.000
K1	0.0152(5)	0.0156(5)	0.0105(4)	0.000	0.0021(3)	0.000
S1	0.0090(5)	0.0084(5)	0.0086(5)	0.000	0.0004(4)	0.000
S3	0.0088(5)	0.0126(5)	0.0091(5)	0.000	−0.0010(4)	0.000
S2	0.0096(5)	0.0115(5)	0.0088(5)	0.000	0.0004(4)	0.000
O5	0.019(1)	0.0114(1)	0.015(1)	−0.0016(9)	−0.0028(9)	0.0020(9)
O4	0.012(2)	0.018(2)	0.011(2)	0.000	0.0022(12)	0.000
O3	0.019(1)	0.0122(1)	0.012(1)	−0.005(1)	0.0056(10)	−0.006(1)
O2	0.013(2)	0.016(2)	0.013(2)	0.000	−0.001(1)	0.000
O8	0.022(2)	0.017(2)	0.022(2)	0.000	0.005(1)	0.000
O6	0.013(2)	0.032(2)	0.011(2)	0.000	−0.001(1)	0.000
O7	0.018(2)	0.038(3)	0.011(2)	0.000	0.001(1)	0.000
O1	0.017(1)	0.039(2)	0.049(2)	−0.035(2)	−0.008(1)	0.007(1)
N1	0.007(2)	0.061(4)	0.008(2)	0.000	0.001(1)	0.000

Table 65: Selected experimental bond lengths [pm] for $K_3[N(SO_3)_3](H_2O)_2$.

Atom–Atom	Length/ pm	Atom–Atom	Length/ pm
S1–O4	145.5(4)	K3–O5	283.1(3)
S1–O3	144.4(3)	K3–O5$^{\#3}$	287.8(3)
S1–N1	169.3(5)	K3–O4$^{\#4}$	293.2(4)
S3–O5	145.0(3)	K3–O4$^{\#2}$	288.02(6)
S3–O6	143.7(4)	K3–O3	296.6(3)
S3–N1	170.0(5)	K3–O7	274.5(4)
S2–O2	143.8(4)	K1–O5$^{\#5}$	277.1(3)
S2–O1	142.5(3)	K1–O8$^{\#7}$	282.9(4)
S2–N1	172.0(5)	K1–O7$^{\#8}$	316.4(2)
K2–O3	279.7(3)	K1–O4$^{\#6}$	283.3(4)
K2–O3$^{\#1}$	287.5(3)	K1–O1	268.0(3)

#1: 1−X, −1−Y, 1−Z; #2: +X, −1+Y, +Z; #3: 2−X, −0.5+Y, 1−Z; #4: 2−X, −Y, 1−Z; #5: 1.5−X, −Y, 0.5+Z; #6: 1.5−X, 1−Y, 0.5+Z; #7: −0.5+X, 0.5−Y, 1.5−Z; #8: 0.5+X, 1+Y.

Table 66: Selected Experimental bond angles [°] for $K_3[N(SO_3)_3](H_2O)_2$.

Atom–Atom–Atom	Angle/ °
S3–N1–S2	120.4(3)
S1–N1–S2	119.7(3)
S1–N1–S3	119.9(3)
O4–S1–N1	103.9(2)
O3–S1–O4	112.56(13)
O3–S1–O3$^{\#1}$	113.8(2)
O5–S3–N1	105.66(13)
O6–S3–O5	113.68(13)
O6–S3–N1	103.9(2)
O5$^{\#6}$–S3–O5	113.1(2)
O2–S2–N1	103.1(2)
O1–S2–O2	114.02(15)
O1$^{\#1}$–S2–O1	115.0(3)
O1–S2–N1	104.46(17)

#1: +X, 0.5−Y, +Z.

7.4.19 $K_2[HN(SO_3)_2]$

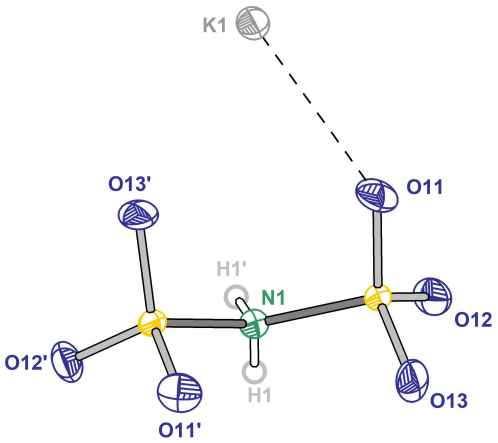

Figure 97: Structure and labeling of $K_2[HN(SO_3)_2]$. The thermal ellipsoids are set to a probability level of 70%.

Table 67: Crystallographic data of $K_2[HN(SO_3)_2]$.

Empirical formula	$HK_2NO_6S_2$
Formula weight	253.34 g · mol^{-1}
Temperature	100.0 K
Wavelength	71.073 pm (Mo-K$_\alpha$)
Crystal system	monoclinic
Space group	*C*2/*c* (15)
Unit cell dimensions	*a* = 1237.55(7) pm
	b = 742.01(4) pm β = 91.578(2)°
	c = 715.87(4) pm
Volume	0.65712(6) nm^3
Z	4
Density (calculated)	2.561 g · cm^{-3}
Absorption coefficient μ	2.057 mm^{-1}
F(000)	504
Crystal size	0.277 × 0.237 × 0.076 mm^3
2θ range/ °	6.40 to 60.00
Index ranges	−17 ≤ h ≤ 17, −10 ≤ k ≤ 10, −10 ≤ l ≤ 10
Reflections collected	19984
Independent reflections	957 [R_{int}= 0.0586, R_σ= 0.0174]
Completeness to theta = 25.24°	100%
Absorption correction	multiscan
Max. and min. transmission	0.7468 and 0.6515
Refinement method	least-squares
Data / restraints / parameters	957/0/56
Goodness-of-fit on F^2	1.167
Final *R* indices [$I \geq 2\sigma(I)$]	R_1 = 0.0172, wR_2 = 0.0447
R indices (all data)	R_1 = 0.0237, wR_2 = 0.0499
Largest diff. peak and hole	0.59/−0.54 e · Å^{-3}
Extinction coefficient	0.0064(6)

Table 68: Atomic coordinates and equivalent isotropic displacement parameters [pm^2 x 10^4] for $K_2[HN(SO_3)_2]$. *U(eq)* is defined as one third of the trace of the orthogonalized U_{ij} tensor**.**

Atom	*x*	*y*	*z*	U_{eq}
K1	0.65285(2)	0.85847(4)	0.35792(4)	0.0145(1)
S1	0.60149(2)	0.67577(4)	0.86199(4)	0.0091(1)
O11	0.64825(8)	0.7991(1)	0.7296(2)	0.0159(2)
O12	0.67241(8)	0.5290(2)	0.9152(2)	0.0173(2)
O13	0.55625(8)	0.7709(2)	1.0192(1)	0.0216(3)
N1	0.500000	0.5702(2)	0.750000	0.0084(3)
H1	0.518(3)	0.488(5)	0.689(4)	0.007(8)

Table 69: Anisotropic displacement parameters [$pm^2 \times 10^4$] for $K_2[HN(SO_3)_2]$. The anisotropic displacement factor exponent takes the form: $-2\pi^2$ [$h^2 a^{*2} U_{11} + 2 h k a^* b^* U_{12} + \ldots$].

Atom	U_{11}	U_{22}	U_{33}	U_{23}	U_{13}	U_{12}
K1	0.0120(2)	0.0185(2)	0.0129(2)	0.0057(1)	−0.0011(1)	−0.0027(1)
S1	0.0077(2)	0.0127(2)	0.0070(2)	−0.0007(1)	0.0005(1)	−0.0007(1)
O11	0.0150(5)	0.0137(5)	0.0191(5)	0.0019(4)	0.0040(4)	−0.0056(4)
O12	0.0105(4)	0.0236(5)	0.0177(5)	0.0069(4)	−0.0006(4)	0.0037(4)
O13	0.0124(5)	0.0386(6)	0.0138(5)	−0.0143(5)	0.0006(4)	0.0009(4)
N1	0.0093(7)	0.0070(6)	0.0090(7)	0.000	0.0004(5)	0.000

Table 70: Selected experimental bond lengths [pm] for $K_2[HN(SO_3)_2]$.

Atom–Atom	Length/ pm	Atom–Atom	Length/ pm
K1–O11	269.9(1)	K1–O13$^{\#6}$	283.15(1)
K1–O11$^{\#1}$	281.1(1)	K1–O13$^{\#2}$	322.50(1)
K1–O11$^{\#2}$	270.2(1)	S1–O11	144.95(1)
K1–O12$^{\#3}$	295.3(1)	S1–O12	144.32(1)
K1–O12$^{\#1}$	307.0(1)	S1–O13	145.38(1)
K1–O12$^{\#4}$	291.3(1)	S1–N1	166.67(8)
K1–O13$^{\#5}$	275.1(1)		

#1: 1.5-X, 1.5-Y, 1-Z; #2: +X, 2-Y, -0.5+Z; #3: 1.5-X, 0.5+Y, 1.5-Z; #4: +X, 1-Y, -0.5+Z; #5: +X, +Y, -1+Z; #6: 1-X, +Y, 1.5-Z.

Table 71: Selected experimental bond angles [°] for $K_2[HN(SO_3)_2]$.

Atom–Atom–Atom	Angle/ °
O11–S1–O13	111.65(7)
O11–S1–N1	106.93(5)
O12–S1–O11	113.46(6)
O12–S1–O13	114.00(7)
O12–S1–N1	102.54(7)
O13–S1–N1	107.42(5)
S1–N1–S1$^{\#1}$	124.0(1)

#1: 1-X, +Y, 1.5-Z.

7.4.20 $K_2Na[N(SO_3)_3]$

Table 72: Crystallographic data of $K_2Na[N(SO_3)_3]$.

Empirical formula	$K_2NNaO_9S_3$
Formula weight	355.38 g · mol^{-1}
Temperature	100.0 K
Wavelength	71.073 pm (Mo-K$_\alpha$)
Crystal system	hexagonal
Space group	$P6_3/m$ (176)
Unit cell dimensions	a = 714.49(3) pm c = 1000.40(5) pm
Volume	0.44228(4) nm^3
Z	2
Density (calculated)	2.669 g · cm^{-3}
Absorption coefficient μ	1.865 mm^{-1}
F(000)	352.0
Crystal size	0.175 × 0.139 × 0.132 mm^3
2θ range/ °	4.072 to 66.888
Index ranges	$-10 \leq h \leq 11$, $-11 \leq k \leq 10$, $-14 \leq l \leq 15$
Reflections collected	21412
Independent reflections	604 [R_{int}= 0.0501, R_σ= 0.0179]
Completeness to theta = 33.44°	99.8%
Absorption correction	multiscan
Max. and min. transmission	0.748 and 0.700
Refinement method	least-squares
Data / restraints / parameters	604/0/31
Goodness-of-fit on F^2	1.167
Final R indices [$I \geq 2\sigma(I)$]	R_1 = 0.0178, wR_2 = 0.0455
R indices (all data)	R_1 = 0.0180, wR_2 = 0.0457
Largest diff. peak and hole	0.50/−0.40 e · Å^{-3}
BASF	0.246(1)
CSD number	2358808

7.4.21 $K_{1.2}Rb_{1.8}[N(SO_3)_3]$

Table 73: Crystallographic data of $K_{1.2}Rb_{1.8}[N(SO_3)_3]$.

Empirical formula	$K_{1.2}NO_9R_{1.8}S_3$
Formula weight	454.96 g · mol^{-1}
Temperature	100.0 K
Wavelength	71.073 pm (Mo-K$_\alpha$)
Crystal system	hexagonal
Space group	*P*6$_3$/*m* (176)
Unit cell dimensions	*a* = 748.21(2) pm
	c = 1011.98(5) pm
Volume	0.49062(4) nm^3
Z	2
Density (calculated)	3.080 g · cm^{-3}
Absorption coefficient μ	10.170 mm^{-1}
F(000)	433.0
Crystal size	0.105 × 0.09 × 0.032 mm^3
2θ range/ °	6.288 to 62.996
Index ranges	−10 ≤ h ≤ 10, −9 ≤ k ≤ 10, −14 ≤ l ≤ 14
Reflections collected	19964
Independent reflections	576 [R_{int}= 0.0599, R_σ= 0.0156]
Completeness to theta = 31.50°	100%
Absorption correction	multiscan
Max. and min. transmission	1.000 and 0.831
Refinement method	least-squares
Data / restraints / parameters	576/0/29
Goodness-of-fit on F^2	1.154
Final *R* indices [$I \geq 2\sigma(I)$]	R_1 = 0.0322, wR_2 = 0.0669
R indices (all data)	R_1 = 0.0356, wR_2 = 0.0689
Largest diff. peak and hole	0.83/−0.81 e · Å^{-3}
CSD number	2358806

7.4.22 $Cs_2K[N(SO_3)_3]$

Table 74: Crystallographic data of $Cs_2K[N(SO_3)_3]$.

Empirical formula	$Cs_2KNO_9S_3$
Formula weight	559.11 g · mol^{-1}
Temperature	100.0 K
Wavelength	71.073 pm (Mo-K$_\alpha$)
Crystal system	trigonal
Space group	*R*3/*c* (161)
Unit cell dimensions	*a* = 778.14(3) pm
	c = 3075.7(2) pm
Volume	1.6129(2) nm^3
Z	6
Density (calculated)	3.454 g · cm^{-3}
Absorption coefficient μ	7.782 mm^{-1}
F(000)	1536.0
Crystal size	0.256 × 0.142 × 0.064 mm^3
2θ range/ °	3.972 to 57.974
Index ranges	−10 ≤ h ≤ 10, −9 ≤ k ≤ 10, −14 ≤ l ≤ 14
Reflections collected	12637
Independent reflections	966 [R_{int}= 0.0440, R_σ= 0.0367]
Completeness to theta = 28.99°	100%
Absorption correction	multiscan
Max. and min. transmission	0.747 and 0.468
Refinement method	least-squares
Data / restraints / parameters	966/1/53
Goodness-of-fit on F^2	1.231
Final *R* indices [$I \geq 2\sigma(I)$]	R_1 = 0.0222, wR_2 = 0.0502
R indices (all data)	R_1 = 0.0230, wR_2 = 0.0503
Largest diff. peak and hole	1.59/−0.91 e · Å^{-3}
BASF	0.08(5); 0,42(4); 0.05(5)
CSD number	2358805

7.5 Thermal Analysis

7.5.1 $K_3[N(SO_3)_3](H_2O)_2$

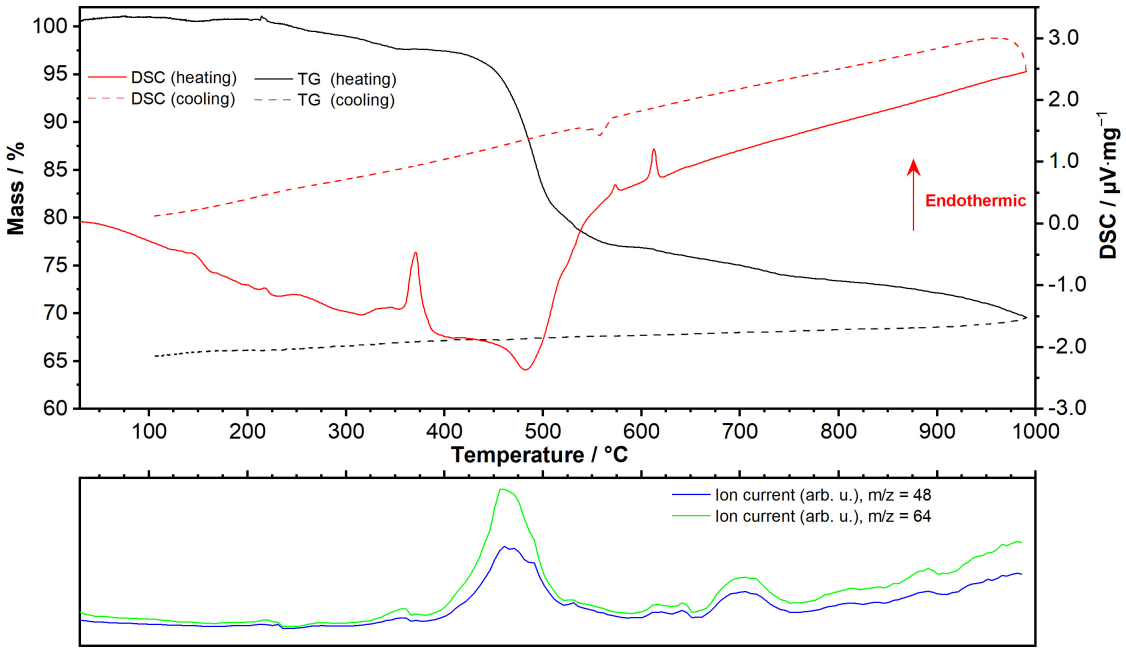

Figure 98: Thermal analysis (TG/DSC) of $K_3[N(SO_3)_3](H_2O)_2$ coupled with an ion current measurement with the predefined m/z values of 48 (SO) and 64 (SO_2). The sample was measured in a corundum crucible with a heating rate of 7 K·min^{-1} (cooling 15 K·min^{-1}) under an argon flow (80 mL·min^{-1}).

Table 75: Assignment of the thermal decomposition steps of $K_3[N(SO_3)_3](H_2O)_2$.

Step/ DSC	T_{onset} / °C	T_{end} / °C	T_{max} / °C	Mass loss/ (obsd./*calc.*) %	Proposed decomposition/ transition
I	213	310	-	4/ *6.3*	Decomposition of $K_3[N(SO_3)_3](H_2O)_2$ to $K_2S_2O_7$
II	360	379.3	370.8	-	Melting of $K_2S_2O_7$
III	463.2	523.7	482.7	31.7/ *31.5*	Exothermic decomposition of $K_2S_2O_7$ to K_2SO_4
Total				35.4/ *35.9*	Residual phase: K_2SO_4

7.6 NMR Spectroscopy

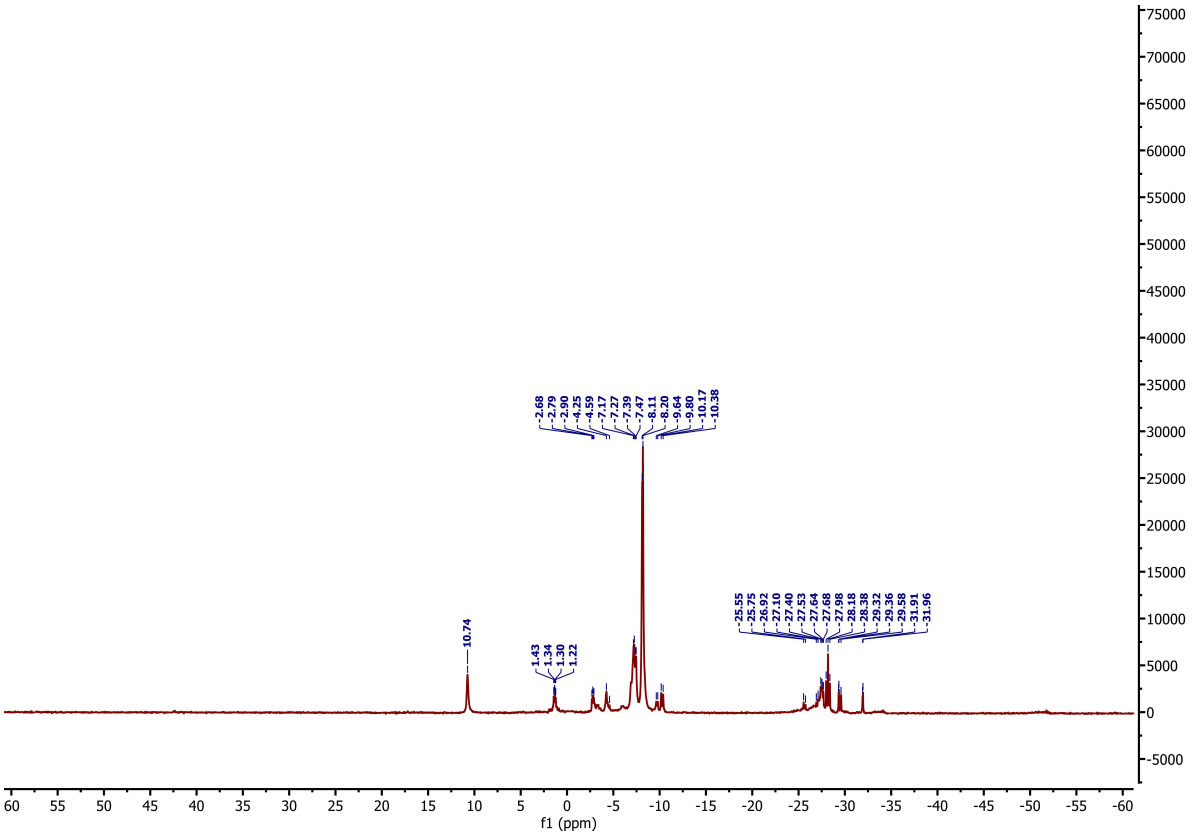

Figure 99: $^{31}P\{^{1}H\}$ NMR of the yellow liquid formed after the reaction between SO_3 (0.04 mL, 0.88 mmol, 10.00 eq.), $P_3N_3Cl_6$ (60 mg, 0.176 mmol, 2.00 eq)) and AuCl (20.4 mg, 0.088 mmol, 1.00 eq.) at 80 °C. The spectrum was recorded in dried CD_2Cl_2 at 162 MHz. H_3PO_4 (85%) was not added as reference standard for preparative reasons.

8 Supporting Information: Publications

The following section contains the supporting information of the submitted manuscript and of the two publications, which have been embedded in this thesis.

8.1 SI: The Unprecedented $[S_4N_2O_{10}]^{2-}$ Anion in the Molecular Gold Complexes $[Au_2Br_2(S_4N_2O_{10})_2]$ and $[Au_2Cl_2(S_4N_2O_{10})_2](S_2O_5Cl_2)$

Chemistry–A European Journal

Supporting Information

The Unprecedented $[S_4N_2O_{10}]^{2-}$ Anion in the Molecular Gold Complexes $[Au_2Br_2(S_4N_2O_{10})_2]$ and $[Au_2Cl_2(S_4N_2O_{10})_2](S_2O_5Cl_2)$

Tobias Rennebaum, David van Gerven, and Mathias S. Wickleder*

SUPPORTING INFORMATION

Table of Contents

A. Syntheses

Preparation of SO_3: SO_3 was obtained in a specially designed apparatus for the generation, distillation and the subsequent transfer into glass ampoules under nitrogen gas. For this purpose, fuming sulfuric acid (10 mL, 65% SO_3, used as received, *VWR Chemicals*, Darmstadt, Germany) was slowly added via a dropping funnel into a 250 mL flask with P_4O_{10} (200 g, > 99%, *Carl Roth*, Karlsruhe, Germany). At the same time, the flask was heated at 135 °C and the generated SO_3 distilled into a connected burette body (scaling 0.01 ml ± 0.01). A connected glass ampoule (l = 200 mm, $ø$ = 16 mm, thickness of the tube wall = 1.80 mm) containing the reaction components was then filled with stoichiometric amounts of freshly distillied SO_3.

$[Au_2Cl_2(S_4N_2O_{10})_2](S_2O_5Cl_2)$: $P_3N_3Cl_6$ (29 mg, 0.082 mmol, 1.0 eq., 99%, *SIGMA-ALDRICH Co*., St. Louis, USA) and $AuCl_3$ (25 mg, 0.082 mmol, 1.0 eq., 99%, *SIGMA-ALDRICH Co*., St. Louis, USA) were placed in a glass ampoule and 422 mg (5.275 mmol, 64.3 eq.) of freshly distilled SO_3 was added. The ampoule was torch sealed and heated to 80 °C within 10 h in a tube furnace. This temperature was maintained for 24 h and the reaction mixture was then allowed to cool down to room temperature within 80 h. The compound could be obtained in form yellow-golden highly moisture sensitive crystals, which had to be handled under inert gas conditions.

$[Au_2Br_2(S_4N_2O_{10})_2]$: $P_3N_3Cl_6$ (8 mg, 0.032 mmol, 99%, *SIGMA-ALDRICH Co.*, St. Louis, USA) and $AuBr_3$ (10 mg, 0.032 mmol, 99.9%, *SIGMA-ALDRICH Co.*, St. Louis, USA) were placed in a glass ampoule and 442 mg (5.516 mmol, 172.4 eq.) SO_3 was added. The torch sealed ampoule was heated to 80 °C within 10 h. The temperature was maintained for 24 h and then cooled down to room temperature within 80 h. The compound could be obtained in form yellow and highly moisture sensitive needles, which had to be handled under inert gas conditions.

Caution! SO_3 is a strong oxidizer which needs careful handling. During the reaction and even after cooling down to room temperature the glass tube might be under pressure. The tube should be cooled with liquid nitrogen before opened.

B. Structure determination and crystallographic details

Single crystal structure determination has been performed on a Bruker D8 venture diffractometer using $MoK_{\square}$ radiation (71.073 pm). The crystals were prepared in perfluorinated ether (Fomblin® YR-180) and selected with the aid of a light microscope with a polarization filter. The crystals were fixed on a micromount with a 150 µm polymer loop and adjusted to the X-ray beam under cooling at 100 K. The intensity data were collected and the images processed using APEX4.[1] The structure solution was performed in the software Olex2 by intrinsic phasing (SHELXT) and the structural model was refined by least squares methods using SHELXL.[2]

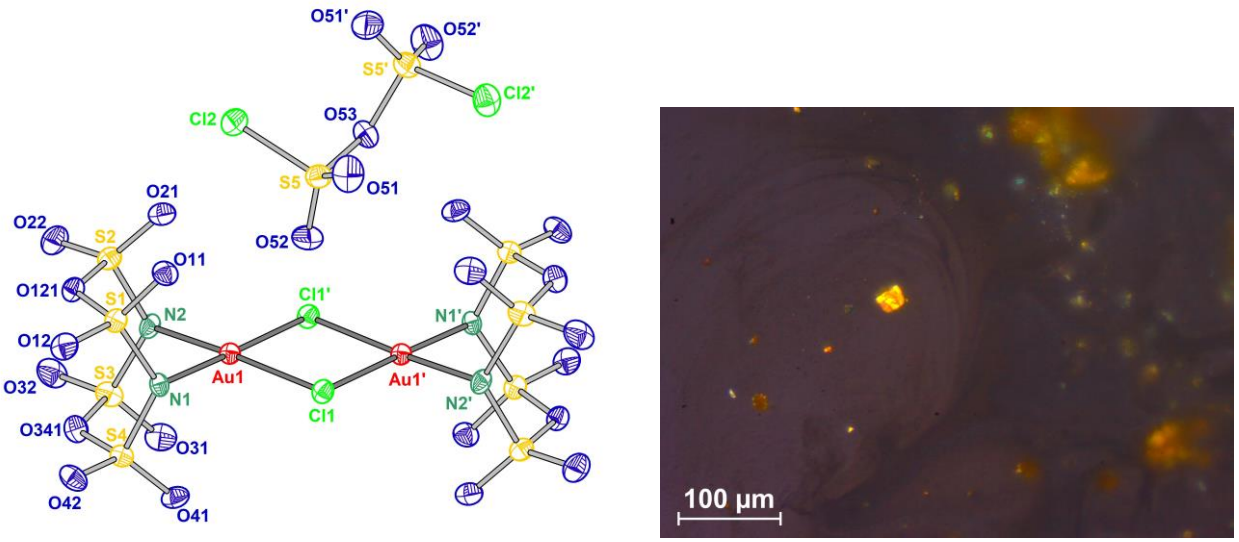

Figure S1. Structure and labelling of $[Au_2Cl_2(S_4N_2O_{10})_2](S_2O_5Cl_2)$ (left) and light microscope image of the single crystal (right). The thermal ellipsoid probability level is set to 70%.

Table S1. Crystal data and structure refinement for $[Au_2Cl_2(S_4N_2O_{10})_2](S_2O_5Cl_2)$.

Empirical formula	$Au_2Cl_4S_{10}N_4O_{25}$	
Formula weight	1312.37 g · mol^{-1}	
Temperature	100.0(2) K	
Wavelength	71.073 pm (Mo-K_α)	
Crystal system	monoclinic	
Space group	*C*2/c	
Unit cell dimensions	*a* = 2442.6(1) pm	
	b = 834.25(4) pm	β = 116.788(2)°
	c = 1505.93(7) pm	
Volume	2.739.3(2) nm^3	
Z	4	
Density (calculated)	3.182 g · cm^{-3}	
Absorption coefficient	11.962 mm^{-1}	
F(000)	2456.0	
Crystal size	0.11 × 0.02 × 0.01 mm^3	
2Theta range for data collection	5.228 to 52.13	
Index ranges	-26 ≤ h ≤ 30, -10 ≤ k ≤ 10, -18 ≤ l ≤ 16	
Reflections collected	10166	
Independent reflections	2702 [*R*(int) = 0.0307, *R*(σ)= 0.0292]	
Completeness to theta = 26.07	99.2%	
Absorption correction	multiscan	
Max. and min. transmission	0.7453 and 0.5801	
Refinement method	least-squares	

SUPPORTING INFORMATION

Data / restraints / parameters	2702/0/205
Goodness-of-fit on F^2	1.073
Final R indices [I>2sigma(I)]	R_1 = 0.0205, wR_2 = 0.0450
R indices (all data)	R_1 = 0.0243, wR_2 = 0.0461
Largest diff. peak and hole	1.28 /-0.63 e · Å^{-3}
CCDC number	2154742

SUPPORTING INFORMATION

Table S2. Atomic coordinates (× 10^4) and equivalent isotropic displacement parameters ($pm^2 \times 10^7$) for $[Au_2Cl_2(S_4N_2O_{10})_2](S_2O_5Cl_2)$. *U(eq)* is defined as one third of the trace of the orthogonalized U^{ij} tensor.

Atom	*x*	*y*	*z*	*U(eq)*
Au1	4287.9(2)	5361.3(2)	4868.1(2)	10.43(7)
S1	3418.3(5)	8151(1)	4755.7(8)	12.2(2)
S2	2988.1(5)	5797(1)	3197.1(8)	13.4(2)
S3	3212.6(5)	3300(1)	4687.8(8)	14.6(2)
S4	3692.7(5)	5642(1)	6249.6(8)	12.2(2)
S5	4791.0(5)	9056(1)	3252.1(8)	16.3(2)
Cl1	5276.4(5)	6243(1)	5905.9(7)	12.7(2)
Cl2	3944.2(5)	9676(1)	2352.9(9)	21.5(3)
N1	3883(2)	6754(4)	5517(3)	10.5(8)
N2	3443(2)	4462(4)	4022(3)	12.9(8)
O11	3755(1)	8897(4)	4329(2)	15.4(7)
O12	3116(2)	8948(4)	5225(2)	16.8(7)
O121	2871(1)	7078(4)	3903(2)	13.0(7)
O21	3357(2)	6492(4)	2812(2)	16.3(7)
O22	2401(2)	5132(4)	2614(2)	19.5(7)
O31	3712(2)	2287(4)	5234(2)	18.8(7)
O32	2613(2)	2766(4)	4086(2)	22.1(8)
O341	3131(2)	4561(4)	5454(2)	15.3(7)
O41	4206(2)	4651(4)	6784(2)	16.0(7)
O42	3418(2)	6590(4)	6705(2)	16.7(7)
O51	5147(2)	10440(4)	3628(3)	25.2(8)
O52	4786(2)	7792(4)	3863(2)	26.6(8)
O53	5000	8172(5)	2500	16(1)

Table S3. Anisotropic Displacement Parameters ($pm^2 \times 10^7$) for $[Au_2Cl_2(S_4N_2O_{10})_2](S_2O_5Cl_2)$. The anisotropic displacement factor exponent takes the form: $-2\pi^2 [h^2 a^{*2} U_{11} + 2 h k a^* b^* U_{12} + \ldots]$.

Atom	U_{11}	U_{22}	U_{33}	U_{23}	U_{13}	U_{12}
Au1	10.8(1)	9.15(1)	11.4(1)	−0.02(6)	5.03(7)	0.51(7)
S1	12.7(6)	9.3(5)	14.1(5)	−0.3(4)	5.7(4)	1.3(4)
S2	13.1(6)	13.3(6)	11.8(5)	−0.5(4)	3.9(4)	0.1(4)
S3	18.5(6)	10.6(5)	15.4(5)	−2.3(4)	8.1(5)	−4.6(4)
S4	14.0(6)	10.6(6)	12.4(5)	−0.2(4)	6.4(4)	−0.4(4)
S5	18.2(6)	16.6(6)	14.7(6)	2.3(4)	8.0(5)	3.2(5)
Cl1	12.2(5)	13.3(5)	12.5(5)	−2.1(4)	5.3(4)	1.8(4)
Cl2	18.2(6)	23.8(6)	22.2(6)	6.8(5)	8.8(5)	5.2(5)
N1	11(2)	10(2)	14(2)	−1(1)	7.0(2)	0.8(1)
N2	8(2)	13(2)	14(2)	0(1)	2.2(2)	−2.4(2)
O11	17(2)	13(2)	17(2)	1.8(1)	8.8(1)	−1.3(1)
O12	20 (2)	13(2)	18(2)	−1(1)	8.8(1)	5.1(1)
O21	19(2)	16(2)	13(2)	2(1)	6.4(1)	1.8(1)
O22	15(2)	22(2)	17(2)	−3(1)	2.5(1)	−2.6(1)
O121	12(2)	13(2)	13(2)	−2(1)	4.1(1)	0.6(1)
O31	25(2)	10(2)	21(2)	1(1)	11(2)	0.0(1)
O32	22(2)	24.(2)	21(2)	−3(1)	10(2)	−11(2)
O341	16(2)	14(2)	18(2)	−2(1)	9(1)	−1(1)
O41	19(2)	14(2)	14(2)	4(1)	6(1)	4(1)
O42	23(2)	13(2)	20(2)	−1(1)	15(1)	1(1)

O51	25(2)	22(2)	28(2)	−11(2)	12(2)	−3(2)
O52	27(2)	32(2)	23(2)	14(2)	14(2)	7(2)
O53	19(2)	11(2)	21(2)	0	13(2)	0

Table S4. Experimental bond lengths (in pm) for $[Au_2Cl_2(S_4N_2O_{10})_2](S_2O_5Cl_2)$.

Atom	Atom	Length	Atom	Atom	Length
Au1	Au1[1]	337.32(4)	S3	O31	140.4(3)
Au1	Cl1[1]	232.4(1)	S3	O32	140.4(3)
Au1	Cl1	232.6(1)	S3	O341	163.8(3)
Au1	N1	203.9(3)	S3	N2	166.5(4)
Au1	N2	201.8(4)	S4	O41	141.1(3)
S1	O11	139.7(3)	S4	O42	140.1(3)
S1	O12	139.9(3)	S4	O341	162.7(3)
S1	O121	164.1(3)	S4	N1	166.0(4)
S1	N1	166.9(4)	S5	O51	140.2(4)
S2	O21	139.9(3)	S5	O52	140.3(3)
S2	O22	140.4(3)	S5	O53	161.5(2)
S2	O121	162.1(3)	S5	Cl2	196.3(2)
S2	N2	166.6(4)			

[1]1-*x*, 1-*y*, 1-*z*

Table S5. Experimental bond angles [°] for $[Au_2Cl_2(S_4N_2O_{10})_2](S_2O_5Cl_2)$.

Atom	Atom	Atom	Angle	Atom	Atom	Atom	Angle
Cl1	Au1	Au1[1]	43.48(3)	S1	N1	Au1	113.3(2)
Cl1[1]	Au1	Au1[1]	43.53(3)	S3	N2	Au1	111.3(2)
Cl1[1]	Au1	Cl1	87.01(4)	S3	N2	S2	123.1(2)
N1	Au1	Au1[1]	138.1(1)	S2	N2	Au1	111.8(2)
N1	Au1	Cl1[1]	178.5(1)	O31	S3	O341	108.8(2)
N1	Au1	Cl1	94.5(1)	O31	S3	N2	105.3(2)
N2	Au1	Au1[1]	135.6(1)	O341	S3	N2	103.4(2)
N2	Au1	Cl1	176.2(1)	O32	S3	O31	124.4(2)
N2	Au1	Cl1[1]	92.2(1)	O32	S3	O341	103.6(2)
N2	Au1	N1	86.3(2)	O32	S3	N2	109.5(2)
Au1[1]	Cl1	Au1	92.99(4)	O41	S4	O341	109.4(2)
O12	S1	O121	103.0(2)	O41	S4	N1	105.2(2)
O12	S1	N1	109.6(1)	O341	S4	N1	102.5(2)
O11	S1	O12	125.0(2)	O42	S4	O41	123.4(2)
O11	S1	O121	108.9(2)	O42	S4	O341	104.1(2)
O11	S1	N1	105.5(1)	O42	S4	N1	110.4(2)
O121	S1	N1	102.7(2)	O53	S5	Cl2	101.8(7)
O21	S2	N2	104.4(2)	O51	S5	Cl2	109.3(2)
O21	S2	O22	124.3(2)	O51	S5	O53	108.9(2)
O22	S2	O121	104.0(2)	O51	S5	O52	122.8(2)
O22	S2	N2	110.4(2)	O52	S5	Cl2	109.4(2)
O121	S2	N2	102.0(2)	O52	S5	O53	102.5(2)
O21	S2	O121	109.6(2)	S5[2]	O53	S5	125.7(3)

[1]1-*x*,1-*y*,1-*z*; [2]1-*x*,+*y*,1/2-*z*

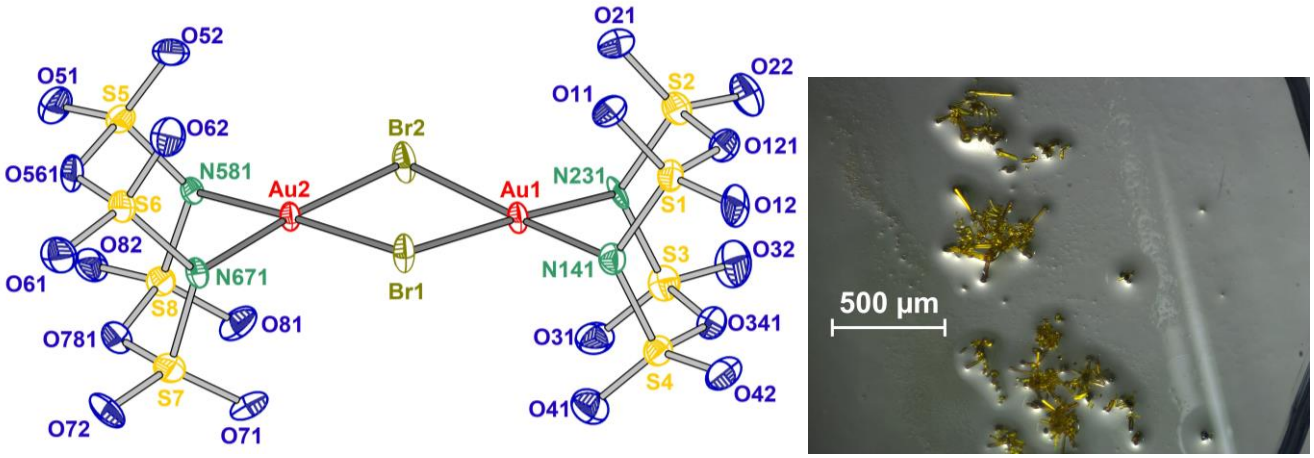

Figure S2. Structure and labelling of $[Au_2Br_2(S_4N_2O_{10})_2]$ and light microscope image of the single crystals (right). The thermal ellipsoid probability is set to 70%.

Table S6. Crystal data and structure refinement for $[Au_2Br_2(S_4N_2O_{10})_2]$.

Empirical formula	$Au_2Br_2S_8N_4O_{20}$	
Formula weight	1186.27 g · mol^{-1}	
Temperature	100.0(2) K	
Wavelength	71.073 pm (Mo-K□)	
Crystal system	triclinic	
Space group	$P\bar{1}$	
Unit cell dimensions	a = 721.6(2) pm	α = 93.392(1)°
	b = 834.25(4) pm	β = 99.71(1)°
	c = 1825.5(5) pm	γ = 107.65(1)°
Volume	1.066.1(5) nm^3	
Z	2	
Density (calculated)	3.695 g · cm^{-3}	
Absorption coefficient	18.382 mm^{-1}	
F(000)	1088.0	
Crystal size	0.319 × 0.142 × 0.14 mm^3	
2Theta range for data collection	5.21 to 61.386	
Index ranges	-10 ≤ h ≤ 10, -12 ≤ k ≤ 12, 0 ≤ l ≤ 26	
Reflections collected	13085	
Independent reflections	13085 [R(int) = 0.0566, R(σ)= 0.0403]	
Completeness to theta = 30.693	97.9%	
Absorption correction	multiscan	
Max. and min. transmission	0.746 and 0.264	
Refinement method	Least-squares	
Data / restraints / parameters	13085/0/326	

Goodness-of-fit on F^2	1.077
Final R indices [I>2sigma(I)]	R_1 = 0.0399, wR_2 = 0.1177
R indices (all data)	R_1 = 0.0435, wR_2 = 0.1265
Largest diff. peak and hole	3.69 /-1.63 e · Å^{-3}
HKLF 5 BASF	0.4996(9)
CCDC number	2154741

Table S7. Atomic coordinates (× 10^4) and equivalent isotropic displacement parameters ($pm^2 \times 10^7$) for $[Au_2Br_2(S_4N_2O_{10})_2]$. *U(eq)* is defined as one third of the trace of the orthogonalized U^{ij} tensor.

Atom	*x*	*y*	*z*	*U(eq)*
Au1	4584.5(5)	6366.2(4)	3168.0(2)	10.50(9)
Au2	381.3(5)	3920.0(4)	1880.6(2)	9.98(9)
Br1	1719(1)	4047(1)	3204.2(5)	14.7(2)
Br2	3016(1)	6469(1)	1886.0(5)	17.0(2)
S1	5761(3)	7929(3)	4804(1)	13.0(4)
S2	7120(3)	9941(3)	3684(1)	15.3(4)
S3	9101(3)	7697(3)	3232(1)	15.6(4)
S4	7746(3)	5684(3)	4354(1)	13.3(4)
S5	−3064(3)	3755(3)	574(1)	13.7(4)
S6	−4002(3)	1593(3)	1681(1)	13.9(4)
S7	−857(3)	283(3)	1455(1)	15.0(4)
S8	−21(3)	2365(3)	294(1)	13.3(4)
N231	7094(11)	8280(9)	3173(5)	13.0(1)
N671	−1630(11)	1684(9)	1867(5)	12(1)
N141	5800(12)	6325(10)	4258(5)	13(1)
N581	−7350(11)	3718(9)	757(4)	11(1)
O11	3867(10)	8070(9)	4575(4)	18(1)
O12	6612(11)	7876(10)	5551(4)	20(1)
O21	5201(11)	10075(9)	3472(4)	19(1)
O22	8883(12)	11212(9)	3703(5)	24(2)
O31	8535(12)	6291(10)	2713(4)	21(1)
O32	10790(11)	9033(10)	3250(5)	26(2)
O41	7221(12)	4288(9)	3834(4)	21(1)
O42	8519(11)	5730(10)	5122(4)	20(1)
O51	−3736(11)	3590(10)	−203(4)	21(1)
O52	−3099(11)	5037(9)	1075(4)	18(1)
O61	−5210(11)	−35(9)	1627(5)	21(2)
O62	−4146(11)	2868(9)	2156(4)	20(1)
O71	1201(11)	749(9)	1749(4)	19(1)
O72	−2164(11)	−1281(8)	1443(4)	20(1)
O81	2039(10)	2751(9)	573(4)	20(1)
O82	−848(11)	2163(9)	−472(4)	18(1)
O561	−4296(10)	2018(9)	820(4)	16(1)
O781	−1175(11)	639(8)	578(4)	17(1)
O121	7387(10)	9426(9)	4540(4)	16(1)
O341	9403(10)	7154(9)	4081(4)	15(1)

Table S8. Anisotropic Displacement Parameters ($pm^2 \times 10^7$) for $[Au_2Br_2(S_4N_2O_{10})_2]$. The anisotropic displacement factor exponent takes the form: $-2\pi^2$ [h^2 $a^{*2}U_{11}$ + 2 h k a* b* U_{12} +…].

Atom	U_{11}	U_{22}	U_{33}	U_{23}	U_{13}	U_{12}
Au1	9.1(2)	9.5(2)	9.3(2)	0.5(1)	−0.2(1)	−1.2(1)
Au2	8.9(1)	8.6(2)	9.3(2)	0.7(1)	−0.9(1)	−0.4(1)
Br1	13.0(4)	14.0(4)	10.4(4)	2.6(3)	−1.7(3)	−3.7(3)
Br2	18.1(4)	13.4(4)	11.4(4)	3.2(3)	−1.9(3)	−4.7(3)
S1	10.2(9)	15(1)	12(1)	−1.1(7)	1.3(7)	2.6(7)
S2	13.8(9)	10.9(9)	19(1)	1.7(8)	3.0(8)	0.4(8)
S3	12.9(9)	17(1)	16(1)	1.8(8)	5.5(8)	2.3(8)
S8	13.4(9)	14(1)	13(1)	0.6(7)	2.0(7)	4.8(8)
S7	15.8(1)	11.5(9)	18(1)	2.9(8)	2.8(8)	4.1(8)
S5	14(1)	15(1)	12(1)	1.5(8)	0.0(8)	6.8(8)
S4	13.4(9)	16(1)	11(9)	0.0(7)	1.9(7)	5.6(8)
S6	10.2(9)	12.1(9)	17(1)	1.0(8)	2.2(8)	0.8(7)
O62	16(3)	22(4)	21(4)	3(3)	5(3)	4(3)
O31	24(4)	24(4)	18(4)	0(3)	4(3)	14(3)
N231	10(3)	6(3)	17(4)	−5(3)	3(3)	−4(2)
N671	7(3)	7(3)	17(4)	1(3)	2(3)	−3(2)
N141	11(3)	13(3)	14(4)	0(3)	2(3)	2(3)
O561	10(3)	16(3)	17(3)	−1(3)	−2(2)	−1(2)
O72	24(4)	6(3)	27(4)	0(3)	6(3)	−1(3)
O41	25(4)	19(3)	20(4)	−1(3)	5(3)	8(3)
O781	17(3)	12(3)	19(3)	−1(2)	2(3)	3(2)
O51	20(3)	25(4)	17(3)	3(3)	−2(3)	9(3)
O52	24(3)	16(3)	18(3)	1(3)	2(3)	12(3)
O12	21(3)	26(4)	9(3)	−5(3)	−2(3)	5(3)
O11	12(3)	21(3)	23(4)	2(3)	3(3)	8(3)
N581	13(3)	12(3)	8(3)	−4(2)	−1(3)	5(3)
O121	10(3)	18(3)	20(3)	1(3)	3(2)	4(2)
O81	11(3)	25(4)	26(4)	8(3)	4(3)	8(3)
O61	16(3)	14(3)	30(4)	4(3)	6(3)	1(3)
O42	19(3)	28(4)	15(3)	1(3)	1(3)	14(3)
O341	14(3)	17(3)	13(3)	2(2)	1(2)	5(2)
O71	17(3)	23(4)	22(4)	7(3)	1(3)	13(3)
O22	23(4)	14(3)	27(4)	−1(3)	4(3)	−3(3)
O82	24(4)	17(3)	13(3)	−2(3)	2(3)	8(3)
O32	14(3)	27(4)	33(4)	3(3)	7(3)	−2(3)
O21	20(3)	18(3)	22(4)	5(3)	1(3)	10(3)

Table S9. Experimental bond lengths (in pm) for $[Au_2Br_2(S_4N_2O_{10})_2]$.

Atom	Atom	Length	Atom	Atom	Length
Au1	Br1	242.2(1)	S8	O781	163.9(7)
Au1	Br2	244.1(1)	S8	N581	166.0(8)
Au1	N231	205.1(7)	S8	O81	141.5(7)
Au1	N141	204.1(8)	S8	O82	140.2(8)
Au2	Br1	242.9(1)	S7	N671	167.4(8)
Au2	Br2	243.8(1)	S7	O72	139.5(7)
Au2	N671	203.6(7)	S7	O781	163.8(8)
Au2	N581	205.0(8)	S7	O71	141.3(7)

S1	N141	167.3(8)	S5	O561	163.3(7)
S1	O12	140.8(7)	S5	O51	140.3(8)
S1	O11	140.5(7)	S5	O52	140.7(7)
S1	O121	162.3(7)	S5	N581	166.8(8)
S2	N231	166.3(8)	S4	N141	164.8(8)
S2	O121	164.7(8)	S4	O41	140.6(8)
S2	O22	140.2(8)	S4	O42	141.1(8)
S2	O21	141.5(8)	S4	O341	163.0(7)
S3	O31	140.8(8)	S6	O62	140.4(8)
S3	N231	166.2(8)	S6	N671	166.4(8)
S3	O341	164.6(7)	S6	O561	163.0(8)
S3	O32	139.8(8)	S6	O61	140.5(7)

Table S10. Experimental bond angles [°] $[Au_2Br_2(S_4N_2O_{10})_2]$.

Atom	Atom	Atom	Angle	Atom	Atom	Atom	Angle
Br1	Au1	Br2	87.20(3)	O72	S7	O781	104.1(4)
N231	Au1	Br1	177.1(2)	O72	S7	O71	123.9(5)
N231	Au1	Br2	95.2(2)	O781	S7	N671	102.3(4)
N141	Au1	Br1	92.0(2)	O71	S7	N671	104.8(4)
N141	Au1	Br2	177.3(2)	O71	S7	O781	108.6(4)
N141	Au1	N231	85.6(3)	O561	S5	N581	102.3(4)
Br1	Au2	Br2	87.10(4)	O51	S5	O561	103.9(4)
N671	Au2	Br1	92.2(2)	O51	S5	O52	124.3(5)
N671	Au2	Br2	174.7(2)	O51	S5	N581	109.7(4)
N671	Au2	N581	86.3(3)	O52	S5	O561	109.4(4)
N581	Au2	Br1	177.6(2)	O52	S5	N581	105.3(4)
N581	Au2	Br2	94.2(2)	O41	S4	N141	106.1(4)
Au1	Br1	Au2	92.73(4)	O41	S4	O42	123.7(5)
Au2	Br2	Au1	92.05(4)	O41	S4	O341	108.9(4)
O12	S1	N141	110.2(4)	O42	S4	N141	109.7(4)
O12	S1	O121	103.9(4)	O42	S4	O341	103.9(4)
O11	S1	N141	105.4(4)	O341	S4	N141	102.8(4)
O11	S1	O12	124.2(5)	O62	S6	N671	105.9(4)
O11	S1	O121	109.0(4)	O62	S6	O561	109.5(4)
O121	S1	N141	102.2(4)	O62	S6	O61	124.0(5)
O121	S2	N231	102.5(4)	O561	S6	N671	102.5(4)
O22	S2	N231	110.6(4)	O61	S6	N671	109.4(4)
O22	S2	O121	103.1(4)	O61	S6	O561	103.6(4)
O22	S2	O21	124.1(5)	S2	N231	Au1	111.6(4)
O21	S2	N231	105.6(4)	S3	N231	Au1	112.2(4)
O21	S2	O121	109.0(4)	S3	N231	S2	121.4(5)
O31	S3	N231	105.2(4)	S7	N671	Au2	108.7(4)
O31	S3	O341	108.4(4)	S6	N671	Au2	115.8(4)
O341	S3	N231	103.2(4)	S6	N671	S7	121.0(5)
O32	S3	O31	123.5(5)	S1	N141	Au1	111.3(4)
O32	S3	N231	110.8(5)	S4	N141	Au1	113.4(4)
O32	S3	O341	104.0(5)	S4	N141	S1	121.8(5)
O781	S8	N581	103.2(4)	S6	O561	S5	122.8(4)
O81	S8	O781	108.5(4)	S7	O781	S8	123.6(4)
O81	S8	N581	105.7(4)	S8	N581	Au2	110.3(4)

O82	S8	O781	103.7(4)	S8	N581	S5	121.8(5)
O82	S8	N581	110.7(4)	S5	N581	Au2	112.8(4)
O82	S8	O81	123.2(5)	S1	O121	S2	122.8(4)
O72	S7	N671	111.1(4)	S4	O341	S3	122.8(4)

C. Results from quantum chemical calculations

A full geometry optimization of the dimer $[Au_2Br_2(S_4N_2O_{10})_2]$ and $[Au_2Cl_2(S_4N_2O_{10})_2]$ was performed within density functional theory (DFT). For $[Au_2Br_2(S_4N_2O_{10})_2]$ the PBE0 exchange-correlation functional with the basis set *cc*-pVDZ for O, N, S and Br and *cc*-pVDZ-PP for Au was used.[3,4] $[Au_2Cl_2(S_4N_2O_{10})_2]$ was optimized with the PBE0 exchange-correlation functional with the basis set *cc*-pVTZ for O, N, S, and Cl and *cc*-pVTZ-PP for Au. The calculations were also used for assigning the Raman frequencies. Throughout the study the TmoleX 18 (Turbomole 7.0) program package was used.[5,6]

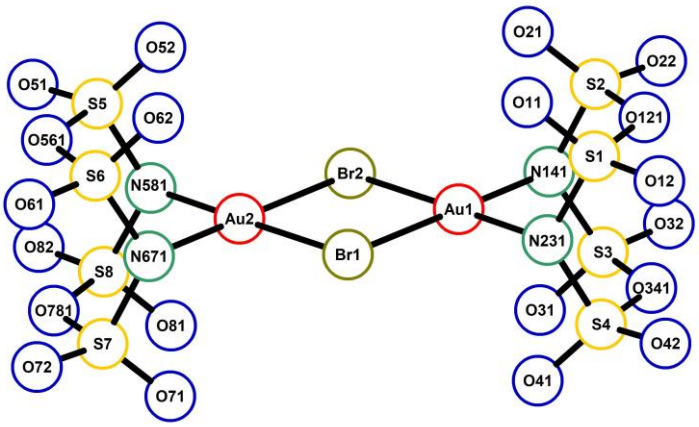

Figure S3: Structure and labelling of $[Au_2Br_2(S_4N_2O_{10})_2]$.

Table S11. Coordinates for the $[Au_2Br_2(S_4N_2O_{10})_2]$ from quantum chemical calculations.

Atom	X	Y	Z
Au1	0.940688	0.943149	1.202218
Au2	−0.940688	−0.943149	−1.202218
Br1	−0.378477	−1.155026	1.203189
Br2	0.378477	1.155026	−1.203189
N141	2.019141	2.666861	1.189157
N231	1.418396	0.751792	3.170261
N671	−2.019141	−2.666861	−1.189157
N581	−1.418396	−0.751792	−3.170261
S1	0.622323	1.906647	4.149022
O12	1.038617	1.777050	5.524852
O11	−0.752390	1.882091	3.681190
O121	1.351161	3.343572	3.648707
S2	1.244113	3.914365	2.066052
O22	2.059685	5.104721	2.077333
O21	−0.139718	3.847446	1.629473
S3	3.699389	2.366390	1.303479

O31	3.928920	1.287118	0.358693
O341	3.836319	1.765402	2.873657
O32	4.436784	3.605990	1.348773
S8	−0.622323	−1.906647	−4.149022
O781	−1.351161	−3.343572	−3.648707
O81	0.752390	−1.882091	−3.681190
O82	−1.038617	−1.777050	−5.524852
S7	−1.244113	−3.914365	−2.066052
O72	−2.059685	−5.104721	−2.077333
O71	0.139718	−3.847446	−1.629473
S5	−3.068385	−0.351487	−3.378941
O561	−3.836319	−1.765402	−2.873657
O51	−3.398263	−0.268409	−4.781323
O52	−3.302619	0.692772	−2.396467
S4	3.068385	0.351487	3.378941
O41	3.302619	−0.692772	2.396467
O42	3.398263	0.268409	4.781323
S6	−3.699389	−2.366390	−1.303479
O62	−3.928920	−1.287118	−0.358693
O61	−4.436784	−3.605990	−1.348773

Table S12. Bond length (in pm) for the $[Au_2Br_2(S_4N_2O_{10})_2]$ from quantum chemical calculations.

Atom	Atom	Length	Atom	Atom	Length
Au1	Br1	247.84	S2	O22	144.3
Au1	Br2	247.93	S2	O21	145.26
Au1	N231	203.33	S3	O31	145.26
Au1	N141	203.42	S3	O341	168.68
Br1	Au2	247.93	S3	O32	144.31
Br2	Au2	247.84	O341	S4	168.65
N231	S2	171.05	S8	O781	168.71
N231	S3	171.07	S8	O81	145.23
N141	S1	171.04	S8	O82	144.33
N141	S4	171.06	O781	S7	168.58
Au2	N671	203.33	S7	O72	144.3
Au2	N581	203.42	S7	O71	145.26
N671	S7	171.05	S5	O561	168.65
N671	S6	171.07	S5	O51	144.31
N581	S8	171.04	S5	O52	145.28
N581	S5	171.06	O561	S6	168.68
S1	O12	144.33	S4	O41	145.28
S1	O11	145.23	S4	O42	144.31
S1	O121	168.71	S6	O62	145.26
O121	S2	168.58	S6	O61	144.31

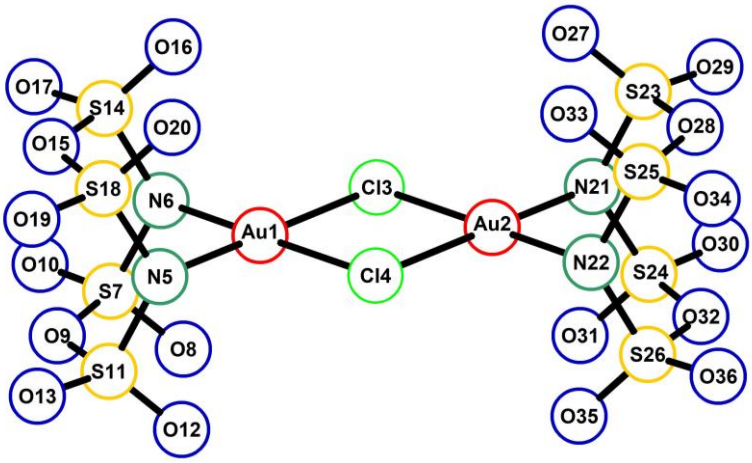

Figure S4. Structure and labelling of $[Au_2Cl_2(S_4N_2O_{10})_2]$.

Table S13. Coordinates for the $[Au_2Cl_2(S_4N_2O_{10})_2]$ from quantum chemical calculations.

Atom	X	Y	Z
Au1	−1.699047	0.243118	−0.150822
Au2	1.699048	−0.243120	0.150823
Cl3	−0.050754	−1.082174	−1.168709
Cl4	0.050756	1.082173	1.168710
N5	−3.107197	1.395525	0.723374
N6	−3.194396	−0.483393	−1.295152
S7	−4.233516	−1.478192	−0.421037
O8	−3.369585	−2.325929	0.332675
O9	−4.964661	−0.409824	0.599003
O10	−5.289916	−1.940641	−1.245081
S11	−4.145210	0.501595	1.701376
O12	−3.285301	−0.344937	2.460809
O13	−5.143326	1.337758	2.261408
S14	−3.720972	0.646925	−2.425366
O15	−4.429751	1.789883	−1.472777
O16	−2.521564	1.181333	−2.981521
O17	−4.794865	0.126033	−3.189774
S18	−3.627351	2.625794	−0.300440
O19	−4.640501	3.397858	0.320879
O20	−2.426948	3.164663	−0.850137
N21	3.107189	−1.395565	−0.723336
N22	3.194406	0.483432	1.295115
S23	4.145201	−0.501688	−1.701386
S24	3.627340	−2.625792	0.300535
S25	4.233516	1.478193	0.420942
S26	3.720992	−0.646834	2.425375
O27	3.285290	0.344808	−2.460859
O28	4.964655	0.409781	−0.599059
O29	5.143312	−1.337882	−2.261378
O30	4.640478	−3.397895	−0.320754
O31	2.426936	−3.164623	0.850268

O32	4.429756	−1.789834	1.472829
O33	3.369576	2.325893	−0.332800
O34	5.289923	1.940682	1.244954
O35	2.521588	−1.181211	2.981567
O36	4.794895	−0.125910	3.189748

Table S14. Bond length (in pm) for the $[Au_2Cl_2(S_4N_2O_{10})_2]$ from quantum chemical calculations.

Atom	Atom	Length	Atom	Atom	Length
Au1	Cl3	234.72	S14	O17	141.74
Au1	Cl4	234.67	O15	S18	164.83
Au1	N5	201.87	S18	O19	141.72
Au1	N6	201.83	S18	O20	142.6
Au2	Cl3	234.67	S21	S23	168.32
Au2	Cl4	234.72	S21	S24	168.3
Au2	N21	201.87	S22	S25	168.33
Au2	N22	201.83	S22	S26	168.29
N5	S11	168.32	S23	O27	142.58
N5	S18	168.29	S23	O28	164.85
N6	S7	168.33	S23	O29	141.74
N6	S14	168.29	S24	O30	141.72
S7	O8	142.59	S24	O31	142.6
S7	O9	164.82	S24	O32	164.83
S7	O10	141.74	S25	O28	164.82
O9	S11	164.85	S25	O33	142.59
S11	O12	142.58	S25	O34	141.74
S11	O13	141.74	S26	O32	164.81
S14	O15	164.81	S26	O35	142.6
S14	O16	142.6	S26	O36	141.74

D. Vibrational spectroscopy

Raman spectroscopic data were collected with *inVia Qotor confocal RAMAN microscope* by *Renishaw GmbH* (Pliezhausen, DE) equipped with 10x, 50x and 100x magnification lenses. The spectra were measured on selected single crystals through the glass ampoule with a green laser (532 nm, 100 mW) with an exposure time of 10000 ms in the range from 1802 cm^{-1} to 102 cm^{-1}. The data were processed and corrected by using the WiRE 5.1 software. Important Raman frequencies in cm^{-1} (exptl./*calcd*.):

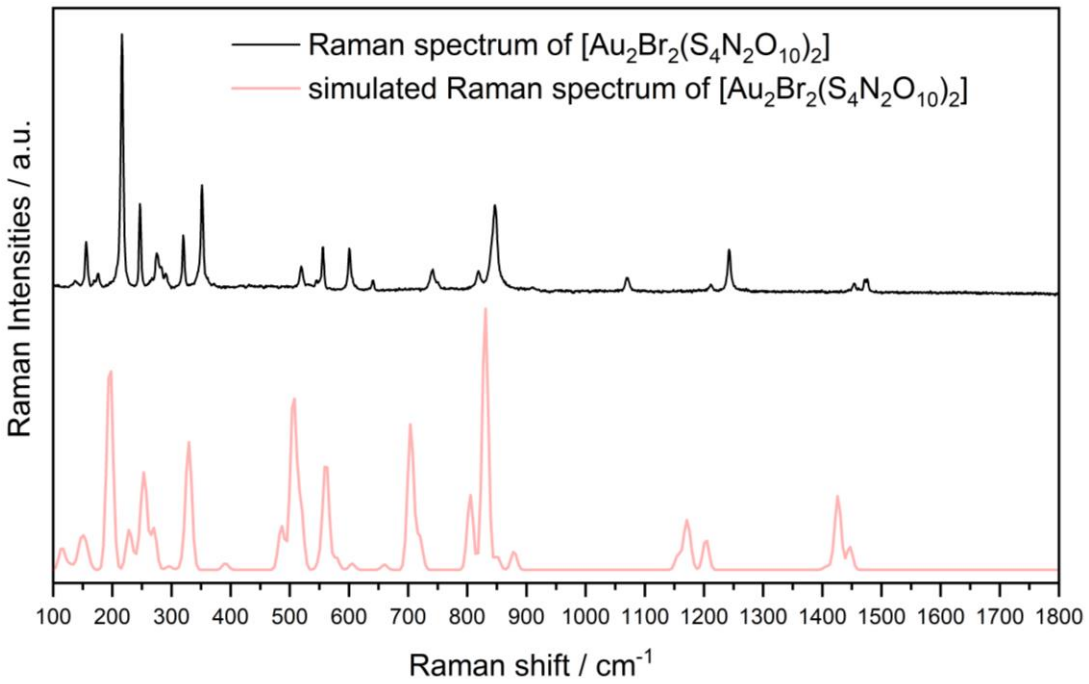

Figure S5. Raman spectrum of a crystal of $[Au_2Br_2(S_4N_2O_{10})_2]$ compared to the respective theoretical simulated spectrum (DFT-PBE0/*cc*-pVDZ for N, O, S, Br and cc-pVDZ-PP for Au) (shown in red). The Intensities are given in arbitrary units, a.u..

Table S8. Assignment of the experimental and simulated Raman bands (in *italics*) of $[Au_2Br_2(S_4N_2O_{10})_2]$.

Assignment	**Raman / cm^{-1}**
$\nu_{sym.}$ S–$O_{terminal}$	1476/*1447*, 1243/*1203*
$\nu_{asym.}$ S–$O_{terminal}$	1453/*1426* 1211/*1175*
ν_{sym} Au-$N_{bridging}$	845/*831,852*
ν_{asym} Au-$N_{bridging}$	818/*805*
ν_{sym} S-$O_{bridging}$	*741/704*
δ_{sym} $[S_4N_2O_{10}]$ units	641/*660* 601/*605* 555/*551* 520/*518*
δ_{asym} $[S_4N_2O_{10}]$ units	320/*329*
δ_{asym} $[S_4N_2O_{10}]$ units - rocking	290/*270*
δ_{sym} $[S_4N_2O_{10}]$ units - scissoring	275/*253*
δ_{sym} $[Au_2Br_2(S_4N_2O_{10})_2]$- wagging	247/*228*
$\nu_{asym.}$ Au-Br $\nu_{sym.}$ Au-Br	216/*197* 216 /*194*
$\delta_{asym.}$ $[Au_2Br_2(S_4N_2O_{10})_2]$- wagging	175/*151*
$\delta_{asym.}$ $[Au_2Br_2(S_4N_2O_{10})_2]$ - twisting	155/*113*
Not assigned frequency	1162

References

[1] Bruker (**2021**). *Apex4*. Bruker AXS Inc., Madison, Wisconsin, USA.
[2] G. Sheldrick. *Acta Crystallogr. A* **2015**. *71*. 3–8.
[3] T. H. Dunning Jr., *J. Chem. Phys.* **1989**, *90*, 1007–1023.
[4] D. E. Woon, T. H. Dunning Jr., *J. Chem. Phys.* **1993**, *98*, 1358–1371.
[5] C. Steffen, K. Thomas, U. Huniar, A. Hellweg, O. Rubner, A. Schroer, *J. Comput. Chem.* **2010**, *31*, 2967–2970.
[6] TURBOMOLE V7.0 **2015**, *a development of University of Karlsruhe and Forschungszentrum Karlsruhe GmbH*, **1989**-**2007**, TURBOMOLE GmbH, since **2007**.

Author Contributions

Tobias Rennebaum performed all of the experimental work in course of his PhD work. David van Gerven assisted in solving the crystal structures. Mathias Wickleder is the supervisor and the leader of the project.

8.2 SI: Hydrazine Sulfonic Acid, $NH_3NH(SO_3)$, the Bigger Sibling of Sulfamic Acid

Chemistry–A European Journal

Supporting Information

Hydrazine Sulfonic Acid, $NH_3NH(SO_3)$, the Bigger Sibling of Sulfamic Acid

Tobias Rennebaum, David van Gerven, Sean S. Sebastian, and Mathias S. Wickleder*

SUPPORTING INFORMATION

Table of Contents

A. Syntheses

NH_3NHSO_3: 9.53 mL $N_2H_4{\cdot}H_2O$ (64% Hydrazine, 0.194 mol, 3.00 eq.) was cooled to −20 °C in an ice/NaCl bath and 10.0 g $Py{\cdot}SO_3$ (0.062 mol, 1.00 eq., *SIGMA-ALDRICH Co.*, St. Louis, USA) was added in portions over a period of one hour. After complete addition, 30 mL of glacial acetic acid was added to the ice cooled solution. The slimy precipitate was isolated and washed with methanol and diethyl ether. The crude product was recrystallized in water and after storage in the fridge a few colourless oval crystals (s. Figure S1) were formed which were analysed by SC-XRD.

$Ba[NH_2NH(SO_3)]_2(H_2O)$: 19.00 mL $N_2H_4{\cdot}H_2O$ (64% Hydrazine, 0.39 mol, 3.00 eq.) was cooled to −20 °C in an ice/NaCl bath and 20.795 g $Py{\cdot}SO_3$ (0.131 mol, 1.00 eq., *SIGMA-ALDRICH Co.*, St. Louis, USA) was added in portions over a period of one hour. The solid $Ba(OH)_2$ (43.70 g, 0.255 mol, 1.95 eq.) was added to the solution and the mixture was stirred for 30 min at rt. The mixture was concentrated to complete dryness under reduced pressure. The residue was mixed with water and the insoluble components were filtered. Gaseous CO_2 was passed into the solution to precipitate the excess of Ba^{2+} in form of $BaCO_3$. To the freed solution ethanol and ether were added to precipitate the product. The separated product was finally washed with ethanol and ether and dried in *vacuo* to afford colourless needles (1.716 g, 4.55 mmol, 3%). **Elemental Analysis:** Calcd. for $BaH_8N_4O_7S_2$: N, 14.84; H, 2.14; S, 16.98. Found N, 14.81; H, 1,99; S, 16.66.

NH_3NHSO_3: For a re-determination of the crystal structure of amidosulfonic acid (sulfamic acid) a crystal selected from the purchased compound (*SIGMA-ALDRICH*) was used.

B. Structure determination and crystallographic details

Single crystal structure determination has been performed on a Bruker D8 VENTURE KAPPA diffractometer with a microfocus sealed tube using a multilayer mirror as monochromator and a Bruker PHOTON III detector. MoK_α radiation (71.073 pm) was used as X-ray source. The crystals were prepared in perfluorinated ether (Fomblin® YR-180) and selected with the aid of a light microscope with a polarization filter. The crystals were fixed on a micromount with a 150 µm polymer loop and adjusted to the X-ray beam under cooling at 100 K. The intensity data were collected and the images processed using APEX4.[1] The integration was done with SAINT and a multi-scan absorption correction using SADABS was applied.[2,3] The structure solution was performed in the software Olex2 by intrinsic phasing (SHELXT) and the structural model was refined by least squares methods using SHELXL.[4]

SUPPORTING INFORMATION

1) NH_3NHSO_3

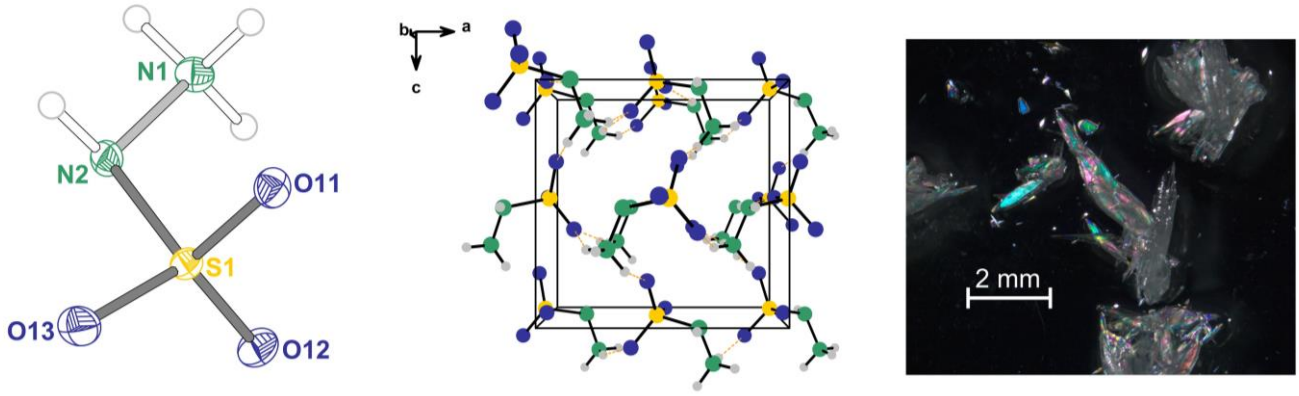

Figure S1: Structure and labelling (left), crystal structure along *b*-axis (middle) and microscope image of crystals (right) of **NH_3NHSO_3**.

Table S1: Crystal data and structure refinement for hydrazine sulfonic acid, **NH_3NHSO_3**

Empirical formula	$H_4N_2O_3S$
Formula weight	112.11 g · mol^{-1}
Temperature	100.0(2) K
Wavelength	71.073 pm (Mo-K_α)
Crystal system	orthorhombic
Space group	$Pca2_1$
Unit cell dimensions	a = 849.59(4) pm
	b = 482.18(2) pm
	c = 832.17(4) pm
Volume	0.34090(3) nm^3
Z	4
Density (calculated)	2.184 g · cm^{-3}
Absorption coefficient	0.788 mm^{-1}
F(000)	232.0
Crystal size	0.11 × 0.02 × 0.01 mm^3
2Theta range for data collection	9.598 to 57.874
Index ranges	$-11 \le h \le 11$, $-6 \le k \le 5$, $-11 \le l \le 11$
Reflections collected	12167
Independent reflections	907 [R_{int}= 0.0523, R_σ= 0.0203]
Completeness to theta = 28.94°	99.7%
Absorption correction	multiscan
Max. and min. transmission	0.6521 and 0.7468
Refinement method	least-squares
Data / restraints / parameters	907/1/73
Goodness-of-fit on F^2	1.164
Final R indices [$I \ge 2\sigma(I)$]	R_1 = 0.0159, wR_2 = 0.0436
R indices (all data)	R_1 = 0.0170, wR_2 = 0.0452
Largest diff. peak and hole	0.38 /−0.28 e · $Å^{-3}$
CCDC number	2225901

SUPPORTING INFORMATION

Table S2: Atomic coordinates and equivalent isotropic displacement parameters (pm^2 x 10^4) for **NH_3NHSO_3.** U_{eq} is defined as one third of the trace of the orthogonalized U_{ij} tensor

Atom	*x*	*y*	*z*	U_{eq}
S1	0.52502(5)	0.32605(8)	0.47728(5)	0.0073(1)
O11	0.6324(2)	0.2552(3)	0.6084(2)	0.0104(3)
O12	0.4912(1)	0.6201(3)	0.4710(3)	0.0111(3)
O13	0.5639(2)	0.2027(3)	0.3240(2)	0.0127(3)
N1	0.2909(2)	0.2462(4)	0.6740(2)	0.0093(3)
N2	0.3511(2)	0.1724(3)	0.5167(2)	0.0090(4)
H1A	0.262(4)	0.445(7)	0.675(4)	0.027(9)
H1B	0.358(4)	0.198(6)	0.762(4)	0.021(8)
H1C	0.208(4)	0.129(8)	0.680(4)	0.030(8)
H2	0.364(4)	-0.023(6)	0.513(4)	0.021(7)

Table S3: Anisotropic displacement parameters ($pm^2 \times 10^4$) for **NH_3NHSO_3**. The anisotropic displacement factor exponent takes the form: $-2\pi^2 [h^2 a^{*2} U_{11} + 2 h k a^* b^* U_{12} + \ldots]$.

Atom	U_{11}	U_{22}	U_{33}	U_{23}	U_{13}	U_{12}
S1	0.0072(2)	0.0064(2)	0.0082(2)	0.0001(2)	0.0004(2)	0.0001(1)
O11	0.0094(6)	0.0103(6)	0.0115(7)	0.0002(5)	−0.0025(6)	0.0001(6)
O12	0.0126(6)	0.0072(5)	0.0134(6)	0.0003(8)	0.0003(8)	0.0010(4)
O13	0.0167(7)	0.0108(7)	0.0107(7)	−0.0011(5)	0.0037(6)	0.0012(6)
N1	0.0085(7)	0.0104(8)	0.0090(7)	0.0003(6)	0.0020(6)	0.0004(6)
N2	0.0096(7)	0.0098(7)	0.0077(9)	−0.0019(5)	0.0018(5)	−0.0013(5)

Table S4: Experimental bond lengths [pm] for **NH_3NHSO_3**

Atom–Atom	Length
S1–O11	146.3(2)
S1–O12	144.8(1)
S1–O13	144.6(2)
S1–N2	168.5(2)
N1–N2	145.0(2)

Table S5: Experimental bond angles [°] for for **NH_3NHSO_3**

Atom–Atom–Atom	Angle [°]
O11–S1–N2	107.42(9)
O12–S1–O11	112.3(1)
O12–S1–N2	105.3(8)
O13–S1–O11	114.8(9)
O13–S1–O12	114.6(1)
O13–S1–N2	101.0(1)
N2–N1–H1A	109.6(2)
N2–N1–H1B	115.0(2)
N2–N1–H1C	100(2)
H1A–N1–H1B	112(3)
H1A–N1–H1C	115(3)
H1B–N1–H1C	106(3)
S1–N2–H2	109(2)
N1–N2–S1	112.2(1)
N1–N2–H2	108(2)

Table S6: Experimental torsion angles for **NH_3NHSO_3**

Atom–Atom–Atom–Atom	Torsion Angle [°]
O11–S1–N2–N1	54.9(2)
O12–S1–N2–N1	−65.0(2)
O13–S1–N2–N1	175.4(1)

Table S7: Hydrogen bonds for **NH_3NHSO_3**: Donor-acceptor distances [pm] and angles [°]

Donor–Acceptor	Length	Angle (N-H...O)
N1–O11	282.1(2)	142.5(3)
N1–O11	280.9(2)	151.5(3)
N1–O12	315.5(3)	143.8(3)
N1–O13	318.5(2)	120.0(2)
N1–O13	278.7(2)	126.7(2)
N2–O11	287.8(2)	111.0(2)
N2–O12	294.2(2)	153.5(2)

2) $Ba[NH_2NH(SO_3)]_2(H_2O)$

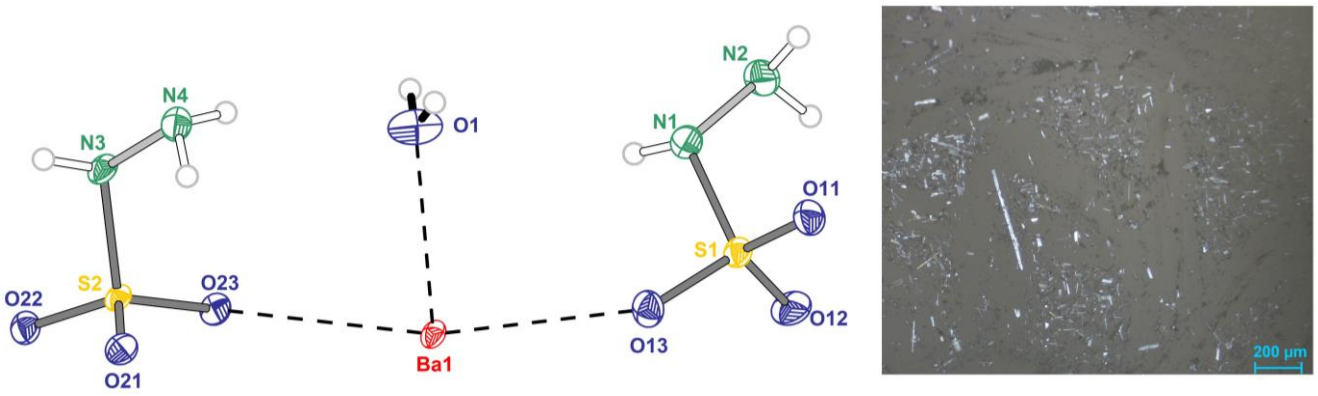

Figure S2: Structure and labelling (left) and microscope image of crystals (right) of **$Ba[NH_2NH(SO_3)]_2(H_2O)$**.

Table S8: Crystal data and structure refinement for **$Ba[NH_2NHSO_3]_2(H_2O)$**

Empirical formula	$BaH_8N_4O_7S_2$
Formula weight	377.56 g · mol^{-1}
Temperature	100.0(2) K
Wavelength	71.073 pm (Mo-K_α)
Crystal system	triclinic
Space group	$P\bar{1}$
Unit cell dimensions	a = 489.75(5) pm, α = 88.238(4)°
	b = 737.52(7) pm, β = 84.761(4)°
	c = 1317.4(1) pm, γ = 79.701(4)°
Volume	0.46618(8) nm^3
Z	2
Density (calculated)	2.690 g · cm^{-3}
Absorption coefficient	4.730 mm^{-1}
F(000)	360.0
Crystal size	0.302 × 0.26 × 0.0077 mm^3
2Theta range for data collection	6.212 to 55
Index ranges	$-6 \le h \le 6$, $-9 \le k \le 9$, $-17 \le l \le 17$
Reflections collected	12862
Independent reflections	2156 [R_{int}= 0.0652, R_σ= 0.0486]
Completeness to theta = 25.242°	99.9%
Absorption correction	multiscan
Max. and min. transmission	0.589 and 0.746
Refinement method	least-squares
Data / restraints / parameters	2156/0/159
Goodness-of-fit on F^2	1.026
Final R indices [$I \ge 2\sigma(I)$]	R_1 = 0.0292, wR_2 = 0.0630
R indices (all data)	R_1 = 0.0331, wR_2 = 0.0649
Largest diff. peak and hole	1.70/−1.13 e · $Å^{-3}$
CCDC number	2225900

Table S9: Atomic coordinates and equivalent isotropic displacement parameters (pm^2 x 10^4) for **$Ba[NH_2NH(SO_3)]_2(H_2O)$**. *U(eq)* is defined as one third of the trace of the orthogonalized U_{ij} tensor.

Atom	*x*	*y*	*z*	U_{eq}
Ba1	0.47226(5)	0.60181(4)	0.16710(2)	0.00783(9)
S2	-0.0001(2)	0.2603(2)	0.05767(7)	0.0077(2)
S1	0.9628(2)	0.7897(2)	0.35550(7)	0.0092(2)
O23	0.0646(6)	0.4114(4)	0.1132(2)	0.0107(6)
O22	-0.2922(6)	0.2891(4)	0.0350(2)	0.0111(6)
O21	0.1933(6)	0.2108(4)	-0.0322(2)	0.0105(6)
O13	0.8732(6)	0.7369(5)	0.2596(2)	0.0126(6)
O1	0.5577(8)	0.3032(6)	0.2914(3)	0.0190(8)
O11	1.2581(6)	0.7154(5)	0.3630(2)	0.0128(6)
O12	0.8920(7)	0.9846(5)	0.3758(2)	0.0157(7)
N3	0.0256(7)	0.0827(6)	0.1388(3)	0.0105(7)
N4	0.3086(7)	0.0090(6)	0.1596(3)	0.0115(7)
N1	0.7940(8)	0.6760(6)	0.4445(3)	0.0128(8)
N2	0.8383(8)	0.7200(6)	0.5466(3)	0.0146(8)
H4A	0.42(1)	0.021(9)	0.098(4)	0.04(2)
H1	0.632(9)	0.685(7)	0.435(3)	0.001(1)
H4B	0.33(1)	0.073(8)	0.204(4)	0.01(1)
H2A	1.01(1)	0.647(8)	0.563(3)	0.02(1)
H3	-0.05(1)	0.008(8)	0.117(4)	0.02(2)
H1A	0.46(1)	0.31(1)	0.342(5)	0.04(2)
H1B	0.67(2)	0.25(1)	0.296(6)	0.06(3)
H2B	0.86(1)	0.837(9)	0.552(4)	0.02(2)

Table S10: Anisotropic displacement parameters ($pm^2 \times 10^4$) for **$Ba[NH_2NH(SO_3)]_2(H_2O)$**. The anisotropic displacement factor exponent takes the form: $-2\pi^2 [h^2 a^{*2} U_{11} + 2 h k a^* b^* U_{12} + \ldots]$.

Atom	U_{11}	U_{22}	U_{33}	U_{23}	U_{13}	U_{12}
Ba1	0.00795(12)	0.0048(2)	0.0109(1)	−0.00025(9)	−0.00117(8)	−0.00146(9)
S2	0.0080(4)	0.0044(6)	0.0107(4)	0.0005(4)	−0.0012(3)	−0.0012(4)
S1	0.0096(4)	0.0067(6)	0.0115(4)	−0.0003(4)	−0.0017(3)	−0.0014(4)
O23	0.014(1)	0.0034(2)	0.015(1)	−0.001(1)	−0.002(1)	−0.001(1)
O22	0.012(1)	0.008(2)	0.014(1)	−0.001(1)	−0.003(1)	−0.002(1)
O21	0.011(1)	0.008(2)	0.012(1)	−0.001(1)	−0.001(1)	−0.001(1)
O13	0.014(1)	0.014(2)	0.011(1)	−0.003(1)	−0.001(1)	−0.004(1)
O1	0.018(2)	0.017(2)	0.018(2)	0.004(1)	0.005(1)	0.004(2)
O11	0.010(1)	0.015(2)	0.013(1)	0.0005(1)	−0.002(1)	−0.003(1)
O12	0.024(2)	0.007(2)	0.016(1)	0.0001(1)	−0.003(1)	−0.003(1)
N3	0.009(2)	0.006(2)	0.016(2)	0.003(1)	−0.003(1)	−0.002(2)
N4	0.010(2)	0.008(2)	0.017(2)	0.001(2)	−0.004(1)	−0.001(1)
N1	0.012(2)	0.012(2)	0.015(2)	0.002(1)	−0.003(1)	−0.003(2)
N2	0.021(2)	0.013(2)	0.011(2)	−0.002(2)	−0.003(1)	−0.004(2)

Table S11: Experimental bond lengths [pm] for **$Ba[NH_2NH(SO_3)]_2(H_2O)$**

Atom–Atom	Length [pm]	Atom–Atom	Length [pm]
S2–O23	144.8(3)	Ba1–O23	279.0(3)
S2–O22	146.5(3)	Ba1–O23$^{\#1}$	302.0(3)
S2–O21	145.9(3)	Ba1–O22$^{\#3}$	292.5(3)
S2–N3	165.9(4)	Ba1–O22$^{\#1}$	293.4(3)
S1–O13	146.1(3)	Ba1–O21$^{\#4}$	280.7(3)
S1–O11	146.3(3)	Ba1–O13	274.7(3)
S1–O12	144.4(3)	Ba1–O13$^{\#2}$	307.6(3)
S1–N1	166.4(4)	Ba1–O1	269.9(4)
		Ba1–O11$^{\#2}$	279.1(3)
N3–N4	144.3(5)	Ba1–N4$^{\#5}$	296.7(4)

N3–H3	79(6)		
N4–H4A	94(6)	O1–H1A	77(7)
N4–H4B	80(5)	O1–H1B	63(8)
N1–N2	143.8(5)		
N1–H1	80(4)		
N2–H2A	95(5)		
N2–H2B	89(6)		

Symmetry transformations used to generate equivalent atoms:
#1: −1+*X*, +*Y*, +*Z*; #2: 1+*X*, +*Y*, +*Z*; #3: −*X*, 1−*Y*, −*Z*; #4: 1−*X*, 1−*Y*, −*Z*; #5: +*X*, 1+*Y*, +*Z*

Table S1: Experimental bond angles [°] for **$Ba[NH_2NH(SO_3)]_2(H_2O)$**

Atom–Atom–Atom	**Angle [°]**	**Atom–Atom–Atom**	**Angle [°]**
O23–Ba1–O23$^{\#2}$	114.9(1)	O13–Ba1–O23$^{\#2}$	64.46(8)
O23–Ba1–O22$^{\#2}$	67.95(8)	O13–Ba1–O23	166.67(9)
O23–Ba1–O22$^{\#3}$	67.72(8)	O13–Ba1–O22$^{\#3}$	125.58(9)
O23–Ba1–O21$^{\#4}$	125.87(8)	O13–Ba1–O22$^{\#2}$	112.48(8)
O23–Ba1–O13$^{\#1}$	63.21(8)	O13–Ba1–O21$^{\#4}$	66.58(8)
O23$^{\#2}$–Ba1–O13$^{\#1}$	167.92(8)	O13–Ba1–O13$^{\#1}$	114.40(9)
O23–Ba1–O11$^{\#1}$	100.98(8)	O13–Ba1–O11$^{\#1}$	71.09(8)
O23–Ba1–N4$^{\#5}$	114.32(9)	O13–Ba1–N4$^{\#5}$	74.2(1)
O22$^{\#2}$–Ba1–O23$^{\#2}$	48.04(8)	O1–Ba1–O23	79.1(1)
O22$^{\#3}$–Ba1–O23$^{\#2}$	101.16(7)	O1–Ba1–O23$^{\#2}$	73.8(1)
O22$^{\#3}$–Ba1–O22$^{\#2}$	74.48(9)	O1–Ba1–O22$^{\#2}$	73.9(1)
O22$^{\#3}$–Ba1–O13$^{\#1}$	89.18(7)	O1–Ba1–O22$^{\#3}$	140.7(1)
O22$^{\#2}$–Ba1–O13$^{\#1}$	131.10(8)	O1–Ba1–O21$^{\#4}$	136(1)
O22$^{\#3}$–Ba1–N4$^{\#4}$	71.53(9)	O1–Ba1–O13$^{\#1}$	94.3(1)
O22$^{\#2}$–Ba1–N4$^{\#5}$	141.01(9)	O1–Ba1–O13	88.2(1)
O21$^{\#4}$–Ba1–O23$^{\#2}$	63.00(8)	O1–Ba1–O11$^{\#1}$	72.8(1)
O21$^{\#4}$–Ba1–O22$^{\#2}$	82.95(8)	O1–Ba1–N4$^{\#5}$	144.7(1)
O21$^{\#4}$–Ba1–O22$^{\#3}$	60.79(8)	O11$^{\#1}$–Ba1–O23$^{\#2}$	124.16(8)
O21$^{\#4}$–Ba1–O13$^{\#1}$	128.47(9)	O11–Ba1–O22	146.38(9)
O21$^{\#4}$–Ba1–N4$^{\#5}$	64.09(9)	O11$^{\#1}$–Ba1–O22$^{\#3}$	132.49(8)
		O11$^{\#1}$–Ba1–O21$^{\#4}$	125.44(9)
O13–S1–O11	110.7(2)	O11$^{\#1}$–Ba1–O13$^{\#1}$	48.1(1)
O13–S1–N1	104.4(2)	O11$^{\#1}$–Ba1–N4$^{\#5}$	72.6(1)
O11–S1–N1	105.0(2)	N4$^{\#5}$–Ba1–O23$^{\#2}$	122.1(0)
O12–S1–O13	114.2(2)	N4$^{\#5}$–Ba1–O13$^{\#1}$	67.1(0)
O12–S1–O11	112.9(2)		
O12–S1–N1	108.9(2)	N4–N3–S2	113.4(3)
		N2–N1–S1	113.3(3)
O21–S2–O22	112.7(2)		
O21–S2–N3	108.9(2)		
O23–S2–O22	112.7(2)		
O23–S2–O21	112.1(2)		
O23–S2–N3	105.5(2)		
O22–S2–N3	103.3(2)		

Symmetry transformations used to generate equivalent atoms:
#1: −1+*X*, +*Y*, +*Z*; #2: 1+*X*, +*Y*, +*Z*; #3: −*X*, 1−*Y*, −*Z*; #4: 1−*X*, 1−*Y*, −*Z*; #5: +*X*, 1+*Y*, +*Z*; #6: +*X*, −1+*Y*, +*Z*

Table S23: Experimental torsion angles for **$Ba[NH_2NH(SO_3)]_2(H_2O)$**

Atom–Atom–Atom–Atom	Torsion Angle [°]
Ba1$^{\#1}$–S2–O23–Ba1	−170.0(4)
Ba1$^{\#1}$–S2–O22–Ba1$^{\#2}$	116.4(2)
Ba1$^{\#1}$–S2–O21–Ba1$^{\#3}$	39.7(4)
Ba1$^{\#1}$–S2–N3–N4	−132.2(3)
Ba1$^{\#4}$–S1–O13–Ba1	146.7(4)
Ba1$^{\#4}$–S1–N1–N2	119.1(3)
S2–N3–N4–Ba1$^{\#5}$	−137.6(2)
O23–S2–O22–Ba1$^{\#1}$	−12.6(2)
O23–S2–O22–Ba1$^{\#2}$	104(1)
O23–S2–O21–Ba1$^{\#3}$	−28.0(3)
O23–S2–N3–N4	−71.0(3)
O22–S2–O23–Ba1	−157.8(3)
O22–S2–O23–Ba1$^{\#1}$	12.1(2)
O22–S2–O21–Ba1$^{\#3}$	101.2(2)
O22–S2–N3–N4	170.5(3)
O21–S2–O23–Ba1	−28.7(4)
O21–S2–O23–Ba1$^{\#1}$	141.3(1)
O21–S2–O22–Ba1$^{\#2}$	−25.5(3)
O21–S2–O22–Ba1$^{\#1}$	−141.9(2)
O21–S2–N3–N4	50.4(4)
O13–S1–O11–Ba1$^{\#4}$	14.2(2)
O13–S1–N1–N2	−175.7(3)
O11–S1–O13–Ba1	134.3(3)
O11–S1–O13–Ba1$^{\#4}$	−12.4(2)
O11–S1–N1–N2	67.8(3)
O12–S1–O13–Ba1	−96.9(4)
O12–S1–O13–Ba1$^{\#4}$	116.4(2)
O12–S1–O11–Ba1$^{\#4}$	−115.3(2)
O12–S1–N1–N2	−53.4(3)
N3–S2–O23–Ba1	90.1(3)
N3–S2–O23–Ba1$^{\#1}$	−99.9(2)
N3–S2–O22–Ba1$^{\#1}$	100.8(2)
N3–S2–O22–Ba1$^{\#2}$	−142.9(2)
N3–S2–O21–Ba1$^{\#3}$	−144.8(2)
N1–S1–O13–Ba1$^{\#4}$	−124.9(2)
N1–S1–O13–Ba1	21.8(4)
N1–S1–O11–Ba1$^{\#4}$	126.3(2)

Symmetry transformations used to generate equivalent atoms:
#1: -1+X, +Y, +Z; #2: -X, 1-Y, -Z; #3: 1-X, 1-Y, -Z; #4: 1+X, +Y, +Z; #5: +X, -1+Y, +Z;

Table S3: Hydrogen bonds for **$Ba[NH_2NH(SO_3)]_2(H_2O)$**: Donor-acceptor distances [pm] and angles [°]

Donor–Acceptor	Length	Angle (N-H...O)
N4–O1	328.3(6)	142(3)
N4–O21	306.6(4)	124(4)
N3–O21	301.6(5)	169(5)
N3–O1	315.7(5)	126(9)
N1–O11	288.9(5)	162(4)
N1–N2	315.0(6)	135(5)
N2–O12	299.1(6)	142(5)
N2–O1	277.2(5)	165(7)
O1–O12	287.0(5)	147(9)

3) NH_3SO_3

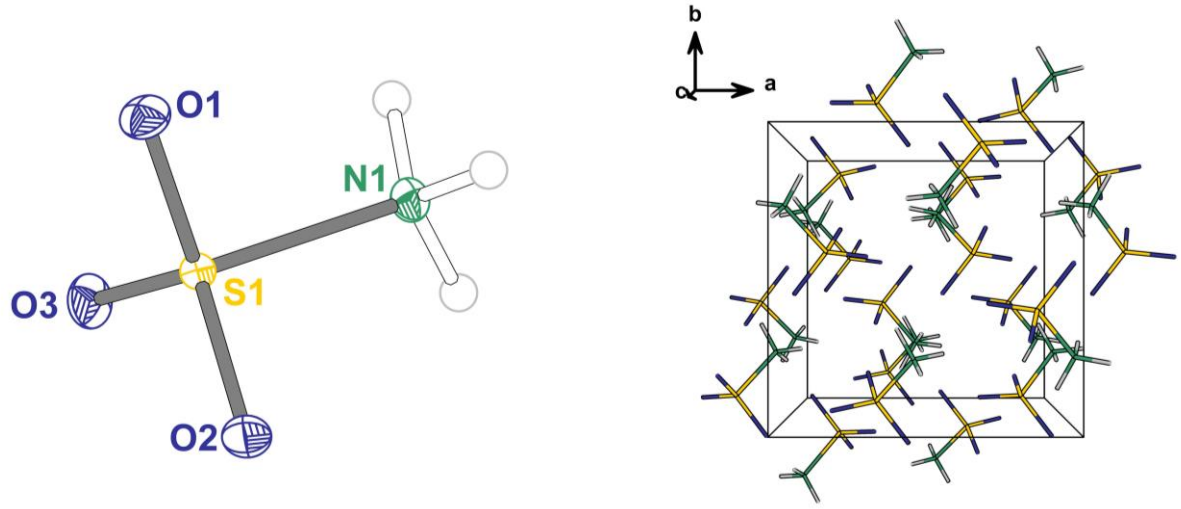

Figure S3: Structure and labelling (left) and crystal structure (right) of sulfamic acid, **NH_3SO_3**.

Table S4: Crystal data and structure refinement of sulfamic acid, **NH_3SO_3**

Empirical formula	H_3NO_3S
Formula weight	97.09 g · mol^{-1}
Temperature	100.0(2) K
Wavelength	71.073 pm (Mo-K_α)
Crystal system	orthorhombic
14Space group	*Pbca* (61)
Unit cell dimensions	*a* = 802.03(2) pm
	b = 800.48(2) pm
	c = 922.10(2) pm
Volume	0.59200(2) nm^3
Z	8
Density (calculated)	2.179 g · cm^{-3}
Absorption coefficient	0.880 mm^{-1}
F(000)	400
Crystal size	0.314 × 0.134 × 0.076 mm^3
2Theta range for data collection	8.44 to 66.97
Index ranges	$-12 \le h \le 12$, $-12 \le k \le 12$, $-14 \le l \le 14$
Reflections collected	14935
Independent reflections	1161 [R_{int}= 0.0425, R_σ= 0.0248]
Completeness to theta = 25.242°	100%
Absorption correction	multiscan
Max. and min. transmission	0.589 and 0.746
Refinement method	least-squares
Data / restraints / parameters	1161/0/47
Goodness-of-fit on F^2	1.098
Final R indices [$I \ge 2\sigma(I)$]	R_1 = 0.0225, wR_2 = 0.0603
R indices (all data)	R_1 = 0.0233, wR_2 = 0.0608
Largest diff. peak and hole	0.50/−0.53 e · $Å^{-3}$

Table S5: Atomic coordinates and equivalent isotropic displacement parameters (pm^2 x 10^4) for **NH_3SO_3**. *U(eq)* is defined as one third of the trace of the orthogonalized U_{ij} tensor

Atom	*x*	*y*	*z*	U_{eq}
S1	0.66685(3)	0.59280(3)	0.67059(2)	0.00484(7)
O3	0.55783(10)	0.44985(9)	0.67837(8)	0.00864(13)
O1	0.70181(9)	0.67484(9)	0.80585(7)	0.00815(13)
O2	0.80675(9)	0.57379(9)	0.57362(8)	0.00859(13)
N1	0.53999(10)	0.73953(10)	0.57905(8)	0.00643(14)
H1A	0.516489	0.701166	0.488432	0.008
H1B	0.594863	0.838743	0.572460	0.008
H1C	0.443349	0.754182	0.629166	0.008

Table S6: Anisotropic displacement parameters ($pm^2 \times 10^4$) for **NH_3SO_3**. The anisotropic displacement factor exponent takes the form: $-2\pi^2 [h^2 a^{*2} U_{11} + 2 h k a^* b^* U_{12} + \ldots]$.

Atom	U_{11}	U_{22}	U_{33}	U_{23}	U_{13}	U_{12}
S1	0.00512(11)	0.00466(11)	0.00473(11)	0.00014(6)	0.00015(6)	0.00022(6)
O3	0.0103(3)	0.0060(3)	0.0096(3)	0.0011(2)	−0.0001(2)	−0.0026(2)
O1	0.0091(3)	0.0098(3)	0.0056(3)	−0.0017(2)	−0.0015(2)	0.0006(2)
O2	0.0074(3)	0.0093(3)	0.0091(3)	0.0005(2)	0.0031(2)	0.0020(2)
N1	0.0065(3)	0.0062(3)	0.0066(3)	0.0007(2)	−0.0005(2)	0.0008(2)

Table S7: Experimental bond lengths [pm] for **NH_3SO_3**

Atom–Atom	Length [pm]
S1–O3	1.4419(8)
S1–O1	1.4372(7)
S1–O2	1.4428(8)
S1–N1	1.7684(8)

Table S8: Experimental bond angles [°] for **NH_3SO_3**

Atom–Atom–Atom	Angle [°]
O3–S1–O2	114.76(4)
O3–S1–N1	101.65(4)
O1–S1–O3	115.96(4)
O1–S1–O2	115.74(5)
O1–S1–N1	102.88(4)
O2–S1–N1	102.81(4)

C. Powder XRD

The powders were prepared in a 3.3 borosilicate glass capillary with an outer diameter of 0.3 mm and glass wall thickness of 0.01 mm. The experimental powder data was measured on a *STOE Stadi P* diffractometer (*STOE & Cie* GmbH, Darmstadt, DE) with Mo-$K_{\alpha1}$ radiation ($\lambda = 70.930$ pm) at room temperature. The reflections were collected on a silicon-based *Dectris Mythen 1K* detector (*Dectris Ltd.*, Baden-Daettwil, CH). The data was processed with *WinXPOW* (version 3.12). The Rietveld refinement was done with TOPAS 5.[5]

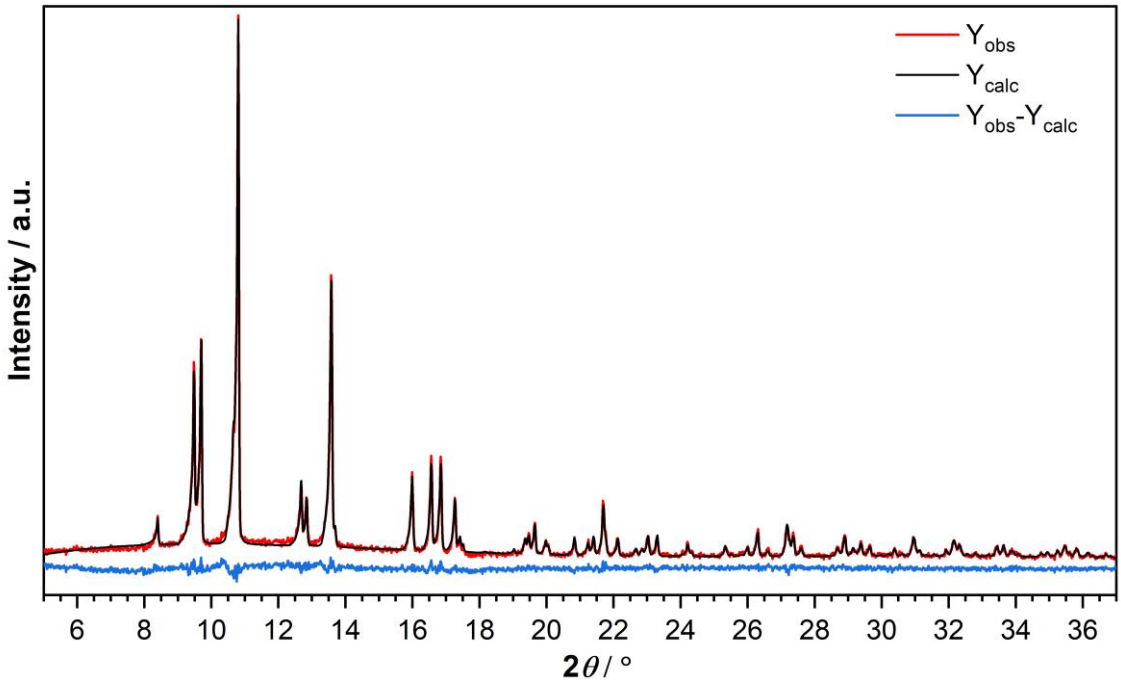

Figure S18: Rietveld refinement plot of **NH_3NHSO_3**. Following profile *R*-factors were received: R_{exp} = 8.48%, R_{wp} = 9.14%, R_p = 6.91%, GOF = 1.08.

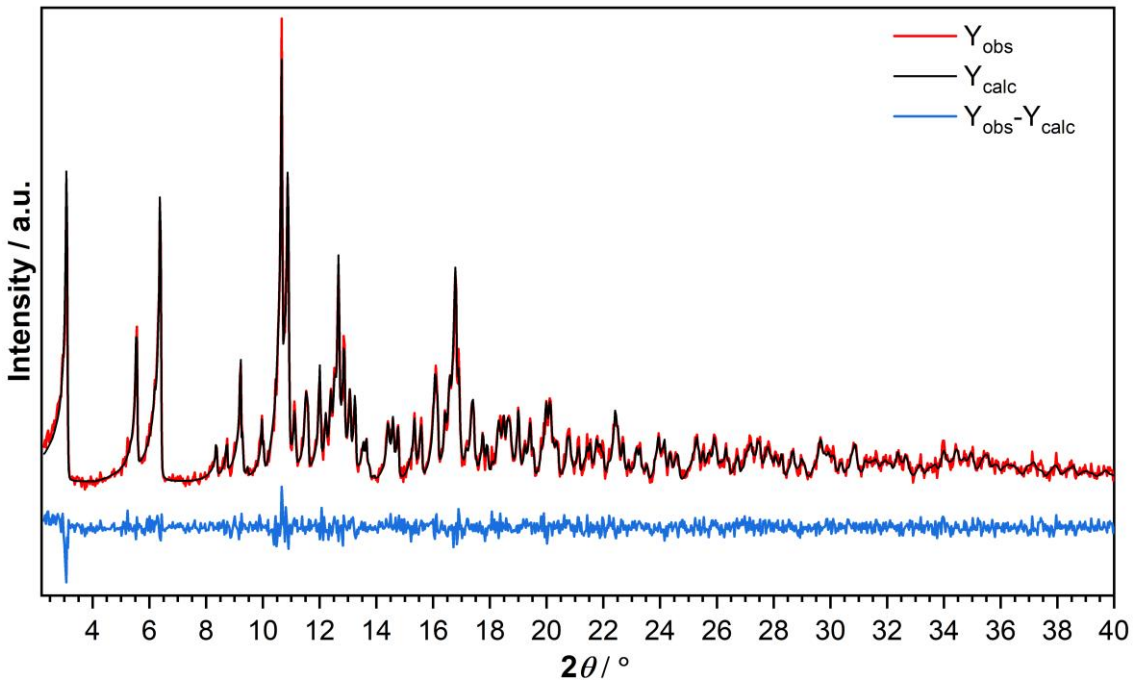

Figure S19: Rietveld refinement plot of **$Ba[NH_2NH(SO_3)]_2(H_2O)$**. Following profile *R*-factors were received: R_{exp} = 12.07%, R_{wp} = 12.48%, R_p = 9.29%, GOF = 1.03.

D. Thermal Analysis

The thermal analysis of NH_3NHSO_3 was performed on a thermal analyser *STA 409* (NETZSCH). The sample was prepared in an Al_2O_3 crucible under ambient conditions. The measurement was performed under an Argon flow (80 mL·min^{-1}) with a heating rate of 2K/min. For comparison, a measurement on $(NH_4)_2SO_4$ was carried out under the same conditions (green curve in Fig. S20).
For $Ba[NH_2NHSO_3]_2(H_2O)$, the thermal analysis was conducted using the same device which was additionally coupled with a quadrupole mass spectrometer (*QMS 421*, BALZERS). The heating rate was 5K/min and the mass analysis was carried out in a scanning mode with predefined m/z values. The solid residue was analyzed by means of powder X-ray diffraction.

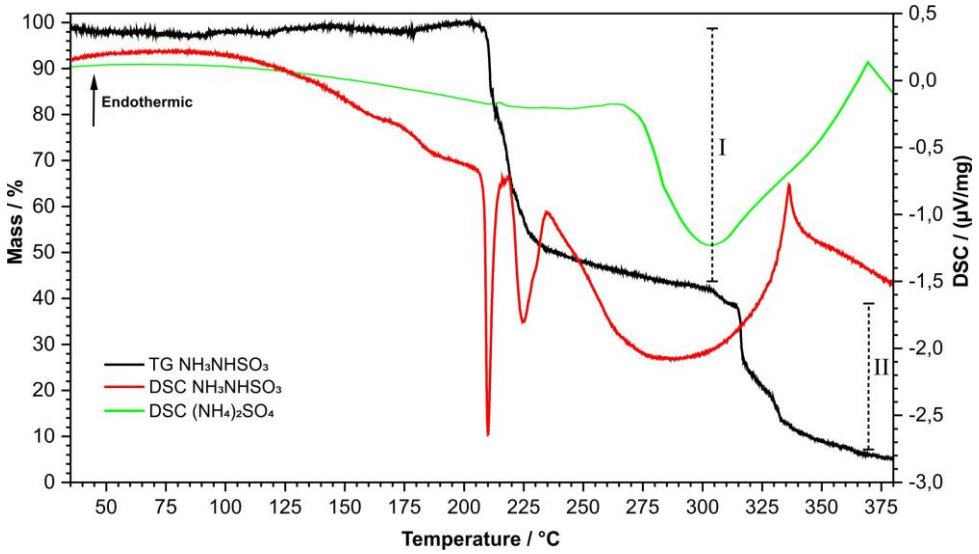

Figure S20: TG/DSC diagram of the thermal decomposition of **NH_3NHSO_3** (heating rate 2 K·min^{-1}). For comparison the DSC curve of the decomposition of $(NH_4)_2SO_4$ is shown (in green).

Table S20: Thermal decomposition data for **NH_3NHSO_3**.

Stage	T_{onset}/ °C	T_{end}/ °C	T_{max}/ °C	Mass loss (calcd.)/ %	Mass loss (obsd.)/ %	Reaction
I	209	241	210/ 224	56	58	$2\ NH_3NHSO_3 \rightarrow (NH_4)_2SO_4 + N_2 + SO_2$ $(NH_4)_2SO_4 \rightarrow H_2SO_4 + 2NH_3$
II	315	333	336	44	38	Endothermic decomposition of H_2SO_4
Total				100	96	

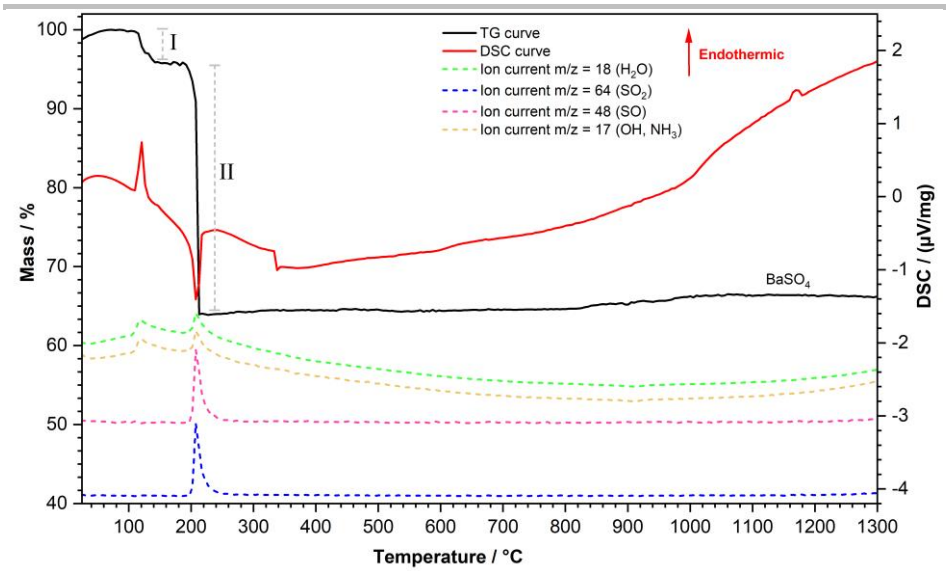

Figure S21: TG/DSC-MS diagram of the thermal decomposition of $Ba[NH_2NH(SO_3)]_2(H_2O)$ (heating rate: 5 $K \cdot min^{-1}$). The ion currents are shown an arbitrary units.

Table S21: Thermal decomposition data for **$Ba[NH_2NH(SO_3)]_2(H_2O)$**

Stage	T_{onset}/ °C	T_{end}/ °C	T_{max}/ °C	Mass loss (calcd.)/ %	Mass loss (obsd.)/ %	Reaction
I	119	186.8	119.8	5	4	$Ba[NH_2NH(SO_3)]_2(H_2O) \rightarrow Ba[NH_2NH(SO_3)]_2 + H_2O$
II	207	207.8	208.4	35	32	$Ba[NH_2NH(SO_3)]_2 \rightarrow BaSO_4 + SO_2 + N_2 + 2\ NH_3$
Total				40	36	

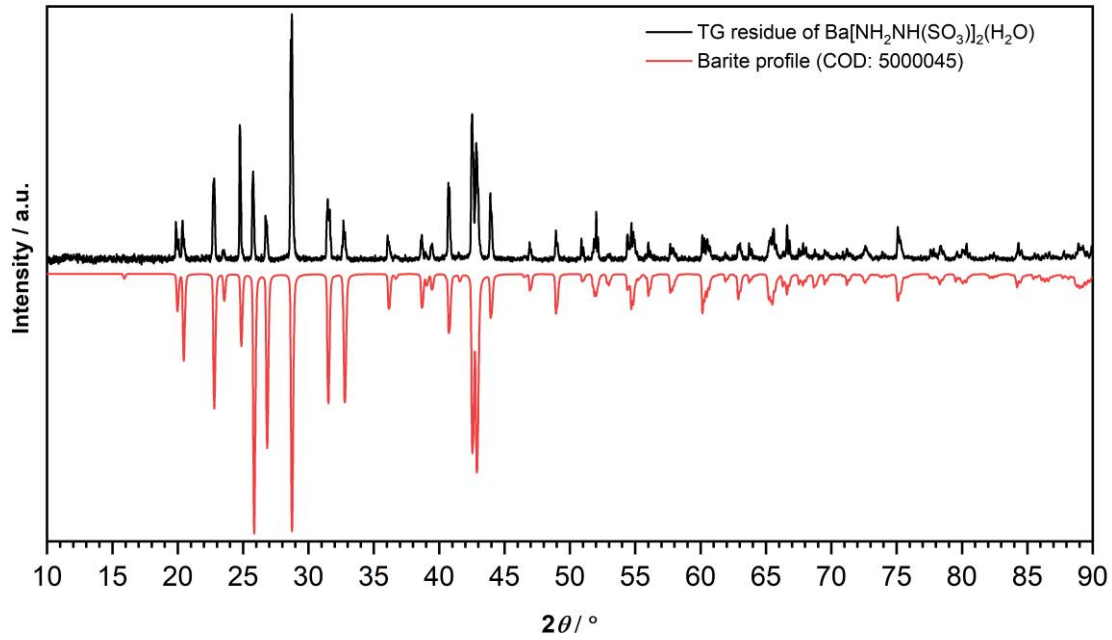

Figure S22: XRD pattern of the TG analysis residue of **$Ba[NH_2NH(SO_3)]_2(H_2O)$** compared to the simulated profile of barite ($BaSO_4$).

E. Vibrational spectroscopy

Raman spectroscopic data were collected with an *inVia Qotor confocal RAMAN microscope* by *Renishaw GmbH* (Pliezhausen, DE) equipped with 10x, 50x and 100x magnification lenses. The spectra were measured on selected single crystals with a green laser (532 nm, 100 mW) with an exposure time of 10000 ms. The data were processed and corrected by using the WiRE 5.1 software. The simulated spectra were simulated according to the geometry-optimized structures (s. chapter **F**)

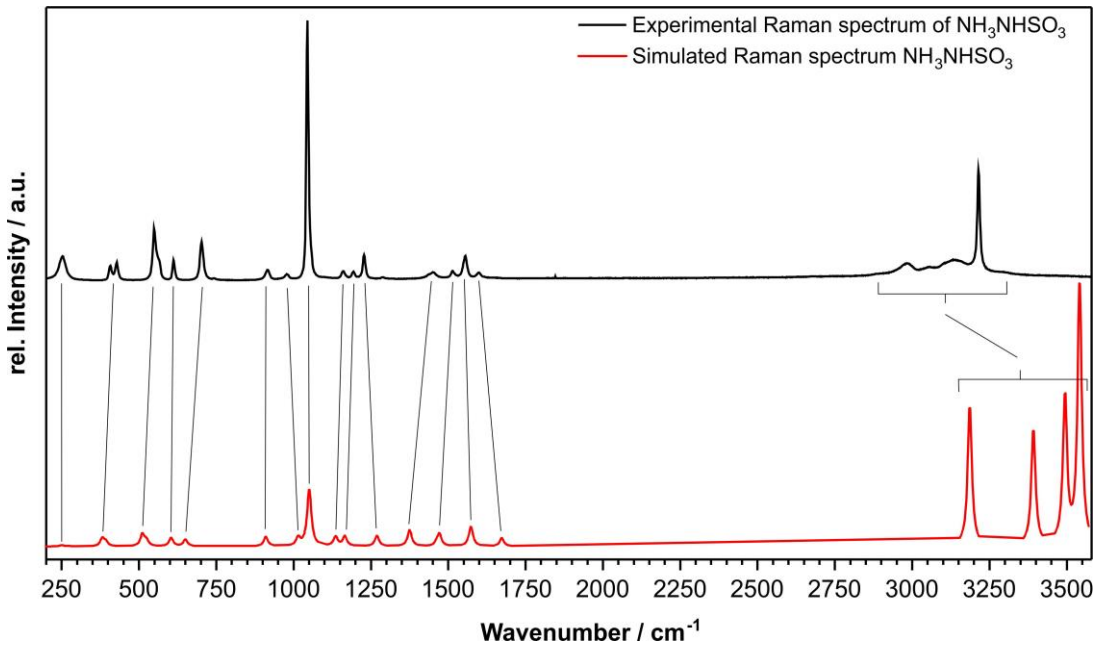

Figure S23: Experimental and simulated Raman spectrum of the zwitterionic NH_3NHSO_3.

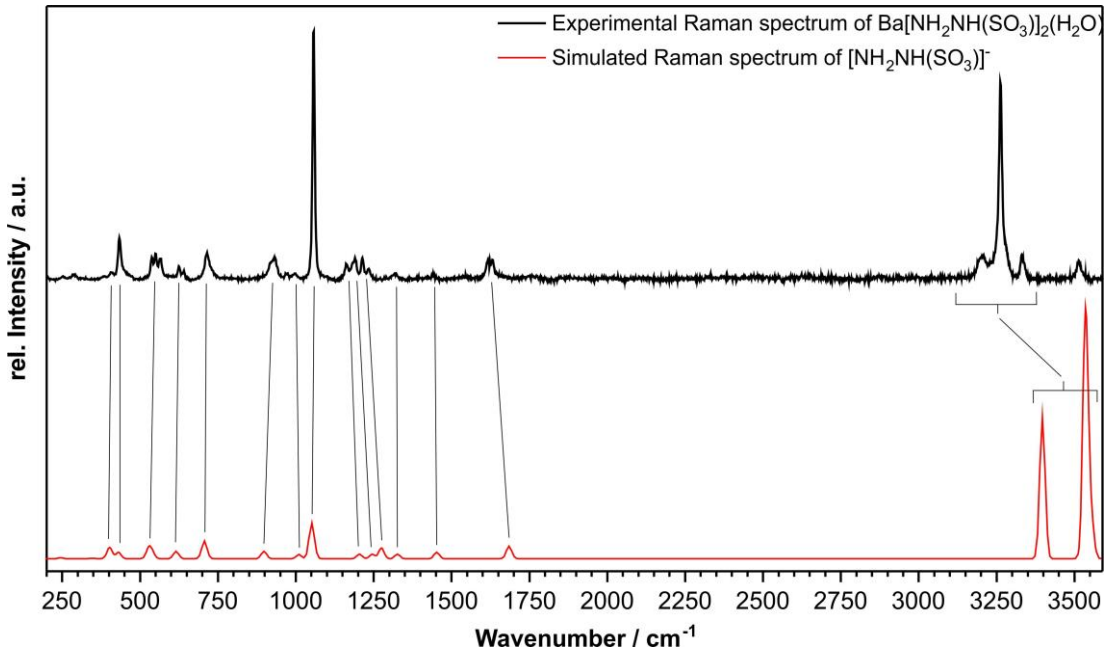

Figure S24: Experimental and simulated Raman spectrum of the $[NH_2NH(SO_3)]^-$ anion

Table S22 Experimental and calculated Raman energies (in cm^{-1}) for NH_3NHSO_3 and the $[NH_2NH(SO_3)]^-$ anion

NH_3NHSO_3	calcd.	$[NH_2NH(SO_3)]^-$	calcd.	assignment
250	249	316	245	$\delta_{rwag}(NH_3)/\delta_{wag}(NH_2)$
405	381	409	402	$\delta(SNHNH_3)$
428	392	433	430	$\tau(NHNH_3)$
548	523	548	539	$\delta_{sym}(SO_3)$
611	603	632	615	$\delta_{asym}(SO_3)$
704	649	714	706	ν(S-NHNH$_3$)
1044	1049	1056	1051	$\nu_{sym}(SO_3)$
1159	1135	1161	1203	$\delta(SNHNH_3)/\delta(SNHNH_2)$
1193	1165	1190	1245	$\delta(NH_3NHSO_3)/\delta(NH_2NHSO_3)$/
1227	1269	1212	1274	$\nu_{asym}(SO_3)$
1448	1374	1234	1326	$\nu_{sym}(SO_3)$
1512	1462	1315	1452	$\delta_{sym}(NHNH_3)$
1555	1573			$\delta_{asym}(NHNH_3)$
1600	1672	1624	1684	$\delta(NH_3)/\delta(NH_2)$
2978	3187	32090	3397	ν(N-H)

F. Results from quantum chemical calculations

Calculation method: A full geometry optimization for NH_3NHSO_3 and the respective ion in $NH_2NHSO_3^-$ from the barium structure, was performed within density functional theory (DFT) using the PBE0 exchange-correlation functional and a cc-pVTZ basis set for all elements. The calculations were also used for assigning the IR and Raman frequencies. Throughout the study the Orca 5.0.3 program package was used.[6]

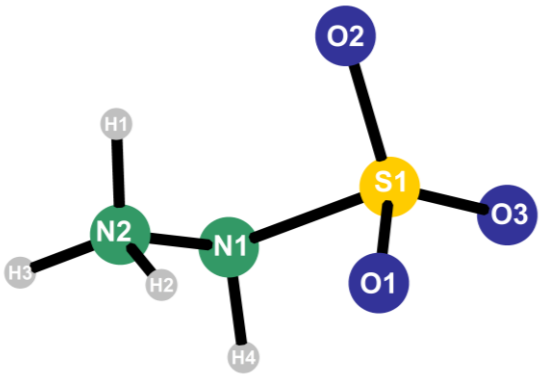

Figure S25 Structure and labelling of the zwitterionic **NH_3NHSO_3** of the geometry optimization.

Table S9: Atomic coordinates for the zwitterionic **NH_3NHSO_3** from the geometry optimization

Atom	x	y	z
S1	4.44367	1.595	3.99202
O1	5.11823	1.13855	5.21545
O2	3.97749	2.97054	4.06766
O3	4.92836	1.08273	2.74139
N1	2.85522	0.75144	4.19000
N2	2.52704	1.16938	5.52764
H1	2.40821	2.18692	5.45177
H2	3.36006	1.01694	6.13204
H3	1.67799	0.72852	5.87158
H4	3.083	−0.24003	4.25547

Table S10: Bond length (in pm) for the zwitterionic NH_3NHSO_3 from the geometry optimization.

Atom–Atom	Length
N2–H1	102.7
N2–H2	104.0
N2–H3	101.7
N1–H4	101.9
S1–N1	180.9
N1–N2	143.9
S1–O1	147.0
S1–O2	145.4
S1–O3	143.6

Table S11: Bond angles (in °) for the the zwitterionic NH_3NHSO_3 from the geometry optimization.

Atom–Atom-Atom	Angle
S1– N1– N2	99.58
O2– S1– N1	98.85
O1– S1– O2	113.43
O1– S1– O3	117.34
O2– S1– O3	119.40
O1– S1– N1	99.62
O3– S1– N1	103.02

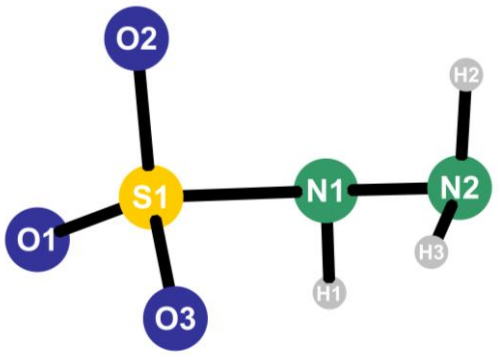

Figure S26 Structure and labelling of the $[NH_2NH(SO_3)]^-$ anion of the geometry optimization.

Table S12: Atomic coordinates for the $[NH_2NH(SO_3)]^-$ anion from the geometry optimization.

Atom	x	y	z
O1	5.51553	5.43756	3.4249
S1	6.24257	5.76654	4.64896
O2	7.60004	5.23426	4.75503
O3	6.13774	7.17771	5.06108
N1	5.36136	4.8817	5.84692
N2	5.69376	5.29501	7.16849
H1	4.38755	5.11135	5.68679
H2	6.57989	4.84404	7.36452
H3	5.90227	6.29528	7.12617

Table S13: Bond length (in pm) for the **$[NH_2NH(SO_3)]^-$** anion from the geometry optimization

Atom–Atom	Length
N1–H1	101.3
N2–H2	101.3
N2–H3	102.3
S1–N1	173.0
N1–N2	142.4
S1–O2	146.2
S1–O3	147.4
S1–O1	146.1

Table S14: Bond angles (in °) for the **$[NH_2NH(SO_3)]^-$** anion from the geometry optimization

Atom–Atom-Atom	Angle
S1– N1– N2	112.04
O3– S1– N1	105.06
O2– S1– O3	113.23
O2– S1– N1	103.68
O1– S1– O2	116.16
O1– S1– O3	114.48
O1– S1– N1	102.21

G. Hirshfeld Surface Analysis

The Hirshfeld surface analysis for the hydrazine sulfonic acid, **NH_3NHSO_3**, was conducted with the program-package *CrystalExplorer 21.5*.[8-9] All covalent hydrogen bond lengths were set to normalized values (1.009 Å for N-H) by the program prior to the calculation. The electron densities for each atom type were taken from the basis sets calculated by Koga et al.[10] and the surfaces were generated on the very high setting for the number of used grid points.

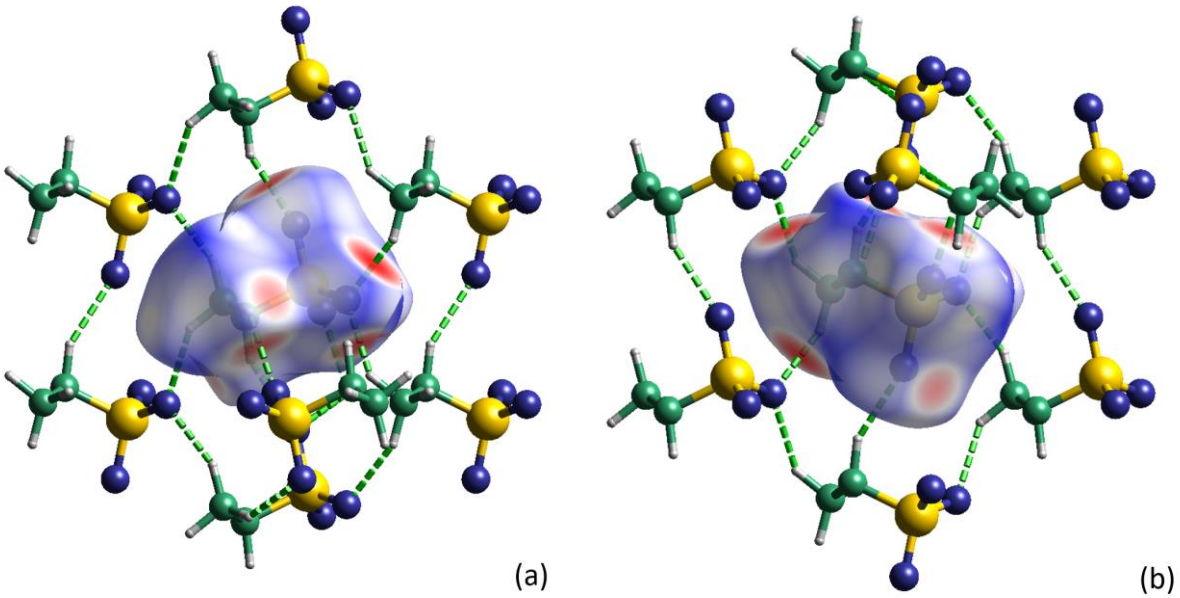

Figure S13: Hirshfeld isosurface around **$[NH_3NH(SO_3)]$** with the d_{norm}-mapping in its crystal structure viewed along with **(a)** and against **(b)** the crystallographic c-axis, with eight contacting **$[NH_3NH(SO_3)]$** units forming hydrogen bonds (green) to the central unit.

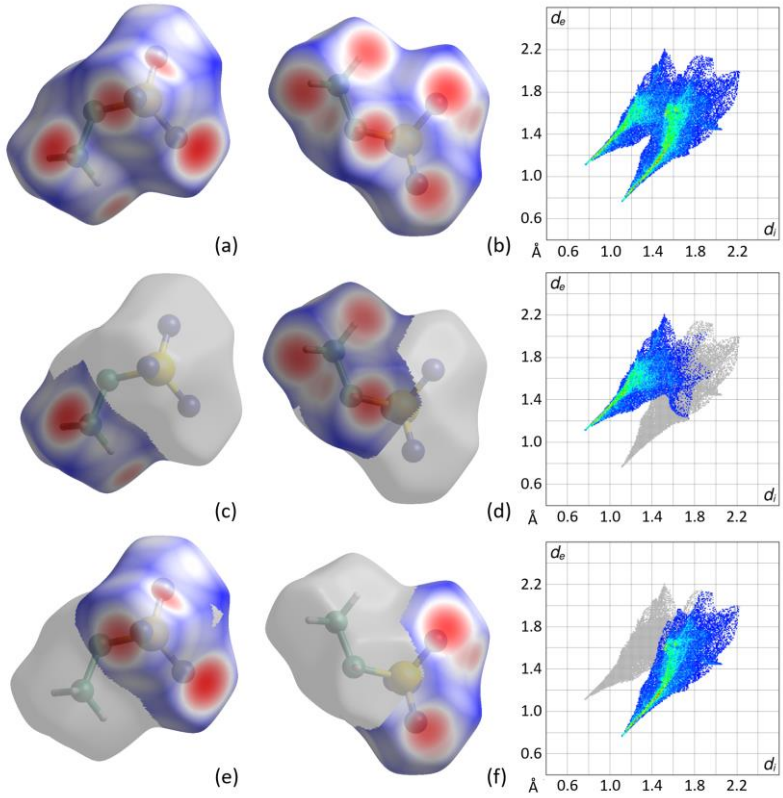

Figure S14: Hirshfeld isosurfaces around **[$NH_3NH(SO_3)$]** with the d_{norm}-mapping in its crystal structure viewed along with **(a, c, e)** and against **(b, d, f)** the crystallographic b-axis, delineated into showing the contacts of all **(a, b**) interior H- **(c, d**) (42.0% of the surface area) and O-atoms **(e, f**) (53.3% of the surface area) to the exteriorwith their respective fingerprint plots.

Table S26: Contributions (in percent %) to the calculated Hirshfeld isosurface by interior and exterior atom types.

		exterior atom				
		S	O	N	H	sum
interior atom	H	.	35.5	3.1	3.4	42.0
	N	.	0.6	.	4.0	4.6
	O	.	6.2	0.6	46.5	53.3
	S	.	.	0.1	0.1	0.2
	sum	0.0	42.2	3.8	54.0	

References

[1] Bruker (**2021**). *Apex4*. Bruker AXS Inc., Madison, Wisconsin, USA.
[2] Bruker, *SAINT V8.40B*, BrukerAXS Inc., Madison, Wisconsin, USA.,
[3] L. Krause, R. Herbst-Irmer, G. M. Sheldrick, D. Stalke, *J. Appl. Crystallogr.* **2015**, *48*, 3–10.
[4] G. M. Sheldrick, *Acta Crystallogr. Sect. A* **2015**, *71*, 3–8.
[5] A. A. Coelho, *J. Appl. Cryst.* **2018**, *51*, 210–218.
[6] T. H. Dunning Jr., *J. Chem. Phys.* **1989**, *90*, 1007–1023.
[7] F. Neese, F. Wennmohs, U. Becker, C. Riplinger, *J. Chem. Phys.* **2020**, *152*, 224108.
[8] P. R. Spackman, M. J. Turner, J. J. McKinnon, S. K. Wolff, D. J. Grimwood, D. Jayatilaka, M. A. Spackman, *J. Appl. Crystallogr.* **2021**, *54*, 1006-1011.
[9] M. A. Spackman, D. Jayatilaka, *CrystEngComm* **2009**, *11*, 19–32.
[10] T. Koga, K. Kanayama, T. Watanabe, T. Imai and A. J. Thakkar, *Theor. Chem. Accounts Theory, Comput. Model. (Theoretica Chim. Acta)*, **2000**, *104*, 411–413.

Author Contributions

Tobias Rennebaum performed all of the experimental work in course of his PhD work. David van Gerven provided the data from quantum chemical calculations. Sean S. Sebastian conducted the Hirshfeld surface analysis. Mathias S. Wickleder is the supervisor and leader of the project.

8.3 SI: N_2H_4 Derived Sulfonic Acids: Hydrazine Disulfonate, $[(SO_3)HNNH(SO_3)]^{2-}$, and Hydrazine *Iso*-disulfonate, $[H_2NN(SO_3)_2]^{2-}$

Chemistry–A European Journal

Supporting Information

N_2H_4 Derived Sulfonic Acids: Hydrazine Disulfonate, $[(SO_3)HNNH(SO_3)]^{2-}$, and Hydrazine *Iso*-disulfonate, $[H_2NN(SO_3)_2]^{2-}$

Tobias Rennebaum, David van Gerven, Felix C. H. Herwede, and Mathias S. Wickleder*

Supporting Information

N_2H_4 derived Sulfonic Acids: Hydrazine Disulfonate, $[(SO_3)HNNH(SO_3)]^{2-}$, and Hydrazine *Iso*-disulfonate, $[H_2NN(SO_3)_2]^{2-}$

Tobias Rennebaum,[a] David van Gerven[a], Felix C. H. Herwede,[a] and Mathias S. Wickleder*[a]

Abstract: The reaction of hydrazinium sulfate and chlorosulfonic acid in pyridine leads to the pyridinium salt of the hydrazine disulfonate anion, $[(SO_3)HNNH(SO_3)]^{2-}$. The salt is the starting material for the preparation of further hydrazine disulfonates, for example of alkaline metals and barium. In all compounds, the $[(SO_3)HNNH(SO_3)]^{2-}$ anion adopts the *gauche* conformation. The conformer is chiral but all of the investigated compounds crystallize as racemates. The disulfonate anion can occur in another constitution with the two sulfonate groups attached to only one nitrogen atom. This so-called hydrazine *iso*-disulfonate, $[H_2NN(SO_3)_2]^{2-}$, has been prepared through a substitution reaction between potassium imidodisulfonate, $K[HN(SO_3)_2]$, and hydroxylamine-*O*-sulfonic acid, H_2NOSO_3H. The hydrazine *iso*-disulfonate anion has been crystallized as potassium and barium compound, respectively. The compounds were characterized by XRD, vibrational spectroscopy, DFT calculations and thermal analyses.

Table of Contents

A Syntheses[1]

Caution!:

Hydrazinium sulfate, $(N_2H_6)SO_4$, is carcinogenic and toxic in contact with skin and causes severe skin burns and eye damage. As a reducing agent, it can react violently with oxidizing agents.
Chlorosulfuric acid, $ClSO_3H$, is a very strong acid which reacts violently with water and causes severe skin burns and eye damage.

$(C_5H_6N)_2[(SO_3)HNNH(SO_3)]$

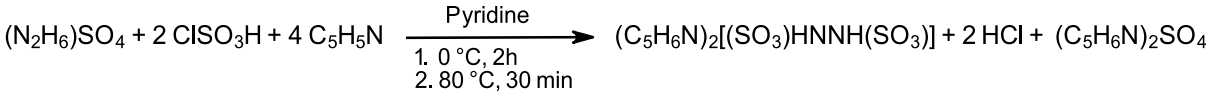

14.31 g (0.11 mol, 1.00 eq.) $(N_2H_6)SO_4$ was suspended in 67 mL dried pyridine. The suspension was cooled with an ice bath and 20.0 mL (0.30 mol, 2.72 eq.) $ClSO_3H$ was added dropwise within 2 h. The mixture was then heated to 80 °C until a yellow solution was formed. After cooling to rt, 120 mL of methanol was added to the mixture. During the storage in refrigerator at 4 °C a colourless precipitate was formed. The crude product was filtered and washed with methanol and diethyl ether and was finally dried under reduced pressure. The product was obtained as a colourless crystalline solid highly soluble in water in a yield of 59% (22.90 g, 0.065 mol).

Elemental Analysis (C/H/N/S; found/ *calcd.* in %): N 15.57/ *15.99*; C 32.75/ *34.28*; H 4.19/ *4.03*, S 15.92/ *18.30*.

$K_2[(SO_3)HNNH(SO_3)](H_2O)$

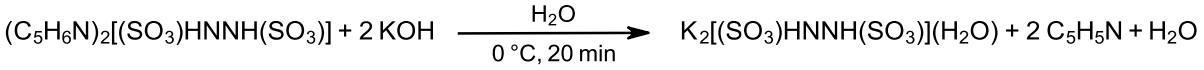

5.00 g (14.28 mmol, 1.00 eq.) $(C_5H_6N)_2[(SO_3)HNNH(SO_3)]$ was dissolved in 15 mL water and the solution was cooled with an ice bath. Then 15 mL of a KOH solution (15%, 40.10 mmol) was added and the mixture was stirred for 20 min. A colourless precipitate was formed which was filtered, washed with cold water and ethanol and was finally dried under reduced pressure. The product was isolated as a colourless crystalline solid in a yield of 31% (1.27 g, 4.45 mmol).

Elemental Analysis (C/H/N/S; found/ *calcd.* in %): N 9.53/ *9.78*; C 0.01/ *0.00*; H 1.31/ *1.41*; S 16.44/ *22.39*.

$Rb_2[(SO_3)HNNH(SO_3)](H_2O)$

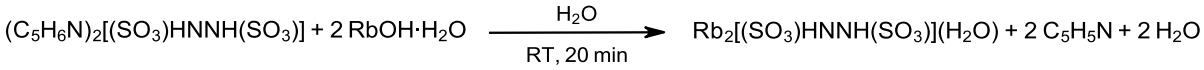

315 mg (0.90 mmol, 1.00 eq.) $(C_5H_6N)_2[(SO_3)HNNH(SO_3)]$ was dissolved in 5 mL water and 190 mg (1.85 mmol, 2.00 eq.) $RbOH{\cdot}H_2O$ were added to the solution. After a few minutes, a colourless precipitate was formed and the precipitation was completed overnight in the refrigerator at 4 °C. The solid was filtered and washed with small portions (5 ml) of cold water, ethanol and diethylether and was finally dried under reduced pressure. The product was obtained as colourless crystalline solid in a yield of 54% (187 mg, 0.49 mmol).

Elemental Analysis (C/H/N/S; found/ *calcd.* in %): N 6.90/ *7.39*; C 0.07/ *0.00*; H 1.05/ *1.06*, S 15.89/ *16.91*.

$Cs_2[(SO_3)HNNH(SO_3)](H_2O)$

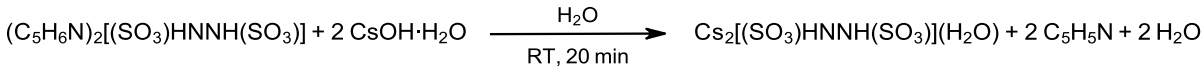

150 mg (0.42 mmol, 1.00 eq.) $(C_5H_6N)_2[(SO_3)HNNH(SO_3)]$ was dissolved in water and the solution was cooled with an ice bath. 127 mg (0.85 mmol, 2.00 eq.) $CsOH{\cdot}H_2O$ were added to the solution under constant stirring. Soon a colourless precipitate was formed and the precipitation was completed in the refrigerator overnight. The crystalline crude product was filtered and

washed with portions of cold water and ethanol and dried under reduced pressure. The product was isolated a colourless crystalline solid in a yield of 41 % (82 mg, 0.173 mmol).

$(NH_4)_2[(SO_3)HNNH(SO_3)](H_2O)$

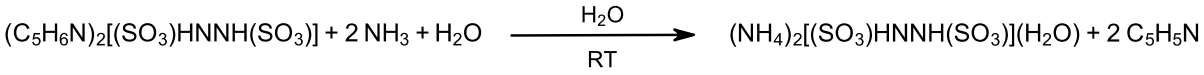

500 mg (1.43 mmol, 1.00 eq.) $(C_5H_6N)_2[(SO_3)HNNH(SO_3)]$ dissolved in 5.0 mL water was treated with an aqueous ammonia solution (25%) until the solution turned alkaline (pH ~ 10). To the clear solution 2.0 mL ethanol (absolute) was added and a colourless precipitate was formed. The suspension was gently heated (~50 °C) until a clear solution was formed again. The recrystallization was then forced in the refrigerator. The colourless crystalline solid was separated and washed with ethanol. The product was isolated in an total yield of 53% (185.3 mg, 0.76 mmol)

Elemental Analysis (C/H/N/S; found/ *calcd.* in %): N 22.88/ *22.94*; C 0.30/ *0.00*; H 4.89/ *4.95*, S 25.69/ *26.25*.

$Ba[(SO_3)HNNH(SO_3)](H_2O)_2$

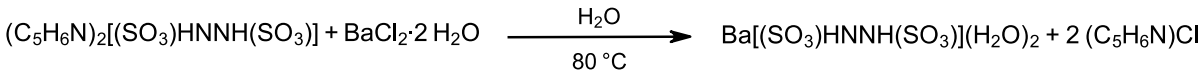

3.00 g (8.56 mmol, 1.00 eq.) $(C_5H_6N)_2[(SO_3)HNNH(SO_3)]$ was dissolved in 10 mL water. Separately 2.13 g (8.71 mmol, 1.02 eq.) $BaCl_2 \cdot 2\ H_2O$ was dissolved in 10 mL water and the solution was heated to 80 °C. The warm solution was poured into pyridinium salt solution and colourless precipitation was formed within 10 min of stirring. After complete precipitation in the refrigerator the solid was filtrated and washed with ethanol. The product was isolated as colourless crystalline solid in a yield of 96 % (3.00 g, 0.825 mmol).

Elemental Analysis (C/H/N/S; found/ *calcd.* in %): N 7.60/ *7.71*; C 0.04/ *0.00*; H 1.62/ *1.66*, S 17.27/ *17.64*.

$K_2[H_2NN(SO_3)_2]$

$K_2[H_2NN(SO_3)_2]$ was prepared in an two-step reaction. First the potassium imidodisulfonate, $K_2[HN(SO_3)_2]$ was synthesized which was further reacted with hydroxylamine-*O*-sulfonic acid, H_3NOSO_3.

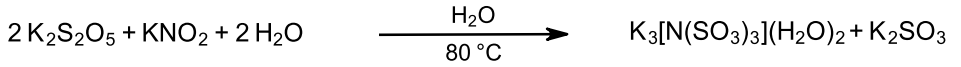

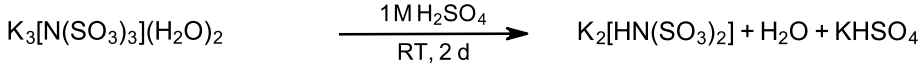

20.00 g (90.00 mol, 2.00 eq.) $K_2S_2O_5$ was dissolved in 40 mL under heating at 80 °C. Separately, 3.83 g (45.00 mol, 1.00 eq.) KNO_2 was dissolved in 10 mL water. Both solutions were combined under stirring and immediately a cloudy precipitate was formed. After filtration the residue was washed with cold ethanol and water and dried under reduced pressure. The crude product was mixed with 20 mL H_2SO_4 (1 mol/L) to form a suspension which was stored in the refrigerator for 2 days. The solid was filtrated and finally washed with water and ethanol. $K_2[HN(SO_3)_2]$ was isolated as colourless solid in a yield of 76% (8.650 g, 34.14 mmol).

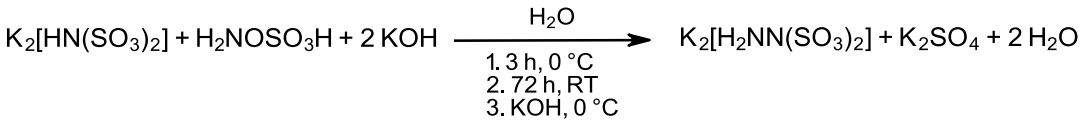

3.00 g (11.84 mmol, 1.00 eq.) $K_2[HN(SO_3)_2]$ and 1.40 g (24.95 mmol, 2.11 eq.) KOH were solved in 10 mL water and the solution was cooled in an ice bath. To this an ice-cold solution of 1.34 g (11.84 mmol, 1.00 eq.) H_2NOSO_3H in 5 mL water was added and the mixture stirred for 3 h at 0 °C and 70 h at RT. During this period a colourless precipitate was formed. 0.55 g (9.80 mmol, 0.85 eq.) KOH were added to the suspension and it was stirred for 30 min. The solid was filtrated and washed with cold water affording the product as a colourless crystalline solid in a yield of 55% (1.76 g, 6.55 mmol).

Elemental Analysis (C/H/N/S; found/ *calcd.* in %): N 10.29/ *10.44*; C 0.00/ *0.00*; H 0.66/ *0.75*, S 24.16/ *23.90*.

$Ba[H_2NN(SO_3)_2](H_2O)_2$

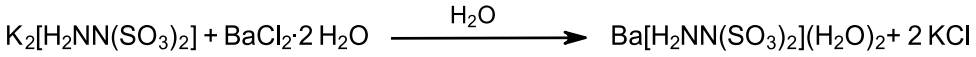

0.14 g (0.52 mmol, 1.00 eq.) $K_2[H_2NN(SO_3)_2]$ was dissolved in 10 mL water and the solution was warmed to 60 °C. 4.45 g (18.2 mmol, 3.30 eq.) $BaCl_2 \cdot 2\ H_2O$ dissolved in 10 mL water and also heated to 60 °C. Both solutions were combined and the resulting reaction mixture was immediately cooled to 0 °C. The formed precipitate was isolated via filtration and the obtained crude product was recrystallized from water at 65 °C. The compound was obtained as a colorless crystalline solid in a yield of 45% (0.85 g, 0.23 mmol).

B Structure determination and single crystal XRD data

Single crystal structure determination has been performed on a Bruker D8 VENTURE KAPPA diffractometer with a microfocus sealed tube using a multilayer mirror as monochromator and a Bruker PHOTON III detector. MoK$_\alpha$ radiation (71.073 pm) was used as X-ray source. The crystals were prepared in perfluorinated ether (Fomblin® YR-180) and selected with the aid of a light microscope with a polarization filter. The crystals were fixed on a micromount with a 150 µm polymer loop and adjusted to the X-ray beam under cooling at 100 K. The intensity data were collected and the images processed using APEX4. The integration was done with SAINT and a multi-scan absorption correction using SADABS was applied.[2-3] The structure solution was performed in the software Olex2 by intrinsic phasing (SHELXT) and the structural model was refined by least squares methods using SHELXL.[4-5]

$(C_5H_6N)_2[(SO_3)HNNH(SO_3)]$

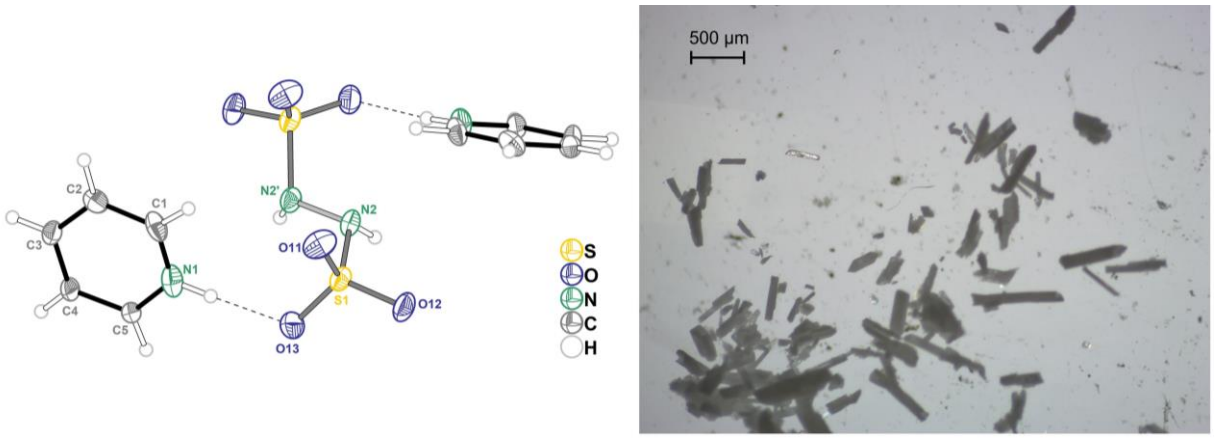

Figure S1: Structure and labelling of **$(C_5H_6N)_2[(SO_3)HNNH(SO_3)]$** (left) and light microscope image of the single crystals (right).

Table S1: Crystal data and structure refinement for **$(C_5H_6N)_2[(SO_3)HNNH(SO_3)]$**.

Empirical formula	$C_{10}H_{14}N_4O_6S_2$
Formula weight	350.37 g · mol^{-1}
Temperature	100.0(2) K
Wavelength	71.073 pm (Mo-K$_\alpha$)
Crystal system	orthorhombic
Space group	*Pccn* (56)
Unit cell dimensions	a = 1844.7(2) pm b = 871.01(8) pm c = 917.71(6) pm
Volume	1.4745(2) nm^3
Z	4
Density (calculated)	1.578 g · cm^{-3}
Absorption coefficient μ	0.396 mm^{-1}
F(000)	728
Crystal size	0.944 × 0.162 × 0.07 mm^3
2θ range for data collection	4.42 to 60.07
Index ranges	−25 ≤ h ≤ 25, −12≤ k ≤ 11, −12 ≤ l ≤ 12
Reflections collected	15497
Independent reflections	2159 [R_{int}= 0.0547, R_σ= 0.0344]
Completeness to theta = 25.242°	100%
Absorption correction	multiscan
Max. and min. transmission	0.973 and 0.926
Refinement method	least-squares
Data / restraints / parameters	2159/0/129
Goodness-of-fit on F^2	1.104
Final R indices [$I \geq 2\sigma(I)$]	R_1 = 0.0426, wR_2 = 0.0950
R indices (all data)	R_1 = 0.0492, wR_2 = 0.0986
Largest diff. peak and hole	0.44 /−0.35 e · Å^{-3}
CCDC number	2292310

Table S2: Atomic coordinates and equivalent isotropic displacement parameters [pm^2 x 10^4] for **$(C_5H_6N)_2[(SO_3)HNNH(SO_3)]$**. *U(eq)* is defined as one third of the trace of the orthogonalized U_{ij} tensor**.**

Atom	*x*	*y*	*z*	U_{eq}
S1	0.17159(2)	0.40305(5)	0.60770(4)	0.0146(1)
O11	0.20587(7)	0.5366(2)	0.5391(2)	0.0206(3)
O12	0.09726(7)	0.3822(2)	0.5621(2)	0.0215(3)
O13	0.18326(8)	0.4010(2)	0.7635(1)	0.0237(3)
N2	0.21165(7)	0.2440(2)	0.5435(2)	0.0157(3)
H2A	0.194(1)	0.221(3)	0.460(3)	0.028(6)
N1	0.34760(9)	0.5843(2)	0.5925(2)	0.0225(3)
H1	0.304(2)	0.568(3)	0.566(3)	0.037(7)
C1	0.3743(1)	0.5200(3)	0.7133(2)	0.0273(4)
H1A	0.341(2)	0.464(3)	0.768(3)	0.041(8)
C2	0.4462(1)	0.5402(2)	0.7488(2)	0.0261(4)
H2	0.467(2)	0.490(3)	0.835(3)	0.040(7)
C3	0.4897(1)	0.6280(2)	0.6578(2)	0.0222(4)
H3	0.536(2)	0.644(3)	0.681(3)	0.032(7)
C4	0.4602(1)	0.6933(2)	0.5336(2)	0.0218(4)
H4	0.489(1)	0.753(3)	0.471(3)	0.028(6)
C5	0.3881(1)	0.6694(2)	0.5029(2)	0.0215(4)
H5	0.365(1)	0.710(3)	0.424(3)	0.034(7)

Table S3: Anisotropic displacement parameters [$pm^2 \times 10^4$] for **$(C_5H_6N)_2[(SO_3)HNNH(SO_3)]$**. The anisotropic displacement factor exponent takes the form: $-2\pi^2$ [$h^2 a^{*2} U_{11}$ + 2 h k a* b* U_{12} +…].

Atom	U_{11}	U_{22}	U_{33}	U_{23}	U_{13}	U_{12}
S1	0.0106(2)	0.0199(2)	0.0132(2)	0.00183(2)	−0.00015(1)	−0.00049(4)
O11	0.0159(6)	0.0201(6)	0.0258(7)	0.0032(5)	0.0021(5)	−0.0022(5)
O12	0.0103(6)	0.0279(7)	0.0263(7)	0.0016(5)	−0.0019(5)	−0.0016(5)
O13	0.0259(7)	0.0324(8)	0.0129(6)	−0.0004(5)	−0.0007(5)	0.0065(6)
N2	0.0103(6)	0.0203(7)	0.0167(7)	−0.0018(6)	−0.0012(5)	−0.0016(5)
N1	0.0172(7)	0.0232(8)	0.0271(8)	−0.0025(6)	0.0018(6)	−0.0072(6)
C1	0.0345(11)	0.0283(10)	0.0191(9)	−0.0014(8)	0.0043(8)	−0.0146(9)
C2	0.0388(11)	0.0220(9)	0.0176(9)	−0.0002(7)	−0.0055(8)	−0.0049(8)
C3	0.0181(9)	0.0239(9)	0.0247(9)	−0.0038(7)	−0.0033(7)	−0.0009(7)
C4	0.0168(8)	0.0238(9)	0.0247(9)	0.0036(7)	0.0015(7)	−0.0050(7)
C5	0.0179(8)	0.0197(9)	0.0270(9)	0.0044(7)	−0.0023(7)	−0.0024(7)

Table S4: Experimental bond lengths [pm] for **$(C_5H_6N)_2[(SO_3)HNNH(SO_3)]$**.

Atom–Atom	Length
S1–O11	146.6(1)
S1–O12	144.5(1)
S1–O13	144.6(1)
S1–N2	167.7(2)
N2–N2^1	141.9(3)
N1–C1	133.6(3)
N1–C5	133.5(2)
C1–C2	137.7(3)
C2–C3	138.7(3)
C3–C4	138.5(3)
C4–C5	137.5(3)

Symmetry transformations used to generate equivalent atoms: 1: 0.5−*X*, 0.5−*Y*, +*Z*;

Table S5: Experimental bond angles [°] for **$(C_5H_6N)_2[(SO_3)HNNH(SO_3)]$**.

Atom–Atom–Atom	Angle [°]
O11–S1–N2	108.32(8)
O12–S1–O11	112.62(8)
O12–S1–O13	115.23(8)
O12–S1–N2	102.26(8)
O13–S1–O11	111.73(9)
O13–S1–N2	105.76(8)
$N2^1$–N2–S1	112.3(1)
C5–N1–C1	122.5(2)
N1–C1–C2	119.9(2)
C1–C2–C3	118.9(2)
C4–C3–C2	119.7(2)
C5–C4–C3	119.1(2)
N1–C5–C4	119.9(2)

Symmetry transformations used to generate equivalent atoms: 1: 0.5−*X*, 0.5−*Y*, +*Z*.

Table S6: Experimental torsion angles [°] for **$(C_5H_6N)_2[(SO_3)HNNH(SO_3)]$**.

Atom–Atom–Atom–Atom	Torsion Angle [°]
O11–S1–N2–$N2^1$	46.26(9)
O12–S1–N2–$N2^1$	165.37(8)
O13–S1–N2–$N2^1$	−73.7(1)
S1–N2–$N2^1$–$S1^1$	135.3(6)

Symmetry transformations used to generate equivalent atoms: 1: 0.5−*X*, 0.5−*Y*, +*Z*.

Table S7: Hydrogen bonds in **$(C_5H_6N)_2[(SO_3)HNNH(SO_3)]$**: Observed donor–acceptor distances (C/N–O) [pm] and angles (C–H/N–H…O) [°].

Donor–Acceptor	Length/	Angle (N-H...O)
N1–O13	269.2(1)	171(1)
N2–O11	291.1(1)	158(1)
C4–O12	314.2(2)	147(2)

$K_2[(SO_3)HNNH(SO_3)](H_2O)$

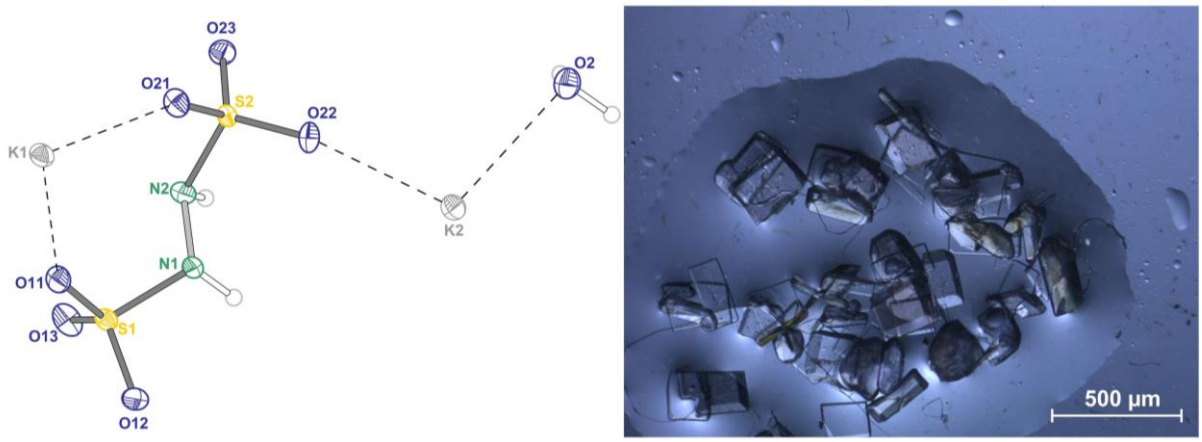

Figure S2: Structure and labelling of **$K_2[(SO_3)HNNH(SO_3)](H_2O)$** (left) and light microscope image of the single crystals (right)

Table S8: Crystal data and structure refinement for **$K_2[(SO_3)HNNH(SO_3)](H_2O)$**.

Empirical formula	$H_4K_2N_2O_7S_2$
Formula weight	286.37 g · mol^{-1}
Temperature	100.0(2) K
Wavelength	71.073 pm (Mo-K$_\alpha$)
Crystal system	orthorhombic
Space group	*Pna*2$_1$ (33)
Unit cell dimensions	*a* = 2060.81(6) pm *b* = 714.36(2) pm *c* = 570.43(1) pm
Volume	0.83976(4) nm^3
Z	4
Density (calculated)	2.265 g · cm^{-3}
Absorption coefficient μ	1.635 mm^{-1}
F(000)	576
Crystal size	0.31 × 0.152 × 0.101 mm^3
2θ range for data collection	3.95 to 56.52
Index ranges	−27 ≤ h ≤ 27, −9≤ k ≤ 9, −7 ≤ l ≤ 7
Reflections collected	13645
Independent reflections	2087 [R_{int}= 0.0351, R_σ= 0.0248]
Completeness to theta = 25.242°	100%
Absorption correction	multiscan
Max. and min. transmission	0.848 and 0.742
Refinement method	least-squares
Data / restraints / parameters	2087/1/135
Goodness-of-fit on F^2	1.162
Final R indices [$I \geq 2\sigma(I)$]	R_1 = 0.0176, wR_2 = 0.0440
R indices (all data)	R_1 = 0.0179, wR_2 = 0.0441
Largest diff. peak and hole	0.29 /−0.34 e · Å^{-3}
Flack X Parameter	0.04(2)
CCDC number	2292309

Table S9: Atomic coordinates and equivalent isotropic displacement parameters [pm^2 x 10^4] for **$K_2[(SO_3)HNNH(SO_3)](H_2O)$**. *U(eq)* is defined as one third of the trace of the orthogonalized U_{ij} tensor**.**

Atom	*x*	*y*	*z*	U_{eq}
K1	0.26554(2)	0.12040(7)	0.3307(1)	0.0115(1)
K2	0.40231(2)	0.99411(7)	0.8551(1)	0.0111(1)
S2	0.32940(2)	0.66645(7)	0.3369(1)	0.0075(1)
S1	0.45385(3)	0.25066(8)	0.3787(1)	0.0088(1)
O23	0.3203(1)	0.7875(3)	0.1354(4)	0.0118(4)
O12	0.49193(9)	0.1957(3)	0.5826(3)	0.0129(4)
O2	0.34029(9)	1.3452(3)	0.8622(4)	0.0149(4)
O21	0.28388(7)	0.5122(2)	0.3503(4)	0.0122(3)
O11	0.39611(7)	0.1387(2)	0.3438(4)	0.0127(3)
O22	0.33486(9)	0.7673(3)	0.5577(4)	0.0123(4)
O13	0.4923(1)	0.2671(3)	0.1665(4)	0.0151(4)
N1	0.4268(1)	0.4619(3)	0.4620(4)	0.0099(4)
N2	0.401(1)	0.5655(3)	0.2695(4)	0.0105(4)
H2A	0.358(2)	1.393(6)	0.754(7)	0.013(9)
H2B	0.364(3)	1.399(9)	0.98(1)	0.07(2)
H1	0.457(2)	0.527(5)	0.543(7)	0.022(1)
H2	0.430(2)	0.654(5)	0.230(7)	0.018(9)

Table S10: Anisotropic displacement parameters [$pm^2 \times 10^4$] for **$K_2[(SO_3)HNNH(SO_3)](H_2O)$**. The anisotropic displacement factor exponent takes the form: $-2\pi^2$ [$h^2 a^{*2} U_{11}$ + 2 h k a* b* U_{12} +…].

Atom	U_{11}	U_{22}	U_{33}	U_{23}	U_{13}	U_{12}
K1	0.0085(2)	0.0104(2)	0.0157(3)	−0.0015(2)	−0.0004(2)	0.0009(2)
K2	0.0119(2)	0.0099(2)	0.0115(2)	0.0009(2)	0.0010(2)	−0.0001(2)
S2	0.0078(2)	0.0066(2)	0.0082(3)	−0.0002(3)	0.0009(3)	−0.0001(2)
S1	0.0074(2)	0.0067(2)	0.0121(3)	0.0003(2)	0.0003(2)	−0.0001(2)
O23	0.0136(9)	0.0106(9)	0.0111(9)	0.0021(7)	−0.0008(7)	0.0002(7)
O12	0.0117(9)	0.0114(9)	0.016(1)	0.0000(7)	−0.0032(7)	0.0021(7)
O2	0.0170(8)	0.0157(8)	0.012(1)	−0.0014(9)	0.0009(9)	−0.0007(6)
O21	0.0107(7)	0.0084(7)	0.0174(8)	0.0001(8)	0.0015(9)	−0.0032(6)
O11	0.0100(7)	0.0094(7)	0.0187(9)	−0.0019(9)	−0.0011(9)	−0.0020(6)
O22	0.0156(9)	0.012(1)	0.0099(9)	−0.0033(8)	0.0016(7)	−0.0015(7)
O13	0.016(1)	0.0122(9)	0.017(1)	0.0018(8)	0.0069(7)	0.0006(8)
N1	0.011(1)	0.0074(9)	0.012(1)	−0.0011(8)	−0.0022(8)	0.0011(8)
N2	0.0091(9)	0.01(1)	0.013(1)	0.0010(8)	−0.0001(7)	0.0013(8)

Table S11: Experimental bond lengths [pm] for **$K_2[(SO_3)HNNH(SO_3)](H_2O)$**.

Atom–Atom	Length
K1–$O23^1$	285.8(2)
K1–$O23^3$	275.2(2)
K1–$O2^4$	294.2(2)
K1–$O21^2$	302.4(3)
K1–O21	282.7(2)
K1–$O21^3$	322.8(3)
K1–O11	269.5(2)
K1–$O22^1$	317.5(2)
K1–$O22^2$	279.4(2)
K2–$O23^8$	275.5(2)
K2–$O12^6$	287.6(2)
K2–$O12^5$	281.1(2)
K2–O2	281.5(2)
K2–$O11^5$	309.7(2)
K2–$O11^7$	297.5(2)
K2–O22	272.7(2)
K2–$O13^6$	305.8(2)
K2–$O13^7$	322.4(2)
S2–O23	145.0(2)
S2–O21	144.9(2)
S2–O22	145.6(2)
S1–O12	145.7(2)
S1–O11	144.8(2)

Atom–Atom	Length
S1–O13	145.2(2)
S2–N2	168.7(2)
S1–N1	167.8(2)
N1–N2	142.6(3)

Symmetry transformations used to generate equivalent atoms: 1: 0.5−*X*, −0.5+*Y*, −0.5+*Z*; 2: 0.5−*X*, −0.5+*Y*, 0.5+*Z*; 3: +*X*, −1+*Y*, +*Z*; 4: 0.5−*X*, −1.5+*Y*, −0.5+*Z*; 5: 1−*X*, 1−*Y*, 0.5+*Z*; 6: +*X*, 1+*Y*, 1+*Z*; 7: +*X*, 1+*Y*, +*Z*; 8: +*X*, +*Y*, 1+*Z*.

Table S12: Selected experimental bond angles [°] for **$K_2[(SO_3)HNNH(SO_3)](H_2O)$**.

Atom–Atom–Atom	Angle [°]
O11–S1–O12	113.8(1)
O11–S1–O13	112.3(1)
O11–S1–N1	105.2(1)
O12–S1–N1	101.3(1)
O13–S1–O12	113.2(1)
O13–S1–N1	110.2(1)
O21–S2–O22	112.4(1)
O21–S2–O23	114.3(1)
O21–S2–N2	104.7(1)
O22–S2–N2	110.0(1)
O23–S2–O22	113.6(1)
O23–S2–N2	100.8(1)
N2–N1–S1	111.9(2)
N1–N2–S2	111.8(2)

Table S13: Selected experimental torsion angles [°] for **$K_2[(SO_3)HNNH(SO_3)](H_2O)$**.

Atom–Atom–Atom–Atom	Torsion Angle [°]
S1–N1–N2–S2	134.3(1)
O11–S1–N1–N2	−75.6(2)
O12–S1–N1–N2	165.7(2)
O13–S1–N1–N2	45.6(2)
O21–S2–N2–N1	−71.3(2)
O22–S2–N2–N1	49.6(2)
O23–S2–N2–N1	169.8(2)
N2–S2–O23–K2[1]	−35.5(2)

Symmetry transformations used to generate equivalent atoms: 1: +*X*,+*Y*, −1+*Z*.

$Rb_2[(SO_3)HNNH(SO_3)](H_2O)$

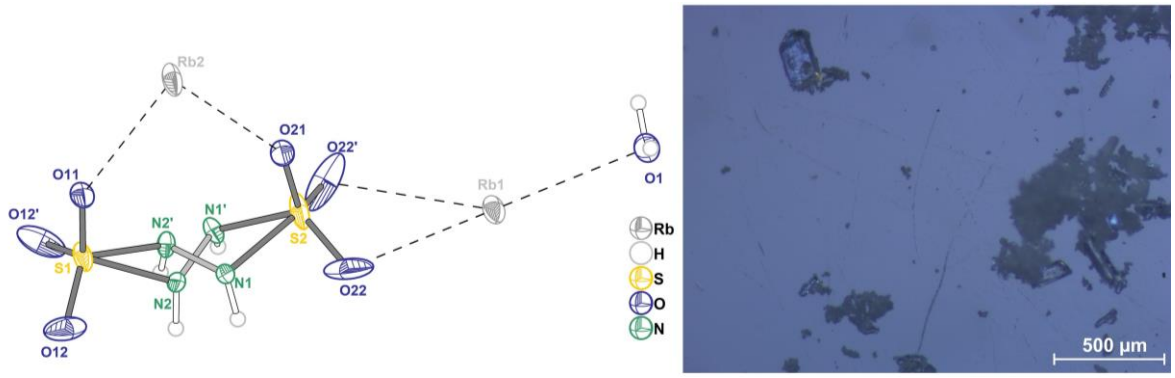

Figure S3: Structure and labelling of **$Rb_2[(SO_3)HNNH(SO_3)](H_2O)$** (left) and light microscope image of the single crystals (right).

Table S14: Crystal data and structure refinement for **$Rb_2[(SO_3)HNNH(SO_3)](H_2O)$**.

Empirical formula	$H_4N_2O_7Rb_2S_2$
Formula weight	379.11 g · mol^{-1}
Temperature	100.0(2) K
Wavelength	71.073 pm (Mo-K$_\alpha$)
Crystal system	orthorhombic
Space group	*Pnma* (33)
Unit cell dimensions	a = 2134.3(1) pm b = 580.23(3) pm c = 734.57(4) pm
Volume	0.90966(9) nm^3
Z	4
Density (calculated)	2.768 g · cm^{-3}
Absorption coefficient μ	11.228 mm^{-1}
F(000)	720
Crystal size	0.17 × 0.054 × 0.053 mm^3
2θ range for data collection	3.82 to 58.98
Index ranges	−29 ≤ h ≤ 29, −8≤ k ≤ 7, −10 ≤ l ≤ 10
Reflections collected	16989
Independent reflections	1367 [R_{int}= 0.0458, R_σ= 0.0234]
Completeness to theta = 25.242°	98.9%
Absorption correction	multiscan
Max. and min. transmission	0.552 and 0.488
Refinement method	least-squares
Data / restraints / parameters	2087/0/90
Goodness-of-fit on F^2	1.090
Final R indices [$I \geq 2\sigma(I)$]	R_1 = 0.0224, wR_2 = 0.0520
R indices (all data)	R_1 = 0.0250, wR_2 = 0.0533
Largest diff. peak and hole	0.63 /−1.01 e · Å^{-3}
CCDC number	2292312

Table S15: Atomic coordinates and equivalent isotropic displacement parameters [pm^2 x 10^4] for **$Rb_2[(SO_3)HNNH(SO_3)](H_2O)$**. *U(eq)* is defined as one third of the trace of the orthogonalized U_{ij} tensor**.**

Atom	*x*	*y*	*z*	U_{eq}
Rb1	0.40743(2)	0.250000	-0.00047(4)	0.0161(1)
Rb2	0.26716(2)	0.750000	0.87591(4)	0.0201(1)
H1	0.360(2)	0.358(6)	-0.405(5)	0.038(1)
S1	0.33187(4)	0.750000	0.3321(1)	0.0159(3)
S2	0.45428(4)	0.750000	0.7344(1)	0.0246(2)
O1	0.3425(1)	0.250000	-0.3550(3)	0.0160(5)
O11	0.2864(1)	0.750000	0.4787(3)	0.0139(4)
O12	0.3312(1)	0.5423(3)	0.2240(2)	0.0275(4)
O21	0.3996(1)	0.750000	0.8498(3)	0.0139(4)
O22	0.49133(9)	0.9574(4)	0.7508(3)	0.0389(6)

Atom	*x*	*y*	*z*	U_{eq}
N1	0.4266(2)	0.8536(7)	0.5278(5)	0.0103(7)
H1A	0.455(3)	0.92(1)	0.466(8)	0.012
N2	0.4002(2)	0.6605(6)	0.4359(5)	0.0094(6)
H2	0.425(3)	0.62(1)	0.343(8)	0.011

Table S16: Anisotropic displacement parameters [$pm^2 \times 10^4$] for **$Rb_2[(SO_3)HNNH(SO_3)](H_2O)$**. The anisotropic displacement factor exponent takes the form: $-2\pi^2$ [$h^2 a^{*2} U_{11}$ + 2 h k a* b* U_{12} +…].

Atom	U_{11}	U_{22}	U_{33}	U_{23}	U_{13}	U_{12}
Rb1	0.0108(1)	0.0288(1)	0.0086(1)	0.000	0.0004(1)	0.000
Rb2	0.0077(1)	0.0441(2)	0.0085(1)	0.000	−0.0005(1)	0.000
S1	0.0076(3)	0.0342(5)	0.0059(3)	0.000	0.0002(2)	0.000
S2	0.0061(3)	0.0618(7)	0.0059(3)	0.000	0.0003(3)	0.000
O1	0.017(1)	0.016(1)	0.015(1)	0.000	−0.003(9)	0.000
O11	0.010(1)	0.024(1)	0.008(0)	0.000	0.0028(8)	0.000
O12	0.043(1)	0.0234(9)	0.0159(8)	0.0052(7)	0.0137(8)	0.0165(9)
O21	0.009(1)	0.023(1)	0.010(1)	0.000	0.0023(8)	0.000
O22	0.0124(8)	0.044(1)	0.060(2)	0.040(1)	0.0096(9)	0.0032(8)
N1	0.011(2)	0.013(2)	0.007(2)	0.001(1)	−0.001(1)	−0.004(1)
N2	0.0071(1)	0.011(1)	0.010(2)	−0.003(1)	−0.002(1)	0.002(1)

Table S17: Experimental bond lengths [pm] for **$Rb_2[(SO_3)HNNH(SO_3)](H_2O)$**.

Atom–Atom	Length
Rb1–O1	295.0(2)
Rb1–O12	287.1(2)
Rb1–$O21^2$	310.70(8)
Rb1–$O22^4$	307.9(2)
Rb1–$O22^1$	307.9(2)
Rb1–$O22^5$	307.0(2)
Rb2–$O1^6$	306.4(2)
Rb2–O11	294.7(2)
Rb2–$O11^7$	320.9(1)
Rb2–$O12^8$	292.1(2)
Rb2–$O12^9$	314.1(2)
Rb2–O21	283.4(2)
S1–O11	144.9(2)
S1–O12	144.3(2)
S1–N2	172.5(4)
S2–O21	144.2(2)
S2–O22	144.5(2)
S2–N1	173.6(4)
N1–N2	142.4(5)

Symmetry transformations used to generate equivalent atoms: 1: 1−*X*, 1−*Y*, 1−*Z*; 2: +*X*, −1+*Y*, −1+*Z*; 3: +*X*, +*Y*, −1+*Z*; 4: 1−*X*, −0.5+*Y*, 1−*Z*; 5: +*X*, 0.5−*Y*, +*Z*; 6: 0.5−*X*, 1−*Y*, 1.5+*Z*; ; 7: +*X*, +*Y*, 1+*Z*; 8: 0.5−*X*, 1−*Y*, 0.5+*Z*; 9: 0.5−*X*, 2−*Y*, 0.5+*Z*.

Table S18: Selected experimental bond angles [°] for **$Rb_2[(SO_3)HNNH(SO_3)](H_2O)$**.

Atom–Atom–Atom	Angle [°]
O11–S1–$N2^1$	103.7(2)
O11–S1–N2	103.7(2)
O12–S1–$N2^1$	120.2(2)
$O12^1$–S1–N2	120.2(2)
O12–S1–N2	90.0(2)
$O12^1$–S1–$N2^1$	90.0(2)
O21–S2–$N1^1$	103.8(2)
O21–S2–N1	103.8(2)
O22–S2–$N1^1$	123.2(2)
$O22^1$–S2–N1	123.2(2)
$O22^2$–S2–$N1^1$	88.3(2)
N2'–N1–S2	106.1(3)
N1'–N2–S1	107.9(3)

Symmetry transformations used to generate equivalent atoms: 1: +*X*, 1/2−*Y*, +*Z*.

Table S19: Selected experimental torsion angles [°] for **$Rb_2[(SO_3)HNNH(SO_3)](H_2O)$**.

Atom–Atom–Atom–Atom	Torsion Angle [°]
S2–N1–N2–S1	139.3(2)
S2–N1–N2–N1^1	−18.1(4)
O11–S1–N2–N1	−80.0(3)
O11–S1–N2–N1^1	−31(1)
O12^1–S1–N2–N1	48.3(3)
O12–S1–N2–N1^1	−145(1)
O12–S1–N2–N1	165.5(3)
O12^1–S1–N2–N1^1	98(1)
O21–S2–N1–N2	−83.4(2)
O22–S2–N1–N2	163.2(3)
O22^1–S2–N1–N2	46.8(3)
N1^1–S2–N1–N2	11.8(3)

Symmetry transformations used to generate equivalent atoms: 1: +*X*, 1.5−*Y*, +*Z*.

$Cs_2[(SO_3)HNNH(SO_3)](H_2O)$

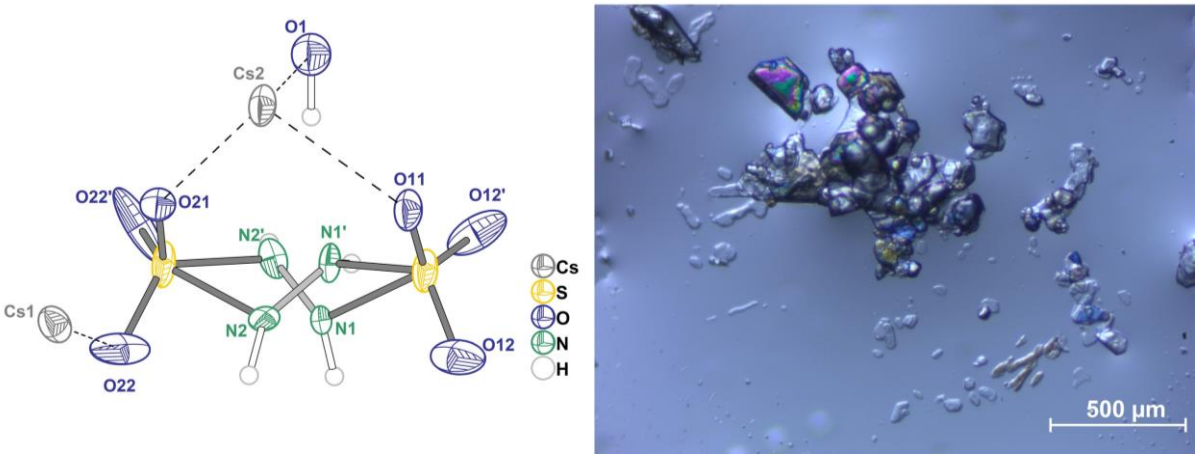

Figure S4: Structure and labelling of **$Cs_2[(SO_3)HNNH(SO_3)](H_2O)$** (left) and light microscope image of the single crystals (right).

Table S20: Crystal data and structure refinement for **$Cs_2[(SO_3)HNNH(SO_3)](H_2O)$**.

Empirical formula	$Cs_2H_4N_2O_7Rb_2S_2$
Formula weight	473.99 g · mol^{-1}
Temperature	100.0(2) K
Wavelength	71.073 pm (Mo-Kα)
Crystal system	orthorhombic
Space group	*Cmc*2$_1$ (33)
Unit cell dimensions	*a* = 590.97(3) pm *b* = 2225.2(1) pm *c* = 764.64(4) pm
Volume	1.00554(9) nm^3
Z	4
Density (calculated)	3.131 g · cm^{-3}
Absorption coefficient μ	7.675 mm^{-1}
F(000)	864
Crystal size	0.495 × 0.184 × 0.08 mm^3
2θ range for data collection	6.47 to 61.00
Index ranges	−8 ≤ h ≤ 8, −31≤ k ≤ 31, −10 ≤ l ≤ 10
Reflections collected	12376
Independent reflections	1587 [R_{int}= 0.0594, R_σ= 0.0381]
Completeness to theta = 25.242°	98.2%
Absorption correction	multiscan
Max. and min. transmission	0.541 and 0.200
Refinement method	least-squares
Data / restraints / parameters	1587/1/84
Goodness-of-fit on F^2	1.188
Final R indices [$I \geq 2\sigma(I)$]	R_1 = 0.0422, wR_2 = 0.0823
R indices (all data)	R_1 = 0.0422, wR_2 = 0.1149
Largest diff. peak and hole	1.71 /−1.23 e · Å^{-3}
Flack X paramter	−0.02(2)
CCDC number	2292313

Table S21: Atomic coordinates and equivalent isotropic displacement parameters [pm^2 x 10^4] for **$Cs_2[(SO_3)HNNH(SO_3)](H_2O)$**. *U(eq)* is defined as one third of the trace of the orthogonalized U_{ij} tensor**.**

Atom	*x*	*y*	*z*	U_{eq}
Cs2	0.000000	0.27046(4)	0.0681(1)	0.0196(3)
Cs1	0.500000	0.41785(4)	0.9320(1)	0.0192(3)
S1	0.000000	0.3337(2)	0.6081(5)	0.0194(9)
S2	0.000000	0.4556(2)	0.2263(5)	0.0214(9)
O11	0.000000	0.2896(5)	0.471(2)	0.020(3)
O1	0.500000	0.3451(7)	0.294(2)	0.025(3)
O21	0.000000	0.4067(5)	0.105(2)	0.017(2)
O22	0.203(2)	0.4919(4)	0.220(2)	0.046(4)
O12	0.205(2)	0.3339(5)	0.713(1)	0.034(2)
N2	0.099(3)	0.4253(7)	0.420(3)	0.014(3)
H2	0.217750	0.447551	0.444749	0.017
N1	0.094(3)	0.4000(8)	0.506(3)	0.014(3)
H1A	0.185283	0.416100	0.584064	0.017
H1	0.60(5)	0.37(2)	0.36(4)	0.09(12)

Table S22: Anisotropic displacement parameters [pm^2 × 10^4] for **$Cs_2[(SO_3)HNNH(SO_3)](H_2O)$**. The anisotropic displacement factor exponent takes the form: $-2\pi^2$ [h^2 a*^{2}U_{11} + 2 h k a* b* U_{12} +…].

Atom	U_{11}	U_{22}	U_{33}	U_{23}	U_{13}	U_{12}
Cs2	0.0347(6)	0.0118(4)	0.0122(4)	0.0014(3)	0.000	0.000
Cs1	0.0152(4)	0.0164(5)	0.0259(6)	0.0061(4)	0.000	0.000
S1	0.039(2)	0.009(2)	0.011(2)	0.001(1)	0.000	0.000
S2	0.048(3)	0.006(2)	0.011(2)	0.001(1)	0.000	0.000
O11	0.032(6)	0.013(5)	0.015(6)	0.003(4)	0.000	0.000
O1	0.026(6)	0.025(6)	0.025(7)	0.002(6)	0.000	0.000
O21	0.021(6)	0.013(5)	0.015(6)	−0.005(4)	0.000	0.000
O22	0.048(6)	0.008(4)	0.08(1)	0.009(5)	−0.046(7)	−0.006(4)
O12	0.028(4)	0.052(7)	0.022(5)	−0.018(5)	0.007(4)	−0.016(4)
N2	0.022(8)	0.006(7)	0.015(9)	−0.002(7)	−0.008(8)	−0.003(6)
N1	0.017(7)	0.013(8)	0.012(8)	0.006(7)	−0.003(7)	−0.005(7)

Table S23: Experimental bond lengths [pm] for **$Cs_2[(SO_3)HNNH(SO_3)](H_2O)$**.

Atom–Atom	Length
Cs2–O11^1	332.7(5)
Cs2–O11	310.7(1)
Cs2–O1^2	331.6(1)
Cs2–O21	305(1)
Cs2–O12^3	329(1)
Cs2–O12^4	311(1)
Cs1–O1^5	321(2)
Cs1–O21^5	324.8(5)
Cs1–O22^6	327(2)
Cs1–O22^7	312(1)
Cs1–O22^5	327(2)
Cs1–O12	306(1)
Cs1–O12^8	306(1)
S1–O11	144(1)
S1–O12	145(1)
S1–N1	177(2)
S2–O21	143(1)
S2–O22	145(1)
S2–N2	173(2)
N2–N1^9	143(3)

Symmetry transformations used to generate equivalent atoms: 1: −1/2−*X*, 1/2−*Y*, −1/2+*Z*; 2: 1/2−*X*, 1/2−*Y*, −1/2+*Z*; 3: +*X*, +*Y*, −1+Z; 4: −1/2+*X*, 1/2−*Y*, −1/2+*Z*; 5: +*X*, +*Y*, 1+*Z*; ; 6: 1−*X*, +*Y*, 1+*Z*; 7: +*X*, 1−*Y*, 1/2+Z; 8: 1−*X*, +*Y*, +*Z*; 9: −*X*, +*Y*, +*Z*.

Table S24: Selected experimental bond angles [°] for **$Cs_2[(SO_3)HNNH(SO_3)](H_2O)$**.

Atom–Atom–Atom	Angle [°]
O11–S1–O12	114.0(5)
O11–S1–N1	104.3(9)
O12–S1–O12^1	112.7(9)
O12^1–S1–N1	120.5(9)
O12–S1–N1	88.9(8)
O21–S2–O22	113.9(7)
O21–S2–N2	104.9(8)
O22–S2–O22^1	111.9(9)
O22–S2–N2	88.0(8)
O22–S2–N2^1	122(1)
O22^1–S2–N2^1	88.0(8)
N1^1–N2–S2	106(1)
N2^1–N1–S1	106(1)

Symmetry transformations used to generate equivalent atoms: 1: *X*, −*Y*+3/2, *Z*.

Table S25: Selected experimental torsion angles [°] for **$Cs_2[(SO_3)HNNH(SO_3)](H_2O)$**.

Atom–Atom–Atom–Atom	Torsion Angle [°]
O11–S1–N1–N2^1	81.6 (14)
O21–S2–N2–N1^1	−85.4 (12)
O22–S2–N2–N1^1	160.3 (13)
O22^1–S2–N2–N1^1	45.7 (15)
O12–S1–N1–N2^1	−163.9 (15)
O12^1–S1–N1–N2^1	−48.0 (17)
S1–N1–N2–S2	143.0(3)

Symmetry transformations used to generate equivalent atoms: 1: *X*, −*Y*+3/2, *Z*.

$(NH_4)_2[(SO_3)HNNH(SO_3)](H_2O)$

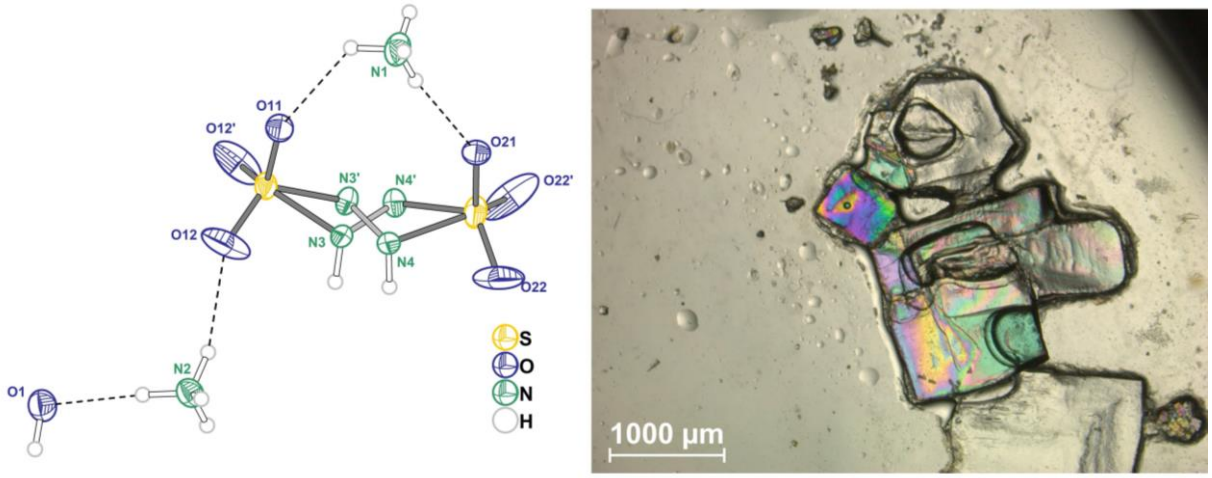

Figure S5: Structure and labelling of **$(NH_4)_2[(SO_3)HNNH(SO_3)](H_2O)$** (left) and light microscope image of the single crystals (right).

Table S26: Crystal data and structure refinement for **$(NH_4)_2[(SO_3)HNNH(SO_3)](H_2O)$**.

Empirical formula	$H_{12}N_4O_7S_2$
Formula weight	244.26 g · mol^{-1}
Temperature	101.0 K
Wavelength	71.073 pm (Mo-Kα)
Crystal system	orthorhombic
Space group	*Pnma* (62)
Unit cell dimensions	a = 2105.4(1) pm b = 579.26(2) pm c = 739.74(3) pm
Volume	0.90216(6) nm^3
Z	4
Density (calculated)	1.798 g · cm^{-3}
Absorption coefficient μ	0.611 mm^{-1}
F(000)	512
Crystal size	0.159 × 0.142 × 0.04 mm^3
2θ range for data collection	3.87 to 57.38
Index ranges	−28 ≤ h ≤ 28, −6≤ k ≤ 7, −9 ≤ l ≤ 9
Reflections collected	16849
Independent reflections	1275 [R_{int}= 0.0465, R_σ= 0.0199]
Completeness to theta = 25.242°	99.9%
Absorption correction	multiscan
Max. and min. transmission	0.976 and 0.907
Refinement method	least-squares
Data / restraints / parameters	1275/0/107
Goodness-of-fit on F^2	1.074
Final R indices [$I \geq 2\sigma(I)$]	R_1 = 0.0365, wR_2 = 0.0897
R indices (all data)	R_1 = 0.0394, wR_2 = 0.0924
Largest diff. peak and hole	0.53 /−0.59 e · Å^{-3}
CCDC number	2292311

Table S27: Atomic coordinates and equivalent isotropic displacement parameters [$pm^2 \cdot 10^4$] for **$(NH_4)_2[(SO_3)HNNH(SO_3)](H_2O)$**. *U(eq)* is defined as one third of the trace of the orthogonalized U_{ij} tensor**.**

Atom	*x*	*y*	*z*	U_{eq}
S1	0.33153(3)	0.250000	0.66416(8)	0.0157(2)
S2	0.45623(3)	0.250000	0.26259(8)	0.0223(2)
O21	0.40175(8)	0.250000	0.1444(2)	0.0160(4)
O11	0.28472(8)	0.250000	0.5214(2)	0.0184(4)
O1	0.34382(9)	0.750000	1.3540(3)	0.0216(4)
O12	0.33120(9)	0.4567(3)	0.7719(2)	0.0378(4)
N2	0.4029(1)	0.750000	1.0105(3)	0.0181(4)
N1	0.2687(1)	0.250000	0.1126(3)	0.0243(5)
O22	0.49356(7)	0.4574(3)	0.2493(3)	0.0461(5)
N4	0.4262(1)	0.3533(5)	0.4651(4)	0.0138(5)
N3	0.3994(1)	0.3400(5)	0.5586(4)	0.0136(5)
H3	0.426165	0.414269	0.628936	0.016
H2A	0.382(2)	0.750000	1.116(5)	0.032(9)
H2B	0.441(3)	0.750000	1.037(7)	0.07(3)
H2C	0.394(2)	0.869(6)	0.945(5)	0.07(1)
H1A	0.245(3)	0.250000	0.210(9)	0.09(2)
H1B	0.306(3)	0.250000	0.135(7)	0.06(1)
H1C	0.257(2)	0.150(9)	0.059(8)	0.13(2)
H4	0.459(2)	0.401(9)	0.528(6)	0.03(1)
H1	0.361(1)	0.865(5)	1.404(4)	0.044(8)

Table S28: Anisotropic displacement parameters [$pm^2 \times 10^4$] for **$(NH_4)_2[(SO_3)HNNH(SO_3)](H_2O)$**. The anisotropic displacement factor exponent takes the form: $-2\pi^2$ [$h^2 a^{*2} U_{11} + 2\ h\ k\ a^*\ b^*\ U_{12} + \ldots$].

Atom	U_{11}	U_{22}	U_{33}	U_{23}	U_{13}	U_{12}
S1	0.0118(3)	0.0256(3)	0.0098(3)	0.000	−0.0004(2)	0.000
S2	0.0101(3)	0.0458(4)	0.0108(3)	0.000	−0.0009(2)	0.000
O21	0.0135(8)	0.0192(8)	0.0153(8)	0.000	−0.0043(6)	0.000
O11	0.0146(8)	0.0267(9)	0.0139(8)	0.000	−0.0032(6)	0.000
O1	0.0238(9)	0.0222(9)	0.0189(9)	0.000	0.0023(7)	0.000
O12	0.070(1)	0.0227(7)	0.0208(7)	−0.0003(6)	−0.0170(7)	−0.0130(7)
N2	0.022(1)	0.018(1)	0.015(1)	0.000	−0.0001(8)	0.000
N1	0.013(1)	0.043(2)	0.017(1)	0.000	0.0002(8)	0.000
O22	0.0154(6)	0.040(1)	0.084(1)	−0.038(1)	−0.0102(7)	0.0008(6)
N4	0.014(1)	0.015(1)	0.013(1)	−0.002(1)	0.0010(11)	−0.004(1)
N3	0.012(1)	0.015(1)	0.015(1)	−0.003(1)	0.0024(11)	−0.002(1)

Table S29: Experimental bond lengths [pm] for **$(NH_4)_2[(SO_3)HNNH(SO_3)](H_2O)$**.

Atom–Atom	Length
S1–O11	144.5(2)
S1–O12	143.8(2)
S1–N3	170.9(3)
S2–O21	144.2(2)
S2–O22	143.9(2)
S2–N4	173.3(3)
N4–N3^1	143.2(4)

Symmetry transformations used to generate equivalent atoms: 1: *+X*, 1/2−*Y*, *+Z*.

Table S30: Selected experimental bond angles [°] for **$(NH_4)_2[(SO_3)HNNH(SO_3)](H_2O)$**.

Atom–Atom–Atom	Angle [°]
O11–S1–N3	103.6(1)
O12–S1–O11	113.69(8)
O12^1–S1–O12	112.7(1)
O12–S1–N3^1	120.7(1)
O12–S1–N3	90.2(1)
O21–S2–N4	103.5(1)
O22–S2–O21	113.12(8)
O22–S2–O22^1	113.2(1)
O22–S2–N4^1	123.2(1)
O22–S2–N4	88.30(12)

Atom–Atom–Atom	Angle [°]
N3[1]–N4–S2	106.9(2)
N4[1]–N3–S1	108.1(2)

Symmetry transformations used to generate equivalent atoms: 1: +*X*, 1/2−*Y*, +*Z*.

Table S31: Selected experimental torsion angles [°] for **$(NH_4)_2[(SO_3)HNNH(SO_3)](H_2O)$**.

Atom–Atom–Atom–Atom	Torsion Angle [°]
S1–N3–N4–S2	141.846
O21–S2–N4–N3[1]	84.52(18)
O11–S1–N3–N4[1]	−80.17(19)
O12–S1–N3–N4[1]	165.36(19)
O12[1]–S1–N3–N4[1]	48.5(2)
O22–S2–N4–N3[1]	−162.09(19)
O22[1]–S2–N4–N3[1]	−45.2(2)

Symmetry transformations used to generate equivalent atoms: 1: +*X*, 1/2−*Y*, +*Z*.

Table S32: Hydrogen bonds in **$(NH_4)_2[(SO_3)HNNH(SO_3)](H_2O)$**: Observed donor–acceptor distances (N–O/O–N) [pm] and angles (N–H…O) [°].

Donor–Acceptor	Length/	Angle (N-H...O)
N1–O21	281.1(3)	170(6)
N1–O11	304.3(3)	125(5)
N2–O1	282.9(3)	174(4)
N2–O12	287.8(3)	149(3)
O1–N4	299.4(3)	162(3)
O1–N3	304.9(3)	173(3)
N3–O22	291.2(3)	164(2)
N4-O22	291.9(4)	156(4)

$Ba[(SO_3)HNNH(SO_3)](H_2O)_2$

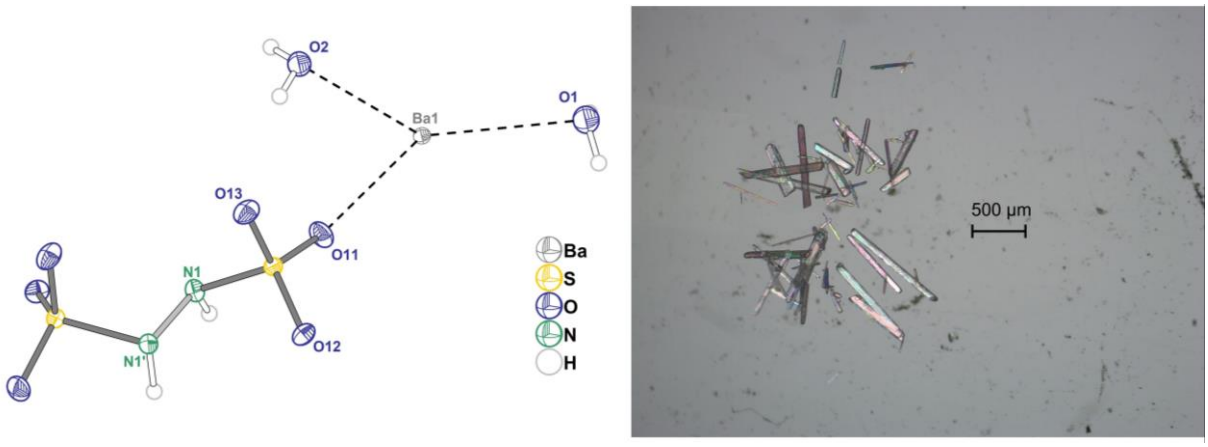

Figure S6: Structure and labelling of **$Ba[(SO_3)HNNH(SO_3)](H_2O)_2$** (left) and light microscope image of the single crystals (right).

Table S33: Crystal data and structure refinement for **$Ba[(SO_3)HNNH(SO_3)](H_2O)_2$**.

Empirical formula	$BaH_6N_2O_8S_2$
Formula weight	363.53 g · mol^{-1}
Temperature	101.0 K
Wavelength	71.073 pm (Mo-Kα)
Crystal system	orthorhombic
Space group	*Ama*2 (40)
Unit cell dimensions	a = 1130.63(5) pm b = 1570.83(8) pm c = 467.45(2) pm
Volume	0.83020(7) nm^3
Z	4
Density (calculated)	2.908 g · cm^{-3}
Absorption coefficient μ	5.308 mm^{-1}
F(000)	688
Crystal size	0.316 × 0.127 × 0.064 mm^3
2θ range for data collection	5.19 to 56.97
Index ranges	−15 ≤ h ≤ 15, −20≤ k ≤ 20, −6 ≤ l ≤ 6
Reflections collected	9015
Independent reflections	1097 [R_{int}= 0.0682, R_σ= 0.0440]
Completeness to theta = 25.242°	100%
Absorption correction	multiscan
Max. and min. transmission	0.712 and 0.450
Refinement method	least-squares
Data / restraints / parameters	1097/1/77
Goodness-of-fit on F^2	0.989
Final R indices [$I \geq 2\sigma(I)$]	R_1 = 0.0142, wR_2 = 0.0249
R indices (all data)	R_1 = 0.0143, wR_2 = 0.0249
Largest diff. peak and hole	0.43 /−0.48 e · Å^{-3}
Flack X parameter	0.03(1)
CCDC number	2292308

Table S34: Atomic coordinates and equivalent isotropic displacement parameters [$pm^2 \cdot 10^4$] for **Ba[(SO$_3$)HNNH(SO$_3$)](H$_2$O)$_2$**. *U(eq)* is defined as one third of the trace of the orthogonalized U_{ij} tensor**.**

Atom	*x*	*y*	*z*	U_{eq}
Ba1	0.750000	0.31268(2)	0.55872(7)	0.00578(8)
S1	0.49987(4)	0.12493(4)	0.4729(2)	0.0069(1)
O1	0.750000	0.494(2)	0.6733(7)	0.0146(5)
H1	0.808(5)	0.497(3)	0.77(2)	0.04(1)
O2	0.750000	0.2030(1)	0.059(2)	0.0118(4)
H2	0.807(4)	0.175(2)	0.070(2)	0.022(9)
O11	0.5907(2)	0.18192(8)	0.574(1)	0.0128(4)
O12	0.4970(2)	0.1130(1)	0.1650(4)	0.0124(3)
O13	0.3815(2)	0.14246(9)	0.5815(6)	0.0098(3)
N1	0.5469(2)	0.03089(1)	0.6038(4)	0.0084(5)
H1A	0.573(4)	0.038(2)	0.791(8)	0.017(9)

Table S35: Anisotropic displacement parameters [$pm^2 \times 10^4$] for **Ba[(SO$_3$)HNNH(SO$_3$)](H$_2$O)$_2$**. The anisotropic displacement factor exponent takes the form: $-2\pi^2$ [$h^2 a^{*2} U_{11}$ + 2 h k a* b* U_{12} +…].

Atom	U_{11}	U_{22}	U_{33}	U_{23}	U_{13}	U_{12}
Ba1	0.00572(9)	0.0062(1)	0.0055(1)	0.0000(1)	0.000	0.000
S1	0.0068(2)	0.0069(2)	0.0066(2)	0.0003(2)	0.0003(1)	0.0005(2)
O1	0.013(1)	0.0136(1)	0.0170(1)	0.0000(9)	0.000	0.000
O2	0.014(0)	0.0111(9)	0.0105(9)	0.000(3)	0.000	0.000
O11	0.0100(7)	0.0102(7)	0.0182(1)	0.0004(9)	−0.0008(1)	−0.0031(5)
O12	0.0163(9)	0.0141(8)	0.0068(7)	0.0014(7)	0.0011(6)	0.0047(6)
O13	0.0077(6)	0.0117(6)	0.0099(9)	−0.0013(8)	0.0007(8)	0.0024(5)
N1	0.0081(8)	0.0068(7)	0.010(2)	0.0003(7)	−0.0013(7)	−0.0005(6)

Table S36: Experimental bond lengths [pm] for **Ba[(SO$_3$)HNNH(SO$_3$)](H$_2$O)$_2$**.

Atom–Atom	Length
Ba1–O1	289.6(2)
Ba1–O2	290.3(8)
Ba1–O2^1	290.4(8)
Ba1–O11^2	273.3(2)
Ba1–O11	273.3(1)
Ba1–O12^3	306.7(2)
Ba1–O12^4	306.7(2)
Ba1–O13^5	277.2 (3)
Ba1–O13^3	294.6(3)
Ba1–O13^4	294.6(3)
Ba1–O13^6	277.2(3)
S1–O11	144.2(2)
S1–O12	145.2(2)
S1–O13	145.8(2)
S1–N1	168.5(2)
N1–N1^7	143.7(4)

Symmetry transformations used to generate equivalent atoms: 1: *X*, *Y*, *Z*+1; 2: −*X*+3/2, *Y*, *Z*; 3: *X*+1/2, −*Y*+1/2, *Z*+1/2; 4: −*X*+1, −*Y*+1/2, *Z*+1/2; 5: −*X*+1, −*Y*+1/2, *Z*−1/2; 6: *X*+1/2, −*Y*+1/2, *Z*−1/2; 7: −*X*+1, −*Y*, *Z*.

Table S37: Selected experimental bond angles [°] for **Ba[(SO$_3$)HNNH(SO$_3$)](H$_2$O)$_2$**.

Atom–Atom–Atom	Angle [°]
N1^1–N1–S1	111.0(2)
O11–S1–N1	101.6(1)
O11–S1–O12	114.8(2)
O11–S1–O13	115.1(2)
O12–S1–N1	104.7 (1)
O12–S1–O13	110.4(1)
O13–S1–N1	109.2(1)

Symmetry transformations used to generate equivalent atoms: 1: −*X*+1, −*Y*, +*Z*.

Table S38: Selected experimental torsion angles [°] for **Ba[(SO$_3$)HNNH(SO$_3$)](H$_2$O)$_2$**.

Atom–Atom–Atom–Atom	Torsion Angle [°]
S1–N1–N1^1–S1^1	134.21
O11–S1–N1–N1^1	162.7(2)
O12–S1–N1–N1^1	−77.5(1)
O13–S1–N1–N1^1	40.7(1)

Symmetry transformations used to generate equivalent atoms: 1: 1−*X*, −*Y*, +*Z*

$K_2[H_2NN(SO_3)_2]$

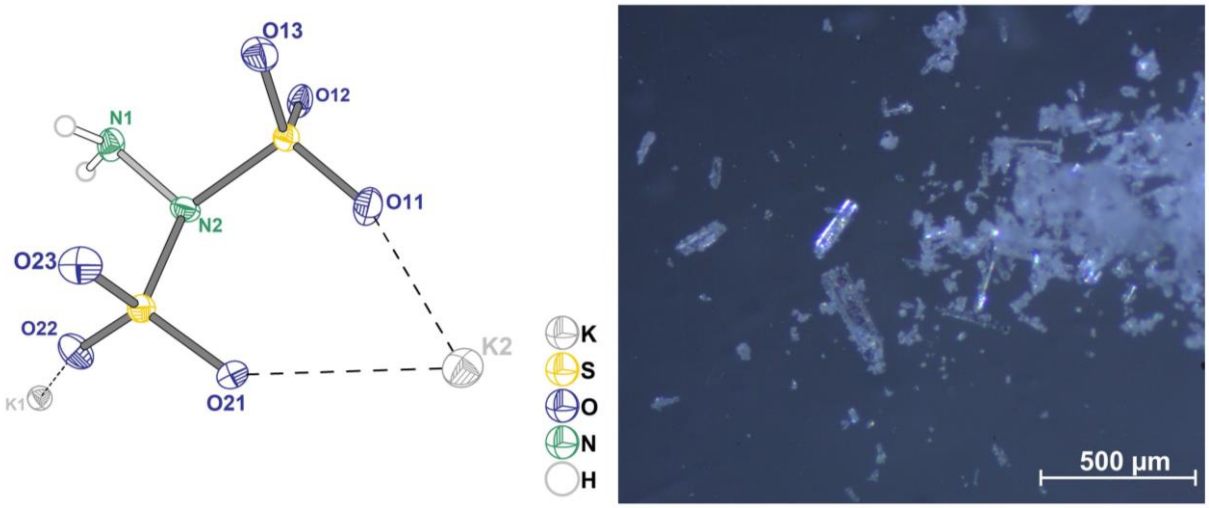

Figure S7: Structure and labelling of **$K_2[H_2NN(SO_3)_2]$** (left) and light microscope image of the single crystals (right).

Table S39: Crystal data and structure refinement for **$K_2[H_2NN(SO_3)_2]$**.

Empirical formula	$H_2K_2N_2O_6S_2$
Formula weight	268.36 g · mol^{-1}
Temperature	100.0 K
Wavelength	71.073 pm (Mo-K$_\alpha$)
Crystal system	orthorhombic
Space group	$P2_12_12_1$ (19)
Unit cell dimensions	a = 551.21(3) pm b = 950.14(4) pm c = 1419.29(7) pm
Volume	0.74332(6) nm^3
Z	4
Density (calculated)	2.398 g · cm^{-3}
Absorption coefficient μ	1.829 mm^{-1}
F(000)	536
Crystal size	0.338 × 0.079 × 0.054 mm^3
2θ range for data collection	5.16 to 62.98
Index ranges	−8 ≤ h ≤ 8, −12≤ k ≤ 13, −19 ≤ l ≤ 20
Reflections collected	13098
Independent reflections	2403 [R_{int}= 0.0484, R_σ= 0.0327]
Completeness to theta = 25.242°	99%
Absorption correction	multiscan
Max. and min. transmission	0.906 and 0.841
Refinement method	least-squares
Data / restraints / parameters	2403/0/118
Goodness-of-fit on F^2	1.097
Final R indices [$I \geq 2\sigma(I)$]	R_1 = 0.0238, wR_2 = 0.0558
R indices (all data)	R_1 = 0.0251, wR_2 = 0.0570
Largest diff. peak and hole	0.40 /−0.49 e · Å^{-3}
Flack X parameter	−0.05(3)
CCDC number	2292297

Table S40: Atomic coordinates and equivalent isotropic displacement parameters [pm^2 · 10^4] for **$K_2[H_2NN(SO_3)_2]$**. *U(eq)* is defined as one third of the trace of the orthogonalized U_{ij} tensor**.**

Atom	*x*	*y*	*z*	U_{eq}
K1	0.4959(1)	1.08976(4)	0.57969(3)	0.0099(1)
K2	-0.0042(1)	0.40119(4)	0.74632(3)	0.0117(1)
S2	0.5167(1)	0.69308(5)	0.68596(3)	0.0083(1)
S1	0.4984(1)	0.45563(4)	0.54693(3)	0.0086(1)
O11	0.2614(3)	0.4286(2)	0.5863(1)	0.0131(3)
O12	0.4997(3)	0.4605(2)	0.4448(1)	0.0124(3)

Atom	*x*	*y*	*z*	U_{eq}
O13	0.6889(3)	0.3666(2)	0.5853(1)	0.0128(3)
O21	0.2717(3)	0.6547(2)	0.7115(1)	0.0138(3)
O22	0.5513(3)	0.8426(2)	0.67107(1)	0.0131(3)
O23	0.7023(3)	0.6339(2)	0.7469(1)	0.0124(3)
N1	0.8101(4)	0.6502(2)	0.5440(1)	0.0112(4)
H1A	0.924(5)	0.634(3)	0.590(2)	0.007(6)
H1B	0.822(6)	0.732(4)	0.522(2)	0.028(9)
N2	0.5666(3)	0.6255(2)	0.5760(1)	0.0099(3)

Table S41: Anisotropic displacement parameters [$pm^2 \times 10^4$] for **$K_2[H_2NN(SO_3)_2]$**. The anisotropic displacement factor exponent takes the form: $-2\pi^2$ [$h^2 a^{*2} U_{11}$ + 2 h k a* b* U_{12} +…].

Atom	U_{11}	U_{22}	U_{33}	U_{23}	U_{13}	U_{12}
K1	0.0101(2)	0.0098(2)	0.0096(2)	−0.0002(1)	0.0011(2)	−0.0006(2)
K2	0.0099(2)	0.0113(2)	0.0140(2)	0.0026(1)	−0.0001(2)	0.0008(2)
S2	0.0085(2)	0.0075(2)	0.0089(2)	0.0002(1)	0.0004(2)	0.0003(2)
S1	0.0084(2)	0.0084(2)	0.0090(2)	−0.0004(1)	−0.0006(2)	−0.0010(2)
O11	0.0097(8)	0.0156(8)	0.0139(7)	−0.0008(6)	0.0016(6)	−0.0044(6)
O12	0.0110(7)	0.0171(7)	0.0090(6)	−0.0020(5)	0.0001(7)	−0.0008(7)
O13	0.0133(8)	0.0084(7)	0.0166(7)	0.0010(6)	−0.0035(6)	0.0014(6)
O21	0.0097(8)	0.0139(8)	0.0177(8)	−0.0048(6)	0.0035(6)	−0.0011(6)
O22	0.0177(9)	0.0082(6)	0.0133(7)	0.0003(5)	−0.0018(6)	−0.0005(5)
O23	0.0130(8)	0.0141(7)	0.0100(7)	0.0016(6)	−0.0006(6)	0.0034(6)
N1	0.0093(9)	0.0123(9)	0.0122(8)	0.0016(7)	0.0028(7)	−0.0030(7)
N2	0.0104(9)	0.0086(7)	0.0106(8)	−0.0009(6)	0.0015(6)	−0.0011(6)

Table S42: Experimental bond lengths [pm] for **$K_2[H_2NN(SO_3)_2]$**.

Atom–Atom	Length
K1–O11[1]	277.9(2)
K1–O12[2]	279.8(2)
K1–O12[1]	283.9(2)
K1–O13[2]	291.9(2)
K1–O13[3]	283.9(2)
K1–O21[4]	328.70(2)
K1–O22	270.04(2)
K1–O23[4]	272.5(2)
K2–O11	271.5(2)
K2–O12[5]	310.8(2)
K2–O13[6]	286.2(2)
K2–O21[7]	283.1(2)
K2–O21	289.2(2)
K2–O22[8]	281.3(2)
K2–O22[7]	328.4(2)
K2–O23[6]	274.0(2)
K2–O23[8]	303.8(2)
K1–N1[2]	305.4(2)
N1–N2	143.6(3)
S2–N2	171.1(2)
S2–O21	144.5(2)
S2–O22	144.9(2)
S2–O23	145.3(2)
S1–N2	170.7(2)
S1–O11	144.4(2)
S1–O12	145.1(2)
S1–O13	145.4(2)

Symmetry transformations used to generate equivalent atoms: 1: *X*+1/2, −*Y*+3/2, −*Z*+1; 2: *X*−1/2, −*Y*+3/2, −*Z*+1; 3: *X*, *Y*+1, *Z*; 4: −*X*+1, *Y*+1/2, −*Z*+3/2; 5: −*X*+1/2, −*Y*+1, *Z*+1/2; 6: *X*−1, *Y*, *Z*; 7: −*X*, *Y*−1/2, −*Z*+3/2; 8: −*X*+1, *Y*−1/2, −*Z*+3/2.

Table S43: Selected experimental bond angles [°] for **$K_2[H_2NN(SO_3)_2]$**.

Atom–Atom–Atom	Angle [°]
O21–S2–O22	114.0(1)
O21–S2–O23	114.3(1)
O21–S2–N2	106.5(1)
O22–S2–O23	112.0(1)
O22–S2–N2	102.35(9)
O23–S2–N2	106.55(9)
O11–S1–O12	113.4(1)
O11–S1–O13	113.9(1)
O11–S1–N2	105.9(9)
O12–S1–O13	112.9(1)
O12–S1–N2	102.1(9)
O13–S1–N2	107.5(1)
S1–N2–S2	122.7(1)
N1–N2–S2	112.2(1)
N1–N2–S1	106.5(1)

Table S44: Selected experimental torsion angles [°] for **$K_2[H_2NN(SO_3)_2]$**.

Atom–Atom–Atom–Atom	Torsion Angle [°]
O11–S1–N2–N1	175.4(1)
O12–S1–N2–N1	−65.7(2)
O13–S1–N2–N1	53.3(2)
O21–S2–N2–N1	−177.0(1)
O22–S2–N2–N1	63.0(2)
O23–S2–N2–N1	−54.6(2)

$Ba[H_2NN(SO_3)_2](H_2O)_2$

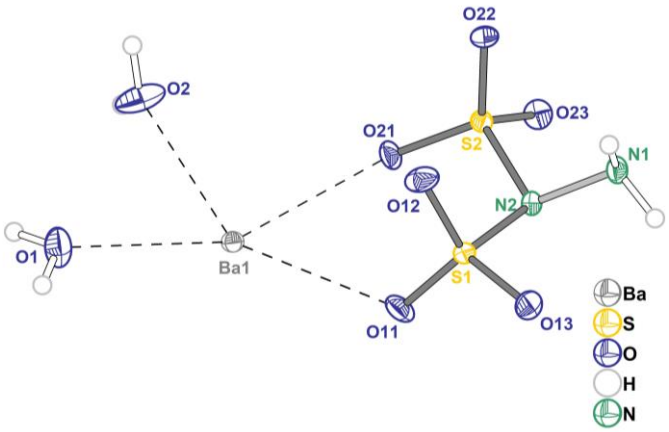

Figure S8: Structure and labelling of **$Ba[H_2NN(SO_3)_2](H_2O)_2$** (left).

Table S45: Crystal data and structure refinement for **$Ba[H_2NN(SO_3)_2](H_2O)_2$**.

Empirical formula	$BaH_6N_2O_8S_2$
Formula weight	363.53 g · mol^{-1}
Temperature	100.0 K
Wavelength	71.073 pm (Mo-K_α)
Crystal system	orthorhombic
Space group	*Pbca* (61)
Unit cell dimensions	a = 980.52(5) pm b = 1026.09(6) pm c = 1668.31(9) pm
Volume	1.6785(2) nm^3
Z	8
Density (calculated)	2.877 g · cm^{-3}
Absorption coefficient μ	5.251 mm^{-1}
$F(000)$	1376
Crystal size	0.283 × 0.281 × 0.158 mm^3
2θ range for data collection	4.88 to 70.00
Index ranges	$-13 \le h \le 15$, $-15 \le k \le 16$, $-26 \le l \le 25$
Reflections collected	22663
Independent reflections	3683 [R_{int}= 0.0403, R_σ= 0.0295]
Completeness to theta = 25.242°	100%
Absorption correction	multiscan
Max. and min. transmission	0.436 and 0.247
Refinement method	least-squares
Data / restraints / parameters	3683/0/143
Goodness-of-fit on F^2	1.135
Final R indices [$I \ge 2\sigma(I)$]	R_1 = 0.0246, wR_2 = 0.0547
R indices (all data)	R_1 = 0.0287, wR_2 = 0.0562
Largest diff. peak and hole	0.95 /−0.76 e · $Å^{-3}$
CCDC number	2292298

Table S46: Atomic coordinates and equivalent isotropic displacement parameters [$pm^2 \cdot 10^4$] for **Ba[$H_2NN(SO_3)_2$](H_2O)$_2$**. *U(eq)* is defined as one third of the trace of the orthogonalized U_{ij} tensor**.**

Atom	*x*	*y*	*z*	U_{eq}
Ba1	0.75388(2)	0.75246(2)	0.21505(2)	0.00707(4)
S1	0.76407(5)	0.53769(4)	0.39351(3)	0.00773(7)
S2	0.49655(5)	0.49159(4)	0.32497(2)	0.00662(7)
O1	0.9312(2)	0.8320(2)	0.1002(1)	0.0167(3)
H1A	0.902(4)	0.870(4)	0.058(3)	0.04(1)
H1B	0.998(5)	0.861(5)	0.111(3)	0.06(1)
O2	0.6469(2)	0.7097(2)	0.0704(1)	0.0198(3)
H2A	0.643(4)	0.649(4)	0.039(2)	0.027(9)
H2B	0.589(5)	0.767(4)	0.056(3)	0.05(1)
O11	0.7640(2)	0.6740(1)	0.37209(9)	0.0138(3)
O12	0.8142(2)	0.4534(2)	0.33000(9)	0.0147(3)
O13	0.8257(2)	0.5109(1)	0.47045(8)	0.0114(2)
O21	0.5398(2)	0.6011(1)	0.27649(8)	0.0106(2)
O22	0.5189(1)	0.3645(1)	0.28820(8)	0.0086(2)
O23	0.3573(1)	0.5041(1)	0.35414(9)	0.0104(2)
N1	0.5762(2)	0.3818(2)	0.45440(9)	0.0090(2)
H1C	0.588(3)	0.403(3)	0.5065(18)	0.015(7)
H1D	0.635(3)	0.324(3)	0.4405(19)	0.019(8)
N2	0.5959(2)	0.4982(1)	0.40823(9)	0.0078(2)

Table S47: Anisotropic displacement parameters [$pm^2 \times 10^4$] for **Ba[$H_2NN(SO_3)_2$](H_2O)$_2$**. The anisotropic displacement factor exponent takes the form: $-2\pi^2$ [$h^2 a^{*2} U_{11}$ + 2 h k a* b* U_{12} +…].

Atom	U_{11}	U_{22}	U_{33}	U_{23}	U_{13}	U_{12}
Ba1	0.00697(6)	0.00713(6)	0.00709(5)	−0.00091(3)	0.00019(3)	−0.00039(3)
S1	0.0094(2)	0.0075(2)	0.0063(1)	−0.0000(1)	−0.00051(13)	−0.0017(1)
S2	0.0073(2)	0.0055(1)	0.0070(1)	0.0002(1)	0.00015(13)	0.0004(1)
O1	0.0118(7)	0.0237(7)	0.0145(6)	0.0073(5)	−0.0011(5)	−0.0035(5)
O2	0.0214(8)	0.0201(7)	0.0179(7)	−0.0108(6)	−0.0087(6)	0.0100(6)
O11	0.0183(7)	0.0090(5)	0.0140(6)	0.0043(4)	−0.0061(5)	−0.0058(5)
O12	0.0110(6)	0.0199(6)	0.0132(6)	−0.0082(5)	0.0043(5)	−0.0043(5)
O13	0.0119(6)	0.0135(6)	0.0088(5)	0.0025(4)	−0.0039(4)	−0.0010(4)
O21	0.0129(6)	0.0091(5)	0.0097(5)	0.0045(4)	−0.0019(4)	−0.0028(4)
O22	0.0092(6)	0.0074(5)	0.0091(5)	−0.0025(4)	−0.0003(4)	0.0008(4)
O23	0.0081(6)	0.0109(6)	0.0122(6)	−0.0003(4)	0.0013(4)	0.0024(4)
N1	0.0115(7)	0.0076(5)	0.0079(5)	0.0019(4)	0.0015(5)	0.0002(5)
N2	0.0095(6)	0.0076(5)	0.0064(5)	0.0012(4)	0.0003(5)	−0.0010(4)

Table S48: Experimental bond lengths [pm] for **Ba[$H_2NN(SO_3)_2$](H_2O)$_2$**.

Atom–Atom	Length
Ba1–O1	271.4(2)
Ba1–O2	266.7(2)
Ba1–O11	274.3(2)
Ba1–O12^1	289.4(1)
Ba1–O21	280.6(1)
Ba1–O21^2	320.8(1)
Ba1–O22^3	291.1(1)
Ba1–O22^1	278.8(1)
Ba1–O23^3	303.1(1)
Ba1–O23^2	297.6(1)
S1–O11	144.3(1)
S1–O12	145.4(2)
S1–O13	144.5(2)
S1–N2	171.6(2)
S2–O21	144.8(1)
S2–O22	145.8(1)
S2–O23	145.5(2)
S2–N2	169.8(2)
N1–N2	143.5(2)

Symmetry transformations used to generate equivalent atoms: 1: 3/2−*X*, 1/2+*Y*, +*Z*; 2: 1/2+*X*, +*Y*, 1/2−Z; 3: 1−*X*, 1/2+*Y*, 1/2−*Z*.

Table S49: Selected experimental bond angles [°] for **Ba[$H_2NN(SO_3)_2$](H_2O)$_2$**.

Atom–Atom–Atom	Angle [°]
O11–S1–O12	113.36(9)
O11–S1–O13	113.87(8)
O11–S1–N2	105.27(8)
O12–S1–N2	106.79(8)
O13–S1–O12	113.11(9)
O13–S1–N2	103.30(8)
O21–S2–O22	114.54(8)
O21–S2–O23	113.15(8)
O21–S2–N2	104.96(8)
O22–S2–N2	107.10(7)
O23–S2–O22	111.12(8)
O23–S2–N2	105.13(8)
S2–N2–S1	116.34(9)
N1–N2–S1	113.8(1)
N1–N2–S2	109.2(1)

Table S50: Selected experimental torsion angles [°] for **Ba[$H_2NN(SO_3)_2$](H_2O)$_2$**.

Atom–Atom–Atom–Atom	Torsion Angle [°]
O11–S1–N2–S2	71.0(1)
O11–S1–N2–N1	−160.8(1)
O12–S1–N2–S2	−49.7(1)
O12–S1–N2–N1	78.5(1)
O13–S1–N2–S2	−169.3(9)
O13–S1–N2–N1	−41.0(1)
O21–S2–N2–S1	−40.5(1)
O21–S2–N2–N1	−170.9(1)
O22–S2–N2–S1	81.7(1)
O22–S2–N2–N1	−48.7(1)
O23–S2–N2–S1	−160.0(8)
O23–S2–N2–N1	69.6(1)

Coordination sphere of the cations of the alkali metal hydrazine disulfonates

Table S51: Listing of A–O distances, coordination numbers and ionic radii observed for the crystallographic unique cations of $A_2[(SO_3)HNNH(SO_3)](H_2O)$ (A = K, Rb, Cs) and $Ba[(SO_3)HNNH(SO_3)](H_2O)_2$. The coordination numbers were determined with *CHARDI2015*.[6]

Atom	A–O [pm]	Coordination Number	Ionic Radius[7] [pm]
K1	269.5(2)-347.8(1)	10	159
K2	272.7(2)-322.4(2)	9	155
Rb1	287.1(2)-310.70(8)	9	163
Rb2	283.4(2)-372.6(2)	11	169
Cs1	306(1)-327(2)	9	185
Cs2	305(1)-380.4(1)	11	178
Ba1	273.3(2)-306.7(2)	11	157

C Powder XRD

Mo-K$_{\alpha1}$ radiation (λ = 70.930 pm) measurements were prepared in 3.3 borosilicate glass capillaries with an outer diameter of 0.3 mm and glass wall thickness of 0.01 mm. The experimental powder data was measured on a *STOE Stadi P* diffractometer (*STOE & Cie* GmbH, Darmstadt, DE) at room temperature. The reflections were collected on a silicon-based *Dectris Mythen 1K* detector (*Dectris Ltd.*, Baden-Daettwil, CH). The data was processed with *WinX*POW (version 3.12). The Rietveld refinement was done with TOPAS 5.[8]

Cu-K$_{\alpha}$ radiation ($\lambda(K_{\alpha1})$ = 154.1 pm, $\lambda(K_{\alpha2})$= 154.4 pm) measurements were prepared on a flat low background monocrystalline silicon holder. The XRD data was measured on a *RIGAKU MiniFlex* diffractometer in Bragg-Brentano geometry in steps of 0.02° and an exposure time of 0.2 to 0.24 seconds per step at room temperature. The data was processed with the program *SmartLab Studio II*.

$(C_5H_6N)_2[(SO_3)HNNH(SO_3)]$

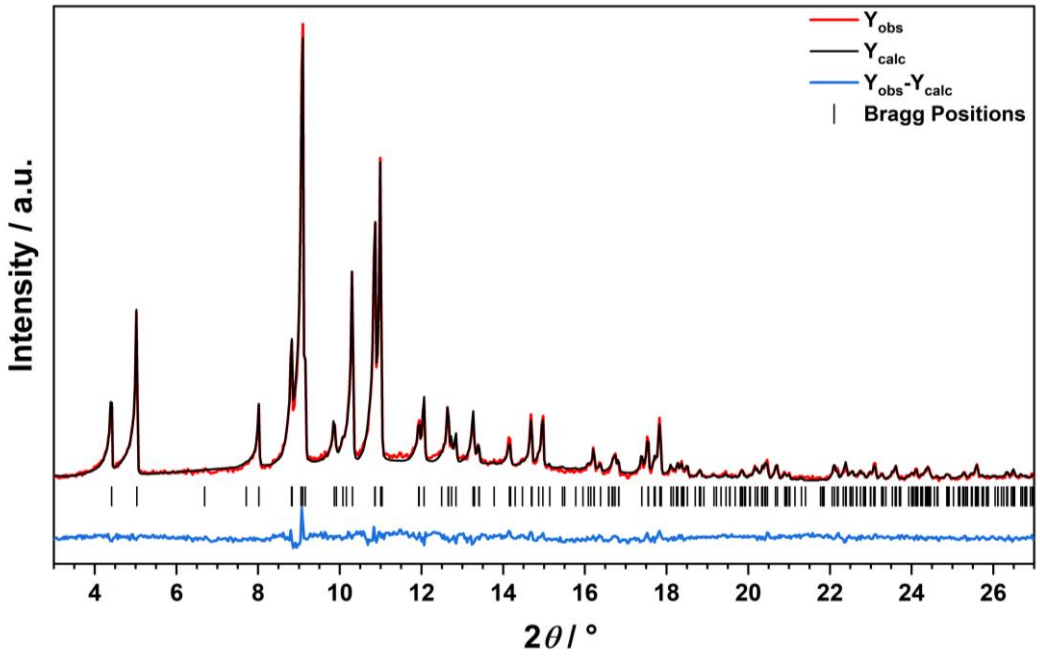

Figure S9: Rietveld refinement plot of **$(C_5H_6N)_2[(SO_3)HNNH(SO_3)]$** (Mo-K$_{\alpha1}$ radiation). Following profile *R*-factors were received: R_{exp} = 4.29%, R_{wp} = 8.43%, R_p = 6.64%, GOF = 1.96. The cell parameter *a*, *b*, *c*, and *V* and the positions of all atoms except the protons were refined. Cell parameters of the refinement are: *a* = 1842.0(2) pm, *b* = 898.48(8) pm, *c* = 922.17(8) pm and *V*= 1.5262(2) nm^3.

$K_2[(SO_3)HNNH(SO_3)](H_2O)$

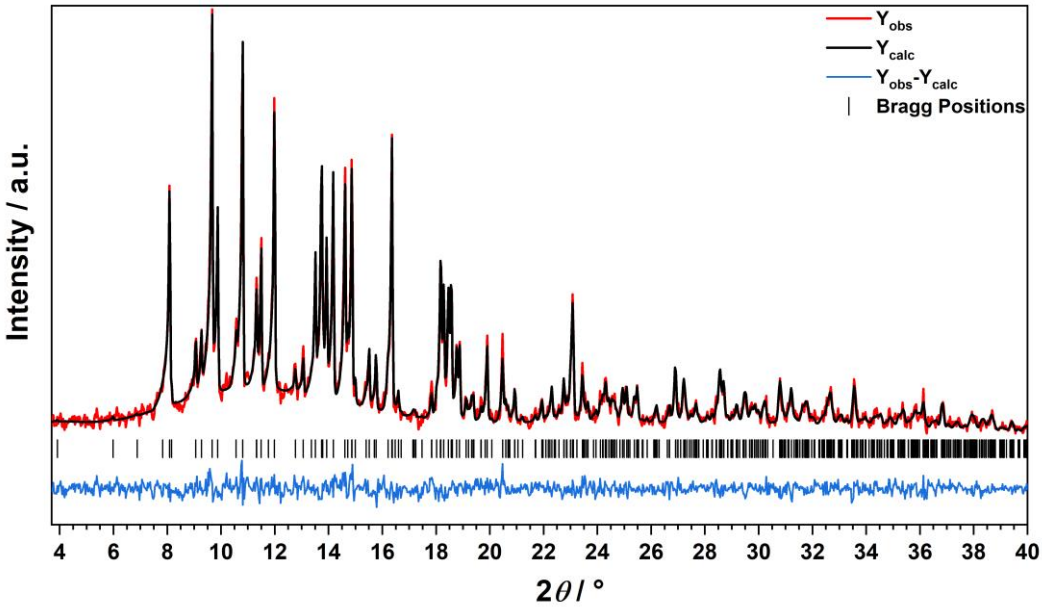

Figure S10: Rietveld refinement plot of **$K_2[(SO_3)HNNH(SO_3)](H_2O)$ (**Mo-$K_{\alpha 1}$ radiation). Following profile *R*-factors were received: R_{exp} = 8.50%, R_{wp} = 8.71%, R_p = 6.69%, GOF = 1.03. The cell parameter *a*, *b* and *c* were refined. Cell parameters of the refinement are: *a* = 2076.6(2) pm, *b* = 718.80(6) pm, *c* = 574.88(6) pm and *V*= 0.8581(1) nm^3.

$Rb_2[(SO_3)HNNH(SO_3)](H_2O)$

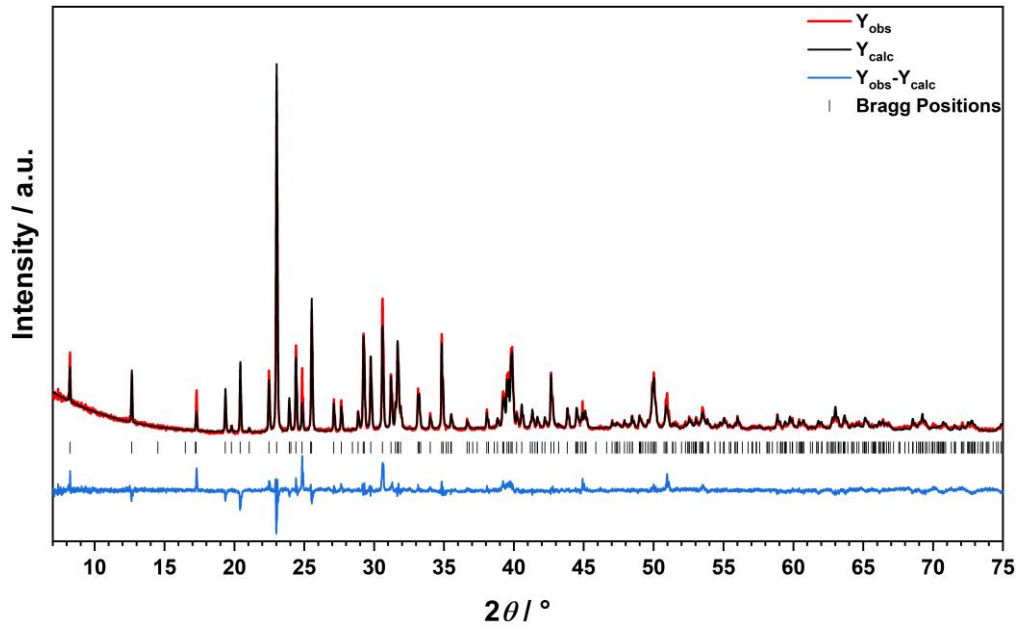

Figure S11: Rietveld refinement plot of **$Rb_2[(SO_3)HNNH(SO_3)](H_2O)$** (Cu-$K_\alpha$ radiation). Following profile *R*-factors were received: R_{exp} = 2.03%, R_{wp} = 6.21%, R_p = 4.36%, GOF = 3.06. The cell parameter *a*, *b* and *c* were refined. Cell parameters of the refinement are: *a* = 2149.04(4) pm, *b* = 584.06(1) pm, *c* = 739.8(2) pm and *V*= 0.92853(3) nm^3.

$Cs_2[(SO_3)HNNH(SO_3)](H_2O)$

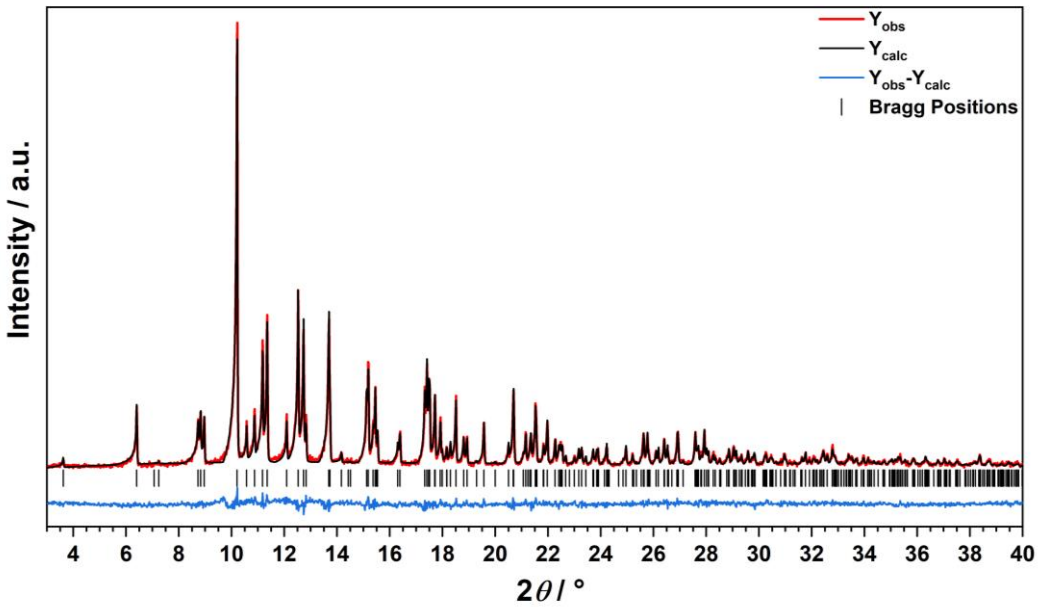

Figure S12: Rietveld refinement plot of **$Cs_2[(SO_3)HNNH(SO_3)](H_2O)$ (**Mo-$K_{\alpha 1}$ radiation). Following profile *R*-factors were received: R_{exp} = 8.15%, R_{wp} = 9.31%, R_p = 6.99%, GOF = 1.14. The cell parameter *a*, *b* and *c* and the positions of the caesium and sulfur atoms were refined. Cell parameters of the refinement are: *a* = 595.11(1) pm, *b* = 2246.43(6) pm, *c* = 769.73(2) pm and *V*= 1.02903(5) nm^3.

$(NH_4)_2[(SO_3)HNNH(SO_3)](H_2O)$

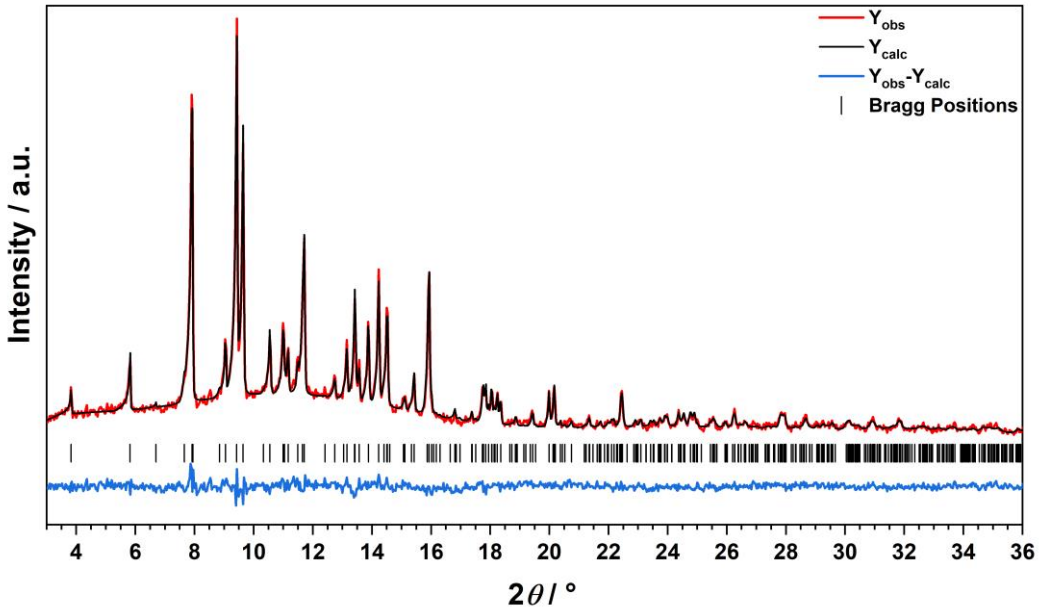

Figure S13: Rietveld refinement plot of **$(NH_4)_2[(SO_3)HNNH(SO_3)](H_2O)$ (**Mo-$K_{\alpha 1}$ radiation). Following profile *R*-factors were received: R_{exp} = 5.26%, R_{wp} = 6.03%, R_p = 4.81%, GOF = 1.15. The cell parameters *a*, *b* and *c* were refined. Cell parameters of the refinement are: *a* = 2126.(2) pm, *b* = 586.90(6) pm, *c* = 740.01(6) pm and *V*= 0.923(1) nm^3.

$Ba[(SO_3)HNNH(SO_3)](H_2O)_2$

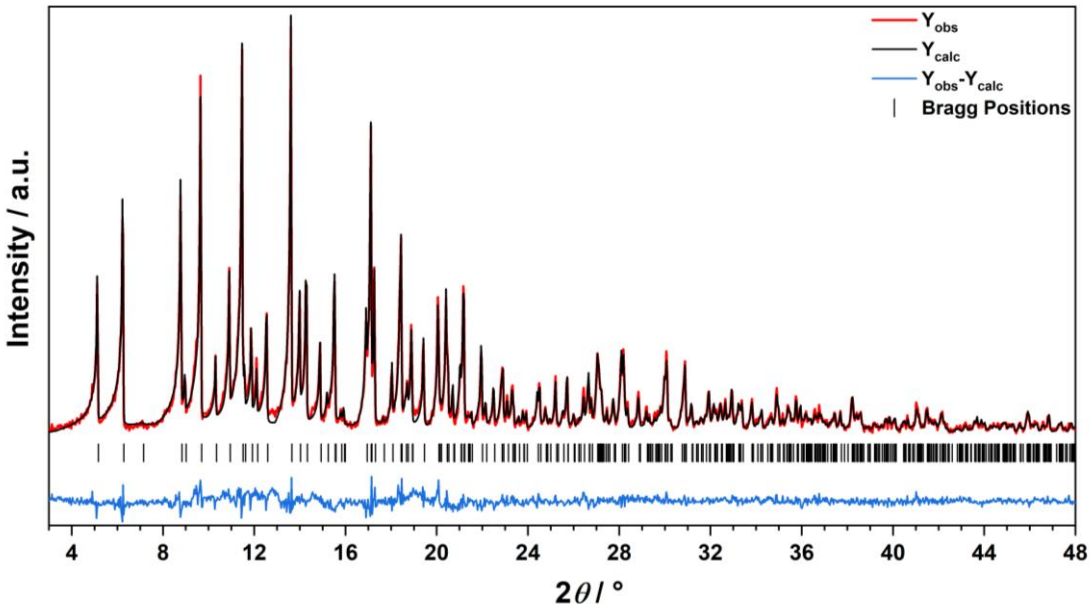

Figure S14: Rietveld refinement plot of **$Ba[(SO_3)HNNH(SO_3)](H_2O)_2$ (**Mo-$K_{\alpha1}$ radiation). Following profile *R*-factors were received: R_{exp} = 7.20%, R_{wp} = 9.43%, R_p = 7.21%, GOF = 1.31. The cell parameter *a*, *b*, *c*, and the positions of the sulfur, oxygen (O11, O12, O13) and nitrogen atoms were refined. Cell parameters of the refinement are: *a* = 1137.62(3) pm, *b* = 1572.95(5) pm, *c* = 471.16(2) pm and *V*= 0.84311(5) nm^3.

$K_2[H_2NN(SO_3)_2]$

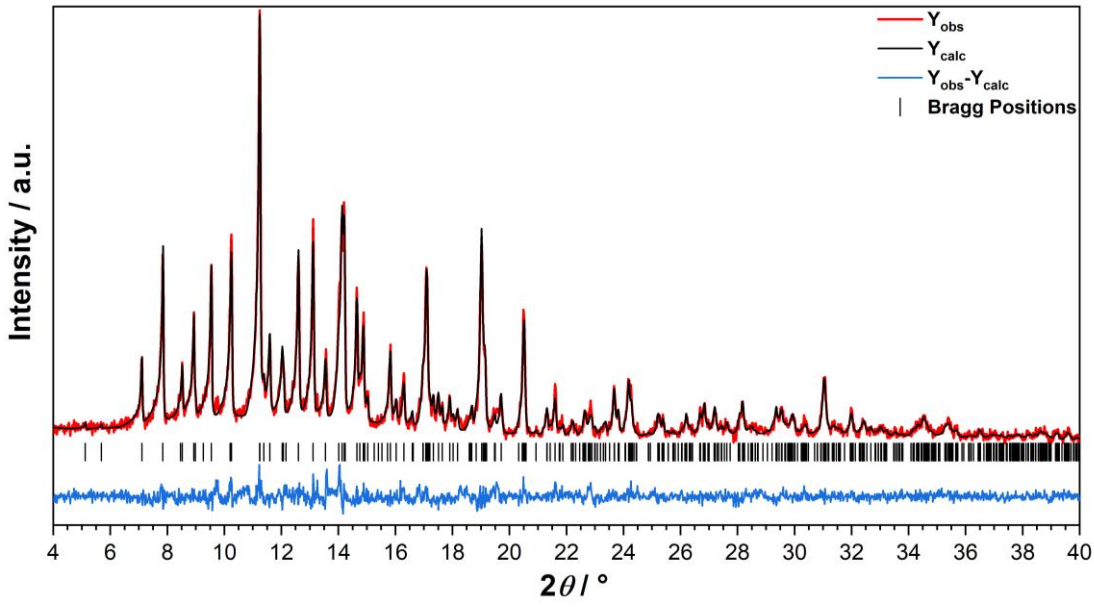

Figure S15: Rietveld refinement plot of **$K_2[H_2NN(SO_3)_2]$ (**Mo-$K_{\alpha1}$ radiation). Following profile *R*-factors were received: R_{exp} = 8.53%, R_{wp} = 8.75%, R_p = 6.78%, GOF = 1.03. The cell parameter *a*, *b*, *c*, and the atomic positions of all atoms except of the protons were refined. Cell parameters of the refinement are: *a* = 556.43(3) pm, *b* = 954.62(5) pm, *c* = 1430.0(9) pm and *V*= 0.75959(7) nm^3.

$Ba[H_2NN(SO_3)_2](H_2O)_2$

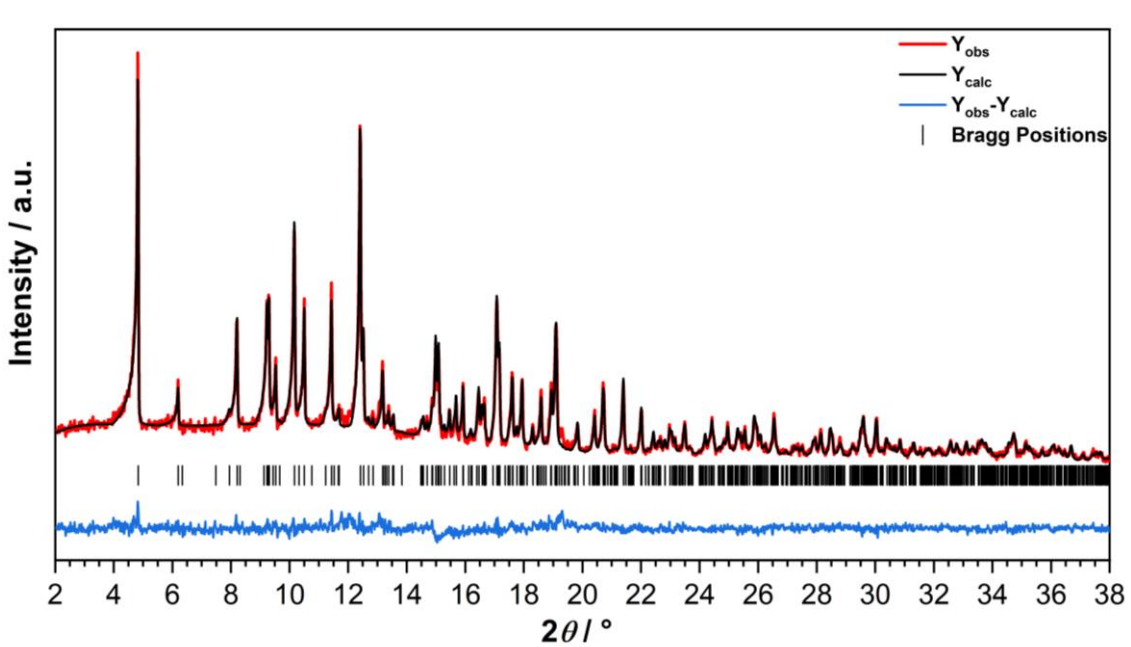

Figure S16: Rietveld refinement plot of **$Ba[H_2NN(SO_3)_2](H_2O)_2$** (Mo-$K_{\alpha1}$ radiation). Following profile *R*-factors were received: R_{exp} = 6.84%, R_{wp} = 7.40%, R_p = 5.60%, GOF = 1.08. The cell parameters *a*, *b*, *c* and the position of the barium atom were refined. Cell parameters of the refinement are: *a* = 990.67(4) pm, *b* = 1023.68(4) pm, *c* = 1683.24(7) pm and *V*= 1.7070(1) nm^3.

D Thermal Analysis

The thermal analyses were performed on a thermal analyzer *STA 409C* (*NETZSCH*) coupled with a quadrupole mass spectrometer (*QMS 421*, *Balzers*). All measurements were done in corundum (Al_2O_3) crucibles on a DSC/TG sample holder under an argon flow of 80 ml·min^{-1}. The ion current measurements were carried out in scanning mode with predefined *m*/*z* values. The collected data was processed with *NETZSCH Proteus*[9].

$(C_5H_6N)_2[(SO_3)HNNH(SO_3)]$

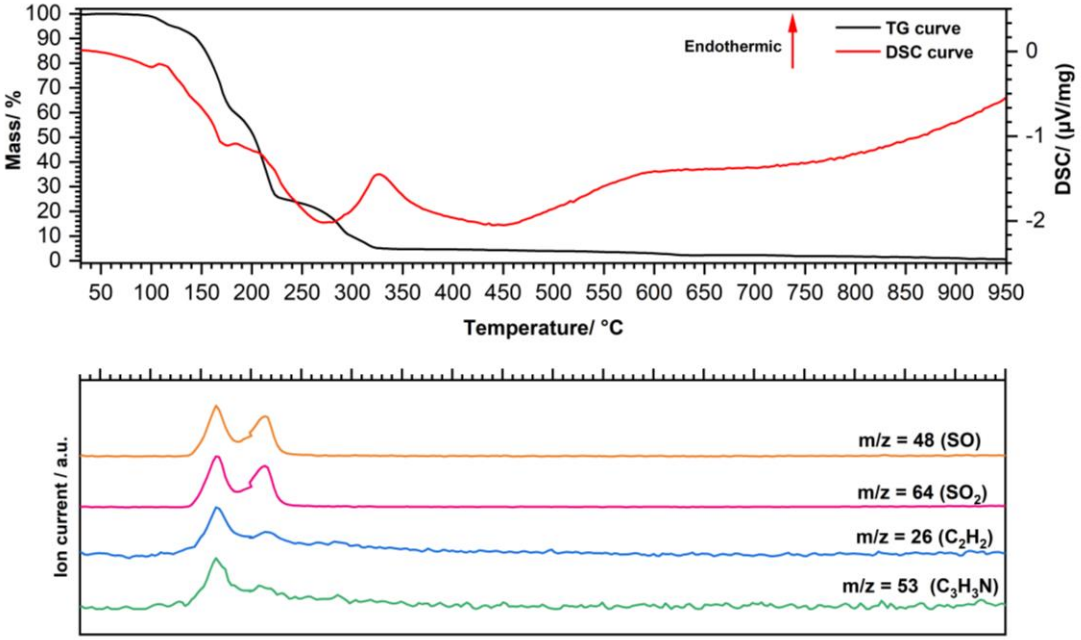

Figure S17: Thermal analysis (on top) of **$(C_5H_6N)_2[(SO_3)HNNH(SO_3)]$** (heating rate 3 K · min^{-1}) combined with an ion current measurement (below) of selected m/z values.

Table S52: Thermal decomposition data of **$(C_5H_6N)_2[(SO_3)HNNH(SO_3)]$**.

Stage	T_{onset}/ °C	T_{end}/ °C	T_{max}/ °C	Mass loss (calcd.)/ %	Mass loss (obsd.)/ %	Decomposition
I	102.5	221	169	72%	76%	Decomposition to H_2SO_4 over one endothermic and one exothermic step
II	274	301	289	28	22.8	Decomposition/ evaporation of H_2SO_4
Total				100	98.8	No residual phase

$K_2[(SO_3)HNNH(SO_3)](H_2O)$

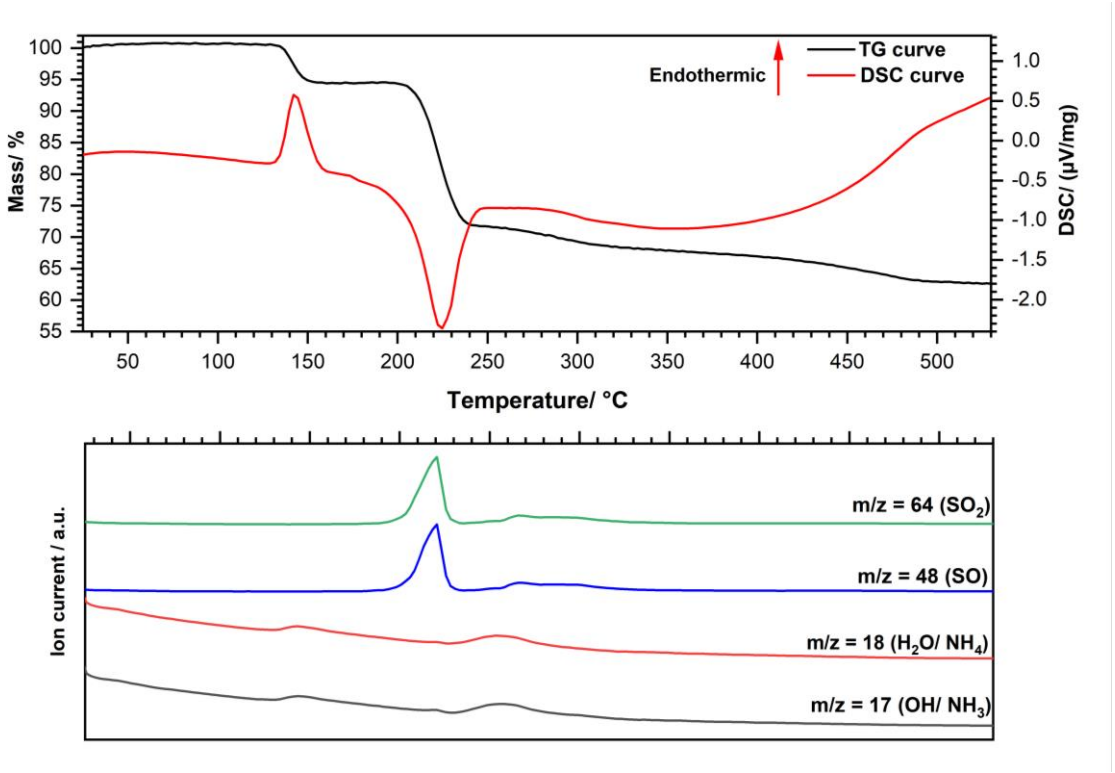

Figure S18: Thermal analysis of **$K_2[(SO_3)HNNH(SO_3)](H_2O)$** (heating rate 5 $K \cdot min^{-1}$) combined with an ion current measurement (below) of selected m/z values.

Table S53: Thermal decomposition data of **$K_2[(SO_3)HNNH(SO_3)](H_2O)$**.

Stage	T_{onset}/ °C	T_{end}/ °C	T_{max}/ °C	Mass loss (calcd.)/ %	Mass loss (obsd.)/ %	Decomposition
I	134.7	155.6	142.9	6.3	6.1	Endothermic releasement of H_2O
II	207.3	238.7	224.3	35.1	31.9	Exothermic decomposition of the hydrazinium disulfonate to SO_4^{2-}
Total				41.4	38	Residual phase: K_2SO_4

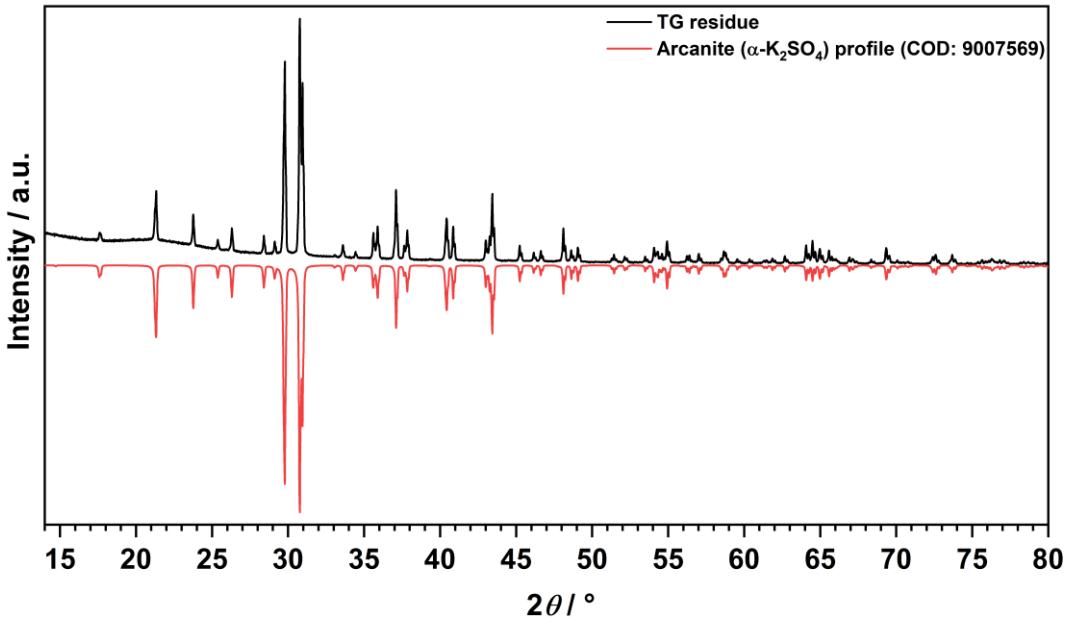

Figure S19: Powder XRD (Cu-Kα radiation, λ = 154.06 pm) of the residue of the thermal analysis of **$K_2[(SO_3)HNNH(SO_3)](H_2O)$** compared to the theoretical pattern of α-K_2SO_4.

$Rb_2[(SO_3)HNNH(SO_3)](H_2O)$

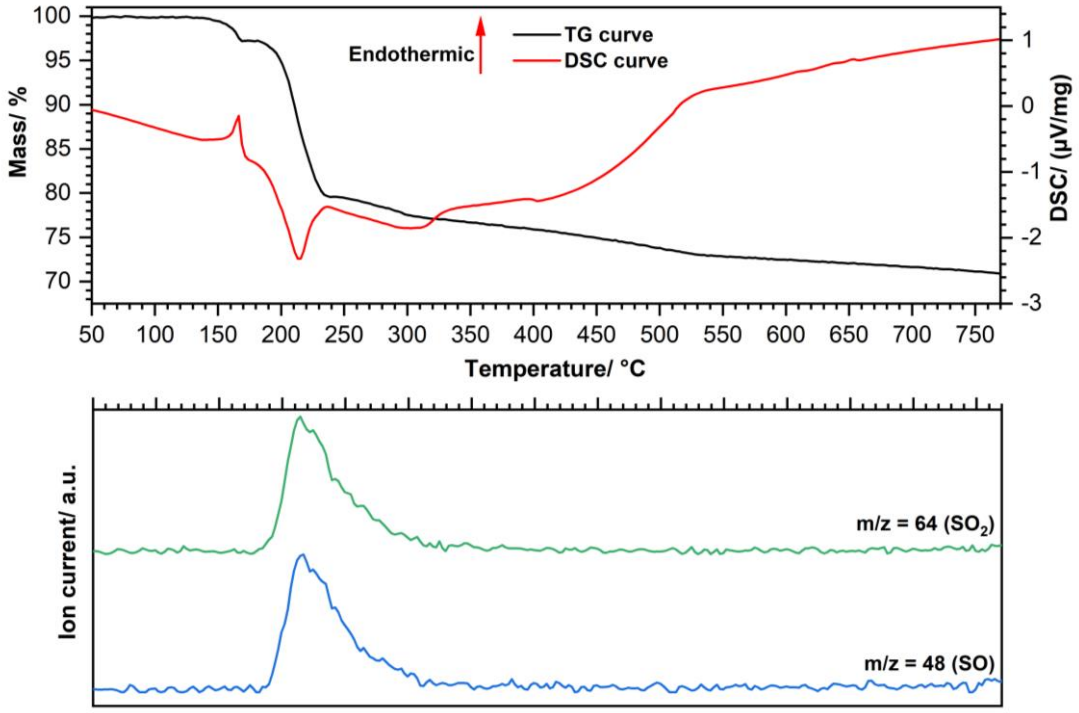

Figure S20: Thermal analysis of **$Rb_2[(SO_3)HNNH(SO_3)](H_2O)$** (heating rate 5 $K \cdot min^{-1}$) combined with an ion current measurement (below) of selected m/z values.

Table S54: Thermal decomposition data of **$Rb_2[(SO_3)HNNH(SO_3)](H_2O)$**.

Stage	T_{onset}/ °C	T_{end}/ °C	T_{max}/ °C	Mass loss (calcd.)/ %	Mass loss (obsd.)/ %	Decomposition
I	160.2	170.0	166	5	3	Endothermic releasement of H_2O
II	193.0	227.1	214.5	26	27	Exothermic decomposition of the hydrazinium disulfonate to SO_4^{2-}
Total				31	30	Residual phase: Rb_2SO_4

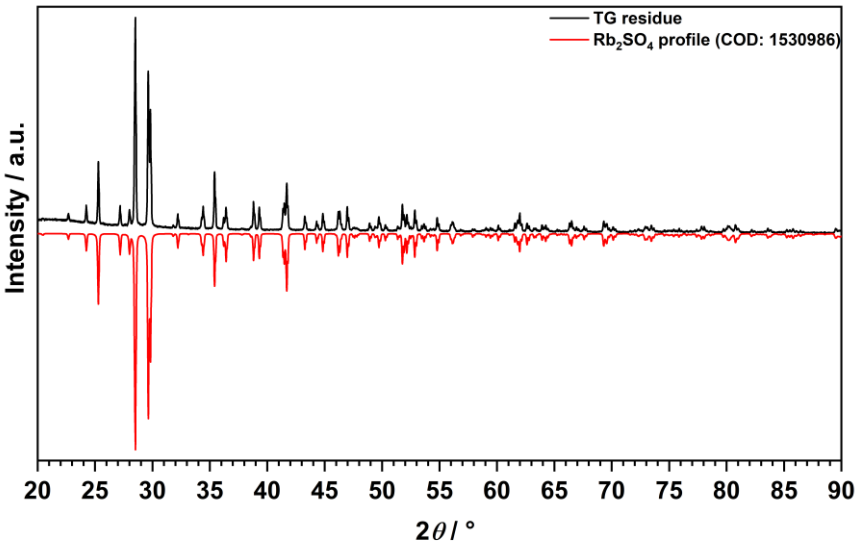

Figure S21: Powder XRD (Cu-Kα radiation, λ = 154.06 pm) of the residue of the thermal analysis of **$Rb_2[(SO_3)HNNH(SO_3)](H_2O)$** compared to the theoretical pattern of Rb_2SO_4.

$Ba[(SO_3)HNNH(SO_3)](H_2O)_2$

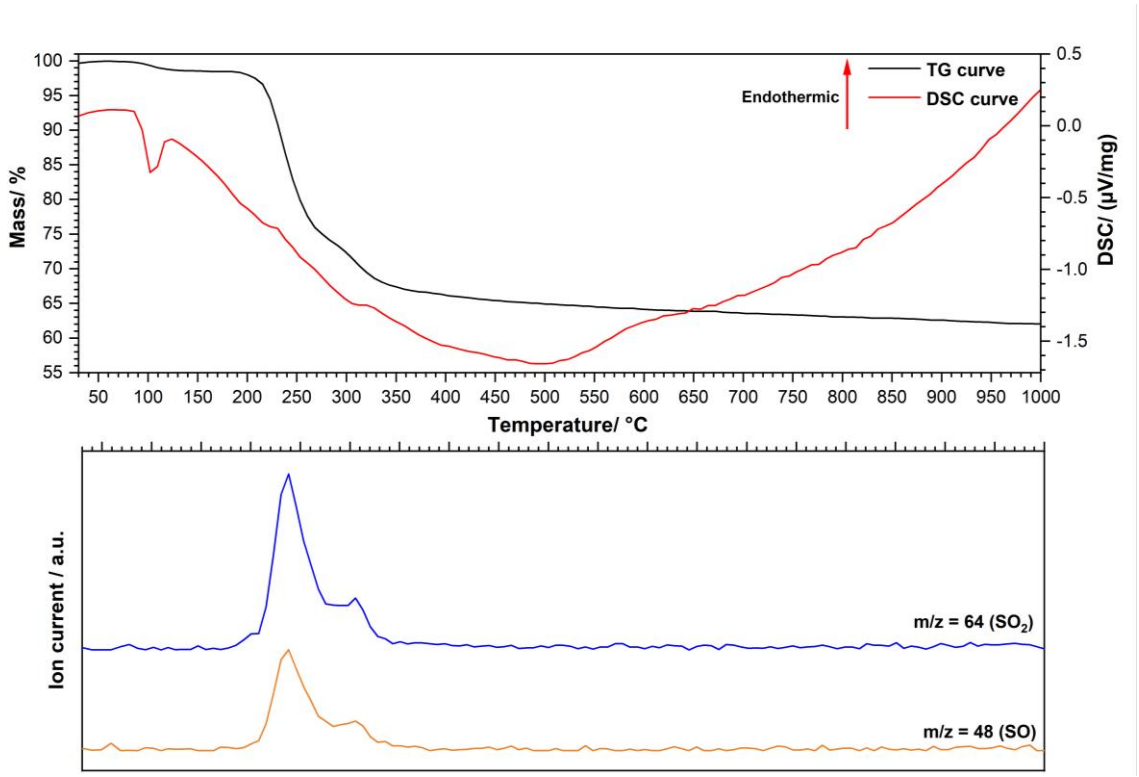

Figure S22: Thermal analysis (on top) of **$Ba[(SO_3)HNNH(SO_3)](H_2O)_2$** (heating rate 3 $K \cdot min^{-1}$) combined with an ion current measurement (below) of selected m/z values.

Table S55: Thermal decomposition data of **$Ba[(SO_3)HNNH(SO_3)](H_2O)_2$**.

Stage	T_{onset}/ °C	T_{end}/ °C	T_{max}/ °C	Mass loss (calcd.)/ %	Mass loss (obsd.)/ %	Decomposition
I	91.7	115.9	104.7	---	2	Exothermic reaction transition to $BaSO_4$ $(N_2H_6)SO_4$
II	155	233.6	277.2	36	36	Melting and decomposition of $(N_2H_6)SO_4$
Total				36	38	Residual phase: $BaSO_4$

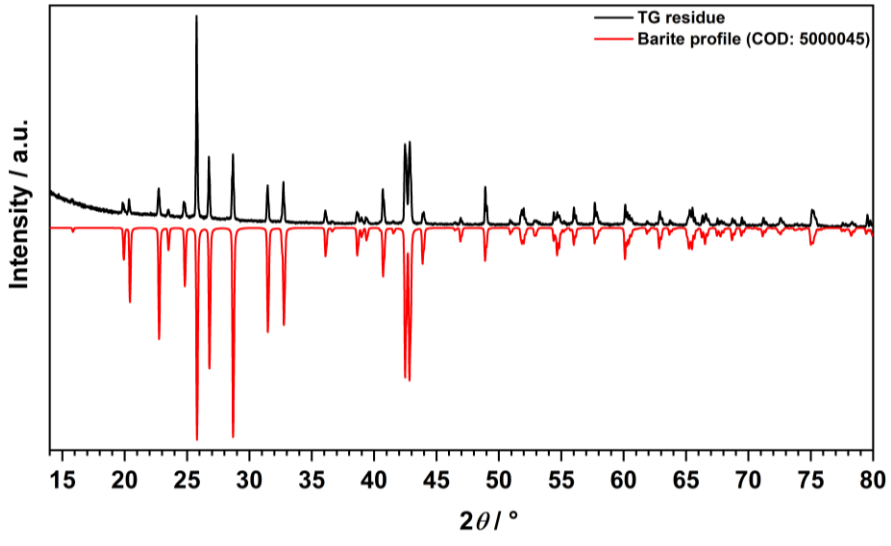

Figure S23: Powder XRD (Cu-K_α radiation, λ = 154.06 pm) of the residue of the thermal analysis of **$Ba[(SO_3)HNNH(SO_3)](H_2O)_2$** compared to the theoretical pattern of $BaSO_4$.

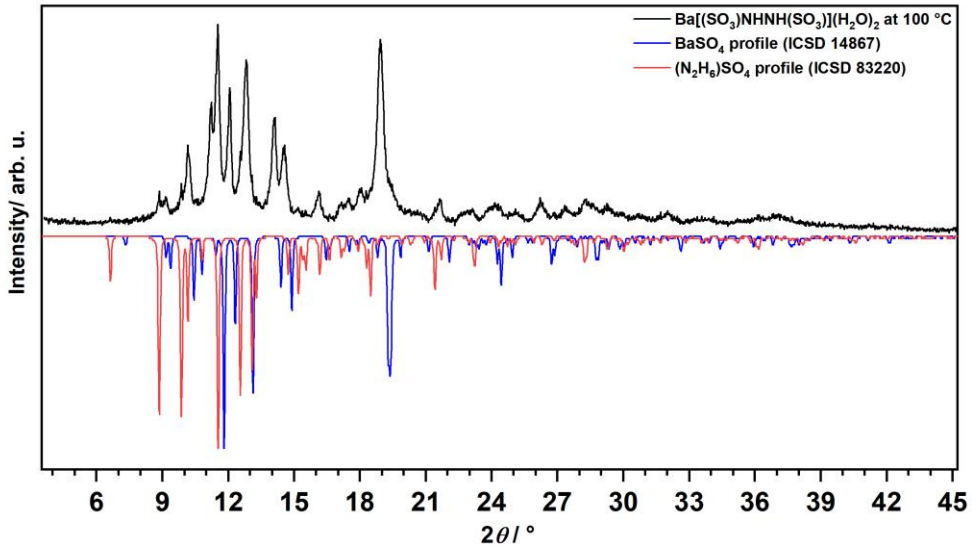

Figure S24: Powder XRD (Mo-$K_{\alpha 1}$ radiation, λ = 70.930 pm) of **Ba[(SO_3)HNNH(SO_3)](H_2O)$_2$** heated at 100 °C for 2h. The simulated diffracograms of $(N_2H_6)SO_4$ and $BaSO_4$ from CIFs are show below.

$K_2[H_2NN(SO_3)_2]$

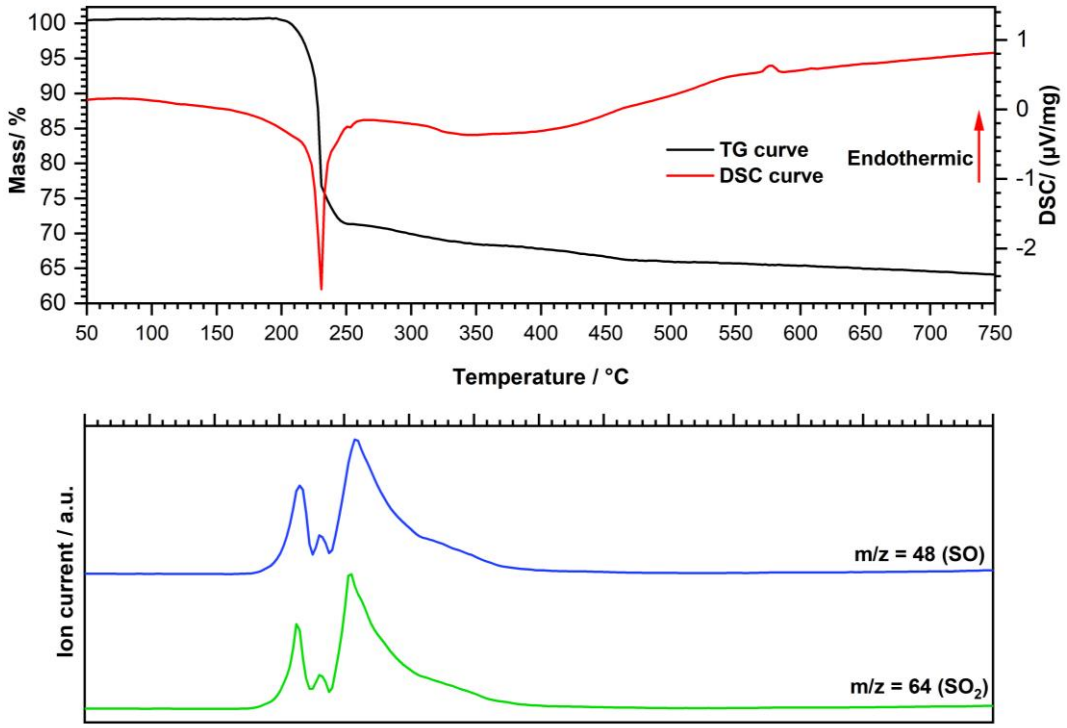

Figure S25: Thermal analysis (on top) of **$K_2[H_2NN(SO_3)_2]$** (heating rate 5 $K \cdot min^{-1}$) combined with an ion current measurement (below) of selected m/z values.

Table S56: Thermal decomposition data of **$K_2[H_2NN(SO_3)_2]$**.

Stage	T_{onset}/ °C	T_{end}/ °C	T_{max}/ °C	Mass loss (calcd.)/ %	Mass loss (obsd.)/ %	Decomposition
I	227.5	234.4	229.6	35.1	36.9	Decomposition to K_2SO_4
Total				35.1	36.9	Residual phase: K_2SO_4

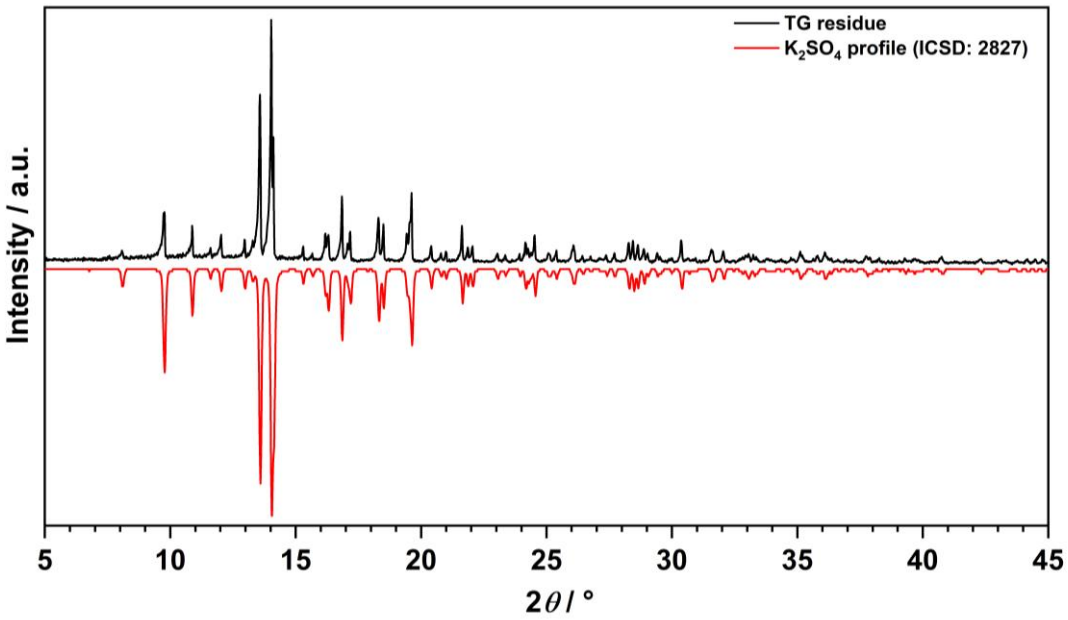

Figure S26: Powder XRD (Mo-$K_{\alpha 1}$ radiation, $\lambda = 70.930$ pm) of the residue of the thermal analysis of **$K_2[H_2NN(SO_3)_2]$** compared to the theoretical pattern of K_2SO_4.

E Vibrational Spectroscopy

The Raman spectroscopic data were collected with an *inVia Qotor confocal RAMAN microscope* from *Renishaw GmbH* (Pliezhausen, DE) equipped with 10x, 50x and 100x magnification lenses. The spectra were measured on selected single crystals with a green laser (532 nm, 100 mW) with an exposure time of 10000 ms. The data were processed and corrected by using the WiRE 5.1 software[10]. The simulated spectra were simulated according to the geometry-optimized structures (s. chapter **F**).

Hydrazine disulfonates

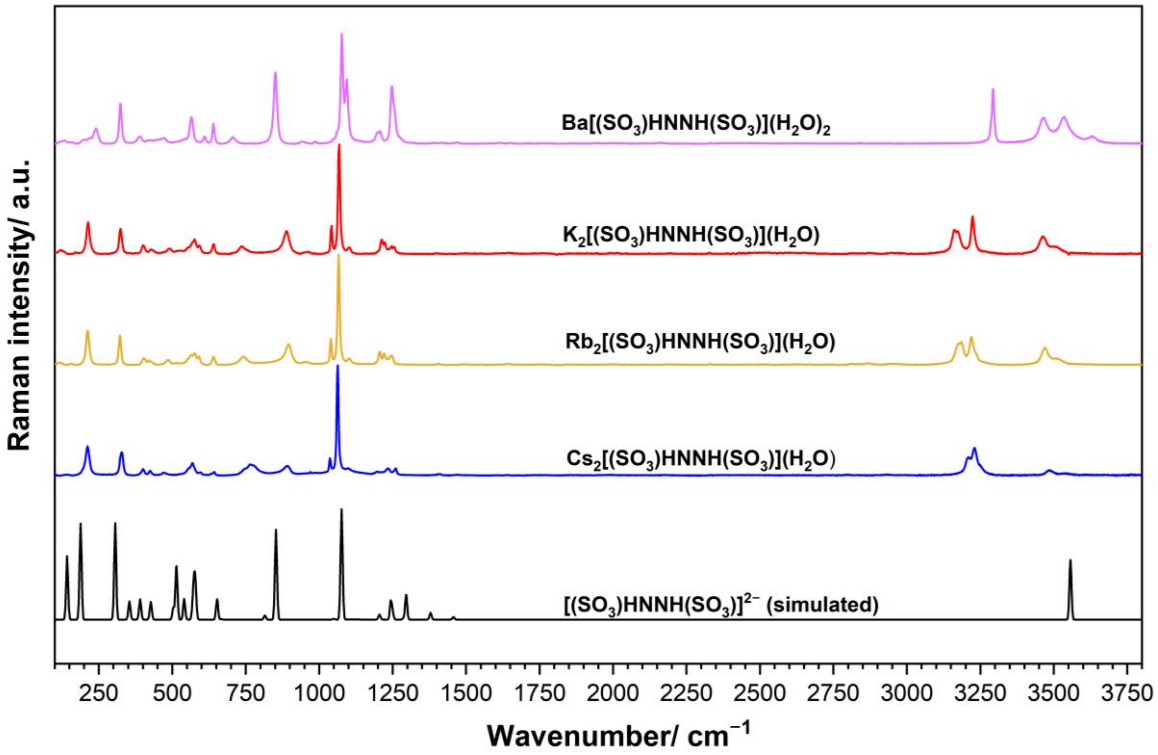

Figure S27: Experimental Raman spectrum of the hydrazine disulfonates of K^+, Rb^+ Cs^+ and Ba^{2+} compared to the theoretical spectrum of the anion $[(SO_3)HNNH(SO_3)]^{2-}$.

Table S57: Assignment of the Raman bands of the hydrazine disulfonates of K^+, Rb^+ Cs^+ and Ba^{2+}.

Assignment	K^+/ cm^{-1}	Rb^+ / cm^{-1}	Cs^+ / cm^{-1}	Ba^{2+} / cm^{-1}	Calcd. / cm^{-1}
$\nu_{s/as}$(NH)	3505(sh) 3462	3521(sh) 3469	3546(sh) 3483	3632 3536 3464	3557 3556
$\nu_{s/as}$(OH)	3224 3175 3161	3220 3179	3231 3208	3293	---
ν_{as}(SO_3)	1255 1246 1223	1246 1222	1260 1235	1248	1295 1287 1249 1244
ν_s(N-N)	1213	1206	1197	1202	1205
ν_s(SO_3)	1068 1042	1066 1040	1063 1037	1094 1077	1076 1050
ν_s(S-N)	889	896	891	851	852
ν_{as}(S-N)	737	742	770	707	815
δ(SO_3) umbrella	640	641	642	640	652
δ(SO_3)	593 574	591 575	597 568	610 565	579 574 570

Assignment	K^+/ cm^{-1}	Rb^+ / cm^{-1}	Cs^+ / cm^{-1}	Ba^{2+} / cm^{-1}	Calcd. / cm^{-1}
					540
τ(NHNH)	490	486	472	471	514
δ[NH(SO_3)NH(SO_3)]	430	422	425	389	427
ω(SO_3NH)	401	403	400	324	390
ω(NHNH)	324	322	327	241	354
δ [NH(SO_3)NH(SO_3)]	214	212	212	196	305
	171	156	140	131	187
	122	116			142

$K_2[H_2NN(SO_3)_2]$

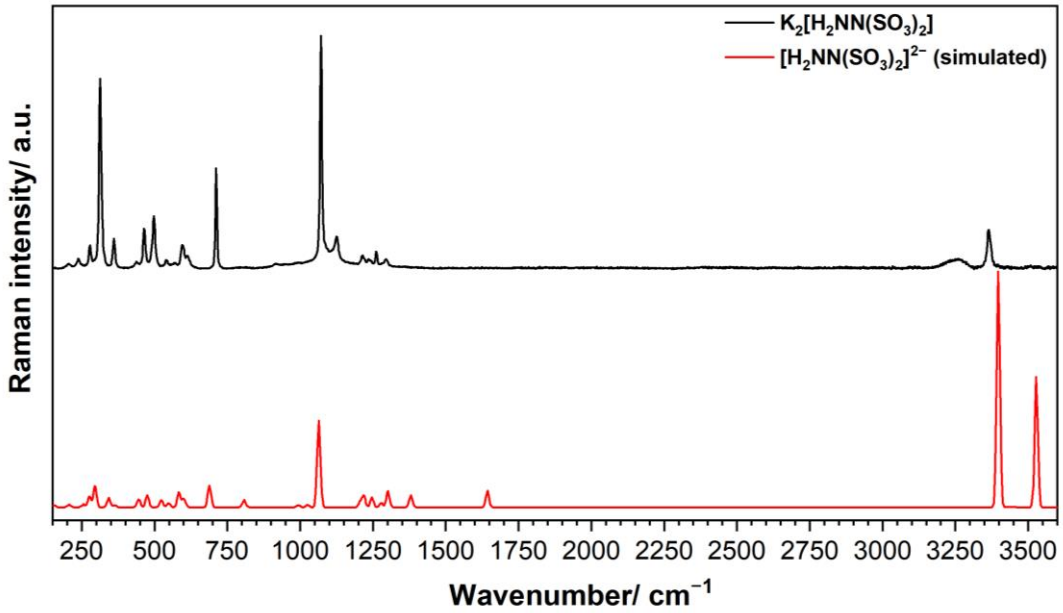

Figure S28: Experimental Raman spectrum of the hydrazine *iso*-disulfonate, **$K_2[H_2NN(SO_3)_2]$**, compared to the theoretical spectrum of the anion $[NH_2N(SO_3)_2]^{2-}$.

Table S58: Assignment of the Raman bands of the hydrazine *iso*-disulfonate, **$K_2[H_2NN(SO_3)_2]$**.l

Assignment	Raman / cm^{-1}	Calcd. / cm^{-1}
ν_{asym}(N-H)	3365	3527
ν_{sym}(N-H)	3258	3397
δ(NH_2) (scissoring)	-	1643
ρ(NH_2)	-	1380
ν_{as}(SO_3)	1296	1301
	1262	1278
	1235	1247
	1214	1218
δ (NH_2)	1125	1206
ν_s(SO_3)	1072	1064
	1021	1025
ν_s(N–N)	914	994
ν_{as}(N–S)	-	807
ν_s(N–S)	712	689
δ(SO_3) umbrella	614	604
δ(SO_3)	596	597
	570	583
	544	549
	489	524

Assignment	Raman / cm^{-1}	Calcd. / cm^{-1}
δ[N(NS_2)]umbrella	465	475
δ(O_3SN)	438	446
ρ(NH_2)	361	364
	313	343
τ(SO_3)	278	295
τ(SO_3)(NH_2)	239	277

F Results from Quantum Chemical Calculations

$[(SO_3)HNNH(SO_3)]^{2-}$

Calculation method: A full geometry optimization for the $[(SO_3)HNNH(SO_3)]^{2-}$ anion of $K_2[(SO_3)HNNH(SO_3)](H_2O)$ was performed within density functional theory (DFT) using the PBE0 exchange-correlation functional and def2-TZVPP basis set for all elements.[11-12] The calculations were also used for assigning the IR and Raman frequencies. Throughout the study the Orca 5.0.3 program package was used.[13] For the calculation a fixed dihedral angle S–N–N–S (134.3(1)°) was set.

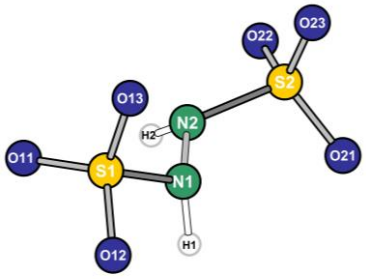

Figure S29: Molecular structure and labelling of the $[(SO_3)HNNH(SO_3)]^{2-}$ anion from the geometry optimization.

Table S59: Atomic coordinates for $[(SO_3)HNNH(SO_3)]^{2-}$ anion from the geometry optimization.

Atom	*x*	*y*	*z*
S2	6.08993	0.75955	5.59195
S1	3.13343	3.59551	5.59195
O23	5.94722	0.73015	7.03097
O22	7.44437	1.03715	5.11696
O21	5.46770	-0.38152	4.92322
O13	3.27613	3.62490	7.03097
O12	1.77898	3.31791	5.11695
O11	3.75567	4.73656	4.92322
N2	5.29770	2.15326	5.03161
N1	3.92565	2.20178	5.03161
H2	5.75788	2.50426	4.20333
H1	3.46546	1.85078	4.20333

Table S60: Bond length for $[(SO_3)HNNH(SO_3)]^{2-}$ from the geometry optimization.

Atom–Atom	Length/ pm
N1–N2	137.3
N1–H1	101.0
N2–S2	169.8
N2–H2	101.0
S1–O11	146.2
S1–N1	169.8
S1–O13	144.6
S1–O12	146.2
S2–O22	146.2
S2–O23	144.6
S2–O21	146.2

Table S61: Bond angles for $[(SO_3)HNNH(SO_3)]^{2-}$ from the geometry optimization.

Atom–Atom–Atom	Angle/ °
S1–N1–N2	119.7
S2–N2–N1	119.7
O11–S1–N1	106.9
O12–S1–N1	99.7
O13–S1–N1	107.4
O21–S2–N2	106.9
O22–S2–N2	107.3
O23–S2–N2	99.7

$[H_2NN(SO_3)_2]^{2-}$

Calculation method: A full geometry optimization for the $[H_2NN(SO_3)_2]^{2-}$ anion of $K_2[H_2NNH(SO_3)_2]$ was performed within density functional theory (DFT) using the PBE0 exchange-correlation functional and cc-pVTZ basis set for all elements.[14-15] The calculations were also used for assigning the IR and Raman frequencies. Throughout the study the Orca 5.0.3 program package was used.[13]

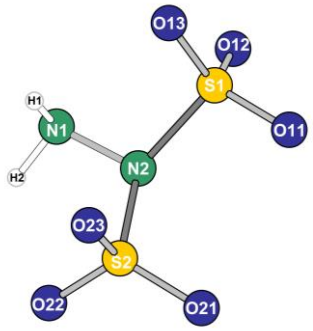

Figure S30: Molecular structure and labelling of the $[H_2NN(SO_3)_2]^{2-}$ anion from the geometry optimization.

Table S62: Atomic coordinates of the $[H_2NN(SO_3)_2]^{2-}$ anion from the geometry optimization.

Atom	*x*	*y*	*z*
S2	2.82962	6.63152	9.70642
S1	2.78235	4.24814	7.73603
O23	3.71851	5.94950	10.65550
O22	3.26846	8.02084	9.44502
O21	1.40688	6.51907	9.99644
O13	4.00616	3.53541	8.13304
O12	2.57667	4.26224	6.28499
O11	1.59707	3.88710	8.50309
N2	3.07496	5.93682	8.10903
N1	4.39511	6.24085	7.65913
H2	4.48407	7.23110	7.86650
H1	5.03813	5.75167	8.28474

Table S63: Bond lengths for $[H_2NN(SO_3)_2]^{2-}$ from the geometry optimization.

Atom–Atom	Length/ pm
N1–H1	102.2
N1–H2	101.6
N2–N1	142.7
N2–S1	175.4
S1–O11	145.7
S2–O21	145.6
S2–O22	148.0
S1–O12	146.6
S1–O13	147.1
S2–O23	146.8
S2–N2	175.9

Table S64: Bond angles for $[H_2NN(SO_3)_2]^{2-}$ from the geometry optimization.

Atom–Atom–Atom	Angle/ °
N1–N2–S1	107.0
N1–N2–S2	109.3
S1–N2–S2	123.4
N2–S2–O21	106.7
N2–S2–O22	99.7
N2–S2–O23	108.6
N2–S1–O11	105.2
N2–S1–O12	103.0
N2–S1–O13	105.7

G References

[1] A. Meuwsen, H. Tischer, *Z. Anorg. Allg. Chem.* **1958**, *294*, 282-293.
[2] Bruker AXS, *Saint V8.40B* **2012**, Madsion, Winconsin, USA.
[3] L. Krause, R. Herbst-Irmer, G. M. Sheldrick, D. Stalke, *J. Appl. Crystallogr.* **2015**, *48*, 3-10.
[4] O. V. Dolomanov, L. J. Bourhis, R. J. Gildea, J. A. K. Howard, H. Puschmann, *J. Appl. Crystallogr.* **2009**, *42*, 339-341.
[5] G. Sheldrick, *Acta Crystallogr. Sec. A* **2015**, *71*, 3-8.
[6] M. Nespolo, B. Guillot, *J. Appl. Crystallogr.* **2016**, *49*, 317-321.
[7] R. Shannon, *Acta Crystallogr. Sec. A* **1976**, *32*, 751-767.
[8] A. Coelho, *J. Appl. Crystallogr.* **2018**, *51*, 210-218.
[9] NETZSCH Gerätebau GmbH, *NETZSCH Proteus 6.1.0* **2019**, Selb, Germany.
[10] Renishaw plc., *WiRE 5.1* **2017**, New Mills, UK.
[11] F. Weigend, R. Ahlrichs, *Phys. Chem. Phys. Chem.* **2005**, *7*, 3297-3305.
[12] F. Weigend, *Phys. Chem. Phys. Chem.* **2006**, *8*, 1057-1065.
[13] F. Neese, F. Wennmohs, U. Becker, C. Riplinger, *J. Chem. Phys.* **2020**, *152*.
[14] T. H. Dunning, Jr., *J. Chem. Phys.* **1989**, *90*, 1007-1023.
[15] D. E. Woon, T. H. Dunning, Jr., *J. Chem. Phys.* **1993**, *98*, 1358-1371.

9 References

[1] L. E. Apodaca, G. E. d'Aquin, R. C. Fell, *Handbook of Industrial Chemistry and Biotechnology* (Eds.: J. A. Kent, T. V. Bommaraju, S. D. Barnicki), Springer International Publishing, Cham, **2017**, pp. 1241-1266.
[2] A. O. Oni, D. A. Fadare, S. Sharma, G. P. Rangaiah, *J. Clean. Prod.* **2018**, *181*, 652-662.
[3] W. Moeller, K. Winkler, *J. Air Pollut. Control Assoc.* **1968**, *18*, 324-325.
[4] R. Westrik, C. H. Mac Gillavry, *Recl. Trav. Chim. Pays-Bas* **1941**, *60*, 794-810.
[5] R. Westrik, C. H. MacGillavry, *Acta Crystallogr.* **1954**, *7*, 764-767.
[6] C. Pascard-Billy, *Acta Crystallogr.* **1965**, *18*, 827-829.
[7] W. S. McDonald, D. W. J. Cruickshank, *Acta Crystallogr.* **1967**, *22*, 48-51.
[8] E. Kemnitz, C. Werner, S. Trojanov, *Acta Crystallogr. Sec. C* **1996**, *52*, 2665-2668.
[9] A. R. Moodenbaugh, J. E. Hartt, J. J. Hurst, R. W. Youngblood, D. E. Cox, B. C. Frazer, *Phys. Rev. B* **1983**, *28*, 3501-3505.
[10] W. Hönle, *Z. Kristallogr. – Cryst. Mater.* **1991**, *196*, 279.
[11] K. Eriks, C. H. MacGillavry, *Acta Crystallogr.* **1954**, *7*, 430-434.
[12] D. W. J. Cruickshank, *Acta Crystallogr.* **1964**, *17*, 684-685.
[13] C. Logemann, T. Klüner, M. S. Wickleder, *Z. Anorg. Allg. Chem.* **2012**, *638*, 758-762.
[14] C. Logemann, T. Klüner, M. S. Wickleder, *Angew. Chem. Int. Ed.* **2012**, *51*, 4997-5000.
[15] L. V. Schindler, A. Becker, M. Wieckhusen, T. Klüner, M. S. Wickleder, *Angew. Chem. Int. Ed.* **2016**, *55*, 16165-16167; *Angew. Chem.* **2016**, *128*, 16399-16401.
[16] L. V. Schindler, M. Struckmann, A. Becker, M. S. Wickleder, *Eur. J. Inorg. Chem.* **2017**, *2017*, 958-964.
[17] J. Bruns, T. Klüner, M. S. Wickleder, *Angew. Chem. Int. Ed.* **2013**, *52*, 2590-2592.
[18] R. Sass, *Acta Crystallogr.* **1960**, *13*, 320-324.
[19] A. F. Cameron, F. D. Duncanson, *Acta Crystallogr. Sect. B* **1976**, *32*, 1563-1564.
[20] J. A. Kurzman, G. Jouan, M. Courty, M. R. Palacín, M. Armand, N. Recham, *Solid State Sci.* **2013**, *25*, 28-32.
[21] V. Zimmermann, M. S. Wickleder, *Z. Kristallogr.* **2015**, *Suppl. 35*, 103.
[22] W. Traube, A. Vockerodt, *Ber. Dtsch. Chem. Ges.* **1914**, *47*, 938-944.
[23] E. Konrad, L. Pellens, *Ber. Dtsch. Chem. Ges.* **1926**, *59*, 135-138.
[24] A. Meuwsen, H. Tischer, *Z. Anorg. Allg. Chem.* **1958**, *294*, 282-293.
[25] D. van Gerven, M. S. Wickleder, *Angew. Chem. Int. Ed.* **2020**, *59*, 17169-17171; *Angew. Chem.* **2020**, *132*, 17320-17323.
[26] T. Rennebaum, *Master Thesis*, University of Cologne, **2020**.
[27] T. L. Muller, *Sulfuric Acid and Sulfur Trioxide; Kirk-Othmer Encyclopedia of Chemical Technology, Vol. 23*, John Wiley & Sons, **2006**.
[28] P. N. Cheremisinoff, *Waste Minimization and Cost Reduction for the Process Industries* (Ed.: P. N. Cheremisinoff), William Andrew Publishing, Park Ridge, NJ, **1995**, pp. 222-284.
[29] N. N. Greenwood, A. Earnshaw, *Chemistry of the Elements* 2ed., Butterworth-Heinemann, Oxford, **1998**.
[30] M. J. King, W. G. Davenport, M. S. Moats, *Sulfuric acid manufacture : analysis, control and optimization*, 2nd ed., Elsevier Amsterdam, Amsterdam, **2013**.
[31] R. W. Lovejoy, J. H. Colwell, D. F. Eggers, Jr., G. D. Halsey, Jr., *J. Chem. Phys.* **2004**, *36*, 612-617.
[32] M. S. Wickleder, C. Logemann, *Handbook on Chalcogen Chemistry, Vol. 1* (Eds.: F. Devillanova, W.-W. du Mont), Royal Society of Chemistry, London, **2013**, pp. 307-345.
[33] E. S. Scott, L. F. Audrieth, *J. Chem. Educ.* **1954**, *31*, 168.
[34] L. Richtera, J. Taraba, J. Toužín, *Collect. Czech. Chem. Commun.* **2006**, *71*, 155-163.
[35] S. Brownstein, E. Gabe, F. Lee, B. Louie, *J. Org. Chem.* **1988**, *53*, 951-954.
[36] E. E. Gilbert, *Chem. Rev.* **1962**, *62*, 549-589.
[37] I. J. Galpin, G. W. Kenner, A. Marston, *Bioorg. Chem.* **1979**, *8*, 323-332.
[38] A. Gieren, B. Dederer, H. W. Roesky, N. Amin, O. Petersen, *Z. Anorg. Allg. Chem.* **1978**, *440*, 119-129.
[39] H.-A. Lehmann, L. Riesel, *Z. Anorg. Allg. Chem.* **1969**, *371*, 281-288.

[40] H.-A. Lehmann, L. Riesel, *Z. Anorg. Allg. Chem.* **1969**, *371*, 281-288.
[41] L. Riesel, H.-A. Lehmann, *Z. Anorg. Allg. Chem.* **1969**, *371*, 289-294.
[42] J. Bruns, M. Eul, R. Pöttgen, M. S. Wickleder, *Angew. Chem. Int. Ed.* **2012**, *51*, 2204-2207.
[43] D. van Gerven, S. Sutorius, J. Bruns, M. S. Wickleder, *ChemistryOpen* **2022**, *11*, e202200122.
[44] R. Steudel, *Chemistry of the Non-Metals*, De Gruyter, Berlin, Boston, **2020**, pp. 521-598.
[45] R. Grau, W. A. Roth, *Z. Anorg. Allg. Chem.* **1930**, *188*, 173-185.
[46] A. N. Campbell, N. O. Smith, *Trans. Faraday Soc.* **1937**, *33*, 545-551.
[47] R. Steudel, *Chemie der Nichtmetalle*, De Gruyter, Berlin, Boston, **2014**.
[48] G. A. Benson, W. J. Spillane, *Chem. Rev.* **1980**, *80*, 151-186.
[49] H. Rose, *Pogg. Anal.* **1834**, *33*, 235.
[50] E. Berglund, *Ber. Dtsch. Chem. Ges.* **1876**, *9*, 252-256.
[51] E. Divers, T. Haga, *J. Chem. Soc., Trans.* **1896**, *69*, 1634-1653.
[52] F. Raschig, *Liebigs Ann. Chem.* **1887**, *241*, 161-252.
[53] P. Baumgarten, *Ber. dtsch. Chem. Ges. A/B* **1936**, *69*, 1929-1937.
[54] K. Yoshikubo, M. Suzuki, *Kirk-Othmer Encyclopedia of Chemical Technology*, John Wiley & Sons, **2000**.
[55] F. A. Kanda, A. J. King, *J. Am. Chem. Soc.* **1951**, *73*, 2315-2319.
[56] A. M. Vuagnat, E. L. Wagner, *J. Chem. Phys.* **1957**, *26*, 77-82.
[57] T. Rennebaum, D. van Gerven, S. S. Sebastian, M. S. Wickleder, *Chem. Eur. J.* **2024**, *30*, e202302526.
[58] F. Belaj, C. Kratky, E. Nachbaur, A. Popitsch, *Monatsh. Chem.* **1987**, *118*, 427-433.
[59] J. Sakurai, *J. Chem. Soc., Trans.* **1896**, *69*, 1654-1662.
[60] M. Cupery, *Ind. Eng. Chem.* **1938**, *30*, 627-631.
[61] L. F. Audrieth, M. Sveda, H. H. Sisler, M. J. Butler, *Chem. Rev.* **1940**, *26*, 49-94.
[62] P. Baumgarten, I. Marggraff, *Ber. Dtsch. Chem. Ges.* **1930**, *63*, 1019-1024.
[63] D. L. H. Williams, *Nitrosation Reactions and the Chemistry of Nitric Oxide* (Ed.: D. L. H. Williams), Elsevier Science, Amsterdam, **2004**, pp. 35-56.
[64] R. Kumar, N. Vijayan, N. Khan, Sonia, M. Kumari, M. Jewariya, R. Srivastava, *J. Mater. Sci.: Mater. Electron.* **2020**, *31*, 14271-14278.
[65] G. W. Cox, T. M. Sabine, V. M. Padmanabhan, N. T. Ban, M. K. Chung, A. J. Surjadi, *Acta Crystallogr.* **1967**, *23*, 578-581.
[66] P. Gross, Y. Zhang, L. Bayarjargal, B. Winkler, H. A. Höppe, *Dalton Trans.* **2022**, *51*, 11737-11746.
[67] R. Manickkavachagam, R. K. Rajaram, *Z. Kristallogr. – Cryst. Mater.* **1984**, *168*, 179-186.
[68] F. Belaj, C. Kratky, E. Nachbaur, A. Popitsch, *Monatsh. Chem.* **1987**, *118*, 947-954.
[69] M. S. Wickleder, *Z. Anorg. Allg. Chem.* **1999**, *625*, 1794-1798.
[70] M. S. Wickleder, *J. Alloys Compd.* **2000**, *303-304*, 445-453.
[71] M. S. Wickleder, *Z. Kristallogr.* **2005**, 192-195.
[72] K. A. Hofmann, E. Biesalski, E. Söderlund, *Ber. Dtsch. Chem. Ges.* **1912**, *45*, 1731-1736.
[73] L. Chaumeton, *C. .r hebd. sèances Acad. sci.* **1936**, 1783-1786.
[74] F. Belaj, C. Kratky, E. Nachbaur, A. Popitsch, *Monatsh. Chem.* **1987**, *118*, 349-354.
[75] E. Divers, T. Haga, *J. Chem. Soc., Trans.* **1892**, *61*, 943-988.
[76] P. Baumgarten, A.-H. Krummacher, *Ber. dtsch. Chem. Ges. A/B* **1934**, *67*, 1257-1260.
[77] H. H. Sisler, L. F. Audrieth, J. A. Lower, W. C. Fernelius, *Inorg. Synth., Vol. 2*, **1946**, pp. 179-181.
[78] H. Sisler, L. F. Audrieth, U. S. Branson, W. C. Johnson, *Inorg. Synth., Vol. 2*, **1946**, pp. 182-183.
[79] J. V. Tillack, C. H. L. Kennard, *J. Chem. Soc. A* **1970**, 1637-1640.
[80] J. R. Hall, R. A. Johnson, *J. Mol. Struct.* **1978**, *48*, 353-361.
[81] J. R. Hall, R. A. Johnson, H. F. Shurvell, *J. Raman Spectrosc.* **1979**, *8*, 145-150.
[82] G. A. Jeffrey, D. W. Jones, *Acta Crystallogr.* **1956**, *9*, 283-289.
[83] D. W. J. Cruickshank, D. W. Jones, *Acta Crystallogr.* **1963**, *16*, 877-883.
[84] P. Barbier, Y. Parent, G. Mairesse, *Acta Crystallogr. Sect. B* **1979**, *35*, 1308-1312.
[85] J. R. Hall, R. A. Johnson, C. H. L. Kennard, G. Smith, B. W. Skelton, A. H. White, *J. Chem. Soc., Dalton Trans.* **1980**, 1091-1097.

[86] F. Mijlhoff, *Acta Crystallogr.* **1965**, *18*, 795-798.
[87] M. Goehring, H. Hohenschutz, J. Ebert, *Z. Anorg. Allg. Chem.* **1954**, *276*, 47-56.
[88] E. Rodek, N. Amin, H. W. Roesky, *Z. Anorg. Allg. Chem.* **1979**, *457*, 123-126.
[89] K. Fischer, K. R. Andress, *Z. Anorg. Allg. Chem.* **1955**, *281*, 169-182.
[90] G. Heinze, A. Meuwsen, *Z. Anorg. Allg. Chem.* **1954**, *275*, 49-58.
[91] C. Leben, M. Jansen, *Z. Naturforsch. B* **1999**, *54*, 757.
[92] D. S. Rustad, *Polyhedron* **2001**, *20*, 2439-2444.
[93] T. Curtius, *Ber. Dtsch. Chem. Ges.* **1887**, *20*, 1632-1634.
[94] T. M. Rattan, K. C. Patil, *Inorganic Hydrazine Derivatives*, **2014**, pp. 1-36.
[95] L. Wolff, *Liebigs Ann. Chem.* **1912**, *394*, 86-108.
[96] L. P. Lessing, *Scientific American* **1953**, *189*, 30-33.
[97] N. L. Munjal, B. L. Gupta, M. Varma, *Propellants, Explosives, Pyrotechnics* **1985**, *10*, 111-117.
[98] F. Raschig, Verfahren zur Darstellung von Hydrazin, DE192783C, 1906.
[99] L. F. Audrieth, B. A. Ogg, *The chemistry of hydrazine*, Wiley, New York, **1951**.
[100] E. Abel, *Monatsh. Chem.* **1956**, *87*, 164-175.
[101] L. Song, M. Liu, W. Wu, Q. Zhang, Y. Mo, *J. Chem. Theory Comput.* **2005**, *1*, 394-402.
[102] R. L. Collin, W. N. Lipscomb, *Acta Crystallogr.* **1951**, *4*, 10-14.
[103] R. Liminga, I. Olovsson, *Acta Crystallogr.* **1964**, *17*, 1523-1528.
[104] L. F. Audrieth, S. F. West, *J. Am. Chem. Soc.* **1955**, *77*, 5000-5002.
[105] T. Curtius, *Ber. Dtsch. Chem. Ges.* **1890**, *23*, 3023-3033.
[106] A. F. Hollemann, E. Wiberg, N. Wiberg, *Lehrbuch der Anorganischen Chemie*, 102 ed., Walter de Gruyter, Berlin, **2007**.
[107] I. C. Tornieporth-Oetting, T. M. Klapötke, *Angew. Chem. Int. Ed.* **1995**, *34*, 511-520.
[108] B. E. Bartlett, F. C. Tompkins, D. A. Young, J. H. L. McAuslan, P. Gray, P. W. Levy, R. A. W. Hill, F. P. Bowden, *Proc. R. Soc. Lond. Ser. A* **1958**, *246*, 206-216.
[109] W. P. Fehlhammer, W. Beck, *Z. Anorg. Allg. Chem.* **2013**, *639*, 1053-1082.
[110] G. Beck, *J. Prakt. Chem.* **1940**, *156*, 227-240.
[111] R. J. Shozda, J. A. Vernon, *J. Org. Chem.* **1967**, *32*, 2876-2880.
[112] H.-A. Lehmann, W. Holznagel, *Z. Anorg. Allg. Chem.* **1958**, *293*, 314-321.
[113] K. O. Christe, J. A. Boatz, M. Gerken, R. Haiges, S. Schneider, T. Schroer, F. S. Tham, A. Vij, V. Vij, R. I. Wagner, W. W. Wilson, *Inorg. Chem.* **2002**, *41*, 4275-4285.
[114] K. O. Christe, M. Gerken, R. Haiges, S. Schneider, T. Schroer, I. Tsyba, R. Bau, *Inorg. Chem.* **2003**, *42*, 416-419.
[115] X. Zeng, H. Beckers, E. Bernhardt, H. Willner, *Inorg. Chem.* **2011**, *50*, 8679-8684.
[116] M. Balci, *Synthesis* **2018**, *50*, 1373-1401.
[117] E. Demarcay, *Compt. Rend* **1881**, *92*, 726.
[118] W. L. Jolly, K. D. Maguire, D. Rabinovich, *Inorg. Chem.* **1963**, *2*, 1304-1305.
[119] A. Zalkin, T. E. Hopkins, D. H. Templeton, *Inorg. Chem.* **1966**, *5*, 1767-1770.
[120] W. L. Jolly, K. D. Maguire, D. F. Martin, J. E. Gano, R. Woehrle, C. Yoshida, *Inorg. Synth.*, **1967**, pp. 102-111.
[121] D. G. Gorenstein, B. A. Luxon, *Encyclopedia of Spectroscopy and Spectrometry (Third Edition)* (Eds.: J. C. Lindon, G. E. Tranter, D. W. Koppenaal), Academic Press, Oxford, **2017**, pp. 294-302.
[122] O. Kühl, *Phosphorus-31 NMR Spectroscopy*, Springer Berlin Heidelberg, **2009**.
[123] R. Keat, R. A. Shaw, M. Woods, *J. Chem. Soc., Dalton Trans.* **1976**, 1582-1589.
[124] M. Goehring, H. Hohenschutz, R. Appel, *Z. Naturforsch. B* **1954**, *9*, 678-681.
[125] G. N. Huntly, *J. Chem. Soc., Trans.* **1891**, *59*, 202-208.
[126] G. Müller-Schiedmayer, H. Harnisch, *Z. Anorg. Allg. Chem.* **1964**, *333*, 260-266.
[127] H. Grunze, *Z. Anorg. Allg. Chem.* **1958**, *296*, 63-72.
[128] J. S. Margo Becke-Goehring, *Angew. Chem.* **1957**, *69*, 640.
[129] H. Gerding, H. Gijben, B. Nieuwenhuijse, J. G. van Raaphorst, *Recl. Trav. Chim. Pays-Bas* **1960**, *79*, 41-45.
[130] W. E. Morgan, T. Glonek, J. R. Van Wazer, *Inorg. Chem.* **1974**, *13*, 1832-1835.
[131] E. Payen, M. Migeon, *C. R. Hebd. Seances Acad. Sci., Ser. C* **1974**, *279*, 687.
[132] K. Olie, *Acta Crystallogr. Sect. B* **1971**, *27*, 1459-1460.

[133] M. D. Ward, I. Y. Chan, S. Lebègue, J. A. Ibers, *Inorg. Chem.* **2014**, *53*, 9969-9975.
[134] G. J. Bullen, *J. Chem. Soc. A* **1971**, 1450-1453.
[135] P. Murray-Rust, J. Murray-Rust, C. I. F. Watt, *Tetrahedron* **1980**, *36*, 2799-2806.
[136] T. Steiner, *Angew. Chem. Int. Ed.* **2002**, *41*, 48-76.
[137] G. A. Jeffrey, *An Introduction to Hydrogen Bonding*, Oxford University Press, **1997**.
[138] G. A. P. Dalgaard, A. C. Hazell, R. G. Hazell, *Acta Crystallogr. Sect. B* **1974**, *30*, 2721-2724.
[139] H. Ondik, *Acta Crystallogr.* **1965**, *18*, 226-232.
[140] M. Bagieu-Beucher, I. Tordjman, A. Durif, J. C. Guitel, *Acta Crystallogr. Sect. B* **1976**, *32*, 1427-1430.
[141] M. Daub, K. Kazmierczak, H. A. Höppe, *Z. Anorg. Allg. Chem.* **2014**, *640*, 46-52.
[142] M. Nespolo, B. Guillot, *J. Appl. Crystallogr.* **2016**, *49*, 317-321.
[143] L. Link, R. Niewa, *J. Appl. Crystallogr.* **2023**, *56*, 1855-1864.
[144] R. D. Shannon, C. T. Prewitt, *Acta Crystallogr. Sect. B* **1969**, *25*, 925-946.
[145] R. Shannon, *Acta Crystallogr. Sec. A* **1976**, *32*, 751-767.
[146] P. W. Pakes, T. C. Rounds, H. L. Strauss, *J. Phys. Chem.* **1981**, *85*, 2469-2475.
[147] R. Faggiani, R. J. Gillespie, C. J. L. Lock, J. D. Tyrer, *Inorg. Chem.* **1978**, *17*, 2975-2978.
[148] U. Thewalt, K. Berhalter, P. Muller, *Acta Crystallogr. Sect. B* **1982**, *38*, 1280-1282.
[149] J. P. Johnson, J. Passmore, P. S. White, A. J. Bannister, A. G. Kendrick, *Acta Crystallogr. Sec. C* **1987**, *43*, 1651-1653.
[150] S. Parsons, J. Passmore, *Acc. Chem. Res.* **1994**, *27*, 101-108.
[151] T. Rennebaum, D. van Gerven, M. S. Wickleder, *Chem. Eur. J.* **2022**, *28*.
[152] P. Schwerdtfeger, P. D. W. Boyd, S. Brienne, A. K. Burrell, *Inorg. Chem.* **1992**, *31*, 3411-3422.
[153] P. M. S.Parsons, P.J.Sadler, R.Johnstone, *CSD Communication* **2006**.
[154] S. A. Brawner, I. J. B. Lin, J.-H. Kim, G. W. Everett, Jr., *Inorg. Chem.* **1978**, *17*, 1304-1308.
[155] M. Mikami, M. Konno, Y. Saito, *Acta Crystallogr. Sect. B* **1979**, *35*, 3096-3098.
[156] S. Sutorius, D. van Gerven, S. Olthof, B. Rasche, J. Bruns, *Chem. Eur. J.* **2022**, *28*, e202200004.
[157] R. J. Gillespie, E. A. Robinson, *Can. J. Chem.* **1961**, *39*, 2189-2200.
[158] M. Pley, M. S. Wickleder, *Z. Anorg. Allg. Chem.* **2004**, *630*, 1036-1039.
[159] A. Moreno Betancourt, J. Schwabedissen, R. M. Romano, C. O. Della Védova, H. Beckers, H. Willner, H.-G. Stammler, N. W. Mitzel, *Chem. Eur. J.* **2018**, *24*, 10409-10421.
[160] B. Krumm, A. Vij, R. L. Kirchmeier, J. n. M. Shreeve, *Inorg. Chem.* **1998**, *37*, 6295-6303.
[161] M. Becke-Goehring, E. Fluck, A. Failli, T. Moeller, *Inorg. Synth.*, **1966**, pp. 105-107.
[162] E. Stanley, *Acta Crystallogr.* **1953**, *6*, 187-196.
[163] W. T. A. Harrison, M. J. Plater, *Acta Crystallogr. E* **2017**, *73*, 188-191.
[164] H. D. Flack, *Helv. Chim. Acta* **2003**, *86*, 905-921.
[165] T. Kasperowicz, D. van Gerven, M. S. Wickleder, *Chem. Eur. J.* **2023**, *29*, e202301761.
[166] T. M. Klapötke, *Chem. Ber.* **1997**, *130*, 443-452.
[167] U. Müller, in *Inorg. Chem.*, Springer Berlin Heidelberg, Berlin, Heidelberg, **1973**, pp. 141-172.
[168] E. Prince, C. S. Choi, *Acta Crystallogr. Sect. B* **1978**, *34*, 2606-2608.
[169] G. E. Pringle, D. E. Noakes, *Acta Crystallogr. Sect. B* **1968**, *24*, 262-269.
[170] G. Hatem, F. Abdoun, M. Gaune-Escard, K. M. Eriksen, R. Fehrmann, *Thermochim. Acta* **1998**, *319*, 33-42.
[171] K. M. Eriksen, R. Fehrmann, G. Hatem, M. Gaune-Escard, O. B. Lapina, V. M. Mastikhin, *J. Phys. Chem.* **1996**, *100*, 10771-10778.
[172] S. Häuhle, A. Meisel, *Z. Chem.* **1968**, *8*, 279-279.
[173] B. J. Meehan, S. A. Tariq, J. O. Hill, *J. Therm. Anal.* **1977**, *12*, 235-244.
[174] A. N. Udaya, *Bachelor Thesis*, University of Cologne, **2023**.
[175] A. Claus, S. Koch, *Liebigs Ann. Chem.* **1869**, *152*, 336-350.
[176] M. Rahm, R. Hoffmann, N. W. Ashcroft, *Chem. Eur. J.* **2016**, *22*, 14625-14632.
[177] V. Zimmermann, L. V. Schindler, D. van Gerven, M. S. Wickleder, *Z. Anorg. Allg. Chem.* **2022**, *648*, e202200238.
[178] E. Buncel, *Chem. Rev.* **1970**, *70*, 323-337.

[179] H.-A. Lehmann, C. R. Ringel, V. Költzsch, *Z. Chem.* **1965**, *5*, 313-313.
[180] D. v. Gerven, *Dissertation Thesis*, University of Cologne **2020**.
[181] D. C. Abercromby, P. F. Tiley, *Journal of the Chemical Society (Resumed)* **1963**, 4902-4904.
[182] webbook.nist.gov/cgi/inchi?ID=C7446119&Mask=4&Type=ANTOINE&Plot=on#ref-1 (NIST Chemistry WebBook, accessed 26.06.2024)
[183] Bruker AXS, *APEX 4 v2021.4-0* **2021**, Madsion, Winconsin, USA.
[184] Bruker AXS, *APEX 5 v2023.9-2* **2023**, Madsion, Winconsin, USA.
[185] Bruker AXS, *Saint V8.40B* **2012**, Madsion, Winconsin, USA.
[186] L. Krause, R. Herbst-Irmer, G. M. Sheldrick, D. Stalke, *J. Appl. Crystallogr.* **2015**, *48*, 3-10.
[187] O. V. Dolomanov, L. J. Bourhis, R. J. Gildea, J. A. K. Howard, H. Puschmann, *J. Appl. Crystallogr.* **2009**, *42*, 339-341.
[188] G. Sheldrick, *Acta Crystallogr. Sec. A* **2015**, *71*, 3-8.
[189] G. Sheldrick, *Acta Crystallogr. Sec. C* **2015**, *71*, 3-8.
[190] Crystal Impact GbR, *Diamond 4.6.8* **2022**, Bonn, Germany.
[191] STOE & Cie GmbH, *WinXPOW 3.6.0.1* **2018**, Darmstadt, Germany.
[192] Rigaku Corporation, *SmartLab Studio II 4.4.295.0* **2014**, Tokyo, Japan.
[193] A. A. Coelho, *TOPAS Academic v6* **2016**,
[194] A. Coelho, *J. Appl. Crystallogr.* **2018**, *51*, 210-218.
[195] B. S. Hulbert, W. M. Kriven, *J. Appl. Crystallogr.* **2023**, *56*, 576.
[196] Renishaw plc., *WiRE 5.1* **2017**, New Mills, UK.
[197] PerkinElmer, *Spectrum 10.6.1.942* **2017**, Waltham, US.
[198] Bruker Optik GmbH, *OPUS 6.5* **2007**, Ettligen, Germany.
[199] NETZSCH Gerätebau GmbH, *NETZSCH Proteus 6.1.0* **2019**, Selb, Germany.
[200] F. Neese, F. Wennmohs, U. Becker, C. Riplinger, *J. Chem. Phys.* **2020**, *152*.
[201] C. Steffen, K. Thomas, U. Huniar, A. Hellweg, O. Rubner, A. Schroer, *J. Comput. Chem.* **2010**, *31*, 2967-2970.
[202] F. Weigend, R. Ahlrichs, *Phys. Chem. Phys. Chem.* **2005**, *7*, 3297-3305.
[203] F. Weigend, *Phys. Chem. Phys. Chem.* **2006**, *8*, 1057-1065.
[204] C. Adamo, V. Barone, *J. Chem. Phys.* **1999**, *110*, 6158-6170.
[205] T. H. Dunning, Jr., *J. Chem. Phys.* **1989**, *90*, 1007-1023.
[206] D. E. Woon, T. H. Dunning, Jr., *J. Chem. Phys.* **1993**, *98*, 1358-1371.
[207] J. Cirera, E. Ruiz, S. Alvarez, *Organometallics* **2005**, *24*, 1556-1562.
[208] M. Pinsky, D. Avnir, *Inorg. Chem.* **1998**, *37*, 5575-5582.
[209] R. Hoppe, *Z. Kristallogr. – Cryst. Mater.* **1979**, *150*, 23-52.
[210] C. R. Groom, I. J. Bruno, M. P. Lightfoot, S. C. Ward, *Acta Crystallogr. Sect. B* **2016**, *72*, 171-179.

10 Danksagung

Diese Arbeit wäre nicht ohne eine Vielzahl an Menschen, die mich während der Promotion begleitet haben, möglich gewesen. Dafür möchte ich einen gesonderten Dank aussprechen.

Beginnen möchte ich mit Prof. Mathias S. Wickleder, der mir die Möglichkeit gegeben hat, in seinem Arbeitskreis an stickstoffhaltigen Sulfaten zu forschen und diese Arbeit zu vollenden. Seine stetige Begeisterung für Forschungsergebnisse aller Art, pflichtbewusste Betreuung und immer vorhandene Ansprechbarkeit bei Problemen haben maßgeblich zum Erfolg dieser Arbeit beigetragen. Nicht zuletzt ermöglichte seine tolerante und liberale Einstellung im Forschungsbetrieb eine facettenreiche Forschung, die geprägt war von einer angenehmen nicht allzu stressigen Atmosphäre.
An nächster Stelle möchte ich Prof. Uwe Ruschewitz für die Übernahme des Zeitgutachtens der Arbeit danken. Als Zweitbetreuer während der Promotion hat er mit wissenschaftlichen Gesprächen und freundlichen Rat zu dieser Arbeit beitragen, wofür ich mich an dieser Stelle auch bedanken möchte.

Dr. David van Gerven möchte ich als ehemaligen Modulbetreuer, Wegbegleiter und Förderer ganz besonders danken. Seine allgegenwärtige Präsenz und immer freundliche Unterstützung haben dazu geführt, dass ich die Masterarbeit sowie dieses Projekt erfolgreich in der Arbeitsgruppe abschließen konnte. Eine besondere Hilfestellung war dabei seine Expertise für kristallographische Probleme sowie für die präparative Schwefeltrioxidchemie.
Dr. Christian Logemann möchte ich ebenfalls als frühen Wegbeleiter herzlich danken, der mir durch seine wissenschaftliche Erfahrung sowie Lösung allerlei anderer Probleme ("Logo kümmert sich") eine bedeutende Hilfestellung war.
Ferner möchte ich J.-Prof. Bertold Rasche danken, der durch sein enormes Wissen und immer entgegenkommenden Hilfsbereitschaft, thematisch und methodisch eine besondere Unterstützung während der Promotion war. Dies gilt auch für PD Dr. Jörn Bruns, der mit seiner seriösen und aufmerksamen Art ebenfalls eine große Hilfe war und diverse Einkristallmessungen durchgeführt und die Arbeit Korrektur gelesen hat. Petra Lux möchte ich danken für Ihr Engagement in organisatorischen Dingen.

Ein wichtiger Bestandteil des Ganzen war außerdem die Arbeit der Analytikplattformen sowie allen anderen Beteiligten mit analytischem Schwerpunkt. Silke Kremer, Dr. Ingo Pantenburg und Daniel Moog gilt ein herzlicher Dank für die durchgeführten röntgenographischen Messungen sowie hilfreichen Einblicke in die Röntgenmethoden, die in dieser röntgenstrukturlastigen Arbeit einen bedeutsamen Teil einnehmen. Außerdem danke ich Dirk Pullem für die C/H/N/S-Probenmessungen. Dr. Daniel Friedrich und Daniela Naumann danke ich für Hilfestellungen in der NMR Spektroskopie. Dr. Christoph Lenting danke ich für eine Einführung in die Ramanspektroskopie und Möglichkeit

selbständig am Ramanspektrometer zu messen. Dr. David van Gerven danke ich für diverse Einkristallmessungen sowie Experimente am OHCD. Niko Flosbach, Tobias Lapić und Seans S. Sebastian danke ich für die Pulverröntgenmessungen an den Flachpräparaten. Sean S. Sebastian danke ich zudem für die Durchführung der *Hirshfeld*-Oberflächenanalyse. Der gesamten Werkstatt danke ich für die kompetente Unterstützung in technischen Fragen sowie Thomas Dautert für die Hilfe bei IT-Angelegenheiten.

Meinen Dank möchte ich außerdem allen ehemaligen und aktuellen Mitgliedern des Arbeitskreises aussprechen. Den ehemaligen Gefährten Dr. Annabelle Mattern, Dr. Laura Straub, Dr. Christopher James und Dr. Markus Zegke danke ich für das gemeinschaftliche Miteinander sowie Hilfestellung in allen Bereichen. Alisha Mertens und Niko Flosbach danke ich besonders als zeitliche synchrone Mitstreiter für den intensiven wissenschaftlichen Austausch und für viele lustige Momente jenseits des Abzuges. Zudem möchte ich Stefan Sutorius, Thomas Kasperowicz, Désirée Badea, Katrin Eppers, Anissa Hnrjic, Tobias Lapić, Iuliia Neumann und Marios Symeonidis für die gemeinsame wissenschaftliche und soziale Zeit herzlich danken. Den studentischen Praktikanten, die ich während der Zeit betreut habe und viel zu dieser Arbeit beitragen haben, gehört auch ein besonderer Dank. Dazu gehören Sebastian Barutzki, Daniel Streup, Felix Croé, Krunal Kanani, Felix Herwede (2x), Aneeta Jose P, Antonia Nkechinyere Udaya und Paula Spengler. Ferner gilt ein Dank allen Beteiligten des Institutes für Anorganische Chemie mit den Arbeitsgruppen von Prof. Axel Klein, Prof. Dr. Dr. (h.c.) Sanjay Mathur und Prof. Uwe Ruschewitz für das gemeinschaftliche und freundliche Miteinander.

Als Kommilitonen und Mitstreiter der ersten Stunde danke ich außerdem Lukas Kletsch, Christopher Wallerius, Andrè Santos, Stefan (Wolf) Sutorius sowie Felix Herwede für die gemeinsame Studienzeit mit vielen lustigen und freundschaftlichen Momenten. Ein Dank gilt auch meinen ehemaligen Chemielehrer Dr. Daniel Schiffbauer, der durch seine fachliche Kompetenz den Weg zum Chemiestudium mitgeebnet hat. Abseits des Studiums möchte ich mich auch bei meinem gesamten Freundeskreis bedanken.

Zuletzt möchte ich bei meinen Eltern, meinem Bruder Flo, meiner Schwägerin Sabine und Neffen Anton für die fortwährende Unterstützung, Liebe und Geduld bedanken.

11 Eidesstattliche Erklärung

„Hiermit versichere ich an Eides statt, dass ich die vorliegende Dissertation selbstständig und ohne die Benutzung anderer als der angegebenen Hilfsmittel und Literatur angefertigt habe. Alle Stellen, die wörtlich oder sinngemäß aus veröffentlichten und nicht veröffentlichten Werken dem Wortlaut oder dem Sinn nach entnommen wurden, sind als solche kenntlich gemacht. Ich versichere an Eides statt, dass diese Dissertation noch keiner anderen Fakultät oder Universität zur Prüfung vorgelegen hat; dass sie - abgesehen von unten angegebenen Teilpublikationen und eingebundenen Artikeln und Manuskripten - noch nicht veröffentlicht worden ist sowie, dass ich eine Veröffentlichung der Dissertation vor Abschluss der Promotion nicht ohne Genehmigung des Promotionsausschusses vornehmen werde. Die Bestimmungen dieser Ordnung sind mir bekannt. Darüber hinaus erkläre ich hiermit, dass ich die Ordnung zur Sicherung guter wissenschaftlicher Praxis und zum Umgang mit wissenschaftlichem Fehlverhalten der Universität zu Köln gelesen und sie bei der Durchführung der Dissertation zugrundeliegenden Arbeiten und der schriftlich verfassten Dissertation beachtet habe und verpflichte mich hiermit, die dort genannten Vorgaben bei allen wissenschaftlichen Tätigkeiten zu beachten und umzusetzen. Ich versichere, dass die eingereichte elektronische Fassung der eingereichten Druckfassung vollständig entspricht."

Köln, 01. Juli 2024
Tobias Rennebaum

12 Teilpublikationen

Tobias Rennebaum, David van Gerven, and Mathias S. Wickleder

The Unprecedented $[S_4N_2O_{10}]^{2-}$ Anion in the Molecular Gold Complexes $[Au_2Br_2(S_4N_2O_{10})_2]$ and $[Au_2Cl_2(S_4N_2O_{10})_2](S_2O_5Cl_2)$

Chem. Eur. J. **2022**, *28*, e202202171, 1-3.

Tobias Rennebaum, David van Gerven, Sean S. Sebastian, and Mathias S. Wickleder

Hydrazine Sulfonic Acid, $NH_3NH(SO_3)$, the Bigger Sibling of Sulfamic Acid

Chem. Eur. J. **2024**, *30*, e202302526, 1-4.

Tobias Rennebaum, David van Gerven, Felix C. H. Herwede, and Mathias S. Wickleder

N_2H_4 Derived Sulfonic Acids: Hydrazine Disulfonate, $[(SO_3)HNNH(SO_3)]^{2-}$, and Hydrazine *Iso*-disulfonate, $[H_2NN(SO_3)_2]^{2-}$

Chem. Eur. J. **2024**, *30*, e202402337, 1-8.